

# Mass Spectrometry in Inorganic Chemistry

A symposium sponsored by  
the Division of Inorganic  
Chemistry at the 152nd  
Meeting of the American  
Chemical Society, New York,  
N. Y. Sept. 15-16, 1966.

**John L. Margrave**

*Symposium Chairman*

ADVANCES IN CHEMISTRY SERIES

72

AMERICAN CHEMICAL SOCIETY  
WASHINGTON, D.C. 1968

Copyright © 1968

American Chemical Society

All Rights Reserved

Library of Congress Catalog Card 68-25995

PRINTED IN THE UNITED STATES OF AMERICA

**American Chemical Society  
Library**

**1155 16th St., N.W.**

**Washington, D.C. 20036**  
In Mass Spectrometry in Inorganic Chemistry; Margrave, J.;  
Advances in Chemistry; American Chemical Society: Washington, DC, 1968.

# Advances in Chemistry Series

Robert F. Gould, *Editor*

## *Advisory Board*

Sidney M. Cantor

Frank G. Ciapetta

William von Fischer

Edward L. Haenisch

Edwin J. Hart

Stanley Kirschner

John L. Lundberg

Harry S. Mosher

Edward E. Smissman

AMERICAN CHEMICAL SOCIETY PUBLICATIONS



## FOREWORD

ADVANCES IN CHEMISTRY SERIES was founded in 1949 by the American Chemical Society as an outlet for symposia and collections of data in special areas of topical interest that could not be accommodated in the Society's journals. It provides a medium for symposia that would otherwise be fragmented, their papers distributed among several journals or not published at all. Papers are refereed critically according to ACS editorial standards and receive the careful attention and processing characteristic of ACS publications. Papers published in ADVANCES IN CHEMISTRY SERIES are original contributions not published elsewhere in whole or major part and include reports of research as well as reviews since symposia may embrace both types of presentation.

## PREFACE

The mass spectrometer has clearly become a basic tool for chemical manipulations and has discontinuously increased in importance from the days when it was regarded primarily as an analytical instrument. New techniques for mass analysis, new designs for sampling, and new electronic accessories have all helped raise the mass spectrometer to a position of prime importance in chemical research. More important than all of these tangible improvements has been a modification of the basic philosophy of chemists toward mass spectrometers. At one time a mass spectrometer would only see a sample after it had been given the ultimate chemical purification and analytical treatments. The chemist was more worried about the mass spectrometer than about his sample. In the modern world the mass spectrometer has become an expensive but rather conventional monitor available to the chemist at any stage in a research problem to help establish what is going on in a chemical process, both quantitatively and qualitatively. Water vapor, fluorine compounds, boron hydrides, sulfur compounds, transition metal chelates, and many other reactive and unusual materials are now being routinely introduced into mass spectrometers for study.

As one might have predicted, the contributions to chemical knowledge by the art of mass spectrometry are directly related to how many different kinds of chemical systems are examined and how many different kinds of studies one can perform on these systems. Gas chromatograph-mass spectrometric units, fast-response systems, high temperature systems, and high precision electronic circuits are only a few of the many new developments which have contributed to the current popularity of mass spectrometers in chemical laboratories.

I wish to acknowledge the promptness and cooperative attitude of the various participants in the original symposium and especially the cooperation of those authors who were able to prepare the papers for this volume. A number of papers which concerned specific topics were submitted for publication in various specialized journals.

The American Chemical Society staff of the *Advances in Chemistry Series* under the direction of Robert F. Gould has been most cooperative

in handling the editorial matters related to this book. In addition, I wish to acknowledge the contributions of Nancy Naomi Craig and B. K. Micklitz in preparing material for publication.

JOHN L. MARGRAVE

Houston, Texas

March 1967

# Mass Spectrometric Studies of Chemionization by Reaction of Electronically Excited Species

J. L. FRANKLIN

Rice University, Houston, Tex.

*During the last few years an increasing number of studies has been carried out on a class of reactions involving the formation of ions in gases by reactions of two neutral atoms or molecules. The reaction  $Ar^* + N_2 \rightarrow ArN_2^+ + e$  is typical. Recently progress has been made toward determining the rate constants of these reactions, which turn out to be in the order of  $10^{-9}$  cc./molecule/sec. In some instances several excited states are known to take part in the reaction.*

The occurrence of diatomic ions of the rare gases has been noted by several experimenters (29, 30, 43), but for a number of years the exact nature of the processes leading to their formation was not understood. In 1951, Hornbeck and Molnar (18) measured the appearance potentials of the homonuclear diatomic ions for all of the rare gases. Their mass spectrometer was not ideally suited to studies of mass spectra of gases at elevated pressures. The instrument had relatively poor resolving power with the result that their appearance potentials were not precise. Nevertheless, they demonstrated that the appearance potentials of the diatomic ions were in all cases 0.7 to 1.5 e. v. below the ionization potentials of the corresponding rare gas atoms. The pressure dependence in each case was found to be second order. Both of these results show that the reaction did not involve atomic ions, and Hornbeck and Molnar concluded that the reaction involved attack of an excited atom upon an atom in the ground state—*i.e.*



where the asterisk signifies electronic excitation. Reactions of this kind, in which an ion is formed by the reaction of two or more neutral entities,

Table I. Appearance Potentials of

<i>Excited Atom, X*</i>	<i>Lowest Excitation Energy</i>	<i>Ionization Potential</i>	<i>Appearance</i>
			<i>He</i>
He	19.8	24.6	23.2 (18) 23.3 (35) 23.4 (22)
Ne	16.8	21.6	
Ar	11.5	15.8	
Kr	9.9	14.7 <sup>b</sup> 14.0 <sup>a</sup>	
Xe	8.3	13.4 <sup>b</sup> 12.1 <sup>a</sup>	

<sup>a</sup> <sup>2</sup>P<sub>3/2</sub> state.

is called chemionization. Following the studies of Hornbeck and Molnar (18), various workers have studied mixtures of certain of the rare gases in an effort to ascertain whether heteronuclear diatomic ions could be formed. Thus, Pahl and Weimer (36, 37) observed HeNe<sup>+</sup> in a glow discharge but failed to find HeAr<sup>+</sup> or NeAr<sup>+</sup> in mixtures of those gases. Fuchs and Kaul (13) studied NeAr<sup>+</sup> and ArKr<sup>+</sup>, and the latter was examined in greater detail by Kaul, Lauterbach, and Fuchs (21). Kaul and Taubert (22) reported ArXe<sup>+</sup> and KrXe<sup>+</sup>. Munson, Franklin, and Field made a rather complete study of the diatomic ions of the rare gases taken alone and in combination (35). They found that all of the possible rare gas diatomic gas ions are formed, and they measured appearance potentials of all except HeXe<sup>+</sup>, which was formed in such small amounts that an appearance potential could not be determined satisfactorily. Table I gives all of the results of these studies as well as of the appearance potentials measured for the rare gas diatomic ions from the literature. It is surprising that, considering the relatively small intensities of these ions, there has been such good agreement among the measured appearance potentials.

Before discussing these measurements it would be of interest to note the shape of a typical ionization efficiency curve for a rare gas diatomic ion (Figure 1). This curve is reminiscent of the excitation curve for optically forbidden transitions by electron impact and is quite different

**the Rare Gas Diatomic Ions in e.v.***Potential of XY<sup>+</sup> where Y is*

<i>Ne</i>	<i>Ar</i>	<i>Kr</i>	<i>Xe</i>
23.4 (35)	17.9 (35)	19.9 (35)	
22.6 (22)	19.9 (35)		
20.9 (18, 35)	16.8 (35)	16.6 (35)	16.0 (35)
	16.5 (13)		
	14.7 (35)	14.0 (35)	13.5 (22, 35)
	15.1 (18, 20)		
		13.0 (35)	12.2 (22)
		13.2 (18, 22)	12.3 (35)
			11.2 (35)
			11.6 (22)

<sup>b</sup> <sup>2</sup>P<sub>1/2</sub> state.

from the typical ionization efficiency curve for the formation of monatomic ions by electrons, also shown in Figure 1 for comparison. As will be discussed in more detail later, the diatomic ions in all cases were second order in pressure. Further, the molecular-ion formation was independent of field strength, and thus the possibility of their formation by ion-molecule reactions is eliminated. Thus, we conclude that Hornbeck and Molnar's (18) interpretation of their observations applies broadly and that the heteronuclear diatomic ions are formed by the following generalized reaction:



It will be of interest to note the appearance potentials of the heteronuclear ions in Table I. In each case the appearance potential is greater than the ionization potential of the constituent atom of lowest ionization potential so that the reaction must always involve an excited state of the atom of highest ionization potential. Possible exceptions to this would be ArKr<sup>+</sup>, ArXe<sup>+</sup>, and KrXe<sup>+</sup>. In the case of KrXe<sup>+</sup> and ArKr<sup>+</sup> the appearance potential is close to the lower (<sup>2</sup>P<sub>3/2</sub>) state of xenon and krypton, respectively. For ArXe<sup>+</sup> the appearance potential is quite close to the higher (<sup>2</sup>P<sub>1/2</sub>) state of xenon. If indeed, a state of the atom of lower ionization potential is involved, it must be an ionic state if the appearance potentials are correct. Since the reaction of an ion with a neutral atom would be third order in pressure and these reactions are second order, it

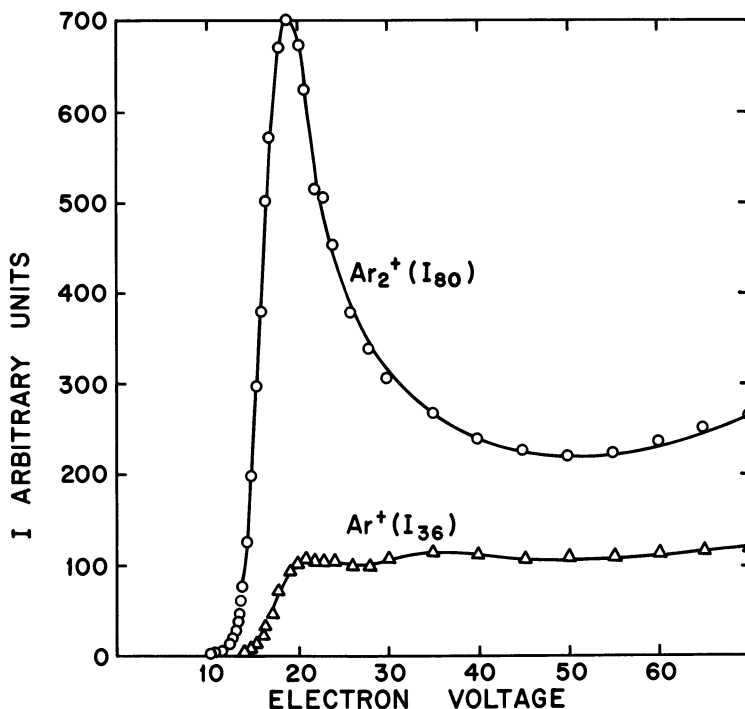


Figure 1. Ionization efficiency curves

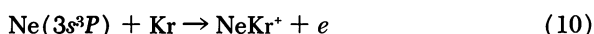
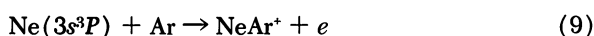
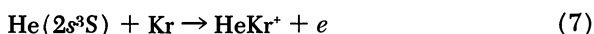
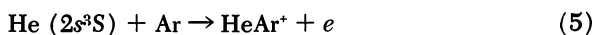
seems certain that the reactions leading to the formation of  $ArKr^+$  and  $ArXe^+$  are reactions of the excited argon, and that for the formation of  $KrXe^+$  involves excited krypton.

In all of the heteronuclear molecular rare gas ions the energy at which the ion appears is greater than one of its possible decomposition asymptotes. There is thus a problem of understanding why such a molecular ion should be stable. There seems no doubt that they are, and we think that Figure 2 will illustrate the reason. Consider the case of  $HeNe^+$ . Presumably, the interaction of  $Ne^+$  with helium is repulsive, whereas that of  $He^+$  with Ne is attractive. However, the noncrossing rule, as illustrated in Figure 2, results in a minimum in the potential energy curve which enables the ion to exist in spite of its energy.

In Table I the  $HeAr^+$  ion has two appearance potentials. The upper one at 19.9 e. v. corresponds closely to the energy of the helium metastable atom. The ionization efficiency curve shows a sharp change in slope at this point. There is, however, a rather long tail to the curve which has a lower appearance potential at around 17.9 e. v. This occurs in an energy range for which there are no known states for either argon or helium, and it is difficult to understand how an ion with this appearance potential

is formed. This was, however, a reproducible value and presumably represented a real phenomenon. There has been some evidence by mass spectrometrists employing electron beams of narrow energy spread which suggest that there are indeed states of argon in the ionization continuum, and one of these has been identified in the neighborhood of 18 e. v. (8). Perhaps it is this state that is responsible for the lower appearance potential of HeAr<sup>+</sup>. A similar result is found with NeXe<sup>+</sup>, whose appearance potential at 16.0 volts is well above the ionization potential of xenon and definitely below the lowest state of neon. Presumably, similar considerations would apply, but there have been no excited states of xenon reported to our knowledge.

The following reactions thus appear to account for the various rare gas diatomic ions:



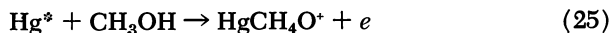
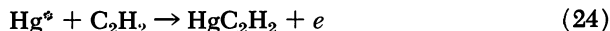
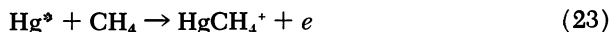
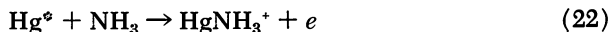
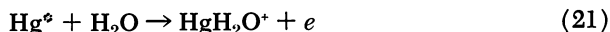
The strength of the bond in He<sub>2</sub><sup>+</sup> has been estimated in various ways with results varying from 0.05 e. v. to 2.2 e. v. Recently, Regan, Browne, and Matsen (38) made a careful and apparently definitive calculation which shows D(He<sub>2</sub><sup>+</sup>) to be at least 2.2 e. v. This bond strength, if correct, would suggest that the appearance potential of He<sub>2</sub><sup>+</sup> should be about 22.4 e. v. In fact, as is seen in Table I, the appearance potential is about 23.2 e. v., and the question arises as to why the potential is not

lower and nearer to 22.4 e. v. The following relevant states of helium atom and their energies (in e. v.) are known (33):

$$2^1P, 21.22; 3^3S, 22.72; 3^1S, 22.92; 3^3P, 23.01; 3^1P, 23.09.$$

At least four of these have sufficient energy to contribute to the formation of the diatomic ion. Recently, St. John *et al.* (39) have studied the cross-section for excitation of various electronic states of helium by electron impact. They find that all of the relevant states except  $^1P$  states dropped to vanishingly small values at about the ionization potential of helium. The  $^1P$  states show appreciable cross sections at voltages considerably below the ionization potential; hence, one concludes that in all probability it is the large cross section for excitation of the  $^1P$  states that determine the appearance potential of the diatomic ion. Thus, the  $3^3P$ , the  $3^1S$  and  $3^3S$ , while being energetically capable of reaction, are present at low energies in such small amounts as to be undetectable. The  $2^1P$  state is of too low an energy to form the diatomic ion and thus, the appearance potential is limited to the  $3^1P$  state whose energy of 23.09 e. v. above the ground state corresponds closely to the average appearance potential determined by various mass spectrometrists for the diatomic ion. States of higher energy may contribute but would not be detected at onset.

Until now the discussion has been limited to rare gases. Although they have indeed played a large part in the development of this field, several other reactions have been reported involving the rare gases with other materials and indeed, involving atoms and molecules, exclusive of the rare gases. Cermak and Herman (6) and Cermak (4) have reported several reactions of the rare gases with mercury and of excited mercury atoms with ammonia, methane, acetylene, and methanol, as well as a reaction with nitrogen in which it could not be determined which reactant was the excited entity. Typical reactions involving mercury are listed below.



More recently Herman and Cermak (17) have found that the reaction of argon and mercury (Reaction 20) involves the metastable state of argon.

Munson, Field, and Franklin (34) have studied reactions of certain rare gases with nitrogen and carbon monoxide, and Field and Franklin (11) have studied reactions of the rare gases with methane, acetylene, and other simple gases. The latter observed the formation, by chemionization reactions, of compounds of xenon with methane, acetylene, oxygen, and water. The former reported reactions of argon, krypton, and xenon with nitrogen and carbon monoxide. In each case it appeared to be the excited rare gas atom that attacked, although this conclusion is somewhat speculative.

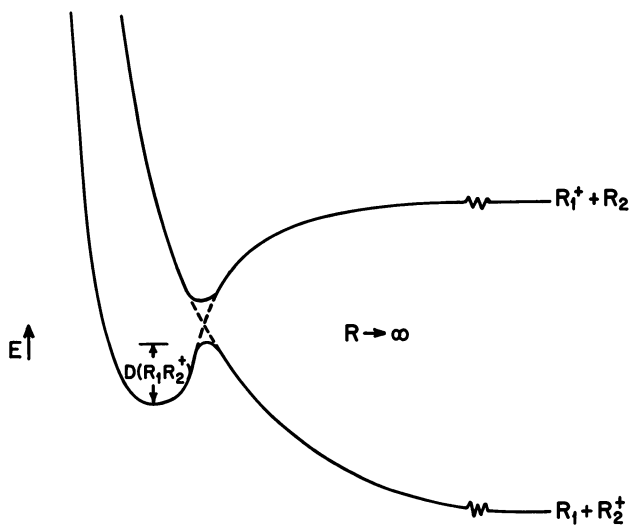
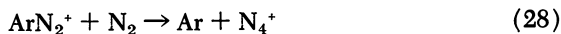


Figure 2. Schematic representation for non-crossing rule for states of  $R_1R_2^+$

Perhaps the earliest studies of chemionization were those of Mohler *et al.* (31, 32) of  $Cs_2^+$  and  $Rb_2^+$ . In these studies monochromatic radiation from line spectra were passed into the vapor of Cs or Rb, and ionization was detected at energies definitely below the ionization potential of the alkali atom in question. Similar studies employing radiation have recently been made by Lee and Mahan (27), who confirmed the results of Mohler *et al.* and also observed the formation of  $K_2^+$  by chemionization.

In further studies Munson, Field, and Franklin (34) observed  $N_4^+$  and  $C_2O_2^+$  respectively in nitrogen and carbon monoxide. Both exhibited ionization efficiency curves having the characteristic sharp maximum a few volts above the onset for forming the product ion. From the shape of the curve it was suspected that an excitation process was involved and

thus that the ions resulted from a chemionization reaction. These ions exhibited second-order dependence on pressure, and their intensities were independent of field strength; hence, they are clearly formed by a chemionization reaction. The  $N_4^+$  and  $C_2O_2^+$  ions were present in rather small intensities even at 300 microns pressure. When the pressure was reduced to 70–80 microns, they could no longer be detected. If, at this pressure of nitrogen, argon was then added in approximately equal amounts,  $N_4^+$  reappeared and along with it  $ArN_2^+$  was observed. A pressure study showed that  $ArN_2^+$  depended on the first power of the pressure of each reactant and that  $N_4^+$  depended on both the first power of the argon pressure and second power of nitrogen pressure. Further,  $N_4^+$  formation depended upon field strength, suggesting that an ion-molecule reaction was involved. Clearly then, the  $N_4^+$  appears to have been formed from the  $ArN_2^+$  ion. The appearance potentials all correspond to that of  $Ar_2^+$ , and indeed the  $Ar_2^+$  ion is reduced as the nitrogen pressure increases. Thus, it is evident that the same states which lead to  $Ar_2^+$  lead also to  $ArN_2^+$ . The sequence of reactions would then appear to be as follows:

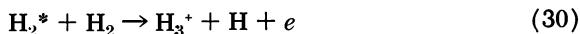


Similar considerations apply to reactions of krypton and CO.

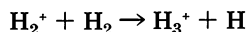
Along similar lines Cermak (5) has reported the formation of  $N_3O^+$  ion by a chemionization process involving reaction of excited  $N_2$  with NO according to Reaction 29.



The ionization efficiency curve showed the same general shape as that for  $N_4^+$ , reported by Munson, Field and Franklin (34). Herman and Cermak (17) have also reported the reaction of excited CO with sodium and potassium vapors to give the ions  $CONa^+$  or  $COK^+$  by chemionization. Recently Keenan and Clarke (23) have reported Reaction 30.



This was a quite surprising result since the formation of  $H_3^+$  had previously been considered to arise only from the reaction:



Similarly, Koyano *et al.* (25), using photoexcitation have observed the formation in acetylene of  $C_4H_3^+$  and  $C_4H_2^+$  by chemionization at energies well below the ionization potential of acetylene. These ions had previously been observed only in ion-molecule reactions between  $C_2H_2^+$  and  $C_2H_2$ .

**Rates of Chemionization Reactions**

In studies of ion-molecule reactions it is relatively simple to obtain explicit determinations of reaction rate because the mass spectrometer clearly identifies and provides quantitative analysis for both reactant and product ions. Unfortunately, in chemionization processes the reactant is not charged and, hence, cannot be observed directly. The reactant must be inferred from other observations, and its quantitative measurement must be obtained indirectly. The most obvious approach is to relate the intensity of the diatomic ion to that of the monatomic ion which cannot undergo reaction at moderate pressures. Dahler *et al.* (10) employed this device in studying the rates of chemionization reactions of helium, neon, and argon to form the diatomic ions. They considered the reaction mechanism to be as follows.



Assuming the steady state to apply to  $\text{Ar}^*$  we find

$$(\text{Ar}^*) = \frac{k_e i_e (\text{Ar})}{k_u + k_r (\text{Ar})} \quad (35)$$

Where  $i_e$  refers to electron current

$$\frac{d(\text{Ar}_2^+)}{dt} = k_r (\text{Ar}) (\text{Ar}^*) = \frac{k_e i_e k_r (\text{Ar})^2}{k_u + k_r (\text{Ar})} \quad (36)$$

$$\frac{d(\text{Ar}^+)}{dt} = k_i i_e (\text{Ar}) \quad (37)$$

Dividing (36) by (35) and recalling that  $\frac{k_i}{k_e} = \frac{\sigma_i}{\sigma_e}$  where  $\sigma$  is cross-section, we find

$$\frac{d(\text{Ar}^+)}{d(\text{Ar}_2^+)} = \frac{\sigma_i}{\sigma_e} \left[ 1 + \frac{k_u}{k_r (\text{Ar})} \right] \quad (38)$$

Since  $(\text{Ar}^+)$  and  $(\text{Ar}_2^+)$  are independent of each other, we can write

$$\frac{(\text{Ar}^+)}{(\text{Ar}_2^+)} = \frac{\sigma_i}{\sigma_e} \left[ 1 + \frac{1}{k_r \tau_u (\text{Ar})} \right] = \frac{I_{\text{Ar}^+}}{I_{\text{Ar}_2^+}} \quad (39)$$

where we assume the observed ion intensities are proportional to concentration and with the same constant of proportionality.

From Equation 39 it will be observed that a plot of  $\frac{I_{Ar^+}}{I_{Ar_2^+}}$  against the reciprocal of pressure should give a straight line whose intercept is  $\frac{\sigma_i}{\sigma_e}$  and whose slope is  $\frac{\sigma_i}{\sigma_e \tau_u k_r}$ . Plots of experimental data did indeed give straight lines, and in Table II the results of Dahler *et al.* (10) for both the ratio of cross sections and the product of  $k_r \tau_u$  are reported. From these results, however, there is no way to determine  $\tau_u$  and  $k_r$  separately. Reasonable values of  $\tau_u$  would be in the range of  $10^{-6}$  to  $10^{-8}$  seconds so that  $k_r$  would necessarily be in the range of  $10^{-10}$  to  $10^{-8}$  cc./molecule sec. Such rate constants would be comparable to those for ion-molecule reactions or at the upper limit would exceed by a factor of 10 the rates of the fastest ion-molecule reactions.

**Table II. Steady State Values for Rates of Diatomic Ion Formation**

Rare Gas	$\sigma_e/\sigma_i$	$k_r \tau_u \times 10^{16}$
He	0.06	0.58
Ne	0.01	11.
Ar	0.055	3.6

In the studies of Dahler *et al.* (10) there was no way to vary the time of reaction, and this necessarily limited the information that could be obtained concerning rates. Lampe and Hess (26) and later Becker and Lampe (1, 2) extended the study of argon by using a time-of-flight mass spectrometer capable of pulsing the electron beam and ion draw-out potential. In this study they could, at various pressures, delay the draw-out pulse and hence vary reaction time in the ionization chamber. As a result they could obtain explicit measurements of reaction rates. The following equations developed this relationship, based upon the mechanism of Dahler *et al.* (10) (Equations 31-34). Since the electron pulse is of short duration, it can reasonably be assumed that excited atoms are formed without reaction and then decay by Reactions 33 and 34. We can then write

$$\frac{-d(Ar^*)}{dt} = [k_u + k_r(Ar)](Ar^*) \quad (40)$$

which integrates to

$$(Ar^*) = (Ar^*)_0 \exp [-[k_u + k_r(Ar)]t] \quad (41)$$

$$d(Ar_2^+) = k_r(Ar^*) \quad (42)$$

substituting Equation 41 into Equation 42 and integrating

$$(\text{Ar}_2^+) = \frac{k_r(\text{Ar}^*)_o(\text{Ar})}{k_u + k_r(\text{Ar})} [1 - \exp [k_u + k_r(\text{Ar})]t] \quad (43)$$

$$(\text{Ar}^*)_o = \frac{ke}{ki} (\text{Ar}^*)_o = \frac{\sigma_e}{\sigma_i} (\text{Ar}^*) \quad (44)$$

$\text{Ar}^+$  being incapable of reaction at the low pressures employed. Finally, then

$$\frac{(\text{Ar}_2^+)}{(\text{Ar}^*)} = \frac{\sigma_e k_r (\text{Ar})}{\sigma_i [k_u + k_r(\text{Ar})]} [1 - \exp [k_u + k_r(\text{Ar})]t] \quad (45)$$

Obviously, studies of  $\frac{(\text{Ar}_2^+)}{(\text{Ar}^*)(\text{Ar})}$  against time at various pressures will permit separation of  $k_u \left( = \frac{1}{\tau_u} \right)$  and  $k_r$ . Lampe and Hess (26) employed the value of  $\sigma_e/\sigma_i$  Dahler *et al.* (10) obtained by the steady-state method, together with their own results to obtain values of  $k_r = 4.3 \times 10^{-10}$  cc. molecule<sup>-1</sup> cm.<sup>-1</sup> and  $\tau_u = 4.76 \pm 0.45 \times 10^{-7}$  sec. The product is in reasonable agreement with that of Dahler *et al.* (10). Cermak and Herman (7), using a beam of excited rare gas atoms found appreciable numbers of long lived ( $\geq 10^{-5}$  sec.) excited atoms with states approaching in energy to the ionization potential. Qualitatively this supports the observations of Lampe (1, 2, 26).

**Table III. Rate Constants for Various States Leading to  $\text{Ar}_2^+$**

Electron Energy, e.v.	$k_r \times 10^9$ cc/molecule/sec.	$\tau_u$ , micro sec.	$\frac{\sigma_e}{\sigma_i} \times 10^2$
18	$1.7 \pm 0.2$	$0.77 \pm 0.07$	$3.0 \pm 0.6$
28	$2.0 \pm 0.1$	$0.55 \pm 0.03$	$0.55 \pm 0.15$
65	$1.3 \pm 0.2$	$0.33 \pm 0.05$	$0.34 \pm 0.4$

Several investigators have recently reported evidence for the participation of several excited states in forming diatomic ions of the rare gases. Kaul (19) observed three states of argon leading to  $\text{Ar}_2^+$ , Comes (8) reported two peaks in the ionization efficiency curve for  $\text{Ar}_2^+$ , and Melton and Hamill (28), employing an RPD method, found three states of argon and of krypton leading to their respective diatomic ions. Becker and Lampe (1, 2) obtained ionization efficiency curves for  $\text{Ar}_2^+$  at several delay times. They found three maxima in each curve—a sharp one at 18 e. v., a somewhat broader one at about 28 e. v., and a very broad one at about 65 e. v. These maxima suggest that three states (or sets of states) are contributing to the formation of  $\text{Ar}_2^+$ . Further, with increasing delay (reaction) time the peaks varied in relative intensity, the 18 e. v.

one becoming increasingly prominent and the 65 e. v. one becoming progressively smaller. The contributions of the various states were not completely separable, but applying a rate treatment similar to that of Lampe and Hess (Equations 40-45) gave reasonable results for the lifetimes and reaction rate constants of the three states involved. Their results are given in Table III.

### *Ions in Flames*

Flames formed by combustion of hydrocarbons with air or oxygen contain an abundance of ions, whereas hydrogen-oxygen flames have few ions, if any. In neither case is the temperature sufficiently high to bring about ionization thermally, and so one must conclude that ionization results from chemical reaction—*i.e.*, from chemionization. The exact nature of the reaction has not been established, but in many cases free radicals formed from hydrocarbons seem to be involved. This suspicion is strengthened by the fact that adding a small amount of hydrocarbon to a hydrogen-oxygen flame brings about a great increase in ionization.

In all flames involving hydrogen or hydrocarbons the most abundant ion is  $\text{H}_3\text{O}^+$  followed by  $\text{NO}^+$  when nitrogen or nitrogen-containing fuels are present. In addition, many hydrocarbon ions are usually present, one of the most interesting being  $\text{C}_3\text{H}_3^+$ , which is suspected of having a cyclic structure. The subject of ions in flames has been extensively studied (24, 40, 42) and will not be reviewed here. However, most scientists concerned with the problem now think that chemionization produces the initial ions and that these then react with various neutral molecules and free radicals present to produce various ionic species.

Although the exact nature of the initial reaction has not been established, there is some evidence and a considerable body of opinion that the initial reaction is (3, 12, 41)



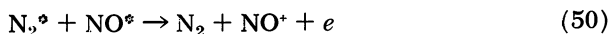
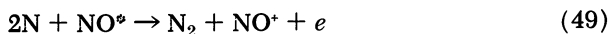
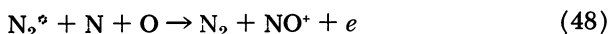
The  $\text{CHO}^+$  ion can react with water as follows



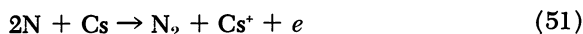
and with other hydrocarbons and oxygen containing compounds in a variety of ways.

Ionization has also been observed in other types of flames or high temperature environments. Thus, Gatz *et al.* (15, 16) have found that ions are formed when NO is added to the nitrogen afterglow and have

attributed their formation to chemionization, probably to one of the following reactions:



Gatz *et al.* (14) have also observed cesium ions when cesium was present in the nitrogen afterglow and attribute it to Reaction 51.



In this laboratory we have found that ionization occurs when benzene is added to the nitrogen afterglow, but neither the ions nor the process of their formation has been identified. Ions also occur in shock waves and probably are formed by chemionization. However, the scope of this paper does not permit a discussion of these processes.

### Literature Cited

- (1) Becker, P. M., Lampe, F. W., *J. Am. Chem. Soc.* **86**, 5347 (1964).
- (2) Becker, P. M., Lampe, F. W., *J. Chem. Phys.* **42**, 3857 (1965).
- (3) Calcote, H. F., "Progress in Astronautics and Aeronautics," Vol. 12, pp. 107-144, Academic Press, New York, 1963.
- (4) Cermak, V., *Proc. Intern. Conf. Phys. Electron At. Collisions, 3rd, Univ. Coll. London, 1963*, 1080.
- (5) Cermak, V., *J. Chem. Phys.* **43**, 4527 (1965).
- (6) Cermak, V., Herman, Z., *Mass Spectrometry Conf., ASTM Committee E-14, New Orleans, La. (June 3-8, 1962)*.
- (7) Cermak, V., Herman, Z., *Collection Czech. Chem. Commun.* **29**, 953 (1964).
- (8) Comes, F. J., *Proc. Intern. Conf. Ionization Phenomena Gases, 6th, Paris, 1963*, 159.
- (9) Comes, F. J., Lessman, W., *Z. Naturforsch* **16A**, 1396 (1961).
- (10) Dahler, J. S., Franklin, J. L., Munson, M. S. B., Field, F. H., *J. Chem. Phys.* **36**, 3332 (1962).
- (11) Field, F. H., Franklin, J. L., *J. Am. Chem. Soc.* **83**, 4509 (1961).
- (12) Fontijn, A., Baughman, G. L., *J. Chem. Phys.* **38**, 1784 (1963).
- (13) Fuchs, R., Kaul, W., *Z. Naturforsch* **15A**, 108 (1960).
- (14) Gatz, C., Young, R. A., Sharpless, R. L., *J. Chem. Phys.* **35**, 1500 (1961).
- (15) Gatz, C., Smith, F. T., Wise, H., *J. Chem. Phys.* **40**, 3743 (1964).
- (16) Gatz, C., Young, R. A., Sharpless, R. L., *J. Chem. Phys.* **39**, 1234 (1963).
- (17) Herman, Z., Cermak, V., *Collection Czech. Chem. Commun.* **31**, 649 (1966).
- (18) Hornbeck, J. A., Molnar, J. P., *Phys. Rev.* **84**, 621 (1951).
- (19) Kaul, W., *Proc. Intern. Conf. Ionization Phenomena Gases, 6th, Paris, 1963*, 169.
- (20) Kaul, W., Fuchs, R., *Z. Naturforsch* **15A**, 326 (1960).
- (21) Kaul, W., Lauterbach, U., Fuchs, R., *Naturwiss* **47**, 353 (1960).
- (22) Kaul, W., Taubert, R., *Z. Naturforsch* **17A**, 88 (1962).
- (23) Keenan, D. J., Clarke, E. M., *Ann. Conf. Mass Spectrometry, 14th, Dallas, May 22-27, 1966*, 42.

- (24) Knewstubb, P. F., "Mass Spectrometry of Organic Ions," F. W. McLafferty, ed., p. 255, Academic Press, New York, 1963.
- (25) Koyano, I., Tanaka, I., Omura, I., *J. Chem. Phys.* **40**, 2734 (1964).
- (26) Lampe, F. W., Hess, G. G., *J. Am. Chem. Soc.* **86**, 2952 (1964).
- (27) Lee, Y. T., Mahan, B. H., *J. Chem. Phys.* **42**, 2893 (1965).
- (28) Melton, C. E., Hamill, W. H., *J. Chem. Phys.* **41**, 1469 (1964).
- (29) Meyerott, R., *Phys. Rev.* **66**, 242 (1944).
- (30) *Ibid.*, **70**, 671 (1946).
- (31) Mohler, F., Foote, P., Chenault, R., *Phys. Rev.* **27**, 37 (1926).
- (32) Mohler, F., Boeckner, C., *J. Res. Nat. Bur. Stds.* **5**, 51, 399 (1930).
- (33) Moore, C. E., *Natl. Bur. Std. Circ.* **467**, I (1949).
- (34) Munson, M. S. B., Field, F. H., Franklin, J. L., *J. Chem. Phys.* **37**, 1790 (1963).
- (35) Munson, M. S. B., Franklin, J. L., Field, F. H., *J. Phys. Chem.* **67**, 1541 (1963).
- (36) Pahl, M., Weimer, U., *Naturwiss.* **44**, 487 (1957).
- (37) Pahl, M., Weimer, U., *Z. Naturforsch* **12A**, 926 (1957).
- (38) Regan, P. N., Browne, J. C., Matsen, F. A., *Phys. Rev.* **132**, 1304 (1963).
- (39) St. John, R. M., Miller, F. L., Lin, Chun C., *Phys. Rev.* **134A**, 888 (1964).
- (40) Shuler, R. E., Fenn, J. B., ed., "Progress in Astronautics and Aeronautics," Vol. 12, Academic Press, New York, 1963.
- (41) Sugden, T. M., "Progress in Astronautics and Aeronautics," p. 145, Vol. 12, R. E. Shuler and J. B. Fenn, eds., Academic Press, New York, 1963.
- (42) Symp. Combust., 10th, Combust. Inst., 1965.
- (43) Tüxen, O., *Z. Physik* **103**, 463 (1936).

RECEIVED October 11, 1966.

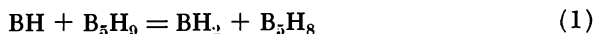
# Ion-Molecule Reactions Involving Pentaborane

G. R. HERTEL<sup>1</sup> and W. S. KOSKI

The Johns Hopkins University, Baltimore, Md.

*In attempting to rationalize some results obtained with rare gas sensitizing agents in the radiolysis of B<sub>5</sub>H<sub>9</sub>, some ion-molecule reactions of D<sup>+</sup>, D<sub>2</sub><sup>+</sup>, and rare gas ions with pentaborane were studied using a tandem mass spectrometer. It was found that the pentaborane fragmentation varied markedly as a function of the recombination energy of the rare gas ion. This variation proceeded as expected except where small ions such as He<sup>+</sup>, D<sup>+</sup>, and D<sub>2</sub><sup>+</sup> were involved. In these latter cases, the fragmentation was considerably less extensive than might be expected purely on the basis of the energy available for excitation as a sole result of the charge transfer process. This behavior was attributed to a field ionization mechanism.*

When certain boron hydrides are irradiated, new products are formed by the coupling of hydride fragments (3). Irradiation of pentaborane-9, for example, leads to decaborane-16 apparently from the coupling of two B<sub>5</sub>H<sub>8</sub> fragments. Studies of the effects of a scavenger (iodine) and sensitizers (the rare gases) have led to the proposal of a mechanism (8). The observed products are believed to arise from the various free radicals and fragments produced as the following scheme suggests:



<sup>1</sup> Present address: Oak Ridge National Laboratory, Oak Ridge, Tenn.

When an excess of a rare gas is added, the deuteron beam ionizes and excites the rare gas atoms which subsequently transfer energy to the pentaborane molecules *via* a variety of processes. As the rare gas, and thus the energy available to the pentaborane, is varied from xenon to helium, more fragmentation is expected to result which will have a corresponding effect on the products. With helium, the diborane yield is at a maximum. The yield decreases as the rare gas is changed to neon, argon, krypton, and xenon. The decaborane-16 yield experiences a broad minimum at argon. When He, Ne, and Ar were used, small amounts of tetraborane-10 and hexaborane-10 were produced. In addition, hydrogen gas and solid polymeric materials were produced in all the radiolysis experiments.

In a complex radiolysis such as this, much can be learned by varying the components of the reaction mixture and the conditions under which the reaction takes place, but it would be of considerable interest to be able to isolate some of the specific reactions which may contribute to the production of the final products. In this study, a two stage, or tandem mass spectrometer is used to study some possibly pertinent ion-molecule reactions involving pentaborane.

### *Experimental*

The instrument used in the experiments has been described elsewhere (4, 10). It consists of two mass spectrometers in tandem. The primary beam of desired ions is produced and selected by the first spectrometer, accelerated or decelerated to the desired energy (from 2 to 200 e. v.) and focused into the reaction chamber containing pentaborane-9. The ionic reaction products are extracted from the reaction chamber at an angle of 90° to the primary beam direction and analyzed by the second mass spectrometer.

The rare gas ions, D<sup>+</sup> and D<sub>2</sub><sup>+</sup>, were used to bombard pentaborane-9 in the energy range 2–200 e. v. to see what further information could be learned about the radiolysis reactions of pentaborane.

### *Results and Discussion*

Table I lists the relative abundances of the ionic products observed when pentaborane is bombarded with 10 e. v. rare gas ions. Xenon is found to produce relatively little fragmentation, as expected, since the recombination energies are low. The ionization potential of B<sub>5</sub>H<sub>9</sub> is 10.4 e. v., and the significant recombination energies of Xe<sup>+</sup> are 12.13 e. v. (<sup>2</sup>P<sub>3/2</sub>) and 13.44 e. v. (<sup>2</sup>P<sub>1/2</sub>). Energy available for the fragmentation of the B<sub>5</sub>H<sub>9</sub><sup>+</sup> ion upon charge transfer, then, is 1.7 e. v. or 3.0 e. v. depending upon the initial energy state of the Xe<sup>+</sup> ion. Krypton with its higher RE's of 14.00 e. v. and 14.67 e. v. changed the distribution of ions toward more fragmented species. With argon, the major product is B<sub>4</sub>H<sub>4</sub><sup>+</sup>, and

there is substantial fragmentation. Neon and helium produced large amounts of highly fragmented species.

**Table I. Relative Abundances of Pentaborane-9 Fragment Ions Produced by Rare Gas Ion Bombardment<sup>a</sup>**

<i>Ion</i>	<i>Xe</i>	<i>Kr</i>	<i>Ar</i>	<i>Ne</i>	<i>He</i>
B <sub>5</sub> H <sub>7</sub>	73				
B <sub>5</sub> H <sub>6</sub>		2	1		
B <sub>5</sub> H <sub>5</sub>	20	76	18		
B <sub>5</sub> H <sub>4</sub>			8	11	7
B <sub>5</sub> H <sub>3</sub>	<1		25	8	7
B <sub>5</sub> H <sub>2</sub>				24	23
B <sub>5</sub> H			3	3	8
B <sub>5</sub>				6	15
B <sub>4</sub> H <sub>6</sub>	3	<1			
B <sub>4</sub> H <sub>5</sub>	<1	2	8		
B <sub>4</sub> H <sub>4</sub>	2	20	31	3	
B <sub>4</sub> H <sub>3</sub>			<1	19	11
B <sub>4</sub> H <sub>2</sub>		<1	2	11	4
B <sub>4</sub> H			<1	1	13
B <sub>4</sub>				1	3
B <sub>3</sub> H <sub>4</sub>			<1	2	
B <sub>3</sub> H <sub>3</sub>			2	4	4
B <sub>3</sub> H <sub>2</sub>			<1	6	3
B <sub>3</sub> H					2

<sup>a</sup> Kinetic energy of rare gas ions = 10 e.v.

Qualitatively, the observed data can be reconciled with the proposed mechanism. When little fragmentation of the pentaborane occurs, as in the case of Xe<sup>+</sup> ion bombardment, very few BH radicals are formed, and since BH is the key to formation of the diborane and decaborane-16 in the proposed mechanism, the yield of products is small. As the rare gas is varied and the energy available to the pentaborane increases, the probability of BH radical formation rises, and the yields of diborane and decaborane-16 reflect this increase. The extensive fragmentation noted can easily account for the large yield of hydrogen observed in the radiolysis experiments. Other minor observations can be tentatively explained from the rare gas ion-pentaborane data, but other than noting that the fragmentation was greater than predicted in all cases, the only conclusion to be drawn from the mass spectrometric data is that the proposed mechanism is a possibility, but the system is complex.

Only the role of positive ions has been considered in this study. It is known that pentaborane and other boron hydrides form negative ions. The role that such ions may play in the radiolysis process is not known but could be significant.

The rare gas ion-pentaborane data taken over an energy range of 2–200 e. v. along with the reported appearance potentials (5) of the various pentaborane fragments were used to construct breakdown curves following the procedure used by Lindholm and his co-workers (1, 2, 6, 9, 11).

A complication of this scheme is the existence in many cases of more than one important recombination energy. This is unfortunately true for all of the rare gases with the exception of helium. Lindholm has studied this problem extensively and has determined recombination energies for many ions. He is often able to assign a specific ion fragment product to a specific recombination energy of the bombarding ion in the course of constructing breakdown curves. Since we were attempting to use a limited amount of data (from only five primary ions) to estimate the breakdown pattern of a rather peculiar and little studied molecule, we could not separate the effects of rare gas ions in the  $^2P_{3/2}$  and  $^2P_{1/2}$  states. To estimate the breakdown curves, the two values for each ion were averaged. The only case in which the difference is sizeable enough to create a problem is that of xenon. The resulting curves do not reflect any anomalies caused by the averaging procedure although, in view of the later results of  $D^+$  and  $D_2^+$  bombardment, it is unfortunate that a more rigorous representation of the breakdown curves in the energy range of 12–14 e. v. is not available. The resulting, admittedly rough, estimates are shown in Figure 1. Data were taken over a primary ion energy range of 2–200 e. v., and it was observed that the relative abundances of the pentaborane fragment ions varied slowly with the kinetic energy of the primary ion beam (4). The solid line segments in Figure 1 represent the experimentally determined points and illustrate the effects of the primary ion energy range.

From these curves it is possible to predict the relative yields of ions expected when bombarding pentaborane with other ions—*e.g.*,  $D^+$  and  $D_2^+$ .  $D^+$  has a recombination energy of 13.5 e. v.; thus, the expected distribution of ions would be no parent peak, little or no  $B_5H_7^+$ , a large and rapidly increasing amount of  $B_5H_5^+$ , less than 20%  $B_4H_4^+$ , and small amounts of  $B_4H_6^+$  and  $B_5H_6^+$ . Instead, one finds that the parent ion,  $B_5H_9^+$ , accounts for over 10% of the products;  $B_5H_7^+$ , over 16%;  $B_5H_5^+$ , 45%;  $B_4H_4^+$ , about 8%; small amounts of other ions are also present. The results at various incident ion energies are tabulated in Table II, and the average results are shown in Figure 2a. Obviously,  $D^+$  does not transfer its full increment of energy upon collision with  $B_5H_9$ , implying that simple charge exchange is not the only mechanism operating. What are the processes which could be involved? It is difficult to ascertain, but some possibilities are (1) hydride ion transfer with HD formation, (2)  $D^+$ -H exchange, (3) an ion-molecule type reaction—*i.e.*, an intimate

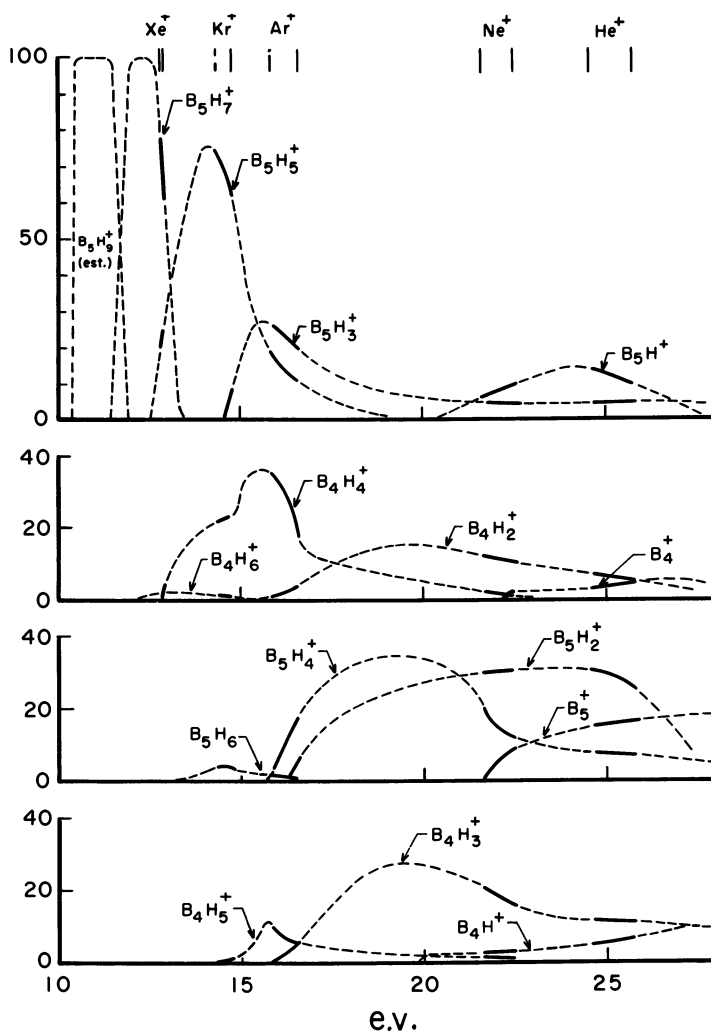


Figure 1. Breakdown pattern of  $B_5H_9^+$ . The relative abundances of fragment ions are plotted as a function of the excitation energy. Solid line segments represent the experimentally determined points

collision, (4) charge transfer, as mentioned, and which cannot explain the observed results in view of the rare gas ion results, and (5) field ionization.

Transfer of a hydride ion would leave an excited  $B_5H_8^+$  ion which could undergo extensive decomposition since the maximum energy available from such a process would be more than that available from simple

charge transfer ( $\sim 18$  as opposed to 13.5 e. v.). This could account for such ions as  $B_5H_2^+$ ,  $B_5H_3^+$ , and  $B_5H_4^+$ , as well as some of the  $B_4H_n^+$  ions which require more energy than that available from  $D^+$  (note the Kr results where none of these ions is formed). Momentum could be transferred by the  $H^-$  and the energy available to the pentaborane fragment reduced to give an even greater spread in product ions. This cannot account for formation of the parent ion in any way, however.

**Table II. Relative Abundances of Product Ions from  $D^+ + B_5H_9$  Reaction at Various  $D^+$  Energies**

Ion	<i>D<sup>+</sup> Incident Ion Energy (e. v.)</i>				
	140	100	40	10	2
$B_5H_9^+$	12.2	11.0	11.8	9.8	11.0
$B_5H_7^+$	23.8	16.6	16.3	17.3	11.4
$B_5H_6^+$	0.9	5.4	3.5	0.5	3.7
$B_5H_5^+$	40.5	34.3	43.1	47.4	52.3
$B_5H_4^+$	6.8	11.2	3.8	5.0	—
$B_5H_3^+$	3.1	3.5	6.5	3.7	7.0
$B_5H_2^+$	3.3	5.0	1.3	3.2	0.8
$B_5H^+$	0.2	1.1	0.5	—	2.7
$B_5^+$	—	—	0.4	—	—
$B_4H_6^+$	—	—	2.0	tr	—
$B_4H_5^+$	tr	2.8	1.3	2.6	4.9
$B_4H_4^+$	8.7	6.3	7.6	8.5	6.5
$B_4H_3^+$	1.0	1.8	1.1	1.3	—
$B_4H_2^+$	—	1.3	0.7	0.8	—

An exchange type reaction in which the  $D^+$  ion replaces an H atom would lead to a parent ion with a mass of 65. This was not observed. To account for the 64 peak, the  $D^+$  would have to replace two hydrogen atoms, but this is just another way of saying that an ion-molecule reaction is taking place. The existence of such an ion as  $B_5H_7D^+$  (mass 64) is difficult to accept since the existence of a stable  $B_5H_8^+$  is questionable in the electron spectrum and was not observed in any of the rare gas ion experiments.

Next, consider the case of an intimate encounter in which the deuterium ion is neutralized and leaves, apparently in some cases, before any excess energy can be redistributed among the bonds of the  $B_5H_9^+$ . The deuterium atom must necessarily carry off some of this excitation energy as kinetic energy or else the parent ion would not be observed. Rosenstock (7) has noted that the fraction of the energy going to the ion depends on the mass of the product ion and the mass of the product neutral; hence, if one assumed that the deuterium ion interacted with

the entire mass of the  $B_5H_9$  molecule (an unlikely situation) on neutralization, the deuterium atom could depart with as much as 97% of the available energy. The distribution of products would then indicate the excess energy imparted to the pentaborane.

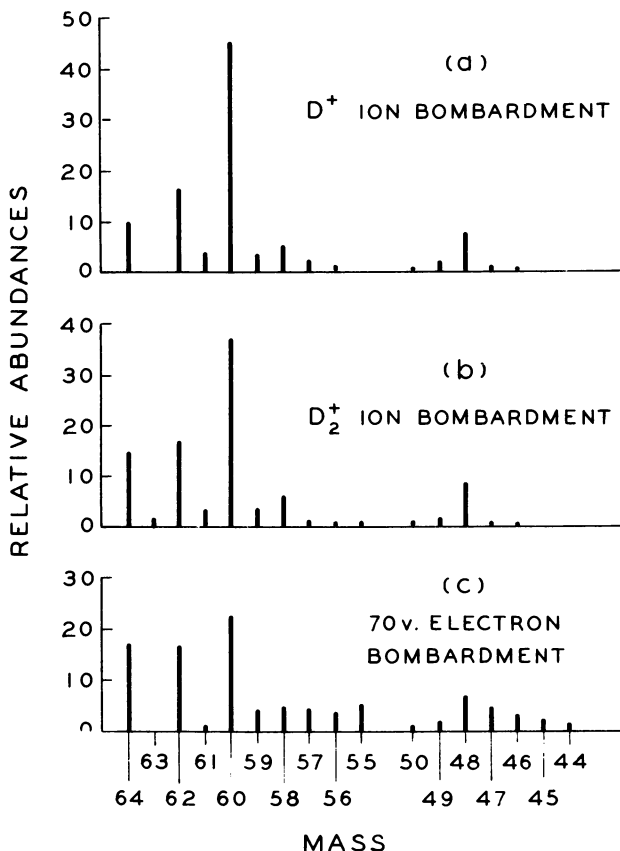


Figure 2. Monoisotopic mass spectra of  $B_5H_9$  produced by  $D^+$ ,  $D_2^+$  and 70 e.v. electron bombardment

Another possible mechanism which could explain the preponderance of parent ion when the bombarding projectile is a small ion is field ionization. In intimate encounters of molecules with small ions, the electric field close to such an ion can be large enough to cause field ionization of the molecule by a quantum mechanical tunnelling process. In the presence of such fields, ionization results with predominantly the parent ions with few fragment ions. This phenomenon appears to be at least qualitatively compatible with the results observed with  $D^+$  in this study.

**Table III. Relative Abundances of Product Ions from  $D_2^+ + B_5H_9$  Reaction at Various  $D_2^+$  Energies**

Ion	$D_2^+$ Incident Ion Energy (e. v.)				
	200	100	40	10	2
$B_5H_9^+$	15.3	13.3	13.4	15.5	14.9
$B_5H_8^+$	0.9 <sub>5</sub>	1.1	1.8	0.4 <sub>5</sub>	1.6
$B_5H_7^+$	19.8	17.6	16.4	16.3	14.8
$B_5H_6^+$	1.7	3.3	3.2	3.7	4.3
$B_5H_5^+$	32.5	35.2	38.2	37.8	37.3
$B_5H_4^+$	3.8	3.5	2.4	4.9	3.9
$B_5H_3^+$	5.8	6.6	8.3	6.1	6.0
$B_5H_2^+$	2.1	1.7	0.1 <sub>8</sub>	0.3 <sub>1</sub>	1.0
$B_5H^+$	0.9 <sub>5</sub>	0.5 <sub>6</sub>	0.3 <sub>5</sub>	0.8 <sub>5</sub>	—
$B_5^+$	1.8	1.3	0.5	0.0 <sub>6</sub>	0.6
$B_4H_6^+$	1.0	1.3	1.0	1.1	1.5
$B_4H_5^+$	1.3	1.3	1.9	1.8	3.1
$B_4H_4^+$	8.1	8.8	9.3	9.5	8.4
$B_4H_3^+$	0.6 <sub>4</sub>	1.2	1.2	0.3 <sub>7</sub>	1.3
$B_4H_2^+$	1.6	0.9 <sub>6</sub>	0.3 <sub>4</sub>	0.7 <sub>8</sub>	0.5 <sub>1</sub>
$B_4H^+$	—	0.3 <sub>6</sub>	0.2 <sub>2</sub>	0.1 <sub>7</sub>	0.1 <sub>2</sub>
$B_4^+$	0.5	0.0 <sub>8</sub>	0.2 <sub>7</sub>	0.0 <sub>1</sub>	—
$B_3H_6^+$	0.2	0.21	0.20	0.06	0.10
$B_3H_5^+$	0.18	0.10	0.08	0.09	0.16
$B_3H_4^+$	0.17	0.29	0.21	0.09	0.08
$B_3H_3^+$	0.72	0.37	0.27	0.13	0.28
$B_3H_2^+$	0.23	0.44	0.16	0.06	—
$B_3H^+$	0.17	—	0.02	—	—
$B_2H_6^+$	0.28	0.16	0.19	0.07	0.13
$B_2H_5^+$	0.03	0.10	0.08	0.03	0.07
$B_2H_4^+$	0.08	0.02	0.05	0.02	0.03
$B_2H_3^+$	0.10	0.07	0.02	0.01	—
$B_2H_2^+$	0.06	0.05	0.03	—	—

The reaction was also run using  $D_2^+$  ions, and similar results were obtained (Table II and Figure 2b). In this case, there was an even greater distribution of products, but an explanation is much more readily available. According to Lindholm (2), the recombination energy of  $H_2^+$  is actually a continuum beginning at the normally accepted value for the ionization potential of 15.44 e. v. and extending upwards several e. v. with a broad maximum probability for transitions between 16.4 and 17.1 e. v. There also exist recombination energies of importance between 13 and 14 e. v. and around 11 e. v. (11). Such a variety of available energies may well account for the distribution of products in the  $D_2^+$  bombardments.

The spectra obtained in these deuterium ion reactions are compared to the electron spectrum (5) in Figure 2. It is obvious that the energy imparted to the pentaborane in the  $D^+$  and  $D_2^+$  reactions does not have

the same wide distribution that the electron spectrum implies. Rather, the distributions appear to peak more sharply in the  $B_5H_5^+$  region.

These results with deuterium ions suggest that one should perhaps reconsider the He data where the mass is also low. It is possible that the helium data are "misplaced" on the breakdown curves and that the actual energy imparted to the pentaborane varies over a wider range than that shown. Since the recombination energy of  $He^+$  is so high and fragmentation is so extensive, any evidence of such behavior is obscured and cannot be detected in the rough estimate of the breakdown pattern in Figure 1.

The data in Table I indicate that fragmentation of  $B_5H_9$  does not vary smoothly as one proceeds through the rare gases. Contrary to what one may expect solely on the basis of the magnitudes of the energy defects, neon produces more extensive fragmentation than helium. This could be explained on the basis of the foregoing discussion that a field ionization mechanism is operating in this case and, consequently, less extensive fragmentation of the  $B_5H_9^+$  occurs.

Whatever the mechanism involved, it appears that the procedure of constructing breakdown patterns from positive ion bombardment data must be approached with caution.

### *Acknowledgment*

The authors wish to thank Marsha S. Hertel who undertook the tedious task of reducing the recorded spectra to the monoisotopic spectra.

### *Literature Cited*

- (1) Chupka, W. A., Lindholm, E., *Arkiv Fysik* **25**, 349 (1963).
- (2) Gustafsson, E., Lindholm, E., *Arkiv Fysik* **18**, 219 (1960).
- (3) Hall, L. H., II, Koski, W. S., *J. Am. Chem. Soc.* **84**, 4205 (1962).
- (4) Hertel, G. R., Koski, W. S., *J. Am. Chem. Soc.* **87**, 404 (1965).
- (5) Kaufman, J. J., Koski, W. S., Kuhns, L. J., Wright, S. S., *J. Am. Chem. Soc.* **85**, 1369 (1963).
- (6) Pettersson, E., Lindholm, E., *Arkiv Fysik* **24**, 49 (1963).
- (7) Rosenstock, H. M., U. S. At. Energy Comm. Rept. JLI-650-3-7, UC-23, Isotopes-Industrial Technology TID-4500, 1959 (unpublished).
- (8) Subbanna, V. V., Hall, L. H., Koski, W. S., *J. Am. Chem. Soc.* **86**, 1304 (1964).
- (9) von Koch, H., Lindholm, E., *Arkiv Fysik* **19**, 123 (1961).
- (10) Weiner, E. R., Hertel, G. R., Koski, W. S., *J. Am. Chem. Soc.* **86**, 788 (1964).
- (11) Wilmenius, P., Lindholm, E., *Arkiv Fysik* **21**, 97 (1962).

RECEIVED September 29, 1966. This work was performed under the auspices of the United States Atomic Energy Commission.

# Mass Spectrometric Study of Ion–Solvent Molecule Interactions in the Gas Phase

P. KEBARLE

University of Alberta, Edmonton, Alberta, Canada

*Important and hitherto unavailable information on ion-solvent molecule interactions can be obtained from the mass spectrometric detection of ion clusters in the gas phase. Individual solvation step enthalpies and entropies for the reactions  $A^+ \cdot (n-1)S + S = A^+ \cdot nS$  can be obtained. The systems where  $A^+ = NH_4^+$ ,  $H_3O^+$ ,  $Na^+$  and  $S = NH_3$  and  $H_2O$  are described. The comparative solvation of  $Cl^-$ ,  $BCl_2^-$ , and  $B_2Cl^-$  by water is described. In a study of the competitive solvation of  $CH_3OH_2^+$  by water and methanol, it is found that methanol is more strongly solvating at close range of the ion. At larger distances (large clusters) water is taken up preferentially. The ammonium ion shows a distinct inner shell of four solvent molecules. Ammonia is taken up preferentially into this shell while water is taken up preferentially into the outer shell.*

Studies of ion-solvent molecule interactions in solution date back to the beginning of physical chemistry and represent a major field in chemical research. In contrast, the systematic study of ion-solvent molecule interactions in the gas phase is only a few years old (10, 12). In this paper we hope to show that a great wealth of significant information on ion-solvent molecule interactions can be obtained from the study of ion-solvent molecule clusters  $A^+ \cdot nS$  or  $B^- \cdot nS$  in the gas phase.  $A^+$  or  $B^-$  is any positive or negative ion, and  $S$  is a solvent molecule—*i.e.*, a molecule with a high dipole moment.

The mass spectrometric gas phase studies are based on measurement of the relative concentrations of the clustered ionic species:  $A^+ \cdot nS$ ,  $A^+ \cdot (n+1)S$  etc. The measurement of the relative concentrations is obtained by bleeding a probe of the gas into an ion mass analysis system—*i.e.*, a vacuum chamber attached to a mass spectrometer. In the vacuum

chamber the gas is pumped out while the ions are captured by electric fields, accelerated, focused, and mass analyzed by some conventional means (magnetic separation, quadrupole filter, etc.). After mass analysis, the ion beam intensities are detected as electrical currents.

Several types of solvation studies can be undertaken if the relative concentrations of the ionic species are known.

**Solvation Enthalpies and Entropies of Individual Solvent Molecule Additions Steps.** Consider the ion  $A^+$  produced in the gas phase by some form of ionizing radiation or thermal means. If the atmosphere surrounding the ion contains the vapor of a polar molecule (solvent  $S$ ), a number of clustering reactions will occur.



At equilibrium the following relations will hold

$$\Delta F^\circ_{0,n} = \Delta F^\circ_{0,1} + \Delta F^\circ_{1,2} + \dots + \Delta F^\circ_{n-1,n} \quad (I)$$

$$\Delta F^\circ_{n-1,n} = -RT \ln \frac{P_{A^+ \cdot nS}}{P_{A^+} \cdot (n-1)S P_S} = -RT \ln K_{n-1,n} \quad (II)$$

where  $P_x$  is the partial pressure of  $X$ .

Thus, knowledge of the equilibrium concentrations of the clustered species  $A^+ \cdot nS$  obtained from experiments at different pressures of  $S$  will allow determination of  $K_{n-1,n}$  and  $\Delta F^\circ_{n-1,n}$ . Such measurements done at different temperatures will lead to the evaluation of  $\Delta H^\circ_{n-1,n}$  and  $\Delta S^\circ_{n-1,n}$ . The availability of such detailed information will, for instance, reveal the shell structure since a discontinuous change of the  $\Delta H^\circ_{n-1,n}$  and  $\Delta S^\circ_{n-1,n}$  values will occur whenever a shell is completed. Finally, the total heat of solvation of the ion can also be obtained from Equation III, with

$$\Delta H_{\text{solv.}} = \sum_{n=0}^{\infty} [\Delta H_{n-1,n} - \Delta H_{\text{evap.}}(S)] \quad (III)$$

equations of the same form holding for the free energy and entropy change of solvation.

It is evident from Equation II, that only the relative concentrations of the ionic species are required. Thus,  $\Delta F^\circ_{n-1,n}$  and  $K_p$  can be obtained from Equation II by assuming that the mass spectrometrically measured ion intensities are proportional to the equilibrium partial pressures of the ions in the ion source. The solvation of  $\text{NH}_4^+$  by  $\text{NH}_3$  and  $\text{H}_3\text{O}^+$  by  $\text{H}_2\text{O}$ , are examples of this type of study.

**Comparative Solvation of Two Different Ions by the Same Solvent.** There are three variants of this type of study.

**COMPARATIVE SOLVATION OF IONS  $A^+$ ,  $C^+$  BY SOLVENT  $S$ .** The two ions are produced in the same system which also contains vapor of the solvent  $S$ . In general, depending on the effective radius and structure of the ion, the relative concentration of clusters  $A^+ \cdot nS$  will be different from that of  $C^+ \cdot mS$ . Thus, for example, in the average  $n$  may be larger by one or two units than  $m$ . This will reveal a stronger interaction of  $A^+$  with  $S$ . Comparison of  $n$  and  $m$  can be done at different temperatures and pressures of  $S$  in order to compare the interactions in the inner shell or in the outer shells. An example of this type of study is the system  $H_3O^+$ ,  $NH_4^+$ , and  $Na^+$  in  $H_2O$  vapor, which is described in the subsequent text.

**COMPARATIVE SOLVATION OF IONS  $A^+$  AND  $B^-$  BY SOLVENT  $S$ .** An example of this type of study would be the system  $K^+$  and  $Cl^-$  with  $H_2O$ . Since the orientation of the water dipoles is reversed in the solvation of positive and negative ions, such a comparative study is of great interest, particularly for isoelectronic pairs as the one quoted above. We have not yet performed studies on such isoelectronic pairs. However, such studies are perfectly possible. The pair  $K^+$  and  $Cl^-$  could be produced in water vapor. By reversing the mass spectrometer controls, the positive and negative ions in the system could be measured within minutes of each other.

**COMPARATIVE SOLVATION OF TWO NEGATIVE IONS BY  $S$ .** An example of this type of study for  $Cl^-$ ,  $BCl^-$  and  $B_2Cl^-$  by  $H_2O$  is given in the subsequent text.

**Competitive Solvation of Ion  $A^+$  (or  $B^-$ ) by Solvent Molecules of Solvents  $S_x$  and  $S_e$ .** A comparison of the solvating power of two different solvents can be obtained by measuring the composition of ion clusters when two different solvents are present at known partial pressures. An example of this type of study is the competitive solvation of  $NH_4^+$  by  $H_2O$  and  $NH_3$  and the solvation of  $CH_3OH_2^+$  by  $CH_3OH$  and  $H_2O$ . A discussion of experiments dealing with these two systems is given later in the text.

### *Apparatus and Method*

The mass spectrometric study of ion-solvent molecule interactions requires mass spectrometric apparatus which can sample ions originating at relatively high pressures. Three somewhat different arrangements are presently in use in this laboratory.

**Alpha Particle Mass Spectrometer (11).** A recent version of this apparatus is shown in Figure 1. The gas, supplied from a conventional gas handling system, which can be backed to  $170^\circ C.$ , is irradiated in the ionization chamber. The radiation is supplied from an enclosed 200-mc.

polonium alpha source. The polonium is deposited on a circular area of about 1/8 inch diameter on the side facing the ion source. To prevent spreading of the polonium, a double container is used. The radiation reaches the ion source through two  $10^{-4}$ -inch stainless steel foils. To prevent early rupture of the foils, two stainless porous plugs are used, allowing pump-out of the alpha source. The irradiated gas bleeds through a leak into the evacuated electrode chamber. There the ions carried by the gas are captured by the electric fields while the gas is pumped away. The ions are focused, accelerated, and then subjected to mass analysis and electron multiplier detection in a  $90^\circ$  sector field analyzer tube.

In "static" runs, gas is supplied to the ion source only at a rate sufficient to compensate the outflow through the leak (0.5 cc./sec. for air, equal to conductance of leak). The gas mixtures were prepared in two 2-liter storage flasks of the gas handling system. Flow runs can be made by passing gas through the ion source.

In the normal runs, one irradiates the total volume over the leak. Provisions are also made for placing a collimating slit between the leak and the alpha source. The collimating slit was cut in a turret of 6-mm. diameter, which screwed onto a leak-carrying cone provided with threads. The slit was elevated over the plane of the leak by unwinding the turret a certain number of revolutions.

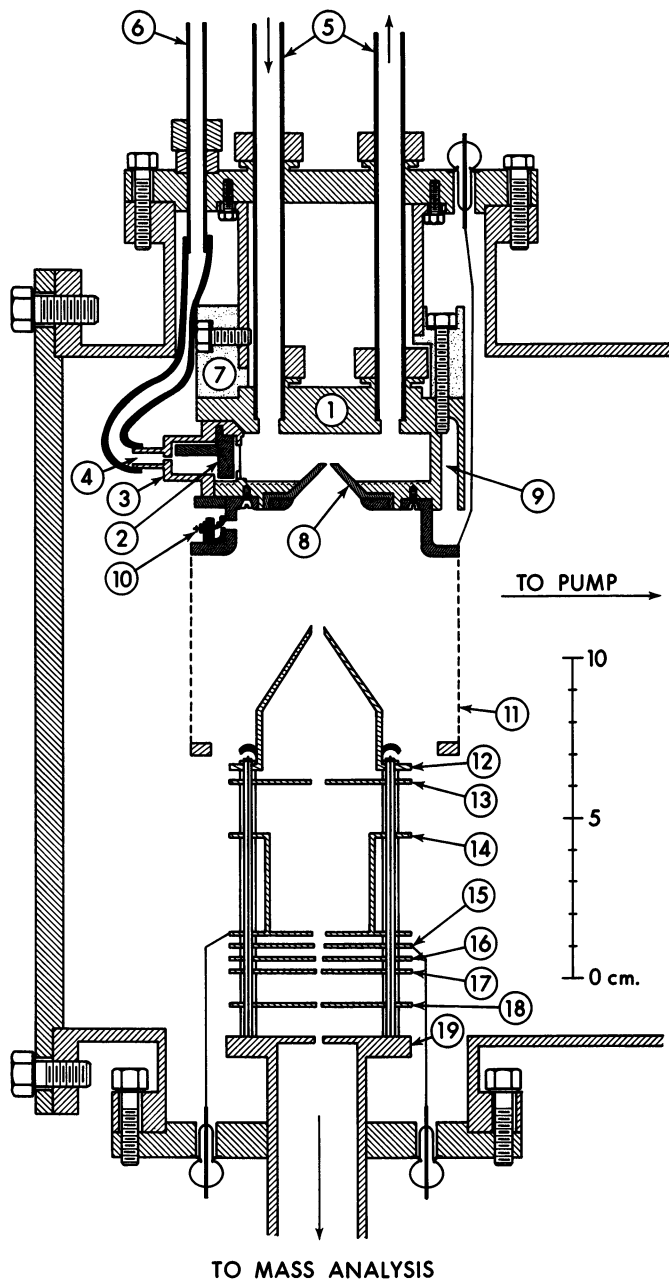
The ion source is normally at room temperature. However, the temperature can be varied up to a maximum of  $200^\circ\text{C}$ . by heaters mounted in the heater walls. These are used either for bake-out or runs at elevated temperatures.

The time for reaction available to the average ion is of the order of a few milliseconds when the uncollimated alpha beam is used (11). This time can be increased by using the collimating slit to screen off a portion immediately above the leak from irradiation.

**Electron Beam Mass Spectrometer (6).** In a more recent apparatus an electron beam is used as ionizing medium. The ion source is identical to that of Figure 1 except that the former alpha source port contains only one thin nickel foil ( $10^{-5}$  inch) window through which the electrons enter the source. The electrons are created by an ordinary electron gun housed in a sidearm of the vacuum chamber opposite the nickel window. The electron filament is kept at *ca.*  $-25000$  volts while the ion source is near ground potential. Absence of radioactive contamination, high intensity ( $\sim 10$  microamps) and possibilities for pulsing (for determining ionic lifetimes) are some of the advantages of the electron beam source. The greater scattering of electrons at high ion source pressures causes a disadvantage which makes beam collimation a problem. A quadrupole mass analyzer is used with this instrument.

**Proton Beam Mass Spectrometer (5).** A 100-kev. proton beam obtained from a Walton-Cockroft accelerator is used as the ionizing medium. The ion source is not like that of Figure 1 but is of the conventional design—*i.e.*, a rectangular box with repeller and narrowed-down ion exit slit. The proton beam enters and exits the ion source through thin nickel foil windows ( $10^{-5}$  inch). The ion optics are of the conventional Nier type, and magnetic analysis is used. A proton beam (preferably of even higher energy than used by us) seems to be the most convenient ionizing

medium for high ion source pressures since it provides high intensity, possibility for pulsing, and little scattering at high pressure. The proton beam can also be deflected electrostatically before entering the ion source.



This permits variation of the proton beam-exit slit distance in the ion source. The cost of Walton-Cockroft accelerators is relatively low.

A high pressure mass spectrometer using m.e.v. protons from a Van de Graaff accelerator has been described by Wexler (14).

**Conditions for Meaningful Measurements and Tests for Equilibrium.** In the discussion given in subsequent sections it is assumed that the measured relative ion intensities represent at least the approximate relative ionic concentrations in the ion source. It is further assumed that ion cluster equilibrium was achieved in the ion source. The validity of these assumptions has been examined in previous publications. It was pointed out that a nonequilibrium growth of the clusters might occur if cooling occurs because of adiabatic expansion past the sampling orifice. To guard against this, one must either have molecular flow in the sampling leak (small diameter of leaks) or keep the partial pressure of the clustering gas low so that the mean free path for clustering reactions is much larger than the diameter of the sampling leak. Adding an inert gas under such conditions should not change the observed relative ion intensities.

Checks for the presence of equilibrium can be made by increasing the ionic reaction time. If the relative intensities remain constant, one may assume that equilibrium or near equilibrium has been achieved since the clustering reactions probably proceed (in the forward direction) rapidly and without activation energy. The ionic reaction times can be increased by moving the ionizing beam away from the sampling leak or slit and by closing down the leak or slit. The latter slows down the mass flow to the sampling orifice and since the ions, at higher pressures and in the absence of electric fields, are carried by mass flow to the orifice, increases the ionic reaction times.

### Results and Discussion

**Heats and Entropies of Individual Steps.** (a)  $\text{NH}_4^+ \cdot (n-1)\text{NH}_3 + \text{NH}_3 = \text{NH}_4^+ \cdot n\text{NH}_3$ . Previous work on ammonia (9, 12) has shown that the primary (positive) ions produced by the alpha radiation are rapidly converted by ion-molecule reactions to the most stable ion, which

←  
Figure 1. Ion source and electrode system

(1) Stainless steel block forming ion source. (2) Alpha source, consisting of polonium deposited on a metal disc. Metal disc enclosed in container with stainless foil window and stainless porous plug allowing pressure equalization across foil. (3) Outer alpha source container with foil window and porous plug. Double container prevents spreading of polonium into pressure equalization system. (4) Porous stainless plug allowing pump-out of alpha source and pressure equalization across foils. (5) Gas supply to ion source and flow system (in the direction of the arrows). (6) Tube leading to vacuum system of alpha source contained. (7) Insulating material allowing voltages different from ground to be applied to ion source. (8) Cone-carrying metal foil at its truncated apex. Foil has one or several leaks through which the gas and ions enter the pumping and electrode chamber. (9) Heater and thermocouple wells for temperature control of ion source. (10) Auxiliary electron gun for gas purity determinations. (11-19) Electrodes focusing ion beam into magnetic mass analyzer

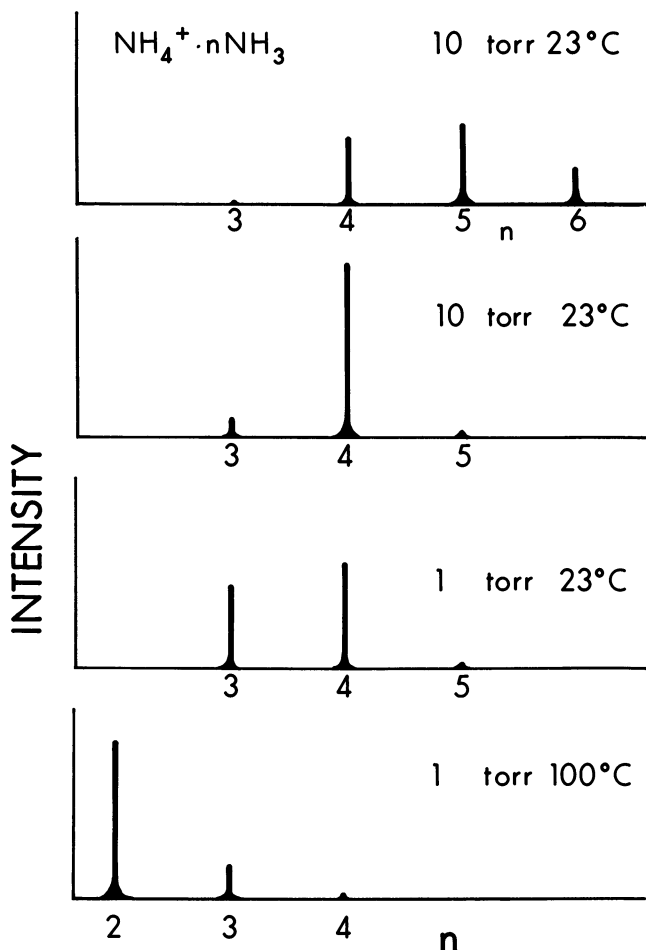


Figure 2. Schematic representation of ion intensities for clustered  $\text{NH}_4^+ \cdot n\text{NH}_3$

Intensities are expressed as fractions of total ion current. Condition of 1 torr and  $100^\circ$  shows cluster of largest concentration to be  $\text{NH}_4^+ \cdot 2\text{NH}_3$ . Reduction of temperature at constant pressure ( $23^\circ$ , 1 torr) causes clusters to grow. Increase of pressure at constant temperature ( $23^\circ$ , 10 torr) produces further cluster growth. Spectrum at top ( $23^\circ$ , 10 torr) shows effect of using large sampling pinhole ( $70\text{-}\mu$  diameter) producing dynamic flow. The resultant adiabatic cooling causes further nonequilibrium growth of clusters. Other three spectra taken with sampling leak consisting of a laser produced array of 30 holes, each of  $10\ \mu$  diameter

is  $\text{NH}_4^+$ . Attachment of ammonia molecules then leads to  $\text{NH}_4^+ \cdot n\text{NH}_3$ . A representation of some typical relative ion intensities observed within

the experimental range used in the measurements is given in Figure 2. The most abundant species at 100°C. and 1 torr ammonia pressure is  $\text{NH}_4^+ \cdot 2\text{NH}_3$ . As the temperature is lowered to 23°C. and 1 torr pressure, the larger clusters  $n = 3$  and  $n = 4$  become more stable. Increasing the pressure at constant temperature also increases the cluster size as is evident from the increase of the  $\text{NH}_4^+ \cdot 4\text{NH}_3/\text{NH}_4^+ \cdot 3\text{NH}_3$  ratio on going from 1 to 10 torr. The ion intensities given at the top of Figure 2 illustrate the effect of the sampling leak size. In this case, a single leak of  $70\mu$  diameter was used. The appearance of clusters of higher mass must be attributed to adiabatic cooling caused by the expansion of the gas jet.

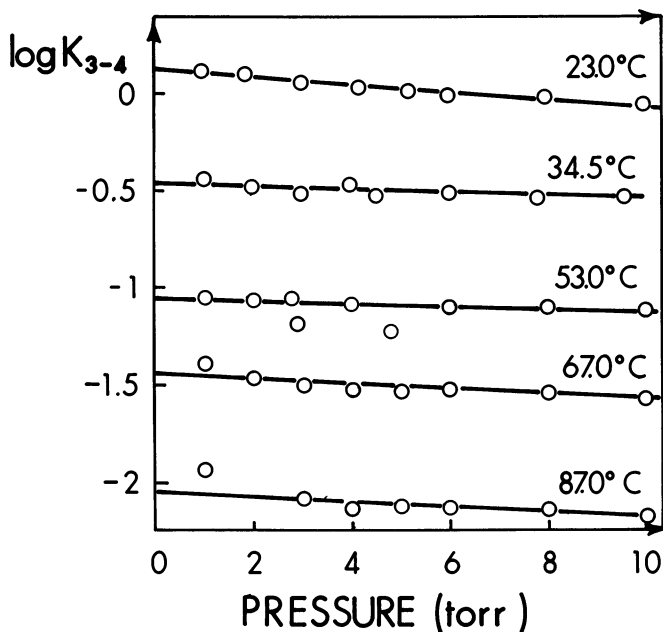


Figure 3. Plot of  $\log K_{3,4}$ , where  $K_{3,4} = I_4/I_3P_{\text{NH}_3}$ , at constant temperatures and variable ammonia pressure (pressure expressed in torr)

Rewriting Equation II for the ammonia system with the assumption that the relative ion intensities  $I_n = I(\text{NH}_4^+ \cdot n\text{NH}_3)$  represent adequately the equilibrium concentration ratios we obtain Equation IV. Plots of  $\log K_{3,4}$

$$RT \log K_{n-1,n} = RT \log \frac{I_n}{I_{n-1} \cdot P_{\text{NH}_3}} \quad (\text{IV})$$

with pressure at different constant temperatures are given in Figure 3.

These data show that Equation IV is obeyed to a good approximation for a pressure change by a factor of 10. A plot of  $\log K_{2,3}$  and  $K_{3,4}$  vs.  $1/T$  is shown in Figure 4. The data used for  $K_{2,3}$  were of similar appearance to those in Figure 3. Since there is a small variation of  $\log K$  with pressure, the values used for the enthalpy plots were taken at zero pressure. This was done only for the sake of consistency. Values taken at 5 torr pressure lead to similar enthalpy data.

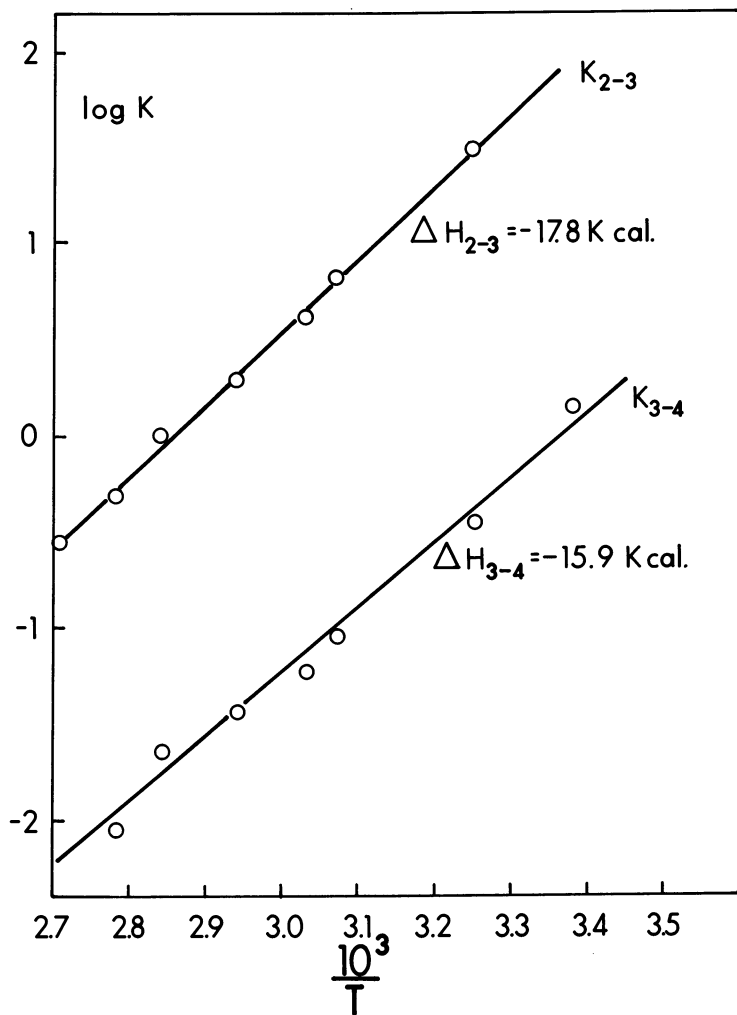


Figure 4. Plots giving enthalpy changes for reaction  $\text{NH}_4^+ \cdot n-1\text{NH}_3 + \text{NH}_3 = \text{NH}_4^+ \cdot n\text{NH}_3$  where  $n-1, n$  is 2,3 and 3,4

The slopes lead to  $\Delta H_{2,3} = -17.8$  and  $\Delta H_{3,4} = -15.9$  kcal./mole. No data were obtained for the clustering Reactions 0,1 and 1,2 which would be observable only at considerably higher temperatures. A  $K_{4,5}$  could still be measured but only at the lowest temperature (25°C.). It is of interest to point out that the range covered even though insufficient for determining a wider set of reactions is still quite extensive. Thus, the measured ratio  $I_2/I_4$  increases in the range (10 torr, 23°C. to 1 torr, 100°C.) by a factor of 100,000. The thermodynamic data obtained are summarized in Table I. It can be shown that the enthalpies and entropies of Table I agree with estimates based on thermodynamic cycles and calculation.

**Table I. Thermodynamic Data on Clustering Reactions**



$n-1,$ $n$	$\Delta F^\circ$ (298°K.) <sup>a</sup>	$\Delta H,$ kcal./mole	$\Delta S^\circ$ (298°K.), e.u.
2,3	-6.4	-17.8	-38
3,4	-3.8	-15.9	-40.5
4,5	-0.5	(-9) <sup>b</sup>	(-33) <sup>c</sup>

<sup>a</sup> Standard state of ammonia, 1 atm.

<sup>b</sup> Obtained from  $\Delta F^\circ$  and the estimated entropy loss.

<sup>c</sup> Estimated.

Figure 5 shows the enthalpies for the first five clustering reactions of  $NH_4^+$  in  $NH_3$ . The values for Steps 2-5 are those from Table I. The Steps 0,1 and 1,2 were estimated from the cycle shown in Figure 6a. From this cycle we obtain Equation V:

$$\Delta H_{0,4} = \Delta H_{\text{amm.}}(NH_4^+) - 4\Delta H_{\text{evap.}}(NH_3) - \Delta H_{\text{amm.}}(NH_4 \cdot 4NH_3) \quad (V)$$

Substituting:  $\Delta H_{\text{amm.}}(NH_4 \cdot 4NH_3) = -30$  kcal./mole (9)  $\Delta H_{\text{evap.}}(NH_3) = -5$  kcal./mole and  $\Delta H_{\text{amm.}}(NH_4^+) = -90$  kcal./mole (9), one obtains  $\Delta H_{0,4} = -80$  kcal./mole. Subtracting from this  $\Delta H_{2,3}$  and  $\Delta H_{3,4}$  (from Table I) one obtains  $\Delta H_{0,2} = -46$  kcal./mole. The magnitudes of  $\Delta H_{0,1}$  and  $\Delta H_{1,2}$  were selected as  $-25$  and  $-21$  kcal./mole which numbers give a continuous increase of  $\Delta H$  in the direction  $\Delta H_{3,4}$  to  $\Delta H_{0,1}$ . While the procedure in obtaining Figure 5 is somewhat arbitrary, we believe that it does give a good qualitative picture of the enthalpy changes in the individual solvation steps.

(b)  $H_3O^+(n-1)H_2O + H_2O = H_3O^+ \cdot nH_2O$ . A system of greater importance than the ammonium ion described above is the water-clustered

hydronium ion,  $\text{H}_3\text{O}^+ \cdot n\text{H}_2\text{O}$ . An early, preliminary study of this system has been published (12). In that study  $K_{n-1,n}$  was determined only at a single (constant) pressure of water, and Arrhenius plots of these  $K$ 's gave  $\Delta H_{3,4} = -20 \pm 5$ ,  $\Delta H_{4,5} = -24 \pm 5$ ,  $\Delta H_{5,6} = -13 \pm 5$  kcal./mole.

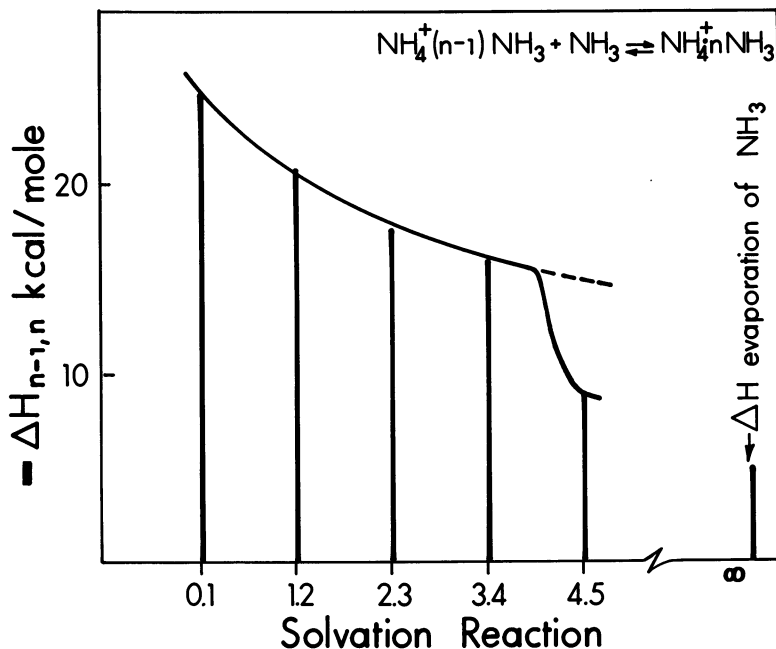


Figure 5. Enthalpy changes for reactions:  $\text{NH}_4^+ \cdot (n-1)\text{NH}_3 + \text{NH}_3 = \text{NH}_4^+ \cdot n\text{NH}_3$  ( $n-1, n$ ). Some of the data are based on estimates as described in the text

Only rough estimates of the expected enthalpies can be made on the basis of available thermodynamic data. The cycle shown in Figure 6b is of the same type as that used for ammonia ( $k$  here is the as of yet unspecified number of inner shell water molecules). From Figure 6b we obtain Equation VI.

$$\Delta H_{0,k} = \Delta H_{\text{hydr.}}(\text{H}_3\text{O}^+) - k\Delta H_{\text{evap.}}(\text{H}_2\text{O}) - \Delta H_{\text{hydr.}}(\text{H}_3\text{O}^+ \cdot k\text{H}_2\text{O}) \quad (\text{VI})$$

To evaluate  $\Delta H_{0,k}$ , we need values for the heats of hydration of  $\text{H}_3\text{O}^+$  and  $\text{H}_3\text{O}^+ \cdot k\text{H}_2\text{O}$ .  $\Delta H_{\text{hydr.}}(\text{H}_3\text{O}^+)$  can be evaluated from the cycle of Figure 6c. The required proton affinity of water,  $PA(\text{H}_2\text{O})$ , is probably 170 kcal./mole (3, 13). Taking the heat of hydration of the proton  $\Delta H_{\text{hydr.}}(\text{H}^+) = -283$  kcal./mole<sup>3</sup> and  $\Delta H_{\text{evap.}}(\text{H}_2\text{O}) = 10.5$ , we obtain  $\Delta H_{\text{hydr.}}(\text{H}_3\text{O}^+) = -123.5$  kcal./mole. An estimate of  $\Delta H_{\text{hydr.}}(\text{H}_3\text{O}^+ \cdot k\text{H}_2\text{O})$  can be obtained from the Born equations (4). (Examples of

calculations with the Born equations are given by Basolo and Pearson (2). Taking 1.5 Å. for the radius of  $\text{H}_3\text{O}^+$  and 2.76 Å. for the diameter of the water molecules (2) in the first shell, one has a total radius of the first shell cluster equal to 3.76 Å. Substituting this value into the Born equations, one obtains the estimate  $\Delta H_{\text{hydr.}}(\text{H}_3\text{O}^+ \cdot k\text{H}_2\text{O}) = -39 \text{ kcal./mole}$ . Substituting into Equation VI, we then obtain:  $\Delta H_{0,k} \approx -123.5 - 10.5k + 39 = -84.5 - 10.5k$ . This yields for the average solvation step in the first shell  $\Delta H_{n-1,n} = \frac{\Delta H_{0,k}}{k} = -(84.5/k) - 10.5 \text{ kcal./mole}$ . For

different values of  $k$  we thus obtain in kcal./mole  $\overline{\Delta H_{n-1,n}} = -31.6$  ( $k = 4$ ),  $-27.4$  ( $k = 5$ ),  $-24.6$  ( $k = 6$ ),  $-22.5$  ( $k = 7$ ), and  $-21$  ( $k = 8$ ). This crude estimate shows that the data obtained in our earlier study are in the right range.

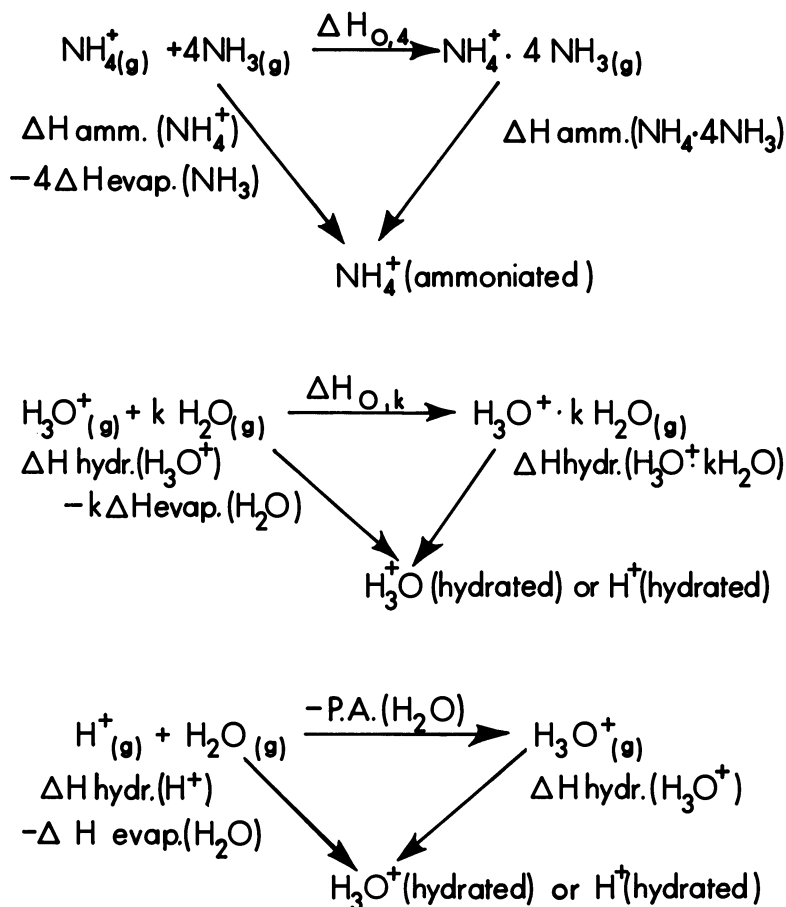


Figure 6. Thermodynamic cycles

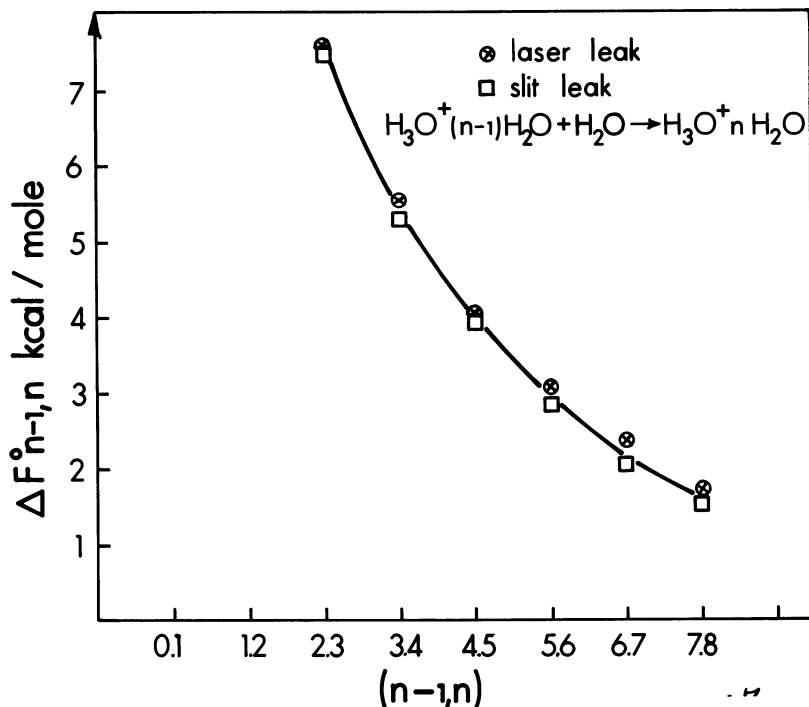


Figure 7. Plot of  $\Delta F^\circ_{n-1,n}$  at 298°K. (Standard state of water 1 atm.)

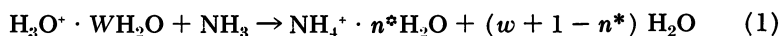
Results obtained with two different leaks, one slit leak with slit width  $7\mu$  and a laser produced array of 30 leaks of  $10\text{-}\mu$  diameter

Since the early study was only preliminary, a second, more extensive research on the hydronium-water system was started in this laboratory a year ago. The alpha particle- and proton beam mass spectrometer are being used. These two instruments provide very different ionic reaction times, and their combination allows a good test for the presence of equilibrium. Unfortunately this study is not yet completed. One result has appeared clearly from the data obtained. It is generally assumed (10) that in aqueous solution the ion  $\text{H}_3\text{O}^+ \cdot 3\text{H}_2\text{O}$  has high stability. Regardless whether this assumption is correct or not, in the gas phase this special stability need not apply since the constraining influence of the surrounding liquid lattice is absent. Thus, the positions above and below the presumably planar trihydrate are free, and since the interaction is largely a purely electrostatic one, the higher hydrates—*i.e.*,  $\text{H}_3\text{O}^+ \cdot 4\text{H}_2\text{O}$  etc. may have stabilities which are not too different. This view is supported by the plot in Figure 7. The standard free energies for the clustering Reactions  $(n-1, n)$  show a continuous change in the range  $n = 2$  to  $n = 8$ . Some further information on the  $\text{H}_3\text{O}^+ \cdot n\text{H}_2\text{O}$  system is given

in the next section which deals with the comparative hydration of  $\text{H}_3\text{O}^+$ ,  $\text{NH}_4^+$ , and  $\text{Na}^+$ .

**Comparative Solvation of Different Ions by the Same Solvent.**

(a) COMPARATIVE HYDRATION OF  $\text{Na}^+$ ,  $\text{H}_3\text{O}^+$ , AND  $\text{NH}_4^+$ . Figure 8 shows ion intensity ratios for water clustering around  $\text{Na}^+$ ,  $\text{H}_3\text{O}^+$ , and  $\text{NH}_4^+$ . The ions  $\text{H}_3\text{O}^+$  and  $\text{NH}_4^+$  were produced simultaneously by irradiating water vapor (at pressures 1–5 torr) containing several parts per million  $\text{NH}_3$ . Under these conditions, the ammonium ion must be produced by proton transfer from hydrated hydronium ions (*see* Reaction 1). Higher concentration of ammonia leads to the complete disappearance of  $\text{H}_3\text{O}^+ \cdot n\text{H}_2\text{O}$ .



In Reaction 1 we have indicated that after adding ammonia to the hydronium cluster (and proton transfer), some water molecules will be "boiled" off. This effect is to be expected since the proton affinity of ammonia is some 35 kcal. higher than that of water. The ammonium hydrate  $\text{NH}_4^+ \cdot n^*\text{H}_2\text{O}$  created by Reaction 1 must engage in further collisions with water molecules before reaching its equilibrium composition  $\text{NH}_4^+ \cdot n\text{H}_2\text{O}$ .

The sodium ions were not introduced intentionally. Their presence was inferred from ion intensities at mass 59, 77, 95, etc. which are of the same mass as  $\text{Na}^+ \cdot 2\text{H}_2\text{O}$ ,  $\text{Na}^+ \cdot 3\text{H}_2\text{O}$ ,  $\text{Na}^+ \cdot 4\text{H}_2\text{O}$ , etc. We attribute this ion series to some sodium containing impurity which in some manner leads to the formation of sodium ions. As pointed out in previous work, ions of low ionization potential originating from trace impurities often represent an appreciable fraction of the total intensity.

The distribution of the hydrates given in Figure 8 is for a water pressure of 1 torr. Data were obtained at pressures from 1–6 torr. The equilibrium constants for the three ions calculated from Equation II remained constant in this pressure range. The distributions of hydronium and sodium clusters (Figure 8) are similar, the average cluster containing five water molecules. The average ammonia cluster contains only four water molecules. Experiments were also performed at higher temperatures where the average ammonium cluster is  $\text{NH}_4^+ \cdot 3\text{H}_2\text{O}$ . The water and sodium clusters were again higher by one unit—*i.e.*,  $\text{H}_3\text{O}^+ \cdot 4\text{H}_2\text{O}$  and  $\text{Na}^+ \cdot 4\text{H}_2\text{O}$ . All water molecules in the ammonium tri- and tetrahydrate are almost certainly "inner shell" molecules. Since the  $\text{Na}^+$  and  $\text{H}_3\text{O}^+$  under the same conditions hold one more water molecule, we may conclude that the fourth and fifth molecules in the sodium and hydronium hydrates are held very strongly and are thus probably inner shell molecules. Concerning the  $\text{H}_3\text{O}^+$ , this conclusion is in agreement with

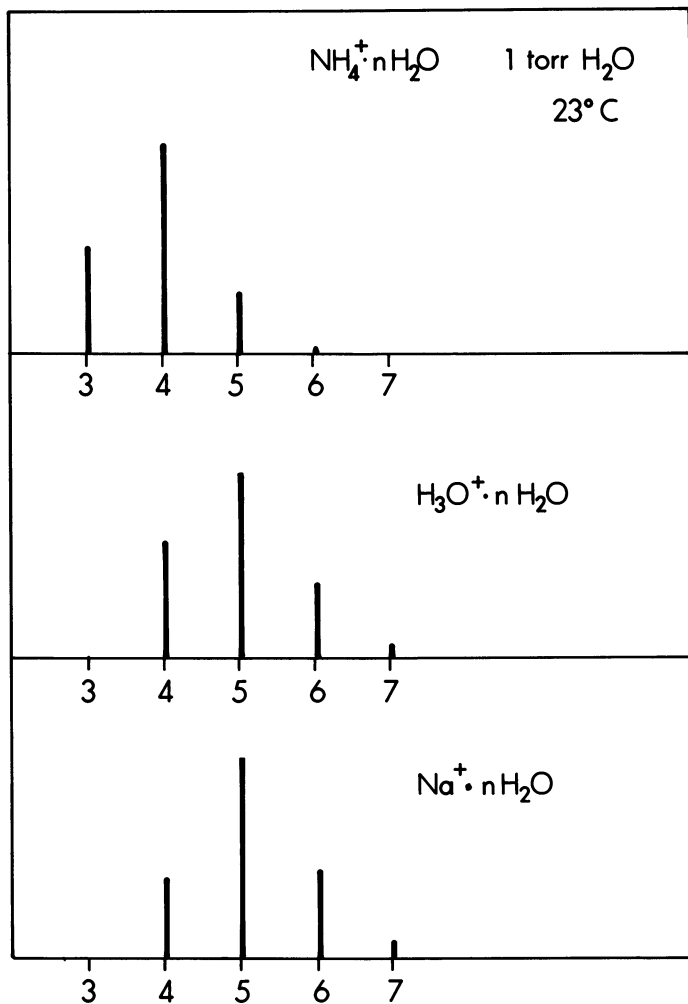


Figure 8. Comparative solvation of  $\text{NH}_4^+$ ,  $\text{H}_3\text{O}^+$ , and  $\text{Na}^+$  by  $\text{H}_2\text{O}$

*The sodium and hydronium ion behave similarly while the ammonium ion holds in the average one less water molecule*

the direct  $\text{H}_3\text{O}^+ \cdot w\text{H}_2\text{O}$  measurements mentioned in the preceding section. From the data of Figure 8 and those at higher temperatures, it follows that for the hydrations

$$-\Delta F^\circ_{4,5}(\text{Na}^+) \approx -\Delta F^\circ_{4,5}(\text{H}_3\text{O}^+) > -\Delta F^\circ_{4,5}(\text{NH}_4^+)$$

and

$$-\Delta F^\circ_{3,4}(\text{Na}^+) \approx -\Delta F^\circ_{3,4}(\text{H}_3\text{O}^+) > -\Delta F^\circ_{3,4}(\text{NH}_4^+)$$

Assuming that these differences reflect  $\Delta H_{n-1,n}$  differences we would expect:  $-\Delta H_{4.5}(\text{Na}^+) \approx -\Delta H_{4.5}(\text{H}_3\text{O}^+) > -\Delta H_{4.5}(\text{NH}_4^+)$  and  $-\Delta H_{3.4}(\text{Na}^+) \approx -\Delta H_{3.4}(\text{H}_3\text{O}^+) > -\Delta H_{3.4}(\text{NH}_4^+)$ . These data can be compared with the total heats of hydration obtained from thermodynamic cycles  $-\Delta H_{\text{hydr.}}(\text{Na}^+) \approx 100^9$ ,  $-\Delta H_{\text{hydr.}}(\text{H}_3\text{O}^+) \approx 130$  (see preceding section) and  $-\Delta H_{\text{hydr.}}(\text{NH}_4^+) \approx 70$  kcal./mole. The difference between the total hydration of  $\text{NH}_4^+$  and  $\text{H}_3\text{O}^+$ ,  $\text{Na}^+$  is reflected in our data but the difference between  $\text{H}_3\text{O}^+$  and  $\text{Na}^+$  is not. Further mass spectrometric work on this system is required before more meaningful comparisons can be made.

COMPARATIVE SOLVATION OF  $\text{Cl}^-$ ,  $\text{BCl}^-$ , AND  $\text{B}_2\text{Cl}^-$  BY  $\text{H}_2\text{O}$ . Figure 9 shows the hydrated negative ions  $\text{Cl}^-$ ,  $\text{BCl}^-$ , and  $\text{B}_2\text{Cl}^-$ . The original intention had been to study only the hydration of  $\text{Cl}^-$ . For this purpose a mixture of a chlorine-containing compound ( $\text{CCl}_4$  and  $\text{Cl}_2$ ), water, and excess of  $\text{N}_2$  were admitted to the ion source. In addition to  $\text{Cl}^- \cdot n\text{H}_2\text{O}$ , two other groups of ions were observed. These ions were identified as  $\text{BCl}^- \cdot n\text{H}_2\text{O}$  and  $\text{B}_2\text{Cl}^- \cdot n\text{H}_2\text{O}$  on the basis of the typical  $^{10}\text{B}$ ,  $^{11}\text{B}$  and  $^{35}\text{Cl}$ ,  $^{37}\text{Cl}$  isotope ratios. The two boron ions obviously arise from some impurity present in the ion source (possibly solder flux). Their presence persisted over many months.

At the low water pressure (Figure 9) the dominant species are  $\text{Cl}^- \cdot \text{H}_2\text{O}$  (with some  $\text{Cl}^- \cdot 2\text{H}_2\text{O}$ ),  $\text{BCl}^- \cdot 2\text{H}_2\text{O}$  and  $\text{B}_2\text{Cl}^- \cdot 4\text{H}_2\text{O}$ . This difference in water content can be understood if it is assumed that all three ions hold about one water molecule as a hydrating species (*i.e.*, with hydrogens toward the negative ion) and  $\text{BCl}^-$  and  $\text{B}_2\text{Cl}^-$  hold respectively one and three water molecules in a dative bond involving the oxygen lone pair. The corresponding electronic structures of the boron ions are given in Figure 10. When the water pressure is increased (Figure 9)  $\text{Cl}^- \cdot \text{H}_2\text{O}$  grows to  $\text{Cl}^- \cdot 4\text{H}_2\text{O}$  and  $\text{Cl}^- \cdot 5\text{H}_2\text{O}$  but the  $\text{BCl}^-$  and  $\text{B}_2\text{Cl}^-$  hydrates grow only by two and one water molecules which could be expected considering that these ions are much bulkier.

#### Competitive Solvation of a Given Ion by Two Different Solvents.

a. COMPETITIVE SOLVATION OF  $\text{CH}_3\text{OH}_2^+$  BY WATER AND METHANOL. A study of the ions in methanol vapor in the pressure range 1–10 torr showed that most of the ions belonged to the series  $\text{CH}_3\text{OH}_2^+ \cdot n\text{CH}_3\text{OH}$ . This suggested the possibility of observing the competitive solvation of  $\text{CH}_3\text{OH}_2^+$  by water and methanol molecules. Figure 11 shows the relative intensities of the mixed clusters obtained when irradiating mixtures of 5% methanol, 95% water and 20% methanol, 80% water both at 5 torr total pressure and  $50^\circ\text{C}$ . ion source temperature. In the mixed methanol-water clusters, the question of the structural assignment arises. Thus, the ion of mass 119 could be assigned as  $\text{H}^+ \cdot 2\text{CH}_3\text{OH} \cdot 3\text{H}_2\text{O}$  or

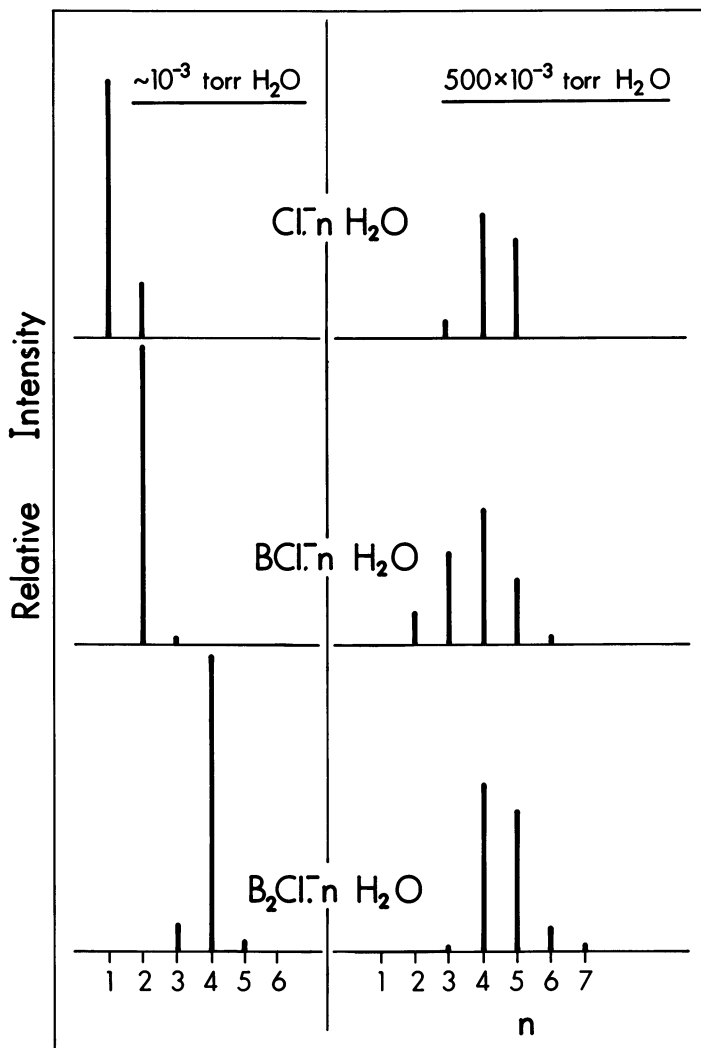


Figure 9. Comparative solvation of  $\text{Cl}^-$ ,  $\text{BCl}^-$ , and  $\text{B}_2\text{Cl}^-$  at two different water vapor pressures and room temperature

Water pressure not accurately known. At lower water pressures  $\text{BCl}^-$  and  $\text{B}_2\text{Cl}^-$  contain one and three water molecules more than  $\text{Cl}^-$ . This excess is probably caused by dative bonds as shown in Figure 10

$\text{CH}_3\text{OH}_2^+ \cdot \text{CH}_3\text{OH} \cdot 3\text{H}_2\text{O}$  or  $\text{H}_3\text{O}^+ \cdot 2\text{CH}_3\text{OH} \cdot 2\text{H}_2\text{O}$ . We have selected the notation  $\text{CH}_3\text{OH}_2^+ \cdot \text{CH}_3\text{OH} \cdot 3\text{H}_2\text{O}$  (or  $\text{CH}_3\text{OH}_2^+ \cdot m\text{M} \cdot w\text{W}$ , for the general cluster where M and W stand for  $\text{CH}_3\text{OH}$  and  $\text{H}_2\text{O}$  and m and w for the number of methanol and water molecules). The proton

was assigned to the methanol oxygen ion since the proton affinity of methanol is some 10–20 kcal./mole (13) higher than that of water.

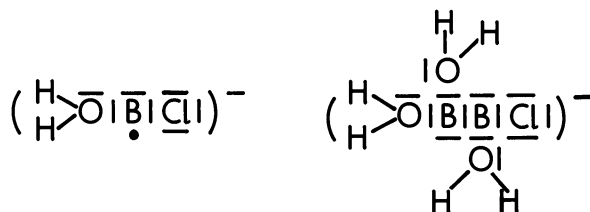


Figure 10. Electronic formulas of  $BCl^- \cdot H_2O$  and  $B_2Cl^- \cdot 3H_2O$  suggested by water content of clusters shown in Figure 9

The clusters obtained with 5% methanol (Figure 11) contain, on the average, considerably more methanol than water even though the partial pressure ratio of water to methanol is 19:1. Thus, methanol is the stronger solvent in the observed clusters—*i.e.*, clusters containing up to six solvent molecules. We shall be able to understand the meaning of this result better after a more detailed treatment of the data. It can be shown that the distribution of water and methanol in the observed clusters follows quite closely a probability distribution. Calling the probabilities for inclusion of water and methanol  $\omega$  and  $\mu$ , for a cluster with a total of  $l$  solvent molecules the probability distribution will be given by the binomial expansion of the term  $(\omega + \mu)^l$ . For example, if a probability distribution is followed, the cluster containing three solvating molecules  $CH_3OH_2^+ \cdot mM \cdot \omega W$ , where  $l = m + \omega = 3$ , should show the following relative intensities:  $CH_3OH_2^+ \cdot 3W : CH_3OH_2^+ \cdot 2WM : CH_3OH_2^+ \cdot W2M : CH_3OH_2^+ \cdot 3M = \omega^3 : 3\omega^2\mu : 3\omega\mu^2 : \mu^3$ . We have obtained values for  $\omega$  and  $\mu$  by fitting binomial expansions to the experimentally observed distribution. The calculated intensities shown in Figure 11 demonstrate that a relatively good fit of the experimental data can be obtained. In order to express the preference for inclusion of methanol and water per unit methanol and water pressure we define  $\gamma = \frac{\mu/P_M}{\omega/P_W}$  as the factor for preferential take up of methanol,  $P_M$  and  $P_W$  being the partial pressures of methanol and water present in the ion source. The  $\gamma$ 's calculated in this manner are given in Figure 11. The results at 5% and 20% methanol show that the  $\gamma$ 's for a cluster of a fixed size (*i.e.*,  $l = \text{const.}$ ) are approximately independent of the methanol-water pressure ratio. This independence was confirmed in a number of other runs with 2, 4, 5, 8, 20, 50% methanol at 2 and 5 torr total pressure. The  $\gamma$ 's are found to decrease as  $l$  increases. Thus, methanol is taken up preferentially by a factor of 55,

21, and 8 for clusters containing three, four, and five solvent molecules. Figure 12 shows a  $\log \gamma$  plot *vs.* the number of solvating molecules. The plot is almost linear and allows an extrapolation to  $\log \gamma = 0$  or  $\gamma = 1$ . This occurs when the cluster contains seven solvating molecules. For  $l > 7$ ,  $\gamma$  becomes less than unity—*i.e.*, water begins to take precedence. Figure 13 also shows results obtained with the proton beam mass spectrometer. The total pressure in these runs was much lower (0.6 torr), and the reaction time was much shorter (several microseconds *vs.* a few milliseconds in the alpha particle ion source). One might suspect that under these conditions clustering equilibrium might not be achieved. However, the results are quite similar to those obtained with the alpha ion source. This might be taken to mean that clustering equilibrium establishes rapidly and that the proton beam results approach equilibrium.

In interpreting the present results considerable help can be obtained from the "electrostatic theory" for metal-ion coordination complexes (2). This theory, using simple electrostatic concepts, allows one to calculate the binding energies of metal complexes in the gas phase. The results of such calculations have been in many cases successful. In general, the potential energy of a complex ion is built up of four terms. These are attributed to the attraction between the ion and the permanent and induced dipole of the ligands, the mutual repulsion of the dipoles, the energy required to form the induced dipoles and the van der Waals repulsions between the ligands and the central ion. Comparing the potential energies of an ion having water or methanol molecules as ligands, it is found that the first term is the decisive one. It contains the sum of the permanent dipole and the polarizability. The dipole moments of water and methanol are 1.85 and 1.69 *D* while the polarizabilities are 1.48 and 3.23  $\text{\AA}^3$ . The potential energy of an ion dipole interaction varies inversely with the square of the distance while the polarizability interaction depends on the fourth power. Therefore, the methanol molecules, with their slightly lower dipole but considerably higher polarizability, will be more strongly solvating than water at close range to the ion. The experimentally observed preference for methanol is thus to be understood as resulting from the higher methanol polarizability.

It can be shown that the possibility of fitting the observed clusters with a given  $l$  by a probability distribution suggests that for  $l < 6$  all solvent molecules belong to an inner solvation shell. Suppose that for  $l = 5$  some of the molecules went into an inner shell (fully occupied) and the rest into an outer shell. The preference for methanol over water in the inner shell will be different from that in the outer shell. It might even be expected that water will be preferentially taken up in the outer shell. It follows that the water-methanol distribution in a cluster containing inner and outer shell molecules could not be fitted by a single

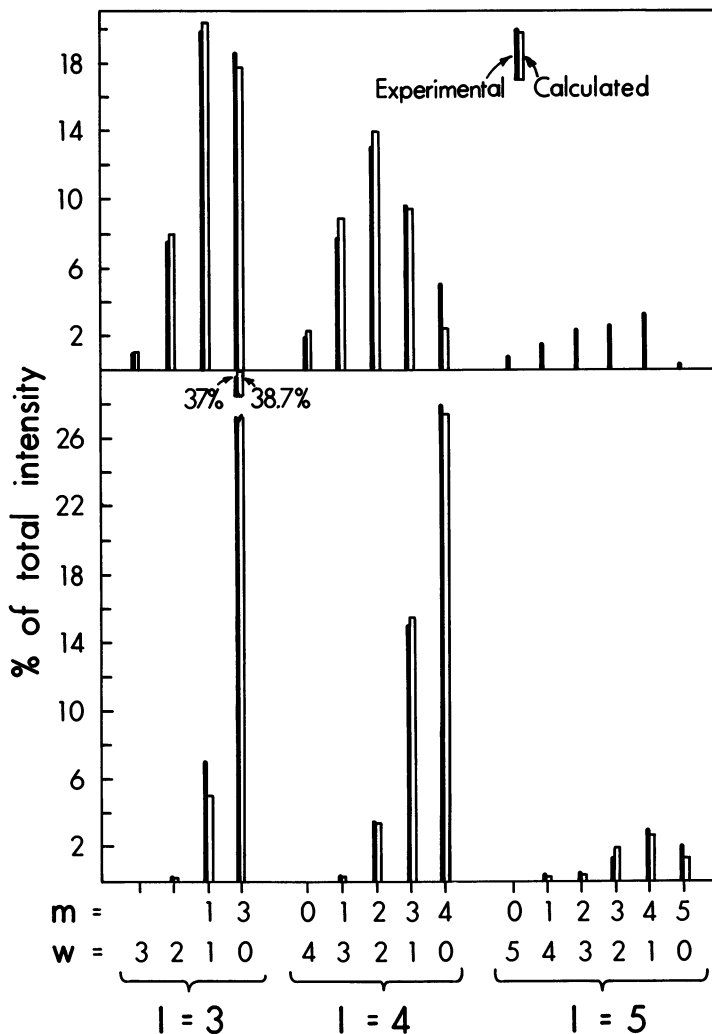


Figure 11. Mixed water and methanol content in  $\text{CH}_3\text{OH}_2^+$   $m\text{CH}_3\text{OH} \cdot w\text{H}_2\text{O}$  clusters. Ion source temperature  $50^\circ\text{C}$ .

probability distribution of the type  $(\omega + \mu)'$  but that the inner and outer shell would have to be fitted separately. Such a case is in fact observed in the competitive solvation of  $\text{NH}_4^+$  by  $\text{H}_2\text{O}$  and  $\text{NH}_3$  which is discussed in the next section. Since the water-methanol clusters of  $l = 3, 4, 5$  can each be fitted with a probability distribution, we can conclude that these clusters do not contain molecules which occupy a distinct outer shell—*i.e.*, that the inner shell contains at least five solvent molecules.

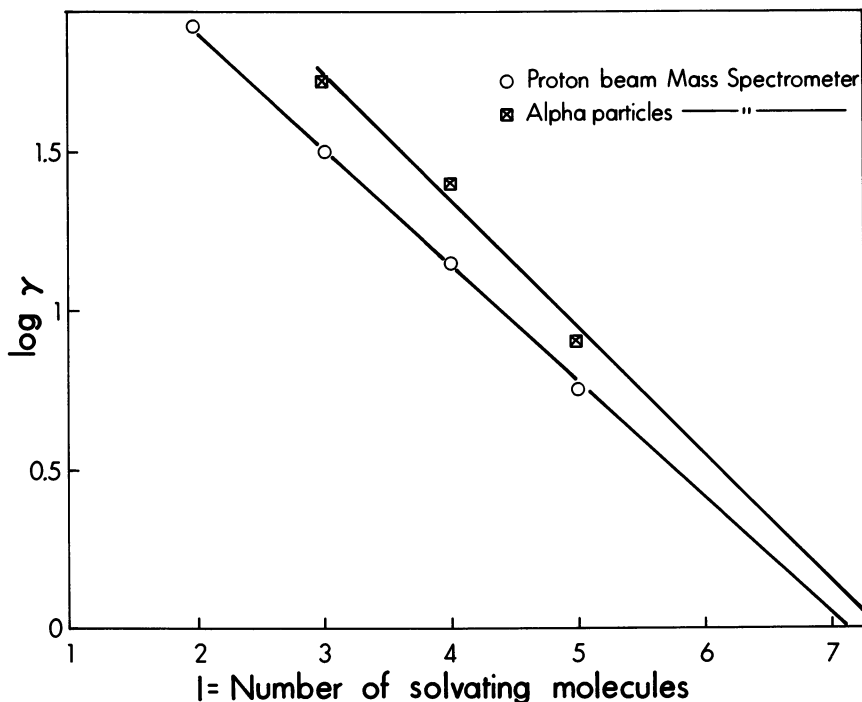


Figure 12. Plot of  $\log \gamma$  vs. number of solvating molecules

$\gamma$  is factor for preferential take up of methanol over water into ion  $\text{CH}_3\text{OH}_2^+ \cdot m\text{CH}_3\text{OH} \cdot w\text{H}_2\text{O}$ , where  $m + w = 1$ . For low  $l$  methanol is taken up preferentially. As size of cluster increases preference for methanol decreases.  $\gamma = 1$  at  $l = 7$  where water and methanol are taken up with equal preference

The ability to fit a cluster of constant  $l$  with a probability distribution is, to a certain extent, surprising even if all molecules belong to the same solvation shell. A probability distribution means, for example, that in the five cluster the preference for methanol over water is the same whether all the remaining four ligands are water or methanol or a mixture of them. Obviously this can not be strictly true. The meaning of the experimental result must be that the nature of the other occupants is, in the first approximation, not important.

While  $\gamma$  remains approximately constant for a cluster distribution with  $l = \text{const.}$ , it was observed that  $\gamma_{l = \text{const.}}$  decreases from  $l = 3$  to  $l = 5$ . This can be understood if one assumes that whenever  $l$  is increased by one unit, the effective radius of the (inner) shell increases. This causes the polarizability to become less important and leads to a decrease of the preference for methanol. An increase of the effective radius might

be expected because of the mutual repulsion attributed to dipole and van der Waal's forces between the ligands.

b. COMPETITIVE INNER AND OUTER SHELL SOLVATION OF  $\text{NH}_4^+$  BY WATER AND AMMONIA MOLECULES. The solvation of  $\text{NH}_4^+$  by  $\text{NH}_3$  was described in a previous section. When water vapor was added to ammonia, new ion peaks could be observed which corresponded to the mixed clusters  $\text{NH}_4^+n\text{NH}_3w\text{H}_2\text{O}$ . Data of three representative runs are shown in Table II. The first experiment is done at very low ammonia pressure where the lower solvates ( $l = 2, 3, 4$ ) are of highest abundance. It can be seen that these ions contain mainly ammonia molecules even though the water-to-ammonia pressure ratio is equal to three. It is also evident that the mixed occupancy follows quite nearly a probability distribution. Calling the probability for ammonia inclusion  $\alpha$  and that for water  $\omega$ , the calculated probabilities for an  $l$  solvate will be equal to the binomial expansion terms of  $(\alpha + \omega)^l$ . Thus, for the  $l = 2$  group the intensities of the ions should be in the ratios  $\alpha^2 : 2\alpha\omega : \omega^2$ . The ratio  $\alpha/\omega$  should be given by the ion intensity ratios  $2I_{52}/I_{53}$ ,  $I_{53}/2I_{54}$  and  $(I_{52}/I_{54})^{1/2}$ . Taking the values from the table we calculate for  $\alpha/\omega$  the values 10.6, 7, and 8.6.

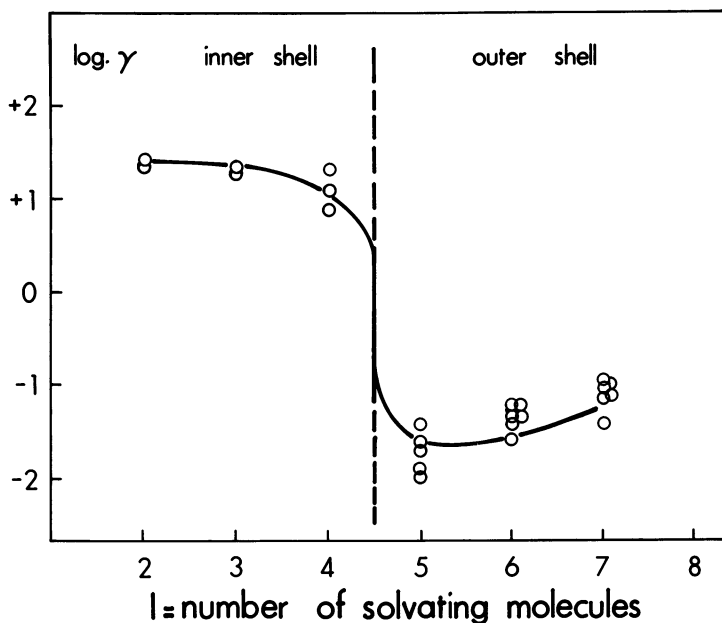


Figure 13. Plot of  $\log \gamma$  for different solvation shells of ion  $\text{NH}_4^+$

$\gamma$  is a factor giving the observed probability for preferential take up of ammonia over water into ion:  $\text{NH}_4^+ \cdot a\text{NH}_3 \cdot w\text{H}_2\text{O}$ , where  $a + w = 1$ . Ammonia is taken up with preference into inner shell ( $l \leq 4$ ), water is taken up with preference into outer shell

**Table II. Mass Spectra of Ammonia-Water Mixtures Showing the Competitive Solvation of the Ammonium Ion by Ammonia and Water Molecules**

$p(\text{NH}_3)$ (torr)		0.05 <sup>a</sup>		1.8		34	
$p(\text{H}_2\text{O})/p(\text{NH}_3)$		3		1.5		0.003	
Ion - Mass		Intensity <sup>b</sup> $\gamma^\circ$		Intensity $\cdot 15^b$ $\gamma^\circ$		Intensity <sup>b</sup> $\gamma^\circ$	
$\text{NH}_4^+ \cdot 2\text{NH}_3$	52	11.1	32				
$\text{NH}_4^+\text{NH}_3 \cdot \text{H}_2\text{O}$	53	2.1	21				
$\text{NH}_4^+ \cdot 2\text{H}_2\text{O}$	54	.15	25				
$\text{NH}_4^+ \cdot 3\text{NH}_3$	69	104.0	23				
etc.	70	40.0	19				
	71	6.3					
	72	<sup>a</sup>					
$\text{NH}_4^+ \cdot 4\text{NH}_3$	86	5.1	7	11.5	15	100	
etc.	87	8.3	12	4.4		<sup>a</sup>	
	88	3.2	11				
	89	0.6					
	90	<sup>a</sup>					
$\text{NH}_4^+ \cdot 4\text{NH}_3 \cdot$	103	<sup>a</sup>		<sup>a</sup>		335	0.027
$1\text{NH}_3$ etc.	104			9		360	
	105			3.2		<sup>a</sup>	
	106						
$\text{NH}_4^+ \cdot 4\text{NH}_3 \cdot$	120					800	0.036
$2\text{NH}_3$ etc.	121					1300	0.047
	122					380	

<sup>a</sup> Contains also 20 torr. xenon to make the signals detectable.

<sup>b</sup> Arbitrary units.

<sup>c</sup> Factor of preferential take up of ammonia to water (*see* text).

<sup>d</sup> Low intensity, not measured accurately.

In order to express the preference for ammonia per unit pressure we define, in analogy with the treatment of the methanol water clusters, a  $\gamma$

which is given by the equation  $\gamma = \frac{\alpha/P_{\text{NH}_3}}{\omega/P_{\text{H}_2\text{O}}}$ . The  $\gamma$ 's calculated in this

way are given in Table II. As  $l$  increases from 2-4 one observes a decrease of  $\gamma$  from about 25 to 10. This change is similar to that observed in the water methanol system. In clusters with  $l = 5, 6$ , etc. a new phenomenon is observed not paralleled by the water methanol system. The ammonia clusters with  $l > 4$  can not be fitted with a simple probability distribution. This is seen clearly from the results at 1.8 and 34 torr of ammonia (Table II). At 1.8 torr of ammonia the calculated  $\gamma$  for the  $l = 4$  group is close to that obtained at the low pressure showing an ammonia preference  $\gamma = 15$ . But the  $\text{NH}_4^+ \cdot 5\text{NH}_3$  ion of mass 103 is essentially missing. The first ion of significant intensity is  $\text{NH}_4^+ \cdot 4\text{NH}_3 \cdot \text{H}_2\text{O}$  (mass 104). This

result can be understood if it is assumed that an inner shell of four molecules has been built up and that water is taken up preferentially in the outer shell. The preference for water in the outer shell can be measured from the result at 34 torr. The much higher ammonia-to-water ratio used in this run leads to a fully ammoniated inner shell so that the ions of higher mass are caused by water presence in the outer shell only. The calculated  $\gamma$ 's for outer shell occupancy are smaller by a factor of nearly 1000. The results from a number of runs at different pressures and water-to-ammonia pressure ratios are summarized in Figure 4, which gives a plot of  $\log \gamma$  for different  $l$ . The values for  $l \leq 4$  represent inner shell  $\gamma$ 's. The values for  $l > 4$  were taken at higher ammonia-to-water pressure ratios where the inner shell was essentially completely made up of ammonia. This allowed the calculation of  $\gamma$ 's for outer shell solvation. The drastic change from  $l = 4$  to  $l = 5$  is evident also from these results. The considerable scatter of the points is believed to be mainly attributed to the difficulty in measuring accurately the ammonia and water pressures in the ion source. The preferential take up of ammonia in the inner shell and of water in the outer shell can be understood on the basis of the polarizabilities and dipole moments of water and ammonia. Ammonia has the higher polarizability but lower dipole; therefore, if it can win over water, it must do so in the inner shell. The result of an inner four shell is in agreement with the  $\Delta H_{n-1,n}$  measurements with pure ammonia described in the section: "Heats and Entropies of Individual Steps."

### Literature Cited

- (1) Altshuller, A. P., *J. Am. Chem. Soc.* **77**, 3480 (1955).
- (2) Basolo, F., Pearson, R. G., "Mechanisms of Inorganic Reactions," p. 64, John Wiley & Sons, New York, 1958.
- (3) Bell, R. P., "The Proton in Chemistry," Cornell University Press, Ithaca, New York, 1959.
- (4) Born, M., *Z. Physik* **1**, 45 (1920).
- (5) Collins, G. J., Kebarle, P. (to be published).
- (6) Durden, D. A., Kebarle, P. (to be published).
- (7) Hamer, W. J., ed., "The Structure of Electrolytic Solutions," Chapter 5, John Wiley & Sons, New York, 1959.
- (8) Hogg, A. M., Kebarle, P., *J. Chem. Phys.* **43**, 449 (1965).
- (9) Hogg, A. M., Haynes, R. M., Kebarle, P., *J. Am. Chem. Soc.* **80**, 28 (1965).
- (10) Kebarle, P., Godbole, E. W., *J. Chem. Phys.* **39**, 1131 (1963).
- (11) Kebarle, P., Haynes, R. M., Searles, S. K., *ADVAN. CHEM. SER.* **58**, 210 (1966).
- (12) Kebarle, P., Hogg, A. M., *J. Chem. Phys.* **42**, 798 (1965).
- (13) Munson, M. S. B., *J. Am. Chem. Soc.* **87**, 2332 (1965).
- (14) Wexler, S., *ADVAN. CHEM. SER.* **58**, 193 (1966).

RECEIVED October 11, 1966.

**American Chemical Society  
Library**

**1155 16th St., N.W.**

**Washington, D.C. 20036**

## The Mass Spectrometer as a Radiolytic and a Catalytic Laboratory

CHARLES E. MELTON

University of Georgia, Athens, Ga., and  
Chemistry Division, Oak Ridge National Laboratory, Oak Ridge, Tenn.

*A research mass spectrometer has been utilized as a self-contained chemical laboratory to investigate decomposition reactions induced by the absorption of ionizing radiation and by a hot metal surface. The investigation provided information not only about the final products but also about the various primary steps and transient species, such as ions and free radicals, which are produced. In the decomposition of ammonia, the most important transient species produced by both modes of excitation were H, NH<sub>2</sub>, and NH<sub>4</sub><sup>+</sup>. By generalizing from the experimental data, the elementary steps of the reaction are specified.*

An ideal study of a chemical reaction induced by any mode of excitation involves a knowledge of (1) the primary products which result from excitation of the electronic system of the individual reactant molecule, (2) transient species such as free radicals which are formed during the course of the reaction, and (3) the reaction of such species in temporal sequence to give final reaction products. This ideal has never been fully realized and consequently the elementary steps of most chemical reactions are uncertain. The advent of the high pressure mass spectrometer (5, 9, 23, 43) offered the possibility of attaining an approximation to this ideal. At first sight there appears to be little connection between a mass spectrometer and an ideal study of a chemical reaction, but the instrument can be suitably modified to obtain most of the information necessary to understand a reaction properly. Since the mass spectrometer can be changed into a combined reaction chamber and analytical tool, transient

species as well as final products can be identified and quantitatively measured during the entire course of the reaction.

The mass spectrometer has often been used to study radiolytic (39, 24) and catalytic reactions (1, 19). But, quantitative studies of the entire reaction were not possible because of inherent limitations on the ion source. In this paper we show how the ion source can be suitably modified to study the complete reaction rather than one or two elementary steps. Ammonia was selected for the investigation. Much work has been carried out on the ammonia system (4, 7, 13, 15, 16, 18, 22, 33, 35, 36, 38, 41, 42), but the elementary steps of the reaction are still obscure. It is the purpose of this report to summarize briefly our progress in an approach to determining the elementary steps of the decomposition of ammonia by the absorption of ionizing radiation and by a hot Pt surface.

### *Experimental*

**Radiolysis.** Our high pressure mass spectrometer, which has been described previously (20), was used for the experiments. The instrument is a 6-inch radius, 60° sector type of magnetic deflection spectrometer. The source region and analyzer region are evacuated separately by Hg diffusion pumps. The ion accelerating voltage is usually maintained at a potential of 5000 volts.

Ions are detected by a 14-stage electron multiplier coupled to both a vibrating reed electrometer (Model 31) and a pulse counter. This arrangement permits a simultaneous measurement of the number of ions detected and the d.c. current produced by each ion beam. The minimum detection sensitivity is about one ion per second with a dynamic range of  $10^7$ . Experimental tests indicated that the detection circuitry was essentially 100% efficient. This conclusion was based on the fact that the count rate reached a plateau well below the maximum gain of the multiplier and the normal energy of the ion beam. Data were taken well above the onset of the plateaus ( $\sim 300$  volts per stage and the 8000 e.v. energy).

A wide-range radiolysis source, shown schematically in Figure 1, was used for the radiolysis experiments. The source consists of three separate compartments constructed of stainless steel, each with an independently controlled electron beam. Ionizing electrons are emitted from the three external thorium-iridium filaments and are collimated by permanent magnets of about 500 gauss strength. The emission from each filament is maintained constant automatically and is normally of the order of 100  $\mu$ amperes, and the collimated electron beams are of the order of 10  $\mu$ amperes each. Electron energies may be varied from essentially zero to 100 e.v. although energies as high as several hundred e.v. may be used. The first compartment contains two electrodes for applying an electric field to the sample during irradiation. The series geometry of the source used in this study is not necessarily the best geometry. Ions could just as easily be extracted at right angles to compartments 1 and 2.

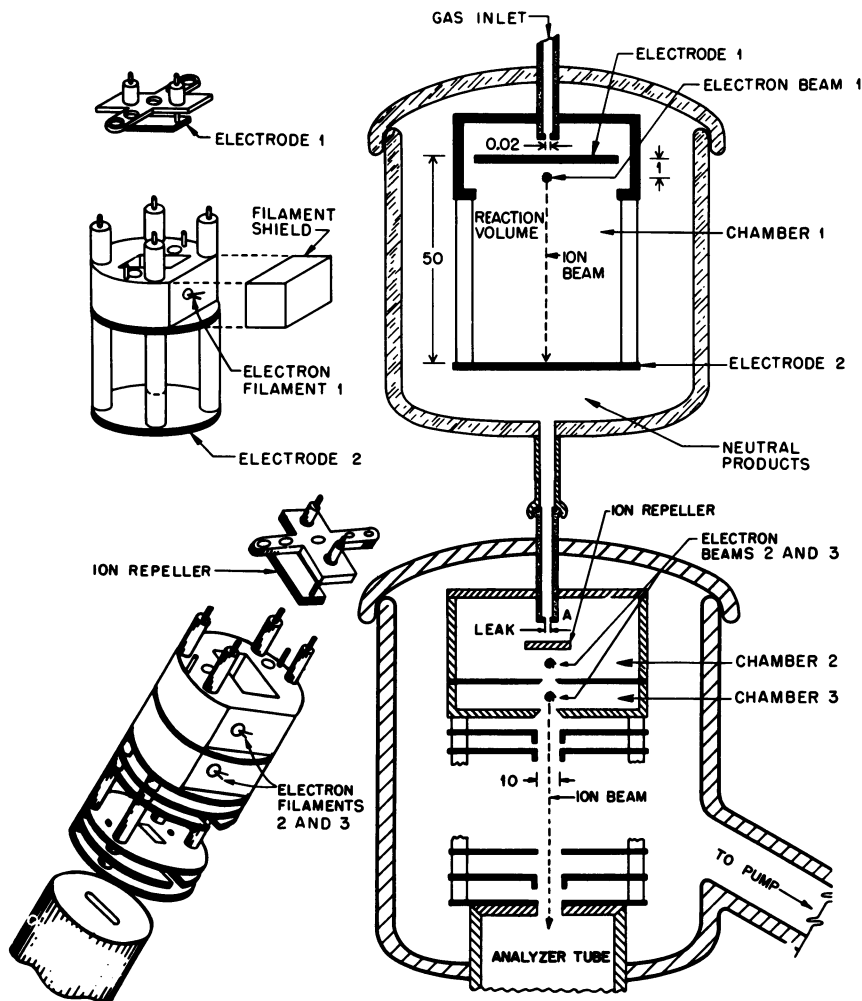


Figure 1. Wide-range radiolysis source for mass spectrometer. Dimensions are given in mm.

The pressure in each compartment was determined using Ar as a standard and the relationship

$$M_o = \frac{M^+}{\sigma N_e l} \quad (1)$$

where  $M_o$  is the number of neutral molecules per c.c.,  $M^+$  is the ion current,  $N_e$  is the electron current,  $\sigma$  is the ionization cross section for electrons of a given energy, and  $l$  is the path length of the electrons.

In operation a gas sample was introduced into the source from a 3-liter gas reservoir through a molecular leak. By energizing certain of

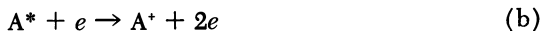
the electron beams (EB), different information about the steps of the reaction could be obtained as discussed below. To avoid confusing the results with thermal reactions, the electron filaments to be used were maintained at a constant high temperature at all times. The EB's were obtained by applying an accelerating potential to the filament.

**PRODUCTS, ENERGETICS, AND G VALUES (EB's, 1 AND 3).** To obtain final products, the threshold energy and G values, EB's 1 and 3 were energized. We define "threshold energy" as the minimum energy of the ionizing medium needed to produce a given neutral product. Irradiation of the sample at high pressure ( $\sim 1$  torr) with EB 1 in compartment 1 produced products which were subsequently ionized by EB 3 in compartment 3 for mass identification. The threshold energy was obtained by gradually increasing the energy of EB 1 until the product appeared as determined by mass analysis using EB 3. Values of  $G(-\text{NH}_3)$  were obtained from measurements of the percentage decomposition, the calculated residence time for the gas in the first compartment (35 sec.), the number of absorbed electrons and the energy of the absorbed electrons. The assumption was made that all secondary and scattered electrons were absorbed in the gas. G values of the products were obtained from  $G(-\text{NH}_3)$  and a material balance. The percent of each product formed in chamber 1 was determined in compartment 3 by EB 3 and normal mass spectrometric procedures. Variation of the pressure in compartment 1 over the range from  $10^{-4}$  to 1 torr gave the pressure dependence for each product.

**PERCENT OF PRODUCT ATTRIBUTED TO ION-MOLECULE REACTIONS (EB's, 1 AND 3, ELECTRODES 1 AND 2).** The percent of final neutral products caused by ion-molecule reactions was determined by using EB's 1 and 3 and electrodes 1 and 2 in compartment 1. EB 1 is very close ( $\sim 1$  mm.) to electrode 1. Consequently, a small negative potential applied to electrode 1 with respect to electrode 2 collects all of the positive ions before they undergo a significant number of ion-molecule reactions. On the other hand, a positive potential applied to electrode 1 causes the positive primary ions to drift toward electrode 2 and to undergo ion-molecule reactions in the gas phase. The difference in the abundance of a given product—e.g.,  $\text{H}_2$ , with electrode 1 positive compared to the abundance with electrode 1 negative was taken as the amount of that product produced by positive ion-molecule reactions.

**CROSS SECTIONS FOR PRIMARY REACTIONS, IONS (EB 3) AND FREE RADICALS (EB's 2 AND 3).** The values of the cross sections for the primary reactions which involve production of positive ions, negative ions and free radicals by electrons were determined by using EB's 2 and 3 and Equation 1. Since counting techniques were used for detection, the number of positive and negative ions detected was independent of the gain of the multiplier (assuming, of course, a gain sufficiently high to produce a count for each ion that strikes the first dynode of the multiplier). From the transmission efficiency of the source and Equation 1, the cross section can be determined for positive and negative ions in compartment 3 by using EB 3 only. To test the accuracy of the method, the cross section of each positive and negative ion was determined separately, and then the sum was compared with the total cross section obtained without mass analysis—i.e., collecting all ions on the ion repeller. Cross sections for

free radicals were determined by using EB's 2 and 3. The procedure involved formulating the mathematical relationships which govern the production of a species such as  $A^+$  by a sequence of reactions



where  $A$  is any atom or molecule and  $A^*$  is an excited molecule or free radical. According to Equation 1, the amount of  $A^*$  produced by Reaction a is given by

$$A^* = \sigma_* AN_e l \quad (2)$$

and that produced by Reaction b is given by

$$A^+ = \sigma_i \eta \frac{A^*}{V^*} N_e l' \quad (3)$$

where  $\sigma_*$  and  $\sigma_i$  are the cross sections for excitation and ionization,  $\eta$  is the transmission coefficient for  $A^*$  from compartment 1 and  $V^*$  is the average velocity of  $A^*$ . Combining Equation 2 and 3, one obtains for the ion current,  $A^+$

$$A^+ = \sigma_* \sigma_i [A] N_e N_e' l l' \frac{\eta}{V^*} \quad (4)$$

By substituting reasonable values for the parameters ( $\sigma_*, \sigma_i = 10^{-16} \text{ cm}^2$ ;  $[A] = 3.5 \times 10^{14}$ ;  $N_e N_e' = 10^{16} \text{ electrons/sec.}$ ;  $l, l' = 1$ ;  $\eta = 10^{-2}$ ;  $V^* = 10^4 \text{ cm./sec.}$ ) in Equation 4, we find that the intensity of  $A^+$  produced by consecutive reactions may be as high as  $10^8 \text{ ions/sec.}$  at a pressure of  $10^{-2} \text{ torr}$  in chamber 2.

The ionization cross section for free radicals  $\sigma_i$  was usually unknown and had to be determined indirectly by calculating the cross section for a similar molecule in accordance with the relationship

$$\sigma = \sigma_0 (E - I) \quad (5)$$

where  $\sigma$  is the cross section for a given value of electron energy,  $E$ ;  $I$  is the ionization potential of the molecule, and  $\sigma_0$  is a constant. Further details of operating a dual electron beam ion source are given elsewhere (25).

**SECONDARY IONS (EB 2) AND SECONDARY FREE RADICALS (EB'S 2 AND 3).** The techniques for studying rate constants for positive and negative ion-molecule reactions at high pressure have been reported by a number of workers (24, 31, 37, 39) and will not be discussed here. We used the same technique and EB 2 for such studies. Secondary free radicals were studied by using EB's 2 and 3. The technique involved scanning the mass spectrum in the mass range of interest (1 to 50 in the present study) first with EB 2 off (filament still hot) and again with a potential on EB 2 sufficient to produce free radicals in the sample. The ion repeller was maintained at a negative potential with respect to the chamber to collect any positive ions formed in compartment 2. Any change in the intensity of a given ion beam or the appearance of a new ion beam was attributed

to the difference in the potential of EB2, and hence indicated the formation of a neutral species from the sample which underwent either radical-molecule or radical-radical reactions.

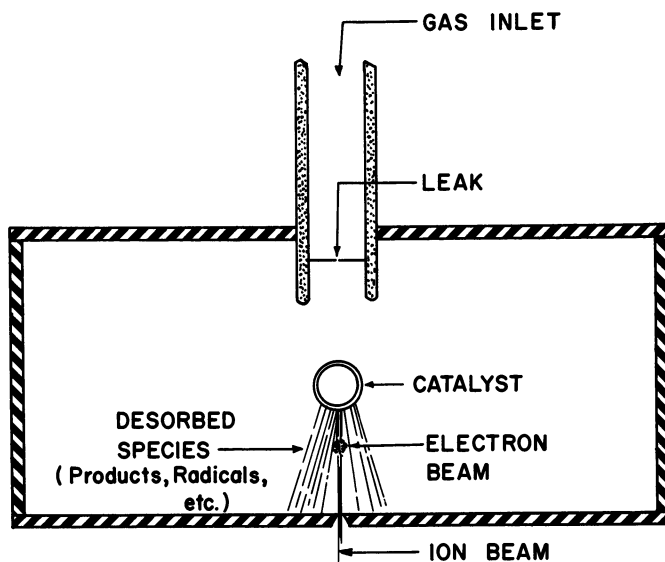


Figure 2. Catalytic reaction chamber for mass spectrometer

**ENERGETICS OF PRIMARY PROCESSES.** The energetics of primary processes which include appearance potentials for positive and negative ions and free radicals were determined by conventional techniques (21, 26).

**Catalysis.** Catalytic reactions were studied by passing reactant gases over a Pt catalyst in the ion source as shown in Figure 2. The catalyst was a spiral of 0.5-mm. Pt wire,  $3 \times 13$  mm. with a surface area of  $\sim 1$  cm.<sup>2</sup>. An optical pyrometer was used to determine the temperature of the catalyst. Products evolved from the catalyst and passed directly into the electron beam where they were ionized and identified by standard methods of mass analysis. Desorbed free radicals were identified by maintaining the energy of the ionizing electrons below that necessary for dissociative ionization of the reactants to give interfering fragment ions. Final and intermediate products were studied as a function of catalyst temperature, pressure, and concentration of each reactant. Product ions from ion-molecule reactions which might confuse the results were minimized by maintaining a 10-e.v. potential, with respect to the exit slit, on the catalyst, thus decreasing the residence time for ions in the ionization chamber. Radicals and intermediates which have a lifetime less than  $1 \mu\text{sec.}$  were not observed because the transit time from the catalyst to the electron beam was of the order of  $1 \mu\text{sec.}$  To be observed by the present method, radicals and intermediates must also be stable either to positive or negative ionization. Furthermore, the resultant ion had to be stable for the order of  $1 \mu\text{sec.}$  (ion transit time from the electron beam to

the detector). The percent abundance of free radicals was determined from the geometry of the reactor and the relationships given in Equation 1.

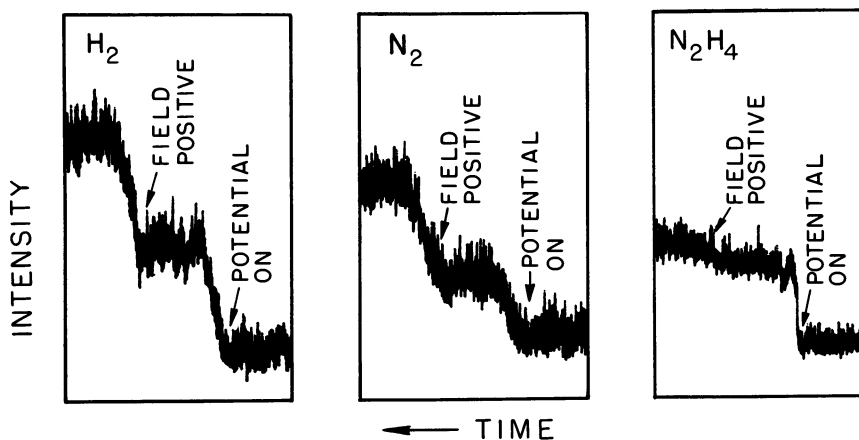
### Results

**Radiolysis. PRODUCTS.** Results from a study of the radiolytic decomposition products of  $\text{NH}_3$  ( $\text{H}_2$ ,  $\text{N}_2$ , and  $\text{N}_2\text{H}_4$ ), are summarized in Table I. The percent of each product was determined by the normal analytical procedures of mass spectrometry. A photograph of actual scans for each of the products is shown in Figure 3. "Potential On" indicates a potential of 100 volts applied to EB 1, Figure 1, and a potential of  $-30$  volts (field negative) applied to electrode 1. "Field Positive" indicates a potential of  $+15$  volts applied to electrode 1.

**Table I. Products Formed by the Irradiation of Ammonia, 100 e.v. Electrons and 1.0 Torr Pressure**

Product	Percent Abundance	Mode of Formation %		G
		Ion-Molecule <sup>a</sup> Reactions	Other Reactions	
$\text{H}_2$	74.9	54	46	8.8
$\text{N}_2$	24.9	63	39	2.9
$\text{N}_2\text{H}_4$	0.2	20	80	.03
$\text{NH}_3$	—	—	—	-6.1

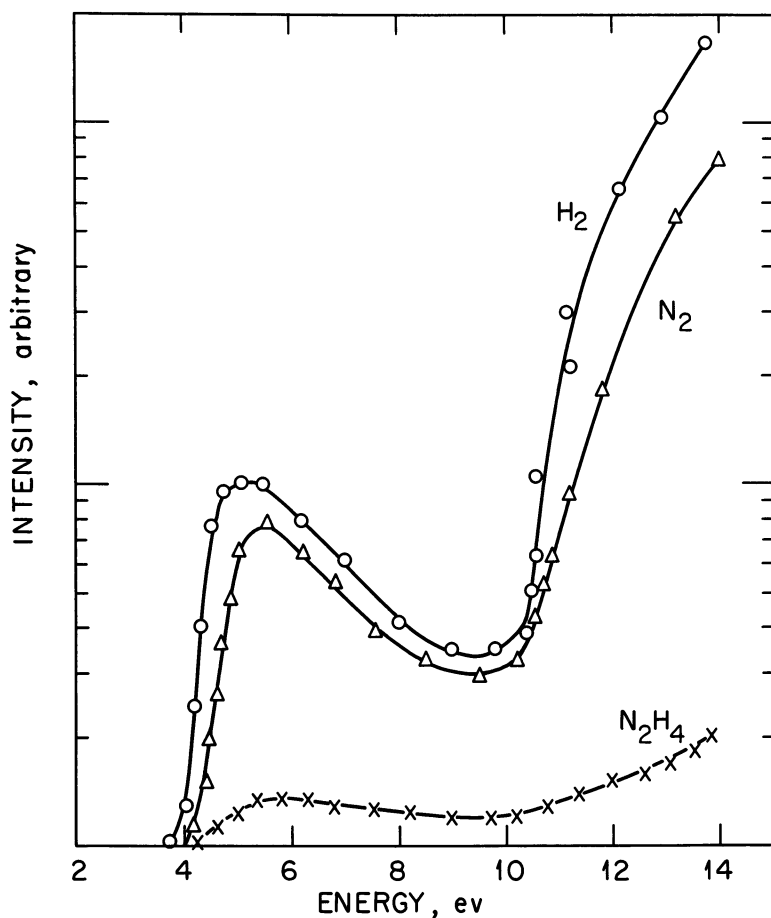
<sup>a</sup> The amount of each product formed by ion-molecule reactions was determined at 0.1 torr pressure.



**Figure 3.** Effect of electric field on the production of  $\text{H}_2$ ,  $\text{N}_2$ , and  $\text{N}_2\text{H}_4$  from the radiolysis of  $\text{NH}_3$  at 0.1 torr pressure

**Table II. Summary of G Values for the Decomposition of  $\text{NH}_3$  in the Gas Phase Obtained by Various Workers**

Product	G Value				This Study
	TBP <sup>a</sup>	H <sup>b</sup>	S <sup>c</sup>	S <sup>d</sup>	
$\text{H}_2$	6.2		10	6.3	8.8
$\text{N}_2$	2			2.1	2.9
$\text{N}_2\text{H}_4$					0.03
$-\text{NH}_3$	4.1	(4-6)			6.1

<sup>a</sup> Ref. 41.<sup>b</sup> Ref. 15.<sup>c</sup> Ref. 34.<sup>d</sup> Ref. 33.

**Figure 4.** Threshold energy and yield curves (abundance of products as a function of the energy of the ionizing radiation) for the products produced by the radiolysis of  $\text{NH}_3$ .

Table III. Primary Products Produced in the First Stage of the

Ion	Positive Ions		Cross Section $\sigma \times 10^{16}$	Species	Neutral
	Relative Abundance	Percent			Relative Abundance
H <sup>+</sup>	2.96	0.77	0.026	·H	100
H <sub>2</sub> <sup>+</sup>	2.96	0.76	0.026	·H <sub>2</sub>	18
N <sup>+</sup>	3.02	0.91	0.03	·N	1
NH <sup>+</sup>	9.07	2.67	0.09	·NH	3
NH <sub>2</sub> <sup>+</sup>	82.17	24.19	0.8	·NH <sub>2</sub>	19
NH <sub>3</sub> <sup>+</sup>	100	29.44	1.0		
Total		58.8	2.0		

To facilitate comparison of the *G*-values obtained in this study with other work, results from four other recent studies (15, 33, 34, 41) are tabulated in Table II. As can be seen, there are no serious disagreements between the various studies, and this agreement might appear surprising since all of the initial excitation in this study was produced by 100 e.v. electrons, whereas that in other studies was produced by high energy radiation (in the k.e.v. to m.e.v. range). However, it is well known that secondary electrons in the 100 e.v. energy range account for most of the chemical change in all radiolysis experiments. Thus, the agreement is really not surprising.

The threshold energy and yield curve for each product is shown in Figure 4. Note that the threshold energy of all of the products corresponds approximately to the appearance potential for H<sup>-</sup> and NH<sub>2</sub><sup>-</sup> (~ 4 e.v.) and NH<sub>3</sub><sup>+</sup> from NH<sub>3</sub> (10.5 e.v.). It appears that these ions and associated radicals lead to the final products.

**PRIMARY REACTIONS.** It is well known that the primary reactions of ionizing radiation with gaseous molecules lead to negative ions, positive ions, excited species, free radicals, and other neutral products. It is apparent that the species and yield will depend on the components of the total collision cross section  $\sigma$  which include the summation of all the excitation cross sections,  $\sigma_{ei}$ , as well as the elastic cross sections

$$\sigma = \sum_i \sigma_{ei} + \int_0^\epsilon \sigma(\epsilon) d\epsilon \quad (6)$$

where  $\sigma_{ei}$  is the cross section for excitation of the *i*th state of the molecule, and  $\sigma \epsilon d\epsilon$  is the cross section for an ionization reaction in which the energy of the ejected electron is between  $\epsilon$  and  $\epsilon + d\epsilon$ . Table III gives

**Irradiation of NH<sub>3</sub> (100 e.v. Electrons and 2 × 10<sup>-7</sup> Torr Pressure)**

Species	Negative Ion					
	Percent	Cross Section $\sigma \times 10^{16}$	Ion	Relative Abundance	Percent	Cross Section $\sigma \times 10^{16}$
	28.98	1	H <sup>-</sup>	100	0.39	0.013
	5.21	0.2				
	0.33	0.01				
	0.72	0.03	NH <sup>-</sup>	0.13	0.001	0.0002
	5.54	0.2	NH <sub>2</sub> <sup>-</sup>	3.71	0.01	0.0006
	40.8	1.41			0.4	0.014

experimental values for the individual and total cross section. The measurements which were made can be summarized as follows:

- (a) Individual and total cross section for the production of a specific ion (positive or negative)  $\sigma_1$

$$\sigma_1 = \int_0^\epsilon \sigma(\epsilon) d\epsilon$$

from NH<sub>3</sub> by 100 e.v. ionizing electrons.

- (b) Individual and total cross sections for the production of a specific free radical or neutral molecule  $\sigma_d$  from NH<sub>3</sub> by 100 e.v. ionizing electrons, *see* Figure 5.

The results from a study of primary reactions shown in Table III show that about 60% of the primary reactions lead to positive and negative ions and 40% to free radicals. These are almost the same as the percentages of reaction products attributed to ions and free radicals as shown by Table I and give a ratio of ionization to dissociation of about 1.5. This is about the same ratio as that for ionization  $\sigma_1$  to excitation ( $\sigma_e$ ) for H ( $\sigma_e/\sigma_e = 1.2$ ) by 100 e.v. electrons calculated using the Born-Bethe approximation (30).

Appearance potentials for the ions from the neutral species are shown in Table IV. Some of the values can be in error because the state of excitation of the neutral species is unknown. Results are in satisfactory agreement with those reported by other workers (2, 11, 12, 17, 27, 32).

ION MOLECULE REACTIONS. A great deal of work has been done on the positive ion-molecule reactions (6, 8, 14, 40) in NH<sub>3</sub>, and it might be thought that there is little need to re-examine the system. In fact, however, the agreement between various workers is only fair, which is scarcely surprising in view of the complexity of such reactions. Furthermore, negative ion-molecule reactions have not been studied even qualitatively.

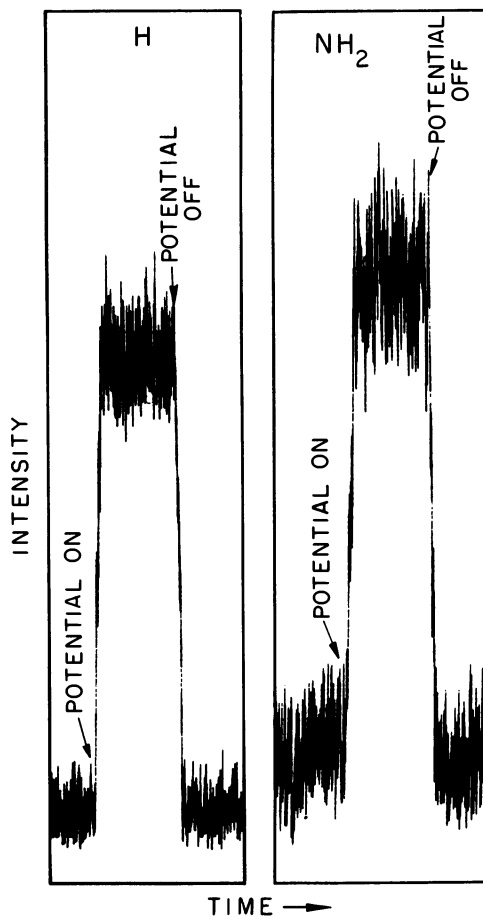


Figure 5. Typical results for the production of H and NH<sub>2</sub> radicals from NH<sub>3</sub> by ionizing radiation

Consequently, we have studied carefully the positive ion-molecule reactions in NH<sub>3</sub> and have examined qualitatively the negative ion-molecule reactions. Results are shown in Table V for positive ions. None of the previous measurements extended up to the pressure region of 1 torr which we used in this study. Derwish *et al.* (6), however, have covered the pressure range up to 0.1 torr. The present results are in reasonable agreement with their measurements except for the reaction



which was observed in the present study but was not reported by them.

However, these workers were unable to account for all of the  $\text{NH}_4^+$  product observed, and it is likely that Reaction C was at least partially responsible for their excess  $\text{NH}_4^+$  ions which account for 83% of the total ion current at 1 torr. The percentage is even higher (97%) when one includes  $\text{NH}_3^+$  and  $\text{NH}_2^+$  which ultimately produce  $\text{NH}_4^+$ . Hence, it is reasonable to assume provisionally that about 99% of the products resulting from ion-molecule reactions are formed from reactions which produce  $\text{NH}_4^+$  and the associated neutrals  $\text{NH}_2$  and H.

**Table IV. Appearance Potentials for Intermediate Neutral Species Produced in the Radiolytic Decomposition of  $\text{NH}_3$**

<i>Species</i>	<i>Relative Abundance</i>	<i>This Study</i>	<i>Previous</i>	<i>Theoretical<sup>a</sup></i>
H	100	13.8		
N	1	14.6		
NH	9	12.8	13.1 <sup>b</sup> 14.0 <sup>c</sup>	
$\text{NH}_2$	13	11.7	11.4 <sup>d</sup> 12.0 <sup>e</sup>	10.5
$\text{NH}_3$	—	10.2	10.5 <sup>f</sup>	(10.2) <sup>g</sup>
$\text{NH}_4$	0.1	5.9		
$\text{N}_2\text{H}_2$	13	9.9	9.9 <sup>d</sup>	10.1
$\text{N}_2\text{H}_3$	1	7.6	7.9 <sup>d</sup>	7.8
$\text{N}_2\text{H}_4$	—	8.8	9.0 <sup>f</sup>	(8.8)

<sup>a</sup> Calculated by our energy calibrated molecular orbital method. Ref. 27.

<sup>b</sup> Ref. 32.

<sup>c</sup> Ref. 12.

<sup>d</sup> Ref. 11.

<sup>e</sup> Ref. 2.

<sup>f</sup> Ref. 17.

<sup>g</sup> Parentheses indicate calibration points.

**DISCUSSION.** The final products— $\text{N}_2$ ,  $\text{H}_2$ , and  $\text{N}_2\text{H}_4$ —produced by the radiolysis of ammonia can be explained on the basis of three reactive species, namely,  $\text{NH}_4^+$ ,  $\text{NH}_2$ , and H as shown in Table VI. The results from Table III show that 97% of all those primary reactions which produce free radicals yield either  $\text{NH}_2$  or H. Furthermore, 99% of all ion-molecule reactions listed in Table V yield either  $\text{NH}_2$  or H as a neutral product. Clearly, these are the principal free radicals to be considered in any reaction mechanism. The results in Table III indicate that  $\text{NH}_4^+$  is the principal ion present at high pressure  $> 0.1$  torr (99% of all ions when  $\text{NH}_2^+$  and  $\text{NH}_3^+$ , which react to produce  $\text{NH}_4^+$ , are included) and therefore must account for the chemical change produced by ion-molecule reactions.

The evidence for mechanisms involving free radical reactions and ion-molecule reactions tabulated in the last column of Table VI is obtained from the threshold energy, the abundance of each species, and the

Table V. Ion Molecule Reactions Observed in the

<i>M./e.</i>	<i>Positive Ion</i>	<i>Percent Abundance</i>	<i>Probable Reaction</i>
1	H	0.1	$\text{NH}_3 + e \rightarrow \text{H}^+ + \text{NH}_2 + 2e$
2	H <sub>2</sub>	0.01	$\text{NH}_3 + e \rightarrow \text{H}_2^+ + \text{NH} + 2e$
14	N	0.1	$\text{NH}_3 + e \rightarrow \text{N}^+ + \text{H}_2 + \text{H} + 2e$
15	NH	0.4	$\text{NH}_3 + e \rightarrow \text{NH}^+ + \text{H}_2 + 2e$
16	NH <sub>2</sub>	4.3	$\text{NH}_3 + e \rightarrow \text{NH}_2^+ + \text{H} + 2e$
17	NH <sub>3</sub>	12.1	$\text{NH}_3 + e \rightarrow \text{NH}_3^+ + 2e$
18	NH <sub>4</sub>	82.9	$\text{NH}_2^+ + \text{NH}_3 \rightarrow \text{NH}_3^+ + \text{NH}_2$
			$\text{NH}_3^+ + \text{NH}_3 \rightarrow \text{NH}_4^+ + \text{NH}_2$
			$\text{H}_2^+ + \text{NH}_3 \rightarrow \text{NH}_4^+ + \text{H}$
29	N <sub>2</sub> H	0.03	$\text{N}^+ + \text{NH}_3 \rightarrow \text{N}_2\text{H}^+ + \text{H}_2$
30	N <sub>2</sub> H <sub>2</sub>	0.01	$\text{NH}^+ + \text{NH}_3 \rightarrow \text{N}_2\text{H}_2^+ + \text{H}_2$
31	N <sub>2</sub> H <sub>3</sub>	0.02	$\text{NH}_2^+ + \text{NH}_3 \rightarrow \text{N}_2\text{H}_3^+ + \text{H}_2$
32	N <sub>2</sub> H <sub>4</sub>	0.01	$\text{NH}_2^+ + \text{NH}_3 \rightarrow \text{N}_2\text{H}_4^+ + \text{H}$
33	N <sub>2</sub> H <sub>5</sub>	0.02	$\text{NH}_3^+ + \text{NH}_3 \rightarrow \text{N}_2\text{H}_5^+ + \text{H}$

Table VI. Summary of

<i>Reaction Product</i>	<i>Percent Abundance</i>	<i>Percent from Positive Ion Molecule Reactions</i>
H <sub>2</sub>	74.9	54
N <sub>2</sub>	24.9	63
N <sub>2</sub> H <sub>4</sub>	0.2	20

identity of the other transient species. For example, the resonance capture type shape of the yield curve for H<sub>2</sub>, N<sub>2</sub>, and N<sub>2</sub>H<sub>4</sub>, Figure 4, strongly suggests that the onset at about 3–4 e.v. is attributed to negative ion formation.

The present results at low pressure show that about 55% of the products are produced by ion-molecule reactions. Toi, Peterson, and Burton (41) suggested, from high pressure work on NH<sub>3</sub>, that 57% to

**Radiolysis of Ammonia at 1.0 Torr Pressure**

<i>Rate Constant</i> $\times 10^9$	<i>Cross Section</i>
<i>Molecules/cc., sec.</i>	$\sigma \times 10^{16} \text{ cm.}^2$

1.9	63
1.5	51
1.1	34
0.06	1.8
0.003	0.9
0.00	0.3
0.0005	0.1
0.001	0.3

**Major Conclusions**

<i>G Value</i>	<i>Threshold Energy</i>	<i>Proposed Mechanism</i>
8.8	3.6	$\text{NH}_3 + e \rightarrow \text{NH}_2^- + \text{H}$ (1)
		$\rightarrow \text{NH}_2 + \text{H}^-$ (1a)
		$\rightarrow \text{NH}_2 + \text{H} + e$ (1c)
	4.2	$\text{H} + \text{NH}_3 \rightarrow \text{NH}_2 + \text{H}_2$ (2)
		$\text{NH}_2 + \text{NH}_2 \rightarrow \text{N}_2\text{H}_4^*$ (3)
	10.2	$\text{N}_2\text{H}_4^* \rightarrow \text{N}_2\text{H}_2 + \text{H}_2$ (4)
		$\text{N}_2\text{H}_2 \rightarrow \text{N}_2 + \text{H}_2$ (5)
		$\text{NH}_3 + e \rightarrow \text{NH}_3^+ + 2e$ (6)
		$\text{NH}_3^+ + \text{NH}_3 \rightarrow \text{NH}_4^+ + \text{NH}_2$ (7)
		$\text{NH}_4^+ + e \rightarrow \text{NH}_2 + \text{H}_2$ (8)
	Continue <i>via</i> (3-5)	
2.9	3.6	Same as (1-5)
	4.2	
	10.2	Same as (6, 7)
0.03	3.6	Same as (1-3)
	4.2	$\text{N}_2\text{H}_4^* + \text{NH}_3 \rightarrow \text{N}_2\text{H}_4 + \text{NH}_3$ (9)
		$\text{NH}_3^- + \text{NH}_3 \rightarrow \text{N}_2\text{H}_6^-$ (10)
	$\text{N}_2\text{H}_6^- \rightarrow \text{N}_2\text{H}_4 + \text{H}_2 + e$ (11)	

76% of the products may be caused by processes involving ions. Takahashi (38) also concluded from r.f. discharge studies that ions are important in the decomposition of  $\text{NH}_3$ . Thus, the present results are in excellent agreement with the results of these investigators who used entirely different techniques. A summary of the types of radiolysis results which can be obtained by mass spectrometry is given in Table VII.

**Table VII. Information Obtained from Radiolysis Experiments**

1. Cross sections for the production of free radicals, ions and excited molecules by elementary reactions.
2. Yield of reactive intermediates (free radicals, ions, etc.).
3. Appearance potentials for ions, free radicals and excited molecules.
4. Positive and negative ion-molecule reactions.
5. Radical-radical, radical-molecule, and excited molecule-molecule reactions.
6. *G* values (molecules formed or decomposed per 100 e.v. of energy absorbed).
7. Abundance of products (intermediates and final).
8. Amount each product produced by ion-molecule reactions.
9. Threshold energy for the appearance of each product.
10. Pressure dependence for each product.

**Catalysis. NEUTRAL TRANSIENT SPECIES.** The free radicals H and NH<sub>2</sub> were the most abundant neutral transient species although N and NH were also observed at low pressure. Results are given in Table VIII. It is interesting to note that H and NH<sub>2</sub>, which are most abundant in this study, were also most abundant in the radiolytic study. These results suggest that the elementary steps are the same for both decomposition reactions.

**Table VIII. Concentration of Neutral Species Observed in the Decomposition of NH<sub>3</sub> at 0.1 Torr Over Pt and 1000°C.**

<i>Species</i>	<i>Concentration (%)</i>
H	0.0021
N	0.0001
NH	0.0003
NH <sub>2</sub>	0.0024
NH <sub>4</sub>	0.0002
N <sub>2</sub>	24.9
H <sub>2</sub>	74.9

**GAS-PHASE IONS.** The existence of charged species in the gas phase during the decomposition reaction is shown by the striking results of Figure 6. In this experiment the temperature of the catalyst was suddenly changed from room temperature to 1000°C. while monitoring the NH<sub>4</sub><sup>+</sup> ion beam with no ionizing electron beam present. The NH<sub>4</sub><sup>+</sup> intensity increases and decreases abruptly, from about 10<sup>4</sup> ions/sec. to less than 1 ion/sec., corresponding to abrupt changes in the catalyst temperature. In previous work (29), it was shown that NH<sub>4</sub><sup>+</sup> is probably formed by a surface reaction between NH<sub>3</sub> and H or H<sub>2</sub> molecules.

A study of the NH<sub>2</sub><sup>-</sup> and H<sup>-</sup> ion beams showed the behavior to be similar to that for NH<sub>4</sub><sup>+</sup>. No other positive or negative ions were observed

in the gas phase with the catalyst hot and the electron beam turned off. The observation of  $\text{NH}_2^-$  and  $\text{H}^-$  was not unexpected because the corresponding free radicals were observed. The abundance of the negative ions can be estimated from the well-known Saha-Langmuir equations

$$\frac{N^+}{N_0} = \frac{(1 - r_i)}{(1 - r_o)} \frac{\omega_i}{\omega_o} \exp\left(\frac{\phi - I}{kT}\right) \quad (8)$$

$$\frac{N^-}{N_0} = \frac{(1 - r_i)}{(1 - r_o)} \frac{\omega_i}{\omega_o} \exp\left(\frac{EA - \phi}{kT}\right) \quad (9)$$

The symbols are defined as:

$N^+/N_0$ ;  $N^-/N_0$  ratio of the charged to the neutral component leaving the surface

$r_i, r_o$  reflection coefficients of the surface for the ion and the neutral

$\omega_i$  and  $\omega_o$  statistical weighting factors for the ion and the neutral

$I$  ionization potential

$EA$  electron affinity

$\phi$  electron work function of the metal

$T$  absolute temperature

$k$  Boltzmann's constant

Although these equations are derived from first principles (28), they should be used with caution because of the effect of different adsorbed materials on the work function,  $\phi$ . Furthermore, the reflection for coefficients for different components for a given surface are usually unknown.

When a  $\text{NH}_3\text{-D}_2$  system was used, the species  $\text{NH}_4^+$  and  $\text{NH}_3\text{D}^+$  were observed. The formation of an  $\text{NH}_3\text{D}^+$  species in an  $\text{NH}_3\text{-D}_2$  system is consistent with the observations of Kemball (16) for the ammonia-deuterium exchange reaction on platinum. His results showed that the initial exchange product is always  $\text{NH}_2\text{D}$  and that  $\text{NHD}_2$  and  $\text{ND}_3$  are formed by subsequent independent reactions. If the intermediate in this exchange reaction were indeed the  $\text{NH}_3\text{D}$  species, the initial product would always be  $\text{NH}_2\text{D}$  because the intermediate on dissociation would give either  $\text{NH}_2\text{D} + \text{H}$  or  $\text{NH}_3 + \text{D}$ .

The absolute rate of ammonia decomposition was found in the present work to be proportional to the partial pressure of ammonia in the pressure range at and below  $10^{-3}$  mm. It was also found to be slowed down by adding hydrogen. The decomposition was approximately inversely proportional to the partial pressure of added hydrogen. Fogel *et al.* (10) have studied the decomposition of  $\text{NH}_3$  by bombarding a Pt

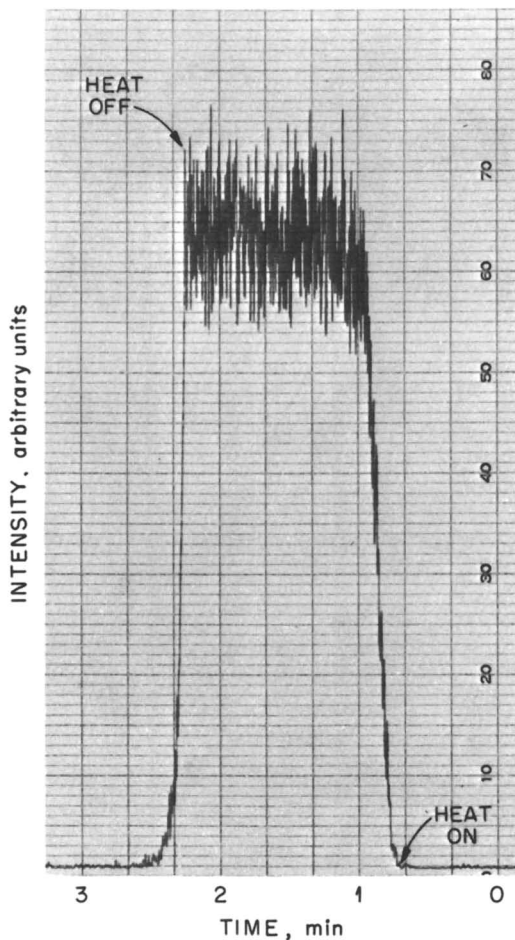


Figure 6. Production of  $\text{NH}_4^+$  ions by the decomposition of ammonia over Pt

catalyst with argon ions to displace species from the surface. The authors conclude that the decomposition of ammonia occurs primarily by the reaction



Certainly the present measurements do not point to such a mechanism. The relative yields of H,  $\text{NH}_2$ , NH, and N radicals in the present work would suggest instead the presence of more  $\text{NH}_2$  groups than NH groups on the surface. However, until one has values for the relative energies of activation for the desorption of H, N, NH, and  $\text{NH}_2$  radicals, one cannot conclude from the observed emissions the relative surface concentrations of these groups. The present experiments seem, however, to

afford definite evidence of the presence of H, N, NH, and NH<sub>2</sub>, and presumably NH<sub>4</sub> or NH<sub>4</sub><sup>+</sup> ions on the surface of the platinum during the catalytic decomposition of ammonia in the temperature range 500° to 1000°C. A summary of the types of information which can be obtained from catalysis studies is given in Table IX.

**Table IX. Information Obtained from Catalytic Experiments**

1. Identity and abundance of final reaction products.
2. Kinetics for the reaction.
3. Activation energy for the reaction.
4. Identity and abundance of reactive species desorbing from the catalyst such as ions and free radicals.
5. Information about elementary steps of the reaction mechanism.

### Conclusions

This mass spectrometric study of the decomposition of ammonia has been principally concerned with the elementary steps which lead to the final products. These steps were postulated on the basis of the identity and behavior of the transient species observed. Several qualitative conclusions about the two modes of decomposition have emerged even though a direct comparison of the absolute abundance of the transient species formed by each mode may be unreliable.

**Table X. Elementary Steps in the Decomposition of Ammonia<sup>a</sup>**

<i>Catalysis</i>	<i>Radiolysis</i>
$\text{NH}_3 \xrightarrow[\text{S}]{\text{S}} \text{NH}_2 + \text{H}$	$\text{NH}_3 \rightarrow \text{NH}_2^a + \text{H}^a$
$\text{NH}_2 + \text{NH}_2 \xrightarrow[\text{S}]{\text{S}} \text{N}_2\text{H}_4$	$\text{NH}_2 + \text{NH}_2 \rightarrow \text{N}_2\text{H}_4^a$
$\text{N}_2\text{H}_4 \xrightarrow{\text{S}} \text{N}_2 + 2 \text{H}_2$	$\text{N}_2\text{H}_4 \rightarrow \text{N}_2 + \text{H}_2$
$\text{H} + \text{NH}_3 \xrightarrow[\text{S}]{\text{S}} \text{NH}_4$	$\text{X}^a + \text{NH}_3 \rightarrow \text{NH}_4^a$
$\text{NH}_4 \xrightarrow[\text{S}]{\text{S}} \text{NH}_2 + \text{H}_2$	$\text{NH}_4^a \rightarrow \text{NH}_2 + \text{H}_2$

<sup>a</sup> S represents a surface, "a" indicates the state, positive, negative, neutral, or excited, and X indicates a reactive species.

The transient species formed by both modes of decomposition were essentially the same. For example, the free radicals H, NH, NH<sub>2</sub>, and NH<sub>4</sub> were observed in about equal relative concentrations (*see* Tables III, VI, and VIII). Even the ions, which might be expected to be completely different, in effect were the same. The ion NH<sub>4</sub><sup>+</sup> was observed desorbing from the catalyst whereas this ion was formed by ion-molecule

reactions in the radiolytic decomposition so that the net result was that  $\text{NH}_4^+$  was the most abundant ion in each reaction at high pressure.

These experimental results lead us to postulate that the elementary steps in the decomposition of ammonia by catalysis may be about the same as those for decomposition by ionizing radiation. However, it should be emphasized that the mode of generation of the primary products ( $\text{NH}_2$ ,  $\text{H}$ , etc.) is completely different and we do not want to imply a similarity in this respect. They are given in Table X.

In this brief discussion, I have tried to show by a specific example how the mass spectrometer can be used as a unique self-contained research laboratory to obtain information necessary for the interpretation of a chemical reaction.

### Acknowledgments

The author wishes to express his appreciation to P. H. Emmett of Johns Hopkins University for many helpful suggestions and stimulating discussions.

### Literature Cited

- (1) Collin, J. E., "Advances in Mass Spectrometry," p. 981, W. L. Mead, ed., The Institute of Petroleum, London, 1966.
- (2) Cook, G. R., Samson, J. A. R., *Bull. Am. Phys. Soc.* **4**, 454 (1959).
- (3) Copley, M. J., Phipps, T. E., *Phys. Rev.* **48**, 960 (1935).
- (4) Dainton, F. S., Skwarski, T., Smithies, D., Wezranowski, E., *Trans. Faraday Soc.* **60**, 1068 (1964).
- (5) Derwish, G. A. W., Galli, A., Giardini-Guidoni, A., Volpi, G. G., *J. Chem. Phys.* **40**, 5 (1964).
- (6) *Ibid.*, **39**, 1599 (1963).
- (7) Devins, J. C., Burton, M., *J. Am. Chem. Soc.* **76**, 2618 (1954).
- (8) Dorfman, L. M., Noble, P. C., *J. Phys. Chem.* **63**, 980 (1959).
- (9) Field, F. H., Franklin, T. L., Munson, M. S. B., *J. Am. Chem. Soc.* **35**, 3575 (1963).
- (10) Fogel, Ya. M., Nadykto, B. T., Rybalko, V. F., Slabospitskii, R. P., Korobchanskaya, I. E., *Dokl. Akad. Nauk SSSR* **147**, 414 (1962).
- (11) Foner, S. N., Hudson, R. L., *J. Chem. Phys.* **29**, 442 (1958).
- (12) Franklin, J. L., Diebeler, V. H., Reese, R. M., Krauss, M., *J. Am. Chem. Soc.* **80**, 298 (1958).
- (13) Hanes, M. H., Blair, E. J., *J. Chem. Phys.* **38**, 672 (1963).
- (14) Hertel, G. R., Koski, W. S., *J. Am. Chem. Soc.* **86**, 1683 (1964).
- (15) Horscroft, R. C., *Trans. Faraday Soc.* **60**, 323 (1964).
- (16) Kemball, C., *Proc. Roy. Soc. (London)* **A217**, 376 (1953).
- (17) Kiser, R. W., "Tables of Ionization Potentials," pp. 68, 72, TID-6142, 1960.
- (18) Laidler, K. J., "Catalysis," p. 138, P. H. Emmett, ed., Reinhold Publishing Corporation, New York, 1954.
- (19) Le Goff, P., Cassuto, A., Pentenero, A., "Advances in Mass Spectrometry," p. 853, W. L. Mead, ed., The Institute of Petroleum, London, 1966.
- (20) Martin, T. W., Rummel, R. E., Melton, C. E., *Science* **138**, 77 (1962).

- (21) McDowell, C. A., "Mass Spectrometry," p. 480, C. A. McDowell, ed., McGraw-Hill Book Co., Inc., New York, 1963.
- (22) McNesby, J. R., Tanaka, I., Okabe, A., *J. Chem. Phys.* **36**, 605 (1962).
- (23) Melton, C. E., *J. Chem. Phys.* **35**, 1751 (1961).
- (24) Melton, C. E., "Mass Spectrometry of Organic Ions," p. 65, F. W. McLafferty, ed., Academic Press, Inc., New York, N. Y., 1963.
- (25) Melton, C. E., *J. Sci. Instr.* **43**, 927 (1966).
- (26) Melton, C. E., Hamill, W. H., *J. Chem. Phys.* **41**, 546 (1964).
- (27) Melton, C. E., Joy, H. W., *Can. J. Chem.* **43**, 1455 (1966).
- (28) Melton, C. E., *J. Catalysis* **5**, 234 (1966).
- (29) Melton, C. E., Emmett, P. H., *J. Phys. Chem.* **68**, 3318 (1964).
- (30) Mott, N. F., Massey, H. S. W., "The Theory of Atomic Collisions," p. 271, Oxford University Press, London, 1950.
- (31) Munson, M. S. B., Franklin, J. L., Field, F. H., *J. Phys. Chem.* **68**, 3098 (1964).
- (32) Reed, R. I., Snedden, W., *J. Chem. Soc.* **IV**, 4132 (1959).
- (33) Salzman, J. D., Blair, E. J., *J. Chem. Phys.* **41**, 3654 (1964).
- (34) Schiek, R. C., *Dissert. Abst.* **24**, 2289 (1963).
- (35) Shiskov, D., Schulte-Frohlinde, D. Z., *Physik Chem.* **44**, 112 (1965).
- (36) Sorokin, Yu. A., Pshchetskii, S. Ya., *Zh. Fiz. Khim.* **39**, 1955 (1965).
- (37) Stevenson, D. P., Schissler, D. D., "Actions Chimiques et Biologiques des Radiations," Cinquieme Serie, p. 167, M. Haissinsky, ed., Masson et C, Edituers, Bris, 1961.
- (38) Takahashi, S., *Bull. Chem. Soc. (Japan)* **33**, 1350 (1960).
- (39) Talrose, V. L., Karacheutsev, G. V., "Advances in Mass Spectrometry," p. 211, W. L. Mead, ed., The Institute of Petroleum, London, 1966.
- (40) Talrose, V. L., Frankevich, E., "Treatise of the All Union Conference on Radiation Chemistry," p. 13, Academy of Sciences of the USSR, Moscow, 1958.
- (41) Toi, Y., Peterson, D. B., Burton, M., *Radiation Res.* **17**, 399 (1962).
- (42) Vsmanov, A. G., Panfilovich, K. B., *Zh. Fiz. Khim.* **39**, 1121 (1965).
- (43) Wells, G. F., Melton, C. E., *Rev. Sci. Instr.* **28**, 1065 (1957).

RECEIVED November 8, 1966. Research sponsored by the U. S. Atomic Energy Commission under contract with the Union Carbide Corporation.

## Direct Mass Spectrometric Sampling of High Pressure Systems

THOMAS A. MILNE and FRANK T. GREENE

Midwest Research Institute, Kansas City, Mo.

*The extension of direct mass spectrometric sampling to inorganic systems at higher pressures offers advantages in the type of species and reactions that can be studied. One method involves an initial expansion as a free jet, which is subsequently collimated into a molecular beam. Knowledge of such free-jet expansions is sufficient to predict the principal phenomena, including mass separation and homogeneous nucleation. A three-stage, differentially pumped sampling system has been applied to the sampling of flames, to the observation of clusters in argon, and to the study of the behavior of Hg and CsCl in Ar and N<sub>2</sub> carrier gases. A preliminary consideration of the kinetics of growth of the species Ar<sub>2</sub> indicates that collisions between molecules at low thermal energies and densities are important.*

Mass spectrometry has proved to be an extremely versatile detector in the study of inorganic gaseous systems, as the papers in this symposium indicate. Most of the systems studied by direct line-of-sight sampling of reactive species, however, have been at relatively low pressures. There are several reasons for wishing to extend direct mass spectrometric sampling to systems at higher pressure. Brewer (5) has pointed out that the complexity of the vapor in equilibrium with a condensed phase frequently increases with increasing temperature and hence increasing pressure. Thus, one may find, and be able to study, many new species at higher pressures. An example is furnished by the class of weakly bound van der Waals' dimers which exist in all gases, with the possible exception of He. Furthermore, both homogeneous and heterogeneous equilibria often must be driven by a high partial pressure of reacting gas to obtain appreciable concentrations of a particular species. The case of steam over NaCl(c) giving a postulated NaCl · 7H<sub>2</sub>O gaseous

molecule (7) is an example. Another process of some interest is that of homogeneous nucleation of both low and high temperature species, which is observable in its earliest molecular stages in the expansion into a vacuum that occurs in direct high pressure sampling. Finally, many practical chemical processes occur in high pressure environments. As an example, it is currently a matter of some concern whether the species which have been shown to be important in the low pressure oxidation of metals, the low pressure decomposition and combustion of solid propellants, and the low pressure equilibria of light metal compounds, are still the important species at the higher pressures and temperatures involved in practical combustion systems.

In the following sections we discuss molecular beam formation from a high pressure gas. High pressure here refers to any sampling condition in which the mean free path of the gas,  $\lambda$ , is substantially smaller than the sampling orifice diameter,  $d$ —*i.e.*, the Knudsen number,  $K_n = \lambda/d$ , is much less than 1. Only the sampling of neutral gases will be considered. Some of the phenomena discussed have a bearing on the direct sampling of ions, but the special problems of ion extraction will not be discussed.

### **Beam Formation Process**

**Free-Jets.** In converting a high pressure gas into a molecular beam which can be introduced into the ion source of a mass spectrometer, the crucial changes in composition or state occur during the initial continuum expansion which occurs downstream (and slightly upstream) of the sampling orifice. If the pressure downstream from the orifice is kept quite low, typically  $10^{-5}$  or  $10^{-6}$  of the pressure of the gas being sampled, one obtains a free-jet expansion. Free-jets are receiving much study currently because of their pertinence to the Kantrowitz-Grey (14) type of supersonic beams for producing high energy, high intensity molecular fluxes and because they can provide a supersonic flow field of known properties for various aerodynamic tests. The problem of high pressure sampling, of course, provides a third motivation for understanding free-jets. The details of free-jet structure and properties are given in many recent papers, particularly those in the proceedings of the Rarefied Gas Dynamics Symposia (6). In addition, several recent review articles are pertinent (2, 3, 8, 15). Only those aspects of immediate concern to direct sampling will be discussed here.

As a basis for understanding the sampling process, it is reasonable to approximate the center-line flow of gas from a knife-edged orifice as consisting of a continuum adiabatic isentropic expansion up to a transition point at which it abruptly enters an essentially collisionless region. Clearly, this is not accurate since the actual transition is gradual, yet the

simple model has proved useful in correlating free-jet data. Direct experimental data for small orifices and monatomic gases give the Mach number of the gas as a result of the continuum expansion and can be fit to an effective terminal Mach number at which collisions essentially cease (1, 25). Over the continuum portion of the expansion, Ashkenas and Sherman (6) give the calculated Mach number as a function of distance downstream as:

$$M = A \left( \frac{x - x_0}{d} \right)^{\gamma-1} - \frac{1}{2} \left( \frac{\gamma + 1}{\gamma - 1} \right) / A \left( \frac{x - x_0}{d} \right)^{\gamma-1}, \quad (1)$$

where  $\gamma$  is the ratio of specific heats,  $d$  is the orifice diameter, and  $x$  is the distance downstream from the orifice.  $A$  and  $x_0$  have the following values for different  $\gamma$ 's:

$\gamma$	$A$	$x_0/d$
5/3	3.26	0.075
7/5	3.65	0.40
9/7	3.96	0.85

At large distances  $M \cong A(x/d)^{\gamma-1}$

$$\rho/\rho_0 = \left( 1 + \frac{\gamma-1}{2} M^2 \right)^{-1/\gamma-1} \cong \left( \frac{\gamma-1}{2} \right)^{-1/\gamma-1} A^{-2/\gamma-1} (x/d)^{-2}$$

which for  $\gamma = 5/3$  reduces to:

$$\rho/\rho_0 = \frac{0.16}{(x/d)^2}, \quad (2)$$

where  $\rho_0$  is the source density and  $\rho$  is the density at a distance  $x$  from the orifice of diameter  $d$ . (Note that the expansion is scaled in orifice diameters.) Standard expressions for isentropic expansion in flowing systems relate the Mach number or density to the local pressure, temperature, and velocity. It is interesting that the flow is source-like and differs relatively little in the rate of density decrease from the rate given by the Knudsen effusion expression (28) were this relationship to apply over the same source conditions.

$$(\rho/\rho_0)_{\text{Knudsen}} = \frac{0.0625}{(x/d)^2}. \quad (3)$$

Prediction of the theoretical beam intensity at a large distance from the orifice, with intervening slits, requires consideration of the terminal Mach number and the geometry of the second slit. With a sufficiently large second slit, or skimmer, Anderson and Fenn (4) have argued that Ashkenas and Sherman's source-flow expression (Equation 2) can be applied at any distance, even into the essentially collisionless regime.

Thus, an upper limit to attainable beam intensities is provided if departures from ideality and scattering are negligible. Anderson, Andres, and Fenn (3) give an expression for intensity in the case of a very small skimmer and a terminal Mach number,  $M_T$ . Likewise, Anderson and Fenn (4) give an expression for large skimmers. The most definitive discussion of beam intensities appears to be that of Hagena and Morton (23). Experimental beam intensities obtained in our system will be compared with those calculated from Equation 2 in the next section.

For monatomic gases, the expansion is relatively simple; only translational degrees of freedom exist, and notwithstanding such refinements as consideration of nonisentropic flow and anisotropic and non-Maxwellian velocity distributions (13), the simple picture above should give a useful description of the history of the sampled gas. It is assumed, of course, that no homogeneous nucleation is occurring during expansion (discussed later). With polyatomic gases one must consider the relaxation of the various internal degrees of freedom during the expansion. Direct experimental data on the translational (1, 25) and rotational states (18, 24) during expansion have been obtained by velocity distribution measurements and by optical spectroscopy. The vibrational behavior has been inferred from the apparent  $\gamma$  which describes the measured free-jet properties. As a first approximation one can predict complete translational relaxation to the terminal Mach number condition (a matter of definition). Rotational relaxation will be considerable, but final rotational temperatures are substantially higher than translational temperatures. Vibrational relaxation will usually be minimal. For excited electronic states, radiative processes will probably dominate over collisional de-excitation. When collisions have essentially stopped, the state of the molecules will remain frozen with the possible exception of unimolecular reactions such as those postulated by Robbins and Leckenby (16), in which weakly bound polyatomic clusters essentially rotate themselves apart in the absence of collisions.

The actual course of the free-jet expansion is shown in Figure 1 for three gases, Ar, N<sub>2</sub>, and CH<sub>4</sub>, initially at 1 atm. and 300°K. The curves labeled "free-jet" show the pressure-temperature conditions of isentropic expansion. The terminal Mach number for argon can be predicted from Anderson and Fenn's criterion (4).

$$M_{T_{\text{erm}}} = 1.17 \left( \frac{\gamma}{d} \right)^{-0.4} \quad (4)$$

The three nearly straight lines show the equilibrium vapor pressure of the condensed phases of the three gases. The significance of these curves will become apparent in the discussion of nucleation. Doubling of the orifice size, for a given pressure, would have two effects. First, the terminal

Mach number would increase according to Expression 4. Second, the time required to reach a given  $T$ - $P$  point on the curves, corresponding to a given Mach number, would double. Times of the order of microseconds are involved over the ranges shown in the figure with orifice sizes of a few mils.

It should be emphasized again that all the above discussion assumes an ideal expansion and the absence of shock effects, either in the free-jet or as a result of the presence of the skimmer in the flow field of the orifice. The validity of these assumptions in our sampler is discussed elsewhere (9, 10).

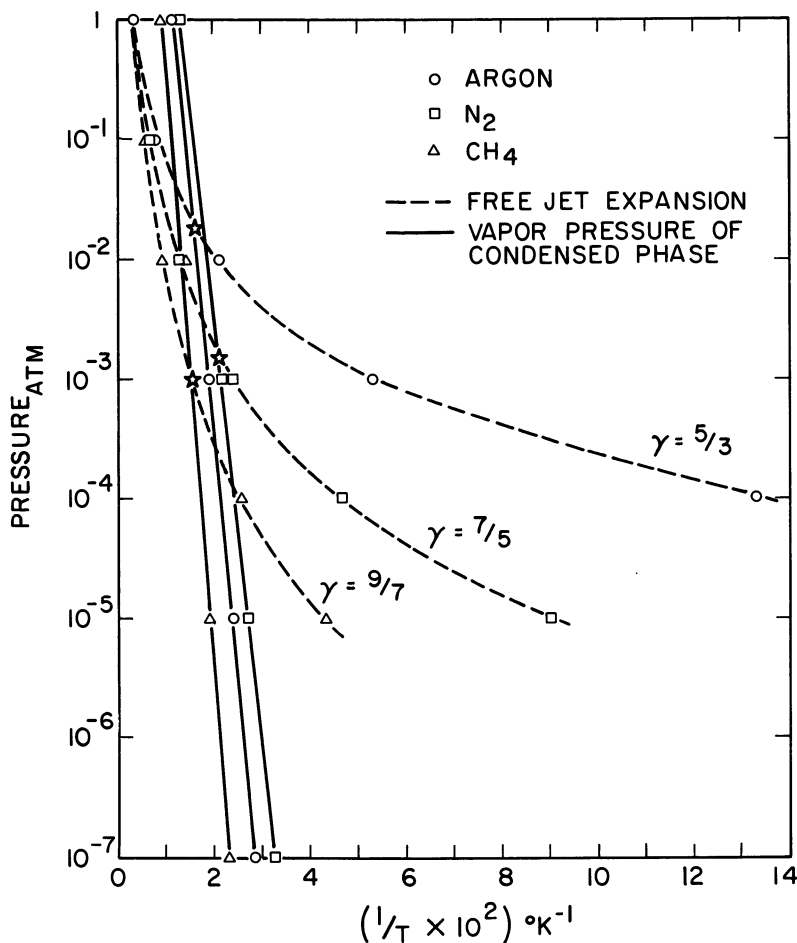


Figure 1. A comparison of calculated free-jet expansion history with saturated vapor pressures for Ar, N<sub>2</sub>, and CH<sub>4</sub> initially at 1 atm. and 300°K.

**Sampling Effects Accompanying Free-Jet Expansion.** There are a number of important consequences of direct free-jet sampling. First, in sampling mixtures of gases, a well developed continuum expansion will result in a nearly unchanged composition of gas at the transition region (26) with all molecules moving along the beam axis with essentially the same velocity. The molecules of different molecular weight will have differing random thermal velocities, however, and as a well collimated molecular beam is formed, the lighter molecules will spread more rapidly than the heavier. The consequence, as first pointed out by Stern, Waterman, and Sinclair (27) and verified by Green, Brewer, and Milne (10) is that the molecular beam reaching the mass-spectrometer ion source will be depleted in lighter molecules in proportion to the first power of their molecular weight. That the different molecules will have essentially the same mean axial velocity has been verified for mixtures of gases by a chopped beam, time-of-flight method (12). For example, in a He-Ar mixture sampled at 1 atmosphere through a 0.002 inch diameter orifice, the Ar and He velocities differed by only a few percent.

One interesting consequence of the above velocity phenomenon, which has been pointed out by Anderson, Andres, and Fenn (2), has significance in terms of beam-surface reaction studies. For a 10% argon-90% He mixture, the final beam composition will be about 50% argon. More important, time-of-flight data show that the argon has a most probable velocity equivalent to an effusive beam with a temperature 2300°K., even though the source temperature is 300°K. A large number of mixtures have been directly studied by Abuaf *et al.* (1) illustrating this feature.

A second effect which occurs in high pressure sampling is really just an example of a failure to preserve the concentrations of species originally present. As Figure 1 shows, even gases which were originally highly unsaturated may become enormously supersaturated in the free-jet and homogeneous nucleation will result (11, 21). In the case of sampling of gases which are initially saturated with respect to a condensed phase of some component, this phenomenon will be exaggerated. Such condensation is a nuisance in sampling and must be suspected in any high pressure study. One way to detect this effect will be mentioned later. Of more importance, however, is the fact that the free-jet presents such a time-temperature-collision history that rapid condensation processes can be studied in their early, molecular stages.

A final point about direct mass spectrometric observations of species from a free-jet is that the internal energy states of the molecule will not be precisely known. Consequently, when dealing with molecules from high temperature sources, the failure of the vibrational degrees of freedom to relax may give rise to fragmentation patterns typical of highly excited

molecules. Such effects have apparently been observed in the sampling of flames (20). A related problem is that with the general ability to sample reactive species, calibrations for mass spectrometer sensitivity will often not be available and one must resort to estimates of cross sections and fragmentation behavior (21).

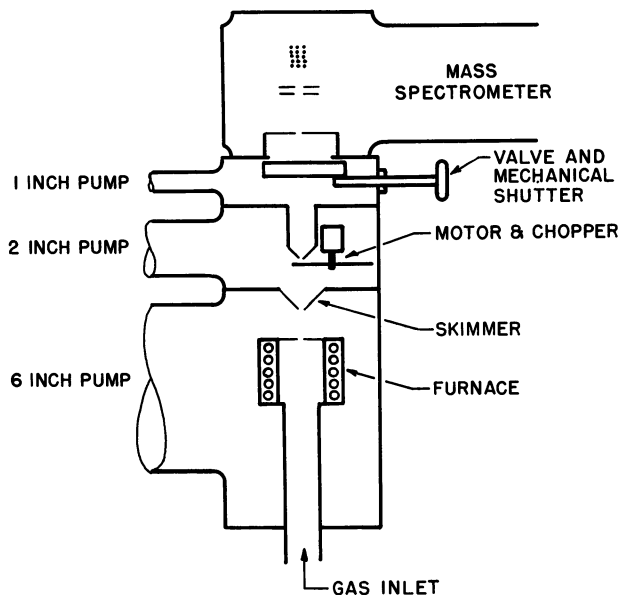


Figure 2. Schematic of a three-stage, high pressure, molecular beam sampling system using a Bendix time-of-flight mass spectrometer as a detector

### Apparatus and Performance

The sampling apparatus that we have developed for high pressure studies of inorganic systems is shown in Figure 2. This system has been improved from that described in our earlier work (10), but uses the same complement of pumps. The orifice-to-electron beam distance has been reduced from 16 to 8 inches, and improved pumping in each stage has resulted in less beam scattering. Typical operating conditions are listed in Table I. This system is not unlike other high pressure beam and sampling systems although of modest pumping capacity. Figure 2 shows a motor-driven chopper in stage two, which has proved to be an essential part of our system. The advantages, problems, and results of using modulated beams for both noise and background-ion discrimination, as well as time-of-flight velocity determinations, have been discussed (12). A graphic indication of one of these advantages is given in Table II. Here the ratio of a noncondensable species, Ar, to a very unstable species, Ar<sub>2</sub>,

is tabulated as a function of chopping frequency. It is seen that even with a well-collimated molecular beam entering the Bendix Model 12 ionization source, data taken with a manual shutter would be in error by a factor of about two and that chopping frequencies of at least 15 c.p.s. are needed to discriminate adequately against beam gases scattered in the ion source. Another advantage of modulation is that high frequency time-of-flight measurements (12) can be used to determine the most probable velocities of the beam components. Valuable information can be deduced about the extent of the free-jet expansion in the case of high pressure beam formation and about the molecular weight of neutral precursors of observed ions in Knudsen effusion studies.

**Table I. Typical Operating Conditions of Molecular Beam Sampling System**

	<i>Pressure, torr</i>	<i>Exit Slit Dimensions, in.</i>	<i>Distance from Ion Source Electron Beam, in.</i>	<i>Typical Scattering Loss, %</i>
Source	760	0.002 diam.	8	—
Stage One	$1 \times 10^{-3}$	0.020 diam.	7-3/4	25
Stage Two	$3 \times 10^{-5}$	$0.10 \times 0.024$	6-1/2	15
Stage Three	$8 \times 10^{-6}$	$0.50 \times 0.030$	2-1/8	10
Ion Source of Bendix Model 12	$< 1 \times 10^{-6}$		0	—

**Table II. The Dependence of the Observed Ratio  $Ar_2/Ar$  on Chopping Frequency**

<i>Frequency (Hz)</i>	$80^+ / 36^+$
0	1.45
2	2.42
8	2.54
15	2.64
50	2.64
100	2.60
160	2.62

Our system has been calibrated to obtain absolute beam fluxes at the ion source by comparing the intensity of  $Ar^+$ , from argon effusing through a system with known geometry under Knudsen conditions, with the intensity observed for a supersonic beam. In this way beam fluxes 8 inches away from the source orifice of about  $5 \times 10^{15}$  molecules/sq. cm. sec. have been demonstrated for a 0.002 inch diameter orifice and 1 atm. argon. The intensity predicted from Equation 2 is  $1.3 \times 10^{16}$  molecules/sq. cm. sec. When scattering corrections of about 60% are applied to the experimental value, the system approaches to within a factor of

two the theoretically predicted maximum intensity. Dynamic ranges of study of  $10^7$  have been obtained in the absence of background peaks. In our practical studies we are limited by fluctuations of the signal from the background hydrocarbons rather than electronic noise.

There is no obvious upper limit to the pressure which can be sampled provided the choice of orifice sizes, distances, and pumping speed allows good free-jet expansion without excessive scattering. We have formed beams from 7 atm. of argon, while Leckenby *et al.* (17) have formed beams from gases at pressures as high as 40 atm. One could conceivably sample fluid systems above the critical conditions. The most probable limitation to the characterization of the actual molecular species present in the fluid will be ambiguities brought on by nucleation phenomena.

The ability of a free-jet expansion to quench chemical reactions with positive activation energies should be nearly optimal owing to the extremely rapid cooling rates. Likewise, reactions such as that of condensation, which have a negative temperature coefficient, should be quenched with maximum efficiency since, for a given orifice size, the free-jet expansion results in the minimum number of collisions during the transition to molecular flow.

### *Application to Inorganic Systems*

There are many applications of high pressure sampling which will occur to inorganic chemists. We describe here only those areas which are currently being pursued in our laboratory.

**Flames.** Our work with the direct sampling of flames is representative of a class of sampling studies in which the sampling orifice is not in thermal equilibrium with the gaseous system being studied. We began our high pressure sampling work with the goal of studying the thermodynamics of gaseous metal-containing species at extremely high temperatures and high partial pressures of  $O_2$  and  $H_2O$ . Such conditions are readily attainable in the burnt gas region of flames. In addition, the ability to follow directly free-radical and other species through the reaction zone was of interest in terms of the kinetic study of flame reactions.

The equilibrium 1-atm. flame work has been presented in some detail previously (20, 22). The present status of this work can be summarized as follows. It appears that 1-atm. flames as hot as  $4000^\circ K$ . can be probed and that free-radical and other noncondensable species can be quantitatively sampled. However, we have been unable to sample highly condensable species with relatively cold sampling orifices. Isothermal furnace studies mentioned below indicate that aerodynamic effects caused by the cold orifice and oxide build-up, and not the inherent homogeneous nucleation or other equilibrium shifts involved in free-jet expansion, are responsible for this limitation.

A promising area for further flame work is indicated in our study of species profiles in reaction zones by means of the direct sampling of

low pressure flames. The low pressure serves mainly to spread out the reaction zone to allow adequate sampling resolution. Very slow burning flames could be studied at one atmosphere. In an apparatus described elsewhere (19), we have obtained a number of profiles through a 1/20th atmosphere, lean  $\text{CH}_4\text{-O}_2$  flame with  $\text{CH}_3\text{Br}$  added. Typical results are shown in Figures 3 and 4. Absolute intensities should not be compared between species, as sensitivity corrections have not been made. The significance of these data lies in the general agreement between the Figure 3 results and previously published quartz microprobe studies (29) for the stable species, combined with our ability as shown in Figure 4 to follow the concentrations of  $\text{HBr}$  and  $\text{Br}$ . These latter species have not previously been studied successfully by indirect sampling techniques.

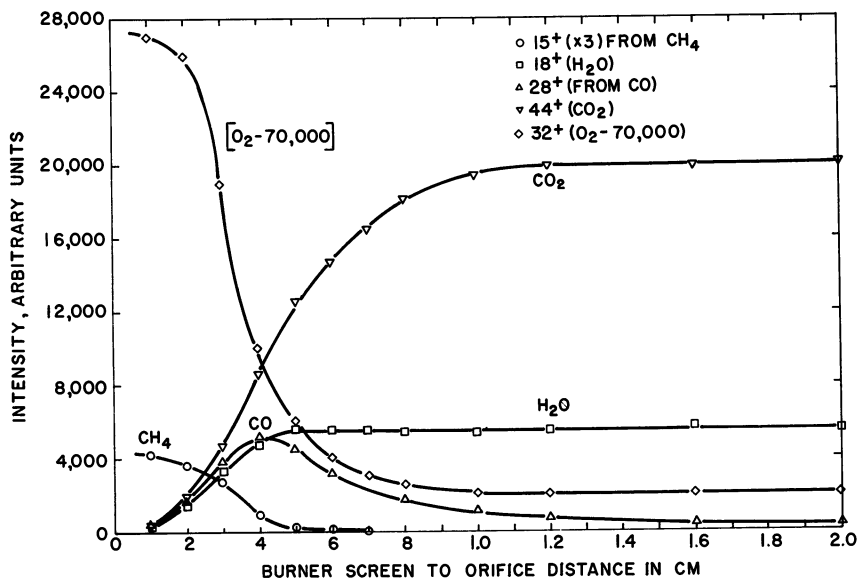


Figure 3. Stable species profiles obtained by direct molecular sampling of a 1/20th-atm., lean,  $\text{CH}_4\text{-O}_2$  flame. Flame composition: 89.6%  $\text{O}_2$ , 10.4%  $\text{CH}_4$ .

**Isothermal Transpiration Cells.** High pressures of gas have been equilibrated with the condensed phases of many materials, in the conventional transpiration experiment, to permit the study often of quite minor vapor species. Because the identification of such species is indirect, and serious complications arise if several gaseous species are present, it would be most desirable to sample the effluent directly with a mass spectrometer. We are doing this by placing a resistance heated Ni transpiration cell in stage one, just below the skimmer, as shown in

Figure 2. Our present cell which uses orifice diameters of 0.0005 to 0.004 inch will handle gas pressures up to 5 atm. Gas flows are determined by the orifice size, for a given pressure, so several orifice sizes may have to be used to establish that equilibrium exists.

With this system we are currently studying the equilibrium  $\text{Li(g)} + 1/2\text{H}_2 \rightarrow \text{LiH(g)}$ , with the intention of going on to other systems such as  $\text{Al} + \text{H}_2$  where higher hydrides may be present and high pressures may be more advantageous in detecting species of interest. The study of such high pressure equilibria will always involve the danger of free-jet nucleation, and appropriate tests, such as the one discussed in the next section, must be carried out.

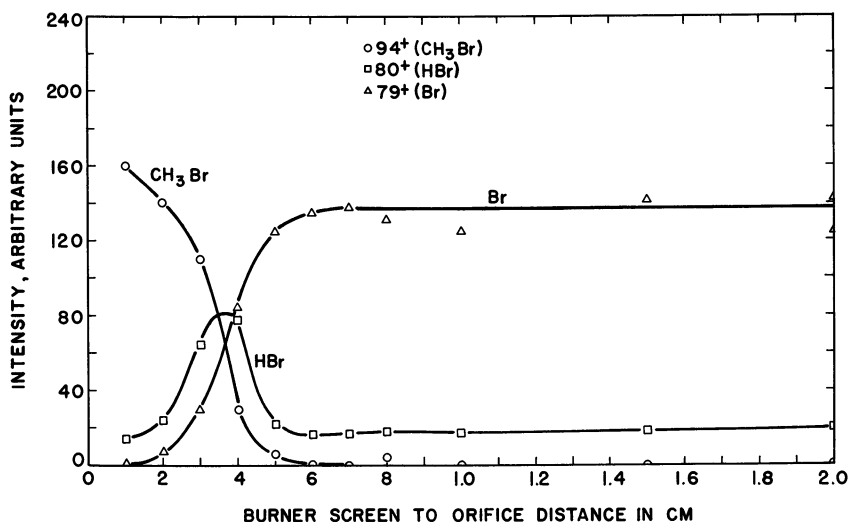


Figure 4. Profiles of bromine species in a 1/20th-atm., lean,  $\text{CH}_3\text{-O}_2$  flame containing about 1%  $\text{CH}_3\text{Br}$ . Flame composition: 89.6%  $\text{O}_2$ , 10.4%  $\text{CH}_4$ .

#### Nucleation and the Thermodynamics of Weakly Bound Clusters.

Whenever a continuum expansion is involved in the sampling process, the danger of supersaturating a species exists and nucleation may occur. Such nucleation will be very sensitive to initial temperature, pressure, and to sampling orifice size. The behavior of argon has been studied in some detail (21). Apart from the complications which nucleation poses for sampling, the mass spectrometric study of free-jet composition provides a unique approach to elucidating the earliest stages of homogeneous nucleation. In fact, the first step in such condensation, the three-body recombination to form a dimer species, can be followed. Studies of this

type are not limited to gases such as argon, and we are now examining higher temperature species as well.

One of the approaches to the interpretation of the  $\text{Ar}_2$  concentrations observed in sampling pure argon is shown in Figure 5, where the observed  $\text{Ar}_2^+$  intensities (attributed solely to simple ionization of  $\text{Ar}_2$ ) are plotted against orifice size at fixed pressure. Note the rather high extrapolated concentration at zero orifice diameter, which we interpret as the equilibrium concentration of  $\text{Ar}_2$  in the static gas (21). The exponential growth with orifice size is governed by nucleation kinetics during the increasing time and decreasing temperatures involved in expansion from larger orifices. This dependence of observed species on orifice size promises to be an indispensable technique in detecting the presence of nucleation effects in sampling.

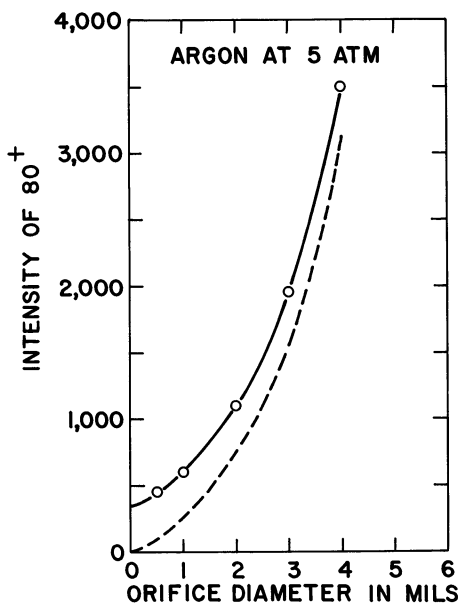


Figure 5.  $\text{Ar}_2^+$  intensities observed after expansion of argon from 5 atm. and  $300^\circ\text{K}$ . through several size orifices

We are not yet prepared to discuss the kinetic significance of the exponential rise of  $\text{Ar}_2$  concentration with orifice size, but it is of interest to consider the nature of the collisional-temperature history of the gas during the free-jet expansion. Table III shows the effect of orifice size on the terminal Mach number, terminal temperature, and number of ternary collisions, as calculated from a simple kinetic model by using

temperature-dependent collision cross sections and assuming Anderson and Fenn's criterion of freezing for all our experimental conditions. The fourth column lists the total number of ternary collisions per molecule from Mach 0.50 to the terminal Mach number. The last column lists the observed mole fractions of  $\text{Ar}_2$  in excess of the zero orifice diameter extrapolated values. Without discussing the assumptions made, it is clear that we are dealing with collisions between molecules of very low relative energy. For example, observe that the number of collisions more than doubles in going from a 0.002 to 0.004 inch diameter orifice. In this model, the increase beyond a factor of two is caused by the extension of the continuum part of the expansion by the larger orifice, as reflected in the larger terminal Mach number and lower temperature. The experimental  $\text{Ar}_2$  mole fractions also more than double from the 0.002 to 0.004 inch case. It seems reasonable, then, to relate this excess dimer to the collisions which occur at very low temperatures. The collisional behavior in this region is not understood at present. Although interpretations may be complicated by such phenomena as long-lived orbiting pairs and lack of information about the transition region, it seems well worth investigating.

**Table III. Calculated Ideal Free-Jet Nucleation History for Argon Initially at 300°K. and 5 Atmospheres**

<i>Orifice Diameter, mils</i>	<i>Terminal Mach No.</i>	<i>Terminal Temp.</i>	<i>Total Ternary Collisions</i>	<i>Observed Excess Mole Fraction of <math>\text{Ar}_2</math></i>
0.5	18.4	2.6	71.70	0.0009
1	24.2	1.5	143.58	0.0027
2	31.9	0.88	287.56	0.0075
3	37.6	0.64	431.46	0.0157
4	42.2	0.51	575.48	0.0310

The above type of correlation represents only one of the ways free-jet nucleation data may be treated. Dilution experiments, comparison of expansions starting with different temperatures and pressures but ending with the same terminal Mach number, and other variations of the initial and final states will help illuminate the important process of homogeneous nucleation over various temperature ranges. It also seems possible to extend the study to higher clusters.

The nucleation behavior of several higher-temperature systems has been examined thus far. Ar and  $\text{N}_2$  have been passed over  $\text{H}_2\text{O}$ ,  $\text{CH}_3\text{OH}$ ,

Li, Hg, and CsCl at pressures up to 2 atm. In these studies the species  $\text{Ar}_2$ ,  $\text{Ar} \cdot \text{Hg}$  and  $\text{Hg}_2$  have been observed in one atmosphere of argon over Hg at  $500^\circ\text{K}$ . These data represent contributions from both equilibrium species and those formed during expansion. A careful measurement of the orifice size dependence of concentrations should allow both a determination of the free energy of the dimers and an indication of their kinetics of formation. In the case of Ar over CsCl, both the monomer and the dimer of the salt were detected in the ratio expected from Knudsen work. In  $\text{N}_2$  the dimer was reduced by a factor of about four; this unexpected behavior is receiving further study. It should be possible to obtain directly the free energies of a number of mixed dimers of the type  $\text{Ar} \cdot \text{Cs}$ ,  $\text{Cs} \cdot \text{Hg}$ , etc. Many clusters were observed in the  $\text{H}_2\text{O}$  and  $\text{CH}_3\text{OH}$  systems. The case of polyatomic molecules may be more complicated because of the possible metastability of the dimers (16). For example, we see several orders of magnitude less dimer in  $\text{N}_2$ ,  $\text{O}_2$ , and  $\text{NO}$  than one would at first expect (12). Nevertheless, direct mass spectrometric verification of such postulated species as the HF hexamer and the methanol tetramer may be feasible. Finally, direct second law heat determinations of weakly bound dimers also appear practicable.

### *Summary*

Direct mass spectrometric sampling of high-pressure systems is possible in many cases, with a tolerable minimum of composition disturbance. The study of flames and heterogeneous reaction systems has shown promise. Also a large class of equilibrium reactions can be elucidated further by combining the transpiration experiment with direct mass spectrometric sampling. The study of gases and gas mixtures will give thermodynamic information about van der Waals', charge-transfer, and hydrogen-bonded species. Finally, nucleation, which is one of the inherent problems in high pressure sampling, can be turned to advantage by allowing a detailed study of the condensation process on the molecular scale.

### *Acknowledgments*

This work was sponsored by the Chemistry Office of the Advanced Research Projects Agency and the Power Branch of the Office of Naval Research.

The authors wish to acknowledge the help of Jacob Beachey and Douglas Day in carrying out the experimental program and the help of Gordon Gross in interpreting the results. Gene Vandegrift has been primarily responsible for the free-jet, collisional-history calculations.

*Literature Cited*

- (1) Abuaf, N., Anderson, J. B., Andres, R. P., Fenn, J. B., Miller, D. R., "Rarefied Gas Dynamics," Vol. 2, p. 1317, C. L. Brundin, ed., Academic Press, New York, 1967.
- (2) Anderson, J. B., Andres, R. P., Fenn, J. B., "Advances in Atomic and Molecular Physics," P. R. Bates, I. Estermann, eds., Vol. I, p. 345, Academic Press, New York, 1965.
- (3) Anderson, J. B., Andres, R. P., Fenn, J. B., p. 281, "Advances in Chemical Physics," Vol. X, J. Ross, ed., Interscience Publishers, New York, 1966.
- (4) Anderson, J. B., Fenn, J. B., *Phys. of Fluids*, 8, 780 (1965).
- (5) Brewer, L., "Chemistry and Metallurgy of Miscellaneous Materials: Thermodynamics," p. 261, Natl. Nucl. Energy Ser. IV—19B, L. Quill, ed., McGraw-Hill, New York, 1950.
- (6) de Leeuw, J. H., "Advances in Applied Mechanics Series," Supplement 1 (1961), Supplement 2 (1963), Supplement 3 (1965), Supplement 4 (1967), "Rarefied Gas Dynamics," Academic Press, New York.
- (7) Elliott, Guy R. B., "Gaseous Hydrated Oxides, Hydroxides, and Other Hydrated Molecules," UCRL-1831, June 1952.
- (8) French, J. B., *AIAA J.* 3, 993 (1965).
- (9) Greene, F. T., Milne, T. A., "Advances in Mass Spectrometry," Vol. 3, p. 841, The Institute of Petroleum, London, 1966.
- (10) Greene, F. T., Brewer, J., Milne, T. A., *J. Chem. Phys.* 40, 1488 (1964).
- (11) Greene, F. T., Milne, T. A., *J. Chem. Phys.* 39, 3150 (1963).
- (12) Greene, F. T., Milne, T. A., 22nd Quart. Tech. Rept., Contract Nonr-3599(00), May 1967.
- (13) Hamel, B., Willis, D. R., *Phys. of Fluids* 9, 829 (1966).
- (14) Kantrowitz, A., Grey, J., *Rev. Sci. Instr.* 22, 328 (1951).
- (15) Knuth, E. L., *Appl. Mech. Rev.* 17, 751 (1964).
- (16) Leckenby, R. E., Robbins, E. J., *Proc. Roy. Soc.* 291, 389 (1966).
- (17) Leckenby, R. E., Robbins, E. J., Trevalion, P. A., *Proc. Roy. Soc. (London)* 280A, 409 (1964).
- (18) Marrone, V., *Univ. Toronto, Inst. Aerospace Studies Rept. No.* 113, (1966).
- (19) Milne, T. A., *Midwest Res. Inst. Rept.* FS-127-P (1966).
- (20) Milne, T. A., Greene, F. T., *J. Chem. Phys.* 44, 2444 (1966).
- (21) Milne, T. A., Greene, F. T., *J. Chem. Phys.*, 47, 4095 (1967).
- (22) Milne, T. A., Greene, F. T., Symp. Combust., 10th, p. 153, The Combustion Institute, 1965.
- (23) Morton, H. S., Jr., Hagen, O. F., "Analysis of Intensity and Speed Distribution of a Molecular Beam from a Nozzle Source," Tech. Rept. UVA-11-P, Contract No. Nonr 3623(00), October 1966.
- (24) Robben, F., Talbot, L., *Phys. of Fluids* 9, 644 (1966).
- (25) Scott, J., Phipps, J. A., "Rarefied Gas Dynamics," Vol. 2, p. 1337, C. L. Brundin, ed., Academic Press, New York, 1967.
- (26) Sherman, F. S., *Phys. of Fluids* 8, 773 (1965).
- (27) Stern, S. A., Waterman, P. C., Sinclair, T. F., *J. Chem. Phys.* 33, 805 (1960).
- (28) Taylor, W. J., *J. Chem. Phys.* 38, 779 (1963).
- (29) Wilson, W. E., Jr., Symp. Combust., 10th, p. 47 (1965).

RECEIVED November 2, 1966.

# Shock Tube Study of a $D_2$ -Ne Mixture From $900^\circ$ - $2300^\circ$ K.

I. D. GAY<sup>1</sup> and R. D. KERN<sup>2</sup>

Gibbs Chemical Laboratory, Harvard University, Cambridge, Mass.

*A theoretical prediction of the fragmentation of deuterium by electron impact as a function of temperature is formulated. This prediction was studied experimentally by coupling a shock tube to a time-of-flight mass spectrometer. The mass peak heights attributed to  $D^+$ ,  $D_2^+$ , and  $D_3^+$  were measured over the temperature range  $900$ - $2300^\circ$ K. The data were represented by a plot of  $\log D^+/D_2^+$  vs.  $1/T$  and were analyzed by considering that the  $D^+$  peak was composed of a  $D^+$  contribution from the fragmentation by electron impact of  $D_2$  molecules which had a Boltzmann distribution of vibrational energy and a  $D^+$  contribution from pressure dependent reactions occurring in the ion source. It is shown that the latter contribution is dominant.*

In view of recent interest in the role of vibrationally excited species in high temperature gas reactions (1, 6), it would be desirable to have a means of monitoring vibrational excitation during such reactions. Since a flexible apparatus for high temperature kinetic studies is the shock tube coupled to a time-of-flight mass spectrometer (5), an attempt has been made to determine whether vibrational excitation can be observed with this apparatus.

It is well known that the mass spectrometric ion fragmentation pattern of molecules varies with temperature, and at least part of this variation is attributable to vibrational excitation. In the simple case of  $H_2$  and its isotopes, the fragmentation pattern has been successfully predicted by assuming the ionization process (for electron energies less than 30 volts) to be a simple Franck-Condon transition from the ground state of  $H_2$  to

<sup>1</sup> Present address: Simon Fraser University, Burnaby, British Columbia, Canada.

<sup>2</sup> Present address: Louisiana State University in New Orleans, New Orleans, La.

the ground state of  $\text{H}_2^+$  (12). These calculations have been improved by Cashion (2) who has also calculated the fragmentation pattern expected from the hydrogen isotopes in vibrational states other than  $v = 0$ . There exists a theoretical prediction of the variance of  $\text{H}^+/\text{H}_2^+$  as a function of temperature which may be tested experimentally.

We chose to do the experiments using  $\text{D}_2$  rather than  $\text{H}_2$  since the observation of masses 2 and 4 was easier than masses 1 and 2. While the calculated fragmentation ratio is small ( $6.96 \times 10^{-3}$  at  $300^\circ\text{K}$ . and  $1.29 \times 10^{-2}$  at  $2400^\circ\text{K}$ .), it increases by a factor of 1.77 over the temperature range  $1000^\circ$  to  $2400^\circ\text{K}$ ., and it was thought that this change would be detectable. There is no interest in working below  $1000^\circ\text{K}$ . since the population of vibrational levels greater than  $v = 0$  is too small to cause a significant change in fragmentation ratio. It is desirable to work below  $2400^\circ\text{K}$ . in order to prevent any contribution from the thermal decomposition of  $\text{D}_2$  and subsequent ionization of D atoms. Possible effects of vibrational relaxation of  $\text{D}_2$  will be discussed.

### Theory

One of the early predictions of the Franck-Condon principle was that the ratio of  $\text{H}^+/\text{H}_2^+$  should be greater than  $\text{D}^+/\text{D}_2^+$  when the atomic ions arise exclusively from dissociation of the  ${}^2\Sigma_g^+$  state of  $\text{H}_2^+$ . This prediction has been confirmed experimentally, and the theoretical magnitude of the ratios has been calculated and compared favorably with experiment (2, 14). At room temperature, the fraction of  $\text{H}^+$  is calculated from the equation

$$f_{\text{H}^+} = \int_0^{r_c} \hat{t} \psi^2(r)_{v=0} dr \quad (1)$$

where  $r_c$  = finite internuclear distance at which dissociation of  $\text{H}_2^+$  into  $\text{H}^+$  and H occurs

$\psi(r)$  = radial wave function for  $\text{H}_2$  multiplied by  $r$

$\hat{t}$  = transition probability operator which is linearly related to the excess energy of the ionizing electrons (12).

To calculate the amount of  $\text{H}^+$  produced from higher vibrational levels, we use the equation

$$f_{\text{H}^+} = \sum_{i=0}^{v_{\max}} f_{v=i} \int_0^{r_c} \hat{t} \psi^2(r)_{v=i} dr \quad (2)$$

where  $i$  = vibrational quantum number

$f_{v=i}$  = Boltzmann population of the  $i^{\text{th}}$  level at temperature  $T$ .

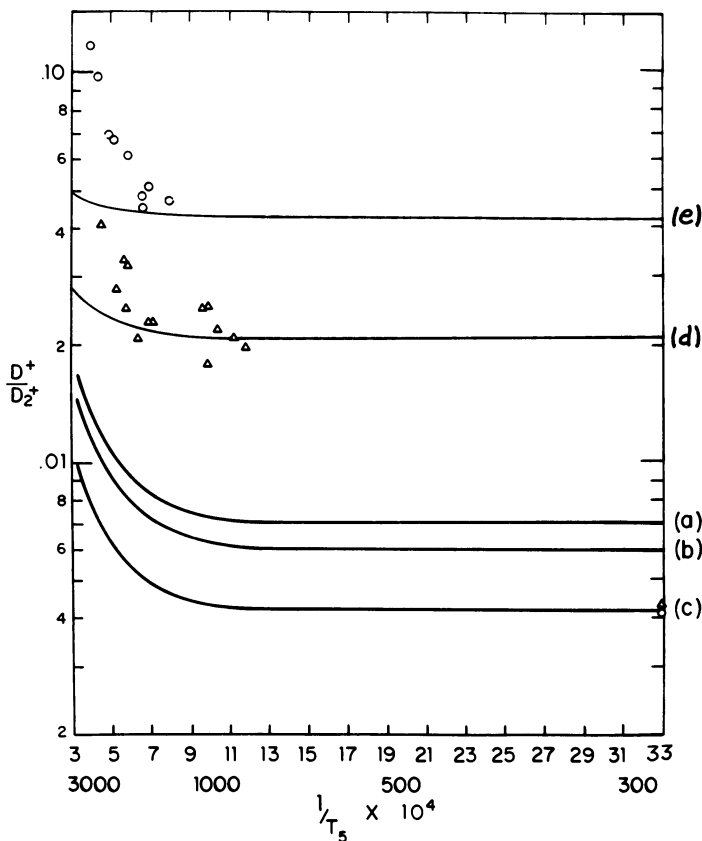


Figure 1. (a)—Theoretical  $D^+/D_2^+$  ratio without excess energy correction. (b)—Curve a corrected for 30 e.v. ionizing energy. (c)—Curve b displaced in order to pass through room temperature experimental ratios.  $\Delta$ —Experimental ratios obtained under shock conditions using a 4-mil diameter nozzle.  $\circ$ —Same as  $\Delta$  except use of a 6-mil diameter nozzle. (d),(e)—Curve c displaced in order to pass through the zero thermal effect points of the 4- and 6-mil data, respectively

The fraction of  $H_2^+$  is obtained by subtracting the right hand side of Equation 2 from unity. The ratio of  $H^+$  to  $H_2^+$  is then formed, and it is a function of temperature only, providing the electron energy is held constant. The  $D^+/D_2^+$  ratio is calculated in exactly the same way using the appropriate wave function and molecular parameters.

Equation 2 was evaluated (2) using the eigenfunctions obtained by numerical solution of the radial wave equation using the accurate adiabatic hydrogen potential of Kolos and Wolnowicz (9). The assumptions involved in this calculation are that Franck-Condon type transitions take

place from  $D_2(^1\Sigma_g^+)$  to  $D_2(^2\Sigma_g^+)$ , that  $D^+$  arises only from those  $D_2$  molecules whose internuclear distance is less than  $r_c$ , and that dissociation from higher electronic states of  $D_2^+$  is negligible when the ionizing electron energy does not exceed 30 e. v. The results of the calculation for various temperatures are shown by curves a and b of Figure 1. Curve a was calculated from Equation 2 without the transition probability operator  $\hat{t}$ . Curve b shows the effect of including  $\hat{t}$  for 30 e. v. electrons.

Calculations of the  $D^+/D_2^+$  ratio were made also as a function of the energy of the ionizing electrons. The results of these calculations show that an electron energy spread of 2 e. v. affects the ratio by only 1.5%.

### Experimental

Experiments were done on a 10% mixture of  $D_2$  in Ne. Both gases were obtained from the Mathieson Co., the neon being research grade and the deuterium C.P. grade.

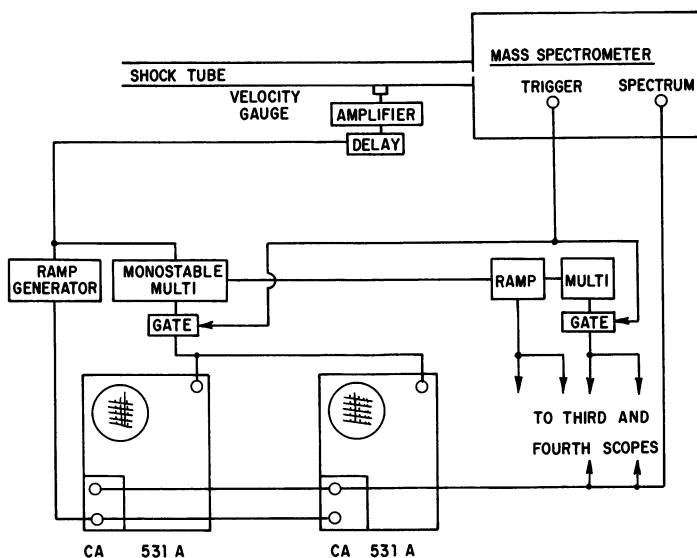


Figure 2. Data collection system

The experiments were performed with the improved apparatus described by Gay *et al.* (6). A modification of the data recording method was necessary because of the small size of the  $D^+$  peak. The data were recorded on two pairs of oscilloscopes, each pair having a gain ratio of 10 or 20. The scopes of each pair were connected in parallel, the  $D^+$  peak being measured on the higher gain member of each pair, and the  $D_2^+$  peak on the lower gain scopes. Seven spectra were recorded on each pair of scopes, at intervals of 30  $\mu$ sec., thus covering a test time of about

420  $\mu\text{sec}$ . The data recording system is shown diagrammatically in Figure 2. Spectra from the first two scopes are presented in Figure 3; the presence of  $\text{D}_3^+$  in an amount about equal to  $\text{D}^+$  was somewhat surprising. The peak at mass 3 is the HD impurity present in the deuterium used.

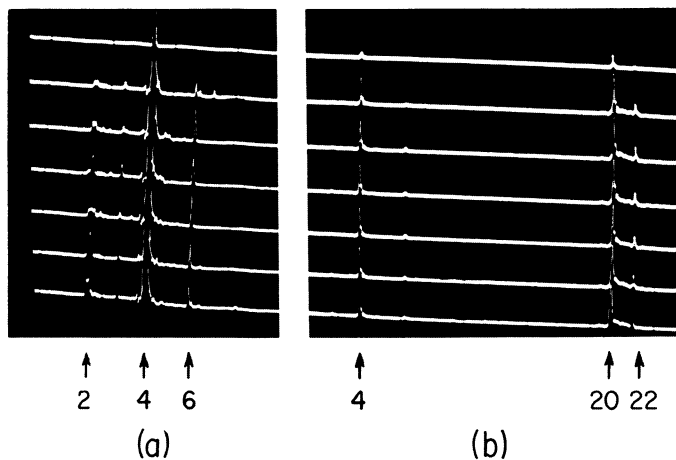


Figure 3. Mass spectra recorded in a typical experiment from two oscilloscopes triggered in parallel. Spectra in a are recorded with 10 times the gain of those in b

Initially, two sets of experiments were performed. One set utilized a 6-mil diameter hole in the nozzle, a +1.5 volt bias on a grid 1 mm. from the nozzle, and +7.5 volt bias on the ion-accelerating grid. The second set of experiments used a 4-mil diameter nozzle, the aforementioned grids at ground potential, and an additional grid biased at -700 volts which was placed between the ion-accelerating grid and the drift tube entrance grid. Molybdenum was installed as the grid material for the second set, resulting in increased sensitivity and decreased statistical fluctuations.

The shocked gas flowed through a divergent nozzle into the ionization region, a distance of some 3 mm. with a transit time on the order of 3  $\mu\text{sec}$ . An ionizing electron energy of 30 volts was used.

The peak heights of  $\text{D}^+$ ,  $\text{D}_2^+$ , and  $\text{D}_3^+$  were measured from the Polaroid pictures. The  $\text{D}_2^+$  peak was reasonably constant during an experiment, while the  $\text{D}^+$  and  $\text{D}_3^+$  peaks were subject to considerable statistical fluctuation. Average values of the  $\text{D}^+/\text{D}_2^+$  and  $\text{D}_3^+/\text{D}_2^+$  ratios were measured as a function of temperature, which was determined from measurements of the incident shock velocity. The experimental  $\text{D}^+/\text{D}_2^+$  ratios are plotted in Figure 1. The reflected shock zone temperature and pressure range covered was 65 torr and 900°K. to 300 torr and 2330°K. Under such conditions the dissociation of  $\text{D}_2$  was negligible, and the vibrational relaxation time of  $\text{D}_2$  in Ne, estimated from literature values (8, 10),

was greater than the transit time through the nozzle at the higher temperatures, and less than the observation time at temperatures above 1200°K. The predicted change in the  $D^+/D_2^+$  ratio from Equation 2 from room temperature to 1200°K. is small enough (0.0007) to be within experimental error.

The  $D^+/D_2^+$  ratio was measured using the Bendix analog output at room temperature at a total reservoir pressure of 5 torr and an ionizing energy of 30 e. v. Optimization of the collimating and compensating magnets produced an experimental peak height ratio of 0.0045, compared with the calculated ratio of 0.0060. This discrepancy is not serious since the same instrumental factor applies to all experiments. Hence, curve c is merely curve b shifted to pass through the room temperature points. The  $D^+/D_2^+$  ratios predicted by Equation 2 should fall on curve c.

The first series of shock experiments at a series of temperatures were performed by filling the shock tube to a constant initial pressure of 5 torr. The  $D^+/D_2^+$  ratios so obtained are plotted in Figure 1 (represented by open circles).

It is clear that the experimental ratios are much higher than the theoretical ratios. The most likely explanation seems to be that  $D^+$  arises from some other source than fragmentation of  $D_2$ , for example, ion-molecule reactions. This conjecture is supported by the appearance of  $m/e = 6$  in the mass spectra which is clearly  $D_3^+$  formed by the well-known reaction:



Further support was obtained by measuring the  $D^+/D_2^+$  ratio as a function of reservoir pressure at room temperature. At a pressure of 50 torr the ratio almost doubled, compared with the ratio at 5 torr. It was obvious that the  $D^+/D_2^+$  ratio consisted of two components—one depending on temperature as predicted by Equation 2 and the second depending on the ion source gas density.

The possibility of a pressure-dependent source of  $D^+$  was further tested by replacing the original 6-mil diameter nozzle with a 4-mil diameter nozzle. This reduced the amount of gas entering the mass spectrometer by approximately a factor of 2 and produced another series of  $D^+/D_2^+$  ratios which are also shown in Figure 1 (denoted by triangles). It is clear that there is indeed a pressure-dependent contribution to the  $D^+$  peak height.

The following procedure was adopted to assess the contribution to  $D^+$  from sources other than Equation 2. Several measurements of  $D^+/D_2^+$  ratio were made near 900°K., and the constant part of the theoretical curve c (300°–900°K.) was raised to pass through these points, thus establishing a zero point for the thermal effect. The predicted high temperature curves d and e were then constructed by adding the increase in  $D^+/D_2^+$  from Equation 2 to the zero points.

In addition to giving too high a  $D^+$  signal, the unknown pressure dependent reactions can also explain the unexpectedly large increase of the  $D^+$  signal with temperature. This is attributed to the fact that when a shock tube is operated with constant initial pressure, the reflected shock density increases sharply with temperature. Hence, an increase of ion source pressure with temperature occurred in the above experiments,

leading to an increase in the amount of  $D^+$  produced by the pressure dependent reaction.

Since it is not practical with this apparatus to decrease the nozzle opening below 4 mils, we decided to do a set of experiments at different temperatures but at constant ion source pressure. Unfortunately, this is not an easy requirement since it is not possible to measure the ion source pressure on the time scale of a shock experiment, and it is not clear what relationship exists between shock tube pressure and ion source pressure.

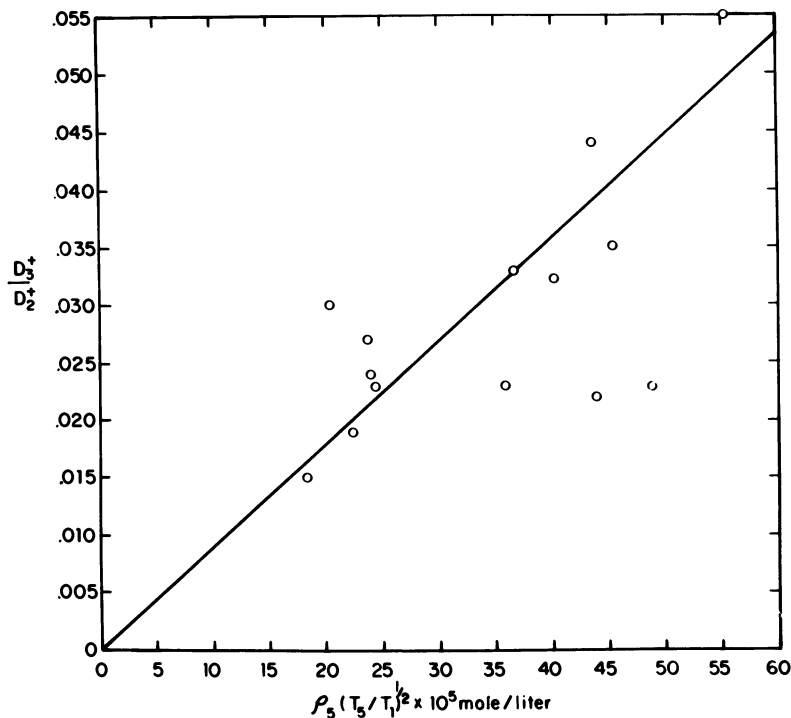


Figure 4. Plot of  $D_3^+/D_2^+$  vs.  $\rho(T_5/T_1)^{1/2}$

Fortunately, the presence of  $D_3^+$  in the mass spectrum gives an indication of the pressure in the ion source. Since  $D_3^+$  is only a few per cent of  $D_2^+$ , it is clear from Reaction 3 that the  $D_3^+/D_2^+$  ratio will vary linearly with ion source gas density. This ratio was therefore plotted against various shock wave parameters in search of a linear relationship. The best linearity was found in a plot of  $D_3^+/D_2^+$  vs.  $\rho_5(T_5/T_1)^{1/2}$  where  $\rho_5$  and  $T_5$  are the density and temperature of the reflected shock zone and  $T_1$  is room temperature. This plot is shown in Figure 4. The scatter in this plot arises from the fact that  $D_3^+$  is a rather small peak, and therefore subject to statistical fluctuation. Nevertheless, a line may be drawn through the data and the origin with a slope of 90 liters/mole. Taking

the residence time in the ion source as 200 nanoseconds and a rate constant for Reaction 3 of  $86.8 \times 10^{10}$  liter/mole/sec. (15), leads to an ion source density of 0.05% of the shock tube density. This percentage is in reasonable agreement with the results of Diesen (4), who arrived at this figure from a consideration of the gas flow into a mass spectrometer during a shock experiment. The residence time estimate is based on the length of the ionizing pulse and the rise time of the ion-accelerating pulse (250 and 100 nanoseconds, respectively).

A test of the suitability of the expression  $\rho_5(T_5/T_1)^{1/2}$  to represent the pressure-dependent processes was made in the following way. The 10% D<sub>2</sub>-90% Ne mixture was shocked at various temperatures with initial pressures adjusted so that  $\rho_5(T_5/T_1)^{1/2}$  was constant, and the D<sup>+</sup>/D<sub>2</sub><sup>+</sup> ratio was measured. An ionizing energy of 22.5 e. v. was used, which made the Ne<sup>+</sup> peak only 1.5 times the height of the D<sub>2</sub><sup>+</sup> peak. The 4-mil diameter nozzle was used. The results of these experiments are shown in Figure 5 along with the D<sup>+</sup>/D<sub>2</sub><sup>+</sup> ratios that were obtained when the initial shock tube pressure was held constant. The theoretical line is curve d of Figure 1 which has been adjusted to the zero point for thermal effects by an experimental point obtained at 900°K. If one assumes that the pressure-dependent contribution to D<sup>+</sup> is now reasonably constant, the agreement of the experimental points with the predicted thermal effect of Equation 2 is good.

Several experiments were performed with a mixture of 5% N<sub>2</sub> and 1% Ar in Ne at an initial pressure of 5 torr in the temperature range 1500°–3100°K., using an ionizing energy of 30 e. v. A calculation of N<sup>+</sup>/N<sub>2</sub><sup>+</sup> was made using a Morse potential for N<sub>2</sub>. A value of  $r_c$  was obtained by requiring the ratio to be 0.067 at room temperature (13). This is an unsatisfactory method of calculation since there are at least five potential curves of N<sub>2</sub><sup>+</sup> which can give N<sup>+</sup> with differing values of  $r_c$  and which are presumably populated to different extents by the ionization of N<sub>2</sub> (7). Nevertheless, using this value of  $r_c$ , the increase of N<sup>+</sup>/N<sub>2</sub><sup>+</sup> with temperature was calculated. At temperatures above 2100°K., the experimental points agree with this crude calculation within 10%. Below 2500°K., the N<sup>+</sup>/N<sub>2</sub><sup>+</sup> ratio grows with time, which we interpret as being caused by the fairly slow vibrational relaxation of N<sub>2</sub> at these temperatures (10). This effect makes accurate ratio measurements uncertain in the N<sub>2</sub> system and results in considerable scatter below 2100°K.

### Discussion

When the effect of pressure-dependent ion source reactions is held constant, it is demonstrated that our D<sup>+</sup>/D<sub>2</sub><sup>+</sup> ratios reproduce the calculated values rather well within inevitable fluctuations associated with small concentrations. Kiefer and Lutz's data (8) shows that vibrational relaxation in the shock tube should be complete under our conditions at temperatures above 1200°K. Since little population of higher vibrational levels would be expected below this temperature, our results are not seriously affected. Although the translational temperature of the gas

decreases sharply on leaving the shock tube (4), the concurrent expansion of the gas lowers the collisional frequency, and there is negligible vibrational relaxation in the 2–3  $\mu\text{sec}$ . transit time between the shock tube and electron beam. We therefore conclude that our  $D^+/D_2^+$  ratios under constant ion source pressure conditions are in fact a measure of the vibrational state of  $D_2$  in the shock tube.

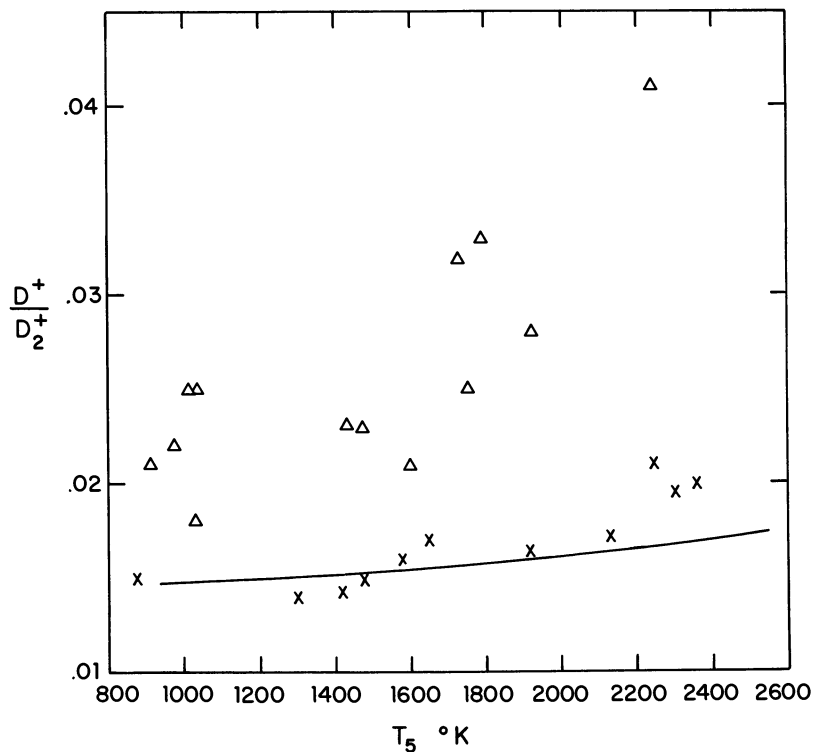


Figure 5. Plot of  $D^+/D_2^+$  vs.  $T_5$ . Solid curve—*theoretical ratios at 22.5 e.v. ionizing energy.* ×—*Experimental ratios obtained with constant ion source gas density, 22.5 e.v.* Δ—*Experimental ratios obtained with constant initial shock tube pressure of 10 torr, 30 e.v.*

Although the thermally induced change in the  $D^+/D_2^+$  ratio is small, it is clear from the results of Cashion (2) that any substantial population of a specific vibrational level other than  $v = 0$  would have a strong effect on the ratio. The shock tube-mass spectrometer method seems quite capable of detecting abnormal vibrational energy distributions in the products of chemical reaction providing the source of  $D^+$  ions from sources other than electron impact fragmentation of  $D_2^+$  can be eliminated or held constant.

The origin of the pressure-dependent  $D^+$  signal observed in these experiments is not certain. It could arise from the dissociative charge transfer reaction



which although exothermic by 3.3 e.v., has a cross section which is too low (11) to explain our results. Another source of  $D^+$  is the collision induced dissociation of  $D_2^+$  (3). A proper assignment of the sources of  $D^+$  from non-thermal origins is beyond the accuracy of the data for experiments performed at constant initial shock tube pressures. In any case since  $D^+$  is always a small fraction of  $D_2^+$ , our method of treating the data will be correct as long as the pressure-dependent  $D^+$  arises from a collision between  $D_2$  or  $D_2^+$  and one other species in the ion source. It is difficult to conceive of the  $D^+$  arising in any other way.

It is interesting to note that the peak shape of mass 2 shows some defocussing under shock conditions, as can be seen in Figure 3. This effect is attributable to greater than thermal kinetic energy possessed by the  $D^+$  ions. This kinetic energy is derived from two sources: those  $D_2^+$  molecules whose internuclear distance is less than  $r_c$  dissociate into  $D^+$  and  $D$  which have kinetic energy, and  $D^+$  produced from exothermic pressure-dependent reactions.

### Acknowledgments

The authors wish to thank the National Science Foundation for the funds which made this work possible. They also wish to thank G. B. Kistiakowsky and J. K. Cashion for their helpful discussions.

### Literature Cited

- (1) Bauer, S. H., Ossa, E., *J. Chem. Phys.* **45**, 434 (1966).
- (2) Cashion, J. K., *J. Chem. Phys.* **45**, 1663 (1966).
- (3) Champion, R. L., Doverspike, L. D., Bailey, T. L., *J. Chem. Phys.* **45**, 4377 (1966).
- (4) Diesen, R. W., *J. Chem. Phys.* **44**, 3662 (1966).
- (5) Dove, J. E., Moulton, D. McL., *Proc. Roy. Soc.* **A283**, 216 (1965).
- (6) Gay, I. D., Kern, R. D., Kistiakowsky, G. B., Niki, H., *J. Chem. Phys.* **45**, 2371 (1966).
- (7) Gilmore, F. R., Memorandum RM-4034-PR, The Rand Corporation, June, 1964.
- (8) Kiefer, J. H., Lutz, R. W., *J. Chem. Phys.* **44**, 658 (1966).
- (9) Kolos, W., Wolnowiecz, L., *J. Chem. Phys.* **41**, 3663 (1964).
- (10) Millikan, R. C., White, D. R., *J. Chem. Phys.* **39**, 3209 (1963).
- (11) Moran, T. F., Friedman, L., *J. Chem. Phys.* **42**, 2624 (1965).
- (12) Schaeffer, O. A., Hastings, J. M., *J. Chem. Phys.* **18**, 1048 (1950).

- (13) Schaeffer, O. A., *J. Chem. Phys.* **18**, 1501 (1950).
- (14) Stevenson, D. P., *J. Chem. Phys.* **15**, 409 (1947).
- (15) Stevenson, D. P., Schissler, D. O., *J. Chem. Phys.* **23**, 1353 (1955).

RECEIVED October 11, 1966.

# Mass Spectrometric Study of Intermediates in the Photochemical Oxidation of Diborane

RICHARD F. PORTER and F. A. GRIMM

Cornell University, Ithaca, N. Y.

*A mass spectrometric technique has been used to study the photolysis of low pressure mixtures of diborane-oxygen. Total sample pressures varied between 5 and 44 mm. Hg with  $B_2H_6/O_2$  ratio between 5/1 and 1/5. The reaction is characterized by two distinct processes—either (a) an explosive reaction leading to gaseous  $H_3B_3O_3$  (boroxine) or (b) a slower initial reaction leading to  $H_2B_2O_3(g)$ . Reaction b accelerates rapidly with irradiation time. Analysis of rate data for the disappearance of  $O_2$  suggests that a chain mechanism is involved. Continued irradiation of  $H_2B_2O_3$  in the presence of  $B_2H_6$  and absence of  $O_2$  results in the formation of  $H_3B_3O_3(g)$  and disappearance of  $H_2B_2O_3$ . A plausible mechanism for the formation of  $H_2B_2O_3$  is discussed.*

Diborane-oxygen reactions have been the subject of numerous investigations. The explosive reaction, which can be initiated thermally, has been studied in some detail. In a recent series of articles (10), early work on this system is reviewed and mechanisms for the explosive oxidation are considered. A pre-explosive reaction has been observed by Goldstein, *et al.* (5). An alternative approach, as described in this paper, is to study the  $B_2H_6-O_2$  reaction photochemically. In these experiments a photochemical technique is used to study low pressure  $B_2H_6-O_2$  mixtures under conditions that do not normally lead to explosions at room temperature. A mass spectrometer was used to analyze gases issuing from a pinhole in a wall of the reaction vessel. This technique has been used before on flow systems to detect free radicals (2, 3, 9). In 1961, Goldfinger *et al.* (4) presented a paper on the adaptation of a mass spectrometer to study high pressure static systems. In this paper we discuss the use of a mass spectrometer to obtain information on the photochemical reaction of  $B_2H_6-O_2$  mixtures in a static system.

### Apparatus and Experimental

The experiments were conducted in a specially designed cell fitted with a quartz immersion well (Figure 1). Joined to the cell was a piece of borosilicate tubing terminating in a pinhole. The pinhole was made by the technique of Lossing and Tickner (9) using a Tesla coil discharge. The size of the pinhole was adjusted until enough gas issued from the hole to give good sensitivity on the mass spectrometer. The pressure in the mass spectrometer never exceeded  $1 \times 10^{-5}$  torr even when the pressure in the reaction vessel was atmospheric. Pinholes prepared in this way were found to be small enough so that the pressure drop during the course of the reaction was less than 2%. The mass spectrometer used was a 10", 60°, direction-focusing instrument. The medium pressure mercury lamp and the quartz immersion well were capable of transmitting the complete spectrum from the 1849-A. line to the infrared. Diborane absorbs in the wavelength region below about 2200 Å. (1, 8) and can also be photosensitized by mercury (6).

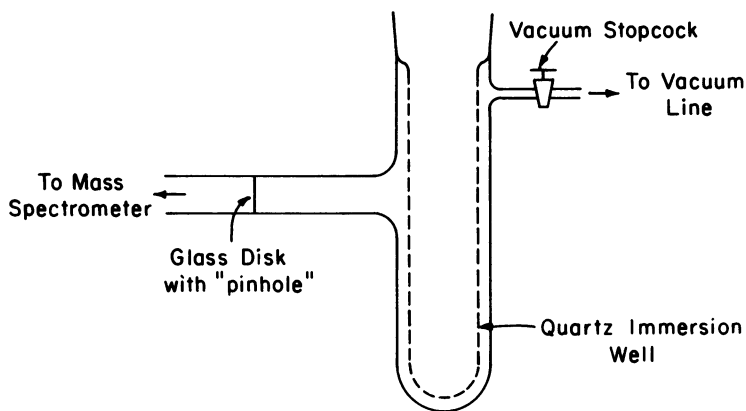


Figure 1. Reaction cell

The reaction cell was maintained at approximately room temperature by flowing pre-cooled  $N_2$  around the lamp and maintaining a vacuum of less than  $1 \times 10^{-4}$  torr between the double walls of the immersion well. A piece of aluminum foil was placed around the lamp to prevent light from reaching the reaction cell until the lamp had stabilized. The experiment was initiated when the foil was removed. Experiments were performed by adding first  $O_2$  and then  $B_2H_6$  to the reaction cell giving a mixture of known composition. Since  $B_2H_6-O_2$  mixtures are extremely unstable, and high pressure mixtures are known to explode, caution must be exercised in preparing and working with these gas mixtures.

The diborane was prepared by the method of Jeffers (7). Reagent grade oxygen was used without further purification.

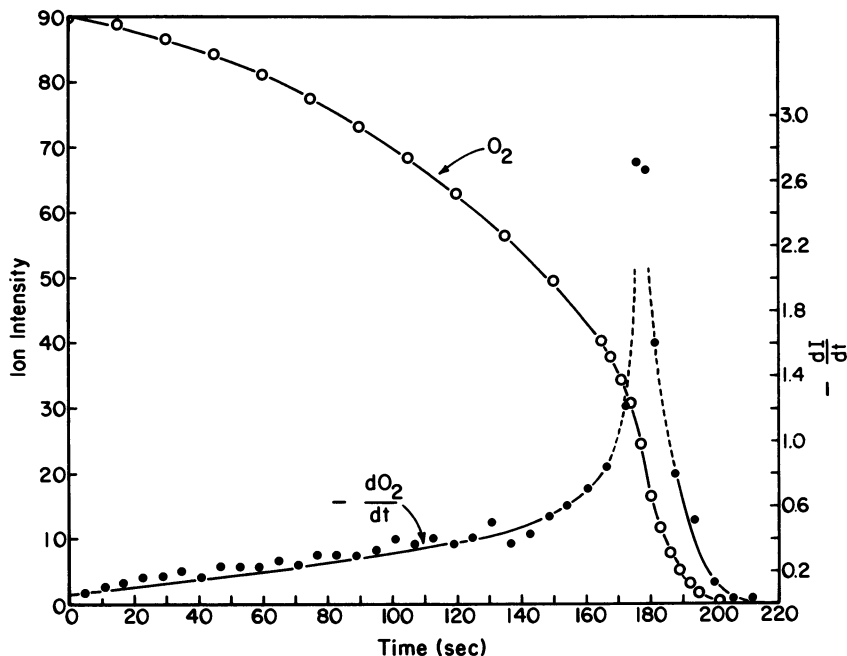


Figure 2. Plot of ion intensity for  $O_2(m/e = 32)$  and first derivative vs. time. Initial  ${}^2B_2$  and  ${}^2O_2$  equal 11.3 and 9.1mm., respectively

### Results

The course of the reaction was followed by continuously monitoring the ion intensity for one of the species as the mixture was irradiated. For  $O_2$  and  $B_2H_6$  ion intensities were observed for mass peaks 32 and 26, respectively. Shown in Figure 2 is a typical plot of ion intensity for  $O_2$  with time along with a plot of the first derivative. Figure 3 illustrates the appearance and disappearance of  $H_2B_2O_3$  and the delayed appearance of  $H_3B_3O_3$ . By obtaining the ion intensities for  $O_2$  and  $B_2H_6$  at the beginning and end of the reaction, it was possible to calculate the stoichiometry (Table I) from a calibration curve of ion intensity vs. pressure. It is important to note that a calibration curve is necessary if one is to relate ion intensity to pressure. Goldfinger *et al.* (4) found that in their apparatus ion intensity vs. pressure for argon showed a break in the plot at about 40 mm. pressure in the reaction cell. The plot was linear to 40 mm. and then changed slope and was linear to 400 mm. In our case all pressures for a single species were below 40 mm. and we obtained a linear plot with no discontinuities. It was noted that the sensitivity of the instrument to  $B_2H_6$  depended on the ratio of  $B_2H_6/O_2$  in the reaction cell. It was found that for a given pressure of  $B_2H_6$  the ion intensity of

the  $m/e = 26$  peak decreased upon addition of  $O_2$ . The  $H_2B_2O_3-O_2$  system showed a more pronounced effect in the opposite direction which made it difficult to obtain an accurate value for the amount of  $H_2B_2O_3$  produced. This effect was not observed for  $B_2H_6-H_2$  mixtures; the ion intensity of the  $m/e = 26$  peak did not change upon adding  $H_2$  to a

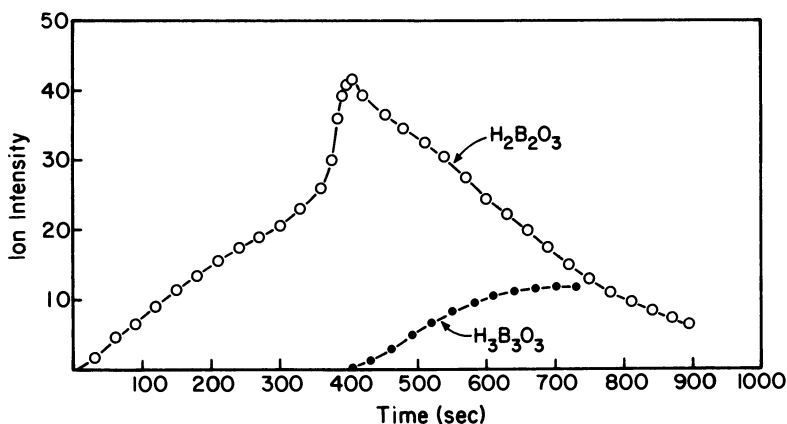


Figure 3. Plot of ion intensity for  $H_2B_2O_3$  ( $m/e = 71$ ) vs. irradiation time for a mixture of  $O_2$  and  $B_2H_6$  of 12.8 and 10.8 mm. pressure respectively, and ion intensity for  $H_3B_3O_3$  ( $m/e = 83$ ) vs. irradiation time for a mixture of  $O_2$  and  $B_2H_6$  of 13.3 and 10.0 mm. pressure, respectively

Table I. Experimental Determination of the Number of Molecules of  $O_2$  Reacting per Molecule of  $B_2H_6$  in Nonexplosive Reaction

Initial $^pO_2$ (mm.)	Initial $^pB_2H_6$ (mm.)	Molecules $O_2$ Reacting per molecule $B_2H_6$
12.8	11.0	2.60
12.8	11.0	2.54 <sup>a</sup>
11.9	9.3	2.04 <sup>a</sup>
11.3	9.1	2.18 <sup>a</sup>
8.2	16.2	2.45
16.1	7.9	2.51 <sup>a</sup>
2.8	2.5	2.60
5.7	5.1	2.96 <sup>a</sup>
11.3	10.3	2.51 <sup>a</sup>
22.7	20.3	2.13 <sup>a</sup>
12.7	9.3	2.86 <sup>a</sup>
5.4	5.0	2.84 <sup>a</sup>
5.7	6.9	2.30
5.5	6.5	2.30 <sup>a</sup>
7.3	5.8	2.10 <sup>a</sup>
		Av. 2.46

<sup>a</sup> Indicates cell had initial coating of  $B_2O_3$ .

given pressure of  $B_2H_6$ . The presence of a small quantity of  $O_2$  in the mass spectrometer from the inlet leak may affect the sensitivity of the electron multiplier and/or the emission characteristics of the ionization filament.

In experiments using unscrambled  $^{16}O_2$ - $^{18}O_2$  in place of ordinary  $O_2$ , it was possible to observe the formation of water, ( $H_2^{18}O$  at  $m/e = 20$  which avoids the usually high background of the  $m/e = 18$  peak), during the reaction and to obtain isotopic distributions in the products. This distribution for  $H_2B_2O_3$  is illustrated in Figure 4.

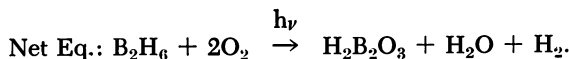
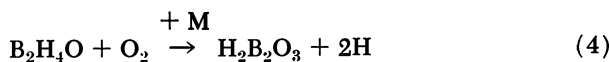
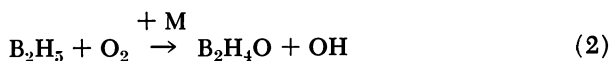
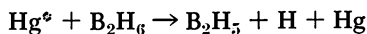
### Discussion

Two types of chemical behavior are observed when low pressure  $B_2H_6$ - $O_2$  mixtures are photolyzed with short wavelength radiation from a medium pressure mercury lamp. These processes are either (a) an explosive reaction producing  $H_3B_3O_3$ ,  $B_2O_3$ , or an unidentified boron hydride (solid) and  $H_2$ , or (b) a slower initial reaction, producing  $H_2B_2O_3$ ,  $H_2$ ,  $H_2O$ , and  $B_2O_3$  followed by the conversion of  $H_2B_2O_3$  to  $H_3B_3O_3$ .

Only Reaction *b* has been studied in any detail, and we will confine our discussion to this phase of the study. The stoichiometry indicated that approximately 2.5 molecules of  $O_2$  are consumed per molecule of  $B_2H_6$  (Table I). The rate of disappearance of  $O_2$  and appearance of  $H_2B_2O_3$  are accelerated with irradiation times, and in some cases an explosion is initiated. The intermediate peroxide,  $H_2B_2O_3$ , obtained when  $B_2H_6$ -( $^{16}O_2$ - $^{18}O_2$ ) mixtures are irradiated, contain oxygen atoms in a non-statistical distribution. This indicated that molecular  $O_2$  is introduced into the molecule without rupture of the O—O bond. The following mechanism is consistent with our observations.



or



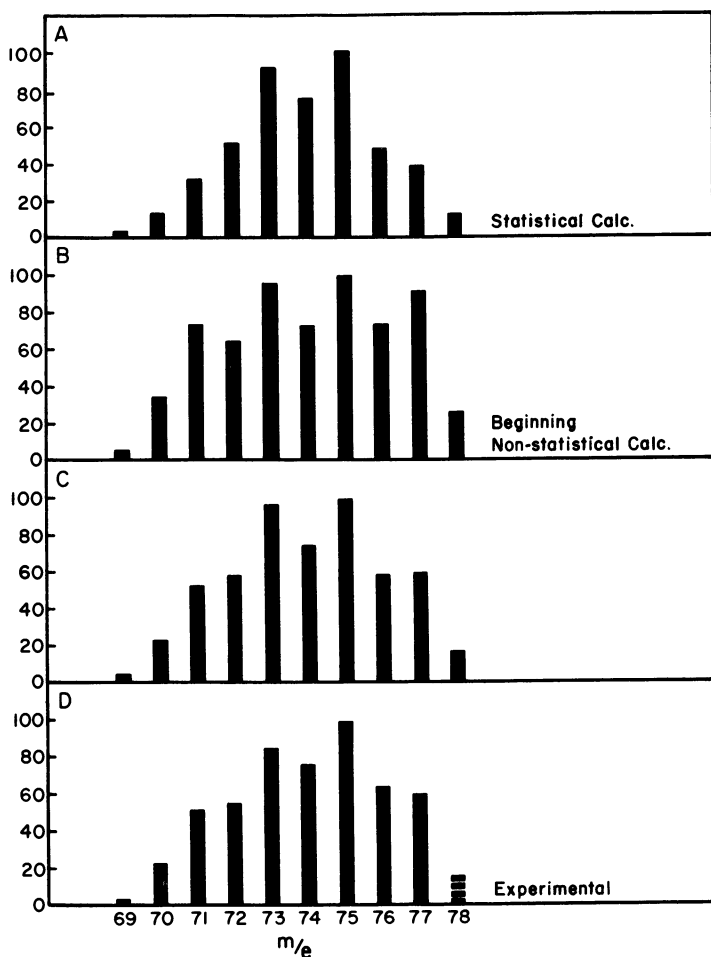


Figure 4. Comparison of calculated  $^{16}\text{O}$ - $^{18}\text{O}$  isotopic distribution in  $\text{H}_2\text{B}_2\text{O}_3$  with experimental results

A. Calculated from  $^{16}\text{O}$ - $^{18}\text{O}$  ratio =  $\frac{0.459}{0.541}$

B. Calculated from initial composition of  $^{16}\text{O}_2$ : $^{16}\text{O}^{18}\text{O}$ : $^{18}\text{O}_2$  = 0.424:0.0696:0.506

C. Calculated from the final composition of  $^{16}\text{O}_2$ : $^{16}\text{O}^{18}\text{O}$ : $^{18}\text{O}_2$  = 0.333:0.272:0.395 determined at the time the distribution in  $\text{H}_2\text{B}_2\text{O}_3$  was obtained. Note: This ratio is different from B since isotopic exchange of  $\text{O}_2$  occurs photochemically

D. Ion intensity at  $m/e = 78$  was corrected for background

The inconsistency of the observed stoichiometry with the expected value by this mechanism is attributed to further oxidation of the products.

The third body ( $M$ ) in Equations 2 and 4 would likely be the surface since we know that the rate of reaction depends upon the condition of the surface. We cannot neglect the possibility that some radicals in Equation 1 may be produced by mercury photosensitization (6) since mercury manometers were used to measure pressure. In several experiments in which oil manometers were used, the rate of reaction appeared to be slower. It is possible to suggest radicals other than  $B_2H_5$  for propagating the chain, but  $B_2H_5$  is a likely product for the primary photochemical step (6, 8).

The mass spectrometric technique as used in this study of the photochemical oxidation of  $B_2H_6$  provided new information on forming intermediates in the chemical reaction. Unfortunately, the technique was not capable of establishing the nature of short lived intermediates which react in a few collisions (*i.e.*,  $B_2H_4O$  as proposed above). The technique did offer advantages over conventional spectroscopic methods which could not be used for observing certain species.

#### Literature Cited

- (1) Blum, E., Herzberg, G., *J. Phys. Chem.* **41**, 91 (1937).
- (2) Eltenton, G. C., *J. Chem. Phys.* **15**, 455 (1947).
- (3) Foner, S. N., Hudson, R. L., *J. Chem. Phys.* **21**, 1374 (1953).
- (4) Goldfinger, P., Huybrechts, G., Verbeke, G., *Proc. Conf. Advan. Mass Spectrometry, 2nd, Oxford, 1961* **2**, 360 (1963).
- (5) Goldstein, *et al.*, "Progress in Astronautics and Rocketry" Vol. 2, Goldfinger, L. E., Goldsmith, M., Lemmon, A. W., Jr., editors, p. 327, Academic Press, New York, 1960.
- (6) Hirata, T., Gunning, H. E., *J. Chem. Phys.* **27**, 477 (1957).
- (7) Jeffers, W., *Chem. Ind. (London)* 431 (1961).
- (8) Kreye, W. O., Marcus, R. A., *J. Chem. Phys.* **37**, 419 (1962).
- (9) Lossing, E. P., Tickner, A. W., *J. Chem. Phys.* **20**, 907 (1952).
- (10) Wolfhard, H. G., Glassman, I., Green, L., Jr., editors, "Progress in Astronautics and Aeronautics," Vol. 15, Academic Press, New York, 1964.

RECEIVED October 11, 1966. Work supported by the Army Research Office—Durham and the Advanced Research Projects Agency.

# Mass Spectrometric Study of the Noble Metal Oxides

## Ruthenium-Oxygen System

J. H. NORMAN, H. G. STALEY, and W. E. BELL

Gulf General Atomic Inc., John Jay Hopkins Laboratory for Pure and Applied Science, San Diego, Calif.

*Mass spectrometric Knudsen cell methods have been used to measure heats of formation of the species  $\text{RuO}_3(\text{g})$ ,  $\text{RuO}_2(\text{g})$ , and  $\text{RuO}(\text{g})$  as  $-17$  kcal./mole at  $1250^\circ\text{K}$ .,  $28.4$  kcal./mole at  $1900^\circ\text{K}$ ., and  $85$  kcal./mole at  $1950^\circ\text{K}$ ., respectively. Entropies of formation of these species have been determined to be  $-20.8$ ,  $-1.5$ , and  $11.8$  e.u., respectively, in the temperature ranges studied. The species  $\text{RuO}_4(\text{g})$  was also observed. Noble metal gaseous oxide heats of formation as measured in transpiration and Knudsen cell studies are found to be in good agreement while some discrepancies in the associated entropies have been noted. A compilation of M—O bond energies for the gaseous noble metal oxides is presented.*

Studies (3, 29, 31, 33) of the ruthenium-oxygen system in the temperature range  $1100^\circ$  to  $1800^\circ\text{K}$ . and at oxygen pressures around 1 atm. have shown  $\text{RuO}_2$  to be the important condensed phase and  $\text{RuO}_3$  and  $\text{RuO}_4$  to be important vapor species. Data on the lower gaseous oxides,  $\text{RuO}_2$  and  $\text{RuO}$ , have not been available.

In the present study, the ruthenium-oxygen system has been investigated by mass spectrometric Knudsen cell methods to determine the important vapor species and associated thermodynamics at oxygen pressures around  $10^{-4}$  atm. between  $1150^\circ$  and  $2050^\circ\text{K}$ .

Thermodynamic values obtained from this study have been compared with values from transpiration studies. In addition, a review of gaseous noble metal oxide thermodynamics as measured using mass

spectrometric Knudsen cell techniques is presented. Where possible these thermodynamics are also compared with results obtained using transpiration studies.

### *Experimental Procedures*

A Consolidated Electrodynamics Corp. Model 21-703 (12-inch radius, 60° sector) mass spectrometer modified for Knudsen cell experiments was employed for this work. Two different cells were used in the study. At temperatures below 1500°K., a quartz Knudsen cell having a 0.7-mm.-diameter orifice was used. The cell, fitted at the top with a quartz oxygen-feed tube, was held in a close-fitting molybdenum cup and was covered with three layers of tantalum. Above 1500°K., an alumina cell of similar dimensions was used. It was similar in geometry except that the orifice was 1.4-mm. diameter and the cell was fed with oxygen through an alumina tube inserted through the base of the cell. This cell also was mounted inside a molybdenum cell.

The assemblies were heated by electron bombardment using tungsten filaments mounted near the side of the cell and above the cell as in the authors' other studies (22). Oxygen flowed into the cell through a viscous-flow inlet from a large reservoir. Oxygen pressure in the cell was determined by the pressure in the reservoir and the cell orifice size. Temperatures below 1500°K. were measured by two Pt/Pt-10% Rh thermocouples attached to the inside of the molybdenum cell, one near the top and the other near the bottom. Temperatures above 1500°K. were measured by making optical pyrometer sightings of the alumina cell through small holes in the outer molybdenum cell near the top and bottom of the alumina cell. Temperatures were equalized by adjusting the potential applied across the top-mounted tungsten filaments. In both cases the cells were charged with Johnson Matthey (99.995% purity) ruthenium metal.

### *Results and Discussion*

Mass peaks attributable to effusate from the Knudsen cells were found to correspond to  $O^+$ ,  $Ru^+$ ,  $O_2^+$ ,  $RuO^+$ ,  $RuO_2^+$ ,  $RuO_3^+$ , and  $RuO_4^+$ , according to masses and isotopic ratios. No other Ru-containing ions were observed. Appearance potentials measured for the ruthenium-containing ions were 7.7, 8.7, 10.6, 11.2, and 12.8 e.v. for, respectively,  $Ru^+$ ,  $RuO^+$ ,  $RuO_2^+$ ,  $RuO_3^+$ , and  $RuO_4^+$ . Near voltage ion appearance thresholds the above-listed peaks were believed to be parent ion peaks. Oxygen pressure sensitivities presented below generally indicate this to be the case. Breaks in the appearance potential curves for  $Ru^+$  and  $RuO^+$  from  $RuO_2$  were measured to occur at 13.0 and 12.8 e.v., respectively.

In an experiment using the quartz cell at 1240°K., the  $O_2$  pressure was varied. Figure 1, a plot of the resulting  $\log I_{RuO_3^+}$  (and  $I_{RuO_2^+}$  and  $I_{RuO^+}$ ) vs.  $\log I_{O_2^+}$  data, shows a 3/2 slope within the uncertainty of the data. This suggests that the  $RuO_3^+$  ion (at  $m/e$  152) is formed from

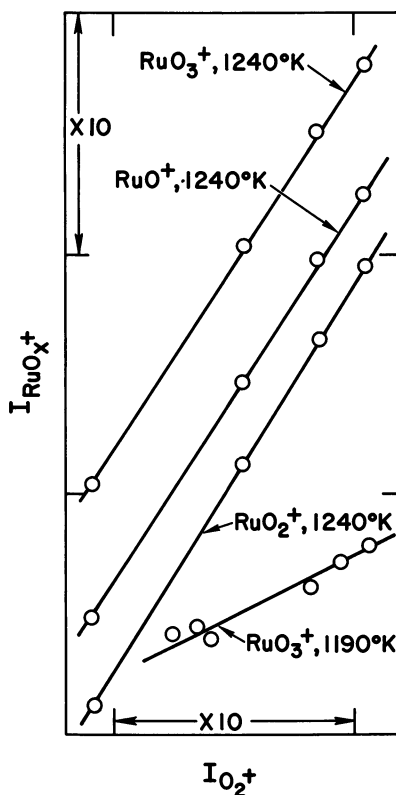
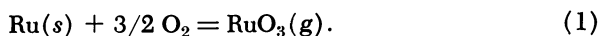
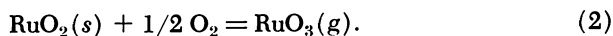


Figure 1. Metal oxide ion intensity dependence on  $O_2^+$  ion intensity

$RuO_3(g)$  since the metal is the solid state present under the experimental conditions (3). That is, the important vaporization reaction is



At  $1190^\circ K$ , the  $I_{RuO_3^+}$  vs.  $I_{O_2^+}$  isotherm, also illustrated in Figure 1, shows a slope close to 0.5. This indicates that  $RuO_2(s)$  was the condensed phase in the  $O_2$  pressure range used and that the important vaporization reaction is



The vapor pressure of  $RuO_4$  over  $RuO_2(s)$  at  $1140^\circ$  and  $10^{-4}$  atm.  $O_2$  as determined by Bell and Tagami (3) should be around  $10^{-8}$  atm. The  $RuO_4^+$  ion was observed in this work but was not intense enough to permit study of its thermal behavior.

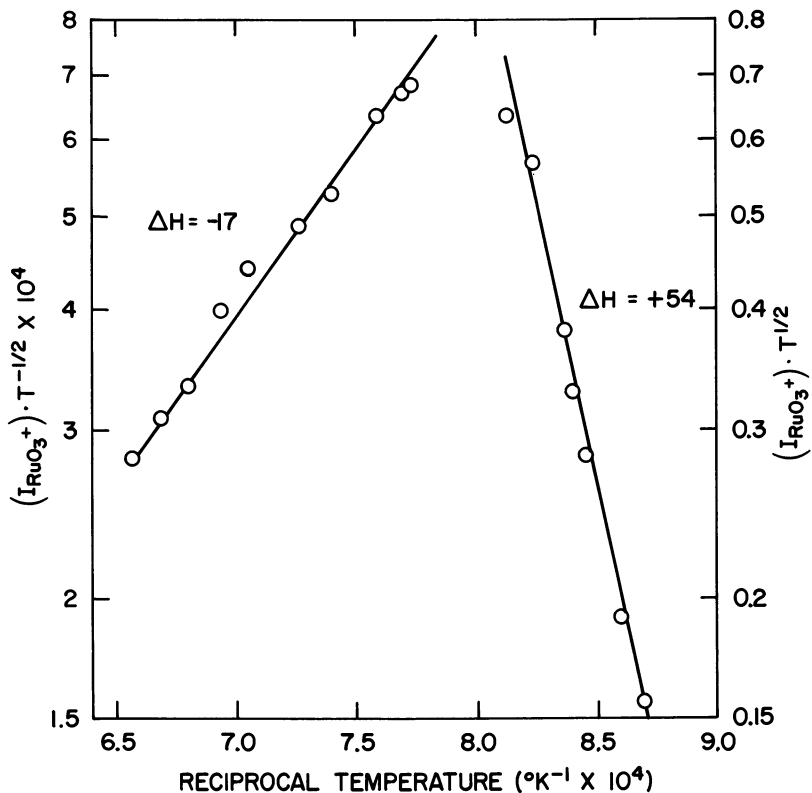
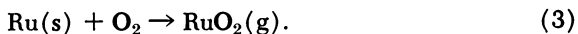


Figure 2. Dependence of  $\text{RuO}_3^+$  intensity functions on temperature

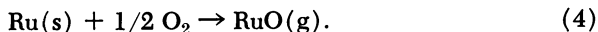
Logarithmic plots of the ion currents of  $\text{RuO}_3^+$  times  $T^{1/2}$  and times  $T^{-1/2}$  as a function of reciprocal temperature are shown in Figure 2. In the experiments from which these data were obtained, the intensity of the  $\text{O}_2^+$  formed from the Knudsen cell effusate was set at a constant high level. Under these conditions, because of the  $IT$  proportionality to pressure, the quantities  $I_{\text{RuO}_3^+}T^{1/2}$  and  $I_{\text{RuO}_3^+}T^{-1/2}$ , respectively, are proportional to the equilibrium constants for Reactions 1 and 2. From slopes of lines drawn through the two sets of data in Figure 2, we calculate  $\Delta H_{1250} = 54$  kcal./mole for Reaction 2 and  $\Delta H_{1250} = -17$  kcal./mole for Reaction 1. These values are in good agreement with  $\Delta H_{1250}$  values of  $+54.7$  and  $-13.9$  kcal./mole calculated for the respective reactions from data reported by Schäfer, Schneidreit, and Gerhardt (31), and  $\Delta H_{1250}$  values of  $+51.6$  and  $-17.0$  kcal./mole calculated for the respective reactions from data reported by Bell and Tagami (3).

Using the alumina cell, the  $\text{RuO}_3(\text{g})$  species can be suppressed by going to higher temperatures, but more important, the pressures of the

lower oxides can be increased. At higher temperatures and a nominal electron energy of 20 e.v., the intensity of the  $\text{RuO}_2^+$  signal from the Knudsen cell effusate was found to depend directly on the square of that portion of the atomic  $\text{O}^+$  signal attributable to Knudsen cell effusate. This suggests that  $\text{RuO}_2^+$  is a parent ion and can be used in describing the vaporization of  $\text{RuO}_2(\text{g})$  in studying the reaction



At a nominal electron energy of 10 e.v., the  $\text{RuO}^+$  signal intensity was found to be proportional to the intensity of the shutterable  $\text{O}^+$ ; therefore,  $\text{RuO}^+$  is a parent ion at this electron energy. At 20 e.v., the  $\text{RuO}^+$  and the  $\text{Ru}^+$  were found to have the same  $\text{O}_2$  dependence as the  $\text{RuO}_2^+$  (at  $m/e$  136), suggesting  $\text{RuO}^+$  (at  $m/e$  120) and  $\text{Ru}^+$  (at  $m/e$  102) were fragments of  $\text{RuO}_2(\text{g})$ . The vaporization reaction for  $\text{RuO}(\text{g})$  is



At 10 e.v., the  $\text{Ru}^+$  peak is found to be independent of the  $\text{O}^+$  signal and thus represents the direct vaporization of ruthenium metal,



Observations of the variation in intensities of the  $\text{RuO}_2^+$  at 20 e.v. and the  $\text{RuO}^+$  and  $\text{Ru}^+$  at 10 e.v. with  $\text{O}^+$  intensity are illustrated in Figure 3.

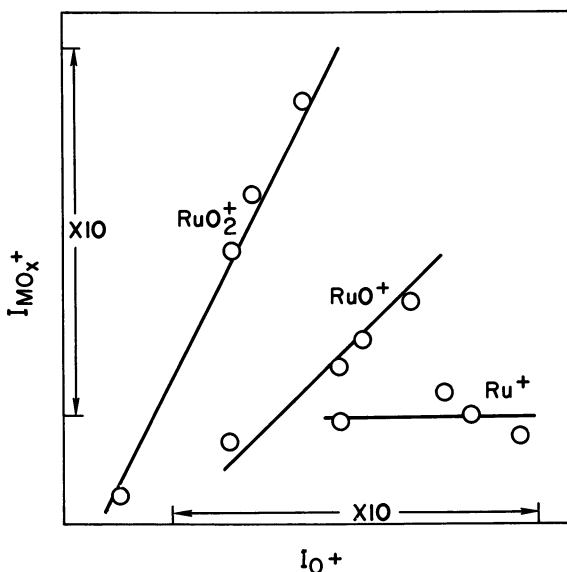


Figure 3. Metal ion intensity dependence on  $\text{O}^+$  ion intensity at 2045°K.

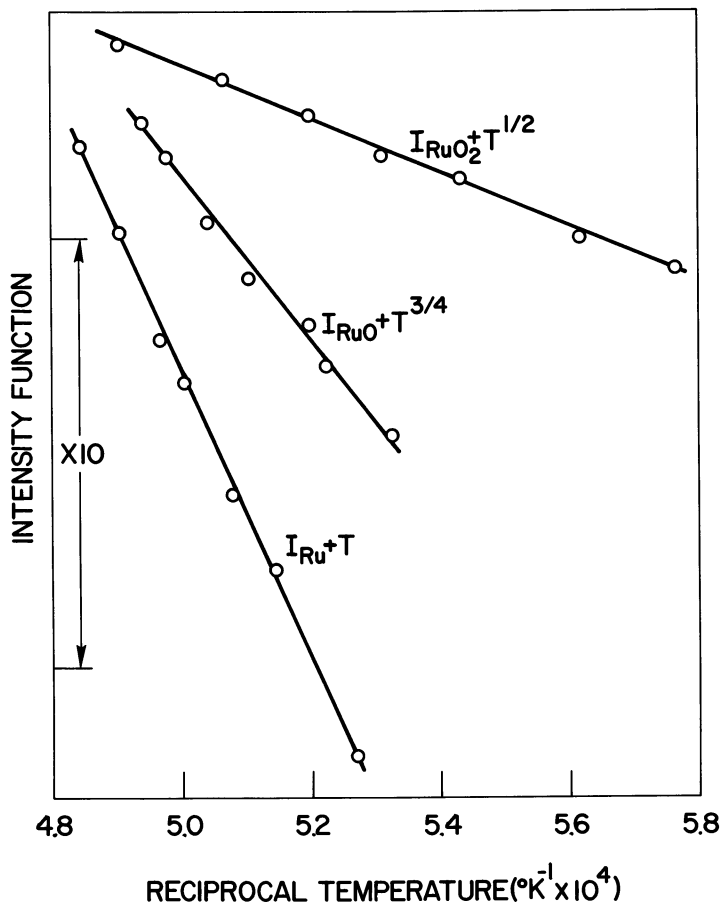
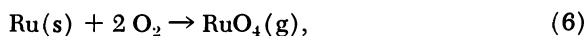


Figure 4. Dependence of ruthenium species ion intensity function on temperature

If the intensities of the  $\text{Ru}^+$ ,  $\text{RuO}^+$ , and  $\text{RuO}_2^+$  ions are studied as a function of temperature at appropriate electron energies and at a high, constant flux of oxygen through the cell ( $P_{\text{O}_2} \gg P_{\text{O}}$ ), the heats of vaporization of the parent species of these ions may be determined from the slopes of ion intensity functions *vs.* reciprocal temperature. Examples of these determinations are presented in Figure 4. Four such determinations were made for each of these species, resulting in values of  $28.4 \pm 1.0$ ,  $85 \pm 5$ , and  $152 \pm 3$  kcal./mole for Reactions 3, 4, and 5, respectively, in the temperature ranges  $1740^\circ\text{--}2040^\circ\text{K.}$ ,  $1870^\circ\text{--}2020^\circ\text{K.}$ , and  $1900^\circ\text{--}2050^\circ\text{K.}$

To estimate the partial pressures of the gaseous species  $\text{RuO}$ ,  $\text{RuO}_2$ ,  $\text{RuO}_3$ ,  $\text{RuO}_4$ ,  $\text{O}$ , and  $\text{O}_2$  present in these systems, a pressure of  $\text{Ru}(\text{g})$

was obtained from the studies of Panish and Reif (26) and of Carrera, Walker and Plante (6) (the Paule and Margrave (27) values differed slightly) and used as a standard in the method described by Inghram and Drowart (13). In this method, total ionization cross sections according to Otvos and Stevenson (24) were employed along with multiplier gains inversely proportional to the square root of the molecular weight and the appearance potentials reported in this study and by Kiser (16). Using these data, entropy values for Reactions 1, 3, and 4 were calculated to be  $-20.8$ ,  $-1.5$ , and  $11.8$  e.u., respectively, in the temperature ranges studied. The heat of vaporization of  $\text{RuO}_4(\text{g})$  ( $-45.4$  kcal./mole) from the studies of Bell and Tagami (3) leads to an entropy of the vaporization reaction,



of  $-33.6$  e.u. from the experimental  $\text{RuO}_4^+$  intensity measured at  $m/e$  166 and a corresponding  $\text{O}_2^+$  ion intensity.

### *Review of Noble Metal Oxide Vaporization Data*

Oxide transpiration studies have been made by Alcock and Hooper (2) (AH), for the metals Pt, Pd, Rh, Ir, and Rh. Other noble metal oxide transpiration studies include a Ru study by Bell and Tagami (3) (BT); a Ru study by Schäfer, Tebben, and Gerhardt (33) (STG); Ir studies by Schäfer and Heitland (30) (SH), Kuriakose and Margrave (17) (KM), and Cordfunke and Meyer (8) (CM); and a Pt study by Schäfer and Tebben (32) (ST). Grimley, Burns, and Inghram (10) (GBI) have investigated the gas phase  $\text{OsO}_4 \rightarrow \text{OsO}_3 + 1/2 \text{O}_2$  equilibrium in a Knudsen cell mass spectrometrically, and Norman, Staley, and Bell (20, 21, 22, 23) have studied the oxides of Ru, Ir, Rh, Pt, and Pd using mass spectrometric Knudsen cell techniques. Schäfer, Tebben, and Gerhardt (33) and Nikolskii and Ryabov (19) have presented reviews of some of this information. The heats of formation from these studies are given in Table I, where the compilation of Coughlin (9) (C) was used to describe the heat of formation of  $\text{OsO}_4(\text{g})$ . In Table I all of the heats have been extrapolated to  $1500^\circ\text{K}$ . by employing, in the absence of structural information on the oxides,  $\text{H}_7$ – $\text{H}_0$  data from the JANAF tables (14) for the appropriate gaseous tungsten oxide except for tetroxides, where Kelley's (15)  $\text{OsO}_4$  heat capacity formula was extrapolated to  $1500^\circ\text{K}$ . The error made by using the heat capacities of these gaseous compounds to describe the same  $\text{MO}_x(\text{g})$  species for other metals at the moderate temperatures involved should be rather small, except where the question of linearity of the  $\text{MO}_2(\text{g})$  molecules is involved—a 1 cal./deg.-mole variance. Appropriate data for the condensed metals and oxygen were

taken from the JANAF tables (14), Stull and Sinke (35), and Hultgren, *et al.* (12). The  $\text{RuO}_2$  data of Alcock and Hooper (2) were corrected to take into account that  $\text{RuO}_2$  was the condensed phase present under their conditions. Also,  $\text{RhO}_2$  was taken as the gaseous rhodium oxide present in their studies. The data of Kuriakose and Margrave (17) were taken to apply to the reaction  $\text{Ir}(s) + 3/2 \text{O}_2 \rightarrow \text{IrO}_3(g)$ .

**Table I. Heats of Formation of the Gaseous Noble Metal Oxides at 1500°K. (kcal./mole)**

Element	Reference <sup>a</sup>	$\text{MO}(g)$	$\text{MO}_2(g)^b$	$\text{MO}_3(g)$	$\text{MO}_4(g)$
Os	GBI		Present	$-11.8 \pm 1$	
	C				-81.5
	NR		(46)	(-25)	
	B		$(39 \pm 20)$		
Ru	NSB	$86.7 \pm 5$	$29.7 \pm 1$	$-17.0 \pm 2$	
	AH			-16.5	
	STG			-13.5	-42.8
	BT			$-16.7 \pm 2$	$-45.4 \pm 3$
	NR		(40)		$-43.1 \pm 2$
	B		$(47 \pm 15)$		
Ir	NSB	Present	$49.7 \pm 1.0$	$6.2 \pm 1.5$	
	AH			4.8	
	CM			4.2	
	SH			4.0	
	KM			$7.1 \pm 1.9$	
	B		$(48 \pm 15)$		
Rh	NSB	$91 \pm 5$	$42.0 \pm 2.0$		
	AH		$45.6 \pm 0.6$		
	B		$(27 \pm 20)$		
Pt	NSB	$102.3 \pm 5$	$37.8 \pm 2.3$		
	AH		$39.4 \pm 0.3$		
	ST		39.9		
	B		$(43 \pm 8)$		
Pd	NSB	$80.0 \pm 1.0$			
	B		$(41 \pm 25)$		

<sup>a</sup> Authors' initials indicate pertinent works.

<sup>b</sup> Values in parentheses are estimated.

The agreement of the experimental values reported in Table I is indeed gratifying. It would seem to give credence to all of the data reported. The agreement between the mass spectrometric and the transpiration results strongly suggests that the same species are being examined in the two different methods, and other evidence substantiates

this. That is, the mass spectrometric studies have not revealed polymers but indicate the presence of the monomer species assumed in the transpiration studies. While the oxygen pressures used in these two types of studies are quite different, this has little to do with the  $P_{M_xO_y}/P_{MO_y}$  ratios—*i.e.*, if  $P_{M_xO_y}$  were important in the transpiration studies, this species probably would have been detected mass spectrometrically. It appears, then, that all these studies, with the possible exception of the Ir studies of Kuriakose and Margrave (17), indicate only the presence of monomeric vapor species of the noble metal oxides.

One might question whether transpiration studies are appropriate for systems as complex as these. Note, however, that the possible presence of several species in the transpiration studies does not seem to have adversely affected the results. For instance, Bell and Tagami obtained thermodynamic information on both  $RuO_3$  and  $RuO_4$  by interpreting ruthenium transport to be caused by both species.

Brewer (5) (B) has estimated the dissociation energies for the dioxides at 0°K. In Table I, his values have been converted into heats of formation at 1500°K. for comparison with the experimental values, where available. While there are discrepancies up to 20 kcal./mole, Brewer's estimates are within his stated uncertainties.

The heat of formation data given in Table I can be converted into bond energy information. Table II presents the heats of formation of the gaseous oxides per oxygen atom at 1500°K. from gaseous metal and atomic oxygen. For self-consistency, the Knudsen cell values are used where available. Data used in constructing this table include the heat of dissociation of oxygen molecules at 1500°K. as presented in the JANAF tables (14) and heats of vaporization of the noble metals at 1500°K. as given by Stull and Sinke (35), Hultgren, *et al.* (12), and/or recent experimental determinations (6, 22, 25, 26, 27). These selected heats of vaporization are also included in Table II.

One noteworthy observation concerning the bond energies presented in Table II is that they exhibit a degree of agreement with an additivity rule. The system with the most extensive pertinent data would be the ruthenium oxides. In this case, 127 kcal. are associated with the bonding of the first gram atom of oxygen, while only 89 kcal. are associated with the fourth—0.7 of the value for the first gram atom. While this does not indicate complete agreement with the additivity rule, this decrease from 1 to 0.7 of the first bond energy across the whole series seems a rather small change and indicates near applicability of the rule. Observed deviations for Os, Ru, and Ir are in the order of decreasing bond strength with additional bonds, while Rh and Pt seem to exhibit a reverse trend by accepting a second gram atom of oxygen somewhat more energetically than the first.

**Table II. Heats of Formation per Oxygen Atom of the Noble Metal Gaseous Oxides at 1500°K. from Atomic Oxygen and M(g) (—kcal./mole)**

Element	Reference	M(g)	MO	MO <sub>2</sub> /2	MO <sub>3</sub> /3	MO <sub>4</sub> /4
Os	(6, 26)	185			145 (GBI)	127 (C)
Ru	This study	152	127	122	117	110
Ir	(25, 27)	156		114	111	
Rh	(12, 35)	131	101	105		
Pt	(12, 35)	134	92	109		
Pd	(22)	89	70			

Nikolskii and Ryabov (19) question the Grimley, Burns, and Inghram (10) value used by Schäfer, Tebben, and Gerhardt (33) in their review to calculate  $-66.2$  kcal./mole for  $\Delta H^\circ_{298}$  of  $\text{OsO}_3(\text{g})$ . This value is related to the degree of departure from additivity of Os—O bonds. Indeed, the GBI 18-kcal./mole difference in oxygen average bond energies for the two higher oxides of osmium presented in Table II is large, but it is difficult to show that it is too large, and it seems unnecessarily preclusive to argue this question from condensed state thermodynamics. It seems best to accept this apparently excellent description of the  $\text{OsO}_3\text{—O}_2\text{—OsO}_4$  equilibrium by reporting the GBI heat of formation of  $\text{OsO}_4(\text{g})$  minus that of  $\text{OsO}_3(\text{g})$ . Nikolskii and Ryabov (19) have also predicted  $\Delta H^\circ_{298}$  for  $\text{OsO}_2$  and  $\text{RuO}_2$ . There is no experimental information concerning  $\text{OsO}_2$ , and their  $\text{OsO}_2$  estimate certainly is subject to the same difficulties as is their  $\text{OsO}_3$  estimate. Their  $\text{RuO}_2$  estimate, converted to 1500°C., would be 9 kcal./mole higher than the experimental value.

The noble metals are presented in Tables I and II essentially in the order of the stability of their oxides and their heats of vaporization. The relation of these properties and their position in the periodic table is evident.

Although the noble metal oxide experimental heats of formation from the mass spectrometric and transpiration techniques are in good agreement, where they can be cross-checked, the vapor pressures determined using the two methods differ considerably. To demonstrate this problem, all of the comparable cases are presented in Table III. While several of the values used cannot be considered well established, two cases,  $\text{IrO}_3$  and  $\text{PtO}_2$ , stand out as reasonable tests. Three transpiration studies, when extrapolated, give  $1.7 (\pm 0.2) \times 10^{-3}$  atm. as the  $\text{IrO}_3$  vapor pressure at 2033°K. and 1 atm.  $\text{O}_2$  pressure in the presence of the metal. The corresponding value from the mass spectrometric method is  $3.5 \times 10^{-4}$ , a factor of five lower. In the platinum oxide transpiration studies cited, the extrapolated vapor pressure of  $\text{PtO}_2(\text{g})$  in 1 atm. oxygen over the metal at 2018°K. was determined to be  $1.0 (\pm 0.1) \times 10^{-4}$  atm. The

mass spectrometric study leads to a value of  $8.5 \times 10^{-6}$  atm., a factor of 11 smaller. The  $\text{RuO}_3$  case is not quite as clear. The two transpiration results at  $1779^\circ\text{K}$ . and 1 atm.  $\text{O}_2$  over the metal give  $4.8 (\pm 3) \times 10^{-2}$  compared with  $4.1 \times 10^{-3}$  obtained mass spectrometrically in this case, a factor of four to 20 lower. In the single comparison of  $\text{RhO}_2$  pressures, the mass spectrometric value is considerably lower than in the other cases. In the  $\text{PdO}$  case, no real comparison can be made except to say that Alcock and Hooper (2) believe, based on their transpiration studies, that  $\text{PdO}$  pressures should be higher than were measured spectrometrically by Norman, Staley, and Bell (22). The one remaining comparison also is not well established since, in the case of  $\text{RuO}_4(\text{g})$ , no mass spectrometric heats were obtained and the transpiration results were based on a minor species determination. In this single case, however, the mass spectrometric pressures were higher than the transpiration pressures.

**Table III. Noble Metal Oxide Comparative Vapor Pressures (atm.)**

<i>Gaseous Species</i>	<i>T(°K.)</i>	<i>Mass Spec. (NSB)</i> $P_{\text{MO}_x}/P_{\text{O}_2}^{x/2}$ <sup>a</sup>	<i>Transpiration</i> $P_{\text{MO}_x}/P_{\text{O}_2}^{x/2}$ <sup>a</sup>	<i>Transpiration</i> <u>Mass Spec.</u>
$\text{RuO}_4$	1729	$(2 \times 10^{-2})$ max	$3.5 \times 10^{-3}$ (STG) $1.1 \times 10^{-3}$ (BT)	(0.5-0.05)
$\text{RuO}_3$	1729	$4.1 \times 10^{-3}$	$6.9 \times 10^{-2}$ (STG) $2.7 \times 10^{-2}$ (BT)	20-5
$\text{IrO}_3$	2033	$3.5 \times 10^{-4}$	$1.6 \times 10^{-3}$ (AH) $1.6 \times 10^{-3}$ (SH) $1.9 \times 10^{-3}$ (CM)	5
$\text{RhO}_2$	2000	$3 \times 10^{-6}$	$1.4 \times 10^{-4}$ (AH)	50
$\text{PtO}_2$	2018	$8.5 \times 10^{-6}$	$8.9 \times 10^{-5}$ (AH) $1.1 \times 10^{-4}$ (ST)	13-10
$\text{PdO}$	1900	$1.0 \times 10^{-6}$	$(4 \times 10^{-5})$ (AH)	(40)

<sup>a</sup>  $P_{\text{O}_2} = \text{atm.}$

These results, then, suggest that generally an underestimation of metal oxide pressures is made in the mass spectrometric studies or an overestimation is made in the transpiration studies. It is difficult to believe that in the transpiration method mass transport was grossly overestimated or diffusional effects were not properly accounted for. For reasons mentioned previously, it is also difficult to believe that polymers cause the differences in the two methods, although under unusual circumstances  $\text{M}_x\text{O}_2$  could be considered to be  $\text{MO}_2$  in the transpiration study, giving excessively high  $\text{MO}_2$  pressures. It seems much more likely

that the crux of this problem is in converting mass spectrometric ion intensities to cell species pressures. Indeed, questions concerning the validity of employing the cross sections of Otvos and Stevenson (24) and the additivity of these quantities have been brought up (7, 18, 28). Stafford (34) has proposed using cross sections derived from Gryzinski's (11) calculational scheme. In several studies (1, 4, 36) attempts were made to avoid the use of calculated cross sections.

Some problems are associated with pressure estimation used in the mass spectrometric method. Mass spectrometric ion intensities are converted to pressures or equilibrium constants by employing ratios of intensities. One either considers a dimensionless pressure ratio as an equilibrium constant or establishes the pressure of a species of interest by comparison with an available pressure standard. For the noble metal  $\text{MO}_2$  gaseous species, it was indeed reasonable to use the  $K_p = P_{\text{MO}_2}/P_{\text{O}_2} = KI_{\text{MO}_2}/I_{\text{O}_2}$  relationship. In other cases, one can utilize dimensionless reactions such as  $\text{M}(s) + 2 \text{O}_2 \rightarrow \text{MO}_3 + \text{O}$  where, in a sense, the  $1/2 \text{O}_2 \rightarrow \text{O}$  equilibrium is employed to calibrate the system. Often the noble metal pressure may be used as a calibrating agent, or some additive to the system, such as silver, may be used in the calibration. While these procedures appear sound and beyond question, they do not circumvent the necessity of estimating relative cross sections and detector sensitivities.

One is often confronted with the problem of the experimentally indeterminate question of how efficiently ions of a particular type can be made from specific neutral species. The method described by Inghram and Drowart (13) for estimating ratios of total ionization efficiencies accepts Otvos and Stevenson's (24) total ionization cross sections and additivity of these cross sections. The method also accepts a linear relationship between cross section and ionizing energy of the exciting electrons above a threshold value to provide these ratios of total ionizing efficiencies. Specific criticisms of the universality of this formula may be directed at:

1. The total atomic cross section values themselves.
2. Additivity of these values to get molecular cross sections.
3. The simplicity of the assumed approach toward the maximum cross sectional values as a function of electron energy.
4. The application of these values to cases where undetected fragmentation may be significant.

Questions of division of transferred energy into excitation and ionization, electronic structure of atoms and molecules, and other basic properties are involved. For instance, Stafford's (34) proposed cross sections differ in many cases from normalized Otvos and Stevenson values by a factor of two or three. His values show deviation from experimentally

determined cross sections, although not as often as do the normalized Otvos and Stevenson values.

Let us consider the situation for the noble metal oxide measurements. Ionization cross sections for oxygen molecules as employed in these studies seem to agree with experimental values—*i.e.*, the ratio of  $O_2$  to M cross sections at the voltages employed is in line with experimental cross section ratios of  $O_2$  and Hg at the employed voltages. If Hg cross section agreement can be taken as indicating noble metal agreement, then the pressure discrepancy problem seems to be concerned with the ionization cross section of  $MO_x$  compared with M and/or undetected fragmentation of  $MO_x$ . One or both might well be the root of the pressure discrepancies presented here.

It appears that although Stafford's (34) approach could help the cross section problem somewhat, considerable doubt will remain even after such an analysis of cross sections of noble metal oxides. Theoretically, the fragmentation problem should not be severe since one should recognize fragments and account for their presence. However, in the real case, the possibility of transmission problems of ions born with high kinetic energy (not considered in this study) and the inability to recognize fragment peaks buried under large system peaks cause considerable uncertainty regarding the degree of fragmentation. Added to this uncertainty, multiplier sensitivities are generally estimated. Accordingly, then, it seems that mass spectrometric pressures using estimated values should be treated with some caution.

The purpose of this portion of the paper is not to imply that mass spectrometric Knudsen cell studies provide inadequate thermodynamics, but to point out that some caution should be employed when using mass spectrometrically determined equilibrium constants based on estimated cross sections, etc. The authors are convinced that, in general, measurements of this type provide and will continue to provide the best available experimental high temperature gaseous system thermodynamics. The authors are also convinced, because of the uncertainties associated with the equilibrium constant "estimation," that good mass spectrometrically determined second law heats have considerable merit when compared with third law heats for complex systems as reported here.

### *Literature Cited*

- (1) Ackermann, R. J., Rauh, E. G., Thorn, R. J., Cannon, M. C., *J. Phys. Chem.* **67**, 762 (1963).
- (2) Alcock, C. B., Hooper, G. W., *Proc. Roy. Soc. (London)* **A254**, 551 (1960).
- (3) Bell, W. E., Tagami, M., *J. Phys. Chem.* **67**, 2432 (1963).
- (4) Berkowitz, J., Marquart, J. R., *J. Chem. Phys.* **39**, 275 (1963).

- (5) Brewer, L., *U. S. At. Energy Comm. Rept. UCRL-8356*, Univ. of Calif. Radiation Lab., July 1958.
- (6) Carrera, N. J., Walker, R. F., Plante, E. R., *J. Res. Natl. Bur. Std.* **68A**, 325 (1964).
- (7) Cooper, J. L., Pressley, G. A., Stafford, F. E., *J. Chem. Phys.* **44**, 3946 (1966).
- (8) Cordfunke, E. P. H., Meyer, G., *Rec. Trav. Chim.* **81**, 495 (1962).
- (9) Coughlin, J. P., *U. S. Bur. Mines Bull.* **542** (1954).
- (10) Grimley, R. T., Burns, R. P., Inghram, M. G., *J. Chem. Phys.* **33**, 308 (1960).
- (11) Gryzinski, M., *Phys. Rev.* **138**, A305, A322, A336 (1965).
- (12) Hultgren, R., Orr, R. L., Anderson, P. D., Kelley, K. K., "Selected Values of Thermodynamic Properties of Metals and Alloys," John Wiley and Sons, New York, 1963.
- (13) Inghram, M. G., Drowart, J., in *Proc. Intern. Symp. High Temp. Technol., Asilomar Conf. Grounds, Calif.*, October 1959 (1960).
- (14) JANAF Thermochemical Tables, The Dow Chemical Co., Midland, Mich., 1963.
- (15) Kelley, K. K., *U. S. Bur. Mines, Bull.* **584**, U. S. Govt. Printing Office, 1960.
- (16) Kiser, R., *U. S. At. Energy Comm. Rept. TID-6142*, University of Kansas, June 20, 1960.
- (17) Kuriakose, A. K., Margrave, J. L., "Kinetics of Oxidation of Iridium at High Temperature," Summary Tech. Rept. No. 2, Rice University (no date).
- (18) Lampe, F. W., Franklin, J. L., Field, F. H., *J. Am. Chem. Soc.* **79**, 6129 (1957).
- (19) Nikolskii, A. B., Ryabov, A. N., *Zh. Neorgan. Khim.* **10**, 1 (1965).
- (20) Norman, J. H., Staley, H. G., Bell, W. E., *J. Chem. Phys.* **42**, 1123 (1965).
- (21) Norman, J. H., Staley, H. G., Bell, W. E., *J. Phys. Chem.* **68**, 662 (1964).
- (22) *Ibid.*, **69**, 1373 (1965).
- (23) *Ibid.*, **71**, 3686 (1967).
- (24) Otvos, J. W., Stevenson, D. P., *J. Am. Chem. Soc.* **78**, 546 (1956).
- (25) Panish, M. B., Reif, L., *J. Chem. Phys.* **34**, 1915 (1961).
- (26) *Ibid.*, **37**, 128 (1962).
- (27) Paule, R. C., Margrave, J. L., *J. Phys. Chem.* **67**, 1896 (1963).
- (28) Pottie, R. F., *J. Chem. Phys.* **44**, 916 (1966).
- (29) Schäfer, H., Gerhardt, W., Tebben, A., *Angew. Chem.* **73**, 27, 115 (1961).
- (30) Schäfer, H., Heitland, H. J., *Z. Anorg. Allgem. Chem.* **304**, 249 (1960).
- (31) Schäfer, H., Schneidereit, G., Gerhardt, W., *Z. Anorg. Allgem. Chem.* **319**, 327 (1963).
- (32) Schäfer, H., Tebben, A., *Z. Anorg. Allgem. Chem.* **304**, 317 (1960).
- (33) Schäfer, H., Tebben, A., Gerhardt, W., *Z. Anorg. Allgem. Chem.* **321**, 41 (1963).
- (34) Stafford, F. E., *J. Chem. Phys.* **45**, 859 (1966).
- (35) Stull, D. R., Sinke, G. C., *ADVAN. CHEM. SER.* **18**, 1956.
- (36) White, D., Seshadri, K. S., Dever, D. F., Mann, D. E., Linevsky, M. J., *J. Chem. Phys.* **39**, 2463 (1963).

RECEIVED October 24, 1966. Supported in part by U. S. Atomic Energy Commission, Contract AT(04-3)-164.

# Calculation of Electron Impact Ionization Cross Sections

FRED E. STAFFORD

Department of Chemistry and the Materials Research Center,  
Northwestern University, Evanston, Ill.

*The Gryzinski theory for electron impact ionization cross sections for atoms is examined with regard to the shape of the total ionization efficiency curve, the relative importance of the contribution to the total cross section of inner electron shells, and agreement with experimental data. The theory agrees well with the available data. The reasons for the systematic differences of the predictions of this theory from those of Otvos and Stevenson are analyzed. Calculations are made for some diatomic molecules. The ratio of the calculated molecular cross section to the sum of the atomic cross sections varies from 0.8 to 1.3. The reasons for this variation are examined.*

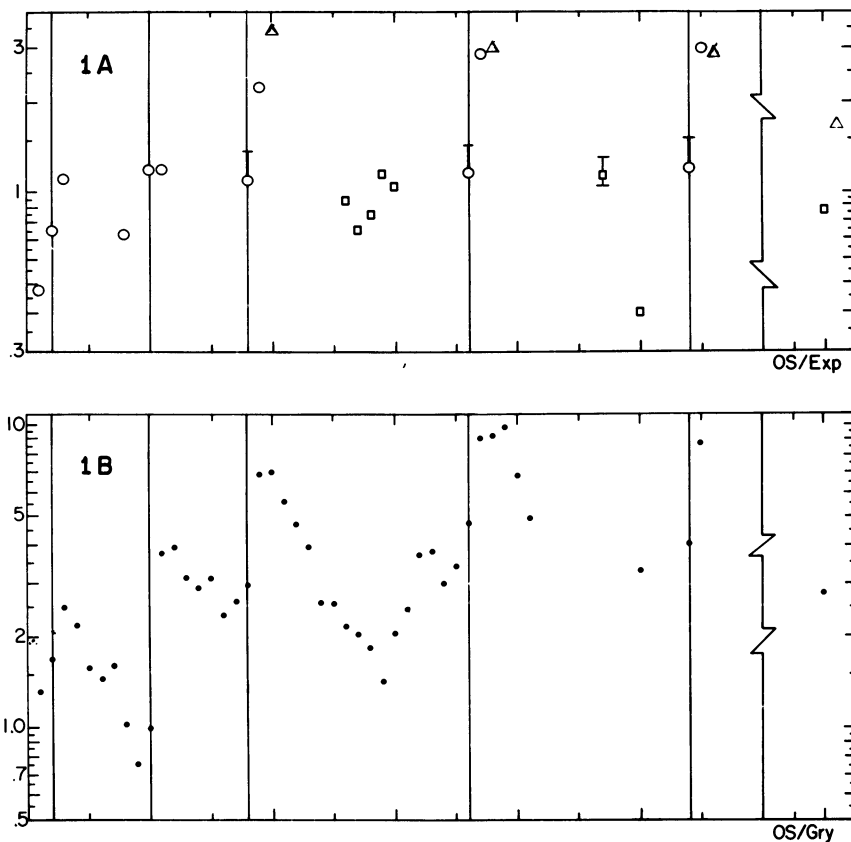
In this paper the reaction



will be considered.  $M$  may be an atom, or it may be a molecule, in which case the problem of fragmentive ionization will have to be considered;  $e^-$  represents an electron with kinetic energy greater than the ionization potential of  $M$ . The rate of this reaction is given by

$$I(M^+) = i(e^-)n(M)l\sigma(E) \quad (2)$$

where  $I$  and  $i$  are the respective currents,  $n(M)$  is the number density of  $M$  in the volume of length  $l$  traversed by the electron beam;  $\sigma$  is a constant characteristic of  $M$ , the energy  $E$  of the impacting electrons, and the particular process being considered—*i.e.*, ionization to a particular state or total ionization. The quantity  $\sigma$  has the units of area and is called a cross section.



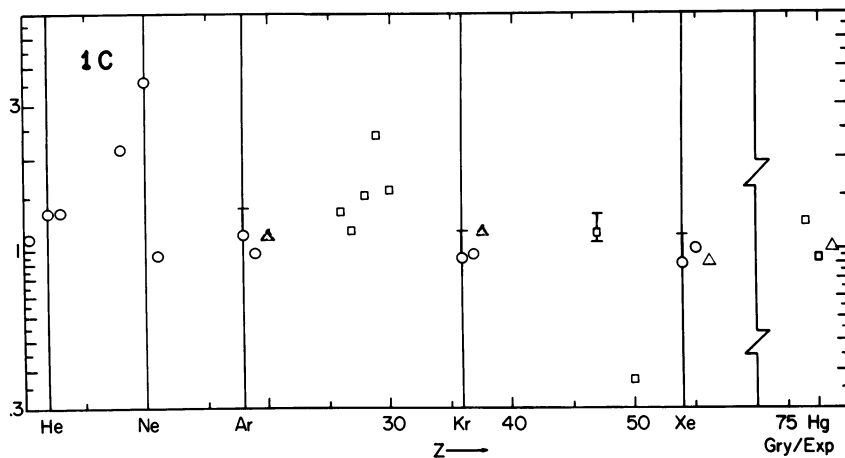
Reaction 1 is of interest in studies of stellar atmospheres, the solar corona, radiation damage, plasmas and nuclear fusion, and in mass spectrometry. The special interest of this paper is the study of high temperature systems where the partial pressure  $P$  of species  $M$  is given by

$$P = I(M^+)T/S\sigma\gamma$$

where  $T$  is the absolute temperature of the crucible or reactor,  $S$  is a constant of the mass spectrometer which is assumed constant with change of mass, and  $\gamma$  is the relative gain of a secondary electron multiplier, if used.

Many species of interest have been observed only by optical and/or mass spectrometry; it is not possible to obtain an independent measure of their cross sections. Estimates of the cross section, or of relative cross sections therefore form an important part of the calculation of thermodynamic properties using the absolute entropy (Third Law) method.

In certain cases, it may be possible to compare Second and Third Law results to obtain cross sections. In addition, particularly where the



Journal of Chemical Physics

**Figure 1.** *a.* Logarithm [(Otvos-Stevenson cross section)/(experimental cross section for single ionization  $\times 3$ )] vs. atomic number  $Z$ .; *b.* Logarithm [(OS cross section)/classical cross section Table I)] vs.  $Z$ .; and *c.* Logarithm [(classical cross section)/(experimental cross section)] vs.  $Z$ .

*Uncertainties in the measured cross sections are not indicated on the figure, but often are large; see especially Kieffer and Dunn (14)*

ratio of intensities varies greatly with temperature, it is possible to combine mass spectrometric measurements with mass flow measurements (1, 2, 3, 4, 6, 7, 8, 20, 24) to deduce relative cross sections. These measurements have proved valuable, but often are limited in that they involve taking small differences between large, uncertain quantities.

The work of Otvos and Stevenson (22) has proved useful in providing cross sections for atoms. These authors suggest also that molecular cross sections be taken equal to the cross sections of the constituent atoms (additivity rule). As our sophistication in mass spectrometry has grown, and as we demand more accurate answers of the technique, the Otvos-Stevenson calculations have been subjected to increasingly more careful experimental verification as is critically reviewed elsewhere (14, 27). Deviations from experiment have been found. The results are shown in Figure 1A (27), where the logarithm of OS to experimental cross section (60 e. v.) is plotted for the atoms as a function of atomic number,  $Z$ . For the most reliable data available—hydrogen, the rare gases, the alkali metals, and the alkaline earth atoms—there is a significant scatter.

Of some interest is the point for Sn ( $Z = 50$ ), for which the calculated cross section is small. The same is true when the calculated cross section for Ge ( $Z = 32$ ) is compared with more recent results. In both of these cases an assumed secondary electron multiplier gain has been used; this may be a significant source of error.

Recently, a theory developed by Gryzinski (10) on classical principles has been used to give detailed predictions of cross sections as a function of impacting electron energy. A summary of the literature as well as new calculations for many of the atoms are given in the preceding paper of this series (27). The theory states that the cross section  $\sigma_j$  for ionization of an electron from the  $j$ th shell is given by

$$\sigma_j = 6.56 \times 10^{-14} (N_j/U_j^2) g(X) \text{ sq. cm.} \quad (3)$$

where  $N_j$  is the number of electrons in the shell,  $U_j$  is the binding energy of the shell in e. v., often taken to be the ionization potential,  $X$  is the energy  $E$  of the impacting electron divided by  $U_j$ , and  $g(X)$  gives the dependence of cross section on  $E$ . The theory states that the shapes of the ionization efficiency curves for all shells are identical when plotted as a function of  $X$ ; maxima of the curves are at  $E \approx 3.7 U_j$ .

The implication of this theory for the mass spectrometrist is great. Cross sections can be predicted if the ionization potential as well as the inner shell electron energies are known. The shape of the ionization efficiency curve can be predicted and variations of cross section with electron energy taken into account.

This paper reviews the application of Equation 3 to atoms, including a comparison of the results from it to those of Otvos and Stevenson. We then make calculations for molecules in order to examine the additivity rule.

### *Results for Atoms*

Of some interest is the agreement between the magnitude (in absolute units) and the shape of ionization efficiency curves. For the heavier alkali metals, the experimental ionization efficiency curve shows two maxima in the region 20–100 e. v., as seen for potassium in Figure 2 (18). The lower three dashed lines show the contributions to the cross section calculated for the  $4s^1$ ,  $3p^6$ , and  $3s^2$  shells. The energy used for each shell is shown in parentheses. The cross sections at the maxima of these three curves are in the ratio indicated by Equation 3. For impacting electrons with energies of  $\sim 300$  e. v. or more, the calculations indicate that the cross section from the  $3p^6$  shell exceeds that from the valence electron. The cross section for single ionization at high electron energies, therefore, should not follow the Bethe equation.

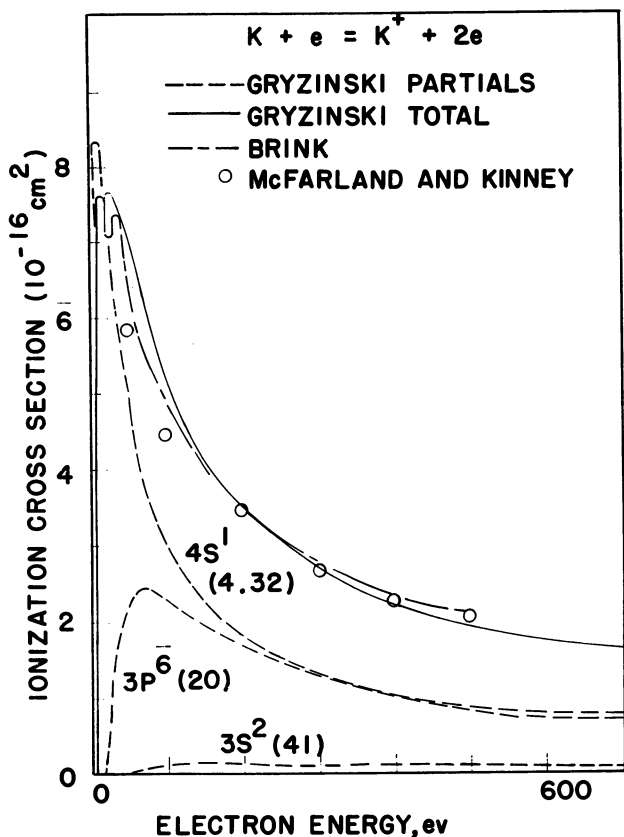


Figure 2. Electron impact cross section for single ionization of potassium as a function of impacting electron energy. The experimental data of Brink, McFarland, and Kinney, as well as the calculated contribution from each of the electronic shells, are shown. (See Ref. 18)

The sum of the partial cross sections is shown by the solid line. While not in perfect agreement, it does give the double maximum observed experimentally. (Note also that the exact shape of the experimental curve is difficult to determine.) Similar results are obtained for the formation of the other alkali metals ions (18) and for doubly charged cesium ion (19), for example. This is the first time that such detailed agreement with experimental cross sections has been obtained. In addition, when contributions from shells with  $U_j$  greater than the ionization potential are considered, Equation 3 replicates the old rule of thumb that the maximum of an ionization efficiency curve lies at 3 to 6 times the onset energy.

A comparison of theory with experiment for all the elements where data are available is given in Figure 1C. The agreement is generally good, except for oxygen (not shown), nitrogen, and neon, where the calculated values are roughly a factor of two high. Gryzinski believes that this may be attributed to an error in the electronic energies of the atoms (11). For Ge and Sn, the calculated values again seem to be quite low. On the whole, the agreement with experiment is significantly better than previously available.

Some of the details of the calculations are given in Table I. For the "easy cases," in general those at the extreme left or right of the Periodic Table, the bulk of the contribution to the total cross section at 60 e. v.

**Table I. Calculation of Cross Sections for 60 e.v. Electrons by Equation 3**

Z		Shell	$U_j(e. v.)^a$	$\sigma_j(A^2)$	$\sigma$
<i>Easy Cases</i>					
1	H	1s <sup>1</sup>	13.6	0.76	0.76
3	Li	2s <sup>1</sup>	5.4	3.3	
		1s <sup>2</sup>	55.0	—	3.3
4	Be	2s <sup>2</sup>	9.3	2.9	2.9
8	O	2p <sub>4</sub>	13.6	3.0	
		2s <sup>2</sup>	32.0	0.2	3.2
9	F	2p <sup>5</sup>	17.4	2.3	
		2s <sup>2</sup>	40.0	0.1	2.4
54	Xe	5p <sup>6</sup>	12.1	5.6	
		5s <sup>2</sup>	25.0	0.3	5.9
<i>Hard Cases</i>					
29	Cu	4s <sup>1</sup>	7.7	2.0	
		3d <sup>10</sup>	11.0	11.0	13.0
	alternate	(3d <sup>10</sup>	10.0	12.6	14.6)
50	Sn	5s <sup>2</sup>	7.3	4.3	
		5p <sup>2</sup>	8.0	3.6	
		4d <sup>10</sup>	10 or 20?	12.6 or 3.4?	
			Total,	20.5 or 11.3?	

<sup>a</sup> From Moore (19) and Slater (24).

comes from the outermost shell, for which the experimentally known ionization potential (21) is used for  $U_j$ . The transition metal atoms are "hard cases." Ignoring that the implicit assumption of Russell-Saunders (*L-S*) coupling may not be valid for the heavier atoms, it is seen that the major contribution to the cross section comes from inner shell electrons. For these, the binding energies (26) are only crudely known and lead to significant uncertainty in the calculated cross sections, as shown. These attempts to apply the present theory clearly indicate a need for further knowledge about atomic structure and levels.

**Comparison with the OS Calculations**

The OS correlation has been discussed previously (9) under the assumptions that the Born approximation and the Bethe equation are valid—*i.e.*, that the impacting electrons have high energy. Under these conditions, the oscillator strength (*f*-value) “sum rules” that apply to photon-induced transitions hold also for electron impact. This led to the conclusion that much of the total cross section for the alkali metals was caused by inner shell ionization. As discussed above for potassium, the Gryzinski theory gives a much more reasonable picture, including that, at higher electron energies, the inner shell cross section does start to exceed that for the valence electron.

Figure 1B shows the logarithm of the ratio of the OS to the present cross sections as a function of atomic number. Discontinuities and/or changes in slope occur, for the most part when subshells or shells are filled. Two explanations may be offered for these observations. First, OS assume that, for ionization from the *j*th shell,  $\sigma_j$  is proportional to the average square radius  $\langle r_j^2 \rangle$  which is in turn proportional to the diamagnetic susceptibility. The formula they use is

$$\langle r_j^2 \rangle \propto n^{*4} (Z - s)^2 \left\{ 1 + 3/2 \left[ 1 - \frac{1(1+1) - 1/3}{n^{*2}} \right] \right\} \quad (4)$$

where  $n^*$  is the effective quantum number,  $(Z - s)$  the effective nuclear charge, and  $l$  the orbital angular momentum quantum number. The first two of these quantities are taken from a paper by Slater (25) who estimates them on the basis of certain approximate wave functions. On the basis of these wave functions, Slater deduced that

$$\langle r_j^2 \rangle \propto n^{*2} (n^* + \frac{1}{2}) (n^* + 1) (Z - s)^2. \quad (5)$$

The advantage of Equation 4 is that it gives a break when the *s* subshells are filled. Equation 5 does not do this. Table II shows that use of Equation 5 with the Slater values for  $n^*$  and  $(Z - s)$  leads to incorrect diamagnetic susceptibilities. The good agreement for the cross sections of the rare gases shown in Figure 1A is attributed to the use of Equation 4 and not a correlation with the diamagnetic susceptibility nor the Slater values for  $\Sigma \langle r_j^2 \rangle$ .

It is interesting to examine the functional relation between the OS and the present calculations. The present calculations assume that  $\sigma_j$  for a single electron is roughly proportional to  $U_j^{2-}$ . In turn, Slater (25) gives that  $U_j^{2-} = n^{*4} (Z - s)^4$ . Substituting into Equation 4 and ignoring the term in the brackets gives

$$\frac{\sigma_j(OS)}{\sigma_j} \approx (Z - s)^2.$$

In addition, the present calculations use empirical values for  $U_j$ . It is likely that use of these corresponds in a purely theoretical calculation to much more sophisticated wave functions than those given by Slater's rules.

**Table II. Diamagnetic Susceptibilities, ( $\Sigma \langle r_j^2 \rangle$ )**

	Slater <sup>a</sup> (Equation 5)	Observed (15)	OS (Equation 4)
He	2.1	1.9	(2.1) <sup>b</sup>
Ne	7.1	6.6	5.4
Ar	23.0	18.0	36.0
Kr	—	29.0	76.0

<sup>a</sup> From J. C. Slater (25).

<sup>b</sup> The OS (22) values for  $\Sigma \langle r_j^2 \rangle$  were normalized to give 2.1 for He.

### Calculations for Molecules

Otvos and Stevenson have suggested that molecular ionization cross sections are equal to the sum of the atomic cross sections. This is called the Additivity Rule, and most workers have used it for lack of something better. The experimental data now becoming available (3, 4, 6, 7, 8, 14), sometimes for rather diverse electron energies, indicate discrepancies from this rule.

The term  $N_j$  in the numerator of Equation 3 suggests that there should be an additivity. The  $U_j^{-2}$  indicates that there will be deviations from the additivity rule because of the shifts in binding energy resulting from the formation of the chemical bond. Table III shows the details of calculations for some simple diatomics, for which the atomic energy levels and cross sections have been given in Table I. Table IV summarizes the results and gives the ratio of the molecular cross section to the sum of those for the atoms. A number of different cases are treated, including those where the last electrons added in a molecular orbital picture go into bonding, or into antibonding orbitals, an isoelectronic series going from homonuclear  $C_2$  to the highly ionic LiF, and formation of free radicals from elements with relatively high ionization potentials.

For the hydrogen molecule, the answer is clear cut, and in excellent agreement with experiment. The ionization potential increases, and the molecular cross section is smaller than the sum of those for the atoms. For  $C_2$ , while the molecular ionization potential is higher than that of the atom, the binding energy (24) of the next lower shell apparently is significantly lowered, and the ratio is predicted to be unity.

An interesting case is LiF, where apparently the transfer of electron density from the Li to the F increases the shielding of the  $p$  electrons,

**Table III. Calculation of Molecular Cross Sections for 60 e.v. Electrons**

<i>n</i>	<i>Species</i>	<i>Shell</i>	$U_j^a$ <i>e. v.</i>	$\sigma_j$ $A^2$	$\sigma$ <i>Total</i> $A^2$
2	H <sub>2</sub>	$\sigma^2$	15.4	1.18	1.18
8	C <sub>2</sub>	$\pi^4$	12.0	3.76	
		$\sigma^2$	15.0	1.26	
8	BeO	$\sigma^2$	23.0	0.5	5.5
		$\pi^4$	13 ± 0.5	3.24	
		$\sigma^2$	14.0	1.36	
		$\sigma^2$	20 ± 5	0.8 ± 0.4	4.6
8	LiF	$\pi^4$	11.2	4.26	
		$\sigma^2$	12.0	1.88	
		$\sigma^2$	20 ± 5	0.8 ± 0.4	6.9
9	BeF	$\sigma^1$	9.0	1.53	
		$\pi^4$	13.1	3.24	
		$\sigma^2$	15.7	1.14	
		$\sigma^2$	40.0	0.08	7.0
10	N <sub>2</sub>	$\sigma^2$	15.6	1.16	
		$\pi^4$	16.6	2.06	
		$\sigma^2$	19.0	0.74	
		$\sigma^2$	30.0	0.26	4.2
11	NO	$\pi^1$	9.3	1.46	
		$\pi^4$	15.1	2.48	
		$\sigma^2$	16.8	1.00	
		2 × $\sigma^2$	—	0.55	5.5
12	O <sub>2</sub>	$\pi^2$	12.1	1.86	
		$\pi^4$	15.8	2.26	
		$\sigma^2$	17.8	0.88	
		2 × $\sigma^2$	32.0	0.36	5.4

<sup>a</sup> The molecular energy levels were taken from or estimated from results given by Robins (24). (See Refs. 12, 13, 23, 37).

**Table IV. Total Ionization Cross Sections, 60 e.v.**

<i>XY</i>	<i>n</i>	$\sigma(XY) A^2$		$\sigma(XY)/[\sigma(X) + \sigma(Y)]$	
		<i>calc.</i>	<i>expt.</i> <sup>a</sup>	<i>calc.</i>	<i>expt.</i>
H <sub>2</sub>	2	1.2	1.1	0.8	0.75
C <sub>2</sub>	8	5.5		1.0	
BeO	8	4.6		0.9	
LiF	8	6.9		1.2	
BeF	9	7.0		1.3	
N <sub>2</sub>	10	4.2 <sup>b</sup>	2.4	0.9	0.9
NO	11	5.5	2.8	1.0	0.9
O <sub>2</sub>	12	5.4	2.5	0.8	0.7

<sup>a</sup> From Kieffer and Dunn (14).

<sup>b</sup>  $\sigma$  for N and O atoms also high by ~80%.

lowers the binding energy of the F  $2p^5$  electrons and consequently increases the calculated cross section. Alternately, the cross section for a highly ionic molecule may be regarded as a weighted average of the cross sections for M, M<sup>+</sup>, X, and X<sup>-</sup>. This molecule illustrates also some of the other problems involved with molecular cross sections. Experimentally (3), the fragment ions are more abundant than the parent, and seem to be formed with kinetic energy so that their intensities are difficult to measure accurately.

For N<sub>2</sub>, NO, and O<sub>2</sub> the calculated ratios are in substantial agreement with experiment, particularly since there may be a large error in the measured cross sections for the atoms. For all three molecules, it is significant that the largest single contribution to the cross section comes from an inner shell—for which energies are not easily determined.

The range of calculated ratios is 0.8 to 1.3, or about  $\pm 30\%$ . This increase in information over the simple additivity rule was made possible by a great deal of information about the electronic energy levels.

Absolute cross sections are known (14) for N<sub>2</sub>, NO, and O<sub>2</sub> as shown in Table IV. In all three cases, the calculated cross sections are about 80% higher than the experimental. No explanation for this is apparent; it may be significant that the calculated atomic cross sections for nitrogen and oxygen as well as neon also are higher than the experimental.

### **Conclusion**

The present calculations for the atoms permit calculation of the contribution from each electronic shell as well as the variation of cross section with electron energy. They are substantially better than those previously available, although significant deviations from experiment seem to exist for oxygen, nitrogen, neon, and possibly germanium. This improvement, as well as the systematic, and often large, differences from the Otvos and Stevenson results are attributed to a difference in the form of the basic equation used and the use of empirical binding energies rather than the equivalent of approximate wave functions.

For molecules, the deviations from the additivity rule seem to be adequately predicted. The largest deviation so far predicted is 30%. For this presumable increase in accuracy of the cross section, a large increase in information for the calculations is needed.

### **Comment**

There exists controversy over the Gryzinski theory and doubt about its validity. The following comment by a reviewer of this paper, indicates some of the criticism of the theory:

The "Gryzinski theory" (really a slightly, and I might add incorrectly, modified classical theory due to J. J. Thompson) is fundamentally an incorrect theory. It does not give the correct high energy behavior or low energy behavior or position of the peak cross section for ionization. This being the case one cannot a priori expect the results using this theory to be more accurate than any other non quantum approximation (or guess?). The fact that in some cases this type of calculation gives apparently better results than other estimates for ionization cross sections is certainly fortuitous and one cannot conclude that this method will then give better results in cases where the cross section is unknown.

Recently, an important set of revised OS calculations has appeared (17) as have experimental cross sections for certain key atoms. The new calculations and the Gryzinski calculations are in agreement except as regards contributions to  $\sigma$  from the  $2p$  and the various  $d$  and  $f$  shells. A detailed discussion and comparison with experiment are given by Lin and Stafford (16).

### *Acknowledgments*

The permission of R. H. McFarland to reproduce Figure 2 is gratefully acknowledged. The work would not have been possible without support from the U. S. Atomic Energy Commission, COO-1147-14.

### *Literature Cited*

- (1) Akishin, P. A., Gorokhov, L. N., Sidorov, L. N., *Dokl. Akad. Nauk SSSR* **135**, 113 (1960).
- (2) Akishin, P. A., Gorokhov, L. N., Sidorov, L. N., *Dokl. Akad. Nauk SSSR* **151**, 163 (1963).
- (3) Berkowitz, J., Tasman, H. A., Chupka, W. A., *J. Chem. Phys.* **36**, 2170 (1962).
- (4) Cater, E. D., Thorn, R. J., *J. Chem. Phys.* **44**, 1342 (1966).
- (5) Chupka, W. A., Inghram, M. G., *J. Phys. Chem.* **59**, 100 (1955).
- (6) Colin, R., Goldfinger, P., Jeunehomme, M., Ann. Summ. Rept. No. 2, March 1960 to February 1961, Contract No. AF 61 (052) 225, WADC, Univ. of Brussels, Brussels, Belgium.
- (7) Colin, R., Goldfinger, P., Jeunehomme, M., Repts. AFML-TR-64-331 and AFML-TR-65-1, Univ. of Brussels, Brussels, Belgium.
- (8) Colin, R., Goldfinger, P., Jeunehomme, M., *Trans. Far. Soc.* **59**, 2851 (1963).
- (9) Cooper, J. L., Jr., Pressley, G. A., Jr., Stafford, F. E., *J. Chem. Phys.* **44**, 3946 (1966).
- (10) Gryzinski, M., *Phys. Rev.* **138**, A336 (1965).
- (11) Gryzinski, M. (private communication, 1966).
- (12) Hildenbrand, D. L., Murad, E., *J. Chem. Phys.* **44**, 1524 (1966).
- (13) Hildenbrand, D. L., Murad, E., *J. Chem. Phys.* **43**, 1400 (1965).
- (14) Kieffer, L. J., Dunn, G. H., *Rev. Mod. Phys.* **38**, 1 (1966).
- (15) Leverenz, H. W., Periodic Chart of the Elements, Radio Corporation of America, Princeton, N. J.

- (16) Lin, S. S., Stafford, F. E., *J. Chem. Phys.* (to be published in March or April 1968).
- (17) Mann, J. B., *J. Chem. Phys.* **46**, 1647 (1967).
- (18) McFarland, R. H., *Phys. Rev.* **139**, A40 (1965).
- (19) McFarland, R. H., *Phys. Rev.* **159**, 20 (1967).
- (20) Milne, T. A., *J. Chem. Phys.* **28**, 717 (1958).
- (21) Moore, C. E., *U. S. Natl. Bur. Std. Circ.* **467**, Washington, D. C.
- (22) Otvos, J. W., Stevenson, D. P., *J. Am. Chem. Soc.* **78**, 546 (1956).
- (23) Price, W. C., Passmore, T. R., Roessler, D. M., *Disc. Far. Soc.* **35**, 201 (1963).
- (24) Robinson, D. W., *J. Phys. Chem.* **69**, 3357 (1965).
- (25) Slater, J. C., *Phys. Rev.* **36**, 57 (1930).
- (26) Slater, J. C., *Phys. Rev.* **98**, 1039 (1955).
- (27) Stafford, F. E., *J. Chem. Phys.* **45**, 859 (1966).

RECEIVED October 5, 1966.

# Automated Data Acquisition and Treatment in Inorganic Mass Spectroscopy

ROBERT J. LOYD and FRED E. STAFFORD

Department of Chemistry and the Materials Research Center,  
Northwestern University, Evanston, Ill.

*Apparatus for various aspects of digital data acquisition and handling are reviewed and reported. These include systems for rapid data throughput, as in high resolution mass spectrometry of gas chromatograph effluents, as well as for systems with less stringent requirements. Data handling, reduction time, and errors are greatly reduced; running time is shortened, and/or the quality of the results is increased in terms of their precision, detail, rapid availability, and variety of possibly informative presentations.*

The capacity of a mass spectrometer to produce information is far greater than that of an individual to receive or reduce it. The need for more detailed and precise results demands that this capacity be used. The capacity for rapid data output must be used when sample size and corrosiveness limit the duration of the experiment. Rapid reduction of data is particularly important in inorganic work where long sample preparation and experimental procedures are involved—the results must be available during the run in order that unforeseen problems be identified and resolved before the experiment is terminated.

For these reasons automated data handling techniques, including direct digital acquisition, computer treatment of data, and on-line computer control of the mass spectrometer are especially attractive. Since Fortran procedures for computation are established and readily accessible, the limiting step is often the acquisition of information directly in computer compatible form. This will be the subject of the present paper.

## *Techniques*

The techniques can be divided into two categories—those for rapid accumulation of large volumes of information, as in high resolution

( $m/\Delta m \sim 10^4 - 10^5$ ) analyses, especially of chromatograph effluents, and those for low flow rates of information.

**High Data Volume Techniques.** Rapid data accumulation and handling techniques are receiving considerable attention from the various mass spectrometer manufacturers, especially for high resolution organic applications. For the spectrometer, spectra with resolution of  $m/\Delta m \sim 10^4$  show that the output of the secondary electron multiplier can be recorded rapidly in analog form directly on magnetic tape (13). The scan rates are fast enough to be usable for gas chromatograph effluent analysis. Equipment must be available for subsequent conversion of the analog tape to computer language.

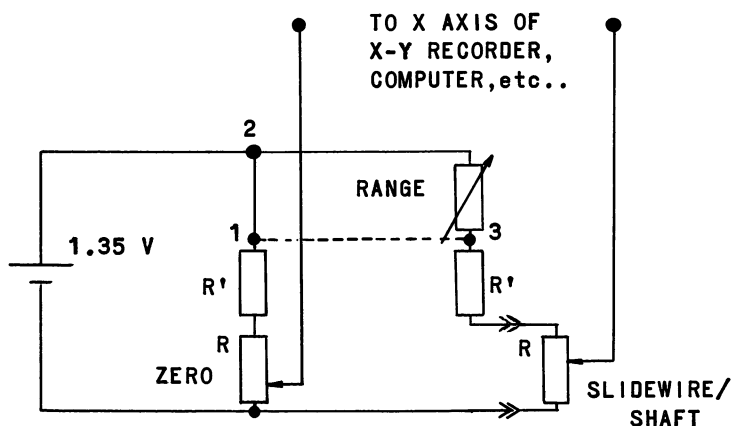


*Figure 1. Retransmitting slidewire circuit used to encode shaft positions. Breaking connection 1-2 and connecting 1-3 may give a more convenient zeroing arrangement*

The mass spectrograph offers the possibility of integrating all of the ion intensities simultaneously on the plate and of translating the plate parallel to the slit to obtain a time-resolved mass spectrum. The data handling problem becomes one of calibrating and rapidly digitizing the vast amount of information (about  $10^6$  readings of optical density per spectrum produced by the microdensitometer used to read the plates), locating the peaks, identifying overlapped (blended) peaks, and computing the masses to one part in about  $10^5$ . Substantial progress has been reported in automating microdensitometers, in writing computer programs, and in devising particularly informative ways to present the information (1, 2, 3, 5, 7, 8, 11, 13, 16, 18, 20). The substantial capital investment involved limits the availability of such facilities.

**Lower Volume Techniques.** In many other experiments, the available ion intensities are so small that measurements must be made over longer

periods of time to obtain usable signal-to-noise ratio. While fast for human acquisition and treatment, this information flow still may be handled easily by apparatus that is becoming readily available to every laboratory.

**Shaft Encoding: Ionization Efficiency Curves.** Various applications require encoding of a shaft position. While digital shaft encoders are available, they are usually prohibitive in price. A simple solution which need not sacrifice accuracy is to use a retransmitting slide wire and the circuit shown in Figure 1.

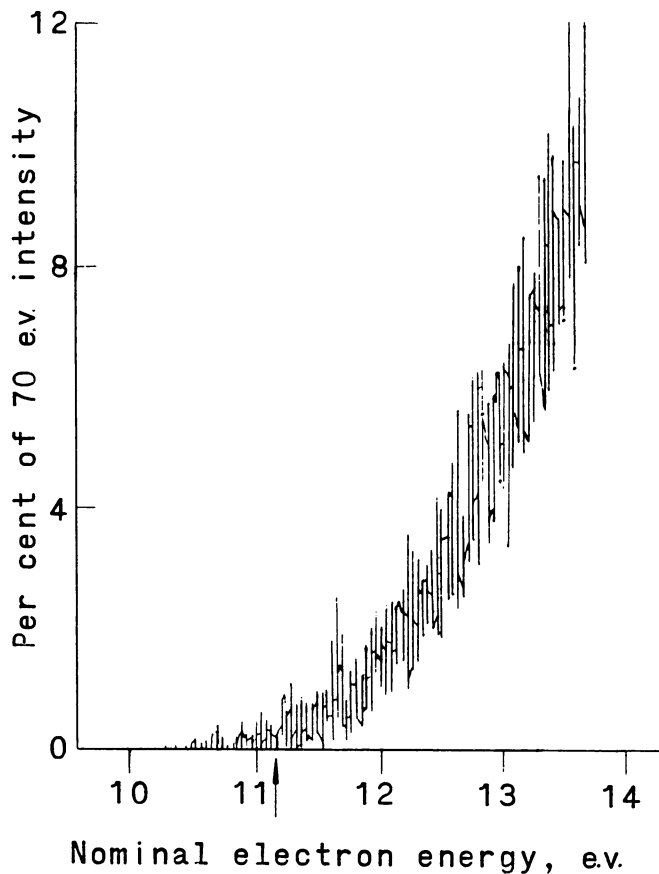
This apparatus will generate an analog signal proportional to the position of any control shaft. Such a circuit has been used in our laboratory for the past two years to record ionization efficiency curves. The range and zero controls were selected to permit any 10-volt segment of ionizing electron energy to give full scale deflection on the X-axis of a 10 millivolt X-Y recorder. The time constant of the entire circuit, comprising the electron voltage regulator, detector, and recorder was large enough that a small timing motor (A. W. Haydon Co., Waterbury, Conn., 1/6 or 1/30 r.p.m.) was used to generate a reproducible sweep. With moderately intense ion currents, appearance potentials could be reproduced to 0.04 e. v. For a weak ion current of about 40 ions per second full scale, a recording is shown in Figure 2. It was produced in about 20 minutes of easy work compared with a hard hour for manual processing.

A buffer memory, a time averaging computer (that of Northern Scientific Corp., Madison, Wisc., is particularly suitable because of facile memory addressing), or a small control computer might be substituted for the X-Y recorder. Such units can provide in-place time averaging as well as input for a large, central computer. An on-line computer for automated determination of appearance potentials also is reported (12).

**Direct Recording of Low Resolution Spectra.** Apparatus is available commercially from Non Linear Systems (Del Mar, Calif.) (19). During a low resolution scan, both the varying ion-accelerating voltage and the ion intensity are digitized and recorded. The mass spectrum is calculated by computer. Mass accuracy of better than 1/4 a.m.u. at  $m/e$  250 is reported (10). For magnetic scanning instruments, both Nuclide Corp. (State College, Pa.) and Varian Associates (Palo Alto, Calif.) have announced new, high accuracy gaussmeters. Of additional interest is using two Hall effect probes in series such that a signal proportional to the magnetic field squared, and linear with mass is produced.

**Averaging and Digitization of Ion Currents.** In many aspects of the mass spectrometry of high temperature systems or of reactive intermediates, the ion intensities are such that the current at each peak must be averaged over a period of time during which the spectrometer settings

must remain constant. An integrating digital voltmeter (DVM) (Vidar Corp., Mountainview, Calif., Model 500) could not be used to measure the electrometer output directly because the integration period of 20 msec. is too short for the small ion currents available. Consequently the system of Figure 3 was built. The integrator circuit is shown in Figure 4; using the high quality operational amplifier makes it easy to construct.



Courtesy S. M. Schildcrout

*Figure 2. Automatically recorded ionization efficiency curve for the metastable process  $\text{Ni}(\text{CO})_2^+ \rightarrow \text{NiCO}^+ + \text{CO}$ : ion intensity vs. ionizing electron energy in e.v. Scan rate, 1/3 volt per minute; maximum ion intensity shown corresponds to about 40 ions per second. The graininess of the low resistance retransmitting slide wire needed to match the recorder available causes the curve to look as if it is composed of a series of vertical lines*

The precision timer is a preset counter set to count the 60-hertz line frequency for 1/4, 1/2, 1, or 2 minutes.

Several advantages accrue from this apparatus. The uniformity of recording the intensities and of time averaging are significantly improved over averaging by eye. Data reduction is less tedious, and the time required is reduced by about 25%.

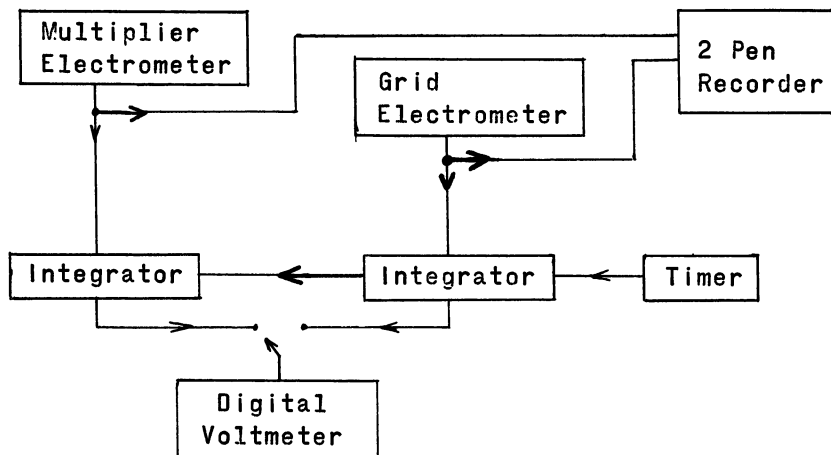


Figure 3. Direct digital data output system. The timer is a preset counter that activates the relays shown in Figure 4. Line frequency is counted

Manual transcription of the data, with its consequent delays and errors, was eliminated by encoding the various spectrometer controls, automatically scanning the various data stations, and writing the information with a 12-line parallel entry tape perforator. The mechanics of the Computing Center now make it desirable to use one of the incremental magnetic recorders that are becoming available at low cost.

The system comprises the following:

- (1) Digital encoding of such identification material as mass or date.
- (2) Digital encoding of such instrument settings as input resistor, electrometer ranges, and emission current as well as time.
- (3) Analog-to-digital conversion of thermocouple readings, electrometer output, shaft encoder output.
- (4) Scanning and "writing" the preceding sources of information with the desired amount of operator intervention.

The identification material is entered directly onto the tape by means of a selector switch and 12 banks of four-pole wafer switches providing binary coded decimal (BCD) output. Instrument settings also are encoded simply by coupling the appropriate control shafts to four-pole wafer switches that produce signals corresponding to 0 through 9 in BCD

output. Analog-to-digital conversion in all cases is accomplished with the DVM.

The heart of the system is the scanner which presents each of the analog signals to the DVM in unvarying sequence. A possible system involving a commercial scanner, and an IBM (Poughkeepsie, N. Y.) card punch is described elsewhere (4). The present unit was built to have facile entry of special control information (Error, End of Data Subset, etc.) and a series of interlocks to minimize operator error. The operation of this unit is shown in Table I. The scanner is activated by Control *a*. This causes a special punch on the tape which the computer is programmed to interpret as "start new subset of data." Three such punches are coded to mean "start new page or new set of data," and five such punches mean "end of run." Pressing this button also readies the scanner to start Cycle I.

The first step of the cycle is to read "preset" information set manually on the 12 wafer switches. Such information includes the ion mass, electron energy, etc. A selector switch on the perforator chooses between the "preset" or the "external" information and is interlocked so that step IA can be performed only if it is in the correct position. Similarly, IB and IC are interlocked with the "external" position.

In the "external" position, three channels accept output from a digital clock; four more channels accept information from the encoders for the secondary electron multiplier output resistance, multiplier electrometer range setting, "grid" (unmultiplied ion current) electrometer range setting, and ionizing electron emission regulator setting. An eighth channel accepts the digital voltmeter (DVM) range, and four more accept the DVM reading itself. The DVM polarity signal is not used.

In position IB, the DVM reads either a thermocouple attached to a Knudsen cell, an automatic optical pyrometer output if available, or a shaft encoder (Figure 1) attached to the slide wire of a manual optical pyrometer.

The scanner is advanced to position IC. The operator then measures the ion current using the integrators. If visual observation of the strip chart recording indicates that the measurement is satisfactory, Control *c* (perform Cycle II) is activated and the two integrator outputs recorded. This cycle may be repeated as many times as desired.

Should an error be made, Control *d* causes a punch which is programmed to make the computer disregard the preceding two frames of information corresponding to the preceding steps II.1 and II.2.

When the appropriate number of readings has been taken, Control *a* is pushed one, three, or five times, and the scanner is set to accept information for the next mass peak, the next set of peaks, or to end the run respectively.

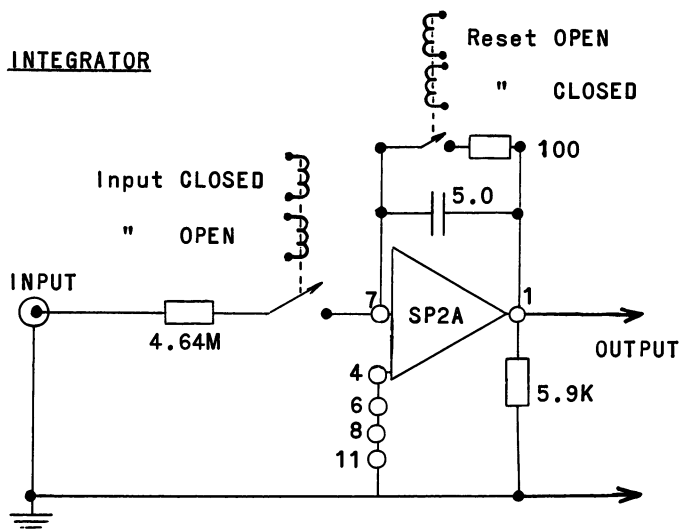


Figure 4. Integrator circuit simply constructed using a high quality operational amplifier. This circuit affords more precision than the pen recorder. The operational amplifier is a Philbrick Researches, Inc. (Dedham, Mass.), Model SP-2A; a Keithley Instruments, Inc. (Cleveland, Ohio), Model 300 also seems suitable

Table I. Operation of the Scanner<sup>a</sup> for Direct Tape Output

#### Cycle I

- A. Record "preset" information (interlocked<sup>b</sup>).
- B. Read with DVM and record "thermocouple" station.
- C. Activate Cycle II.

#### Cycle II

1. (a) Read with DVM and (b) print integrator 1 output.
2. (a) Read with DVM and (b) print integrator 2 output.
3. Hold.

#### Controls

- a. Go to Cycle I, A.
- b. Advance in Cycle I.
- c. Perform Cycle II.
- d. Error.

<sup>a</sup> The scanner comprises two counting rings—Silicon Controlled Rectifiers. Cycle I can be initiated only if the perforator interlock is activated, and if Control *a* is pushed. It advances one step at a time. Cycle II has five steps and once activated is advanced through all steps back to "Hold" by an R-C timing network. Additional steps might be added to permit "shutter position," electron energy, gaussmeter reading, etc. to be recorded. Clare Corp. HGSM-1016, bistable, single pole mercury relays are used for switching.

<sup>b</sup> See text.

<sup>c</sup> Circuits may be obtained from "Motorola Semiconductor Circuits Manual," Motorola, Inc., Phoenix, Arizona, 1964.

Each of the time steps II.1 and II.2 are repeated, the five channels of information representing the encoder positions and the DVM range are recorded. The computer is programmed to scan these and print out a special signal if any one should change within a particular subset of data. This has proved useful in spotting operator or recorder errors.

As a result of this system, almost all manual treatment is eliminated and the CDC 3400 computer reduces in one minute of running time data that previously required 100 man hours simply to obtain a table of ion intensities. These intensities are provided in tabular form and on punched cards, and must be compared with the original strip chart recording because of various instrumental and operator errors. (Such comparison is relatively fast but need not be done immediately if rough results are needed during a run.) The cards are corrected and reprocessed to make any necessary calculations and to present the results in a variety of potentially informative ways.

Apart from the obvious time saving and the more thorough data treatment, there are other benefits. Operator fatigue is diminished, probably because of the rhythm imposed by the apparatus. There is a tendency to take more data. Most important, the results are available soon enough to be used for planning the remainder of the run and thus permit the worker to take a more efficient role in designing his experiment.

**On-line Computer Control.** The various steps as well as the decisions described above under Computer Compatible Output can and have (7, 8) been performed by a small, on-line control computer. Such an instrument would completely replace both the scanner and data-writer in the system described above, as well as any time averaging computer. New units with increasing memory capacity and decreasing cost are continually becoming available; their cost may be lower than that of the scanner/time averaging systems. In addition, they can provide buffer memory for a central, shared-time computer and can continually monitor pressure, inlet temperature, etc., for possibly abnormal conditions. Convenient programming permits any of a wide variety of sequences to be designed and interchanged as necessary. Fortran packages are available on many units.

In a system operating for isotopic analyses, only moderate resolution and a relatively narrow mass range are required (7, 8). A gauss meter is used to obtain a mass indication, and the computer is programmed to identify and record only the top of the peak. Electrometer ranges are computer controlled by means of relays. The computer also decides when enough scans over the spectrum have been made to obtain preselected reproducibility limits. The new high accuracy gauss meters mentioned previously may improve performance where wider mass ranges and/or accuracy are desired.

Programs and interfaces developed (6) to enable a small PDP computer (Digital Equipment Corp., Maynard, Mass.) to control a four-circle x-ray diffractometer should be readily adaptable to the mass spectrometer. The programs developed include those for preliminary scans to find significant intensities in a new system, and a routine to maximize intensity on the detector. Such a maximization routine is essential in cases, as implied elsewhere (17) for a simple inorganic system, where the gauss meter does not give a sufficiently accurate indication of mass.

A system for on-line computer controlled and processed determination of appearance potentials by the retarding potential difference (RPD) method has been reported (12). Data reduction using a shared time computer also is reported (9).

### **Conclusion**

Various systems with differing capabilities have been described. Using one or several of these has greatly improved the quality of information available from the mass spectrometer. Precision is increased by increased systematicity and by reducing human error. Precision is increased also by in-place time averaging. A large volume of significant information in various potentially informative forms is made available rapidly, and it becomes possible to more effectively study gas chromatograph effluent, and corrosive, unstable, or otherwise transitory systems. Results become available while the experiment is in progress, permitting the unexpected to be identified rapidly, and pertinent modifications of the experiment to be made.

### **Acknowledgments**

Much of the capital equipment for this project was acquired for us at minimum cost as "excess" or as gifts by Joseph Downey of the Northwestern University Purchasing Department. The extensive collaboration of James B. Bruce, John E. Fedyski, George A. Pressley, Jr., Sara J. Steck, Joan C. Kaye, and Pamela M. Bro were of great value. Vogelback Computing Center (Northwestern University) and its staff, especially J. Richard Walston, provided both aid and computing time. We gratefully appreciate support from the Northwestern University Materials Research Center, The University, and the Atomic Energy Commission, Document COO-1147-12.

### **Literature Cited**

- (1) Biemann, K., Bommer, P., Desiderio, D. M., McMurray, W. J., *Advan. Mass Spectrometry, Proc. Conf., 3rd, Paris, 1964*, 639 (Pub. 1966).

- (2) Biemann, K., Bommer, P., Desiderio, D. M., McMurray, W. J., *Tetrahedron Letters* 1964, 1725.
- (3) Biemann, K., Bommer, P., Desiderio, D. M., McMurray, W. J., *Tetrahedron Letters* 1965, 647.
- (4) Brown, E. R., Smith, D. E., DeFord, D. D., *Anal. Chem.* 38, 1130 (1966).
- (5) Burlingame, A. L., *Advan. Mass Spectrometry, Proc. Conf., 3rd, Paris, 1964*, 701 (Pub. 1966).
- (6) Busing, W. R., Woody, J. W., Roseberry, R. T. (private communication).
- (7) Cook, H. D., Barker, F. B., Hudgens, J. E., *5th Natl. Meeting Soc. Appl. Spectr., Chicago, June 13-17, 1966*, Abst. 202.
- (8) Cook, H. D., Barker, F. B., Hudgens, J. E., *Conf. Mass Spectr. Allied Topics, 13th, St. Louis, 1965*, p. 220.
- (9) Hogan, P. J., DeLaeter, R. J., *J. Sci. Inst.* 43, 662 (1966).
- (10) Howard, H. E., *Anal. Chem.* 38, 946 (1966).
- (11) Kohl, D. A., Dissertation, Indiana Univ., Dec., 1966, pp. 62 ff.
- (12) Martignoni, P., Morgan, R. L., Cason, C., *Rev. Sci. Inst.* 36, 1783 (1965).
- (13) McLafferty, F. W., *Science*, 151, 641 (1966).
- (14) McMurray, W. J., Greene, B. N., Lipsky, S. R., *Anal. Chem.* 38, 1194 (1966).
- (15) Merrit, Charles, Jr., Issenberg, I., Bazinet, M. L., Green, B. N., Merron, T. O., Murray, J. G., *Anal. Chem.* 37, 1037 (1965).
- (16) Olsen, R. W., *Conf. Mass Spectr. and Allied Topics, 13th, St. Louis, 1965*, p. 191.
- (17) Stafford, F. E., Pressley, G. A., Baylis, A. B., *ADVAN. CHEM. SER.* 72, 137 (1967).
- (18) Steinhaus, D. W., Engelman, R., Jr., Briscoe, W. L., *U. S. At. Energy Comm. LA 3100* (1964).
- (19) Thomason, E. M., *Anal. Chem.* 35, 2155 (1963).
- (20) Venkataraghavan, R., McLafferty, F. W., Amy, J. W., *Anal. Chem.* 39, 178, 278 (1967).

RECEIVED October 5, 1966.

# Mass Spectrometric Studies of Unstable Species

FRED E. STAFFORD, GEORGE A. PRESSLEY, JR.,  
and ANTHONY B. BAYLIS

Department of Chemistry and the Materials Research Center,  
Northwestern University, Evanston, Ill.

*Several aspects of the application of mass spectrometry to the study of unstable inorganic species, including boron hydrides and nickel tetracarbonyl, are presented: (1) molecular beam mass spectrometry: important effects of pyrolysis in the conventional ion source, which acts as a flow reactor, are shown for  $B_4H_{10}$ ,  $B_4H_8CO$ , and  $H_2BNH_3$ . (2) The detection and characterization of otherwise elusive reactive intermediates, including  $BH_3$ ,  $B_4H_8$ , and  $H_2BNH_2$ . (3) Measurement of the partial pressures of some of these intermediates and other species under equilibrium conditions at high temperatures: stepwise bond dissociation energies are indicated for  $BH_3$ ; when graphite and hydrogen are heated under flow conditions at  $\sim 2000^\circ C$ ., moderately high molecular weight ions are observed and implications raised for the genesis of life related molecules.*

The problem of using the mass spectrometer to identify and characterize labile molecules and/or reactive intermediates can be broken into three parts. First is obtaining the mass spectra of those labile species that can be prepared and "stored in a bottle." The problem is that some of these species such as  $BH_3CO$ ,  $B_4H_8CO$ ,  $B_4H_{10}$ , and  $Ni(CO)_4$ , decompose at measurable rates near or at room temperature and would therefore be expected to decompose in either the inlet system (8) or in the ion source which is heated by the electron emitting filament. Decomposition in the source is insidious; the analytical chemists recognized the problem early and carefully thermostatted the ion sources of the mass spectrometer, often at  $250^\circ C$ . This means that the source can act as a reproducible flow reactor. Thus, it may be difficult to identify the result-

ing steady state mixture of subject molecule, reactive intermediates, and pyrolysis products (27, 34). This may cause a particularly severe problem in obtaining the mass spectra of isotopically labelled materials—scrambling could occur without there necessarily being any decomposition. In any case, it should be of vital concern to those who make theoretical calculations of mass spectra.

Once the mass spectra of the “stable” molecules are firmly established, a second phase is to identify the reactive intermediates responsible for the polymerization or degradation of a given starting molecule. Such direct identification is valuable for systems where the kinetic data are intractably complex, as for the boron hydrides or for nickel carbonyl.

Finally, it is possible that some of these reactive intermediates may be “high temperature molecules.” Although unstable with respect to decomposition at ordinary temperatures, they may exist in measurable concentrations at elevated temperatures. In this case, equilibrium constants and thermodynamic properties may be determined—*e.g.*, for  $\text{BH}_3$  in equilibrium with boron and hydrogen at  $2000^\circ\text{K}$ . Such thermodynamic data can then be used to verify a proposed reaction mechanism. In this paper, all three aspects are discussed.

### *Experimental*

**Inlet System.** The essential parts of the flow reactor and ion source apparatus assembly are shown in Figure 1 (Nuclide Associates, State College, Pa. Model 12-60-HT8). This is a modification of the arrangement of Chupka and Inghram (4, 7, 18). A reactant material is distilled from a low temperature container into the tube *T* in the bottom. It then flows through the reactor *A*, which contains a series of baffles, and then effuses out of the orifice into a high vacuum region. A septum divides this reactor compartment from the separately pumped ion source chamber, where the neutral species are ionized by an electron beam at the center of the plate marked *J1*. The slit just below *J1* is narrow. It and the movable beam-defining slit *D* define a line that molecules must travel to be ionized. Thus, by scanning the slit *D* from right to left, one obtains a shutter profile (18) which permits determination of whether the ions originated from residual background, neutrals coming from the radiation screens *C*, the wall of the reactor, or the reactor interior. The slit in the ionization chamber, *J1*, is large enough to permit the molecular beam to escape without any collisions with the chamber walls. It is believed that the molecular beam mass spectrum corresponds to one with “zero ion source contact.”

We discuss below how this arrangement helps us to distinguish between—*e.g.*  $\text{BH}_3$  ions formed by fragmentive ionization of diborane,  $\text{B}_2\text{H}_6$ , or from the neutral reactive intermediate  $\text{BH}_3$ .

In its present state of evolution, this apparatus is similar to that used by Eltenton (9, 10) and Lossing (24). One significant difference is that here the reactor is far from the electron beam. Intensity has been delib-

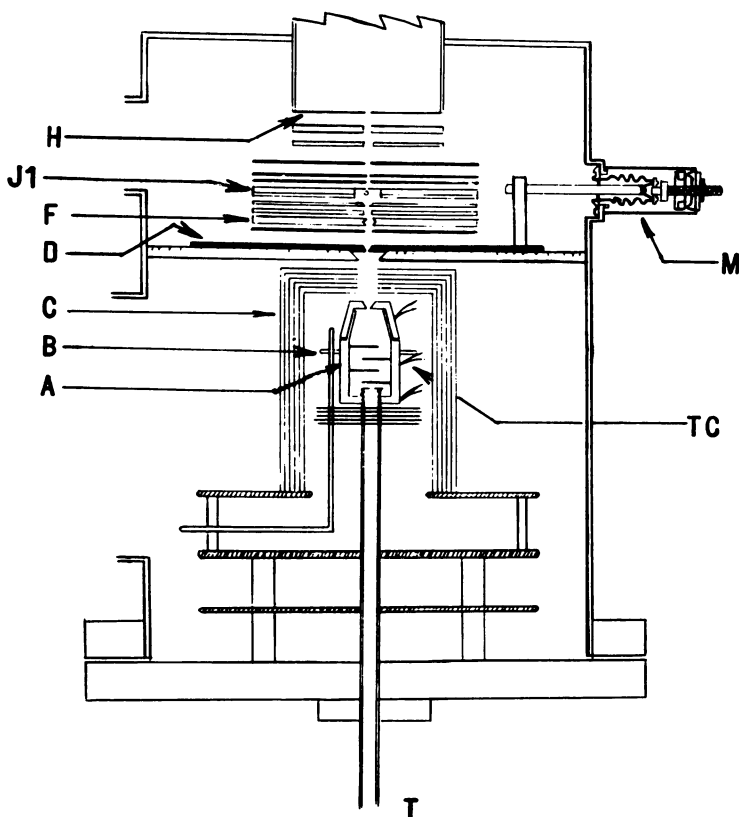


Figure 1. Flow reactor and ion source assembly

(A) Flow reactor, (B) Tungsten heating filament, (C) Radiation shields, (D) Movable beam defining slit ("shutter"), (F) Deflector for charged species in the molecular beam, (J1) Ionization chamber, (H) Ion beam defining slit, (T) Inlet tube, (TC) Thermocouples, and (M) Micrometer

erately sacrificed for differential pumping, the movable beam-defining slit, and the resulting shutter profiles.

Foner and Hudson (15, 16), Fite and Brackmann (14), Milne and Green (28), and Fehlner and Callen (11) have a similar arrangement except that a chopper, perhaps without the differential pumping, is used in place of movable slit *D*. A phase-sensitive detector is then used, and the tedious manual operation of *D* is eliminated.

**The Mass Analyzer.** This is of moderately high resolution. It certainly is not true that work at low masses requires only low resolution. Figure 2 shows how the boron hydride peaks at mass 12 [ $^{12}\text{C}$ ,  $^{11}\text{BH}$ , and  $^{10}\text{BH}_2$ ] are uniquely identified by their mass defects. This is especially useful in searching for tri- and tetraborane pyrolysis products. Mass resolution of a factor of 3 to 6 higher than that shown here would be desirable.

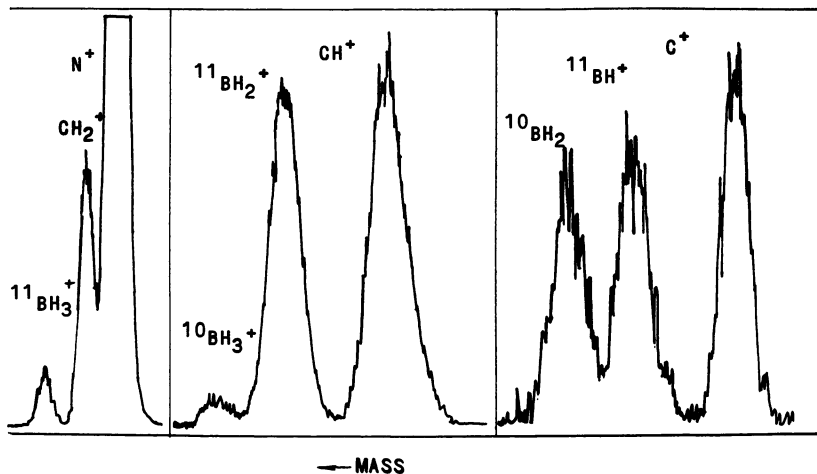


Figure 2. Resolution of the triplets at mass peaks 14, 13, and 12 showing how boron and/or carbon hydrides can be unambiguously identified and measured. The highest intensity at mass 12 corresponds to about 30 ions per second, and the scan time for the triplet is about 3 minutes

**Automatic Data Reduction.** In a typical run on  $^{10}\text{B}_4\text{H}_{10}$  (3) it was necessary to monitor 27 ion peaks between masses 10 and 50. Seven species are postulated that would have parent peaks in this region. In addition, polymerization product peaks were observed at every mass between 50 and 110, and could be attributed to any of eight additional neutrals. Thus, a total of 87 mass peaks, attributable to 15 possible neutrals, had to be studied.

In general, a 40-consecutive hour run required an additional 120 hours (not consecutive!) for reading the charts and reducing the data.

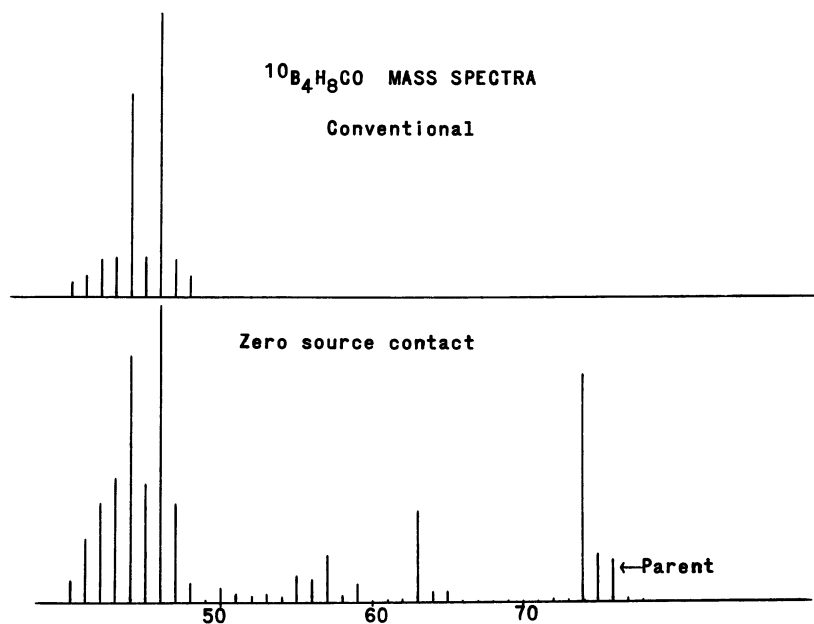
To eliminate some of this massive repetitive labor, automatic data treatment devices have been developed and are discussed elsewhere (25). In addition to reducing the human labor, this apparatus has in fact improved the extent and precision of the data and the range of the apparatus, making feasible experiments that would otherwise not be possible. In addition, results are available to the workers during the run so that they may be used for planning the next step. Perhaps the most important advantage is that our students experience first hand that unless absolutely necessary, no human being should do repetitive labor that could be done equally well, or in this case, much better by machine.

## Results

**Molecular Beam Mass Spectra of Labile Materials.** In the experimental arrangement shown in Figure 1, the slit by which the molecular beam leaves the ionization chamber *I1* is larger than the collimating slit just below it. Consequently, the molecular beam is believed to pass through the ionization chamber with no wall contacts or scattering.

Operating the slit *D* permits measurement of the ion intensities associated with the molecular beam species. A molecular beam mass spectrum so obtained should correspond to "zero ion source contact."

Workers, using source geometries different from the present one, have chopped the molecular beam at various frequencies. Observation of the chopped ion current led to the conclusion that it may arise from ions attributed to both straight-through and scattered components of the molecular beam. We believe that the contribution of the latter does not affect the results in the present case.

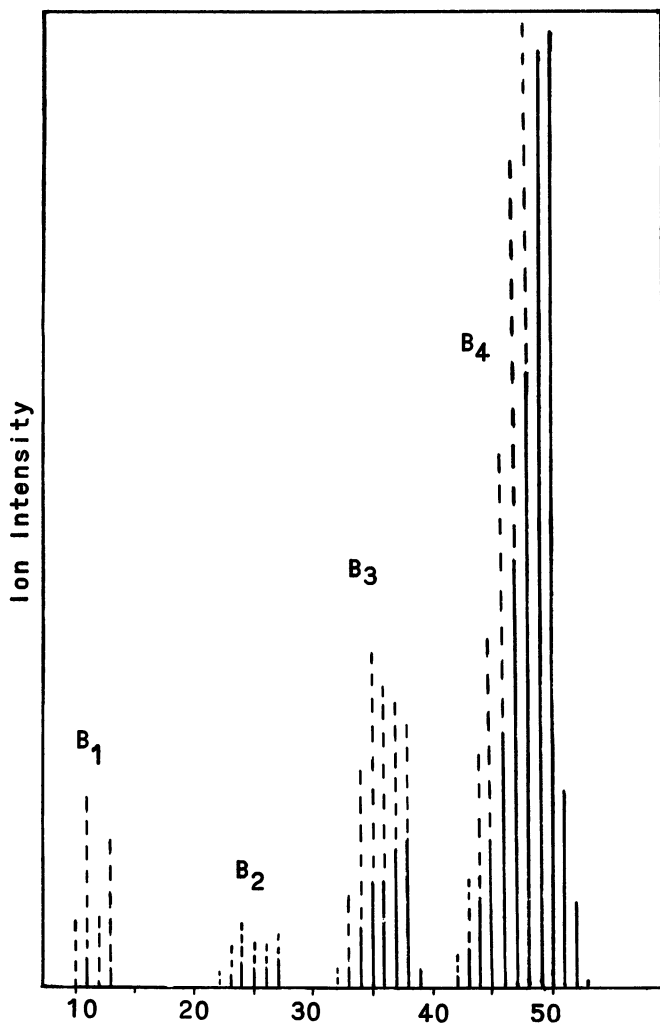


Top, courtesy G. L. Brennan and R. Schaeffer

Figure 3. (Top) Mass spectrum of tetraborane carbonyl,  $\text{B}_4\text{H}_8\text{CO}$ , taken with a conventional analytical mass spectrometer. Small contributions of pentaborane ions are subtracted out. (Bottom) Mass spectrum taken with the molecular beam spectrometer (17). It is believed that the difference is caused by complete pyrolysis in the conventional spectrometer ion source, which is about  $250^\circ\text{C}$ .

$\text{B}_4\text{H}_8\text{CO}$ . A striking example of the value of this technique is shown in Figure 3. The upper mass spectrum is that of tetraborane carbonyl,  $\text{B}_4\text{H}_8\text{CO}$ , taken with a conventional analytical mass spectrometer (courtesy of G. L. Brennan and Riley Schaeffer). The lower spectrum is of the same compound taken with zero ion source contact [by R. E. Hollins *et al.* (17)]. The latter shows intense parent and parent-minus- $\text{H}_2$  peaks. Of some interest is that  $m/e$  63,  $^{10}\text{B}_3\text{H}_5\text{CO}^+$ , is relatively large; it is the

analog of the proposed species  $B_3H_7$ . The former does not show these peaks. All evidence indicates that the former is caused by a mixture of pentaboranes (subtracted out in the figure), tetraborane -10, and the



Journal of the American Chemical Society

*Figure 4. Conventional mass spectrum compared to molecular beam mass spectrum of tetraborane-10. The difference is attributed to pyrolysis to form  $B_1H_8$  and probably diborane and other species in the conventional ion source (29)*

--- Conventional mass spectrum  
 — Molecular beam mass spectrum

intermediate to be discussed below, tetraborane-8. This carbonyl, which is known to pyrolyze at 0°C., has been completely decomposed during the short contact with the ion source.

$B_4H_{10}$ . Figure 4 shows a comparison of the molecular beam mass spectrum of tetraborane-10 with that taken with a conventional analytical mass spectrometer. When Arlan D. Norman prepared this sample, he found that his conventional mass spectra always showed pentaborane peaks. Other mass spectra in the literature (2) show also hexaboranes. The molecular beam mass spectrum shows none, indicating pyrolysis in the conventional source.

The remaining discrepancies might be attributed to temperature-induced changes in mass spectra—*i.e.*, as the temperature is raised, higher vibrational levels are populated. Because of the role of the Franck-Condon principle in the primary ionization process, this could lead to the observed change in the fragmentation pattern. A rather exhaustive study (discussed below) shows that the conventional mass spectrum arises from a mixture of tetraborane-10, the intermediate tetraborane-8, probably diborane, and possibly other species.

From these results it is clear that any theoretical calculation of the mass spectrum of tetraborane-10, or of similarly labile molecules must be compared with the molecular beam mass spectra.

ISOTOPICALLY LABELED  $B_4H_{10}$ . A particularly important case of a labile compound is an isotopically labeled molecule, particularly with *H* or *D* labels. The label atoms could be scrambled without any indication of decomposition. A molecular beam mass spectrometric investigation of such labeled tetraboranes has been reported recently (29) and has given results significantly different from those previously in the literature. The apex (2, 4) boron atoms are lost in a preferred manner, but not deuterium in a bridge position.

$BH_3CO$ . The mass spectrum of borane carbonyl (taken by S. M. Schildcrout) is shown in Figure 5 and compared with the conventional mass spectrum (6). The fragmentation pattern of this molecule is similar to that of the tetraborane carbonyl in that there is a relatively intense parent peak and a still larger parent-minus-two peak. The elimination of ions from  $B_2H_6$ , neutral in the molecular beam spectrum allowed us to identify various  $BH_nC^+$  fragment peaks. These peaks are so small that they are not seen in the figure.

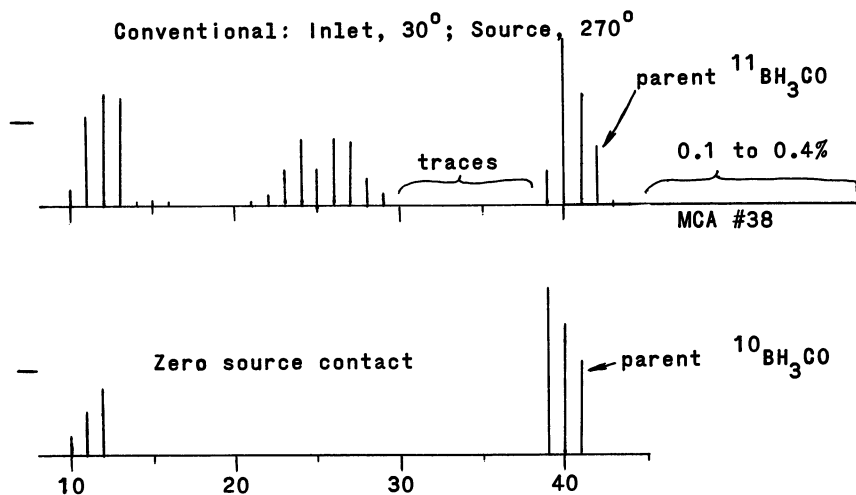
$B_2H_6$ . Of other species studied, the molecular beam mass spectrum of diborane is essentially the same as that measured with the conventional mass spectrometer (1).

$Ni(CO)_4$ . The mass spectrum of nickel carbonyl,  $Ni(CO)_4$ , has been of some interest recently (35, 36). For this compound, Schildcrout *et al.* (32) have shown that the conventional spectrometer does not

give detectable amounts of intermediates such as the tricarbonyl. In some respects, this is a surprise because the literature (32) postulates such an intermediate in the gas-phase pyrolysis and other reactions. It does confirm the validity of the previous studies (35, 36) in which the positive and negative ion mass spectra were measured and compared with theoretical calculations. The present results (32) give the first rearrangement ions, C—O scissions, and metastable transitions reported for this molecule.

$\text{H}_3\text{BNH}_3$ . The vapors above ammonia borane solid have been studied and the molecule  $\text{H}_3\text{BNH}_3$  identified as the principle vaporization product (22). Study of the hemideutero compound  $\text{H}_3\text{BND}_3$  shows that in electron impact fragmentation a B—H bond is broken in preference to a N—D bond.

Because of a solid-state decomposition, the vapor contains also other decomposition products. Its low vapor pressure and instability would make ammonia borane extremely difficult to study by conventional mass spectrometric techniques.



Courtesy S. M. Schildcrout

Figure 5. (Bottom) Molecular beam mass spectrum of borane carbonyl,  $\text{BH}_3\text{CO}$  (Top) Conventional spectrum (6) shows diborane and does not permit measurement of the  $\text{BH}_2\text{C}^+$  peaks

**Studies of Reactive Intermediates. BORON HYDRIDES.** The boron hydrides have been of interest for some years because of their high specific heats of combustion and because of their "electron deficient"

structures involving bridge hydrogen bonds and the great variety and diversity of the molecules formed. Chemical, and particularly kinetic, studies (1, 23, 33) have been greatly complicated by the reactivity of the boron hydrides and by the complex, quasi-equilibrium mixture of products.

**BORANE,  $BH_3$ .** Although many workers have sought borane, it has largely eluded detection. The first reported identifications came approximately simultaneously by Fehlner and Koski, who identified it in the pyrolysis of diborane (12, 13) and of borane carbonyl,  $BH_3CO$  (12, 13), and by our own group (4). We have obtained a complete mass spectrum, free of possible  $BH_2$ , for this molecule. We have only sparsely investigated the pyrolysis of  $BH_3CO$ , and this has led to polymerization. Studies using shorter flow times and lower reactor pressures are under way.

The pyrolysis of  $B_2H_6$  has been studied (4) using a variation of more than  $10^2$  in flow time and  $10^3$  in diborane pressures. One group of results is shown in Figure 6 where the ratios of mass peaks 13 ( $^{10}BH_3^+$ ) and 12 ( $^{10}BH_2^+$ ) to mass peak 25 ( $^{10}B_2H_5^+$ ) are plotted as a function of temperature. The monomer ion intensities increase in both absolute and relative ion intensity.

Some of the deformation frequencies of  $B_2H_6$  are such that one might argue that these modes are becoming excited and causing a change in fragmentation pattern. The data in Figure 7 indicate that this is not the case. Here the percentage shutter effect, that is, the amount of molecules caused by molecular beam species compared with the amount existing as a stable background, is plotted for the diborane and the monoborane ion peaks. At the temperature where the monoborane/diborane ion peak ratios start to increase, there is also an increase in the monoborane ion shutter effects. The shutterable fraction of  $B_2H_5^+$  ion remains constant. This is a good indication that at the higher temperatures these ions have different neutral progenitors. Furthermore, the neutral progenitor of the monoborane ions must be much more reactive since it is more rapidly pumped. It may still be that the progenitor of the  $BH_3$  ions is in fact an excited diborane molecule,  $B_2H_6^*$ . The mass spectrum of  $BH_3$  obtained from  $BH_3CO$ , for example, is therefore highly desirable for comparison with the one given below.

The mass spectrum of monoborane obtained (4) in this fashion from  $B_2H_6$  is  $BH_3^+$  (31%),  $BH_2^+$  (100%),  $BH^+$  (16%), and  $B^+$  (8%). It is similar to those of the boron trihalides (21, 30) as well as to those of certain aluminum (31) and scandium (26) trihalides.

This technique of discerning reactive species should continue to prove valuable. Alternately, Klemperer, Buchler, and co-workers (5) have used a strong inhomogeneous electric field alternately to select those molecules with (*e.g.*  $LiOH$ ) and without (*e.g.*  $(LiOH)_2$  a dipole

moment. This probably would not have worked in the present case, because of the low ion intensity attributed to  $\text{BH}_3$  and its probable  $D_{3h}$  symmetry.

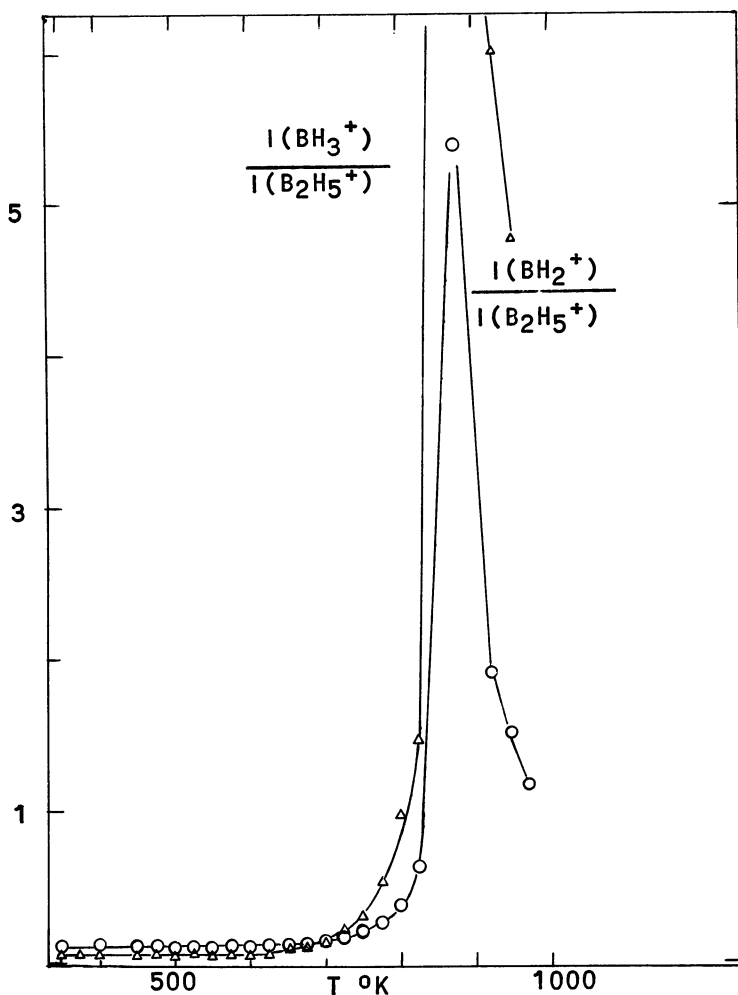


Figure 6. Formation of  $\text{BH}_3$ : Ratio of mass peak intensities  $I(^{10}\text{BH}_2^+)/I(^{10}\text{B}_2\text{H}_5^+)$  and  $I(^{10}\text{BH}_3^+)/I(^{10}\text{B}_2\text{H}_5^+)$

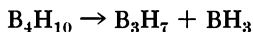
In the study of the pyrolysis of diborane (4), equations were developed for deducing the rate constant for pyrolysis under low pressure conditions—*i.e.*, those conditions where material leaves the reactor by molecular flow, and where, in addition, the mean free path is sufficiently large that the composition throughout the reactor is constant. It was shown also that anomalous effects seem to occur if the conductance of

the exit orifice is comparable with the conductance of the body of the reactor.

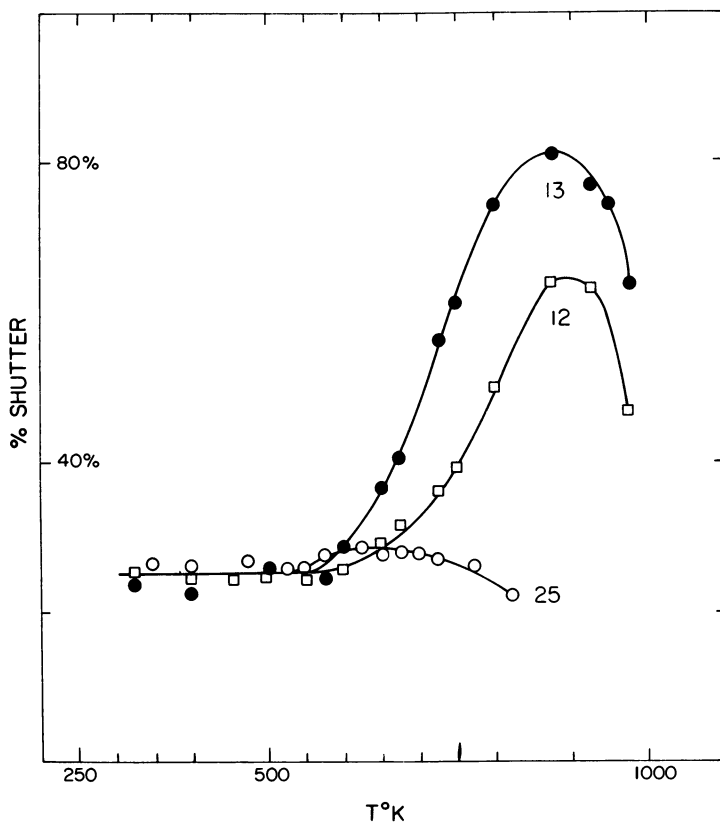
**TETRABORANE-8.**  $B_4H_8$  poses more complicated problems. It could be formed by dehydrogenation of tetraborane-10.



Even if this reaction were shown to occur, another reaction also has been postulated.



Thus, if  $B_4H_8$  were formed from tetraborane-10, the formation of the neutral triborane and monoborane species could not necessarily be precluded; with the low ion intensities available it would be difficult to



Journal of the American Chemical Society

Figure 7. Formation of  $BH_3$  (continued): Percent shutter effect vs. reactor temperature showing that the monoborane ions have a different, more reactive neutral progenitor than mass 25 ( $B_2H_5^+$ ) from diborane.<sup>(4)</sup>

American Chemical Society

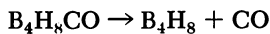
Library

1155 16th St., N.W.

Washington, D.C. 20036

In Mass Spectrometry, *Journal of the American Chemical Society*, Vol. 90, No. 1, p. 147, 1968.  
 Advances in Chemistry; American Chemical Society: Washington, DC, 1968.

make sufficiently accurate determinations of these appearance potentials. Accordingly, alternate routes to the tetraborane-8 intermediate would be desirable. These include



and

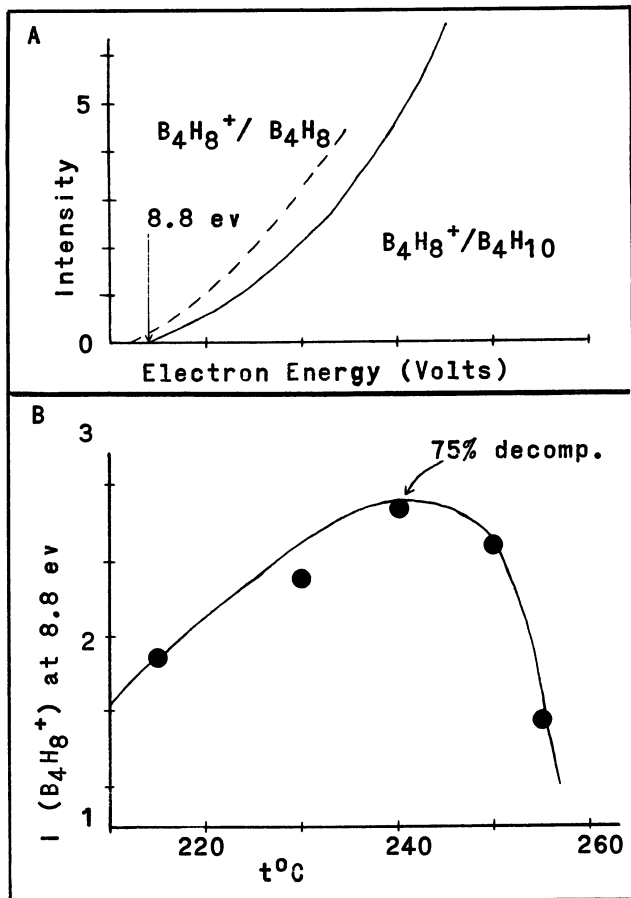


Figure 8. Formation of  $\text{B}_4\text{H}_8$  from  $\text{B}_4\text{H}_{10}$ :  $\text{B}_4\text{H}_8^+$  ion current at low ionizing electron energy vs. reactor temperature. This increase in ion current with temperature, parallel increases in percent shutter effect, and other data indicate the formation of  $\text{B}_4\text{H}_8$  neutral

Figure 8 shows some of the results for the pyrolysis of tetraborane-10 (3). In this case, there was enough ion intensity so that the change in intensity of the parent for the reactive intermediate could be followed at

low ionizing electron energy. These results, indicating the presence of the tetraborane-8 reactive intermediate, are corroborated by observation of the ratios of other ion peaks, and by the percentage shutter effect.

It is this body of evidence that indicates that the difference between the zero source contact and the conventional mass spectrum, shown in Figure 4, is in fact caused by the tetraborane-8.

In addition, the difficulties in studying these species are well illustrated by the observation that even at these low pressures with the reactor at 200°C. every mass peak from 55 to 110 showed the presence of boron hydride pyrolysis products. The most intense of these was only 2% of the  $B_4H_8^+$  ion intensity, so it is not likely that they made an appreciable contribution to the  $B_4H_8$  mass spectrum observed.

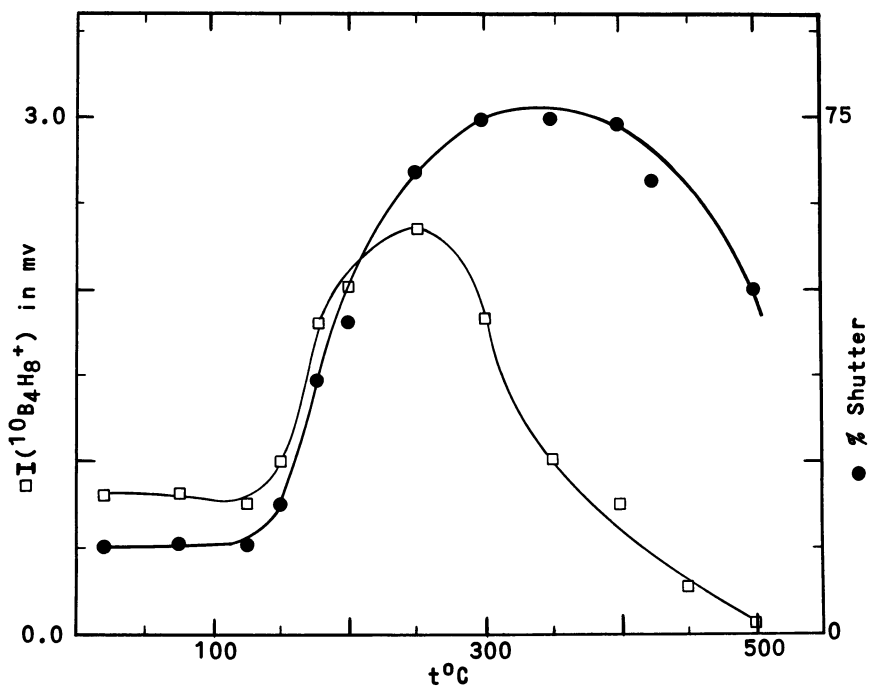


Figure 9. Formation of  $B_4H_8$  from  $B_4H_8CO$ : Ion current at mass peak 48 (squares) and percentage shutter effect (circles), both as a function of reactor temperature (17)

In subsequent work, Hollins *et al.* (17) have followed the pyrolysis of tetraborane carbonyl. Although this compound is extremely unstable and explosive, the tetraborane-8 intermediate could be clearly identified (Figure 9) by the change in mass spectra, and by the shutter effects. Appearance potentials were measured.

A similar study of pentaborane-11 has not yet been reported. It will be interesting to see the results.

**NICKEL TETRACARBONYL.**  $\text{Ni}(\text{CO})_4$  has been reported to form a tricarbonyl during its gas-phase pyrolysis and has been the subject of recent lively interest (32, 35, 36). Schildcrout *et al.* (32) have studied the pyrolysis of this molecule extensively but have not been able to find any evidence for intermediate formation in agreement with the recent work of Kangas *et al.* (20).

**AMMONIA BORANE.**  $\text{H}_3\text{BNH}_3$  yields  $\text{BNH}_4$  as well as diborane and ammonia when vaporized. Pyrolysis of  $\text{H}_3\text{BND}_3$  shows that the structure of the product is most likely  $\text{H}_2\text{BND}_2$ .

**High Temperature Studies.** Some of the problems in the pyrolysis mechanism of the boron hydrides could be solved if  $\text{BH}_2$  or  $\text{BH}_3$  could be studied in equilibrium with hydrogen and boron. Thermodynamic predictions indicate that one or both of these should be present in observable quantities under mass spectrometric conditions at about  $2000^\circ\text{C}$ . For this study the previously determined mass spectrum of borane-3 should be particularly valuable.

The available data (19) can be combined to give the bond dissociation energy  $D(\text{BH}-\text{H})$  for  $\text{BH}_3$ , in kcal./mole:



It is quite likely that at least two of the three bond dissociation energies must be in error. The middle one seems to be much too large.

S. J. Steck has undertaken equilibrium studies of the boron hydrogen system at about  $2000^\circ\text{C}$ . Her preliminary results corroborate these speculations in that  $\text{BH}_3$  is readily observed but not  $\text{BH}_2$ . For the conditions used, the bond dissociation energies quoted above lead to the prediction that  $\text{BH}_2$  should be  $\sim 10^3$  more abundant, in striking disagreement with the observations.

**MODERATELY HIGH MOLECULAR WEIGHT AND LIFE RELATED CARBON SPECIES.** When hydrogen is allowed to flow through a graphite reactor heated to about  $2000^\circ\text{C}$ ., Steck observes ions of the type  $\text{C}_x\text{H}_y$  containing up to seven or more carbon atoms. The mass spectra indicate that the neutral progenitors probably are noncyclic; low appearance potentials in some cases indicate the presence of free radicals.

This result is exciting because it affects calculations of the amount of material present in stellar sources and because it suggests a mechanism for the formation of organic substances leading to the origin of life. The

possibility also is suggested that if nitrogen were added to the reaction mixture, nitriles and eventually amines could be formed.

### **Conclusion**

Our various activities in applying mass spectrometry to inorganic chemistry have been summarized in this report. First, and perhaps most unique, is the measurement of molecular beam mass spectra of such labile molecules as tetraborane-10, tetraborane carbonyl, ammonia borane, and nickel carbonyl. In this work, the effects of interfering mass spectra from pyrolysis on the ion source are eliminated. Such effects have been shown to be significant in interpreting certain mass spectra (29). The reactive intermediates  $\text{BH}_3$  and  $\text{B}_4\text{H}_8$  have been clearly identified and to some extent characterized. Some data have been obtained also for the stepwise bond dissociation energies of gaseous  $\text{BH}_3$ . Higher molecular weight hydrocarbon ions have been identified coming from species in the vapor above graphite and hydrogen.

### **Acknowledgments**

The significant contributions of M. E. Gordon, R. E. Hollins, S. M. Schildcrout, E. J. Sinke, S. J. Steck, Riley Schaeffer, A. D. Norman, D. F. Shriver, and P. M. Kuznesof are gratefully acknowledged. The assistance of R. J. Loyd, J. A. Brabec, J. B. Bruce, E. Falkenberg, Joan C. Kaye, and Pamela M. Bro also has been invaluable.

Support for the various projects described has come from the Northwestern University Materials Research Center (supported by the U. S. Advanced Research Projects Agency), and from the U. S. Atomic Energy Commission for which this bears document number COO-1147-11. This support is very much appreciated.

### **Literature Cited**

- (1) Adams, R. M., "Boron, Metallo-Boron Compounds, and Boranes," p. 507 ff., Interscience Publishers, New York, 1964.
- (2) API Project 44, "Selected Values of Properties of Hydrocarbons and Related Compounds," A. & M. College of Texas, College Station, Tex., 1955.
- (3) Baylis, A. B., Pressley, G. A., Jr., Gordon, M. E., Stafford, F. E., *J. Am. Chem. Soc.* **88**, 929 (1966).
- (4) Baylis, A. B., Pressley, G. A., Jr., Stafford, F. E., *J. Am. Chem. Soc.* **88**, 2428 (1966).
- (5) Büchler, A., Stauffer, J. L., Klemperer, W., *Bull. Am. Phys. Soc.* **11**, 202 (1966).
- (6) *Carnegie Inst. Technol.*, Pittsburgh, Pa., *Serial No. 38*, "Manufacturing Chemists' Association Project on Properties of Chemical Compounds." (Data submitted by Callery Chemical Co., Callery, Pa.), (June 1960).
- (7) Chupka, W. A., Inghram, M. G., *J. Phys. Chem.* **59**, 100 (1955).

- (8) Ditter, J. F., Spielman, J. R., Williams, R. E., *Inorg. Chem.* **5**, 118 (1966).
- (9) Eltenton, G. C., *J. Chem. Phys.* **10**, 403 (1942).
- (10) *Ibid.*, **15**, 455 (1947).
- (11) Fehlner, T. P., Callen, R. B., *ADVAN. CHEM. SER.* **72**, 181 (1967).
- (12) Fehlner, T. P., Koski, W. S., *J. Am. Chem. Soc.* **86**, 2733 (1964).
- (13) *Ibid.*, **87**, 409 (1965).
- (14) Fite, W. L., Brackmann, R. T., *Phys. Rev.* **113**, 1141 (1958).
- (15) Foner, S. N., Hudson, R. L., *J. Chem. Phys.* **21**, 1374 (1953).
- (16) *Ibid.*, **36**, 2681 (1962).
- (17) Hollins, R. E., Pressley, G. A., Jr., Baylis, A. B., Stafford, F. E., "Abstracts of Papers," 152nd Meeting ACS, Sept. 1966, V4.
- (18) Inghram, M. G., Drowart, J., "Proc. Intern. Symp. on High Temperature Technology," p. 219, McGraw-Hill, New York, 1960.
- (19) "JANAF Thermochemical Tables," Dow Chemical Co., Midland, Mich.
- (20) Kangas, L. R., Heck, R. F., Henry, P. M., Breitschaft, S., Thorsteinson, E. M., Basolo, F., *J. Am. Chem. Soc.* **88**, 2334 (1966).
- (21) Koski, W. S., Kaufman, J. J., Pachuki, C. F., *J. Am. Chem. Soc.* **81**, 1326 (1959).
- (22) Kuznesof, P. M., Shriver, D. F., Stafford, F. E. (unpublished work).
- (23) Lipscomb, W. N., "Boron Hydrides," W. A. Benjamin, Inc., New York, 1963.
- (24) Lossing, F. P., "Mass Spectrometry," ed. by C. A. McDowell, p. 442, McGraw-Hill, New York, 1963.
- (25) Loyd, R. J., Stafford, F. E., *ADVAN. CHEM. SER.* **72**, 127 (1967).
- (26) McKinley, J. D., *J. Chem. Phys.* **42**, 2245 (1965).
- (27) McLafferty, F. W., Purdue University (private communication).
- (28) Milne, T. A., Greene, F. T., *ADVAN. CHEM. SER.* **72**, 68 (1967).
- (29) Norman, A. D., Schaeffer, R., Baylis, A. B., Pressley, G. A., Jr., Stafford, F. E., *J. Am. Chem. Soc.* **88**, 2151 (1966).
- (30) Osberghaus, O., *Z. Physik* **128**, 366 (1950).
- (31) Porter, R. F., Zeller, E. E., *J. Chem. Phys.* **33**, 858 (1960).
- (32) Schildcrout, S. M., Pressley, G. A., Jr., Stafford, F. E., *J. Am. Chem. Soc.* **89**, 1617 (1967).
- (33) Stock, A., "Hydrides of Boron and Silicon," Cornell Univ. Press, Ithaca, N. Y., 1933.
- (34) Wada, Y., Kiser, R. W., *Inorg. Chem.* **3**, 174 (1964).
- (35) Winters, R. E., Kiser, R. W., *J. Chem. Phys.* **44**, 1964 (1966).
- (36) Winters, R. E., Kiser, R. W., *Inorg. Chem.* **3**, 699 (1964).

RECEIVED October 5, 1966.

# Mass Spectrometry of Inorganic Halides

ROBERT W. KISER,<sup>1</sup> JOHN G. DILLARD<sup>2</sup> and DONALD L. DUGGER<sup>3</sup>

Kansas State University, Manhattan, Kan.

*A mass spectrometric study has been made of  $TiCl_4$ ,  $NbCl_5$ ,  $TaCl_5$ ,  $ZnCl_2$ ,  $ZnBr_2$ ,  $HgCl_2$ ,  $HgBr_2$ ,  $HgI_2$ ,  $PCl_3$ ,  $PBr_3$ ,  $POCl_3$ , and  $PSF_3$ . Heats of formation for the various ions in the mass spectra are calculated from the appearance potentials measured. Clastograms and metastable transition studies have aided in the assignments of the fragmentation pathways. Ion-pair processes were found to be unimportant in the formation of positive ions from all compounds studied except thiophosphoryl fluoride. Ionization of the metal-containing molecules involves the removal of the electron from a molecular orbital to which the halogen atom orbitals contribute significantly.*

The study of gaseous inorganic ions using mass spectrometric analysis dates back to the classic studies conducted by Thomson (203) and Aston (2). Thomson was the first to recognize the applicability of the mass spectrometer as a powerful analytical tool and was successful in identifying inorganic species formed by decomposition in electrical discharges. Aston's pioneering work concerned the determinations of the relative abundances of naturally-occurring isotopes of the chemical elements (2). Interest in the study of electron impact processes and the formation of gaseous ions was stimulated by Dempster's (23) design and construction of a mass spectrometer equipped with an ion source capable of forming ions with nearly the same energy and using a magnetic field to carry out the mass analysis of the ions.

During the ensuing development of mass spectrometry, the investigation of inorganic compounds assumed a secondary importance to the design and improvement of analytical methods for organic materials,

<sup>1</sup> Present address: University of Kentucky, Lexington, Ky.

<sup>2</sup> Present address: Virginia Polytechnic Institute, Blacksburg, Va.

<sup>3</sup> Present address: Texas Instruments, Dallas, Texas.

particularly those of primary interest to the petroleum industry. This decreased emphasis on inorganic studies also was probably caused in part by a lack of more sophisticated supplementary equipment needed for studying the generally less volatile inorganic materials.

Within the last two decades, mass spectrometric studies of the nature of the vaporized species and the ionization and dissociative ionization processes for these gaseous inorganic substances have received renewed attention. This has been primarily caused by the advances in high temperature mass spectrometry and the significance such studies have had for inorganic chemistry. Too, the renaissance of inorganic chemistry that has occurred in the past decade or so, owing to increased utilization of physical methods and theoretical approaches, has occasioned the inorganic chemist to rediscover the utility of mass spectrometry as a means of attacking his varied problems. Although, as is noted below, many of the relatively "simple" inorganic species have been subjected to mass spectrometric study, there is no reason that the more "complex" molecules should not be scrutinized to yield valuable information that is either difficult or impossible to obtain by other methods.

In subsequent paragraphs we present a brief review of the variety of studies of inorganic halides in which mass spectrometry has played a significant rôle, particularly with respect to mass spectral identification and energetics. Neither isotopic abundances nor isotopic separations are included. Because of the importance of photoionization studies, first done by Terenin and Popov (199, 200, 201) to the energetic data, references to such work have also been included. The ordering of this treatment follows the periodic arrangement. The remainder of this paper is concerned with current studies of related halogen-containing systems that have been conducted in our laboratory.

**Group IA.** Numerous investigators have examined all of the fluorides and/or chlorides of this family save francium (6, 134, 135, 137, 183). Studies have also been reported of individual alkali metal halides; these are: lithium (9, 44, 72, 153, 154, 156), sodium (72, 77, 154), and potassium (72, 77). A large number of investigations of hydrogen halides have been reported (4, 5, 17, 19, 25, 42, 44, 46, 51, 57, 64, 73, 76, 80, 83, 97, 99, 115, 116, 117, 143, 144, 145, 147, 148, 149, 158, 159, 160, 161, 162, 165, 166, 204, 211, 212, 213, 214).

**Group IIA.** Aside from the examinations that the alkaline earth fluorides have received (8, 11, 15, 35, 36, 54, 66, 67, 68, 216), only the magnesium halides have been studied mass spectrometrically (8).

**Group IIIB and Transitional Metals.** Apparently yttrium chloride is the sole member of Group IIIB that has been studied (132, 133). The only investigation of the lanthanides and actinides that were found in

the present literature search involve uranium fluoride and chloride (16, 210, 214).

Marriott, Thorburn and Craggs (128) investigated titanium tetrachloride and Sidorov, Akishin, and Belousov (188) have studied zirconium tetrafluoride. Dillard (31) has examined the biscyclopentadienyltitanium and -zirconium dichlorides. We report herein an additional study of the titanium tetrachloride system. Our own recent studies (31) of niobium and tantalum chlorides are reported in this work.

Numerous other investigations of first row transition element halides have been made (15, 31, 41, 86, 90, 91, 92, 130, 131, 155, 177, 178, 179, 185, 204, 219). Additional members of Group IIB that have been studied include cadmium chloride (87) and mercury chloride, bromide, and iodide (15, 31, 41, 53, 204). Recent reports have appeared concerning rhenium chloride systems (14, 173).

**Group IIIA.** Aside from the recent considerations of the thallium halides (7, 93), studies have been limited to the halides of boron (55, 66, 69, 84, 85, 98, 100, 107, 108, 122, 124, 125, 127, 129, 150, 164, 175, 186, 190) and aluminum (11, 35, 153, 156, 216).

**Group IVA.** There have been many investigations of energetics in the organic halogen systems (10, 28, 29, 30, 38, 39, 53, 58, 59, 61, 65, 70, 71, 78, 81, 95, 109, 110, 111, 118, 123, 126, 139, 146, 157, 167, 168, 176, 189, 190, 192, 202, 212, 213). Studies of the fluorides and chlorides of two additional members of this group include work on silicon and germanium (24, 36, 43, 62, 81, 125, 176, 191, 202, 206, 212, 213, 215, 216, 219).

**Group VA.** Nitrogen fluorides have been rather extensively examined (13, 18, 33, 62, 63, 88, 106, 113, 169), whereas little attention has been given to other nitrogen halides (61, 152). Several investigators have reported the results of their investigations of phosphorus fluorides and chlorides (51, 56, 89, 94, 104, 163, 180, 207). No additional work appears to have been done on antimony halides since the early efforts of Kusch, Hustrulid and Tate (51, 104). Only a little more attention has been given to arsenic fluoride and chloride (51, 104, 179).

**Group VIA.** The principal studies of the halides of this group have been concerned with sulfur (3, 22, 24, 34, 43, 68, 101, 102, 119, 151, 174, 176, 184, 217), although reports of oxygen-fluorine systems (26, 120, 121) have appeared recently.

**Group VIIA.** Various interhalogen compounds and negative halide ion studies are to be found in the literature (48, 60, 79, 152, 193, 194, 216).

**Noble Gas Halides.** Mass spectrometric studies have been of prime importance in the exciting investigations of this new class of compounds (12, 75, 196, 197, 218).

**Oxyhalides and Thiohalides.** In addition to the above systems, various oxyhalides and a few thiohalides have been examined mass spectrometrically (26, 27, 31, 40, 56, 69, 86, 114, 120, 121, 138, 145, 170, 171, 172, 174, 176, 184, 207).

The present work is a report of a portion of current mass spectrometric studies in these laboratories of inorganic halides and oxy- (and thio-) halides. It has been found that there are some similarities as well as differences between metal and non-metal halides. Additionally, caution is urged in the assignment of ion pair processes involving these halides. After describing the experimental procedures and techniques employed in this work, the results of our investigations are presented and discussed.

### *Experimental Apparatus and Procedures*

**Mass Spectrometers and Data Reduction.** The mass spectrometer used principally in this study was a Bendix model 12-100 time-of-flight which has been partially described previously (48, 49). The instrument has been modified to permit studies of negative ions and equipped with a Hewlett-Packard model 175A 50Mc oscilloscope with capabilities for recording the oscilloscope trace. The signal from the Wiley magnetic electron multiplier was fed through an HP model 1759B dual trace vertical amplifier plug-in. Negative ion spectra were recorded directly with a heated-pen galvanometer on 5 cm. strip chart paper by scanning the oscilloscope trace with a ramp pulse generated in the HP model 1784A recorder plug-in.

An Associated Electrical Industries MS-9 double-focusing mass spectrometer was also employed in this study. A rhenium ribbon filament was heated to give a trap current of 100  $\mu$ amp. The ion repeller was nominally 2 volts. At a medium resolution of 1100 (using the 2.08  $\Gamma_{1/2}$  definition) the mass spectrum was scanned in 31 seconds/octave by decreasing the magnetic field. High resolution spectra ( $> 20,000$ ) were also obtained. After signal amplification with an 11-stage electron multiplier, the spectra were traced with a six-galvanometer recorder mirroring ultraviolet light onto a photosensitive paper. Other details of this instrument have been reported (50).

Pressures, as determined by Alpert ionization gauges, were maintained between  $1 \times 10^{-7}$  and  $1 \times 10^{-6}$  torr in the ion source and below  $1 \times 10^{-7}$  torr in the MS-9 analyzers. Samples were introduced to the ion source of the MS-9 by heating a 4  $\mu$ l. cavity in a quartz probe. The 0.07 mm. orifice of this cavity is 2.1 cm. from the electron beam. The temperature of the sample in the cavity was controlled by electrically heating the nichrome windings. An iron-constantan thermocouple and a Leeds and Northrup potentiometer was used to monitor the temperature of the cavity.

A nominal ionizing energy of 70 e.v. was employed in determining the positive ion mass spectra in both instruments. The relative abundances reported herein are those for the monoisotopic mass spectra and therefore

include the contributions from ion currents for all the isotopes in a particular ion. Negative ion mass spectra were taken with the time-of-flight instrument at a voltage where the ions were the most intense. This voltage varied from compound to compound.

Metastable transitions were investigated using the MS-9 instrument in the usual manner. By applying a variable retarding potential to the electron multiplier stack in the time-of-flight instrument, it also has been possible to employ this spectrometer for metastable transition studies.

Clastograms were determined by scanning the entire mass spectrum as a function of the electron energy. At higher electron energies the stepping interval was approximately 5 e.v. This interval was reduced to about 1 e.v. for electron energies below 25 e.v. Logarithmic clastograms were constructed by plotting the logarithm of the fractional abundance of each ion at any given electron energy as a function of the electron energy. Figure 1 shows a typical clastogram. Included in the present

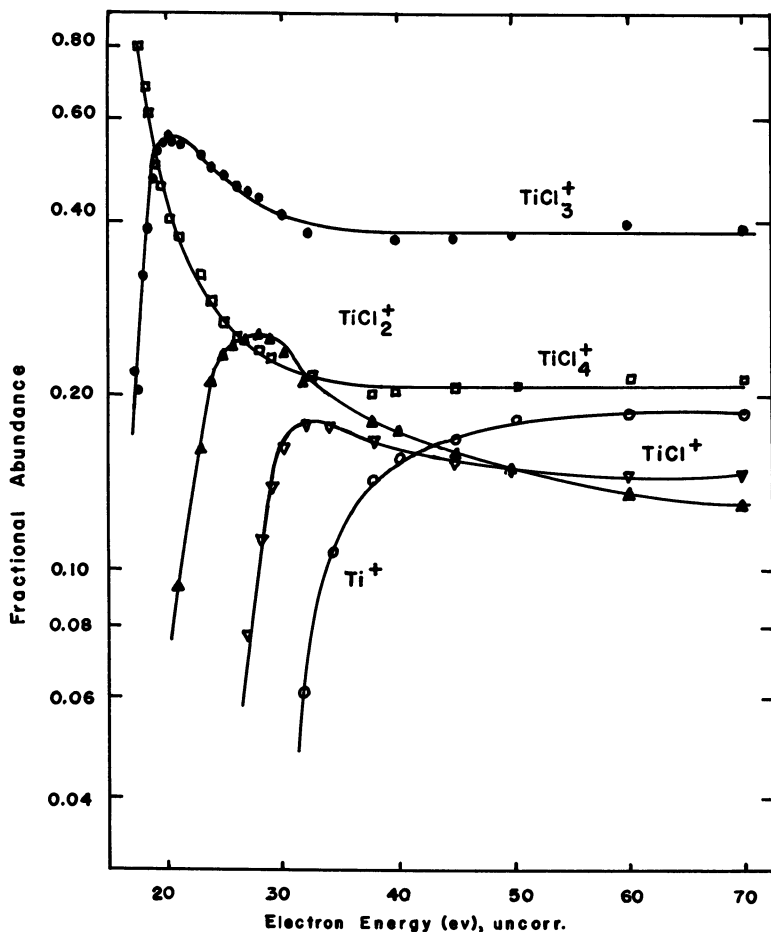
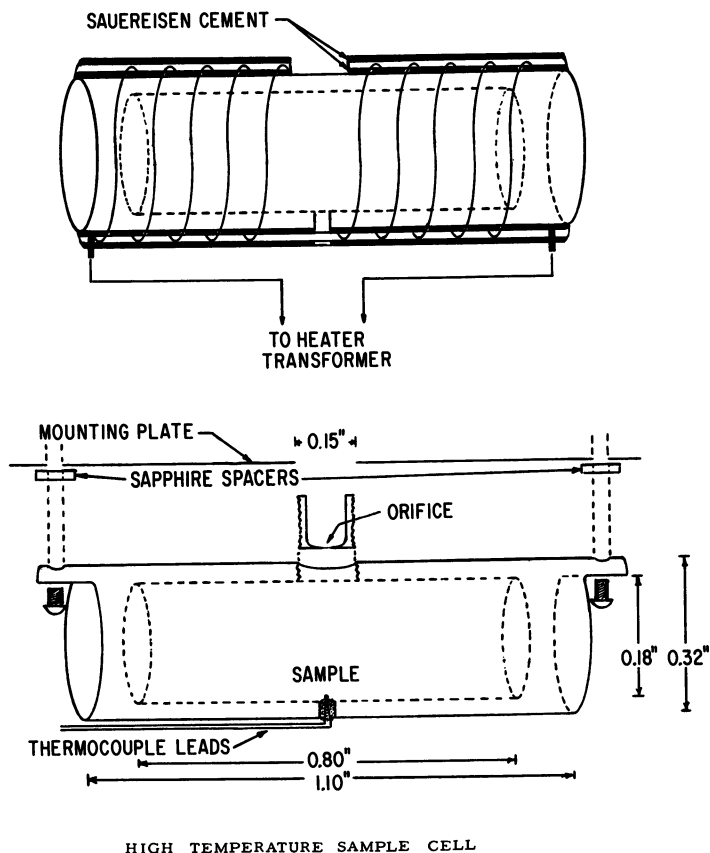


Figure 1. *Logarithmic Clastogram for Titanium Tetrachloride*

study is the first reported negative ion clastogram, determined for  $\text{POCl}_3$  in essentially the same manner by recording the oscilloscope trace.

Ionization and appearance potentials were determined from ionization efficiency curves by the semi-logarithmic plot technique of Lossing, Tickner, and Bryce (112) and by the extrapolated voltage difference procedure outlined by Warren (209). Energy calibrants used in these studies were nitrogen ( $I = 15.58$  e.v.) (64), mercury ( $I = 10.43$  e.v.) (140, 141, 142), and water ( $I = 12.59$  e.v.) (213). Good internal agreement was obtained using the different calibrants. Error values quoted in this work represent the reproducibility at one standard deviation.



HIGH TEMPERATURE SAMPLE CELL

Figure 2. High Temperature Sample Cell

**Heats of Sublimation.** An additional modification in the time-of-flight instrument was made (31) in the ion source to permit installation of a high temperature cell. The following design is an improvement to the earlier model reported by Shadoff (185). The cell (*see* Figure 2), constructed from solid brass stock, had an enclosed cavity 0.8 inches in length and 0.18 inches in diameter and two metal wings for mounting the

cell on the lower side of the ion source. Sauereisen #31 cement was used as insulation and as a means of holding the nichrome heater coil and chromel-alumel thermocouple (sealed by silver solder through the wall of the chamber) in place. An effusion insert plug about 0.2 inches in length, contained a hole centered through the plug which terminated in a 5 mil orifice. Fifty to one hundred milligrams of sample were placed in the cavity and the cell was sealed by tightening the brass effusion plug. After attaching the cell to the ion source, the source assembly was inserted in the flight tube, appropriately sealed, and the mass spectrometer was evacuated to about  $10^{-6}$  torr. Heating of the cell and its contents was accomplished by passing a current from a variable powerstat (0-12.6 volts) through the heater coil. The temperature of the cell was determined with a Tempco portable pyrometer and millivoltmeter (model PM-1K17) using a room temperature junction as the reference for the thermocouple.

The experiments for determining the heats of sublimation were usually carried out by heating the sample rather than cooling because of the deleterious effects of the vaporized species on the sensitivity of the multiplier dynode strip. Preliminary measurements with  $ZnBr_2$  showed no deviation outside the precision limits between heating and cooling curves.

The heats of sublimation were calculated using the form of the Clausius-Clapeyron equation given by Honig and coworkers (32, 74). Using this technique, a plot of the ion current multiplied by the absolute temperature as a function of the reciprocal of the absolute temperature yields a straight line. Typical plots for two halides are shown in Figures 3 and 4. The accuracy in our measurements is about 2-3 kcal./mole, as may be seen from Table I and Figures 3 and 4.

Shadoff (185) used the earlier design of this cell to follow the thermal decomposition of *cis*, and *trans*- $[Co(en)_2Cl_2]Cl$ . The present design is much superior to the earlier model for the study of "mass thermal analysis" (52, 105).

**Materials.** Most of the compounds investigated herein were obtained from commercial sources, although several were prepared by techniques published in the literature.

The pentachlorides of niobium and tantalum were obtained from City Chemical Co., and transferred under a dry nitrogen atmosphere to break-seal containers, evacuated, and sealed. Mercury bromide and iodide, zinc bromide, and phosphorus trichloride were Baker and Adamson products. Mercury and zinc chlorides were received from Fisher Scientific Co. Phosphorus tribromide and thiophosphoryl chloride were purchased from K & K Laboratories and the titanocene and zirconocene dichlorides were obtained from Arapahoe Chemicals, Inc.

The addition compound  $TaCl_5 \cdot S(C_2H_5)_2$  was synthesized as outlined by Fairbrother and Nixon (37). Diethyl sulfide was distilled from  $P_2O_5$  and fractionated in an 18-inch column packed with borosilicate glass rings. An intermediate fraction boiling at  $90^\circ C$ . was used in the preparation. The reaction between the organic sulfide and tantalum pentachloride was carried out inside a polyethylene glove bag under a dry nitrogen atmosphere. The resulting dark red solution was vacuum distilled at about  $5 \times 10^{-3}$  torr. Small volumes of yellow liquid were

collected in borosilicate vials equipped with glass break seals. Elemental analysis by Galbraith Laboratories gave good agreement with the calculated elemental compositions:  $\text{TaCl}_5 \cdot \text{S}(\text{C}_2\text{H}_5)_2$ ; Calc: Ta, 40.58, Cl, 39.24; H, 2.24; C, 10.76%. Found: Ta, 40.19; Cl, 39.31; H, 2.14; and C, 10.62%.

The sample of thiophosphoryl fluoride,  $\text{PSF}_3$ , was prepared by the technique outlined by Tullock and Coffman (205). One mole of NaF was stirred with 0.65 mole tetramethylene sulfone. After evacuation of the system, 0.25 mole  $\text{PSCl}_3$  was slowly added and the mixture was heated to  $150^\circ \text{C}$ . The thiophosphoryl fluoride gas evolved was subsequently collected in a  $-78^\circ \text{C}$  trap. The sample, without further distillation, was found to be greater than 95% pure by mass spectrometric analysis.

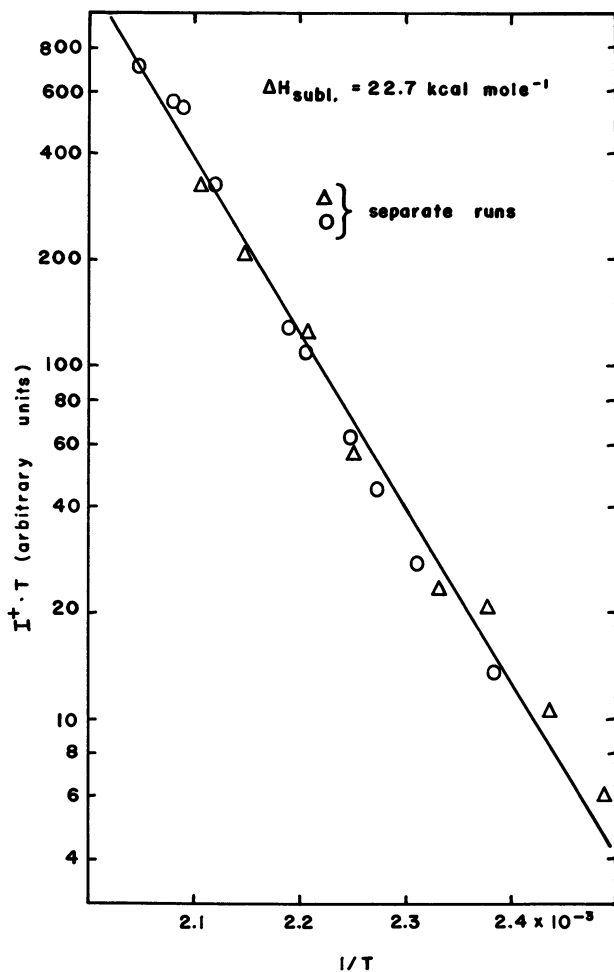


Figure 3. Second-Law Heat of Sublimation of Biscyclopentadienyltitanium Dichloride

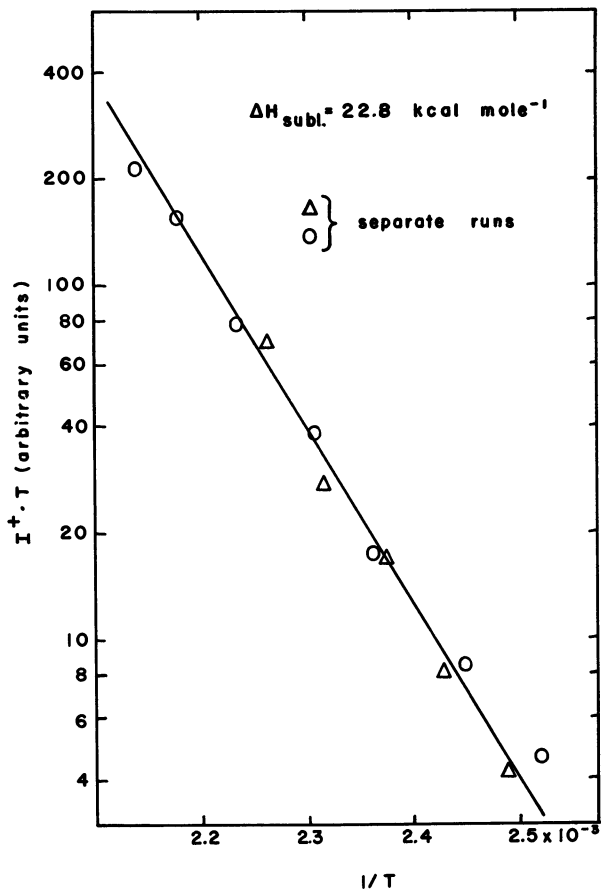


Figure 4. Second-Law Heat of Sublimation of Biscyclopentadienylzirconium Dichloride

**Auxiliary Thermochemical Data.** The following heats of formation were utilized in calculations of ionic heats of formation from the appearance potential data. All values refer to the gaseous species. F, 18.88 (208); F<sup>-</sup>, -64.7 (208); Cl, 29.08 (208); Br, 26.74 (208); I, 25.54 (208); O, 59.55 (208); S, 66.64 (208); S<sup>-</sup>, 17.42 (208); Zn, 31.19 (178); and Hg, 14.54 (178) kcal./mole.

**Experimental Results.** The experimental data obtained in these studies are grouped together and presented below; a brief discussion of these data is incorporated into this presentation.

**TITANIUM TETRACHLORIDE.** The appearance potentials and relative abundances for the positive ions formed from TiCl<sub>4</sub> are given in Table II. Marriott, Thorburn, and Craggs (128) used a Lozier tube to study TiCl<sub>4</sub> and found the ionization potential of TiCl<sub>4</sub> to be 11.7 e.v. and observed the appearance potentials of TiCl<sub>3</sub><sup>+</sup> and Cl<sup>-</sup> in an ion pair process to be 12.9 e.v. It is readily seen upon examining Table II, that these appearance

**Table I. Comparison of Measured and Accepted Heats of Sublimation**

Molecule	$\Delta H_{\text{subl.}}$ (kcal./mole)		
	This Study	Others	References
ZnBr <sub>2</sub>	30.0	30.1	(178)
HgCl <sub>2</sub>	19.3	18.50, 19.85	(20, 178)
HgI <sub>2</sub>	20.5	20.46	(178)
Ti(C <sub>5</sub> H <sub>5</sub> ) <sub>2</sub> Cl <sub>2</sub>	22.7		
Zr(C <sub>5</sub> H <sub>5</sub> ) <sub>2</sub> Cl <sub>2</sub>	22.8		
Fe(C <sub>5</sub> H <sub>5</sub> ) <sub>2</sub>		16.81	(82)

**Table II. Appearance Potentials and Heats of Formation for Positive Ions Produced from Titanium Tetrachloride<sup>a</sup>**

Ion	Relative Abundance at 70 e.v.	Appearance Potential (e.v.)	Probable Process	$\Delta H_f$ (ion) (kcal./mole)
TiCl <sub>4</sub> <sup>+</sup>	53.5	11.6 <sub>5</sub> ± 0.1 <sub>5</sub>	TiCl <sub>4</sub> → TiCl <sub>4</sub> <sup>+</sup>	87
TiCl <sub>3</sub> <sup>+</sup>	100.0	13.3 ± 0.3	→ TiCl <sub>3</sub> <sup>+</sup> + Cl	96
TiCl <sub>2</sub> <sup>+</sup>	33.0	16.7 ± 0.3	→ TiCl <sub>2</sub> <sup>+</sup> + 2Cl	145
TiCl <sup>+</sup>	39.0	20.6 ± 0.3	→ TiCl <sup>+</sup> + 3Cl	206
Ti <sup>+</sup>	40.8	25.0 ± 0.3	→ Ti <sup>+</sup> + 4Cl	279
TiCl <sub>3</sub> <sup>2+</sup>	1.9	30.0 ± 0.5	→ TiCl <sub>3</sub> <sup>2+</sup> + Cl	481
TiCl <sub>2</sub> <sup>2+</sup>	6.9	32.1 ± 0.8	→ TiCl <sub>2</sub> <sup>2+</sup> + 2Cl	500
TiCl <sup>2+</sup>	13.0	35.6 ± 0.9	→ TiCl <sup>2+</sup> + 3Cl	552
Ti <sup>2+</sup>	3.0	39.1 ± 1.3	→ Ti <sup>2+</sup> + 4Cl	604

<sup>a</sup>  $\Delta H_f(\text{TiCl}_{4(g)}) = -181.6$  kcal./mole (1).

potentials are in reasonable agreement with the data reported herein. There is no doubt concerning the process corresponding to the appearance potential for the TiCl<sub>4</sub><sup>+</sup> ion; however, our assignment of the probable process for the formation of TiCl<sub>3</sub><sup>+</sup> ion from TiCl<sub>4</sub> does not agree with that of Marriott, *et al.* (128).

Using the appearance potential given in Table II for Ti<sup>+</sup>, a heat of formation of Ti<sup>+</sup> is calculated to be 279 kcal./mole, in good agreement with a value of 269 kcal./mole determined by combining  $I(\text{Ti}) = 6.83$  e.v. (140, 141, 142) with  $\Delta H_f(\text{Ti})_{(g)} = 112$  kcal./mole (176). We conclude, therefore, that the process for the formation of Ti<sup>+</sup> can not involve a Cl<sup>-</sup> ion. It is difficult to understand why the TiCl<sub>3</sub><sup>+</sup> ion should be formed with Cl<sup>-</sup> ion in an ion pair process. The ion intensity of TiCl<sub>3</sub><sup>+</sup> is significantly greater than (it was not possible to obtain a quantitative ratio) that observed for the Cl<sup>-</sup> ion; this too is difficult to understand if the TiCl<sub>3</sub><sup>+</sup> and Cl<sup>-</sup> ions should be formed in an ion pair process. Further, if the TiCl<sub>3</sub><sup>+</sup> ion were formed in an ion pair process  $\Delta H_f(\text{TiCl}_3^+)$  would be ~ 180 kcal./mole rather than the 96 kcal./mole assigned in Table II; in this case the heats of formation of the TiCl<sub>x</sub><sup>+</sup> ions would not exhibit a reasonably monotonic increase as *x* is varied from four to zero.

A low intensity metastable ion at  $m^* = 126.45$  (for the most abundant isotopic species) was observed in the mass spectrum of  $\text{TiCl}_4$ . This corresponds to the metastable transition



Such a transition is in agreement with the clastogram for  $\text{TiCl}_4$ , shown in Figure 1, in which the  $\text{TiCl}_3^+$  ion is observed to increase sharply, pass through a maximum, and decrease slowly simultaneous with a monotonic decrease in the intensity of the  $\text{TiCl}_4^+$  ion as the ionizing energy of the electrons is increased. That is,  $\text{TiCl}_3^+$  is formed from  $\text{TiCl}_4^+$  and further decomposes to other species. Thus, we are forced to conclude the probable process for the formation of  $\text{TiCl}_3^+$  ion given in Table II, and the accompanying  $\Delta H_f(\text{TiCl}_3^+)$ . Interestingly, the data of Marriott, Thornburn, and Craggs (128) can be made compatible with the assignments given in Table II by employing the ion pair process



Two negative ions,  $\text{Cl}^-$  and  $\text{TiCl}_3^-$ , were observed to be formed in resonance processes from  $\text{TiCl}_4$ . These are listed in Table III. The intermediate values determined for the resonance potentials (at the peak maxima) are in agreement with the nature of a dissociative electron capture reaction. The data indicate also a high electron affinity of  $\text{TiCl}_3$ .

Figure 1 also suggests that the  $\text{TiCl}_3^+$  ion unimolecularly decomposes to form  $\text{TiCl}_2^+$  through the loss of a Cl atom; in turn, the  $\text{TiCl}_2^+$  ion consecutively decomposes to  $\text{TiCl}^+$ , and finally to  $\text{Ti}^+$ .

The energetic data given in Table II suggest the same consecutive unimolecular decomposition of the rather abundant doubly-charged ions. The  $\text{TiCl}_4^{2+}$  ion was not observed; it is suggested that  $\text{TiCl}_5^{2+}$  is a "pseudo-parent" doubly-charged ion formed in the initial electron impact process. The clastogram data support this mechanism.

**Table III. Negative Ion Processes for Some Group IVB and VB Metal Chlorides**

Ion	Resonance Potential (e.v.)	Resonance Process
$\text{TiCl}_3^-$	5.5	$\text{TiCl}_4 \rightarrow \text{TiCl}_3^- + \text{Cl}$
$\text{Cl}^-$	6.5	$\text{TiCl}_4 \rightarrow \text{Cl}^- + \text{TiCl}_3$
$\text{NbCl}_4^-$	2.3	$\text{NbCl}_5 \rightarrow \text{NbCl}_4^- + \text{Cl}$
$\text{Cl}^-$	4.7	$\text{NbCl}_5 \rightarrow \text{Cl}^- + \text{NbCl}_4$
$\text{TaCl}_4^-$	2.6	$\text{TaCl}_5 \rightarrow \text{TaCl}_4^- + \text{Cl}$
$\text{Cl}^-$	5.5	$\text{TaCl}_5 \rightarrow \text{Cl}^- + \text{TaCl}_4$

**NIObIUM AND TANTALUM PENTACHLORIDES.** The appearance potentials for the principal ions from and mass spectra of niobium and tantalum pentachloride are given in Tables IV and V, respectively. The clastogram for tantalum pentachloride is shown in Figure 5; that for niobium pentachloride is similar and therefore has not been included here.

Unlike the titanium tetrachloride, the parent ions from these compounds are extremely low intensity ions ( $\text{TaCl}_5^+$  was not detected).

**Table IV. Appearance Potentials and Heats of Formation for Positive Ions Produced from Niobium Pentachloride<sup>a</sup>**

<i>Ion</i>	<i>Relative Abundance at 70 e.v.</i>	<i>Appearance Potential (e.v.)</i>	<i>Probable Process</i>	$\Delta H_f$ ( <i>ion</i> ) (kcal./mole)
NbCl <sub>5</sub> <sup>+</sup>	0.3	(11.0) <sup>b</sup>	NbCl <sub>5</sub> → NbCl <sub>5</sub> <sup>+</sup>	(80) <sup>b</sup>
NbCl <sub>4</sub> <sup>+</sup>	100.0	11.3 <sub>4</sub> ± 0.2 <sub>2</sub>	→ NbCl <sub>4</sub> <sup>+</sup> + Cl	59
NbCl <sub>3</sub> <sup>+</sup>	30.0	(14.3) <sup>b</sup>	→ NbCl <sub>3</sub> <sup>+</sup> + 2Cl	(99) <sup>b</sup>
NbCl <sub>2</sub> <sup>+</sup>	27.1	18.8 ± 0.3	→ NbCl <sub>2</sub> <sup>+</sup> + 3Cl	173
NbCl <sup>+</sup>	24.9	22.8 ± 0.5	→ NbCl <sup>+</sup> + 4Cl	236
Nb <sup>+</sup>	19.8	28.0 ± 0.7	→ Nb <sup>+</sup> + 5Cl	327
NbCl <sub>4</sub> <sup>2+</sup>	0.8			
NbCl <sub>3</sub> <sup>2+</sup>	trace			
NbCl <sub>2</sub> <sup>2+</sup>	8.5			
NbCl <sup>2+</sup>	7.5			
Nb <sup>2+</sup>	1.8			

<sup>a</sup>  $\Delta H_f(\text{NbCl}_{5(g)}) = -173.3$  kcal./mole (178, 187).

<sup>b</sup> Estimated values.

**Table V. Appearance Potentials and Heats of Formation for Positive Ions Produced from Tantalum Pentachloride<sup>a</sup>**

<i>Ion</i>	<i>Relative Abundance at 70 e.v.</i>	<i>Appearance Potential (e.v.)</i>	<i>Probable Process</i>	$\Delta H_f$ ( <i>ion</i> ) (kcal./mole)
TaCl <sub>5</sub> <sup>+</sup>		(11.6) <sup>b</sup>	TaCl <sub>5</sub> → TaCl <sub>5</sub> <sup>+</sup>	(84) <sup>b</sup>
TaCl <sub>4</sub> <sup>+</sup>	100.0	12.0 ± 0.28	→ TaCl <sub>4</sub> <sup>+</sup> + Cl	64
TaCl <sub>3</sub> <sup>+</sup>	22.9	15.0 ± 0.4	→ TaCl <sub>3</sub> <sup>+</sup> + 2Cl	104
TaCl <sub>2</sub> <sup>+</sup>	23.9	19.6 ± 0.6	→ TaCl <sub>2</sub> <sup>+</sup> + 3Cl	181
TaCl <sup>+</sup>	17.9	25.0 ± 0.5	→ TaCl <sup>+</sup> + 4Cl	277
Ta <sup>+</sup>	13.0	29.5 ± 0.4	→ Ta <sup>+</sup> + 5Cl	352
TaCl <sub>4</sub> <sup>2+</sup>	2.3			
TaCl <sub>3</sub> <sup>2+</sup>	11.5			
TaCl <sub>2</sub> <sup>2+</sup>	7.2			
TaCl <sup>2+</sup>	3.9			
Ta <sup>2+</sup>	1.9			

<sup>a</sup>  $\Delta H_f(\text{TaCl}_{5(g)}) = -183.3$  kcal./mole (103, 178).

<sup>b</sup> Estimated values.

Typical of the halides is the fact that the (parent minus one halogen)<sup>+</sup> ion is the most intense ion in the mass spectrum. Also typical of the metal halides is the relatively large intensities of the doubly-charged ions.

The fragmentation mechanisms are proposed to be similar to the mechanism suggested for the titanium tetrachloride study. This proposal is supported by the clastograms. The clastograms for the doubly-charged ion, although not as well defined as for the singly-charged ions, similarly argue for such mechanisms.

On this basis, and on the basis of the energetic data, the processes shown in Table IV and V have been assigned and heats of formation for

the ions calculated. From arguments similar to those employed in the titanium tetrachloride case, we do not believe that  $\text{Cl}^-$  formed by an ion pair process is significant in any of the processes studied here. Because of the very low abundance of the parent ions, ionization potentials were not determined. However, by utilizing the statistical theory of mass spectra it is possible to estimate that the ionization potentials will be 0.3 to 0.4 e.v. below the lowest appearance potential. Therefore, we estimate  $I(\text{NbCl}_5) \approx 11.0$  e.v. and  $I(\text{TaCl}_5) \approx 11.6$  e.v. Because the mercury background interfered with a direct determination,  $AP(\text{NbCl}_3^+) \approx 14.3$  e.v. has been estimated by interpolation from the regular variation in the appearance potentials and heats of formation.

Table III records the negative ions observed and their energetics of formation. It is easily seen that these molecules behave very much like titanium tetrachloride under electron impact.

From the ionic heats of formation for the various  $\text{MCl}_n^+$  species in Tables II, IV, and V, the ionization potentials of the  $\text{MCl}_n$  were calculated using the heats of formation for the  $\text{TiCl}_n$  (1, 176) and  $\text{TaCl}_n$  (103, 176) moieties. The second ionization potentials of the  $\text{TiCl}_n$  species were determined in like manner.  $\Delta H_f(\text{NbCl}_5)$  and  $\Delta H_f(\text{Nb})$  are quite similar

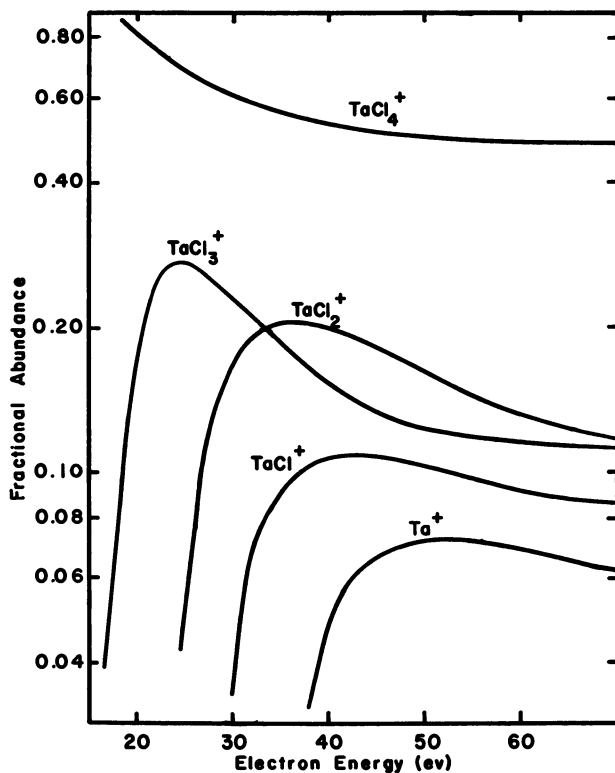


Figure 5. *Logarithmic Clastogram for Tantalum Pentachloride*

to  $\Delta H_f(\text{TaCl}_5)$  and  $\Delta H_f(\text{Ta})$ , respectively, so that  $\Delta H_f(\text{NbCl}_n)$  were readily estimated by comparison to the  $\Delta H_f(\text{TaCl}_n)$  values. The results of the calculations are presented in Table VI and compared to the first ionization potentials of the metals. It is observed that  $I(\text{MCl}) \approx I(\text{M})$ , but as chlorine atoms are successively added,  $I(\text{MCl}_n)$  increases, and that for  $\text{TiCl}_4$ ,  $\text{NbCl}_5$  and  $\text{TaCl}_5$  the ionization potentials are much greater and approach  $I(\text{Cl})$ . Although exhibiting the same trend, the second ionization potentials of  $\text{TiCl}_n$  do not approach the second ionization potential of chlorine as distinctly.

**Table VI. Ionization Potentials for Some Group IVB and VB Metal Chlorides**

Molecule	Spectroscopic Values			Second Ionization Potential (e.v.)
	First Ionization Potential (e.v.)	First Ionization Potential (e.v.)	Ref.	
$\text{TiCl}_4$	$11.65 \pm 0.15$			
$\text{TiCl}_3$	$9.7 \pm 0.3$			$16.7 \pm 0.6$
$\text{TiCl}_2$	$9.3 \pm 0.3$			$15.4 \pm 0.9$
$\text{TiCl}$	$8.1 \pm 0.4$			$15.0 \pm 1.0$
Ti		6.82	(140, 141, 142)	$14.1 \pm 1.4$
$\text{NbCl}_5$	11.0 <sup>a</sup>			
$\text{NbCl}_4$	$8.3 \pm 0.3$			
$\text{NbCl}_3$	$7.5 \pm 0.3$			
$\text{NbCl}_2$	$7.6 \pm 0.4$			
$\text{NbCl}$	$6.7 \pm 0.5$			
Nb		6.84	(140, 141, 142)	
$\text{TaCl}_5$	11.6 <sup>a</sup>			
$\text{TaCl}_4$	$8.9 \pm 0.3$			
$\text{TaCl}_3$	$8.1 \pm 0.3$			
$\text{TaCl}_2$	$7.9 \pm 0.6$			
$\text{TaCl}$	$8.2 \pm 0.5$			
Ta		7.88	(140, 141, 142)	

<sup>a</sup> Estimated values.

It is suggested from these results that the molecular orbital from which the electron is withdrawn upon ionization is one in which both the metal and the halogen orbital contributions are important. It would be expected that the metal orbitals make a greater contribution to the lower oxidation states of the metal, and that the halogen orbital contributions would be more important for higher oxidation states of the metal; this expectation appears to be borne out by these results and also by the results of previous mass spectrometric studies of the metal carbonyls.

**ZINC CHLORIDE AND BROMIDE.** The mass spectra of zinc chloride and bromide (Tables VII and VIII) were obtained by heating samples of the compounds to approximately 400°C. in the high temperature sample

**Table VII. Appearance Potentials and Heats of Formation for Positive Ions Produced from Zinc Chloride (at 683°K.)<sup>a</sup>**

<i>Ion</i>	<i>Relative Abundance at 70 e.v.</i>	<i>Appearance Potential (e.v.)</i>	<i>Probable Process</i>	$\Delta H_f$ ( <i>ion</i> ) (kcal./mole)
ZnCl <sub>2</sub> <sup>+</sup>	100.0	11.7 <sub>5</sub> ± 0.2 <sub>3</sub>	ZnCl <sub>2</sub> → ZnCl <sub>2</sub> <sup>+</sup>	208
ZnCl <sup>+</sup>	12.3	13.7 ± 0.2	→ ZnCl <sup>+</sup> + Cl	224
Zn <sup>+</sup>	18.6	14.6 ± 0.3	→ Zn <sup>+</sup> + 2Cl	216
Cl <sup>+</sup>	74.3	19.6 ± 0.3	→ Cl <sup>+</sup> + Zn + Cl	329

<sup>a</sup>  $\Delta H_f(\text{ZnCl}_{2(g)}) = -63.0$  kcal./mole (178).

**Table VIII. Appearance Potentials and Heats of Formation for Positive Ions Produced from Zinc Bromide (at 673°K.)<sup>a</sup>**

<i>Ion</i>	<i>Relative Abundance at 70 e.v.</i>	<i>Appearance Potential (e.v.)</i>	<i>Probable Process</i>	$\Delta H_f$ ( <i>ion</i> ) (kcal./mole)
ZnBr <sub>2</sub> <sup>+</sup>	100.0	10.3 <sub>9</sub> ± 0.3 <sub>3</sub>	ZnBr <sub>2</sub> → ZnBr <sub>2</sub> <sup>+</sup>	192
ZnBr <sup>+</sup>	11.3	13.4 ± 0.2	→ ZnBr <sup>+</sup> + Br	234
ZnBr <sub>2</sub> <sup>2+</sup>	4.8			
Zn <sup>+</sup>	12.4	14.7 ± 0.3	→ Zn <sup>+</sup> + 2Br	237
Br <sup>+</sup>	23.0	17.7 ± 0.3	→ Br <sup>+</sup> + Zn + Br	302

<sup>a</sup>  $\Delta H_f(\text{ZnBr}_{2(g)}) = -48.1$  kcal./mole (178).

cell shown in Figure 2. No apparent variations in the 70 e.v. monoisotopic mass spectrum were noted over the temperature range studied; this indicates that these materials vaporized as monomers under the equilibrium conditions (probably undersaturated) obtained with the high temperature cell. As a result, the ions observed are caused by the fragmentation of the parent molecule ion and are not ionized decomposition products. This is also borne out by the magnitude of the appearance potentials determined for these ions.

The processes assigned for the dissociative ionization are consistent with the appearance potentials measured, with the processes assigned for the other metal halides studied in this work, and with the heats of formation of the metal ions. The ionization potential determined for ZnCl<sub>2</sub> is lower than the value of 12.9 e.v. found by Foote and Mohler (41).

The heat of sublimation determined with the Second Law for ZnBr<sub>2</sub> (see Table I) is in good agreement with the literature value (176). It is of particular interest to note that in the mass spectra of both molecules the parent-molecule ion is the most intense ion. The proposed fragmentation process for these compounds is that the ZnX<sup>+</sup>, formed unimolecularly from ZnX<sub>2</sub><sup>+</sup>, decomposes *via* competitive paths to form Zn<sup>+</sup> and X<sup>+</sup>.

The negative halide ions were observed in the mass spectrum of both compounds at very low electron energies (resonance potentials of approximately 5 e.v.). Only in zinc bromide was ZnX<sup>-</sup> observed; this ion was determined to have a sharp resonance capture peak at 4.5 e.v. and

was not found to be produced in any ion pair process. No  $\text{ZnCl}^-$  was noted at any electron energy.

**MERCURIC CHLORIDE, BROMIDE, AND IODIDE.** The mass spectra and appearance potentials for mercuric chloride, bromide, and iodide are reported in Tables IX–XI. In each of these studies the  $\text{Hg}^+$  ion formed by dissociative ionization could not be determined because of the mercury background spectra caused by the use of a mercury diffusion pump with the time-of-flight mass spectrometer. However, the  $\text{Hg}^+$  peaks observed were much less intense than the parent molecule ion. In every case, the

**Table IX. Appearance Potentials and Heats of Formation for Positive Ions Produced from Mercuric Chloride (at 460°K.)<sup>a</sup>**

<i>Ion</i>	<i>Relative Abundance at 70 e.v.</i>	<i>Appearance Potential (e.v.)</i>	<i>Probable Process</i>	$\Delta H_f(\text{ion})$ (kcal./mole)
$\text{HgCl}_2^+$	72.7	$10.86 \pm 0.25$	$\text{HgCl}_2 \rightarrow \text{HgCl}_2^+$	214
$\text{HgCl}^+$	9.2	$12.06 \pm 0.26$	$\rightarrow \text{HgCl}^+ + \text{Cl}$	213
$\text{HgCl}_2^{2+}$	1.6	$28.3 \pm 0.5$	$\rightarrow \text{HgCl}_2^{2+}$	616
$\text{HgCl}^{2+}$	0.2	$32.0 \pm 0.5$	$\rightarrow \text{HgCl}^{2+} + \text{Cl}$	672
$\text{Cl}^+$	100.0	$17.7 \pm 0.3$	$\rightarrow \text{Cl}^+ + \text{Hg} + \text{Cl}$	328

<sup>a</sup>  $\Delta H_f(\text{HgCl}_{2(g)}) = -36.5$  kcal./mole (178).

**Table X. Appearance Potentials and Heats of Formation for Positive Ions Produced from Mercuric Bromide (at 454°K.)<sup>a</sup>**

<i>Ion</i>	<i>Relative Abundance at 70 e.v.</i>	<i>Appearance Potential (e.v.)</i>	<i>Probable Process</i>	$\Delta H_f(\text{ion})$ (kcal./mole)
$\text{HgBr}_2^+$	100.0	$9.94 \pm 0.15$	$\text{HgBr}_2 \rightarrow \text{HgBr}_2^+$	208
$\text{HgBr}^+$	17.5	$12.09 \pm 0.17$	$\rightarrow \text{HgBr}^+ + \text{Br}$	230
$\text{HgBr}_2^{2+}$	6.4	$25.7 \pm 0.3$	$\rightarrow \text{HgBr}_2^{2+}$	571
$\text{HgBr}^{2+}$	2.0	$31.1 \pm 0.7$	$\rightarrow \text{HgBr}^{2+} + \text{Br}$	669
$\text{Br}^+$	34.3	$16.7 \pm 0.2$	$\rightarrow \text{Br}^+ + \text{Hg} + \text{Br}$	322

<sup>a</sup>  $\Delta H_f(\text{HgBr}_{2(g)}) = -21.7$  kcal./mole (178).

**Table XI. Appearance Potentials and Heats of Formation for Positive Ions Produced from Mercuric Iodide (at 445° and 493°K.)<sup>a</sup>**

<i>Ion</i>	<i>Relative Abundance at 70 e.v.</i>	<i>Appearance Potential (e.v.)</i>	<i>Probable Process</i>	$\Delta H_f(\text{ion})$ (kcal./mole)
$\text{HgI}_2^+$	100.0	$8.87 \pm 0.22$	$\text{HgI}_2 \rightarrow \text{HgI}_2^+$	200
$\text{HgI}^+$	18.8	$11.3 \pm 0.4$	$\rightarrow \text{HgI}^+ + \text{I}$	230
$\text{HgI}_2^{2+}$	7.6	$21.4 \pm 0.5$	$\rightarrow \text{HgI}_2^{2+}$	489
$\text{I}_2^+$	1.7		$\rightarrow \text{I}_2^+ + ?$	
$\text{I}^+$	41.6	$15.5 \pm 0.4$	$\rightarrow \text{I}^+ + \text{Hg} + \text{I}$	313

<sup>a</sup>  $\Delta H_f(\text{HgI}_{2(g)}) = -4.8$  kcal./mole (178).

parent molecule ions were the most intense ions except for the  $\text{HgCl}_2$  study, in which the parent molecule ion is second-most intense after the  $\text{Cl}^+$  ion.

The probable processes are consistent with the determined appearance potentials and with the heats of formation of  $\text{Cl}^+$ ,  $\text{Br}^+$ , and  $\text{I}^+$ . It is interesting to note that the ionization potential of  $\text{HgBr}_2$  and  $\text{HgI}_2$  are less than the ionization potential of their constituent atoms. In the  $\text{HgCl}_2$  case, the ionization potential is only slightly greater than that of mercury, but is significantly less than the ionization potential of the chlorine atom, and is also lower than the value of  $I(\text{HgCl}_2)$  reported by Foote and Mohler (41).

The parent doubly-charged species in Table IX to XI are noted to be relatively intense and that this intensity increases from the chloride to the iodide. The second ionization potentials calculated from the data in these tables for the chloride, bromide and iodide are  $17.4 \pm 0.6$ ,  $15.8 \pm 0.3$ , and  $12.5 \pm 0.6$  e.v., respectively. This decrease in the second ionization potentials as one goes from the chloride to the iodide parallels the decrease in the first ionization potentials of these molecules, as well as the variation in the second ionization potentials of  $\text{HgCl}$  and  $\text{HgBr}$  ( $19.9 \pm 0.6$  and  $19.0 \pm 0.7$  e.v., respectively.)

In a study of negative ion formation from these three compounds we observed no  $\text{HgX}^-$  ion at any electron energy, although the  $\text{Cl}^-$ ,  $\text{Br}^-$ , and  $\text{I}^-$  ions were found to be formed by dissociative resonance capture at 2–4 e.v. No negative ions were noted to be formed in ion pair processes.

**Table XII. Appearance Potentials and Heats of Formation for Positive Ions Produced from Phosphorus Trichloride<sup>a</sup>**

<i>Ion</i>	<i>Relative Abundance at 70 e.v.</i>	<i>Appearance Potential (e.v.)</i>	<i>Probable Process</i>	$\Delta H_f$ ( <i>ion</i> ) (kcal./mole)
$\text{PCl}_3^+$	37.0	$10.7_5 \pm 0.2$	$\text{PCl}_3 \rightarrow \text{PCl}_3^+$	179
$\text{PCl}_2^+$	100.0	$12.3 \pm 0.2$	$\rightarrow \text{PCl}_2^+ + \text{Cl}$	186
$\text{PCl}^+$	19.0	$16.8 \pm 0.3$	$\rightarrow \text{PCl}^+ + 2\text{Cl}$	261
$\text{Cl}^+$	31.2	$20.2 \pm 0.5$	$\rightarrow \text{Cl}^+ + \text{PCl} + \text{Cl}$	(37) <sup>b</sup>
$\text{P}^+$	10.0	$21.2 \pm 0.5$	$\rightarrow \text{P}^+ + 3\text{Cl}$	333

<sup>a</sup>  $\Delta H_f(\text{PCl}_{3(g)}) = -68.6$  kcal./mole (208).

<sup>b</sup>  $\Delta H_f(\text{PCl}_{(g)})$ .

**PHOSPHORUS TRICHLORIDE AND TRIBROMIDE.** The energetic data given in Table XII for phosphorus trichloride are results reported by Sandoval, Moser, and Kiser (180). The heats of formation for the positive ions have been recalculated using more recent thermochemical data (208). Both the monoisotopic mass spectral cracking pattern and the energetic values are in good agreement with data reported subsequently by Halmann and Klein (56). The mass spectrum reported herein, obtained at 70 e.v., is in fair agreement with that reported by Kusch, Hustrulid, and Tate (104) using 120 e.v. ionizing energy.

The monoisotopic mass spectrum, appearance potentials of the positive ions, and heats of formation of the positive ions from phosphorus

tribromide are presented in Table XIII. A comparison of Tables XII and XIII reveals a marked similarity in the mass spectral cracking patterns of the chloride and bromide compounds, and in the processes for the formation of these ions in their threshold regions.

It is to be noted that the probable processes assigned for the formation of the positive ions do not involve ion pair formation processes. Halmann and Klein (56) have suggested that  $\text{PCl}_2^+$  is formed from  $\text{PCl}_3$  in the reaction



Using the arguments outlined above (even though a metastable transition was not observed) we conclude that Reaction 3 does not assume a significant rôle in the forming of  $\text{PX}_2^+$  ions from  $\text{PCl}_3$  and  $\text{PBr}_3$ . Although a careful search for metastable transitions in these compounds was made using both the time-of-flight and the MS-9 instruments, no "metastable peaks" were observed. The behavior of the  $\text{PX}_2^+$  curve in the clastograms indicates that  $\text{PCl}_2^+$  arises from  $\text{PCl}_3^+$ . These facts are compatible with a "fast" metastable transition.

**Table XIII. Appearance Potentials and Heats of Formation for Positive Ions Produced from Phosphorus Tribromide<sup>a</sup>**

<i>Ion</i>	<i>Relative Abundance at 70 e.v.</i>	<i>Appearance Potential (e.v.)</i>	<i>Probable Process</i>	$\Delta H_f$ ( <i>ion</i> ) (kcal./mole)
$\text{PBr}_3^+$	60.0	$10.0 \pm 0.2$	$\text{PBr}_3 \rightarrow \text{PBr}_3^+$	197
$\text{PBr}_2^+$	100.0	$11.4 \pm 0.2$	$\rightarrow \text{PBr}_2^+ + \text{Br}$	203
$\text{PBr}^+$	30.7	$15.6 \pm 0.3$	$\rightarrow \text{PBr}^+ + 2\text{Br}$	273
$\text{Br}^+$	—	$17.1 \pm 0.5$	$\rightarrow \text{Br}^+ + \text{PBr} + \text{Br}$	(33) <sup>b</sup>
$\text{P}^+$	19.0	$20.1 \pm 0.5$	$\rightarrow \text{P}^+ + 3\text{Br}$	350

<sup>a</sup>  $\Delta H_f(\text{PBr}_{3(g)}) = -33.3$  kcal./mole (208).

<sup>b</sup>  $\Delta H_f(\text{PBr}_{(g)})$ .

Two features which warrant attention concerning these phosphorus halide systems in contrast with the metal halide systems discussed above concern doubly-charged ions and negative ions. As pointed out earlier, the metal halides show a tendency to form relatively intense doubly-charged ions, whereas only a few doubly-charged ions are observed in phosphorus trichloride and tribromide and they are of a much lower intensity. The relative intensities of the  $\text{X}^-$  ions (the only negative ions observed) formed by both dissociative resonance capture and by ion pair formation, are much greater in the phosphorus halides than in the metal halides. The phosphorus halides are similar to the metal halides in one important respect: they all have as their base peak the (parent-halogen)<sup>+</sup> ion.

**PHOSPHORYL CHLORIDE AND THIOPHOSPHORYL FLUORIDE.** Halmann and Klein (56) have reported mass spectral data for  $\text{POCl}_3$ . The data reported in this work (Table XIV) differs in several important respects from the studies of the earlier investigations.

**Table XIV. Appearance Potentials and Heats of Formation for Positive Ions Produced from Phosphorus Oxytrichloride<sup>a</sup>**

Ion	Relative Abundance at 70 e.v.	Appearance Potential (e.v.)	Probable Process	$\Delta H_f$ (ion) (kcal./mole)
$\text{POCl}_3^+$	44.2	$11.4 \pm 0.3$	$\text{POCl}_3 \rightarrow \text{POCl}_3^+$	129
$\text{POCl}_2^+$	100.0	$12.8 \pm 0.3$	$\rightarrow \text{POCl}_2^+ + \text{Cl}$	133
$\text{POCl}^+$	4.1	$15.6 \pm 0.3$	$\rightarrow \text{POCl}^+ + 2\text{Cl}$	168
$\text{PCl}^+$	6.9	$20.2 \pm 0.4$	$\rightarrow \text{PCl}^+ + \text{O} + \text{Cl}_2$	273
$\text{PO}^+$	37.3	$16.6 \pm 0.4$	$\rightarrow \text{PO}^+ + 3\text{Cl}$	162
$\text{P}^+$	12.6	$28.1 \pm 0.5$	$\rightarrow \text{P}^+ + \text{O} + 3\text{Cl}$	369
$\text{Cl}^+$	23.7		$\rightarrow \text{Cl}^+ + ?$	

<sup>a</sup>  $\Delta H_f(\text{POCl}_3(g)) = -133.48$  kcal./mole (208).

The mass spectral cracking patterns from the two investigations are in fair agreement, with the exception of the data for three ions. Halmann and Klein have reported a 3% abundance of the  $\text{PCl}_3^+$  ion and 8% abundance of the  $\text{PCl}_2^+$  ion. We observed no  $\text{PCl}_3^+$  and only a very small  $\text{PCl}_2^+$  ion intensity. We did find the  $\text{POCl}^+$  ion (with about 4% relative abundance) and were able to obtain energetic data for this ion; Halmann and Klein did not report the presence of this ion in their investigations of  $\text{POCl}_3$ . It is believed that their sample contained some amount of  $\text{PCl}_3$  as impurity, as evidenced also from the low appearance potentials reported for the  $\text{PCl}_3^+$  and  $\text{PCl}_2^+$  ions.

Although these few discrepancies in the mass spectrum of  $\text{POCl}_3$  exist, the more important disagreement between the two studies concerns the energetic data. We recall from the inorganic halide results discussed above that an increase of approximately 1.5 to 2.0 e.v. occurs for the lowest appearance potential above the ionization potential if any significant amount of the parent-molecule ion is observed. In Table XIV we show that this holds true as well for  $\text{POCl}_3$ . The results do not agree with those obtained by Halmann and Klein (56) where only a 0.2 e.v. difference in the ionization potential and the lowest appearance potential was reported. If the appearance potential of the  $\text{POCl}_2^+$  ion, reported to be 13.3 e.v., is accepted, then the ionization potential of  $\text{POCl}_3$  is expected to be  $\sim 11.5$  e.v., in agreement with our results.

From preliminary studies of  $\text{POF}_3$  and  $\text{POBr}_3$  in this laboratory, we find the ionization potentials of these molecules to be 13.4 e.v. and 10.46 e.v., respectively. The ionization potential of  $\text{POCl}_3$  is expected to be intermediate between these two values, again substantiating an ionization potential of  $\text{POCl}_3$  distinctly lower than 13 e.v.

The value of the appearance potential of  $\text{PCl}^+$  obtained by Halmann and Klein is much lower than the value we report in Table XIV. This is to be expected if they have  $\text{PCl}_3$  contaminating their  $\text{POCl}_3$  sample. In fact, the appearance potential of  $\text{PCl}^+$  from  $\text{PCl}_3$  and from  $\text{POCl}_3$  reported by Halmann and Klein agree. We conclude, therefore, that many of the processes assigned by Halmann and Klein are in error.

The positive ion clastogram for  $\text{POCl}_3$  is shown in Figure 6. It is interesting to note that the consecutive unimolecular decomposition reac-

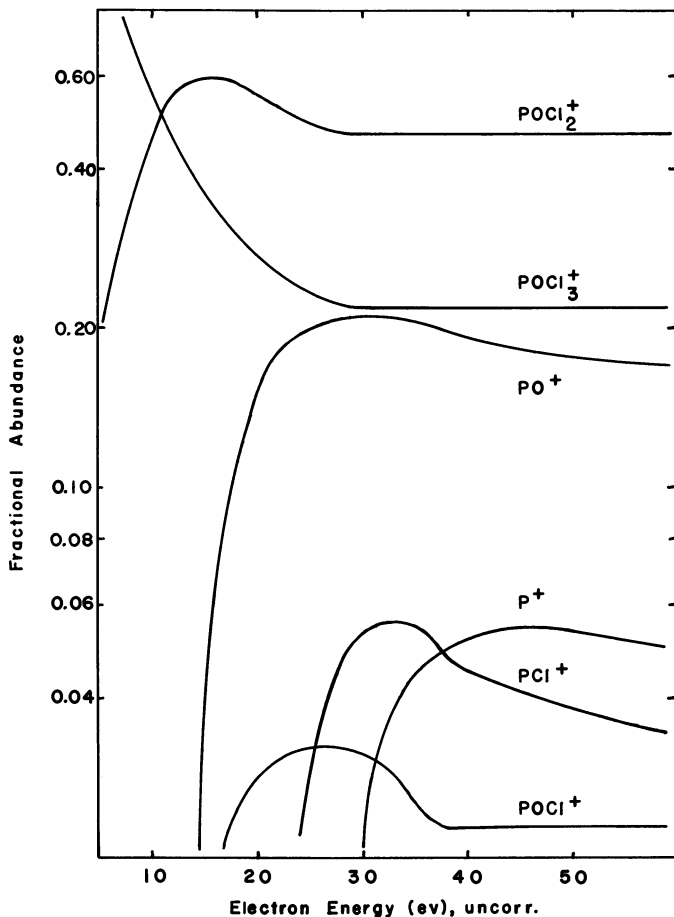
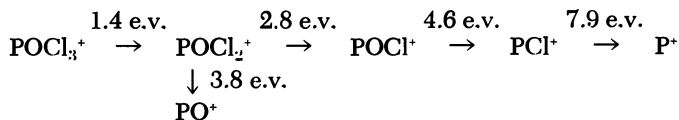


Figure 6. *Logarithmic Clastogram for Phosphoryl Chloride*

tions which appear to be the major decomposition paths in the metal and phosphorus halide systems no longer are the only pathways occurring in  $\text{POCl}_3$ . A decomposition scheme which includes both consecutive and competitive modes of decomposition is more probable. The clastogram and energetic data suggest the following decomposition scheme:



Although a search was made for metastable transitions in  $\text{POCl}_3$ , none were identified. Thus, the clastogram information is of particular importance to this study.

The following negative ions were observed from  $\text{POCl}_3$ :  $\text{POCl}_2^-$ ,  $\text{POCl}^-$ ,  $\text{PCl}^-$ ,  $\text{PO}^-$ , and  $\text{Cl}^-$ . Except for the  $\text{PO}^-$  ion, Halmann and Klein (56) observed these same ions and  $\text{PCl}_3^-$ ,  $\text{PCl}_2^-$ , and  $\text{O}^-$  in addition to those we report. Figure 7 is a negative ion clastogram of  $\text{POCl}_3$ . One may observe that this negative ion clastogram, the first such treatment of negative ion spectra as a function of the electron energy, is basically different from the positive ion clastograms discussed above. The ion intensities vary in a manner unlike the positive ion analogs because of the two different types of ionization processes which occur with negative ions; namely, resonance processes and ion pair formation. Absolute energetic data were not obtained for these ions because of the difficulties encountered in the calibration of the energy axis. It is not possible to assign a unique decomposition mechanism of the negative ions from Figure 7.

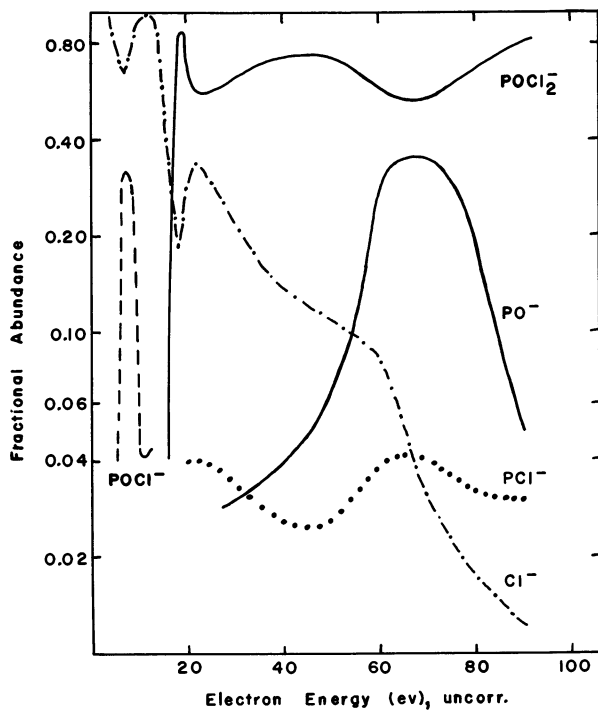


Figure 7. *Logarithmic Clastogram of Negative Ions from Phosphoryl Chloride*

Similar to the other halides discussed in this work, the (parent-minus one halogen)<sup>+</sup> ion is a very intense ion in the mass spectrum of  $\text{POCl}_3$ . In contrast to  $\text{POCl}_3$  and many of the other halides, thiophosphoryl fluoride, exhibits a large parent ion (*see* Table XV). More unusual is the observation that the  $\text{S}^+$  ion is the second most intense ion in the mass spectrum. The ionization potential of  $\text{PSF}_3$  is quite low suggesting the

**Table XV. Appearance Potentials and Heats of Formation for Positive Ions Produced from Thiophosphoryl Fluoride<sup>a</sup>**

<i>Ion</i>	<i>Relative Abundance at 70 e.v.</i>	<i>Appearance Potential (e.v.)</i>	<i>Probable Process</i>	$\Delta H_f(\text{ion})$ (kcal./mole)
PSF <sub>3</sub> <sup>+</sup>	100.0	11.1 ± 0.3	PSF <sub>3</sub> → PSF <sub>3</sub> <sup>+</sup>	2
PSF <sub>2</sub> <sup>+</sup>	27.1	16.0 ± 0.2	→ PSF <sub>2</sub> <sup>+</sup> + F	96
PF <sub>3</sub> <sup>+</sup>	6.9	14.3 ± 0.2	→ PF <sub>3</sub> <sup>+</sup> + S <sup>-</sup>	58
PF <sub>2</sub> <sup>+</sup>	26.0	17.2 ± 0.3	→ PF <sub>2</sub> <sup>+</sup> + F + S <sup>-</sup>	106
PF <sup>+</sup>	6.8	22.9 ± 0.4	→ PF <sup>+</sup> + F <sub>2</sub> + S	207
PS <sup>+</sup>	2.4	19.2 ± 0.5	→ PS <sup>+</sup> + 2F + F <sup>-</sup>	216
F <sup>+</sup>	trace			
S <sup>+</sup>	73.5			

<sup>a</sup>  $\Delta H_f(\text{PSF}_{3(g)}) = -254$  kcal./mole (196).

removal of an electron from an orbital on the phosphorus or sulfur rather than the halogen atoms.

We have had to treat the PSF<sub>3</sub>, shown in Table XV, in a manner different from the preceding compounds; ion pair formations have been written for three of the processes assigned. F<sup>-</sup> was observed from PSF<sub>3</sub> at higher electron energies.  $\Delta H_f(\text{PS}^+) = 216$  kcal./mole agrees with values of 209 and 240 kcal./mole determined from PSCl<sub>3</sub> and PSBr<sub>3</sub> by Wada (207). No S<sup>-</sup> ion was observed at any electron energy in our studies; however, it is postulated in Table XV to give agreement of  $\Delta H_f(\text{PF}_3^+) = 58$  kcal./mole with values of 78 kcal./mole from Wada's PF<sub>5</sub> study (202), and an unpublished value of 40 kcal./mole from PF<sub>3</sub>. If the process yielded S rather than S<sup>-</sup>, the calculated  $\Delta H_f(\text{PF}_3^+)$  would be much lower (~9 kcal./mole). Similar reasoning was used in making the assignment for the PF<sub>2</sub><sup>+</sup> ion in Table XV.

In an effort to attempt to observe TaSCl<sub>n</sub><sup>+</sup>, where  $n = 0$  to 3, TaCl<sub>5</sub> · S(C<sub>2</sub>H<sub>5</sub>)<sub>2</sub> was prepared and studied. Fairbrother and Nixon (38) report that this compound withstands decomposition at reduced pressure and elevated temperatures. Upon introduction of this material to the mass spectrometer ion source, fragmentation did occur; however, only fragment ions indicative of TaCl<sub>5</sub> and S(C<sub>2</sub>H<sub>5</sub>)<sub>2</sub> were observed. The S(C<sub>2</sub>H<sub>5</sub>)<sub>2</sub> fragmentation pattern agreed with the known mass spectrum of diethyl sulfide, and the TaCl<sub>5</sub> pattern was identical to that observed for TaCl<sub>5</sub> (see above discussion). The clastogram and appearance potentials determined confirmed that we were observing only the decomposition products of TaCl<sub>5</sub> · S(C<sub>2</sub>H<sub>5</sub>)<sub>2</sub> and that TaSCl<sub>3</sub> was not formed in the decomposition. Therefore, a comparison of this system to other MYX<sub>3</sub> compounds was not possible.

### Conclusions

In the metal halides, a significant contribution of the halogen orbitals to the highest molecular orbital is deduced from the values of the ionization potentials of these compounds. Commonly, the most intense ion

observed in the 70 e.v. mass spectrum is the (parent minus one halogen)<sup>+</sup> ion, although several of the metal halides have the (parent)<sup>+</sup> ion as the base peak. Ion pair processes are found generally not to play a significant rôle in the formation of positive ions. Many of the fragmentation mechanisms, as suggested from the clastograms and energetic data, may be described by consecutive unimolecular decompositions of the parent ion.

Although a large number of studies of inorganic halide systems have been made, many more investigations are required before detailed generalizations of the fragmentation pathways and predictions of the energetics can be made, and these compounds constitute only a small fraction of inorganic chemistry. Studies of the metal carbonyl, various metal alkyls, and sandwich compounds (45) have been reported. Currently, studies of Werner complexes such as the metal acetylacetonates (and substituted acetylacetonates) (198), glyoximates (96), and 8-quinolinolates are underway. What is required to aid in understanding the reaction of gaseous inorganic ions (and the effects of the variation of the metal atoms in similar compounds) is a large effort in studying many systems mass spectrometrically. The techniques and instrumentation are now available to permit these investigations which should be of particular value in inorganic chemistry; it would indeed be worthwhile to attempt to obtain routinely at least the mass spectrum of each new inorganic compound synthesized for these purposes.

### *Acknowledgments*

The authors wish to thank R. M. Teeter and E. J. Gallegos and Chevron Research Company for aid in obtaining some of the metastable transition data with the MS-9 at the Richmond Laboratories. This work has benefited from the financial support of the U.S. Atomic Energy Commission and the Department of the Army. One of us (J.G.D.) held a National Aeronautics and Space Administration Fellowship during the tenure of these studies and wishes to extend his appreciation for this aid.

### *Literature Cited*

- (1) Altman, D., Farber, M., Mason, D. M., *J. Chem. Phys.* **25**, 531 (1956).
- (2) Aston, F. W., "Mass Spectra and Isotopes," 2nd ed., Edward Arnold and Co., London, 1942.
- (3) Asundi, R. K., Craggs, J. D., *Proc. Phys. Soc. (London)* **83**, 611 (1964).
- (4) Barton, H. A., *Phys. Rev.* **25**, 469 (1925).
- (5) Barton, H. A., *Phys. Rev.* **30**, 614 (1927).
- (6) Berkowitz, J., Chupka, W. A., *J. Chem. Phys.* **29**, 653 (1958).
- (7) Berkowitz, J., Chupka, W. A., *J. Chem. Phys.* **45**, 1287 (1966).
- (8) Berkowitz, J., Marquart, J. R., *J. Chem. Phys.* **37**, 1853 (1962).
- (9) Berkowitz, J., Tasman, H. A., Chupka, W. A., *J. Chem. Phys.* **36**, 2170 (1962).

- (10) Blanchard, L. B., LeGoff, P., *Can. J. Chem.* **35**, 89 (1957).
- (11) Botter, R., "Advances in Mass Spectrometry," R. M. Elliott, ed., Vol. 2, pp. 540-554, Pergamon Press, Oxford, England, 1963.
- (12) Boudreaux, E. A., *J. Chem. Phys.* **40**, 246 (1964).
- (13) Bralsford, R., Harris, P. V., Price, W. C., *Proc. Roy. Soc. (London)* **A258**, 459 (1960).
- (14) Büchler, A., Blackburn, P. E., Stauffer, J. L., *J. Phys. Chem.* **70**, 685 (1966).
- (15) Büchler, A., Stauffer, J. L., Klemperer, W., *J. Chem. Phys.* **40**, 3471 (1964).
- (16) Burhop, E. H. S., Massey, H. S. W., Watt, C., in "The Characteristics of Electrical Discharges in Magnetic Fields," Guthrie and Wakerling, eds., Div. I, Vol. 5, p. 145, McGraw-Hill Book Co., New York, 1949.
- (17) Burns, J. F., *Carbide and Carbon Chemical Co.*, K-25 Plant, Rept. **K-1147**, Oct. 8, 1954.
- (18) Colburn, C. B., Johnson, F. A., *J. Chem. Phys.* **33**, 1869 (1960).
- (19) Coope, J. A. R., Frost, D. C., McDowell, C. A., *Nature* **179**, 1186 (1957).
- (20) Cubicciotti, D., Eding, H., Johnson, J. W., *J. Phys. Chem.* **70**, 2989 (1966).
- (21) Cullen, W. R., Frost, D. C., *Can. J. Chem.* **40**, 390 (1962).
- (22) Curran, R. K., *J. Chem. Phys.* **34**, 1069 (1961).
- (23) Dempster, A. J., *Phys. Rev.* **11**, 316 (1918).
- (24) Dibeler, V. H., Mohler, F. L., *J. Res. Natl. Bur. Stds.* **40**, 25 (1948).
- (25) Dibeler, V. H., Reese, R. M., *J. Chem. Phys.* **31**, 282 (1959).
- (26) Dibeler, V. H., Reese, R. M., Franklin, J. L., *J. Chem. Phys.* **27**, 1296 (1957).
- (27) Dibeler, V. H., Reese, R. M., Mann, D. E., *J. Chem. Phys.* **27**, 176 (1957).
- (28) Dibeler, V. H., Reese, R. M., Mohler, F. L., *J. Chem. Phys.* **20**, 761 (1952).
- (29) Dibeler, V. H., Reese, R. M., Mohler, F. L., *J. Res. Natl. Bur. Stds.* **57**, 113 (1956).
- (30) Dibeler, V. H., Reese, R. M., Mohler, F. L., *J. Chem. Phys.* **26**, 304 (1957).
- (31) Dillard, J. G., Ph.D. Dissertation, Kansas State Univ., Manhattan, Kan., 1967.
- (32) Drowart, J., Honig, R. E., *J. Phys. Chem.* **61**, 980 (1957).
- (33) Dubov, S. S., Khokhlova, A. M., *Zh. Obshch. Khim.* **34**, 586 (1964).
- (34) Duncan, A. B. F., *J. Chem. Phys.* **20**, 951 (1952).
- (35) Ehlert, T. C., Blue, G. D., Green, J. W., Margrave, J. L., *J. Chem. Phys.* **41**, 2250 (1964).
- (36) Ehlert, T. C., Margrave, J. L., *J. Chem. Phys.* **41**, 1066 (1964).
- (37) Fairbrother, F., Nixon, J. F., *J. Chem. Soc.* **1962**, 150.
- (38) Farmer, J. B., Henderson, I. H. S., Lossing, F. P., Marsden, D. G. H., *J. Chem. Phys.* **24**, 348 (1956).
- (39) Fisher, I. P., Homer, J. B., Lossing, F. P., *J. Am. Chem. Soc.* **87**, 957 (1965).
- (40) Flesch, G. D., Svec, H. J., *J. Am. Chem. Soc.* **81**, 1787 (1959).
- (41) Foote, P. D., Mohler, F. L., *Phys. Rev.* **17**, 394 (1921).
- (42) Fox, R. E., *J. Chem. Phys.* **32**, 385 (1960).
- (43) Fox, R. E., Curran, R. K., *J. Chem. Phys.* **34**, 1595 (1961).
- (44) Friedman, L., *J. Chem. Phys.* **23**, 477 (1955).
- (45) Friedman, L., Irsa, A. P., Wilkinson, G., *J. Am. Chem. Soc.* **77**, 3689 (1955).
- (46) Frost, D. C., McDowell, C. A., *Can. J. Chem.* **36**, 39 (1958).
- (47) Frost, D. C., McDowell, C. A., *Can. J. Chem.* **38**, 407 (1960).

- (48) Gallegos, E. J., Kiser, R. W., *J. Am. Chem. Soc.* **83**, 733 (1961).  
(49) Gallegos, E. J., Kiser, R. W., *J. Phys. Chem.* **65**, 1177 (1961).  
(50) Gallegos, E. J., Klaver, R. F. (unpublished data).  
(51) Glockler, G., Lind, S. C., "The Electrochemistry of Gases and Other Dielectrics," pp. 333-371, John Wiley and Sons, Inc., New York, 1939.  
(52) Gohlke, R. S., Langer, H. G., *Anal. Chem.* **37** (10), 25A (1965).  
(53) Gowenlock, B. G., Haynes, R. M., Majer, J. R., *Trans. Faraday Soc.* **58**, 1905 (1962).  
(54) Green, J. W., Blue, G. D., Ehlert, T. C., Margrave, J. L., *J. Chem. Phys.* **41**, 2245 (1964).  
(55) Hall, L. H., Subbanna, V. V., Koski, W. S., *J. Am. Chem. Soc.* **86**, 3969 (1964).  
(56) Halmann, M., Klein, Y., *J. Chem. Soc.* **1964**, 4324.  
(57) Hamano, H., *Bull. Chem. Soc. Japan* **30**, 741 (1957).  
(58) Harrison, A. G., Kebarle, P., Lossing, F. P., *J. Am. Chem. Soc.* **83**, 777 (1961).  
(59) Harrison, A. G., Shannon, T. W., *Can. J. Chem.* **40**, 1730 (1962).  
(60) Henglein, A., Muccini, G. A., *J. Chem. Phys.* **31**, 1426 (1959).  
(61) Herron, J. T., Dibeler, V. H., *J. Am. Chem. Soc.* **82**, 1555 (1960).  
(62) Herron, J. T., Dibeler, V. H., *J. Chem. Phys.* **33**, 1595 (1960).  
(63) Herron, J. T., Dibeler, V. H., *J. Res. Natl. Bur. Stds.* **65A**, 405 (1961).  
(64) Herzberg, G., "Molecular Spectra and Molecular Structure. I. Spectra of Diatomic Molecules," 2nd ed., pp. 456-534. D. Van Nostrand Co., Inc., New York, 1950.  
(65) Herzberg, G. (private communication to C. Lifshitz and F. A. Long) 1965.  
(66) Hildenbrand, D. L., Murad, E., *J. Chem. Phys.* **43**, 1400 (1965).  
(67) Hildenbrand, D. L., Murad, E., *J. Chem. Phys.* **44**, 1524 (1966).  
(68) Hildenbrand, D. L., Theard, L. P., *J. Chem. Phys.* **42**, 3230 (1965).  
(69) Hildenbrand, D. L., Theard, L. P., Saul, A. M., *J. Chem. Phys.* **39**, 1973 (1963).  
(70) Hobrock, D. L., Ph.D. Dissertation, Kansas State Univ., Manhattan, Kan., 1965.  
(71) Hobrock, D. L., Kiser, R. W., *J. Phys. Chem.* **68**, 575 (1964).  
(72) Hobson, R. M., *J. Chem. Phys.* **23**, 2463 (1955).  
(73) Hogness, T. R., Lunn, E. G., *Phys. Rev.* **26**, 44 (1925).  
(74) Honig, R. E., *J. Chem. Phys.* **22**, 126 (1954).  
(75) Hoppe, R., Dähne, W., Mattauch, H., Rodden, K. M., *Angew. Chem.* **74**, 903 (1962).  
(76) Hughes, A. L., Dixon, A. A., *Phys. Rev.* **10**, 495 (1917).  
(77) Ionov, N. I., *Doklady Akad. Nauk SSSR* **59**, 467 (1948).  
(78) Irsa, A. P., *J. Chem. Phys.* **26**, 18 (1957).  
(79) Irsa, A. P., Friedman, L., *J. Inorg. Nucl. Chem.* **6**, 77 (1958).  
(80) Isaacs, L. D., Price, W. C., Ridley, R. G., "The Threshold of Space," M. Zelikoff, ed., pp. 143-151, Pergamon Press, Ltd., London, 1957.  
(81) Johns, J. W. C., Barrow, R. F., *Proc. Phys. Soc. (London)* **A71**, 476 (1958).  
(82) Kaplan, L., Kester, W. L., Katz, J. J., *J. Am. Chem. Soc.* **74**, 5531 (1952).  
(83) Karo, A. M., Allen, L. C., *J. Chem. Phys.* **31**, 968 (1959).  
(84) Kaufman, R., *Phys. Rev.* **78**, 332 (1950).  
(85) Kaufman, R., *Trans. N. Y. Acad. Sci.* **15**, 131 (1953).  
(86) Keneshea, F. J., Cubicciotti, D., *J. Chem. Phys.* **40**, 191 (1964).  
(87) Keneshea, F. J., Cubicciotti, D., *J. Chem. Phys.* **40**, 1778 (1964).  
(88) Kennedy, A., Colburn, C. B., *J. Chem. Phys.* **35**, 1892 (1961).  
(89) Kennedy, T., Payne, D. S., Reed, R. I., Snedden, W., *Proc. Chem. Soc.* **1959**, 133.

- (90) Kent, R. A., Margrave, J. L., *J. Am. Chem. Soc.* **87**, 3582 (1965).  
(91) Kent, R. A., Margrave, J. L., *J. Am. Chem. Soc.* **87**, 4754 (1965).  
(92) Kent, R. A., McDonald, J. D., Margrave, J. L., *J. Phys. Chem.* **70**, 874 (1966).  
(93) Khvostenko, V. I., Sultanov, A. S., *Zh. Fiz. Khim.* **39**, 475 (1965).  
(94) Kiser, R. W., Clark, R. J., Krassoi, M. A. (unpublished work) 1966.  
(95) Kiser, R. W., Hobrock, D. L., *J. Am. Chem. Soc.* **87**, 922 (1965).  
(96) Kiser, R. W., Sullivan, R. E. (unpublished work) 1966.  
(97) Knipping, P., *Z. Physik* **7**, 328 (1921).  
(98) Koski, W. S., Kaufman, J. J., Pachucki, C. F., *J. Am. Chem. Soc.* **81**, 1326 (1959).  
(99) Krauss, M., *J. Chem. Phys.* **28**, 1021 (1958).  
(100) Kreuzer, H., *Z. Naturforsch.* **12A**, 519 (1957).  
(101) Kuczowski, R. L., *J. Am. Chem. Soc.* **86**, 3617 (1964).  
(102) Kuczowski, R. L., Wilson, E. B., Jr., *J. Am. Chem. Soc.* **85**, 2028 (1963).  
(103) Kurbanov, A. R., Suvorov, A. V., Shchukarev, S. A., *Zh. Neorg. Khim.* **9**, 513 (1964).  
(104) Kusch, P., Hustrulid, A., Tate, J. T., *Phys. Rev.* **52**, 840 (1937).  
(105) Langer, H. G., Gohlke, R. S., Smith, D. H., *Anal. Chem.* **37**, 433 (1965).  
(106) LaPaglia, S. R., Duncan, A. B. F., *J. Chem. Phys.* **34**, 1003 (1961).  
(107) Law, R. W., Margrave, J. L., *J. Chem. Phys.* **25**, 1086 (1956).  
(108) Law, R. W., Margrave, J. L., *J. Chem. Phys.* **34**, 1003 (1961).  
(109) Lifshitz, C., Long, F. A., *J. Chem. Phys.* **41**, 2468 (1964).  
(110) Lifshitz, C., Long, F. A., *J. Phys. Chem.* **69**, 3731 (1965).  
(111) Lossing, F. P., Kebarle, P., De Sousa, J. B., "Advances in Mass Spectrometry," J. D. Waldron, ed., pp. 431-441, Pergamon Press, Ltd., London, 1959.  
(112) Lossing, F. P., Tickner, A. W., Bryce, W. A., *J. Chem. Phys.* **19**, 1254 (1951).  
(113) Loughran, E. D., Mader, C., *J. Chem. Phys.* **32**, 1578 (1960).  
(114) Lustig, M., Cady, G. H., *Inorg. Chem.* **2**, 388 (1963).  
(115) Mackay, C. A., *Phil. Mag.* **46**, 828 (1923).  
(116) Mackay, C. A., *Phys. Rev.* **23**, 553 (1924).  
(117) Mackay, C. A., *Phys. Rev.* **24**, 319 (1924).  
(118) Majer, J. R., Patrick, C. R., *Nature* **201**, 1022 (1964).  
(119) Malik, W. U., Salahuddin, *Naturwiss.* **50**, 402 (1963).  
(120) Malone, T. J., McGee, Jr., H. A., *J. Phys. Chem.* **69**, 4338 (1965).  
(121) Malone, T. J., McGee, Jr., H. A., *J. Phys. Chem.* **70**, 316 (1966).  
(122) Margrave, J. L., *Symp. Valence Chem. Binding*, Madison, Wisconsin, June 22, 1956.  
(123) Margrave, J. L., *J. Chem. Phys.* **31**, 1432 (1959).  
(124) Margrave, J. L., *J. Chem. Phys.* **32**, 1889 (1960).  
(125) Marriott, J., Ph.D. Dissertation, Univ. of Liverpool, 1954.  
(126) Marriott, J., Craggs, J. D., *J. Electron.* **1**, 405 (1956).  
(127) Marriott, J., Craggs, J. D., *J. Electron. Control* **3**, 194 (1957).  
(128) Marriott, J., Thorburn, R., Craggs, J. D., *Proc. Phys. Soc. (London)* **B67**, 437 (1954).  
(129) Massey, A. G., Urch, D. S., *Chem. Ind.* **1965**, 607.  
(130) McKinley, J. D., *J. Chem. Phys.* **40**, 120 (1964).  
(131) McKinley, J. D., *J. Chem. Phys.* **40**, 576 (1964).  
(132) McKinley, J. D., *J. Chem. Phys.* **41**, 2814 (1964).  
(133) McKinley, J. D., *J. Chem. Phys.* **42**, 2245 (1965).  
(134) Miller, R. C., Kusch, P., *J. Chem. Phys.* **25**, 860 (1956).  
(135) Milne, T. A., Cubicciotti, D., *J. Chem. Phys.* **29**, 846 (1958).  
(136) Milne, T. A., Klein, H. M., *J. Chem. Phys.* **33**, 1628 (1960).

- (137) Milne, T. A., Klein, H. M., Cubicciotti, D., *J. Chem. Phys.* **28**, 718 (1958).
- (138) Mitra, G., *J. Am. Chem. Soc.* **80**, 5639 (1958).
- (139) Momigny, J., *Bull. Soc. Roy. Sci. Liege* **28**, 251 (1959).
- (140) Moore, C. E., *Natl. Bur. Stds. Cir.* **467**, 1949.
- (141) *Ibid.*, 1952.
- (142) *Ibid.*, 1958.
- (143) Morrison, J. D., *J. Chem. Phys.* **19**, 1305 (1951).
- (144) Morrison, J. D., Hurzeler, H., Inghram, M. G., Stanton, H. E., *J. Chem. Phys.* **33**, 821 (1960).
- (145) Morrison, J. D., Nicholson, A. J. C., *J. Chem. Phys.* **20**, 1021 (1952).
- (146) Murakawa, K., *Z. Physik* **109**, 173 (1938).
- (147) Nicholson, A. J. C., *J. Chem. Phys.* **43**, 1171 (1965).
- (148) Nier, A. O., Hanson, E. E., *Bull. Am. Phys. Soc.* **10**, 10 (1935).
- (149) Nier, A. O., Hanson, E. E., *Phys. Rev.* **50**, 722 (1936).
- (150) Osberghaus, O., *Z. Physik* **128**, 366 (1950).
- (151) Paulett, G. S., Lustig, M., *J. Am. Chem. Soc.* **87**, 1020 (1965).
- (152) Petry, R. C., *J. Am. Chem. Soc.* **82**, 2400 (1960).
- (153) Porter, R. F., *J. Chem. Phys.* **33**, 951 (1960).
- (154) Porter, R. F., Schoonmaker, R. C., *J. Chem. Phys.* **29**, 1070 (1958).
- (155) Porter, R. F., Schoonmaker, R. C., *J. Phys. Chem.* **63**, 626 (1959).
- (156) Porter, R. F., Zeller, E. E., *J. Chem. Phys.* **33**, 858 (1960).
- (157) Pottie, R. F., Lossing, F. P., *J. Am. Chem. Soc.* **85**, 269 (1963).
- (158) Price, W. C., *Bull. Am. Phys. Soc.* **10**, 9 (1935).
- (159) Price, W. C., *Phys. Rev.* **47**, 419 (1935).
- (160) Price, W. C., *Phys. Rev.* **47**, 510 (1935).
- (161) Price, W. C., *Proc. Roy. Soc. (London)* **A167**, 216 (1938).
- (162) Price, W. C., *Chem. Revs.* **41**, 257 (1947).
- (163) Price, W. C., Passmore, T. R., *Discussions Faraday Soc.* **35**, 232 (1963).
- (164) Price, W. C., Passmore, T. R., Roessler, D. M., *Discussions Faraday Soc.* **35**, 201 (1963).
- (165) Price, W. C., Teegan, J. P., Walsh, A. D., *Proc. Roy. Soc. (London)* **A201**, 600 (1950).
- (166) Price, W. C., Tuttle, W. T., *Proc. Roy. Soc. (London)* **A174**, 207 (1940).
- (167) Reed, R. I., Snedden, W., *Trans. Faraday Soc.* **54**, 301 (1958).
- (168) Reed, R. I., Snedden, W., *Trans. Faraday Soc.* **55**, 876 (1959).
- (169) Reese, R. M., Dibeler, V. H., *J. Chem. Phys.* **24**, 1175 (1956).
- (170) Reese, R. M., Dibeler, V. H., private communication to B. G. Hobrock and R. W. Kiser.
- (171) Reese, R. M., Dibeler, V. H., *J. Phys. Chem.* **66**, 155 (1962).
- (172) Reese, R. M., Dibeler, V. H., Franklin, J. L., *J. Chem. Phys.* **29**, 880 (1958).
- (173) Rinke, K., Schäfer, H., *Angew. Chem.* **77**, 131 (1965).
- (174) Roberts, J. E., Cady, G. H., *J. Am. Chem. Soc.* **81**, 4166 (1959).
- (175) Robinson, D. W., *J. Mol. Spectry.* **11**, 275 (1963).
- (176) Rosenbaum, O., Neuert, H., *Z. Naturforsch.* **9A**, 990 (1954).
- (177) Rosenstock, H. M., Sites, J. R., Walton, J. R., Baldock, R., *J. Chem. Phys.* **23**, 2442 (1955).
- (178) Rossini, F. D., Wagman, D. D., Evans, W. H., Levine, S., Jaffe, I., *Natl. Bur. Stds. Circ.* **500**, 1952.
- (179) Ruff, J. K., Paulett, G., *Inorg. Chem.* **3**, 998 (1964).
- (180) Sandoval, A. A., Moser, H. C., Kiser, R. W., *J. Phys. Chem.* **67**, 124 (1963).
- (181) Schoonmaker, R. C., Friedman, A. H., Porter, R. F., *J. Chem. Phys.* **31**, 1586 (1959).
- (182) Schoonmaker, R. C., Porter, R. F., *J. Chem. Phys.* **29**, 116 (1958).
- (183) Schoonmaker, R. C., Porter, R. F., *J. Chem. Phys.* **30**, 283 (1959).

- (184) Seel, F., Budenz, K., *Ber.* **98**, 251 (1965).
- (185) Shadoff, L. A., Ph.D. Dissertation, Kansas State Univ., Manhattan, Kan., 1966.
- (186) Shapiro, I., Landesman, H., *J. Chem. Phys.* **33**, 1590 (1960).
- (187) Shchukarev, S. A., Oranskaya, M. A., Shemyakina, T. S., *Zh. Neorg. Khim.* **5**, 2135 (1961).
- (188) Sidorov, L. N., Akishin, P. A., Belousov, V. I., Shol'ts, V. B., *Zh. Fiz. Khim.* **38**, 146 (1964).
- (189) Steele, W. C., *J. Phys. Chem.* **68**, 2359 (1964).
- (190) Steele, W. C., Nichols, L. D., Stone, F. G. A., *J. Am. Chem. Soc.* **84**, 1154 (1962).
- (191) Steele, W. C., Stone, F. G. A., *J. Am. Chem. Soc.* **84**, 3599 (1962).
- (192) Streitwieser, A., Jr., *J. Am. Chem. Soc.* **82**, 4123 (1960).
- (193) Stuckey, W. K., Ph.D. Dissertation, Kansas State Univ., Manhattan, Kan., 1966.
- (194) Stuckey, W. K., Kiser, R. W., *Nature* **211**, 963 (1966).
- (195) Stull, D. R., "JANAF Thermochemical Tables," **PB-168**, 370.
- (196) Studier, M. H., Sloth, E. N., "Noble-Gas Compounds," H. H. Hyman, ed., pp. 47-49, Univ. of Chicago Press, Chicago, Ill., 1963.
- (197) Svec, H. J., Flesch, G. D., *Science* **142**, 954 (1963).
- (198) Teeter, R. M., Kiser, R. W., unpublished work (1966).
- (199) Terenin, A., *Phys. Rev.* **36**, 147 (1930).
- (200) Terenin, A., Popov, B., *Z. Physik* **75**, 338 (1932).
- (201) Terenin, A., Popov, B., *Physik. Z. Sowjetunion* **2**, 299 (1932).
- (202) Thompson, J. C., Margrave, J. L., Timms, P. L., *Chem. Commun.* **1966**, 566.
- (203) Thomson, J. J., *Phil. Mag.* **24**, 209 (1912).
- (204) Thomson, J. J., Thomson, G. P., "Conduction of Electricity through Gases," 3rd ed., p. 81, Cambridge at the University Press, London, 1933.
- (205) Tullock, C. W., Coffman, D. D., *J. Org. Chem.* **25**, 2016 (1960).
- (206) Vought, R. H., *Phys. Rev.* **71**, 93 (1947).
- (207) Wada, Y., Ph.D. Dissertation, Kansas State University, Manhattan, Kan., 1964.
- (208) Wagman, D. D., Evans, W. H., Halow, I., Parker, V. B., Bailey, S. M., Schumm, R. H., *Natl. Bur. Std. (U.S.) Tech. Note* **270-1**, Oct. 1, 1965.
- (209) Warren, J. W., *Nature* **165**, 810 (1950).
- (210) Warren, V. L., Horton, J. C., *U. S. At. Energy Comm.* **K-1429** (1959).
- (211) Watanabe, K., *J. Chem. Phys.* **26**, 542 (1957).
- (212) Watanabe, K., Nakayama, T., Mottl, J., *Dept. Army #5B99-01-004 ORD-#TB2-0001-OOR-#1624*, Contract No. DA-04-200-ORD 480 and 737 (December 1959).
- (213) Watanabe, K., Nakayama, T., Mottl, J. R., *J. Quant. Spectry. Radiative Transfer* **2**, 369 (1962).
- (214) White, J. R., Cameron, A. E., *Phys. Rev.* **71**, 907 (1947).
- (215) Wilkinson, P. G., *J. Mol. Spectry.* **6**, 1 (1961).
- (216) Wilkinson, P. G., *Astrophys. J.* **138**, 778 (1963).
- (217) Wilson, E. B., Jr., Kuczkowski, R. L., *Doc. N63-17725* (1962).
- (218) Wilson, E. G., Jortner, J., Rice, S. A., *J. Am. Chem. Soc.* **85**, 813 (1963).
- (219) Zubkov, V. I., Tikhomirov, M. V., Andrianov, K. A., Golubtsov, S. A., *Doklady Akad. Nauk SSSR* **159**, 599 (1964).

RECEIVED November 14, 1966. Taken in part from the doctoral dissertations of John G. Dillard and Donald L. Dugger, submitted to the Graduate School of Kansas State University, Manhattan, Kansas.

# Mass Spectrometry of Phosphorus Hydrides

T. P. FEHLNER and R. B. CALLEN

Department of Chemistry and Radiation Laboratory, University of Notre Dame, Notre Dame, Ind.

*Appearance potentials, heats of formation, and relative abundances of the principal positive ions from phosphine, diphosphine-2, and diphosphine-4 have been determined using a mass spectrometer with collision-free sampling. A value for the heat of formation of  $26 \pm 8$  kcal./mole for diphosphine-2 has been calculated from the data. It is shown that in conventional ion sources decomposition completely obscures the mass spectrometry of diphosphine-4.*

As the source of a mass spectrometer operates at elevated temperatures, the mass spectrometry—*i.e.*, relative abundances and appearance potentials of the principal ions produced by electron impact—of thermally unstable substances can be obscured by decomposition occurring in the ion source. Diphosphine-4 is a compound that decomposes rapidly at room temperature. In order to obtain unambiguous information, some method of collision-free sampling must be used (5). The results are interesting since it appears that the mass spectrometry of pure diphosphine-4 has not been previously observed.

## *Experimental*

The mass spectrometer and sampling system used here are basically similar to instruments previously described (4, 5, 16), and only a brief characterization is given below.

The sampling system is illustrated in Figure 1. The gas or mixture of gases to be examined flows from a cold reservoir through the center tube of the quartz flow reactor, whose temperature may be varied from room temperature to about 800°K. The center portion of the efflux of the reactor is sampled by means of a circular orifice leading into a separately pumped chamber. The pressure on the high side of the leak is kept below the value where the mean free path is comparable to the orifice dimensions. The beam is collimated and then ionized in a separately pumped mass spectrometer chamber. The total beam length is

3.1 cm. To introduce discrimination against background and other source effects, the neutral beam is modulated in the second chamber at 590 c.p.s., using a vibrating reed driven by an audio oscillator. The total output of the mass spectrometer, which is a normal circle,  $90^\circ$ , 8.75 cm. radius of curvature, magnetic sector machine having a quadrupole ion lens, and using electron multiplier detection, is fed into a narrow-band amplifier locked-in to the frequency and phase of the chopper. By employing a modulated beam system, any unmodulated signals arising from background gas, residual beam molecules (molecules which enter the source as beam molecules and are ionized after being scattered and before being pumped away) pyrolysis products, etc. are eliminated although they still compete with the modulated signal as noise.

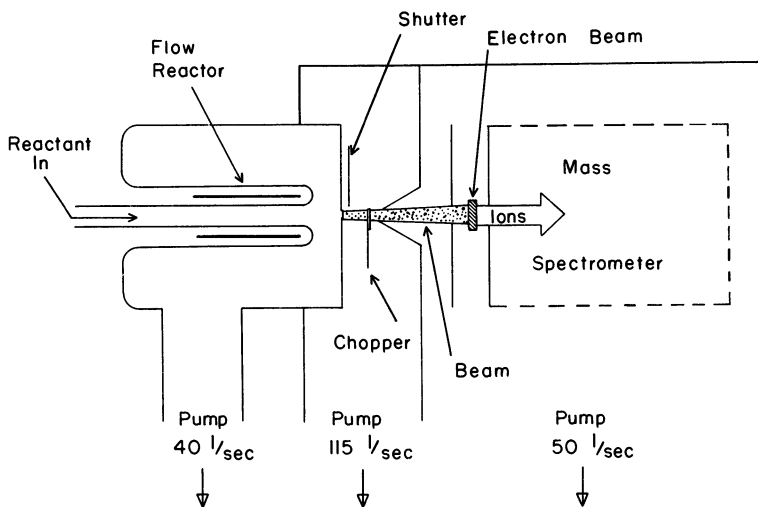


Figure 1. Schematic drawing of sampling system

There are three other effects which can result in signals coherent with the beam signal (4). Large pressure fluctuations in the source can have substantial components at the chopping frequency. These are minimized by using a differentially pumped beam collimation system. However, with the differentially pumped system there is a net flow between the different chambers. Part of this flow will coincide with the beam, will be chopped, and will be indistinguishable from the beam. A solenoid-operated shutter, which blocks the beam but does not affect the flow, allows this extraneous signal to be determined. With nitrogen as a test gas this signal was only 3% of the total modulated signal in this apparatus. Finally, when the neutral beam is introduced into the ionization chamber, a density of residual molecules is built up owing to the finite pumping speed at the source exits. In the present apparatus the density of these residual molecules is about 0.1 times the density of beam molecules at the steady state for nitrogen gas even though a rather open source construction was employed. When the beam is modulated, there is a tendency for the residual gas density to follow the beam density

changes. This effect is not important provided the modulation period is short with respect to the time constant of the vacuum system (4, 5). Here a modulation period of 1.7 msec. and a vacuum time constant of 50 msec. gave an inphase component of the total pressure variation of  $3 \times 10^{-5}$ .

With this system the ion signal observed is attributed to gas introduced into the source in an essentially collision-free manner. This contrasts with conventional sampling where gas is simply leaked into the source and suffers many collisions with the hot walls of the source before being ionized or pumped away.

### *Appearance Potentials*

Appearance potentials of the parent ions of phosphine and diphosphine-4 were determined using a model 12-107 Bendix time-of-flight mass spectrometer, which was previously modified for retarding potential difference (RPD) appearance potential measurements (6, 10). Xenon and krypton were used as calibrating gases, and the ionization potentials, determined for both the protonated and deuterated molecules, were identical within experimental error. Results by the RPD method can be compared with those obtained by photoionization since a value of 10.18 e. v. was obtained here for the ionization potential of  $\text{NH}_3$ ; this is in good agreement with the photoionization value of 10.154 e. v. (18).

Appearance potentials of the fragment ions were determined on the mass spectrometer using molecular beam sampling using a semilog technique (5). The parent ion was used to calibrate the voltage scale. The  $\text{PH}_x^+$  ions from  $\text{P}_2\text{H}_4$  were an exception to this since the vanishing current method (8) was used because of the low intensity of these ions and the presence of small  $\text{PH}_3$  impurities. The stated error in the appearance potentials is an estimate based on the precision of each measurement, the number of determinations, and the method used to determine the value.

In order to calculate the ionic heats of formation, the process for forming the ion must be known. Determining the correct process is not easy; however, appearance potentials can generally be estimated, and the most probable process can be chosen by comparison with the experimental values. By assuming that the appearance potential measured refers to the ion formed in its ground state with no excess energy, the heat of formation can be calculated (9).

### *Phosphine*

Phosphine was prepared as described previously (1). The results of this study along with those of the previous studies (3, 11, 13, 15, 17) are given in Table I. A ( $\text{P}^+/\text{PH}_3$ )—*i.e.*, the appearance potential of  $\text{P}^+$

**Table I. Relative Abundances and Appearance Potentials of the**  
*Relative abundance*

	<i>m/e</i>	<i>Relative abundance</i>			
		<i>This work</i> (50 e. v.)	<i>Others (70 e. v.)</i>		
<i>Phosphine</i>	34	61	75.2 <sup>a</sup>	85.0 <sup>d</sup>	68.0 <sup>c</sup>
	33	30	21.8 <sup>a</sup>	27.6 <sup>d</sup>	25.4 <sup>c</sup>
	32	100	100.0 <sup>a</sup>	100.0 <sup>d</sup>	100.0 <sup>c</sup>
	31	35	24.1 <sup>a</sup>	26.4 <sup>d</sup>	40.2 <sup>c</sup>
<i>Diphosphine-2</i>	64	70			
	63	60			
	62	100			
<i>Diphosphine-4</i>	66	100	100 <sup>a</sup>	100 <sup>b</sup>	
	65	8	12 <sup>a</sup>	16 <sup>b</sup>	
	64	52	68 <sup>a</sup>	69 <sup>b</sup>	
	63	46	59 <sup>a</sup>	67 <sup>b</sup>	
	62	60	77 <sup>a</sup>	1190 <sup>b</sup>	
	34	1 max. <sup>f</sup>	70 <sup>a</sup>	(5) <sup>b</sup>	
	33	3 <sup>f</sup>	28 <sup>a</sup>	61 <sup>b</sup>	
	32	8 <sup>f</sup>	134 <sup>a</sup>	2 <sup>b</sup>	
	31	8 <sup>f</sup>	88 <sup>a</sup>	14 <sup>b</sup>	

<sup>a</sup> See (17).

<sup>b</sup> See (14).

<sup>c</sup> See (15).

<sup>d</sup> See (11).

from  $\text{PH}_3$ , is somewhat doubtful since the ion efficiency curve exhibited considerable tailing.

For this molecule the spectrum obtained on the machine with collision-free sampling was nearly identical to that obtained with conventional sampling. Within experimental error, two of the ionization potentials previously measured (11, 17) agree with the RPD value reported here.

From A ( $\text{PH}_2^+/\text{PH}_3$ ) and the ionization potential of  $\text{PH}_3$  one notes that  $D(\text{H}_2\text{P}-\text{H}) = 3.2$  e. v. in the  $\text{PH}_3^+$  ion. By assuming that the average PH bond energy,  $E(\text{P}-\text{H})$ , in the ions is 3.2 e. v., appearance potentials of the fragment ions can be estimated for various processes. The results given in Table II for the most probable process are consistent with the measured appearance potentials. For  $\text{P}^+$  an alternative value of 15.9 is obtained using an ionization potential of  $\text{P} = 10.5$  e. v. (8) and a PH bond energy in  $\text{PH}_3$  of 77 kcal./mole (7).

With the heat formation of  $\text{PH}_3$  taken to be 1.3 kcal./mole (7), the ionic heats of formation given in Table II are calculated from the measured appearance potentials.

**Principal Ions from Phosphine, Diphosphine-2, and Diphosphine-4***Appearance potential, e. v.*

<i>This work</i>	<i>Others</i>			
10.05 ± 0.05	10.2 <sup>a</sup>	10.0 <sup>d</sup>	11.5 <sup>e</sup>	10.4 <sup>f</sup>
13.2 ± 0.2	13.2 <sup>a</sup>	13.9 <sup>d</sup>	14.4 <sup>e</sup>	14.0 <sup>f</sup>
12.6 ± 0.2	13.3 <sup>a</sup>	12.0 <sup>d</sup>	12.4 <sup>e</sup>	13.1 <sup>f</sup>
15.9 (P)	17.2 <sup>a</sup>	16.7 <sup>d</sup>	16.5 <sup>e</sup>	16.0 <sup>f</sup>
10.2 ± 0.2				
13.3 ± 0.4				
11.9 ± 0.4				
9.17 ± 0.05	8.7 ± 0.3 <sup>a</sup>		10.6 <sup>b</sup>	
12.2 ± 0.2	9.1 <sup>a</sup>		11.3 <sup>b</sup>	
11.1 ± 0.2	10.5 <sup>a</sup>		12.7 <sup>b</sup>	
14.6 ± 0.3	13.2 <sup>a</sup>		13.6 <sup>b</sup>	
13.2 ± 0.2	12.2 <sup>a</sup>		13.7 <sup>b</sup>	
—	(10.1) <sup>a</sup>			
15.3 ± 0.5	(13.2) <sup>a</sup>		12.5 <sup>c</sup>	
17.4 ± 0.5	(13.4) <sup>a</sup>			
19.4 ± 0.5	(17.3) <sup>a</sup>		16.7 <sup>b</sup>	

<sup>e</sup> See (13).<sup>f</sup> See (14).<sup>a</sup> Uncorrected for multiplier discrimination.***Diphosphine-2***

$P_2H_2$  was originally prepared by pyrolyzing  $P_2H_4$  in the flow reactor shown in Figure 1 (2). Later it was found that the steady-state concentration of  $P_2H_2$  formed from  $P_2H_4$  at room temperature and low pressures using a nearly static system was sufficient to study this molecule.  $P_2H_2$  has not been isolated in a pure state, and consequently its mass spectrometry is incomplete.

The results on this molecule are given in Table I. The relative abundances for  $P_2H_2$  given here are somewhat different from the approximate values reported previously (2). The former were obtained by subtracting the room temperature spectrum of pure  $P_2H_4$  from the room temperature spectrum of a mixture of  $P_2H_4$  and  $P_2H_2$ , while the latter were obtained by subtracting the room temperature spectrum from a high temperature spectrum of the mixture. A small temperature effect in the spectrum of  $P_2H_4$  could easily account for the difference observed, and the values reported here are the better values.

The ionization potential of  $P_2H_2$  was determined using the semi-log technique and is less certain than the other ionization potentials. When

Table II. Calculated Appearance Potentials and Heats of Formation

	Ion	Process	
<i>Phosphine</i>	$\text{PH}_3^+$	$\text{PH}_3 \rightarrow \text{PH}_3^+$	
	$\text{PH}_2^+$	$\text{PH}_3 \rightarrow \text{PH}_2^+ + \text{H}$	
	$\text{PH}^+$	$\text{PH}_3 \rightarrow \text{PH}^+ + \text{H}_2$	
	$\text{P}^+$	$\text{PH}_3 \rightarrow \text{P}^+ + \text{H}_2 + \text{H}$	
<i>Diphosphine-2</i>	$\text{P}_2\text{H}_2^+$	$\text{P}_2\text{H}_2 \rightarrow \text{P}_2\text{H}_2^+$	
	$\text{P}_2\text{H}^+$	$\text{P}_2\text{H}_2 \rightarrow \text{P}_2\text{H}^+ + \text{H}$	
	$\text{P}_2^+$	$\text{P}_2\text{H}_2 \rightarrow \text{P}_2^+ + \text{H}_2$	
<i>Diphosphine-4</i>	$\text{P}_2\text{H}_4^+$	$\text{P}_2\text{H}_4 \rightarrow \text{P}_2\text{H}_4^+$	
	$\text{P}_2\text{H}_3^+$	$\text{P}_2\text{H}_4 \rightarrow \text{P}_2\text{H}_3^+ + \text{H}$	
	$\text{P}_2\text{H}_2^+$	$\text{P}_2\text{H}_4 \rightarrow \text{P}_2\text{H}_2^+ + \text{H}_2$	
	$\text{P}_2\text{H}^+$	$\text{P}_2\text{H}_4 \rightarrow \text{P}_2\text{H}^+ + \text{H}_2 + \text{H}$	
	$\text{P}_2^+$	$\text{P}_2\text{H}_4 \rightarrow \text{P}_2^+ + 2\text{H}_2$	
	$\text{PH}_2^+$	(a)	$\text{P}_2\text{H}_4 \rightarrow \text{PH}_2^+ + \text{PH}_2$
		(b)	$\rightarrow \text{PH}_2^+ + \text{P} + \text{H}_2$
		(c)	$\rightarrow \text{PH}_2^+ + \text{PH} + \text{H}$
	$\text{PH}^+$	(a)	$\text{P}_2\text{H}_4 \rightarrow \text{PH}^+ + \text{PH}_3$
		(b)	$\rightarrow \text{PH}^+ + \text{PH} + \text{H}_2$
		(c)	$\rightarrow \text{PH}^+ + \text{PH}_2 + \text{H}$
		(d)	$\rightarrow \text{PH}^+ + \text{P} + \text{H}_2 + \text{H}$
$\text{P}^+$	(a)	$\text{P}_2\text{H}_4 \rightarrow \text{P}^+ + \text{PH}_2 + \text{H}_2$	
	(b)	$\rightarrow \text{P}^+ + \text{PH}_3 + \text{H}$	
	(c)	$\rightarrow \text{P}^+ + \text{P} + \text{H}_2 + \text{H}_2$	
	(d)	$\rightarrow \text{P}^+ + \text{PH} + \text{H}_2 + \text{H}$	

$E(\text{P}-\text{H}) = 3.2$  e. v. is used for the ions, the estimated appearance potentials are consistent with the measured values for the chosen processes. The heats of formation of the ions for these processes are given in Table II in terms of the heat of formation of  $\text{P}_2\text{H}_2$ .

### *Diphosphine-4*

$\text{P}_2\text{H}_4$  was prepared as previously described (1). The results of this study along with those of the other two studies (14, 17) are given in Table I. The relative intensity of  $\text{PH}_3^+$  from  $\text{P}_2\text{H}_4$  is a maximum value as the appearance potential measurement for this ion showed the presence of a small  $\text{PH}_3$  impurity. No good value for  $A(\text{PH}_3^+/\text{P}_2\text{H}_4)$  could be obtained. A comparison of the fragmentation pattern obtained with collision-free sampling and those reported previously for conventional sampling shows clearly that decomposition occurs in the spectrometer source.

The ionization potential reported here does not agree well with either of the previous values (14, 17). A tentative explanation may be

**of Ions from Phosphine, Diphosphine-2, and Diphosphine-4**

<i>Calculated appearance potential e. v.</i>	$\Delta H_f^+$ <i>kcal./mole</i>
	233
13.2	254
12.0	291
15.2, 15.9	316
	$235 + \Delta H_f(P_2H_2)$
13.4	$254 + \Delta H_f(P_2H_2)$
12.1	$274 + \Delta H_f(P_2H_2)$
	216
12.4	234
11.1	261
14.3	289
13.0	309
12.0	
14.1	
15.2	
12.4	
14.6	
15.8	
17.8	
14.6	
15.8	
16.8	
18.0	

put forth on the basis of the shape of the ionization efficiency curve. From Figure 2 one sees that the ion efficiency curve for diphosphine-4 will exhibit considerably more "tailing" than the rare gas curve. A close look at the methods (8) shows that the linear extrapolation technique will yield a high ionization potential, and the energy compensation technique will give a low value. Saalfeld and Svec used the former method and obtained a high ionization potential, while Wada and Kiser used the latter and obtained a low result.

Once again using  $E(P-H) = 3.2$  e. v. for the ions, the estimated appearance potentials for the  $P_2H_x^+$  ions are consistent with the chosen processes and the measured values. Taking the heat of formation of  $P_2H_4$  to be 5.0 kcal./mole (7) the ionic heats of formation are calculated. Combining the values for  $P_2H_4$  and  $P_2H_2$  yields the heat of formation of  $P_2H_2$ , the best value being  $26 \pm 8$  kcal./mole.

The  $A(PH_x^+/P_2H_4)$  values are rather uncertain. Since these values have been previously used to derive bond energies (15), it is of interest to estimate the appearance potentials of the various processes. This can be done using the heats of formation of the  $PH_x^+$  ions from Table II, the

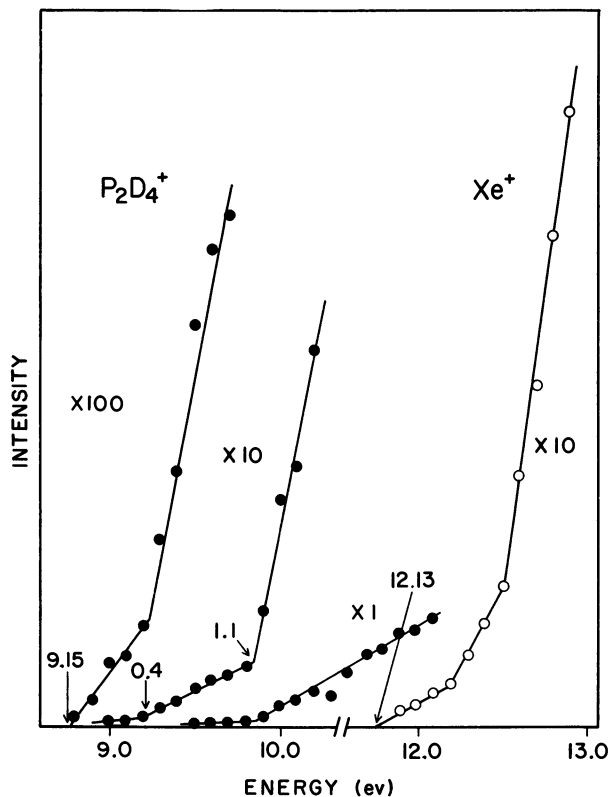


Figure 2. Typical RPD ionization potential measurement for diphosphine-4

heats of formation of H and P (12), and by assuming  $D(\text{H}_2\text{P}-\text{H}) = D(\text{P}-\text{H}) = E(\text{P}-\text{H}) = 77$  kcal./mole (7). The results given in Table II show that the measured appearance potentials are not consistent with the lowest energy processes. In particular, it appears that  $\text{PH}_2^+$  is formed by process *c* with no excess energy or by process *b* with 1.2 e. v. excess energy rather than by process *a* as previously assumed (15).

The substantial disagreement between the results of this study and the previous studies can be explained in terms of decomposition of  $\text{P}_2\text{H}_4$  in the mass spectrometer source. Comparing fragmentation patterns shows that production of  $\text{PH}_3$  explains the difference between  $A(\text{PH}_x^+/\text{P}_2\text{H}_4)$  values reported by Wada and Kiser and the values reported here. It also probably accounts for the low values of Saalfeld and Svec.

The disagreement for  $\text{P}_2\text{H}_r^+$  ions is not as easily explained. Table I shows that there is a distinct similarity in Wada and Kiser's values for

A ( $P_2H_2^+/P_2H_4$ ), A ( $P_2H^+/P_2H_4$ ), and A ( $P_2^+/P_2H_4$ ), and the values for the same ions from  $P_2H_2$  determined here. This was an indication that in addition to  $PH_3$ ,  $P_2H_2$  was formed in the source.

To test this, the following experiment was carried out. The appearance potentials of ions from  $P_2H_4$  were measured using the energy compensation technique (the method of Wada and Kiser) and using the modulated molecular beam sampling system. The mass spectrometer was then switched over to operation in the unmodulated mode with the shutter closed to approximate the operating conditions of Wada and Kiser. The appearance potentials were determined both by the energy compensation and the vanishing current techniques. The results are given in Table III.

**Table III. Appearance Potentials of Ions from Diphosphine-4 for Beam and Conventional Sampling**

Ion	Modulated Beam	Unmodulated		Ref. 17 <i>e. c.</i> <sup>a</sup>
	<i>e. c.</i> <sup>a</sup>	<i>e. c.</i> <sup>a</sup>	<i>v. c.</i> <sup>b</sup>	
$P_2H_3^+$	12.4 ± 0.3	12.0 ± 0.3	11.8 ± 0.3	9.1 ± 0.3
$P_2H_2^+$	11.1	10.8	10.2	10.5
$P_2H^+$	14.6	13.7	13.6	13.2
$P_2^+$	13.2	12.2	11.8	12.2

<sup>a</sup> *e. c.* refers to energy compensation technique.

<sup>b</sup> *v. c.* refers to vanishing current technique.

Within experimental error the values determined by the energy compensation technique in the modulated case agree with those in Table I listed under this work. In the unmodulated case the measured appearance potentials of  $P_2H_2^+$ ,  $P_2H^+$ , and  $P_2^+$  are identical to those of  $P_2H_2$ . It may be concluded then that  $P_2H_2$  was present in Wada and Kiser's source, and the best values for the appearance potentials of these ions from  $P_2H_4$  are those reported in Table I for this research.

The last experiment also shows that the appearance potential of  $P_2H_3^+$  is the same in both the modulated and unmodulated cases, and the low value reported by Wada and Kiser is not confirmed. It is possible that the  $P_2H_3$ , which they suggest is present in their source, was produced by a surface reaction on the walls or filament and consequently depends rather specifically on the source conditions. It may be noted that the pressure in the source used here was  $2 \times 10^{-7}$  torr during operation which is probably a factor of 10 less than the pressure in Wada and Kiser's source. Also the simulated conventional spectrum obtained in this experiment shows less  $PH_3$  than does the spectrum of Wada and Kiser.

Finally, it is not completely clear why the appearance potentials reported by Saalfeld and Svec (14, 15) differ from both those given here

and from those of Wada and Kiser. One notes that with one exception the differences in  $A(P_2H_x^+) - A(P_2H_4^+)$  reported by Saalfeld and Svec are the same within experimental error to those reported by Wada and Kiser. If one makes the *ad hoc* assumption that the former's voltage scale calibration was in error owing to the use of the linear extrapolation method, then they too were probably observing a mixture of pyrolysis products. The magnitude of the  $P_2^+$  ion intensity suggests that in this case  $P_4$  was one of the products.

### Acknowledgments

This work was supported in major part by the National Science Foundation, grant NSF-GP-4186. Partial support of the Radiation Laboratory of the University of Notre Dame which is operated under contract with the U. S. Atomic Energy Commission is also acknowledged. This is AEC Document No. COO-38-513.

### Literature Cited

- (1) Evers, E. C., Street, E. H., Jr., *J. Am. Chem. Soc.* **78**, 5726 (1956).
- (2) Fehlner, T. P., *J. Am. Chem. Soc.* **88**, 1819 (1966).
- (3) Fischler, J., Halmann, M., *J. Chem. Soc.* **1964**, 31.
- (4) Fite, W. L., Brackmann, R. T., *Phys. Rev.* **112**, 1141 (1958).
- (5) Foner, S. N., Hudson, R. L., *J. Chem. Phys.* **21**, 1374 (1953); **36**, 2676 (1962).
- (6) Fox, R. E., Hickam, W. M., Grove, D. J., Kjeldaas, T., Jr., *Rev. Sci. Instr.* **26**, 1101 (1955).
- (7) Gunn, S. R., Green, L. G., *J. Phys. Chem.* **65**, 779 (1961).
- (8) Kiser, R. W., "Introduction to Mass Spectrometry and Its Applications," pp. 168-169, Prentice-Hall Inc., Englewood Cliffs, N. J., 1965.
- (9) McDowell, C. A., Ed., "Mass Spectrometry," pp. 553-564, McGraw-Hill Book Co., Inc., New York, N. Y., 1963.
- (10) Melton, C. E., Hamill, W. H., *J. Chem. Phys.* **41**, 3464 (1964).
- (11) Neuert, H., Clasen, H., *Z. Naturforsch.* **7a**, 410 (1952).
- (12) Rossini, F. D., *et al.*, "Selected Values of Chemical Thermodynamic Properties," *Circular of the NBS*, No. 500, 1952.
- (13) Saalfeld, F. E., Svec, H. J., *Inorg. Chem.* **2**, 46 (1963).
- (14) *Ibid.*, **2**, 50 (1963).
- (15) *Ibid.*, **3**, 1442 (1964).
- (16) Talrose, V. L., *et al.*, *Prib. i Tekhn. Experim.* **6**, 78 (1960).
- (17) Wada, Y., Kiser, R. W., *Inorg. Chem.* **3**, 174 (1964).
- (18) Watanabe, K., Mottl, R., *J. Chem. Phys.* **26**, 1773 (1957).

RECEIVED October 11, 1966.

# Analysis of Boranes and Carboranes by Mass Spectrometry

J. F. DITTER, F. JAMES GERHART, and ROBERT E. WILLIAMS

Space-General Corporation, Center for Research and Education,  
Los Angeles, Calif.

*Boranes and carboranes each have their own characteristic mass spectral patterns. Boranes under electron impact fragment rather severely, the "unstable" ones somewhat more so than the "stable," and consequently they, as well as their alkylated derivatives, display broad, rounded mass spectral profiles. Conversely, the stable class of compounds, the closo-carboranes (and their alkyl derivatives), are quite resistant to fragmentation, and hence their spectral profiles have sharp cut-off points at their high mass numbers. A useful technique for determining the exact number of boron and carbon atoms in carboranes involves careful measurement of the intensity of the mass spectral peak owing to the  $^{13}\text{C}$ -containing ion that appears above the normal cut-off peak, as illustrated for  $\text{C}_4\text{B}_6\text{H}_{12}$ , the dimethyl derivative of  $\text{C}_2\text{B}_6\text{H}_8$ .*

Various ion groups in the mass spectral patterns of boron hydrides (natural abundance of  $^{11}\text{B}/^{10}\text{B} = 4.0$ ) have characteristically broad, rounded profiles that generally allow easy identification in chemical mixtures (24). In each ion group the boron isotopes are essentially distributed in a statistical manner, and, as a consequence, the greater the number of borons in a particular ion group, the farther removed will be the peak of maximum intensity from the top mass number. An even more influential factor in determining the point of maximum intensity, however, is the ease of abstraction of hydrogen atoms, and in boranes this abstraction occurs relatively easily. Without exception, at normal ionizing voltages, the ion of highest intensity has fewer hydrogens than the parent molecule. Furthermore, these same spectral characteristics are carried over to alkyl derivatives of the boranes.

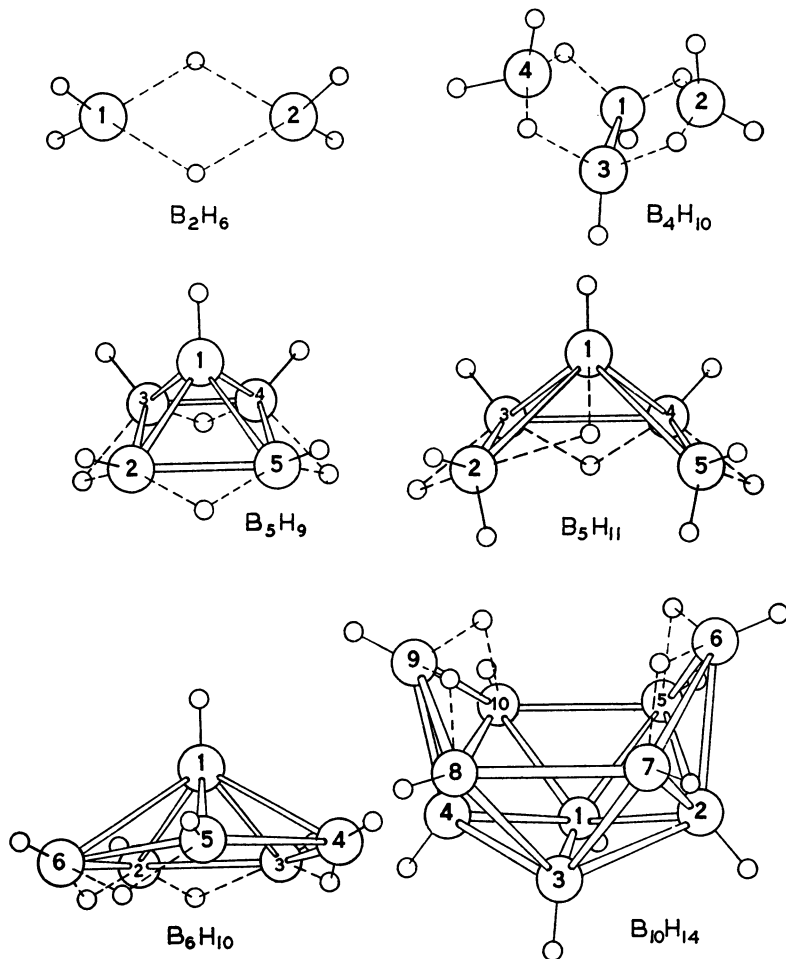


Figure 1. Molecular configurations of typical boron hydrides

On the other hand, for the stable closed-cage *closo*-carboranes the fragmentation patterns are representative of minimal hydrogen abstraction. (The terms *closo*- and *nido*-, pertaining to carboranes, were adopted at the latest meeting of the Boron Nomenclature Committee, American Chemical Society Meeting, New York City, September 12-16, 1966.) The spectral patterns display sharp cut-offs at the highest mass numbers, and the highest intensity peak almost invariably is that of the parent ion; in a few cases the ion with one or two hydrogens abstracted is of slightly higher intensity than the parent ion. The second, third, etc. generations of ions (those with one, two, etc. boron and/or carbon atoms abstracted) have intensities that are only small percentages of their parent group

intensities. As with boranes, these characteristics are reflected in the related alkylated *closo*-carboranes, and once again the over-all profile serves as a ready "fingerprint" for quick identification. Because of the

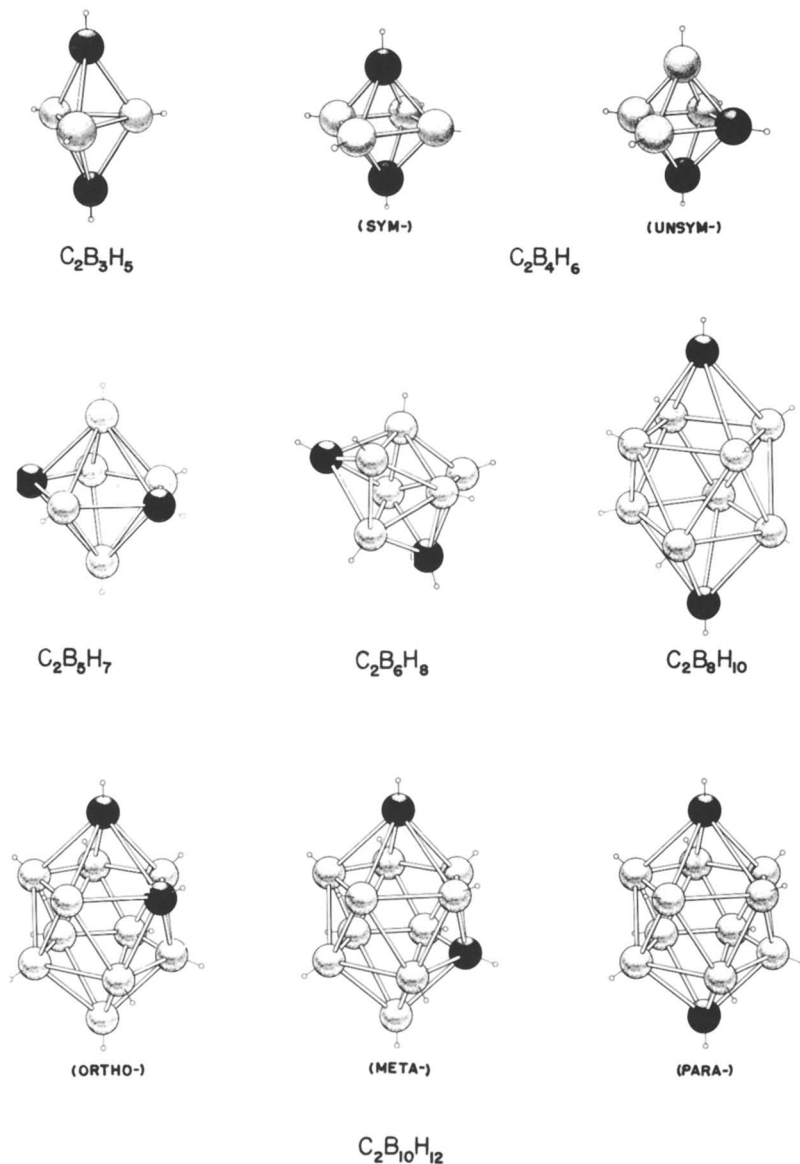


Figure 2. Molecular configurations of typical *closo*-carboranes

resistance to hydrogen abstraction, *closo*-carborane spectra resemble, somewhat, the spectrum of elemental boron.

*Nido*-carboranes, which have open molecular structures and which generally contain hydrogen bridge bonding, resemble boranes more than they resemble *closo*-carboranes in their fragmentation patterns. At least this is the case with the few *nido*-carboranes that have been synthesized and analyzed mass spectrally.

In the following discussion the structural configurations of boranes will be compared with the two classes of carboranes, and structural differences will then be related in a general way to mass spectral fragmentation patterns. The mass spectra of all *closo*-carboranes and derivatives and the spectrum of the methyl derivative of the *nido*-carborane,  $\text{CB}_5\text{H}_9$ , were obtained with a Perkin-Elmer Hitachi RMU-6D spectrometer (80 volts ionizing potential) located at West Coast Technical Service, San Gabriel, Calif. The remaining spectra were obtained with a Consolidated Model 21-620 spectrometer. Although there are some dissimilarities in fragmentation patterns with different instruments and with different voltages, the over-all mass spectral profiles—which are our main interest here—do not change appreciably. In several instances, as indicated, the exact isomeric structures of some of the *closo*-carboranes were unknown, but it is highly doubtful whether isomeric differences could effect any gross changes in spectral patterns.

### ***Borane Structures***

Molecular structures of some typical boron hydrides are shown in Figure 1. Those having the more condensed structures ( $\text{B}_5\text{H}_9$ ,  $\text{B}_6\text{H}_{10}$ , and  $\text{B}_{10}\text{H}_{14}$ ) have one terminal hydrogen for each boron atom, while those with open structures ( $\text{B}_4\text{H}_{10}$  and  $\text{B}_5\text{H}_{11}$ ) also have  $\text{BH}_2$  groups. The former are the so-called "stable" boranes, while the latter, excepting diborane, are the "unstable" boranes, denoted as such in accordance with their relative thermal stabilities (25). A better designation is the formula  $(\text{BH})_n(\text{BH}_3)_x$ , where  $n$  has an integral value, and  $x = 2$  for stable boranes and 3 for unstable boranes (6). One significant characteristic of all boranes is the presence of three-center B—H—B (hydrogen bridge) bonding (12). On electron impact there is a pronounced tendency for the hydrogen atoms to be abstracted in pairs, and some mass spectral evidence with bridge-deuterated decaborane (23) and labeled tetraborane (7) indicated that the first pair of hydrogens abstracted consists of a terminal hydrogen and its adjacent hydrogen bridge atom. Later work with zero source contact mass spectrometry (14), however, suggests that, for tetraborane at least, this mechanism may be incorrect.

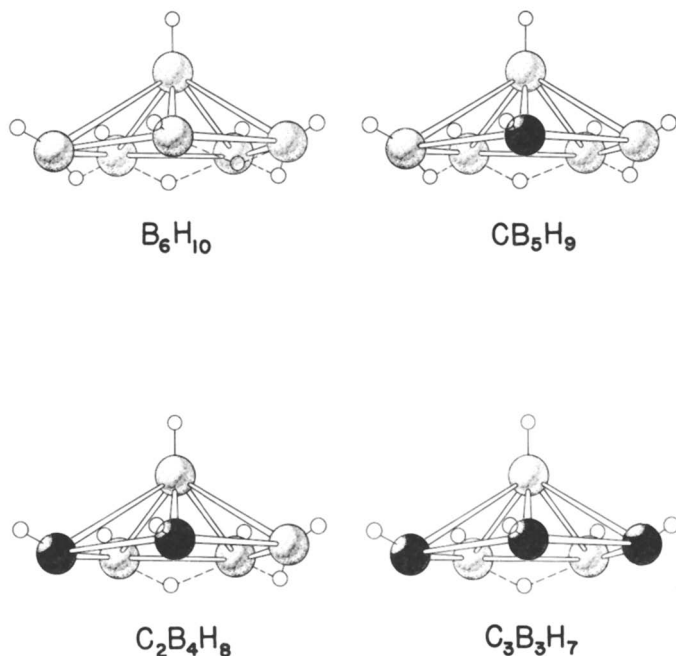


Figure 3. Structural similarities of hexaborane-10 and three of the nido-carboranes. The structure of  $C_1B_2H_6$ , which is analogous to the others, is not shown

### *Closo-Carborane Structures*

As mentioned previously, two general classes of carboranes are known: closed cage (*closo*-) and open (*nido*-) compounds. The *closo*-compounds as a class are significantly more stable under electron impact, are less reactive chemically, and are thermally more stable than either the boranes or *nido*-carboranes. Additionally, each boron and each carbon in a *closo*-carborane has a single terminal hydrogen, and generally there are no hydrogen bridges. With one exception,  $CB_5H_7$  (15), the *closo*-carboranes reported to date contain two carbon atoms and have the general formula  $C_2B_nH_{n+2}$ . The structures of representative compounds of this type are shown in Figure 2.

The simplest member of the series and the one first discovered is  $C_2B_3H_5$ , *closo*-1,5-dicarbapentaborane (5, 10, 13, 19, 21), a trigonal bipyramid with a carbon in each of the two apex positions. Recently Grimes (9) has presented evidence for an alkyl derivative of the 1,2-isomer in which one skeletal carbon is in an apex position and the other is equatorial. The second carborane in the *closo*-series is  $C_2B_4H_6$ , a

tetragonal bipyramid, of which two isomers are known: the 1,2- and the 1,6-dicarb-compounds (10, 13, 17, 19, 22). Similarly, going up the scale by successive addition of BH units, there are  $C_2B_5H_7$  (1, 10, 11, 13, 17, 19, 21),  $C_2B_6H_8$  (13, 28, 31),  $C_2B_7H_9$  (13, 28),  $C_2B_8H_{10}$  (13, 20, 28),  $C_2B_9H_{11}$  (8, 13, 26), and  $C_2B_{10}H_{12}$  (5, 12, 13, 19). In each case there are known or potential isomers with carbons arranged in various positions in the molecular skeletons. In the case of  $C_2B_{10}H_{12}$ , the structure is a closed icosahedron, and all atoms occupy equivalent positions; the numbering system is such that one arbitrarily selects one of the carbons as the apex (No. 1), and the equatorial positions are then numbered clockwise in each plane.

Monocarbahexaborane (7), the only reported *closo*-carborane with one carbon atom (15), is isoelectronic with  $C_2B_4H_6$ . It has a bridge hydrogen and is the only *closo*-carborane to date with this feature.

### *Nido-Carborane Structures*

The *nido*-carboranes that have been discovered and characterized to date include four,  $CB_5H_9$  (16),  $C_2B_4H_8$  (18, 19),  $C_3B_3H_7$  (4), and  $C_4B_2H_6$  (3), that arise from systematic substitution of CH groups for  $BH_2$  groups within  $B_6H_{10}$  with which they are isoelectronic. All of these species, including  $B_6H_{10}$ , have pentagonal pyramid structures.  $B_6H_{10}$  has

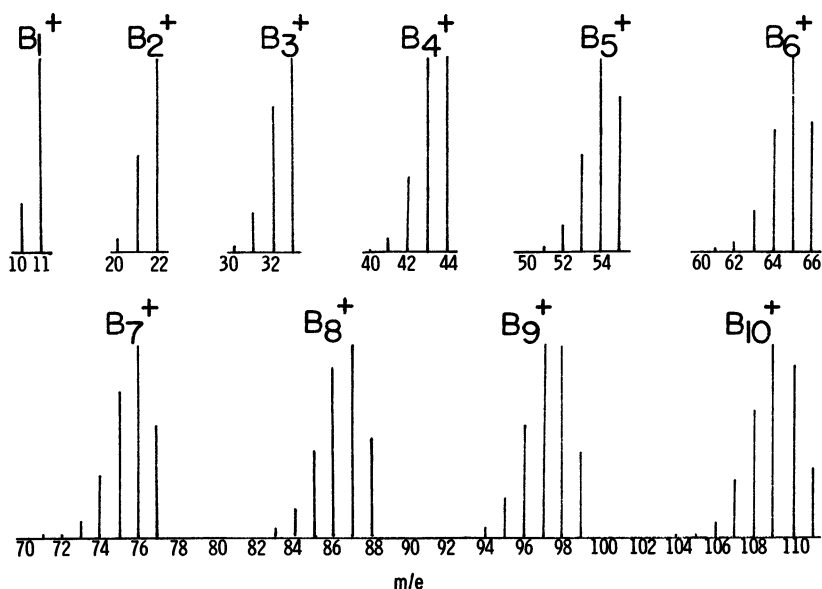


Figure 4. Synthetic polyisotopic mass spectrum of boron of naturally occurring abundance

four bridge hydrogens, while the *nido*-carboranes have three, two, one, and zero bridge hydrogens, respectively; excepting  $C_4B_2H_6$  the structures of these compounds are shown in Figure 3. In the case of  $CB_5H_9$ , only methyl derivatives have been reported, while the parent species itself remains undetected. Similarly, evidence for the parent compound  $C_3B_3H_7$  is still tentative, but three C-methyl derivatives have been isolated and characterized. A fifth *nido*-carborane,  $C_2B_9H_{13}$  (19, 29), presumably containing two bridge hydrogens and having an open icosahedral structure, also has been prepared.

Tebbe, Garrett, and Hawthorne (27) have reported an example of a third type of carborane,  $C_2B_7H_{13}$ , which tentatively has been determined to contain two methylene groups and two hydrogen bridges. It does not fall into either the *closo*- or *nido*- categories.

### General Characteristics of Boron Spectra

If elemental boron consisting only of  $^{10}B$ -isotope were subjected to electron impact and then analyzed mass spectrometrically, one would observe only monoisotopic species at  $m/e$  10, 20, 30, etc., corresponding to  $^{10}B^+$ ,  $^{10}B_2^+$ ,  $^{10}B_3^+$ , etc. Similarly, the  $^{11}B$ -isotope in pure elemental form would generate peaks at  $m/e$  11, 22, 33, 44, etc. ( $^{11}B^+$ , . . .). In boron of naturally occurring composition ( $^{11}B/^{10}B = 4.0$ ), however, the result would be a polyisotopic mass spectrum of essentially statistically distributed  $^{11}B$  and  $^{10}B$ , as depicted in Figure 4. For ion groups containing small numbers of borons (say  $B_1^+$  to  $B_4^+$ ) the spectral profile is statistically weighted in favor of the higher mass numbers of the group, because of the high concentration (80%) of  $^{11}B$ ;—*i.e.*, in the  $B_3$ -group,  $^{11}B_3^+$  is the most abundant ion, while in the  $B_4$ -group,  $^{11}B_4^+$  and  $^{11}B_3^{10}B_1$  are in equal abundance. As the number of borons increases beyond four, however, the maximum intensity peak (or peaks) begins to shift away from the cut-off peak. In the  $B_5$ -group,  $^{11}B_4^{10}B_1^+$  is the most abundant ion, while in the  $B_{10}$ -group, it is  $^{11}B_8^{10}B_2^+$ , which is 2.81 times as abundant as  $^{11}B_{10}^+$ .

The abundance ratios of all the isotopic species in a particular ion group are readily calculated by simple statistics. If the boron occurs in natural abundance, the concentration of any ion,  $^{11}B_x^{10}B_y$ , is given by

$$[^{11}B_x^{10}B_y] = W(.80)^x(.20)^y.$$

In this expression,  $W$  is the statistical weight—the number of different ways  $^{11}B$  and  $^{10}B$  atoms can be arranged in the available skeletal positions—numerically equal to  $(x + y)!/x!y!$ . The values of  $W$  are tabulated in mathematical handbooks as “binomial coefficients.”

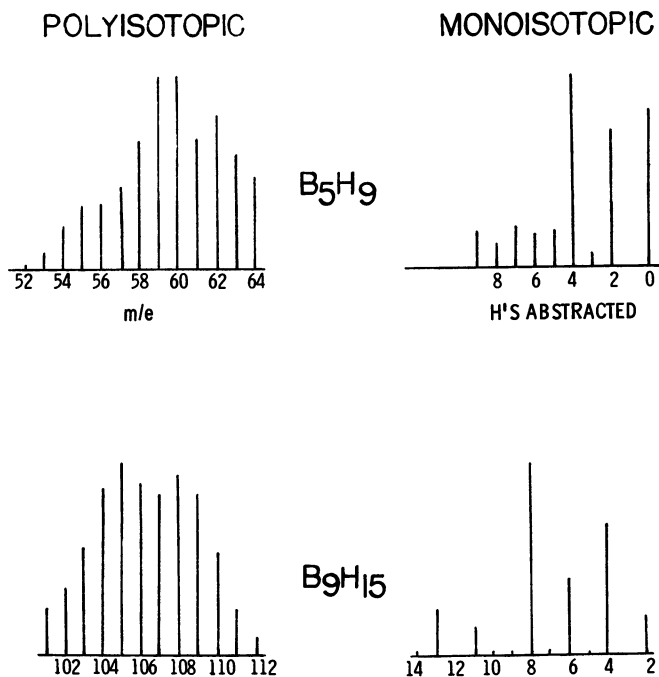


Figure 5. Parent group mass spectra of pentaborane-9 and nonaborane-15

As an example, consider a compound with five boron atoms. Based on the above equation the concentrations and isotopic abundance ratios, relative to  $^{11}\text{B}_5$ , are as follows:

Isotopic Species	Concentration	Abundance Ratio
$^{11}\text{B}_5$	$1(.80)^5$	1.0
$^{11}\text{B}_4^{10}\text{B}$	$5(.80)^4(.20)$	$5/4 = 1.25$
$^{11}\text{B}_3^{10}\text{B}_2$	$10(.80)^3(.20)^2$	$10/4^2 = 0.625$
$^{11}\text{B}_2^{10}\text{B}_3$	$10(.80)^2(.20)^3$	$10/4^3 = 0.156$
$^{11}\text{B}^{10}\text{B}_4$	$5(.80)(.20)^4$	$5/4^4 = 0.0195$
$^{10}\text{B}_5$	$1(.20)^5$	$1/4^5 = 0.00098$

Similar calculations can be carried out for all other ion groups (already tabulated in Table I of Ref. 24), and the elemental boron spectrum in Figure 4 is based on these data. The utility of such data lies in calculating monoisotopic spectra from polyisotopic data since the concentrations of all isotopic species can be determined by measuring only those ions containing  $^{11}\text{B}$ -atoms.

For example, the monoisotopic spectrum of  $\text{B}_5\text{H}_9$  is obtained by first measuring  $^{11}\text{B}_5\text{H}_9^+$  (m./e. 64), then subtracting  $^{11}\text{B}_4^{10}\text{BH}_9^+$ ,  $^{11}\text{B}_3^{10}\text{B}_2\text{H}_9^+$ ,

etc. (relative values 1.0, 1.25, 0.625, etc.) from  $m/e$  63 down to  $m/e$  59 ( $^{10}\text{B}_5\text{H}_9^+$ ). The residual of  $m/e$  63 then is  $^{11}\text{B}_5\text{H}_8^+$ , and from this the intensities of  $^{11}\text{B}_4^{10}\text{BH}_8^+$ ,  $^{11}\text{B}_3^{10}\text{B}_2\text{H}_8^+$ , etc., and ultimately all ions,  $\text{B}_5\text{H}_9^+$ ,  $\text{B}_5\text{H}_8^+$ ,  $\text{B}_5\text{H}_7^+$ , . . .  $\text{B}_5^+$  are determined. Next in line is the  $\text{B}_4\text{H}_x^+$  group, then  $\text{B}_3\text{H}_x^+$ , etc.

In each group, if the correct number of boron atoms is assumed, the data should reduce to a neat monoisotopic spectrum. If the number of boron atoms assumed is smaller than the actual number present, the data also may reduce to negligibly small residuals, but if the number assumed is greater than the actual number present, inordinately large negative residuals will occur during the reduction process. The criterion, therefore, is the largest number of boron atoms that will suitably reduce the data.

### Mass Spectra of Boranes

If, to the boron ion species in Figure 4 we could add hydrogens, the cut-off peak would shift upward in proportion to the number of hydrogens added, and the profiles would be the same as for elemental boron. For

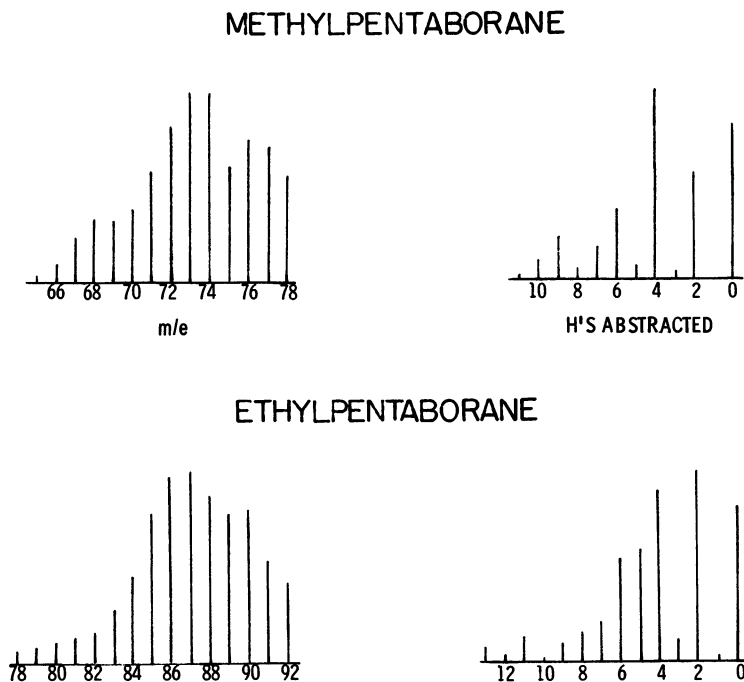


Figure 6. Parent group mass spectra of two alkyl derivatives of pentaborane-9

example,  $B_5H_9^+$  would occupy the regime from  $m/e$  59 to  $m/e$  64, corresponding to the mass range of  $^{10}B_5H_9^+$  to  $^{11}B_5H_9^+$  rather than the range  $m/e$  50 to  $m/e$  55 of the  $B_5^+$  species; the highest intensity peak would be  $m/e$  63 because the species  $^{11}B_4^{10}BH_9^+$  would be statistically most probable. However, since electron impact also knocks hydrogens off some of the pentaborane molecules, the entire spectrum of ions from  $m/e$  50 ( $^{10}B_5^+$ ) to  $m/e$  64 ( $^{11}B_5H_9^+$ ) shows up. Furthermore,  $B_5H_5^+$  is the ion of highest intensity, and varied yields of the various  $B_5H_n^+$  ions combined with the statistical distribution of boron isotopes causes the profile to peak at  $m/e$  59 to  $m/e$  60, as shown in Figure 5. The effect is even more pronounced for the  $BH_2$ -containing "unstable" borane,  $B_9H_{15}$ , which has its maximum intensity peak nine mass numbers below its molecular weight of 114. Also, the two ions  $B_9H_{15}^+$  and  $B_9H_{14}^+$  are of negligibly small intensities, a characteristic which holds true for all "unstable" boranes. In essence, then, the boron isotope distribution and the ease of abstraction of hydrogens give boranes their broad, rounded profiles, and this contributes to easy identification.

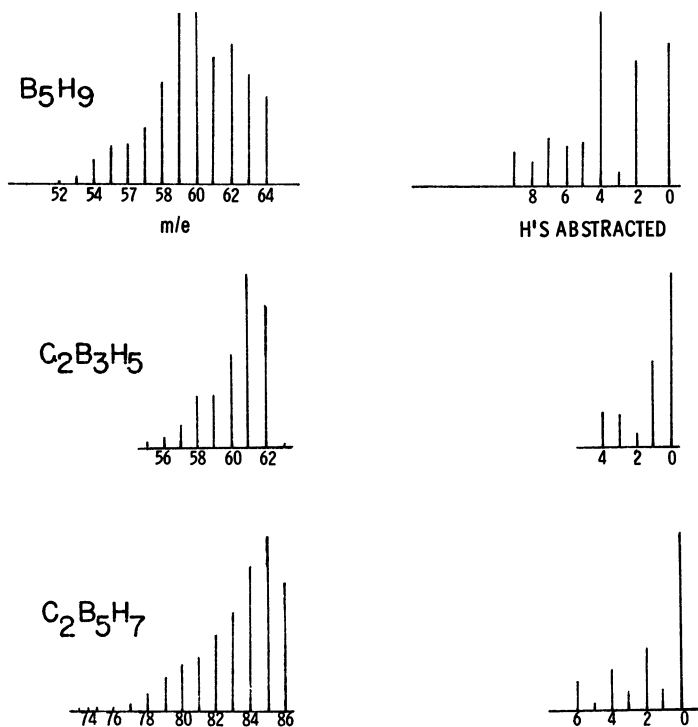


Figure 7. Comparison of mass spectra of 1,5- $C_2B_3H_5$  and 2,4- $C_2B_5H_7$  closo-carboranes with that of  $B_5H_9$ .

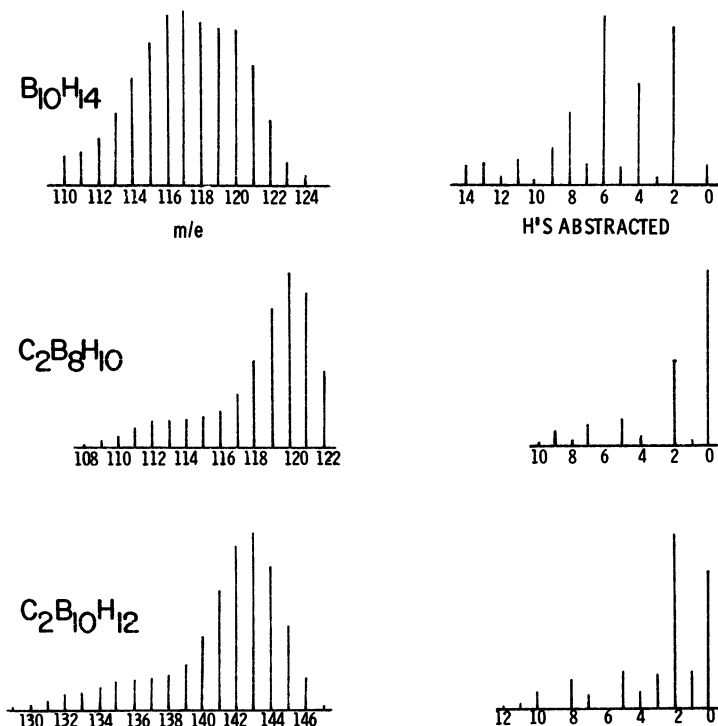


Figure 8. Comparison of mass spectra of  $C_2B_8H_{10}$  and 1,2- $C_2B_{10}H_{12}$  closo-carboranes with that of  $B_{10}H_{14}$

The same general fragmentation patterns hold true for the related alkyl-boranes, and two typical examples are shown in Figure 6. Adding methyl and ethyl groups merely shift the cut-offs upward 14 and 28 mass numbers, respectively, reflecting the addition of  $CH_2$  and  $C_2H_4$  to the molecular weight. The fact that the parent group profile is changed only slightly suggests that the hydrogen abstraction upon electron impact occurs preferentially on the borane skeleton, not on the alkyl side chains, and this has been verified by mass spectral analysis of compounds with deuterated alkyl groups (30).

### Mass Spectral Profiles of Carboranes

**Closo-Carboranes.** In Figure 7 the parent group spectra of two closo-carboranes, 1,5- $C_2B_3H_5$  and 2,4- $C_2B_5H_7$ , are compared with the spectrum of  $B_5H_9$ . ( $C_2B_5H_7$  has the same number of borons as  $B_5H_9$ , while  $C_2B_3H_5$  has the same number of skeletal atoms.) The spectral

differences are quite pronounced. The small degree of hydrogen abstraction in the *closo*-carboranes can be seen in their monoisotopic spectra; in each case the parent ion is of considerably greater intensity than any of its offspring. The same general profile is evident for the carborane,  $C_2B_8H_{10}$ , shown in comparison with  $B_{10}H_{14}$  in Figure 8.  $C_2B_8H_{10}$  was prepared in yields of less than 1%, and we do not know which isomer was formed. The spectrum of 1,2- $C_2B_{10}H_{12}$ , also shown in Figure 8, has a fairly intense parent ion, but its highest intensity peak for some reason is two mass numbers below that of its parent. The reason for this apparent discrepancy is not known. In Figure 9 are spectra of the 1,2- and 1,6-isomers of *closo*- $C_2B_4H_6$ , and here we see that the  $C_2B_4H_5^+$  ion is the one of highest intensity. In general, however, the over-all spectral characteristics closely resemble other *closo*-carboranes.

As with boranes, alkyl derivatives of carboranes fragment nearly the same as do the nonalkylated parents. The hydrogens from the alkyl side chains and those from the carborane skeleton appear to have about the same general resistance to abstraction. Figure 10 compares the spectrum of 2,4- $C_2B_5H_7$  with that of a C-methyl derivative,  $CH_3C_2B_5H_6$ , while Figure 11 shows spectra of the dimethyl derivatives of  $C_2B_8H_{10}$ ,  $C_2B_7H_9$ ,

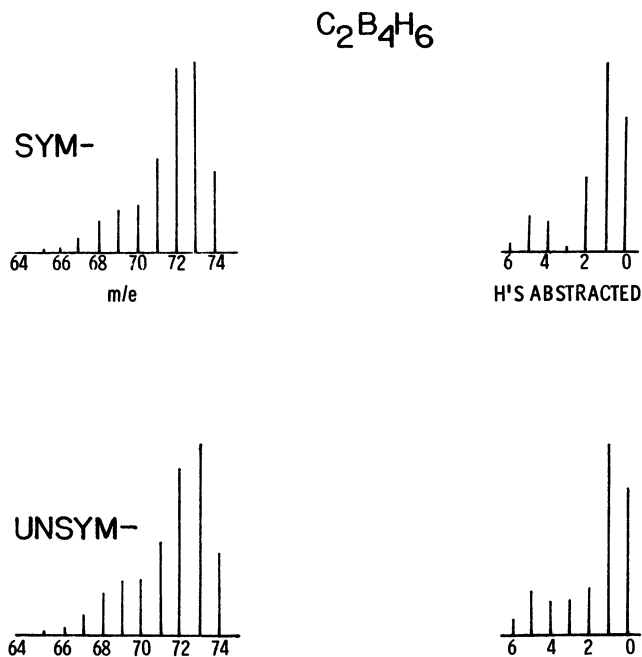


Figure 9. Parent group mass spectra of the 1,6- and 1,2-isomers of  $C_2B_4H_6$

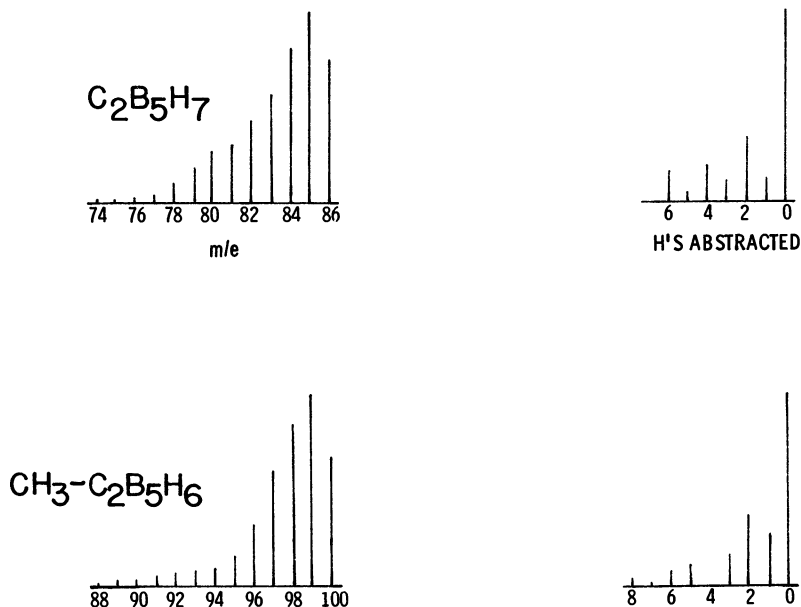


Figure 10. Similarities in the mass spectra of 2,4- $C_2B_5H_7$  and a C-methyl derivative

$C_2B_6H_8$  (exact isomeric structures as yet unknown). The spectra are self-explanatory.

**Nido-Carboranes.** As mentioned previously the *nido*-carboranes contain hydrogen bridges, and they are not as thermally or chemically stable as their *closo*-counterparts. Figure 12 shows the spectra of  $C_2B_4H_8$  and the methyl derivative of  $CB_5H_9$ , and it is apparent that their fragmentation patterns are more closely allied with boranes than with the *closo*-carboranes. This is also demonstrated rather dramatically by comparison with the spectra of the two *closo*-carborane isomers of  $C_2B_4H_6$  in Figure 9.

### Over-all Comparison of Boranes and Carboranes

To show in a general way how the polyisotopic mass spectra of the borane and carborane series change as the number of boron atoms increases, we have plotted in Figure 13 the relative positions of the maximum intensity peaks for all the compounds for which we have spectra. For example, for the lower molecular weight *closo*-carboranes the maximum intensity peak occurs one mass number less than the molecular weight of the parent molecule, while for  $B_{10}H_{14}$ , which is a "BH"-type borane, the relative position of this peak is seven mass numbers below the mass number of the parent. In several instances—*e.g.*,  $B_5H_9$ , the

spectra show two peaks of essentially equal "maximum" intensity, and we chose to use average (nonunit) values in the plot.

In the plot we note a general trend upward for all boron compounds owing to the way in which boron isotopic species are distributed; however, the predominant factor governing the position of the maximum intensity peak arises from the ease of abstraction of hydrogens from parent ions.  $\text{BH}_2$ -containing boranes lose hydrogens most readily, while the "stable"  $\text{BH}$ -boranes and the *nido*-carboranes are somewhat more resistant to hydrogen abstraction. The *closo*-carboranes are without question the most stable of these species. One would predict that the mass spectra of such related species as  $\text{B}_{10}\text{H}_8(\text{CO})_2$  would also resemble the *closo*-carboranes.

### Determination of Boron and Carbon by $^{13}\text{C}$ -Isotope Analysis

With any carbon-containing compound of natural isotopic abundance, there will be mass spectral contributions from ion species containing the

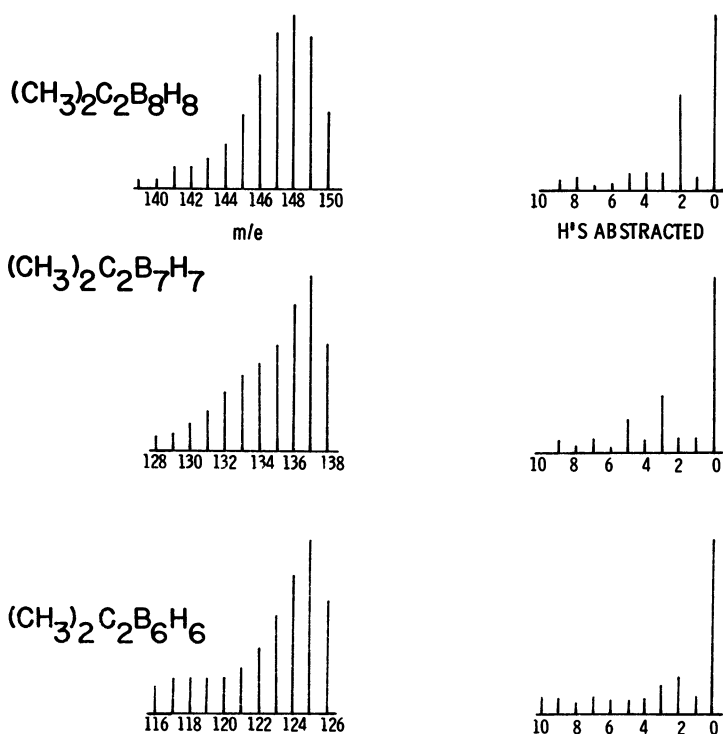


Figure 11. Parent group mass spectra of three dimethylated *closo*-carboranes

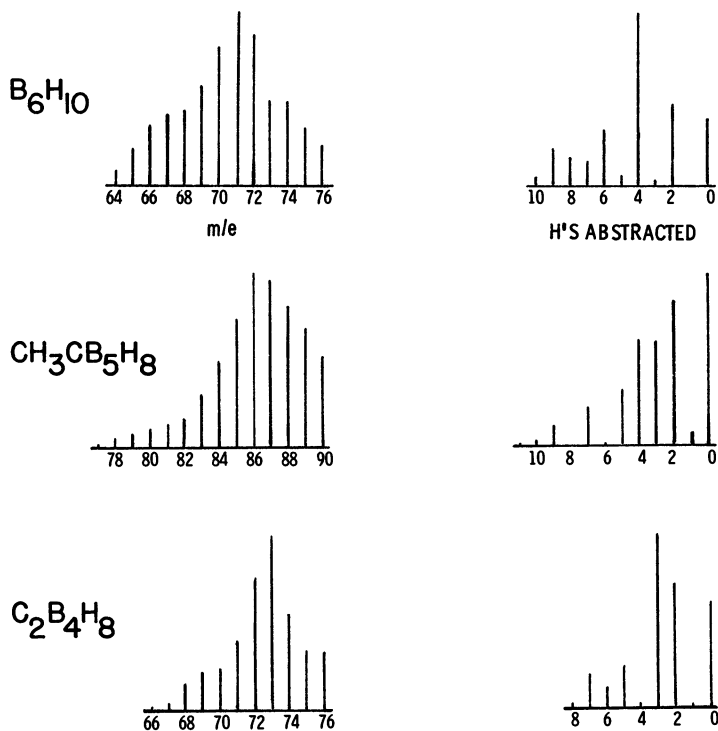


Figure 12. Comparison of the spectra of two nido-carboranes with that of hexaborane-10

$^{13}C$ -isotope. There also will be small contributions from deuterium-containing species, but in calculating abundance ratios the deuterium can be conveniently lumped together with the  $^{13}C$ -species. In some cases, where the number of hydrogen atoms is small, it can be neglected entirely. For a compound with an unknown combination of carbon, boron, and hydrogen (or other elements, for that matter), mass spectral analysis generally can be used to determine the exact number of boron and carbon atoms in the parent compound. The requirements are: (1) a mass spectrometer that gives good peak definition, and (2) negligible contributions from impurities in the vicinity of the parent ion mass number. Sharp cut-offs at the parent ion  $m/e$  are also desirable, and in this respect the *closo*-carboranes are almost ideally suited. The method can be illustrated with  $C_4B_6H_{12}$ , the dimethyl derivative of  $C_2B_6H_8$ .

**First Approximation.** The compound in question has a *closo*-carborane profile and, excepting a small  $^{13}C$ -isotope peak at  $m/e$  127 (relative intensity 1.0), the high mass cut-off occurs at  $m/e$  126 (intensity

23.9). Now the cut-off peak would have to be attributed to  $^{11}\text{B}$ -containing ions from species such as  $\text{C}_3\text{B}_7\text{H}_{13}$ ,  $\text{C}_4\text{B}_6\text{H}_{12}$ , or  $\text{C}_5\text{B}_5\text{H}_{11}$ , etc. Consequently, the  $^{13}\text{C}$ -isotope peak at  $m/e$  127 would then have to be  $^{13}\text{C}_1^{12}\text{C}_2^{11}\text{B}_7\text{H}_{13}^+$ ,  $^{13}\text{C}_1^{12}\text{C}_3^{11}\text{B}_6\text{H}_{12}^+$ , or  $^{13}\text{C}_1^{12}\text{C}_4^{11}\text{B}_5\text{H}_{11}^+$ , etc. As with boron isotopes, it is a fairly simple matter to calculate relative abundances of ions containing  $^{13}\text{C}$  and  $^{12}\text{C}$ ; based on natural abundance of the two isotopes, the calculations are as follows:

$$\text{General formula: } [^{12}\text{C}_x^{13}\text{C}_y] = W(.98931)^x(.01069)^y$$

$$\text{For } \text{C}_3\text{B}_7\text{H}_{13}: \frac{[^{12}\text{C}_2^{13}\text{C}_1]}{[^{12}\text{C}_3]} = \frac{3(.98931)^2(.01069)}{1(.98931)^3} = 0.03242$$

$$\text{For } \text{C}_4\text{B}_6\text{H}_{12}: \frac{[^{12}\text{C}_3^{13}\text{C}_1]}{[^{12}\text{C}_4]} = \frac{4(.98931)^3(.01069)}{1(.98931)^4} = 0.04322$$

$$\text{For } \text{C}_5\text{B}_5\text{H}_{11}: \frac{[^{12}\text{C}_4^{13}\text{C}_1]}{[^{12}\text{C}_5]} = \frac{5(.98931)^4(.01069)}{1(.98931)^5} = 0.05402$$

The observed ratio of  $m/e$  127 to  $m/e$  126 is 1/23.9, or 0.0418, pointing to  $\text{C}_4\text{B}_6\text{H}_{12}$  as the correct formula for the compound in question. We could also have included the deuterium isotope contribution,  $^{12}\text{C}_4^{11}\text{B}_6^1\text{H}_{11}^2\text{H}_1^+$ , to  $m/e$  127, although this is unnecessary when the

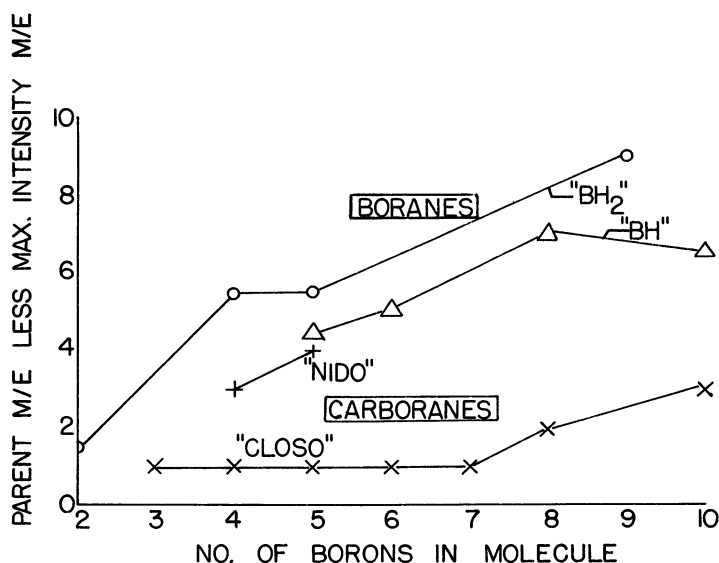


Figure 13. Comparison of spectral profile characteristics of boranes and carboranes

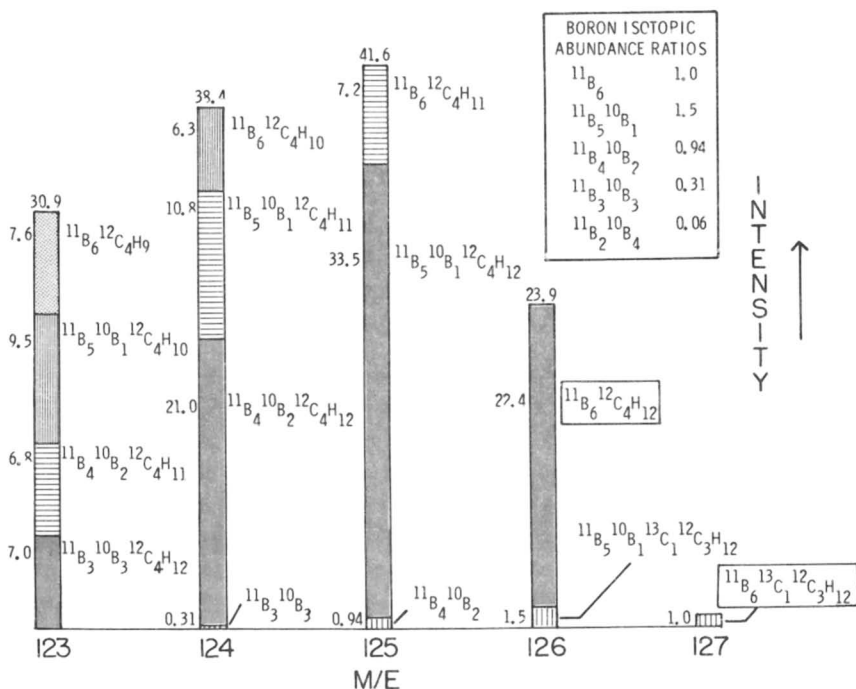


Figure 14. Distribution of ion species in the mass spectrum of  $\text{B}_6\text{C}_4\text{H}_{12}$ —“second approximation”

(Legend: Similar cross-hatched areas represent related boron isotopic species; ion formulas in boxes represent related carbon isotopic species of interest)

calculation is only a first approximation. Just for the sake of completeness, however, the contribution of this ion would be

$$\frac{[{}^1\text{H}_{11}{}^2\text{H}_1]}{[{}^1\text{H}_{12}]} = \frac{12(.99984)^{11}(.00016)}{(.99984)^{12}} = 0.00192$$

Added to the previous result for  $^{13}\text{C}$  we get a total calculated contribution of  $.04322 + .00192 = .04514$ , compared with the observed intensity ratio of 0.0418.

It is not necessary to derive these values for each situation, however, since tables of isotopic abundance ratios are already available. Beynon (2) for example, has tabulated them for various combinations of carbon, hydrogen, nitrogen, and oxygen (no boron, unfortunately) up to mass 250. In some cases (including the  $\text{C}_4\text{H}_{12}$  portion of  $\text{C}_4\text{B}_6\text{H}_{12}$ ), it is necessary to extrapolate (linearly) the data in his table.

**Second Approximation.** In the first approximation we assumed that only one ion was contributing to  $m/e$  126, namely  $^{12}\text{C}_4^{11}\text{B}_6\text{H}_{12}^+$ . This is

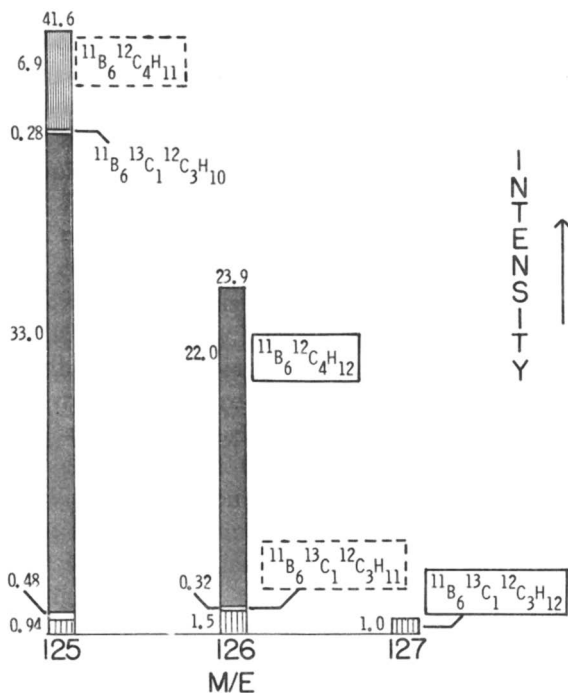


Figure 15. Distribution of ion species in the mass spectrum of  $\text{B}_6\text{C}_4\text{H}_{12}$ —“third approximation” (Legend: same as in Figure 14)

not strictly true, however, because two  $^{13}\text{C}$ -containing isotopes (deuterium neglected again for simplicity) also are present. One is the  $^{11}\text{B}_5^{10}\text{B}_1$ -counterpart of  $m/e$  127 and, from statistical calculations, it is 1.5 times the intensity of  $m/e$  127; the other ion is the  $^{13}\text{C}$ -counterpart of  $\text{C}_4^{11}\text{B}_6\text{H}_{11}^+$ —the principal ion of  $m/e$  125. As shown in Figure 14, subtraction of 1.5 from the intensity of  $m/e$  126 leaves a residual value of 22.4, which, as a second approximation, we can attribute to the  $^{12}\text{C}_4^{11}\text{B}_6\text{H}_{12}^+$  ion. The observed ratio of  $^{13}\text{C}^{12}\text{C}_3/^{12}\text{C}_4$  now is 1.0/22.4, or 0.0446. This is closer to our calculated value (deuterium included) of 0.04514 than was our first approximation (.0418).

Similarly, if it were necessary to perform these same computations for  $\text{C}_3\text{B}_7\text{H}_{13}$  and  $\text{C}_5\text{B}_5\text{H}_{11}$ , the amount subtracted from  $m/e$  126 would be 1.75 and 1.25, respectively, since these are the  $^{11}\text{B}_6^{10}\text{B}_1$  and  $^{11}\text{B}_4^{10}\text{B}_1$  counterparts of  $m/e$  127. The residuals of  $m/e$  126 then would be 22.1 and 22.6, respectively, and the ratios of  $m/e$  127 to these residuals would be 0.0452 and 0.0442, respectively; these figures deviate by about 25% from the required abundance ratios of 0.032 and 0.054 (derived by methods given in the “first approximation” section).

**Further Refinement of Spectral Data.** As mentioned in the previous section and as shown in Figure 15, the data can be further refined by taking into account the  $^{13}\text{C}$ -analog of  $\text{C}_4^{11}\text{B}_6\text{H}_{11}^+$ , the principal contributor to  $m/e$  125. Moreover, several iterative processes can be utilized to "zero in" on the exact contribution of this ion, from which one can calculate precisely the intensity of  $^{13}\text{C}_1^{12}\text{C}_3^{11}\text{B}_6\text{H}_{11}^+$  in  $m/e$  126. We performed this task with the data at hand and obtained nearly exact checks with the statistically calculated value of 0.04514 for the abundance ratio of  $^{13}\text{C}_1^{12}\text{C}_3^{11}\text{B}_6\text{H}_{12}^+$ .

The point of this whole procedure is that given good spectra, one can use them to determine the exact numbers of borons, carbons, hydrogens, etc. (barring the absence of parent ions) in a compound. In many instances this technique can preclude the necessity for elemental chemical analyses. If the material in question is impure, the mass spectral analyses may not give correct answers—but, then, neither will elemental analyses. Furthermore, with a small amount of fractionation, it is generally easy to tell by shifts of spectral peaks whether or not it is a relatively pure compound. The technique can be utilized with any isotopic elements of known abundance.

### *Acknowledgment*

This investigation was sponsored by the Office of Naval Research.

### *Literature Cited*

- (1) Beaudet, R. A., Poynter, R. L., *J. Am. Chem. Soc.* **86**, 1258 (1964).
- (2) Beynon, J. H., "Mass Spectrometry and Its Applications to Organic Chemistry," p. 486, Elsevier Publishing Co., New York, 1960.
- (3) Binger, P., *Tetrahedron Letters* **24**, 2675 (1966).
- (4) Bramlett, C. L., Grimes, R. N., *J. Am. Chem. Soc.* **88**, 4269 (1966).
- (5) Clark, C. C., U.S. Patent No. 3,062,756 (November 6, 1962).
- (6) Ditter, J. F., Spielman, J. R., Williams, Robert E., *Inorg. Chem.* **5**, 118 (1966).
- (7) Fehlner, T. P., Koski, W. S., *J. Am. Chem. Soc.* **85**, 1905 (1963).
- (8) Garrett, P. M., Tebbe, F. N., Hawthorne, M. F., *J. Am. Chem. Soc.* **86**, 5016 (1964).
- (9) Grimes, R. N., *J. Am. Chem. Soc.* **88**, 1070 (1966).
- (10) Grimes, R. N., *J. Am. Chem. Soc.* **88**, 1895 (1966).
- (11) Köster, R., Grassburger, M. A., *Angew Chem., Internat. Ed.* **4**, 439 (1965).
- (12) Lipscomb, W. N., "Boron Hydrides," W. A. Benjamin, Inc., New York, 1963.
- (13) Lipscomb, W. N., *Science* **153**, 373 (1966).
- (14) Norman, A. D., Schaeffer, R., Baylis, A. B., Pressley, G. A., Jr., Stafford, F. E., *J. Am. Chem. Soc.* **88**, 2151 (1966).
- (15) Onak, T. P., Drake, R., Dunks, G. B., *J. Am. Chem. Soc.* **87**, 2505 (1965).

- (16) Onak, T. P., Dunks, G. B., Spielman, J. R., Gerhart, F. J., Williams, Robert E., *J. Am. Chem. Soc.* **88**, 2061 (1966).
- (17) Onak, T. P., Gerhart, F. J., Williams, Robert E., *J. Am. Chem. Soc.* **85**, 3378 (1963).
- (18) Onak, T. P., Williams, Robert E., Weiss, H. G., *J. Am. Chem. Soc.* **84**, 2830 (1962).
- (19) Onak, T. P., "Advances in Organometallic Chemistry," Vol. 3, p. 263, F. G. A. Stone, R. West, eds., Academic Press, New York, 1965.
- (20) Potenza, J. A., Lipscomb, W. N., *Inorg. Chem.* **5**, 1301 (1966).
- (21) Shapiro, I., Good, C. D., Williams, Robert E., *J. Am. Chem. Soc.* **84**, 3837 (1962).
- (22) Shapiro, I., Keilin, B., Williams, Robert E., Good, C. D., *J. Am. Chem. Soc.* **85**, 3167 (1963).
- (23) Shapiro, I., Lustig, M., Williams, Robert E., *J. Am. Chem. Soc.* **81**, 838 (1959).
- (24) Shapiro, I., Wilson, C. O., Ditter, J. F., Lehmann, W. J., *ADVAN. CHEM. SER.* **32**, 127 (1961).
- (25) Stock, Alfred, "Hydrides of Boron and Silicon," Cornell University Press, Ithaca, New York, 1933.
- (26) Tebbe, F. N., Garrett, P. M., Hawthorne, M. F., *J. Am. Chem. Soc.* **86**, 4222 (1964).
- (27) Tebbe, F. N., Garrett, P. M., Hawthorne, M. F., *J. Am. Chem. Soc.* **88**, 607 (1966).
- (28) Tebbe, F. N., Garrett, P. M., Young, D. C., Hawthorne, M. F., *J. Am. Chem. Soc.* **88**, 609 (1966).
- (29) Wiesboeck, R. A., Hawthorne, M. F., *J. Am. Chem. Soc.* **86**, 1642 (1964).
- (30) Williams, Robert E., unpublished data.
- (31) Williams, Robert E., Gerhart, F. J., *J. Am. Chem. Soc.* **87**, 3513 (1965).

RECEIVED October 24, 1966.

# High Molecular Weight Boron Sulfides

## IV. Mass Spectrometric Investigation of the Conversion of Metathioboric Acid to Boron Sulfide

JIMMIE G. EDWARDS and PAUL W. GILLES

University of Kansas, Lawrence, Kan.

*The decomposition of metathioboric acid,  $\text{HBS}_2(\text{s})$ , to produce boron sesquisulfide,  $\text{B}_2\text{S}_3(\text{glass})$ , and the vaporization of the latter have been studied mass spectrometrically in the temperature range  $50^\circ$  to  $665^\circ\text{C}$ . At temperatures below  $100^\circ\text{C}$ . relative intensities, appearance potentials, and shutter effects of the ions from partly decomposed  $\text{HBS}_2$  have been measured. Six metastable ionic reactions have been found, and other ionic fragmentations have been studied. The vapor species below  $100^\circ\text{C}$ . are  $\text{H}_2\text{S}(\text{g})$ ,  $(\text{HBS}_2)_3(\text{g})$ ,  $\text{H}_3\text{BS}_3(\text{g})$ , and  $\text{H}_2\text{B}_2\text{S}_5(\text{g})$ . The existence of gaseous boron sulfides having molecular weights over 800 has been confirmed by studies of the vaporization of  $\text{B}_2\text{S}_3$  at temperatures over  $250^\circ\text{C}$ . Many new ionic species, including polymers of  $\text{BS}_2^+$ , are reported. Variations of ionic intensity ratios with temperature indicate that several neutral molecules exist in the vapor of  $\text{B}_2\text{S}_3$ .*

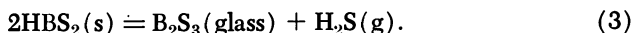
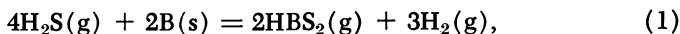
Recent investigations of the vaporization of condensed materials in the  $\text{H}_2\text{S}-\text{B}_2\text{S}_3$  system have revealed a variety of gaseous molecules. The important condensed phases in this system are  $\text{HBS}_2$  and  $\text{B}_2\text{S}_3$ . The infrared spectra of  $\text{HBS}_2(\text{s})$  and of the gaseous products of reactions between  $\text{H}_2\text{S}(\text{g})$  and  $\text{B}_2\text{S}_3(\text{glass})$  have been investigated by Greene (3, 4). He attributed some of the bands to  $(\text{HBS}_2)_2(\text{g})$  and some to a  $\text{HBS}_2-(\text{HBS}_2)_3$  mixture. Sommer, Walsh, and White (12) examined the mass spectrum of vapor from a mixture of  $\text{ZnS}$  and boron at  $700^\circ$  to  $800^\circ\text{C}$ ., but found no ion more massive than  $\text{B}_2\text{S}_3^+$ .

Three new series of high molecular weight molecules were discovered by Greene and Gilles (5, 6) in their mass spectrometric investigations of the vaporization of boron sulfide prepared by decomposition of  $\text{HBS}_2(\text{s})$ . Series I ions contained boron and sulfur only; Series II contained boron, sulfur, and a third element or radical, probably silicon; and Series III contained boron, sulfur, and oxygen. The decomposition of  $\text{HBS}_2(\text{s})$  was studied mass spectrometrically by Edwards, Wiedemeier, and Gilles (2); they discovered the vapor to be composed of  $\text{H}_2\text{S}(\text{g})$ ,  $(\text{HBS}_2)_3(\text{g})$ ,  $\text{H}_3\text{BS}_3(\text{g})$ , and  $\text{H}_2\text{B}_2\text{S}_5(\text{g})$ .

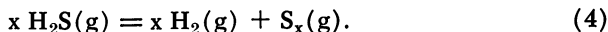
The purpose of this paper is to report new mass spectrometric results on this system and to bring these together with previous results to reach conclusions about the number and nature of the neutral molecules in the vapor, about their dependence on temperature and sample composition, and about their ionic fragmentation reactions.

### Experimental

**Samples.** Preparation of  $\text{HBS}_2$  and  $\text{B}_2\text{S}_3$  was by the method used by Greene and Gilles (6) and is illustrated by the following chemical equations,



Reaction 1 was accomplished at 600° to 800°C. in a 96% silica glass tube; the  $\text{H}_2\text{S}$  was carried over B in a stream of  $\text{H}_2$  to restrict the decomposition reaction,



Reaction 2 occurred in the cooler regions of the preparation tube.

The boron in Reaction 1 was a sample with an isotopic composition of 93%  $^{10}\text{B}$  and 7%  $^{11}\text{B}$  obtained from Oak Ridge National Laboratory. Hydrogen sulfide was obtained from commercial cylinders of the compressed material and was dried before use.

**Apparatus.** A detailed investigation of the decomposition Reaction 3 constituted a major part of this study. The reaction was performed in the stainless steel mass spectrometer vacuum enclosure at residual gas pressures below  $10^{-6}$  torr.

The mass spectrometer was a Nuclide, 12 inch radius, 60° magnetic sector, high temperature mass spectrometer. The vacuum enclosure consisted of three regions separately pumped by mercury diffusion pumps with liquid nitrogen traps:—(1) The molecular source region contained the sample in a graphite Knudsen cell; (2) The ionization region contained the ion source and ion beam forming plates; (3) The analyzer and collector region was crossed by the analyzing magnetic field, and contained the ion collector and electron multiplier. Regions 2 and 3 were separated by the final ion focussing slit.

Regions 1 and 2 were separated by an externally moveable slit which could be used to interrupt or scan the molecular beam before it entered the ionization region. With this beam shutter closed, the molecular source and the ionization source were effectively isolated. Pressures in the three regions were measured with hot cathode ionization gauges.

The sample was contained in a graphite Knudsen cell which had been outgassed *in vacuo* at 1500°C. The cell contained an effusion orifice which was 0.4 mm. in diameter and 6.3 mm. long, and was heated by radiation from tungsten resistance filaments. Temperature uniformity was achieved by use of tantalum radiation shields. Temperatures were measured with a Pt, Pt-10% Rh thermocouple, the hot junction of which was inserted into a well in the bottom of the crucible.

**Procedure.** The incongruent vaporization of a sample of about 0.5 grams of HBS<sub>2</sub> was studied in detail at progressively increasing temperatures up to 665°C. This sample was the one used in an earlier study (2). The sample was heated to the temperature desired for a given study, and was maintained constant at this temperature while measurements were being made. While observations were not being made—*i.e.*, overnight or on weekends, the sample was not heated and was kept under high vacuum at room temperature. When maintenance of the mass spectrometer required shutdown of the vacuum system, dry helium was introduced, but the sample was not exposed to the atmosphere.

Initial studies were made at temperatures from 55° to 95°C. for about three months, from 70° to 80°C. for about one month, and from 80° to 90°C. for two weeks. At this point the crucible with the sample was removed from the mass spectrometer for the first time and stored for four months in a plastic vial in a desiccator.

The final measurements were made at higher crucible temperatures. Studies were performed during a one-month period at 25 different temperatures from 100° to 665°C. The sample was studied for several hours at a given temperature, and then the temperature was increased by 10° to 40°C. for a new study. As in the initial studies, the sample was heated only while observations were being made; between experiments the sample was often cooled to room temperature.

The crucible with the sample was weighed immediately before introduction into or after removal from the mass spectrometer. Ionic intensities were measured as functions of magnetic field strength, ion accelerating potential, crucible temperature, energy of ionizing electrons, and position of the beam shutter. In addition, the monotonic manner in which the temperature was varied allowed deductions about the dependence of intensities on the degree of sample decomposition.

The studies of intensity as a function of magnetic field strength and ion accelerating voltage yielded simple scans of the mass spectrum, the mass to charge ratio,  $m/e$ , of a given ion being determined by its position in the mass spectrum. Intensity of an ion as a function of ionizing electron energy yielded the ionization efficiency curve, from which the appearance potential,  $AP$ , was determined by the vanishing current method. The energy axis was calibrated from the  $AP$  of Hg<sup>+</sup>. Intensity as a function of shutter position gave shutter profiles and total shutter effects—*i.e.*, percentage intensity decrease upon closing the shutter. When the shutter

effect was less than 100, it was also measured on isotope peaks to establish the extent to which permanent background gases contributed to the intensity.

Measurements of ion intensity as a function of temperature yield temperature coefficients for the parent molecules if the composition of the condensed phase in the Knudsen cell is constant. Studies of intensity ratios as functions of temperature yielded information about ionic decomposition in the ion source of the mass spectrometer.

Normal ions were identified from their  $m/e$  values. The identifications were confirmed by comparing the observed intensities with the theoretical intensity distribution calculated from the proposed chemical formula and the known isotopic compositions of the elements. The confirmation procedure is illustrated in Figure 1 with the use of data presented by Greene and Gilles (6) for the ion  $B_8S_{14}^+$ . The solid line on the right connects the observed intensities for the band of peaks which was proposed to represent  $B_8S_{14}^+$  containing natural boron, and the one on the left is for the same band containing 93%  $^{10}B$ -enriched boron. The dashed lines represent isotopic intensity distributions calculated from the ionic formulas shown and the known isotopic contents of the samples.

The excellent agreement for the formula  $B_8S_{14}^+$  identifies the ion. The slight disagreement at low  $m/e$  values for the ions with natural boron arose because of overlap with a weak band of Series III ions with the formula  $B_9S_{13}O^+$ .

When isotopic ions of two or more species overlapped in the mass spectrum, the contributions were separated by a stripping technique. The first peak in the band was attributed to a single species composed only of the lightest isotope of each element. Contributions from this species at higher  $m/e$  values were then calculated and subtracted from the observed intensities to obtain intensities caused by the remaining species. This process was repeated until all contributions were separated.

In scans of the mass spectrum the shapes of the peaks and the regions between peaks were studied closely to discover the presence of "metastable" ions. These result from ionic fragmentations of the type,



occurring after the ion  $A^+$  has entered the electric acceleration field, but before it enters the analyzing magnetic field. Hipple, Fox, and Condon (7) have shown that if the fragmentation occurs after acceleration is complete then the  $m/e$  value,  $m^*$ , at which the metastable ion appears in the mass spectrum is related to the  $m/e$  values of  $A^+$  and  $B^+$  by

$$m^* = m_B^2/m_A. \quad (6)$$

Metastable ions were distinguished from others in the mass spectrum by their diffuse appearance and by the fact that they might appear at nonintegral  $m/e$  values. To identify the ions  $A^+$  and  $B^+$  in Reaction 5 for a particular metastable ion, the observed apparent mass  $m^*$  was compared with values calculated from Equation 6 for all possible decompositions among the ions in the mass spectrum. It was required that Equation 6 be satisfied, that the ions  $A^+$  and  $B^+$  have relatively high intensities, and that the neutral product  $C$  be a reasonable chemical species.

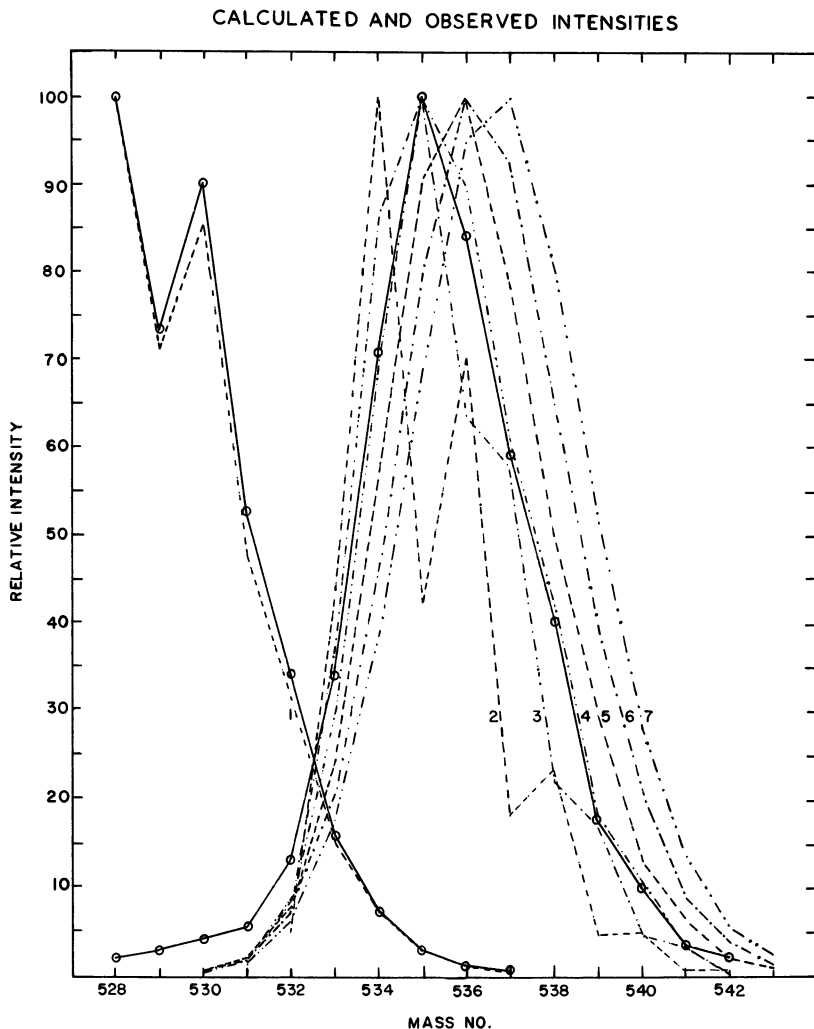


Figure 1. Observed and Calculated Intensity Distributions for Identification of  $B_8S_{14}^+$ . On the Left—Ions Containing Boron Enriched in  $^{10}B$ . On the Right—Ions Containing Natural Boron. Solid Lines—Observed Relative Intensities, Broken Lines—Calculated Relative Intensities for the Following Formulas. 1— $B_8S_{14}^+$ , 2— $B_2S_{16}^+$ , 3— $B_5S_{14}^+$ , 4— $B_8S_{14}^+$ , 5— $B_{11}S_{13}^+$ , 6— $B_{14}S_{12}^+$ , 7— $B_{17}S_{11}^+$

## Results

The  $HBS_2$  was obtained from Reactions 1 and 2 as white needle crystals among some gray and less clearly crystalline product. The mass spectra observed at all temperatures in these experiments consisted of a large number of well resolved peaks grouped in bands. Some bands

consisted of ions with a single stoichiometry but different isotopic compositions. More complex bands resulted from overlap of two or more simple bands.

Even though the same sample was used for all measurements, the results are grouped according to the temperature of the crucible. In the lowest region the vaporizing substance was  $\text{HBS}_2(\text{s})$  and in the highest region, predominantly  $\text{B}_2\text{S}_3(\text{gl})$ . Separating these regions is a transition one extending from  $100^\circ$  to  $250^\circ\text{C}$ .

**Table I. Ions Observed from  $60^\circ$  to  $100^\circ\text{C}$ . During Vaporization of  $\text{H}^{10}\text{BS}_2$**

<i>Mass of Prominent Peak</i>	<i>No. of Atoms/Molecule</i>			<i>Relative Intensity <math>85^\circ\text{C}</math>., <math>70\text{ e.v.}</math></i>	<i>Appearance Potential (<math>\text{e.v.} \pm 0.3</math>)</i>	<i>Shutter Effect (%) at <math>60^\circ\text{C}</math>.</i>
	<i>H</i>	<i>B</i>	<i>S</i>			
32	0	0	1	8.4	15.3	11
33	1	0	1	8.4	15.9	11
34	2	0	1	20	10.2	10
64	0	0	2	8.0	19	58
10	0	1	0	2.2	23.1	76
42	0	1	1	1.3	25.8	65
43	1	1	1	0.41	24.3	47
74	0	1	2	18	16.4	76
75	1	1	2	16	12.4	62
76	2	1	2	20	11.8	67
106	0	1	3	2.5	16.1	74
107	1	1	3	3.0	11.6	65
108	2	1	3	1.7	14.0	77
109	3	1	3	1.3	9.9	21
84	0	2	2	2.4	22.1	87
85	1	2	2	6.1	16.6	84
116	0	2	3	9.4	13.1	89
117	1	2	3	17	13.1	89
148	0	2	4	3.1	13.0	92
149	1	2	4	13	11.4	94
150	2	2	4	98	10.5	92
182	2	2	5	0.68	8.9	50
126	0	3	3	1.0	13.0	93
158	0	3	4	0.70	15.0	92
190	0	3	5	0.34	15.2	93
191	1	3	5	3.3	11.2	93
192	2	3	5	3.3	11.5	93
193	3	3	5	0.10		91
224	2	3	6	1.8	12.3	98
225	3	3	6	100	9.3	95

**Vaporization of HBS<sub>2</sub> Below 100°C.** These studies have been reported by Edwards, Wiedemeier, and Gilles (2). The mass loss of their sample during the investigations below 100°C. was 19.7% of the initial mass. If H<sub>2</sub>S were the only volatile substance;—*i.e.*, if the decomposition occurred only by Reaction 3, the mass loss on complete decomposition would be 22.8%; because other gases were observed, the extent of conversion was less than 86%.

Thirty ions which appeared in the mass spectrum at temperatures from 60° to 100°C. are listed in Table I, columns 2-4. In columns 1 and 5 are listed the *m/e* values and relative intensities observed in a typical investigation at 85°C. The intensities given were obtained as intensity decreases produced by closing the beam shutter, and are the sum of all isotopic intensities for each ion relative to (HBS<sub>2</sub>)<sub>3</sub><sup>+</sup> which was taken to be 100.

Appearance potentials were measured for all ions which were sufficiently intense, and are reported in column 6 of Table I. The indicated uncertainty of ±0.3 e.v. in these values was deduced by measuring some of the values several times.

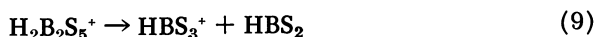
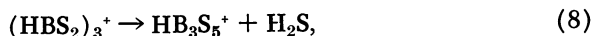
The shutter effect for the ions varied with time. When the HBS<sub>2</sub>(s) was placed in the mass spectrometer, the shutter effects of most ions were initially approximately 100. However, after several hours of vaporization the shutter effects decreased noticeably, and this decrease continued throughout the experiments below 100°C. The shutter effect for each of the ions, given in column 7 of Table I, was obtained early in the decomposition but after the shutter effects had decreased considerably. The temperature was 60°C.

Six metastable ions were discovered in the studies below 100°C. The relative intensities of these were less than 0.2 with the intensity of (HBS<sub>2</sub>)<sub>3</sub><sup>+</sup> taken as 100. The metastable decomposition reactions which were deduced are listed in Table II in which the first two columns give apparent and calculated *m/e* values. The next three sets of three columns identify the reactions.

Appearance potentials of four metastable ions were measured and are listed in Column 14 of Table II; the intensities of the other two identified metastable ions were too low to obtain dependable *AP* values. In columns 12 and 13 of Table II are listed *AP* values of the proposed parents and fragments for all six metastable reactions.

Three different groups of two metastable reactions are designated by the letters A, B, and C in the last column of Table II. For group A the metastable ion and the proposed fragment have the same *AP*; the *AP* values for group B were not determined. For group C the *AP* of the metastable ion is lower than that of the proposed fragment, an occurrence for which no satisfactory explanation readily appears.

Other metastable ions were carefully sought, but not found. A special search which proved to be unsuccessful was devoted to the reactions,



Quantitative information about ionic fragmentation processes can be obtained by consideration of shutter effects. A simple derivation yields the equation

$$S_j = \frac{\sum_{i=1}^n I_i S_i}{\sum_{i=1}^n I_i} \quad (10)$$

in which  $S_j$  is the shutter effect of ion  $j$  to whose intensity  $n$  ionic fragmentation processes contribute, and  $S_i$  is the shutter effect of ion  $i$ , one of the  $n$  ions which fragment to yield ion  $j$ . The part contributed by ion  $i$  to the intensity of ion  $j$  is symbolized by  $I_i$ . Thus, when the shutter effects are known, one has a relationship among the contributions from various fragmentations to a given ionic intensity.

Equation 10 is especially useful when  $n = 2$ , because one obtains the ratio of intensities from the two fragmentations. Such is surely the case for  $\text{B}_2\text{S}_2^+$ , since there are only two neutral molecules with two or more boron atoms,  $\text{H}_2\text{B}_2\text{S}_5$  and  $(\text{HBS}_2)_3$ . For this case,  $n$  in Equation 10

**Table II. Metastable Decompositions from  $\text{H}^{10}\text{BS}_2$  below  $100^\circ\text{C}$ .**

Mass	No. Atoms/Molecule			Appearance Potential ( <i>e.v.</i> $\pm$ 0.3)			Identifi- cation Group <sup>a</sup>	
	Calcu- lated	Parent H B S	Frag- ment H B S	Neutral H B S	Par- ent	Frag- ment		Meta- stable
38.5 $\pm$ 0.08	38.50	2 2 4	2 1 2	0 1 2	10.5	11.8	11.8	A
46.8 $\pm$ 0.1	46.77	1 2 3	0 1 2	1 1 1	13.1	16.4	13.5	C
48.5 $\pm$ 0.08	48.49	1 2 4	1 2 2	0 0 2	11.4	16.6	14.9	C
71.3 $\pm$ 0.1	71.27	2 3 5	1 2 3	1 1 2	11.5	13.1	ND <sup>b</sup>	B
89.7 $\pm$ 0.2	89.66	2 2 4	0 2 3	2 0 1	10.5	13.1	ND <sup>b</sup>	B
100.0 $\pm$ 0.08	99.95	3 3 6	2 2 4	1 1 2	9.3	10.5	10.4	A

<sup>a</sup> Group A. Identification established by mass, intensity, and AP.

Group B. Identification indicated by mass and intensity.

Group C. Identification indicated by mass and intensity, but contraindicated by AP.

<sup>b</sup> Not Detected.

is 2, ion  $j$  is  $B_2S_2^+$ , ion 1 is  $H_2B_2S_5^+$ , and ion 2 is  $(HBS_2)_3^+$ . With shutter effects from Table I we have

$$87 = \frac{50I_1 + 95I_2}{I_1 + I_2} \quad (11)$$

which reduces to  $I_2/I_1 = 4.5$ . Thus, four to five times as much  $B_2S_2^+$  results from fragmentations of  $(HBS_2)_3^+$  as from  $H_2B_2S_5^+$ . A similar calculation for  $B_2S_3^+$  yields  $I_2/I_1 = 6.5$ , and the result is the same for  $HB_2S_3^+$ , because its shutter effect is the same. For only one other ion in Table II is it clear that  $n = 2$ . This is  $HB_2S_2^+$ , but application of Equation 10 to this ion is complicated by the fact that isotopic ions of  $B_2S_2^+$ , with a different shutter effect appear at the same  $m/e$  value and must be taken into account.

**Vaporization From 100° to 250°C.** Scans of the mass spectrum were successively performed in the transition region at 100°, 110°, 130°, 155°, 170°, 190°, 215°, and 240°C. They were usually taken in the decreasing mass direction and required several hours each. These scans were characterized by changing relative intensities of ions and by the absence of high molecular weight ions.

All ions present below 100°C. were observed in these scans. The intensities for most ions varied irregularly with temperature, even to the extent that some intensities sometimes were less than in the preceding scan at lower temperature. The general trend for the intensities of all the ions except  $H_2S^+$  was to attain a maximum at about 155°C., then to decrease with increasing temperature. The intensity of  $H_2S^+$  also did not vary smoothly, but always increased with increasing temperatures.

Two ions not observed below 100°C. were found in this temperature range. The ion  $S_8^+$  was present in all scans, and  $H_2B_4S_9^+$  was found in the scans above 150°C. The intensity of  $S_8^+$  was always less than 10% relative to that of  $(HBS_2)_3^+$ , and its variation with temperature was similar to that of the majority of the ions. The intensity of  $H_2B_4S_9^+$  was low; at 155°C. it was less than 0.3% that of  $(HBS_2)_3^+$ . It increased monotonically with temperature and at 240°C. was 2.5 times as large as at 155°C. No new metastable transition was observed, and no boron sulfide ion larger than  $B_3S_5^+$  was found in this temperature range.

Few measurements requiring constant ionic intensities at a given temperature were performed because of rapid sample decomposition. The appearance potential of  $H_2B_2S_5^+$  at 202°C. was found to be 8.9 e.v.  $\pm$  0.3 e.v.

**Vaporization Above 250°C.** Scans of the mass spectrum were made at 265°, 275°, 300°, 330°, 360°, 370°, 400°, 430°, 465°, 490°, 510°, 540°, 565°, 590°, 615°, 640°, and 665°C. The high molecular weight ions discovered by Greene and Gilles (6) were observed, and many new ions

containing no hydrogen were discovered. A few low molecular weight, hydrogen-containing ions,—*e.g.*,  $\text{H}_2\text{S}^+$  and  $\text{HBS}_2^+$  remained in the mass spectrum at these temperatures, and their intensities relative to those of the high molecular weight ions were very high.

The Series I ions with formulas simpler than  $\text{B}_3\text{S}_6^+$  were present with significant intensities at  $265^\circ\text{C}$ . and remained in the spectrum at the highest temperature. Three larger Series I ions,  $\text{B}_7\text{S}_{12}^+$ ,  $\text{B}_8\text{S}_{14}^+$ , and  $\text{B}_8\text{S}_{16}^+$  were observed at  $265^\circ\text{C}$ ., and one larger, hydrogen-containing ion,  $\text{H}_2\text{B}_4\text{S}_9^+$ , was still present. No Series II or III ion was detectable at  $265^\circ\text{C}$ . A few ions containing five and six borons were first detected at  $275^\circ\text{C}$ .

At  $300^\circ\text{C}$ . the mass spectrum was much richer in ions;  $\text{B}_8\text{S}_{15}^+$  appeared along with  $\text{B}_7\text{S}_{14}^+$ ,  $\text{B}_7\text{S}_{13}^+$ ,  $\text{B}_8\text{S}_{12}^+$ ,  $\text{B}_6\text{S}_{12}^+$ , and several others. In addition, two Series III ions,  $\text{B}_8\text{S}_{15}\text{O}^+$  and  $\text{B}_8\text{S}_{13}\text{O}^+$ , became detectable.

As the temperature was increased above  $300^\circ\text{C}$ . the mass spectrum became very rich. Many Series I and III ions were found, and above  $400^\circ\text{C}$ . the Series II ions appeared. At about  $350^\circ\text{C}$ . ions with as many as ten boron atoms achieved detectable intensities.

In all three series of ions the intensities of the low molecular weight ions varied with temperature differently than did the intensities of the high molecular weight ions. The intensities of most Series I ions with  $m/e$  less than 250 increased monotonically with temperature, but for heavier ions the intensities reached a maximum at about  $400^\circ$  to  $500^\circ\text{C}$ . then decreased. At temperatures slightly above  $250^\circ\text{C}$ . and also above  $600^\circ\text{C}$ . the intensities of low  $m/e$  ions were greater than those for the heavier ions, but in the region  $300^\circ$  to  $600^\circ\text{C}$ ., the heavier ions were more intense than the lighter ions except for  $\text{H}_2\text{S}^+$ ,  $\text{HBS}_2^+$ ,  $\text{S}_2^+$ , and  $\text{B}_2\text{S}_3^+$ .

Intensities of Series II ions with  $m/e$  below about 450 increased with increasing temperature. Ions with high  $m/e$  values had intensities that reached a maximum between  $550^\circ$  to  $650^\circ\text{C}$ ., then decreased with increasing temperature. Series III ions with  $m/e$  less than about 300 increased in intensity with increasing temperature. The others reached a maximum intensity between  $400^\circ$  and  $600^\circ\text{C}$ . then decreased with temperature. Although many of the new ions were present in the spectrum over only short temperature ranges,  $\text{B}_8\text{S}_{16}^+$  was observed in all scans above  $250^\circ\text{C}$ .

In Figure 2 the intensities of the boron-sulfur ions relative to that of  $\text{B}_8\text{S}_{16}^+$  as 100 which were observed in the scan at  $490^\circ\text{C}$ . are shown graphically. The location of each number represents an ion with the formula  $\text{B}_n\text{S}_m^+$ , in which  $n$  and  $m$  are, respectively, the ordinate and abscissa of the location. The two dashed lines on the graph connect locations of the ionic polymers of  $\text{B}_2\text{S}_3$  and  $\text{BS}_2$ , respectively. Most ions fall within the region enclosed by these lines. Not shown are ions containing

only one element, although  $B^+$  as well as all ionic sulfur polymers up to  $S_8^+$  were observed. A relative intensity of zero means that the ion was not observed at  $490^\circ\text{C}$ . but was observed in one or more of the other scans; a  $G$  represents an ion observed by Greene and Gilles (6) but not observed in this work; and underlining indicates an ion not observed by them.

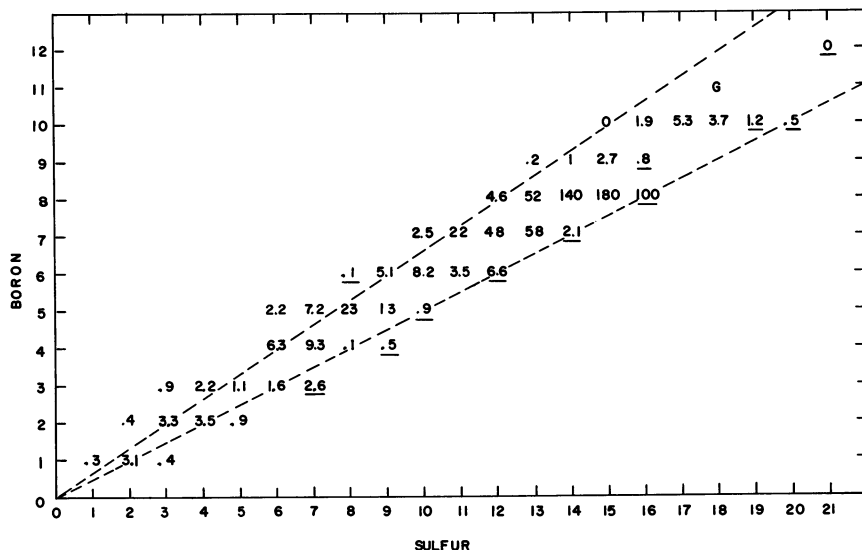


Figure 2. Relative Intensities of Series I Boron Sulfide Ions at  $490^\circ\text{C}$ . The numbers of boron and sulfur atoms in the ion are given as ordinate and abscissa. Intensity of  $B_8S_{16}^+$  equals 100. Underlining indicates an ion not observed by Greene and Gilles, and a  $G$  represents each ion observed by them but not observed in this work

Relative intensities of the Series I ions observed at the same temperature,  $490^\circ\text{C}$ ., are also represented on a schematic mass spectrum in Figure 3. The ordinate gives on a logarithmic scale the percentage intensity relative to that of  $B_8S_{16}^+$ . The abscissa identifies the ion, first by the number of boron atoms, then by the number of sulfur atoms; thus it is not continuous in  $m/e$ .

In Figures 4 and 5 are shown, respectively, the Series II or silicon-containing ions which were observed in the scan at a higher temperature,  $640^\circ\text{C}$ ., and their relative intensities on a schematic mass spectrum of the same type as in Figure 3. Figures 6 and 7 illustrate in the same way the Series III, or boron-sulfur-oxygen ions, and their relative intensities in the scan at  $565^\circ\text{C}$ .

Composition variations in the samples prevented direct use of intensity *vs.* temperature data to obtain thermodynamic quantities, but

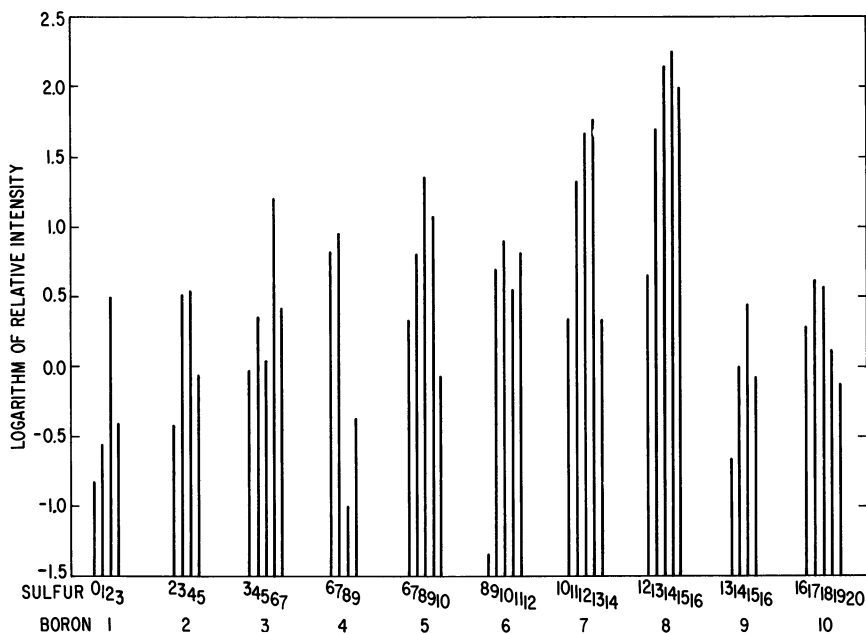


Figure 3. *Logarithms of Relative Intensities of Series I Boron Sulfide Ions at 490°C. Intensity of  $B_8S_{16}^+$  Equals 100*

information on fragmentation processes can be obtained. Consider the ionic fragmentation reaction



If only one molecular source yields  $A^+$ , and if Reaction 12 is the only source of  $B^+$ , then the intensity ratio  $I(A^+)/I(B^+)$  is independent of sample composition. However, if more than one molecular source exists for either ion  $A^+$  or ion  $B^+$ , then the value of the intensity ratio will depend on sample composition and temperature.

In Figure 8 logarithms of three intensity ratios,  $I(B_8S_{15}^+)/I(B_8S_{16}^+)$ ,  $I(B_7S_{12}^+)/I(B_8S_{14}^+)$ , and  $I(B_8S_{12}^+)/I(B_8S_{14}^+)$  are plotted as functions of the inverse temperature. The variations of these three ratios with temperature are typical of those found for other ions. At Knudsen cell temperatures below 750°K. ( $1/T = 1.33 \times 10^{-3}$ ) intensity ratios  $I(B_8S_{12}^+)/I(B_8S_{14}^+)$  and  $I(B_7S_{12}^+)/I(B_8S_{14}^+)$  were effectively independent of temperature and composition, and, therefore, both ions whose intensities appear in the ratio probably had a single molecular precursor. Above this temperature a new source arose for the ion whose intensity appears in the numerator in each of these two ratios as indicated by the increasing value of the intensity ratio with increasing temperature.

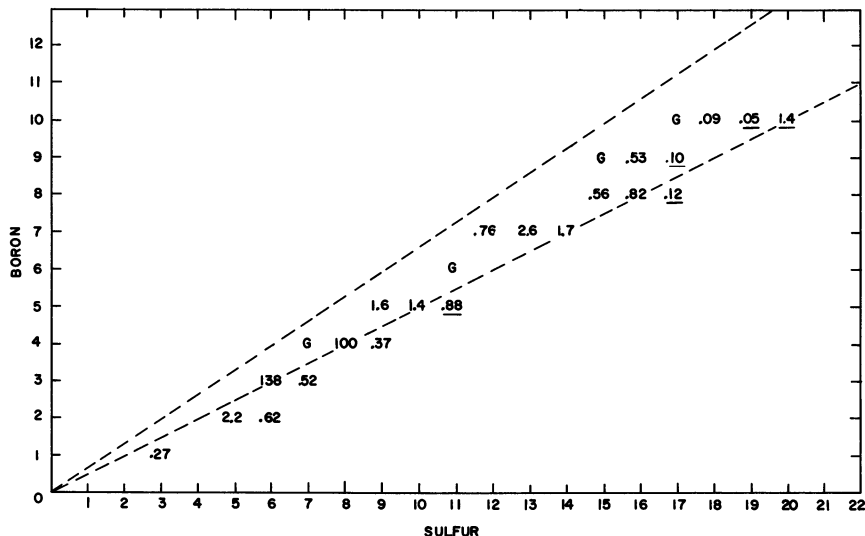


Figure 4. *Relative Intensities of Series II Boron Sulfide Ions at 640°C. Each ion contains one silicon atom. The numbers of boron and sulfur atoms are given as ordinate and abscissa. Intensity of  $B_4S_3Si^+$  equals 100. Underlining indicates an ion not observed by Greene and Gilles, and a G represents each ion observed by them but not observed in this work*

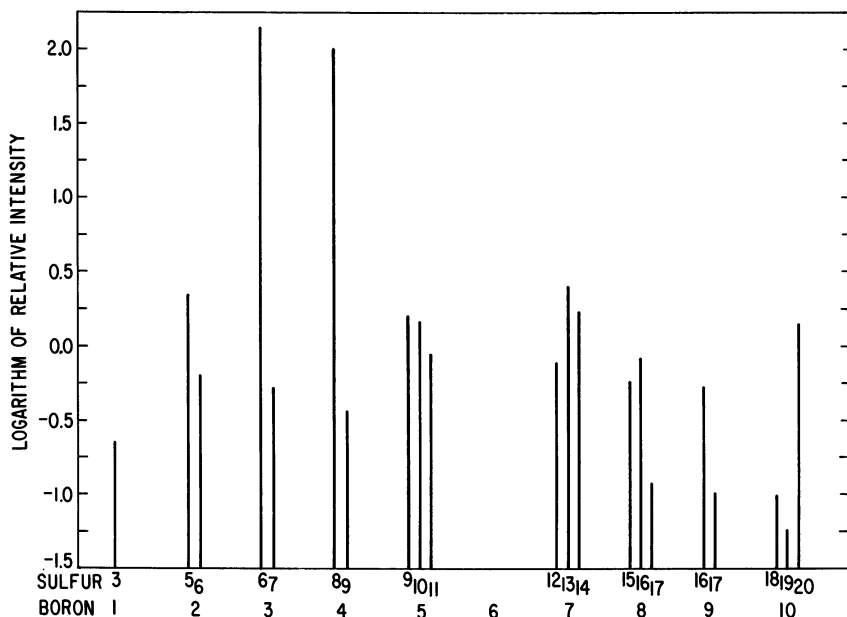


Figure 5. *Logarithms of Relative Intensities of Series II Boron Sulfide Silicide Ions at 640°C. Intensity of  $B_4S_3Si^+$  Equals 100*

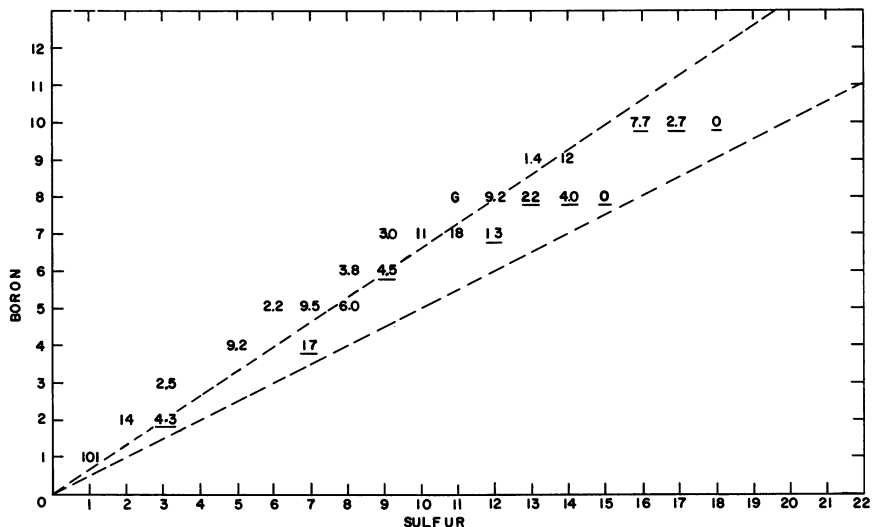


Figure 6. Relative Intensities of Series III Boron Sulfide Ions at 565°C. Each ion contains one oxygen atom. The numbers of boron and sulfur atoms are given as ordinate and abscissa. Intensity of  $B_8S_{16}^+$  equals 100. Underlining indicates an ion not observed by Greene and Gilles, and a G represents each ion observed by them but not observed in this work

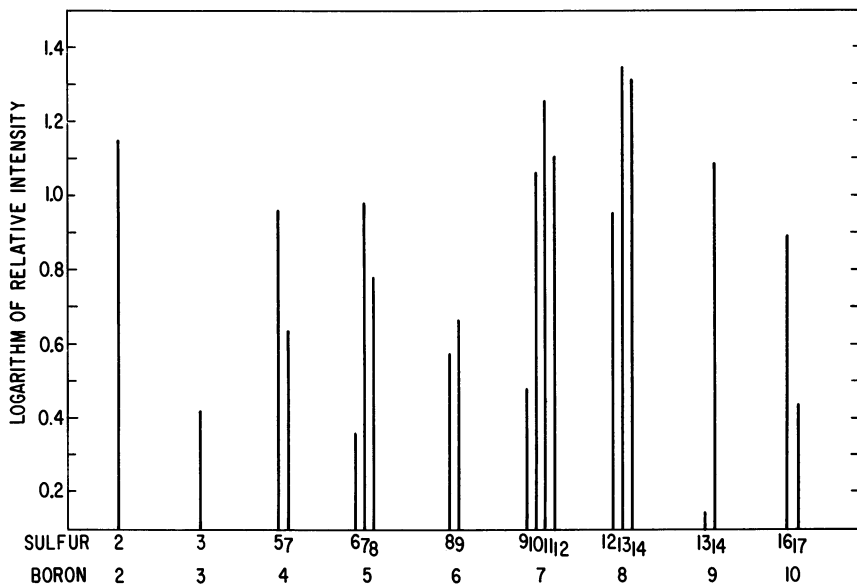


Figure 7. Logarithms of Relative Intensities of Series III Boron Sulfide Oxide Ions at 565°C. Intensity of  $B_8S_{16}^+$  equals 100

The observed variation of the intensity ratio  $I(\text{B}_8\text{S}_{15}^+)/I(\text{B}_8\text{S}_{16}^+)$  in Figure 8 shows that at least two molecular precursors for one or both of these ions existed over the entire range of temperatures represented, and that the nature of these sources did not change appreciably at temperatures below  $600^\circ\text{K}$ . ( $1/T = 1.55 \times 10^{-3}$ ). The curvature at high temperatures is probably caused by a disappearance of a source of  $\text{B}_8\text{S}_{15}^+$ .

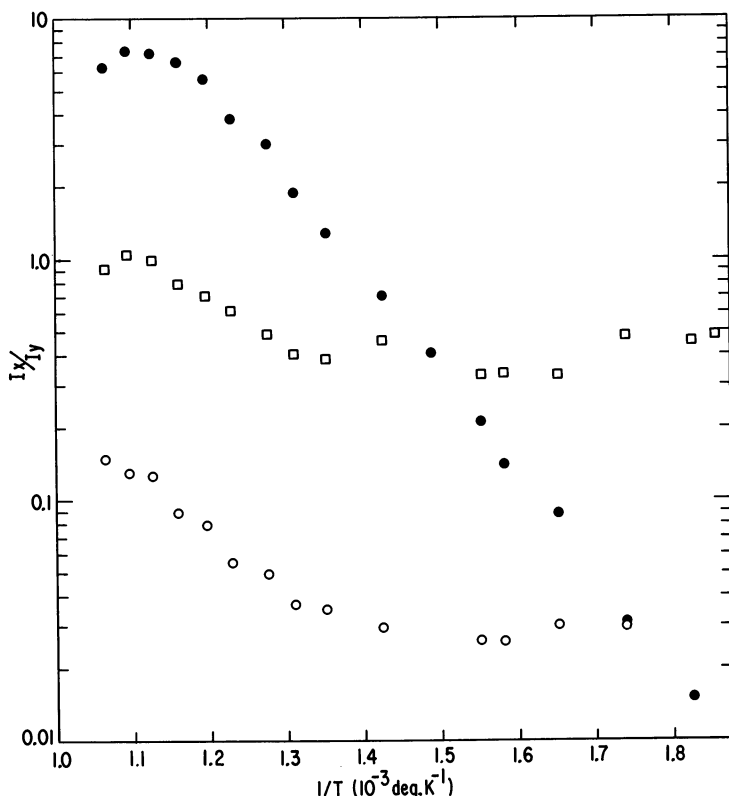


Figure 8—Logarithms of Intensity Ratios as Functions of  $1/T$ . Thermodynamic quantities should not be taken from slopes because composition of samples was changing. ●— $I(\text{B}_8\text{S}_{15}^+)/I(\text{B}_8\text{S}_{16}^+)$ , □— $I(\text{B}_7\text{S}_{12}^+)/I(\text{B}_8\text{S}_{14}^+)$ , ○— $I(\text{B}_8\text{S}_{12}^+)/I(\text{B}_8\text{S}_{14}^+)$

Molecular precursors of ions cannot be deduced unequivocally from information about intensity ratios such as that discussed above. Other changes which occurred in the mass spectrum at temperatures of the breaks in the curves suggest, however, some fragmentation relationships. For example, at about  $370^\circ\text{C}$ ., which is also the temperature at which a break occurs in two curves in Figure 8, the first ions containing ten boron

atoms appeared in the mass spectrum. One deduces from this observation the possibility that molecules with ten or more borons are neutral precursors for some of the ions in Figure 8.

### Discussion

**Vaporization of HBS<sub>2</sub> Below 100°C.** The information which has been obtained from the low temperature vaporization experiments is sufficient to allow identification of the important neutral molecules in equilibrium with HBS<sub>2</sub>(s) at temperatures below 100°C. This evidence includes the identification, intensities, *AP* values, and shutter effects of the ions and the metastable reactions. Figure 9 illustrates the mass spectrum and relative intensities by means of vertical lines. Appearance potentials and shutter effects are represented by circles and triangles, respectively. One sees that the most intense ions originating from the crucible region below 100°C. are (HBS<sub>2</sub>)<sub>3</sub><sup>+</sup>; the pair (HBS<sub>2</sub>)<sub>2</sub><sup>+</sup> and HB<sub>2</sub>S<sub>4</sub><sup>+</sup>; the group H<sub>2</sub>S<sup>+</sup>, HS<sup>+</sup>, and S<sup>+</sup>; the group H<sub>2</sub>BS<sub>2</sub><sup>+</sup>, HBS<sub>2</sub><sup>+</sup>, and BS<sub>2</sub><sup>+</sup>; and the pair HB<sub>2</sub>S<sub>3</sub><sup>+</sup> and B<sub>2</sub>S<sub>3</sub><sup>+</sup>. The ions with lowest *AP* values are H<sub>2</sub>B<sub>2</sub>S<sub>5</sub><sup>+</sup>, (HBS<sub>2</sub>)<sub>3</sub><sup>+</sup>, H<sub>3</sub>BS<sub>3</sub><sup>+</sup>, and (HBS<sub>2</sub>)<sub>2</sub><sup>+</sup>.

The agreement of the measured *AP* of H<sub>2</sub>S<sup>+</sup> with the known value, the unique shutter effect of H<sub>2</sub>S<sup>+</sup>, and the known decomposition of HBS<sub>2</sub> to B<sub>2</sub>S<sub>3</sub> show that H<sub>2</sub>S<sup>+</sup> results from ionization of H<sub>2</sub>S. The low *AP* and high intensity of (HBS<sub>2</sub>)<sub>3</sub><sup>+</sup>, the absence of any higher molecular weight hydrogen containing species, and the fact that the trimer has the same composition as HBS<sub>2</sub>(s) show that it also is a neutral molecule. The low *AP* and low shutter effect of H<sub>3</sub>BS<sub>3</sub><sup>+</sup> and the fact that H<sub>3</sub>BS<sub>3</sub>, orthothio-boric acid, lies on the join containing H<sub>2</sub>S, HBS<sub>2</sub>, and B<sub>2</sub>S<sub>3</sub> of the ternary H-B-S system indicate that H<sub>3</sub>BS<sub>3</sub> is an important neutral molecule in this system.

The ion with the lowest *AP* is H<sub>2</sub>B<sub>2</sub>S<sub>5</sub><sup>+</sup>, and this fact indicates that it also is a parent ion. The only higher molecular weight ions, and, therefore, those to which it might be related by a fragmentation process involving negative ion formation, all have much larger shutter effects, thus substantiating the conclusion that it is a parent ion.

The low *AP*, high intensity, and the composition of (HBS<sub>2</sub>)<sub>2</sub><sup>+</sup> suggest that it too is a parent ion. On the other hand, the observation of the metastable decomposition from the trimer to the dimer at *m/e* = 100, the agreement of the *AP* values for the metastable and the dimer ions, and the fact that the dimer and trimer have the same shutter effect all suggest that (HBS<sub>2</sub>)<sup>+</sup> is a fragment. The dimer molecule probably is not important at temperatures below 100°C.

The other ions with *m/e* values greater than 110 have *AP* values greater than 11 e.v. and large shutter effects, and they most likely arise

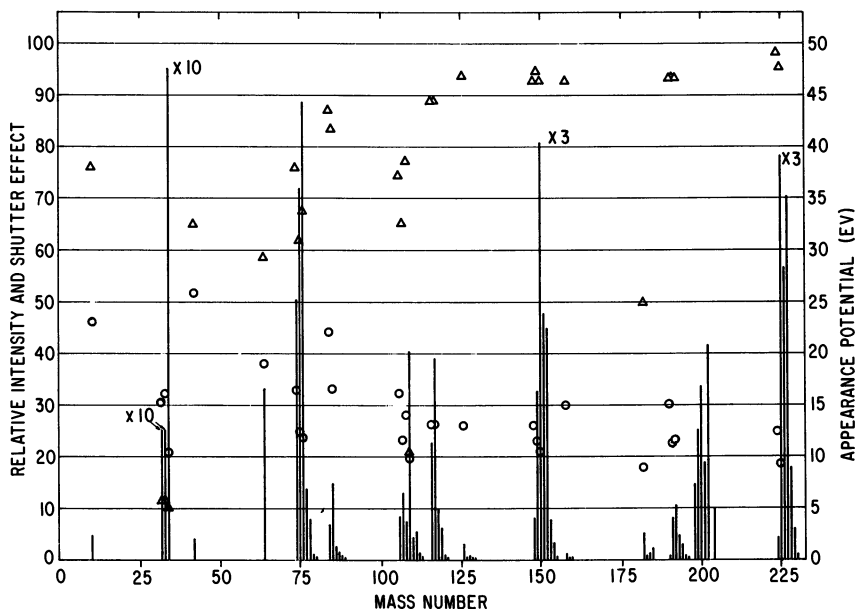


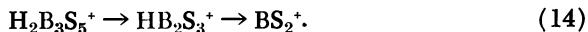
Figure 9. Relative Intensities, Appearance Potentials, and Shutter Effects of Ions Observed from  $H^{10}BS_2$  (s) at  $60^\circ$  to  $100^\circ C$ . The lengths of vertical lines give the relative intensities and the triangles give the shutter effects on the left scale. The circles give the appearance potentials on the right scale

from fragmentation of  $(HBS_2)_3^+$ . The ions with  $m/e$  values between 50 and 108 also have AP values greater than 11 e.v. and intermediate shutter effects, and they probably arise from two or more processes from parent molecules with different shutter effects—*e.g.*,  $(HBS_2)_3$ ,  $H_3BS_3$ , and  $H_2B_2S_5$ .

Some of these decompositions were observed as metastable ions. In particular, the observations prove the existence of two fragmentation series.



and



From the AP values and shutter effects of  $(HBS_2)_3^+$  and  $H_2B_3S_5^+$  one may deduce that the latter series also originates with  $(HBS_2)_3$ , but no other evidence of this has been found.

The AP reported here for  $B_2S_3^+$  is  $13.1 \pm 0.3$  e.v. and that given previously (6) was  $10.4 \pm 0.3$  e.v. The difference arises from the fact that at crucible temperatures below  $100^\circ C$ . the ion is a fragment from

one of the acid species, and in the earlier, higher temperature studies on  $B_2S_3$  the ion is a parent.

Inasmuch as both the initial reactant  $HBS_2$  and the principal ultimate product  $B_2S_3$  lie on the  $H_2S$ - $B_2S_3$  join, the *a priori* hypothesis is that the main gaseous product of the decomposition will be  $H_2S$ . The results show that  $H_2S(g)$ ,  $H_3BS_3(g)$ , and  $(HBS_2)_3(g)$  are indeed the principal gaseous products of the low temperature vaporization; thus the overall result is a loss of  $H_2S$  as well as  $HBS_2$  from the condensed phase. The parent ion  $H_2B_2S_3^+$  does not lie on the  $H_2S$ - $B_2S_3$  join, but its intensity is small below  $100^\circ C$ .

**Vaporization at Higher Temperatures.** The observations from  $100^\circ$  to  $250^\circ C$ . revealed only additional ions,  $S_8^+$  and its fragments and  $H_2B_4S_9^+$ . The fact that hydrogen-containing species remained important shows that decomposition of the  $HBS_2(s)$  was not yet complete.

At higher temperatures, above  $250^\circ C$ ., the observations of high molecular weight ions by Greene and Gilles (6) were confirmed in many experiments under a variety of conditions. In addition, new ions were discovered. The fact that many of these new ions were present in the mass spectrum only in relatively short temperature ranges explains why they were not observed earlier. The vapor at temperatures above  $250^\circ C$ . probably contains many neutral molecules, their variety and concentrations depending on the temperature and sample composition.

The presence of ions with formulas up to  $B_{12}S_{21}^+$  and the impossibility of significant ion-molecule reactions at the low pressures in the ion source and analyzer prove that molecules at least as large as  $B_{12}S_{21}$  must exist. It is probable that  $B_{12}S_{21}^+$  is a fragment of a still larger, but undetected ion. The observation of relatively intense  $B_8S_{16}^+$  over a wide temperature range is significant because it had been predicted (6) that  $B_8S_{16}$  should be an important neutral molecule.

Greene and Gilles (6) attributed the existence of high molecular weight boron sulfide molecules in the vapor to excess sulfur in the condensed state. The sample used in this work was prepared by their method and produced  $S_8^+$ ; thus this sample also was sulfur-rich. Their failure to observe  $BS_2$  polymers may have arisen because their sulfur activity was not as high as ours. The failure by Sommer, Walsh, and White (12) to observe any boron-sulfide ion more complex than  $B_2S_3^+$  was probably caused by the much lower sulfur activity in their system.

Few conclusions about the Series II and Series III ions can be obtained from these investigations. The Series III ions most likely result from substitution of one oxygen for one sulfur in Series I ions. Supporting this chemical argument is the fact that if one sulfur is added to each ion in Figure 6 their locations with respect to the  $B_2S_3$  and  $BS_2$  polymer lines become much like those of the Series I ions in Figure 2.

The same type of comparison of Figures 2 and 4 reveals that the two representations almost superimpose if one sulfur is removed from each Series II ion. Thus, these ions could be obtained by adding one silicon atom and one sulfur atom to the appropriate Series I ions.

Our results obtained below 100°C. appear to indicate that  $(\text{HBS}_2)_3$  is the only important gaseous molecule with the stoichiometry of  $\text{HBS}_2$ . Greene (3, 4) in his investigations of the infrared spectrum of this system interpreted his results in terms of  $\text{HBS}_2(\text{g})$ ,  $(\text{HBS}_2)_2(\text{g})$ , and  $(\text{HBS}_2)_3(\text{g})$ . However, his work was done at higher temperatures, where the monomer achieves importance.

Work on the H-B-O system can be divided into two categories, one containing the several papers by Porter (1) and his coworkers on boroxine  $\text{H}_3\text{B}_3\text{O}_3(\text{g})$  and its derivatives, and the other containing work on the spectra and thermodynamic properties of substances in the  $\text{H}_2\text{O}-\text{B}_2\text{O}_3$  system,  $\text{HBO}_2(\text{g})$ ,  $(\text{HBO}_2)_3(\text{g})$ ,  $\text{B}_2\text{O}_3(\text{s})$ , and  $\text{B}_2\text{O}_3(\text{g})$ , by Greene (3, 4), Meschi, Chupka, and Berkowitz (8), by Randall and Margrave (9), and by White, Mann, Walsh, and Sommer (13).

There is little analogy between the present work and that on the boroxine system. The principal neutral species in the present study lie on the  $\text{H}_2\text{S}-\text{B}_2\text{S}_3$  join or slightly to the sulfur-rich side, but the boroxine compounds are on the oxygen-deficient side of the corresponding join in the H-B-O system.

A major difference between the studies on the boric acids and this work on the thioboric acids lies in the temperature range. The present experiments on the hydrogen containing species were performed mostly below 100°C., where the principal species were  $(\text{HBS}_2)_3(\text{g})$  and  $\text{H}_2\text{S}(\text{g})$ , but the experiments on the boric acids employed the reaction between water and boric oxide above 800°C., where the principal species is  $\text{HBO}_2(\text{g})$ . The difference in volatilities arises presumably because of greater hydrogen bonding in the boric acids.

No oxygen analog of  $\text{H}_2\text{B}_2\text{S}_5$  has been discovered. The structure of this new molecule is not known but it probably contains the five membered 1,3,4-trithiadiborolane ring (10, 11), which includes a S-S bond. On the basis of this structure, the absence of  $\text{H}_2\text{B}_2\text{O}_5$  is explained by the instability of the required peroxide bond.

The second major difference between the sulfur and oxygen systems is that in the latter no high molecular weight species has yet been discovered. Probably the reason for the difference lies in the greater tendency of sulfur to catenate. Possibly the greater difficulty of forming oxygen-rich solutions of  $\text{B}_2\text{O}_3$  and the necessity of working at higher temperatures both militate against the existence of high molecular weight boron oxides.

### *Acknowledgment*

The authors are pleased to acknowledge the support of this work by the United States Atomic Energy Commission through its contract No. AT(11-1)-1140 with the University of Kansas, and by the National Aeronautics and Space Administration under Sustaining Grant No. NsG-298 to the University of Kansas. They thank the University of Kansas Computation Center for aid in the isotopic distribution calculations. They also wish to thank Heribert Wiedemeier for preparing the sample, contributing to the lowest temperature measurements, and providing illuminating suggestions and comments.

### *Literature Cited*

- (1) Barton, L., Wason, S. K., Porter, R. F., *J. Phys. Chem.* **69**, 3160 (1965).
- (2) Edwards, J. G., Wiedemeier, H., Gilles, P. W., *J. Am. Chem. Soc.* **88**, 2935 (1966).
- (3) Greene, F. T., Ph.D. Thesis, Univ. of Wisconsin, 1961.
- (4) Greene, F. T., *Univ. Microfilms No. 61-5933*, Ann Arbor, Michigan.
- (5) Greene, F. T., Gilles, P. W., *J. Am. Chem. Soc.* **84**, 3598 (1962).
- (6) Greene, F. T., Gilles, P. W., *J. Am. Chem. Soc.* **86**, 3964 (1964).
- (7) Hipple, J. A., Fox, R. E., Condon, E. U., *Phys. Rev.* **69**, 347 (1946).
- (8) Meschi, D. J., Chupka, W. A., Berkowitz, J., *J. Chem. Phys.* **33**, 530 (1960).
- (9) Randall, S. P., Margrave, J. L., *J. Inorg. Nucl. Chem.* **16**, 29 (1960).
- (10) Schmidt, M., Siebert, W., *Angew. Chem.* **76**, 687 (1964).
- (11) Schmidt, M., Siebert, W., *Angew. Chem. Internat. Edit.* **3**, 637 (1964).
- (12) Sommer, A., Walsh, P. N., White, D., *J. Chem. Phys.* **33**, 296 (1960).
- (13) White, D., Mann, D. E., Walsh, P. N., Sommer, A., *J. Chem. Phys.* **32**, 488 (1960).

RECEIVED January 9, 1967.

# A Modified Mass Spectrometer Ion Source for the Study of High Temperature Vaporization

Vaporization of Zinc, Cadmium, Arsenic, Selenium, Cadmium Arsenide, and Cadmium Selenide.

J. B. WESTMORE

University of Manitoba, Winnipeg, Canada

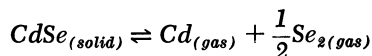
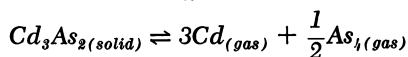
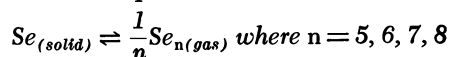
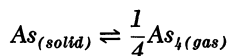
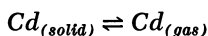
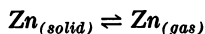
H. FUJISAKI

Research Institute for Scientific Measurements, Tohoku University, Sendai, Japan

A. W. TICKNER

Division of Applied Chemistry, National Research Council, Ottawa, Canada

*The construction of an ion source for vaporizations in the range 100° to 400°C. is described. The conditions under which the vaporizations occur are analyzed and some results presented. Thermodynamic data are presented. The vaporizations studied were*



*The accommodation coefficient for the vaporization of As<sub>4</sub> from solid arsenic or from Cd<sub>3</sub>As<sub>2</sub> is small and also may be small for the vaporization of Se<sub>2</sub> from CdSe.*

The most commonly used method of studying relatively involatile materials in a mass spectrometer is by means of a Knudsen or effusion cell. These are now available as accessories to commercial instruments. A molecular beam from the cell intersects an electron beam in the ionizing region. The recorded ion current is proportional to the concentration of a particular molecular species in the beam and can be related to its partial pressure inside the effusion cell. By varying the temperature of the effusion cell and recording the ion current owing to the various species emerging from the cell at each temperature, thermodynamic data can be obtained. If the effusion cell can be calibrated so that absolute partial pressures can be determined, then free energies and entropies as well as enthalpies can be obtained for the vaporization reactions.

A modified ion source has been constructed in which the ionizing electron beam actually passes through a chamber containing vapor above the condensed phase as shown in Figure 1. The details of its construction will be given in the experimental section. The partial pressure of the vapor in the ionizing region is directly controlled by the temperature of the sample.

One advantage of this ion source over the conventional Knudsen cell source arises because the sample vapor is actually generated in the ionizing region. This results in greater sensitivity and the ability to work at lower vapor pressures. Using a Faraday cup collector and vibrating reed amplifier, ion currents were measured at pressures estimated to be in the range  $10^{-7}$  to  $10^{-4}$  torr. Greater sensitivity should be achieved with an electron multiplier detector. It becomes possible to study systems at lower temperatures and different conditions than previously, and in some cases different behavior has been observed. Since at these pressures the mean free path is much larger than the cell dimensions it is possible to work at conditions where collisions in the vapor are of negligible importance.

A disadvantage of this ion source is that because of the relatively large area of the slits some vapor can diffuse back into the ionization region from outside the cell. Although the amount of back diffusion is relatively small, in some cases it prevented an unambiguous conclusion as to whether a smaller molecule arose by vaporization from the condensed phase or by thermal decomposition of a larger molecule on the mass spectrometer filament. A further consequence of the relatively large slit area is the effect on the steady state pressure in the sample chamber. This effect will be analyzed in the theoretical section.

The potential of the sample chamber could be varied with respect to the filament. In this way the current caused by a particular ion could be

determined as a function of the electron energy, and an ionization efficiency curve could be obtained. Although the curves did not have the idealized shape, appearance potentials obtained from them agreed well with literature values when a direct comparison was possible. The electron energy scale was calibrated with an inert gas, usually krypton or xenon.

### *Experimental*

**Description of the Ion Source.** The ion source was originally described by Mann and Tickner (11) and later modified (17). The details of the modified apparatus now follow.

The ion source of a conventional 90° magnetic sector mass spectrometer was modified as shown in Figure 1. Originally the normal pumping on the mass spectrometer tube was supplemented by a 70 liters/sec. mercury diffusion pump equipped with a liquid nitrogen trap attached directly to the ion source chamber to reduce the background of residuals in the ion source. However, there were appreciable variations in pumping speed, and hence this extra diffusion pump was only used for initial heating of the sample chamber. Copper cooling coils were added to the ends of the source chamber to prevent the rubber O-rings from being overheated.

The entire furnace assembly was mounted on plate  $P_1$  which was attached to the same mounting posts as the focusing and collimating plates of the mass spectrometer. Plate  $P_2$  was supported with respect to  $P_1$  by four rods. All of the plates and supporting rods were made of Chromel A.

The electron beam was supplied by a tungsten filament  $F$ . It entered the ion source furnace through a small slit and emerged through a slightly larger slit to be measured by means of trap  $T$ . Permanent magnets mounted externally supplied a collimating field of about 400 gauss. An exit slit was provided in the end of the furnace, and a circular hole 1 cm. in diameter in plate  $P_1$  opposite the slit allowed sufficient penetration of the field from the focusing plates to withdraw the ions. The two slits for the electron beam and the ion exit slit were defined by pieces of Chromel foil spot-welded onto the ion source furnace. The sizes of the slits could consequently be varied, and their total area averaged between 4 to 6 sq. mm. Three tool steel pins 0.5 mm. in diameter mounted on  $P_1$  and corresponding holes in the end of the ion source furnace located the exit slit with respect to the collimating slits of the mass spectrometer. Electrons from the filament were accelerated by a potential applied between the filament and the furnace. This potential could be varied between about 5 to 100 volts and was measured with a digital voltmeter when ionization efficiency curves were being determined.

The furnaces were machined from molybdenum which, in addition to its low vapor pressure and high melting point, possessed high thermal conductivity and was not attacked by the vapors of the metals to be examined. Each furnace had its own heating element of a noninductive type cut from Chromel A sheet and wound on with mica insulation. Since it was not necessary to know the temperature of the ion source furnace

with great accuracy, it was convenient to place a thermocouple on its wall inside the heating element. The radiation shields were made of tantalum and were supported by stainless steel screws and borosilicate glass spacers. All electrical leads were brought out at the end of the ion source chamber by means of feed-through insulators.

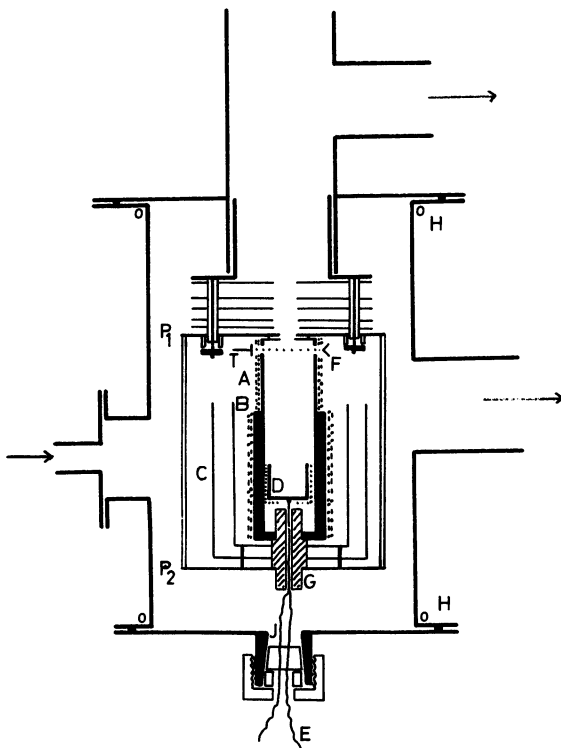


Figure 1. Mass spectrometer ion source

A. Ion source furnace; B. Sample furnace; C. Radiation shields; D. Molybdenum crucible; E. Thermocouple; F. Filament; G. Sample support; H. Cooling coils; J. Feed through insulator of Teflon; P<sub>1</sub> and P<sub>2</sub>. Mounting plates; and T. Electron beam trap

A regulated a.c. power supply with an output voltage constant to 0.1% was used to supply power for heating the furnaces. Each furnace received its power from the secondary winding of an isolating transformer which allowed the furnace heating elements to operate at the potential of the ion source, approximately 2000 volts above ground. The temperature of each furnace was controlled manually by adjusting a variable auto-transformer which supplied the voltage to the primary winding. This

arrangement allowed different temperatures to be maintained in the two furnaces over a sufficiently wide range.

Powdered samples were placed in crucibles machined from molybdenum. One crucible had a single large compartment while another had seven compartments of equal size drilled in it. Samples could be placed in different numbers of holes to vary the effective sample area, as will be discussed in the theoretical section. The crucible was fitted into a specially made quartz cup which had a circular hole in the bottom so that it could be mounted on a support machined from boron nitride or quartz. A hole drilled in the axis of the sample support allowed the insertion of a Chromel P-Alumel thermocouple which measured the sample temperature. The thermocouple wires were brought out of the vacuum without joins by passing them through small holes in a Teflon plug which was compressed by forcing it into a tapered hole by screwing down a threaded nut onto it.

The thermocouple was calibrated at the melting points of zinc, lead, and tin and at the boiling point of water. Recalibration after use showed that the calibrations had changed by less than  $0.6^\circ$  in all cases. The e.m.f.'s were measured on a potentiometer with an accuracy of  $\pm 0.002$  mv.

Temperature equilibrium could be attained in a few minutes, and the temperature was held constant to within  $0.5^\circ$  while the ion currents were being measured. It was found that the amount by which the temperature of the ion source furnace exceeded that of the sample furnace had little effect on the results. Since the temperatures of the two furnaces were interdependent to some extent, a relatively small temperature difference of about  $5^\circ$  was used in most of the experiments to extend the range of the sample furnace temperature to as low a value as possible.

To correct for any variation in the over-all efficiency of the ion source during a series of measurements a small reference pressure of krypton or xenon was maintained in the ion source chamber by allowing the gas to leak in from a reservoir in the sample line. Krypton and xenon were chosen because they were chemically inert, their ionization potentials are accurately known and are the lowest of the inert gases, and their atomic weights were closer to those of the samples than were the other inert gases. At each temperature the ion current corresponding to the inert gas was measured as well as the ion current caused by the sample.

### *Theoretical*

**Evaluation of Steady State Conditions in the Sample Cell.** At the steady state the rate of evaporation of molecules from the surface of the sample is equal to the sum of the rate of loss of molecules from the cell and the rate of condensation of vapor molecules onto the sample surface. The theoretical maximum rate of evaporation of molecules of molecular weight  $M$  from a surface is given by the well-known Langmuir-Knudsen equation (4, 7, 9) as

$$\text{rate of evaporation} = P(2\pi MRT)^{-1/2} \text{ moles cm.}^{-2} \text{ sec.}^{-1}$$

where  $P$  is the saturated vapor pressure. Similar expressions are obtained for condensation and effusion:

$$\text{rate of condensation} = p(2\pi MRT)^{-1/2} \text{ moles cm.}^{-2} \text{ sec.}^{-1}$$

$$\text{rate of effusion} = p(2\pi MRT)^{-1/2} \text{ moles cm.}^{-2} \text{ sec.}^{-1}$$

where  $p$  is the pressure of vapor above the surface.

In many cases rates of evaporation and condensation are much smaller than these theoretical maximum rates. An evaporation coefficient,  $\alpha_e$ , or a condensation coefficient,  $\alpha_c$ , is defined as the ratio of the actual rate of evaporation or condensation to the theoretical maximum rate given by the Langmuir-Knudsen equation. These coefficients are also known as accommodation coefficients. In general, small values of evaporation coefficients are observed when a surface reaction takes place prior to the desorption step, the rate of which can be appreciably slower than the desorption rate. This subject has been discussed in some detail by Somorjai (5).

The steady state conditions in the mass spectrometer ion source are given by—rate of evaporation = rate of condensation + rate of effusion

$$\alpha_e PA(2\pi MRT)^{-1/2} = \alpha_c pA(2\pi MRT)^{-1/2} + pa(2\pi MRT)^{-1/2}$$

which simplifies to

$$\alpha_e PA = \alpha_c pA + pa \quad (1)$$

where  $p$  is now the steady state pressure in the sample cell.

$A$  is the effective sample area

$a$  is the effective effusion area

The effective area of the sample is difficult to estimate. Two limiting cases can be discussed. When  $\alpha_e$  and  $\alpha_c$  are large—*i.e.*, approaching unity, and the sample completely covers the bottom of the crucible,  $A$  is given by the cross section of the crucible. By using a crucible having a number of compartments,  $A$  can be varied by filling different numbers of compartments. The other limiting case is obtained when  $\alpha_e$  and  $\alpha_c$  are small. Once molecules have left the surface, the probability of condensation on the surface is small, and  $A$  will be given by the surface area of the sample.  $A$  can be varied in a known way by altering the mass of the sample or by altering its particle size, but absolute values of the surface area can only be roughly estimated, except perhaps for single crystal samples.

The effective effusion area will be smaller than the total area of the electron and ion slits because of the Clausing factor. This correction is negligible for the present work since, as will be seen, it is the order of magnitude of the ratio effusion area to sample area which is required.

Equation 1 can be rearranged to give

$$p = \left( \frac{P}{1 + f/\alpha_c} \right) \frac{\alpha_e}{\alpha_c} \quad (2)$$

where  $f = a/A$ .

When the condensation coefficient is large and  $f$  is small, then

$$p \simeq P \cdot \frac{\alpha_e}{\alpha_c} \simeq P \quad (3)$$

since  $\alpha_e$  will be of the same order of magnitude as  $\alpha_c$ . In this case

$$\frac{d \ln p}{d(1/T)} \simeq \frac{d \ln P}{d(1/T)} = - \frac{\Delta H}{R} \quad (4)$$

where  $\Delta H$  is the enthalpy of the vaporization process.

When the condensation coefficient is smaller than  $f$ , then

$$p \simeq \frac{P \alpha_e}{f} \quad (5)$$

and  $p$  is much smaller than  $P$ .

In this case

$$\frac{d \ln p}{d(1/T)} = - \frac{(\Delta H + \Delta H')}{R} \quad (6)$$

where  $\Delta H'$  is the enthalpy of a surface reaction which occurs before evaporation.

The present apparatus can be used to decide whether evaporation and condensation coefficients for a given vaporization are large or small. By varying  $f$  it can be determined whether the steady state pressure is given by Equation 3 or Equation 5. Some effect on the slope of the  $d \ln p$  against  $1/T$  plot may also be observed (compare Equations 4 and 6) but this is a less sensitive test.

When two or more different species evaporate from the surface their steady state pressures can be compared. When their accommodation coefficients are large, Equation 3 applies, and no relative change in their steady state pressures occurs as  $f$  is varied. When their accommodation coefficients are both small, Equation 5 applies. Even if their accommodation coefficients are different, no relative change in their partial pressures occurs as  $f$  is varied. A variation should be observed if one species has a large value of  $\alpha$  and the other a small value of  $\alpha$  so that the steady state pressure for one species is given by Equation 3 and for the other by Equation 5.

The ion current caused by a vapor in the sample chamber can be used as a quantity proportional to its concentration over a considerable

temperature range as long as conditions in the ion source do not change. In practice, the efficiency of the ion source was found to vary with temperature, and a reference concentration of krypton or xenon was maintained by allowing the gas to leak in from a reservoir in the sample line. The ion currents used to determine variations in partial pressure were obtained from Equation 7

$$I = I_m \cdot \frac{I_{IG}^0}{I_{IG}} \left( \frac{T^0}{T} \right)^{1/2} \frac{P_{IG}}{P_{IG}^0} \quad (7)$$

where  $I_m$  is the measured ion current at temperature  $T$ ,  $I_{IG}$  is the inert gas ion current at temperature  $T$  and reservoir pressure  $P_{IG}$ , and the superscript zero indicates the corresponding quantities under the reference conditions. The temperature correction term arises as follows. The steady state inert gas concentration in the ion source is given when the rate of its flow into the source is equal to its rate of flow out. At constant reservoir pressure and assuming constant pumping speed in the ion source region the rate of flow into the ion source is constant. The rate of outflow is also constant. Under conditions of molecular flow  $CT^{1/2}$  is constant, where  $C$  is the concentration of inert gas in the ion source. Hence

$$\frac{C}{C^0} = \left( \frac{T^0}{T} \right)^{1/2}$$

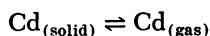
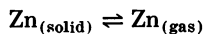
The steady state pressure of a given species in the ion source is proportional to  $IT$  and hence the variation in partial pressure referred to some standard condition is given by

$$p = k I_m \cdot \frac{I_{IG}^0}{I_{IG}} \left( \frac{T}{T^0} \right)^{1/2} \frac{P_{IG}}{P_{IG}^0} \quad (8)$$

where  $k$  is a constant of the mass spectrometer, and the ionization cross section of the species. This equation does not permit calculation of absolute pressures.

### Results and Discussion

**Zinc and Cadmium.** The apparatus was used to determine the heats of sublimation of zinc and cadmium (11). The sublimations can be represented

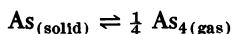


No dimeric or polymeric molecules could be detected.

For zinc,  $\Delta H_{298}$  was found to be  $30.05 \pm 0.42$  kcal. per mole and for cadmium  $\Delta H_{298}$  was  $26.48 \pm 0.20$  kcal. per mole. These values are in

satisfactory agreement with literature values (16) and indicate that the apparatus is suitable for determination of heats of sublimation of materials having accommodation coefficients which are not small. For metals vaporizing as atoms the accommodation coefficient is not less than 0.1, and consequently Equation 4 applies.

**Arsenic.** The sublimation of arsenic was studied by Westmore, Mann, and Tickner (17). In the temperature range 220° to 280°C. the only process that could be definitely detected was



with an apparent heat of sublimation of  $43.0 \pm 0.4$  kcal. per mole at 298°K. This is much higher than the value of 34.5 kcal. per mole obtained by equilibrium methods (16), but agrees with the value reported by Kane and Reynolds (6) for large orifice sublimation. The latter authors found that at about 280°C. the accommodation coefficient was small, about  $10^{-4}$ , and hence Equation 6 should apply. Kane and Reynolds suggested that the small accommodation coefficient resulted from a surface rearrangement to form  $\text{As}_4$  molecules which are not present as such in the solid phase. Similar behavior is exhibited by phosphorus (1, 6).

**Selenium.** The sublimation of selenium was studied by Fujisaki, Westmore, and Tickner (2) between 102° and 187°C. At these temperatures the only stable solid phase is grey, metallic, or hexagonal selenium which is comprised of long helical chains of selenium atoms. Several references are given by Fujisaki *et al.* (2). The mass spectrum of the vapor is very complex, containing the ions  $\text{Se}_n^+$  where  $n = 1$  to 10. Appearance potentials of the ions suggest that  $\text{Se}^+$ ,  $\text{Se}_2^+$ ,  $\text{Se}_3^+$ , and  $\text{Se}_4^+$  arise from fragmentation of heavier ions and that  $\text{Se}_5^+$ ,  $\text{Se}_6^+$ ,  $\text{Se}_7^+$ , and  $\text{Se}_8^+$  arise mainly from the corresponding parent molecules. Probably  $\text{Se}_9^+$  and  $\text{Se}_{10}^+$  arise from  $\text{Se}_9$  and  $\text{Se}_{10}$ , but this conclusion could not be verified. The vapor may also contain small amounts (less than 0.5%) of  $\text{Se}_2$ , but whether it comes from the selenium surface or from thermal decomposition of a heavier molecule on the mass spectrometer filament or the walls of the sample chamber cannot be determined.

Since the ratios of the currents attributed to the various ions did not change as the sample area or effusion area was changed, it was thought that the accommodation coefficients for the sublimation of the molecules  $\text{Se}_5$ ,  $\text{Se}_6$ ,  $\text{Se}_7$ , and  $\text{Se}_8$  were all fairly large so that their partial pressures did not change (Equation 3), or all small, not necessarily equal, so that they changed by a similar factor (Equation 5). It was not possible for some species to have large coefficients and some to have small coefficients. Furthermore, although day-to-day variations are to be expected, at a given temperature it seemed that the ion currents of the various species

were insensitive to variation in effusion and sample area, indicating that conditions appropriate to Equation 3 applied. This equation is valid when the accommodation coefficients are fairly large. Support for this view is given by the data of Table I which show that a weighted mean of the heats of sublimation of  $\text{Se}_5$ ,  $\text{Se}_6$ ,  $\text{Se}_7$ , and  $\text{Se}_8$  will be close to the value for the heat of sublimation given by Stull and Sinke (16). This latter value was selected by them to give the best fit with entropy and vapor pressure of numerous workers, assuming the vapor to be mainly  $\text{Se}_6$ . Consequently, the equation which is valid for large accommodation coefficients, holds.

**Table I. Heats of Sublimation and Relative Abundances of Subliming Selenium Molecules**

<i>Species</i>	$H_{418}$ <i>kcal./mole</i>	<i>Relative abundance at 175°C.</i>	<i>% in vapor at 175°C.</i>
$\text{Se}_5$	$36.2 \pm 0.5$	50.6	29.1
$\text{Se}_6$	$33.8 \pm 0.5$	100.0	57.5
$\text{Se}_7$	$38.4 \pm 0.5$	19.7	11.4
$\text{Se}_8$	$39.9 \pm 0.7$	3.5	2.01
$\text{Se}_9$	—	0.02	0.012

The results are interpreted in terms of the sublimation from the selenium surface of cyclic molecules formed by breaking of the chains of selenium atoms. Cyclic molecules should be formed more readily than diradical chain molecules, and once formed would only be held by van der Waals forces. Cyclic molecules having 3 or 4 atoms would be considerably strained whereas  $\text{Se}_5$ ,  $\text{Se}_6$ ,  $\text{Se}_7$ , and  $\text{Se}_8$  would be relatively unstrained, and it is suggested that this is why  $\text{Se}_3$  and  $\text{Se}_4$  are absent from the vapor.

**Table II. Thermodynamic Data for the Sublimation of Grey Selenium**

<i>Species</i>	<i>Average <math>C_p</math> from 298° to 418° K. cal. deg.<sup>-1</sup></i>	<i>Average <math>\Delta C_p</math> cal. deg.<sup>-1</sup></i>	$\Delta H^{\circ}_{298}$ <i>kcal./mole</i>	$\Delta F^{\circ}_{298}$ <i>kcal./mole</i>	$\Delta S^{\circ}_{298}$ <i>cal. mole<sup>-1</sup> deg.<sup>-1</sup></i>
$\text{Se}_5$	23.9	-8.2	37.2	21.8	51.7
$\text{Se}_6$	29.5	-9.0	34.9	20.6	48.0
$\text{Se}_7$	35.1	-9.9	39.6	23.2	55.1
$\text{Se}_8$	40.7	-10.6	41.2	24.8	55.1

The present apparatus does not allow measurement of absolute vapor pressures. However, estimates of other thermodynamic quantities were

made by estimating the relative partial pressures of the various species and comparing them with vapor pressure data given by Stull and Sinke. The results are given in Table II.

**Cadmium Arsenide,  $Cd_3As_2$ .** The vapor pressure diagram of the cadmium-arsenic system shows a minimum corresponding to  $Cd_3As_2$ . This material can be vaporized and recondensed with no change in composition. The vaporization of  $Cd_3As_2$  has been described by Westmore, Mann, and Tickner (17). The vapor was shown to consist of Cd and  $As_4$ . On initial vaporization the arsenic vaporized slowly. Eventually, steady state conditions were reached where the arsenic seemed to be vaporizing more readily, and reproducible results were obtained.

It was found that the ratio of cadmium to arsenic in the vapor varied as the sample and effusion areas were varied. Furthermore, their temperature coefficients varied. The results were consistent with a much smaller accommodation coefficient for the vaporization of arsenic than for cadmium. It can be seen from Equations 3 to 6 that such variations are possible if different values of  $\alpha$  are used for cadmium and for arsenic.

The experimental results were interpreted in terms of the surface reactions

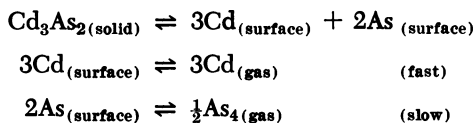


**Table III. Temperature Coefficients for the Vaporization of Cadmium Arsenide**

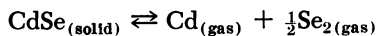
Conditions	Temperature range, °C.	$^{114}Cd$ slope, deg. $^{-1}$	As slope, deg. $^{-1}$	$\Delta$ slope, deg. $^{-1}$
A	218–274	8080 $\pm$ 150	8300 $\pm$ 150	220 $\pm$ 65
B	220–285	8065 $\pm$ 70	8385 $\pm$ 150	320 $\pm$ 130
C	228–287	7730 $\pm$ 130	8650 $\pm$ 130	930 $\pm$ 140
D	240–375		8292	
E	434–578		6800	

Sample size: A, 0.35 gram approx.; B, 0.172 gram; C, 0.012 gram. Estimated sample area: A, 3000 sq. mm.; B, 1600 sq. mm.; C, 100 sq. mm. Estimated effusion area: A, 6.3 sq. mm.; B, 4.0 sq. mm.; C, 4.0 sq. mm. D, Nesmeyanov (12), Knudsen cell, unstated conditions. E, Lyons and Silvestri (10), equilibrium studies.

The temperature coefficients obtained were higher than those obtained from equilibrium vapor pressure measurements (10) but agreed with the effusion measurements of Nesmeyanov *et al.* (12). A summary of the results is given in Table III. The composition of the vapor varied with the sample size and effusion area. For example, at 500°K. the ion

current ratio  $I_{\Sigma As}/I_{114 Cd}$  was 2.69 for condition A, 2.46 for condition B, and 1.41 for condition C. These conditions are explained in Table III.

**Cadmium Selenide.** Preliminary results indicate that the vaporization proceeds according to the reaction:

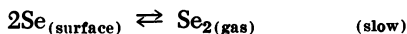
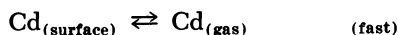
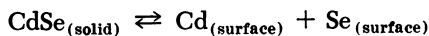


However, in the temperature range 440° to 600°C., the vaporization is noncongruent, as the vapor is selenium deficient, and the temperature coefficient for vaporization of  $Se_2$  is higher than for Cd. This is in contrast to the claim of Goldfinger and Jeunehomme (3) that the intensity ratios of  $Cd^+$ ,  $Se_2^+$ , and  $Se^+$  were constant at different temperatures and during complete evaporation of the samples. These authors used open crucibles or quartz Knudsen cells and worked in the temperature range 550° to 800°C. corresponding to sample pressures of  $10^{-3}$  to  $10^{-1}$  torr. A summary of the vaporization studies on cadmium selenide is shown in Figure 2. Some uncertainty is involved in the positions of the lines for the results of this work since steady state pressures could not be determined and had to be estimated. The temperature coefficients obtained were as follows:

Somorjai (14)	10,020 deg. <sup>-1</sup>	Equilibrium, 700°–935°C.
Korneeva (8)	10,950	Knudsen cell, 500°–750°C.
Somorjai (15)	12,220	Free vaporization, 570°–800°C.
Goldfinger (3)	10,770	Mass spectrometric and Knudsen cell, 550°–800°C.
Wosten (18)	11,470	Transpiration, 740°–900°C.
This work	10,360 for Cd 11,130 for $Se_2$	440°–600°C.

On initial vaporization of the sample, it was found that cadmium vaporizes more readily than selenium (as  $Se_2$ ), but the relative amount of selenium increased with time until a steady state appeared to be attained. Even at this steady state, comparison of the ion currents at 500°C. from  $Se^+ + Se_2^+$  and  $Cd^+$  gives, assuming stoichiometric vaporization, the ratio for the ionization cross sections  $\sigma_{Se_2}/\sigma_{Cd}$  as 0.59 compared with 1.38 for the higher temperature work of Goldfinger and the ratio  $\sigma_{Se}/\sigma_{Cd} = 0.84$  (13). In this work, the vapor is therefore, selenium deficient.

The results are interpreted in terms of the reactions:



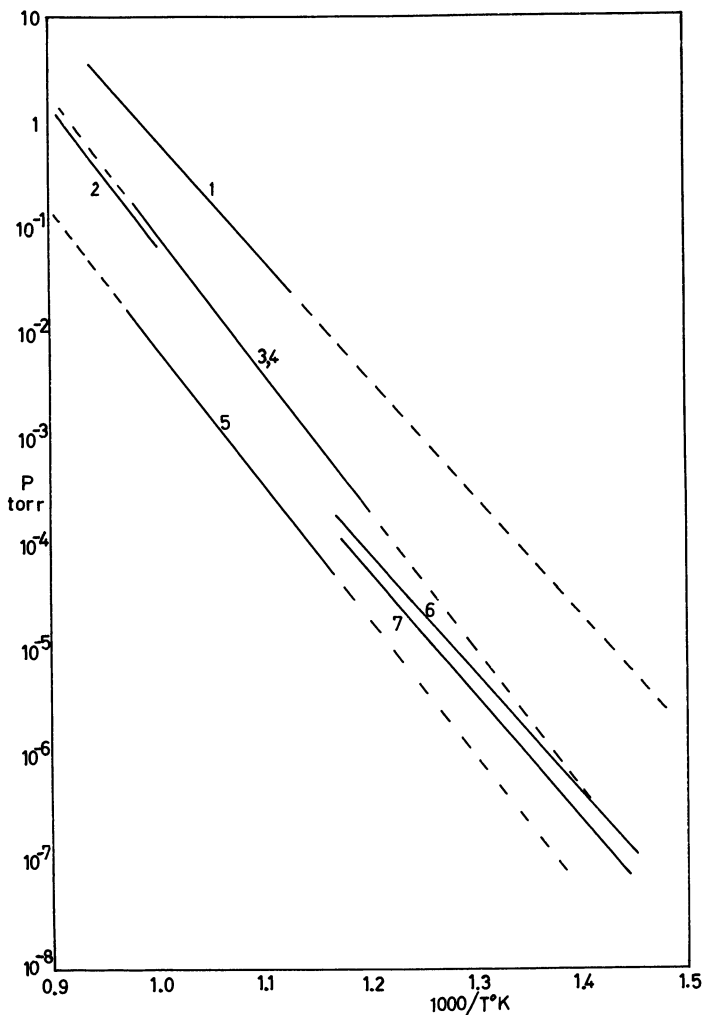


Figure 2. Apparent vapor pressure of cadmium selenide

1. Somorjai (14), equilibrium; 2. Wosten (18), transpiration; 3. Korneyeva (8), Knudsen cell; 4. Goldfinger (3), Knudsen cell; 5. Somorjai (15), free vaporization; 6. This work, Cd; and 7. This work,  $\text{Se}_2$

where the slow step is speculated to be diffusion of Se atoms on the surface to form  $\text{Se}_2$  molecules. The surface of the sample becomes cadmium deficient, and cadmium atoms must diffuse to the surface from the interior. Hence, the steady state condition of a sample in a Knudsen cell will depend upon many factors including particle size, sample size, effusion area, and temperature. Further work on cadmium selenide is now in progress. It appears that equilibrium studies, such as those of Somorjai

(14), would be the only studies to yield reliable thermodynamic data. It is significant that the temperature coefficient for Cd vaporization from CdSe in this work is closest to Somorjai's equilibrium value and that Goldfinger's temperature coefficient lies between the values for Cd and Se<sub>2</sub> obtained here.

Cadmium selenide in thin films is used in solid state devices. These films are prepared by vaporizing CdSe onto a substrate in vacuum. The films tend to be Cd rich, and production of films with reproducible properties is difficult. This is not surprising in the light of the results described here.

### Conclusions

The mass spectrometer ion source was used to study a number of different types of vaporization. It can yield much of the information obtainable by the conventional Knudsen effusion method but can sometimes yield information of a different type. This has been illustrated by a study of cadmium arsenide and cadmium selenide. In the latter case, a comparison with results obtained by the conventional techniques was possible. Caution is necessary when interpreting the results of Knudsen cell work.

### Literature Cited

- (1) Brewer, L., Kane, J. S., *J. Phys. Chem.* **59**, 105 (1955).
- (2) Fujisaki, H., Westmore, J. B., Tickner, A. W., *Can. J. Chem.* **44**, 3063 (1966).
- (3) Goldfinger, P., Jeunehomme, M., *Trans. Far. Soc.* **59**, 2851 (1963).
- (4) Hertz, H., *Ann. Phys. (Leipzig)* **17**, 177 (1882).
- (5) Jepson, D. W., Somorjai, G. A., *J. Chem. Phys.* **39**, 1665 (1963).
- (6) Kane, J. S., Reynolds, J. H., *J. Chem. Phys.* **25**, 342 (1956).
- (7) Knudsen, M., *Ann. Phys. (Leipzig)* **47**, 697 (1915).
- (8) Korneyeva, I., Sokolov, V. V., Novoselova, A. V., *Zhur. Neorg. Khim.* **5**, 241 (1960).
- (9) Langmuir, I., *J. Am. Chem. Soc.* **35**, 931 (1913).
- (10) Lyons, V. J., Silvestri, V. J., *J. Phys. Chem.* **64**, 251 (1960).
- (11) Mann, K. H., Tickner, A. W., *J. Phys. Chem.* **64**, 251 (1960).
- (12) Nesmeyanov, A. N., Iofa, B. Z., Strel'nikov, A. A., Fursov, V. G., *Russ. J. Phys. Chem.* **30**, 1250 (1956).
- (13) Otvos, J. W., Stevenson, D. P., *J. Am. Chem. Soc.* **78**, 546 (1956).
- (14) Somorjai, G. A., *J. Phys. Chem.* **65**, 1059 (1961).
- (15) Somorjai, G. A., "Condensation and Evaporation of Solids," p. 417-433, Gordon and Breach, New York, 1964.
- (16) Stull, D. R., Sinke, G. C., "Thermodynamic Properties of the Elements," *ADVAN. CHEM. SER.* **18** (1956).
- (17) Westmore, J. B., Mann, K. H., Tickner, A. W., *J. Phys. Chem.* **68**, 606 (1964).
- (18) Wosten, W. J., *J. Phys. Chem.* **65**, 1949 (1961).

RECEIVED October 11, 1966.

# Mass Spectrometry of Molecules of the Nitrogen Family

K. DOUGLAS CARLSON, FRED J. KOHL, and O. MANUEL UY

Case Institute of Technology, University Circle, Cleveland, Ohio

*Mass spectrometric studies of the gaseous molecules produced from solid compounds of the nitrogen family of elements are briefly summarized. The variety and nature of the solids are examined first to demonstrate the possibilities for observing complex molecules in these systems at elevated temperatures. Then the detection and characterization of these molecules by mass spectrometry are described. It is shown that a wide variety of both parent and fragmented ion species are observed. The problems of differentiating between parent and fragmented species and of estimating absolute partial pressures of the parent molecules are described with some specific examples. The existence of the various homonuclear and heteronuclear molecules can be correlated with the polymeric nature of the solids and the comparable binding energies of the molecules.*

Atoms of the Group VA family of elements N, P, As, Sb, and Bi combine among themselves to form an interesting class of diatomic and tetraatomic molecules and perhaps molecules of a more complex nature. The homonuclear species, such as  $P_2$ ,  $As_2$ ,  $P_4$ , and  $As_4$ , are well known from early vapor density and more recent mass spectrometric investigations of the vaporization properties of the solid elements. The heteronuclear species, such as  $As_2P_2$ , have been observed only recently in studies of the vaporization of mixtures and binary compounds of the elements. This paper presents a brief introduction and summary of current systematic studies of these molecules by mass spectrometry.

Because the solid-vapor systems of the pnictides are complex, and for various reasons are intrinsically difficult to study quantitatively, there

are many details that cannot be covered in this paper. Instead, our intention is to present here a broad but brief survey of these systems, drawing upon both our work and that of others and emphasizing the applications of mass spectrometry.

The inter-pnictide molecules are of general interest as additional examples of the complexity of the vapor phase above solid inorganic materials at elevated temperatures. Specifically, they are of interest here as examples of systems that require the full application of mass spectrometric techniques combined with subsidiary experiments. Most important, these molecules provide a useful class of related molecules for a systematic study of the chemical bonding effects in a series of inorganic species having similar chemical bonds and related symmetry properties.

### **Solid Phases**

Characteristics of the solids of the Group VA elements are fairly well known. There are several allotropic forms and both stable and metastable phases. An interesting feature of many of these solids is their polymeric composition involving chains of tetrahedral units. Because of this kind of atomic arrangement, their vaporization at elevated temperatures produces tetrameric and dimeric vapor molecules. There is much less known about the binary and higher compounds of these elements. The best known solid inter-pnictide compound is  $P_3N_5$ , but the other solid nitrides  $AsN$ ,  $SbN$ , and  $BiN$  have been reported in the older literature. Combinations of As and P, Sb and As, Bi and As, and Bi and Sb form various solid solution phases. No solid phosphides of Sb or Bi have been reported.

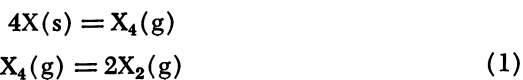
Although the first homogeneous solid phosphorus nitride,  $P_3N_5$ , was prepared in 1903 from a reaction of  $P_2S_5$  and  $NH_3$  (53), chemists have long been synthesizing various solids containing both nitrogen and phosphorus, such as phosphonitrilic compounds, metaphosphimic acids and phosphorus amides. Amorphous solids with N/P ratios ranging from unity to 1.7 have been reported (34, 35, 36, 38, 39, 44). The inconsistency of nomenclature and analysis in published research makes it difficult to ascertain "whether or not the material described as phospham by one is the same as the material described as phosphorus nitride by another" (34, 55), or whether they were not  $(PNCl_2)_n$  (43, 44) and  $P_2(NH_2)_3$  (37), which are products formed from the reaction used to prepare  $P_3N_5$  from  $NH_3$  and  $PCl_5$ . It seems rather certain at this time that  $P_3N_5$  is the only crystalline binary solid phase in the P-N system. Crystalline  $P_3N_5$  has a faint orange color, is inert at room temperature, non-hygroscopic, and exhibits no appreciable decomposition in vacuum up to  $\sim 700^\circ C$ . Although it exhibits sharp x-ray diffraction powder patterns, it is complex, and a crystallographic analysis has not been carried



is less than 1% As in Bi (54). In no system is there any strong evidence for the formation of any definite stoichiometric compounds.

### Vapor Species

The group VA elements and inter-pnictides vaporize to yield gaseous species which are predominantly tetratomic or diatomic. Thus, the mass spectrometer used in conjunction with the Knudsen effusion method may be used to study both solid-vapor and vapor-vapor equilibria. Investigations of the vaporization of the elements have yielded thermodynamic data for the following types of reactions:



Here X represents P (5, 9, 18, 28), As (9, 18, 28), Sb (2, 8, 18), and Bi (31, 56). It has been shown that at temperatures below 1000°C., the equilibrium vaporization of the elements, except bismuth, yields mainly the  $X_4$  gaseous molecule (4, 18, 28). Although one observes ion currents for the monatomic, diatomic, and triatomic species (5), the data suggest that these result mainly from fragmentation of the tetramers during the ionization process. In many cases careful appearance potential studies can differentiate the parent and fragment species, although the results are not always unambiguous.

Several careful studies of the vaporization of red phosphorus (4, 5) have been carried out. However, the exact ratios of tetramer to dimer molecules are still not certain. Many studies of the vaporization of phosphorus, arsenic, and antimony from alloys with cadmium (59), indium (9, 18, 19), and gallium (9, 18) at moderately high temperatures, have shown that  $P_2$ ,  $As_2$ , and  $Sb_2$  vaporize as parents along with  $P_4$ ,  $As_4$ , and  $Sb_4$ . Also, nonequilibrium vaporization conditions have yielded both diatomic and tetratomic molecules along with triatomic and larger molecules. In several of these studies,  $P_8$  (5, 29) and  $As_8$  (28) were observed. Nevertheless, the concentrations of these species are believed to be small under equilibrium conditions. The previous thermal history of the sample is also critical for the species which can be observed upon initial vaporization (5, 11, 40).

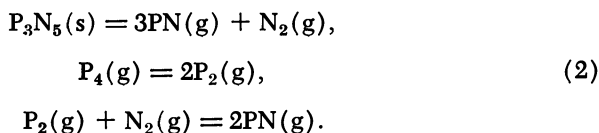
The congruent vaporization of  $P_3N_5(s)$  has been studied by Knudsen cell mass spectrometry (31). The positive ion species formed by electron impact ionization of the neutral molecules were found to be  $P_1^+$ ,  $P_2^+$ ,  $P_3^+$ ,  $P_4^+$ ,  $N_1^+$ ,  $N_2^+$ ,  $PN^+$ , and  $PN^{2+}$ . Ions of more complex molecules were not observed. Relative ion intensities of these various species are given in Table I. The very large apparent intensity of  $N_2^+$  suggests that the partial pressure of the nitrogen molecule is very much larger than that

of any other molecule. Actually, it turns out that the partial pressures of  $N_2$  and PN are, in fact, comparable and that the differences in apparent intensities arise from the differences in the condensability of PN on the surfaces of the mass spectrometer system and the pumping rate of  $N_2$ . There is also a similar problem of noncondensability of  $P_2$  and  $P_4$ . We shall return to these problems later.

**Table I. Approximate Relative Intensities of Ion Species from the Vapor of  $P_3N_5(s)$  at  $850^\circ C$ . with an Ionizing Electron Energy of 50 e.v. (31)**

<i>Species</i>	<i>Relative Intensity</i>
$N_1^+$	2.8
$PN^{2+}$	negligible
$N_2^+$	100.0
$P_1^+$	2.6
$PN^+$	50.0
$P_2^+$	5.4
$P_3^+$	1.5
$P_4^+$	1.1

Detailed appearance potential measurements are necessary to determine the neutral molecules in equilibrium with  $P_3N_5(s)$ . These are found to be  $P_4$ ,  $P_2$ , PN, and  $N_2$ . Thus, three equilibrium reactions characterize this system, and these may be written as



Although the existence of the molecules  $AsN(g)$ ,  $SbN(g)$ , and  $BiN(g)$  has been demonstrated by optical spectroscopy (16, 22), no mass spectrometric investigations have yet been made of the vaporization characteristics of the solids. These solids may be expected to vaporize similarly to  $P_3N_5$  although at lower temperatures.

The As-P system is one of great complexity. This system has been studied by the vaporization of As and P from a mixture of the elements (31) and from the alloy  $In(P_{0.56}As_{0.44})$  (19). The expected parent gaseous molecules in this system are  $As_2$ ,  $P_2$ ,  $AsP$ ,  $As_4$ ,  $P_4$ ,  $As_3P$ ,  $As_2P_2$ , and  $AsP_3$ , while the expected fragments produced by electron impact ionization of the vapor molecules are  $As^+$ ,  $P^+$ ,  $As_3^+$ ,  $As_2^+$ ,  $P_3^+$ ,  $P_2^+$ ,  $As_2P^+$ ,  $AsP_2^+$ , and  $AsP^+$ . All of the ions expected for the parent and fragment species have been observed in both studies.

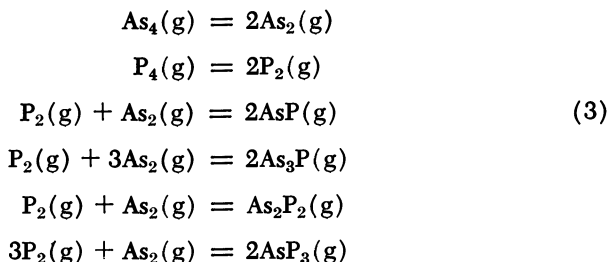
Relative intensities of the ions of the vapors above a mixture of  $As(s)$  and  $P(s)$  are given in Table II. The intensity ratios are somewhat

puzzling, because on the basis of the relative vapor pressures of phosphorus and arsenic, one would expect the vapor to consist predominantly of phosphorus-containing species. The results obtained may be attributed to the existence of very small vaporization coefficients for the elements and the absence of true equilibrium in the vapor. One also has a problem of the partial noncondensability of the vapor molecules, similar to the circumstance mentioned earlier for the P-N system. Further work is being carried out on the vaporization of solid AsP itself.

**Table II. Approximate Relative Intensities of Ion Species from the Vapor of a Mixture of P(red,s) and As(s) at 216°C. with an Ionizing Electron Energy of 50 e.v. (31)**

<i>Species</i>	<i>Relative Intensity</i>
P <sup>+</sup>	2.0
As <sup>+</sup>	38.0
P <sub>2</sub> <sup>+</sup>	1.0
As <sub>2</sub> <sup>+</sup>	57.0
AsP <sup>+</sup>	3.0
P <sub>3</sub> <sup>+</sup>	negligible
As <sub>3</sub> <sup>+</sup>	29.0
P <sub>2</sub> As <sup>+</sup>	0.4
PAs <sub>2</sub> <sup>+</sup>	1.0
P <sub>4</sub> <sup>+</sup>	2.0
As <sub>4</sub> <sup>+</sup>	100.0
PAs <sub>3</sub> <sup>+</sup>	6.0
P <sub>2</sub> As <sub>2</sub> <sup>+</sup>	2.0
P <sub>3</sub> As <sup>+</sup>	2.0

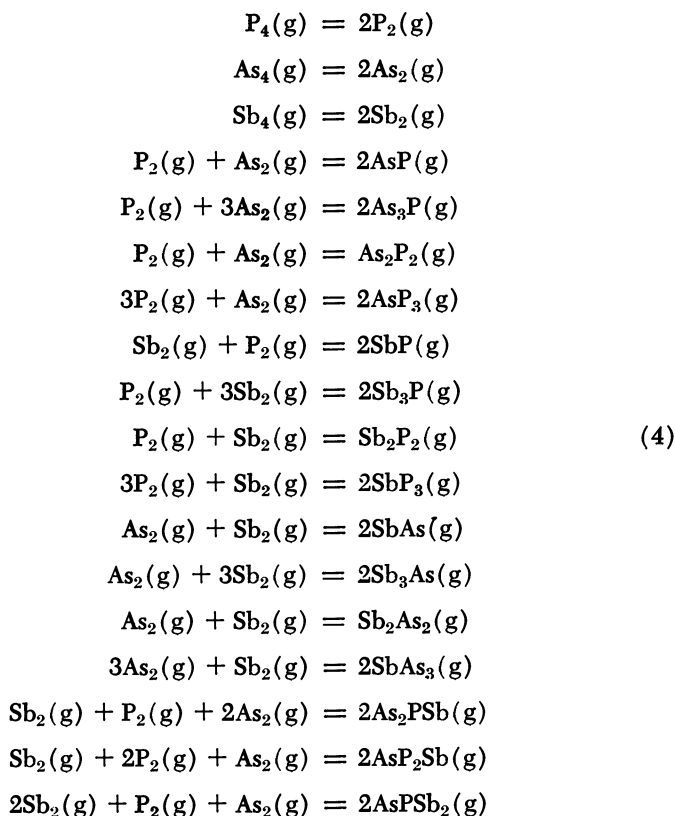
The gaseous equilibria of interest in the As-P system are the following:



Preliminary experiments (31) on the Sb-As system give evidence for the existence of the molecules SbAs, Sb<sub>3</sub>As, Sb<sub>2</sub>As<sub>2</sub>, and SbAs<sub>3</sub> over the Sb-As solid phase. Although no complete mass spectrometric studies have been made of the vaporization of Bi-As or Bi-Sb, gaseous molecules of SbBi and Sb<sub>3</sub>Bi have been observed vaporizing from liquid bismuth

contaminated with slight amounts of antimony (31). It would be interesting to determine whether or not other possible tetratomic molecules containing bismuth, such as  $\text{Sb}_2\text{Bi}_2$ ,  $\text{SbBi}_3$ , and the corresponding arsenic analogs, are stable, since it has been conjectured that in view of the weakness of the "triple" bond in  $\text{Bi}_2$ , the single bonds in such tetratomic molecules would be even weaker and probably unstable (49). The existence of the  $\text{SbBi}$  diatomic molecule has been observed in optical spectroscopy (16, 22).

Another interesting study, but one not yet carried out, would be that concerned with producing polymeric molecules containing three or possibly four different pnictide elements. Molecules of this kind may be expected to form between P, As, Sb, and possibly Bi. The molecule  $\text{As}_2\text{PSb}$  has been observed mass spectrometrically (23). The treatment of data obtained from these complex ternary and quaternary systems would be much more difficult than that of the binary systems. For example, the system  $\text{Sb-As-P}$  would be characterized in part by the following gaseous equilibria:



*Parent Molecules and Absolute Pressures*

The previous summary demonstrates that vaporization of the pnictides produces a complex vapor phase and that the mass spectrometer detects ion species of both parent and fragmented molecules. It is necessary then to differentiate between the parents and fragments to establish the vaporization equilibria and to estimate scaling factors that convert ion intensities to absolute partial pressures for thermodynamic analyses. We wish to discuss here some of the techniques found particularly useful in these studies.

**Table III. Appearance Potentials of Ion Species of the Vapor of  $P_3N_5(s)$  (31), in e.v. Units<sup>a</sup>**

<i>Ion Species</i>	<i>Linear Extrapolation</i>	<i>R.P.D.</i>	<i>Literature</i>
$N_2^+$	$15.5 \pm 0.3$	$15.4 \pm 0.01$	$15.6^{\circ}$
$P_2^+$	$9.6 \pm 0.3$		$10.0$ (from $P_2^*$ ) <sup>o</sup>
	$11.7 \pm 0.3$		$12.0$ (from $P_2$ ) <sup>o</sup>
$P_4^+$	$9.2 \pm 0.3$		$9.0^d$
$PN^+$	$11.6 \pm 0.3$	$11.8 \pm 0.1$	
$P_1^+$	$17.5 \pm 0.3$ (from $P_2, P_4, PN$ )		$16.0$ (from $P_2$ ) <sup>o</sup>
			$18.0$ (from $P_4$ ) <sup>o</sup>
			$18.5$ (from $PN$ ) <sup>f</sup>
$P_3^+$	$14.3 \pm 0.3$ (from $P_4$ )		$14.5^{\circ}$
$N_1^+$	$24.0 \pm 0.3$ (from $N_2$ )	$23.6 \pm 0.1^h$	$24.3^g$
		$26.0 \pm 0.1^i$	$26.8^g$
	$20.0 \pm 0.5$ (from $PN$ )		
$PN_2^+$	$40.7 \pm 0.5$		

<sup>a</sup> A.P. ( $H_2O^+$ ) =  $12.60^b$  as standard.

<sup>b</sup> Ref. (45).

<sup>c</sup> Ref. (5).

<sup>d</sup> Refs. (28, 20).

<sup>e</sup> Refs. (13, 58).

<sup>f</sup> Ref. (31).

<sup>g</sup> Ref. (41).

<sup>h</sup> The products are  $N_1^+(^3P) + N(^4S)$ .

<sup>i</sup> The products are  $N_1^+(^3P) + N(^2D)$ .

The problem of differentiating parent and fragment ions can be handled reasonably well for these systems by very careful measurements of appearance potentials, both by the linear extrapolation method (57) and the retarding potential difference (R.P.D.) method (14). As examples, we list appearance potentials of the various ions observed in the  $P_3N_5$  study in Table III and discuss their interpretation. Some points of the discussion are illustrated by the appearance potential curves given in Figures 1 and 2.

The appearance potential of  $N_2^+$  compares very well with the value of 15.6 e.v. obtained by photoionization (58) and electron impact ionization (13). Two linear portions are observed in the ionization efficiency

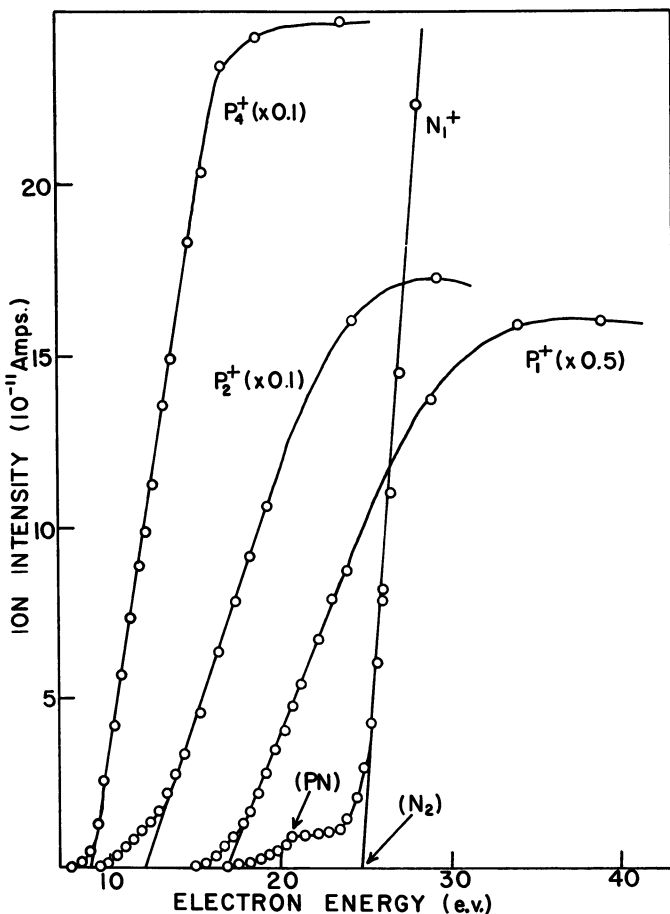
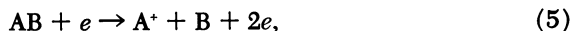


Figure 1. Ionization efficiency curves for  $P_4^+$ ,  $P_2^+$ ,  $N_1^+$ , and  $P_1^+$

curve for  $P_2^+$  (Figure 1). The values of the appearance potentials correspond well with the value of  $10.0 \pm 0.05$  e.v. for the ionization of an appreciably populated excited state of  $P_2$  and the value of  $12.0 \pm 0.5$  e.v. for that of the ground state (5). The appearance potential of  $P_4^+$  compares well with the ionization potential of 9.0 e.v. determined by electron impact (28) and photoionization (20) studies. The appearance potential of  $11.8 \pm 0.1$  e.v. for  $PN^+$  can be compared with those of the isoelectronic ions:  $AsP^+$  ( $11.2 \pm 0.5$  e.v.) (19),  $P_2^+$  and  $N_2^+$ . Therefore, the observed appearance potentials for  $P_2^+$ ,  $P_4^+$ ,  $N_2^+$ , and  $PN^+$  indicate that these ions, at least in part, are formed by direct ionization of neutral molecules.

For the fragmentation reaction



the appearance potential of  $A^+$  may be written (26) as

$$A.P.(A^+) \geq I.P.(A) + D_T^\circ(AB). \quad (6)$$

The appearance potential of  $17.5 \pm 0.3$  e.v. for  $P_1^+$  is appropriate to either of the two processes written below. Using the values  $I.P.(P_1) = 10.98$  e.v. (21),  $D^\circ_{1100}(P_4 = 2P_2) = 2.30$  e.v. (51), and  $D^\circ_{1100}(P_2) = 5.09$  e.v. (51), we obtain

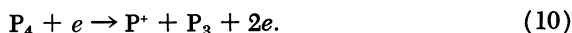


We have considered also the process



It seems probable, therefore, that all the neutral molecules  $P_2$ ,  $P_4$ , and  $PN$  are equally important parents of the  $P_1^+$  ion.

The  $P_3^+$  ion can be produced directly from  $P_4$ , or by ionization of  $P_3$  from the solid. However, the appearance potential of  $14.3 \pm 0.3$  e.v. corresponds well with the value  $14.5 \pm 0.5$  e.v. (5) for the process,



If  $P_3$  vaporizes from the solid, the appearance potential would occur at 11.5 e.v. (5). Thus  $P_3^+$  is a fragment.

The ionization efficiency curve for  $N_1^+$  gives an appearance potential of  $24.0 \pm 0.3$  e.v., which compares with 24.3 e.v. for the appearance potential  $N_1^+$  from  $N_2$  (41). A shoulder appearing at about 20 e.v. (Figure 1) shows a small contribution from  $PN$ , according to the process



The *R.P.D.* curve of  $N_1^+$  (Figure 2) gives two linear portions beginning at 23.6 and 26.0 e.v. These correspond specifically to the two processes suggested by Reed (41):



Owing to weak intensities, *R.P.D.* measurements on  $P_1^+$ ,  $P_2^+$ ,  $P_3^+$ , and  $P_4^+$  could not be made. Doubly charged positive ions, other than  $PN^{2+}$  with an appearance potential of 40.7 e.v., were undetected in this study. Polymeric species such as  $P_8^+$  also were not observed. Thus, we conclude that the only important parent molecules vaporizing from  $P_3N_5(s)$  are  $P_4$ ,  $P_2$ ,  $PN$ , and  $N_2$ . This confirms that the three reactions defined by Reaction 2 totally characterize the solid-vapor equilibria of this system.

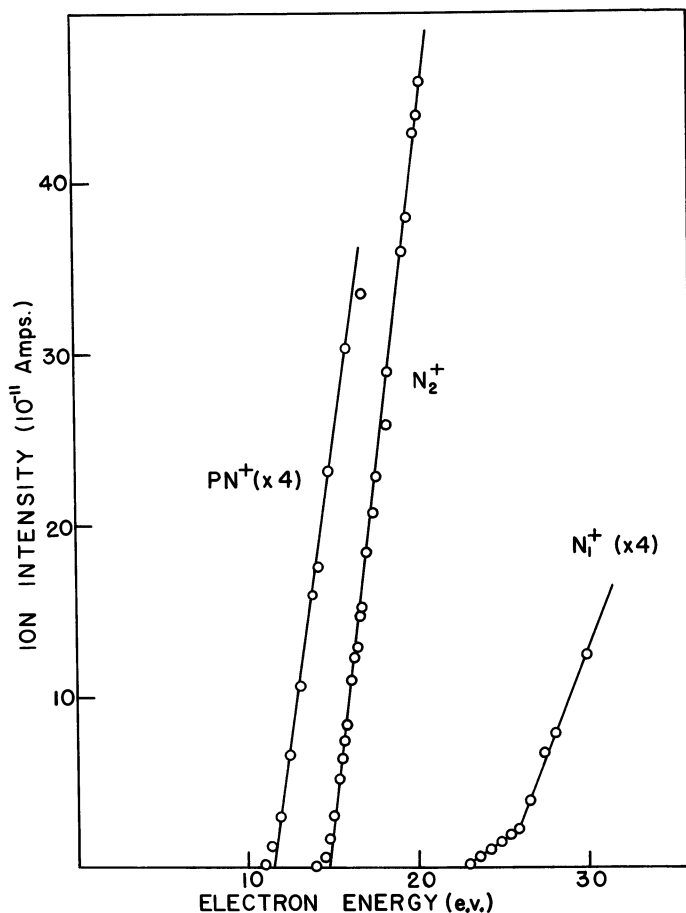


Figure 2. R.P.D. curves for  $PN^+$ ,  $N_2^+$ , and  $N_1^+$

After identifying the molecules involved in the equilibrium vaporization, one wishes to derive thermodynamic properties for the various processes. Of course, one can proceed to obtain second law heats from the relative ion intensity measurements, but it is more useful to obtain absolute vapor pressures so that entropy data can be employed in third law analyses. Absolute vapor pressures of the molecules of the pnictide systems, however, are difficult to obtain because of the problem of non-condensability mentioned earlier.

Consider this problem for the  $P_3N_5$  solid-vapor system. Gaseous  $N_2$  is totally noncondensable unless special cooling apparatus or efficient pumping of the Knudsen cell source is provided. Even with the latter possibility, it is difficult to pump out all  $N_2$  that is not a part of the primary molecular beam. Furthermore, our experiments have shown

that  $P_2(g)$  and  $P_4(g)$  are only partially condensable, whereas  $PN(g)$  is essentially totally condensable. These characteristics are understandable in view of the thermal stability of  $P_3N_5(s)$  and the temperatures of  $700^\circ C$ . to  $1000^\circ C$ . required for its vaporization. As a result of these differences in condensability of the various molecules, one measures ion intensities  $I_1^+$  which, except for  $PN$ , are abnormally high and which are related to the partial pressures  $P_1$  by considerably different overall instrument sensitivity factors  $K_1$  in the usual relationship,

$$P_1 = K_1 I_1^+ T. \quad (14)$$

Similar circumstances are found for studies on the other pnictide systems.

Thus, it is not possible in these cases to obtain reliable pressures completely from estimates of relative ionization cross-sections. Instead, we have found that total absolute effusion measurements, combined with arguments concerning the major parent species and mass balance relationships, are a necessary adjunct to the mass spectrometric investigations to provide estimates of absolute pressures. In this case, the total mole rate of effusion  $N_s$  of the solid phase of molecular weight  $M_s$  is measured over a temperature range from  $T^{(1)}$  to  $T^{(2)}$ . These mole rates are converted to apparent total pressures  $P_s$  and adjusted by least-squares.

It is often useful to extend this procedure to the method proposed by Cater and Thorn (6). Consider the  $P_3N_5$  vaporization to the molecules  $P_4$ ,  $P_2$ ,  $PN$ , and  $N_2$ . The individual partial pressures  $P_i$  and the apparent pressures  $P_s$  are related to mole rates by the effusion law,

$$P_i = N_i \sqrt{2\pi M_i RT}. \quad (15)$$

Therefore, we have from the nitrogen mole balance relationship,

$$5P_s = P_{PN} \sqrt{M_s/M_{PN}} + 2P_{N_2} \sqrt{M_s/M_{N_2}} \quad (16)$$

and from the phosphorus mole balance relationship,

$$3P_s = P_{PN} \sqrt{M_s/M_{PN}} + 2P_{P_2} \sqrt{M_s/M_{P_2}} + 4P_{P_4} \sqrt{M_s/M_{P_4}}. \quad (17)$$

Provided that the scaling constant  $K_1$  of Equation 14 is independent of temperature (not necessarily true for noncondensable substances), then one can write

$$P_1^{(1)}/P_1^{(2)} = I_1^{(1)}T^{(1)}/I_1^{(2)}T^{(2)}. \quad (18)$$

Equations 16, 17, and 18 for each species  $i$  at two temperatures  $T^{(1)}$  and  $T^{(2)}$  can be solved to obtain absolute pressures  $P_i$ , and thus absolute scaling factors  $K_1$  for Equation 14. There are difficulties in applying this method to data of finite precision, but the concept is quite useful to account for anomalous intensities of the kind found in the pnictide studies (31).

**Table IV. Atomization Energies of some Inter-Pnictide Molecules**

<i>Molecule</i>	$E_0^\circ(e.v.)$	<i>Method</i>	<i>Reference</i>
N <sub>2</sub>	9.756	Spectra	(22)
P <sub>2</sub>	5.031	Spectra	(22)
	4.95	Mass Spect.	(17)
As <sub>2</sub>	3.94	Spectra	(16)
Sb <sub>2</sub>	3.0	Spectra	(16)
	3.1	Mass Spect.	(8)
	(3.7)	Spectra	(22)
Bi <sub>2</sub>	1.70	Spectra	(16, 22)
	2.04	Torsion Effusion	(1, 3, 60)
	2.06	Mass Spect.	(31)
PN	6.0	Spectra	(16)
	(6.3), 7.8	Spectra	(22)
	7.1	Static	(24)
	7.5	Spectra	(33)
	7.57	Mass Spect.	(31)
AsN	5 ± 1	Spectra	(16)
	(6.5)	Spectra	(22)
SbN	3.1	Spectra	(16)
	(4.8)	Spectra	(7, 22)
SbBi	3 ± 2	Spectra	(16)
	(3.0)	Spectra	(22)
P <sub>4</sub>	12.4	Mass Spect.	(9, 18)
As <sub>4</sub>	10.9	Mass Spect.	(9, 18)
Sb <sub>4</sub>	9.0	Mass Spect.	(2, 8, 18)
Bi <sub>4</sub>	6.0	Mass Spect.	(31)

### Discussion

It is of interest now to consider briefly the reasons why the pnictide elements and compounds vaporize to complex molecules, and to speculate on the bonding itself in the vapor molecules. There are however, several useful reviews and discussions published by others (20, 40, 49) pertinent to these considerations, and we wish to refer the reader to these for detailed information. For the elements, of course, it appears to be the atomic arrangement of molecular units in the solid that permit the condensed phase to vaporize to dimers and tetramers. Because the bonding and geometry of the molecular units in the solid govern the overall thermodynamic properties, the structural arguments are qualitatively equivalent to rationalizations based on free energy considerations.

The polymeric nature of the binary solid phases, likewise, must influence their vaporization processes. Solid P<sub>3</sub>N<sub>5</sub> consists of a network of P-N molecular units with single and double bonds (50). It seems

natural than that PN molecules should occur in the vapor. Because the solid is richer in nitrogen, however, appreciable amounts of  $N_2$  occur in the vapor. The binding energy of  $N_2$  is about 2 e.v. greater than that of PN, so that there is a competition between phosphorus and nitrogen for bonding with atomic nitrogen, and it is in favor of  $N_2$  both in the solid and vapor. The large value of the binding energy of  $N_2$  explains the absence of heteronuclear tetramers in this system. The existence of PN molecules in the vapor is really an interesting circumstance in relation to the normal absence of such molecules in other nitride systems. For these other systems, the equilibrium is vastly in favor of  $N_2$ .

Known values of atomization energies for various homonuclear and heteronuclear molecules of the Group VA elements are summarized in Table IV. One can find here pairs of homonuclear molecules with comparable energies and corresponding heteronuclear analogues with energies comparable to those values. These characteristics obviously correlate with the existence of the various species found in the vapor above the condensed phases. So it is not at all surprising that the vapors of the solid pnictides may contain a large variety of homonuclear and heteronuclear species. One hopes that mass spectrometric and other investigations of these molecules may eventually yield reliable dissociation energies, sufficiently precise that important subtle differences are well-defined. It should then be possible to begin to understand the chemical bonding in such molecules at a quantitative level.

### Acknowledgments

It is a pleasure to acknowledge support of this research by the Army Research Office—Durham, The Olin Center for the Study of Materials, Case Institute, and the Case Research Fund.

### Literature Cited

- (1) Aldred, A. T., Pratt, J. N., *J. Chem. Phys.* **38**, 1085 (1963).
- (2) Boerboom, A. J. H., Reyn, H. W., Vugts, H. F., Kistemaker, J., *Physica* **30**, 2137 (1964).
- (3) Bracket, E., Brewer, L., *U.S. At. Energy Comm. UCRL-3712* (1957).
- (4) Brewer, L., Kane, J. S., *J. Phys. Chem.* **59**, 105 (1955).
- (5) Carette, J., Kerwin, L., *Can. J. Phys.* **39**, 1300 (1961).
- (6) Cater, E. D., Thorn, R. J., *J. Chem. Phys.* **44**, 1342 (1966).
- (7) Coy, N. H., Sponer, H., *Phys. Rev.* **58**, 709 (1940).
- (8) DeMaria, G., Drowart, J., Inghram, M. G., *J. Chem. Phys.* **31**, 1076 (1959).
- (9) Drowart, J., Goldfinger, P., *J. Chem. Phys.* **55**, 721 (1958).
- (10) Ehret, W. F., Abramson, M. B., *J. Am. Chem. Soc.* **56**, 385 (1934).
- (11) Farr, T. D., *Tenn. Valley Authority, Chem. Eng. Rept. No. 8* (1950).
- (12) Fischer, F., Schröter, F., *Ber.* **43**, 1465 (1910).

- (13) Fox, R. E., Hickam, W., *J. Chem. Phys.* **22**, 2059 (1954).
- (14) Fox, R. E., Hickam, H., Kjeldaas, Jr., T., Grove, D. J., *Phys. Rev.* **84**, 859 (1951).
- (15) Franklin, E. C., *J. Am. Chem. Soc.* **27**, 820 (1905).
- (16) Gaydon, A. G., "Dissociation Energies and Spectra of Diatomic Molecules," Chapman and Hall, Ltd., London, 1953.
- (17) Gingerich, K. A., *J. Chem. Phys.* **44**, 1717 (1966).
- (18) Goldfinger, P., Jeunehomme, M., "Advances in Mass Spectrometry," p. 534-546, J. D. Waldron, ed., Pergamon Press, New York, 1959.
- (19) Gutbier, H. B., *Z. Naturforsch.* **16a**, 268 (1961).
- (20) Hart, R. R., Robin, M. B., Kuebler, N. A., *J. Chem. Phys.* **42**, 3631 (1965).
- (21) Herzberg, G., "Atomic Spectra and Atomic Structure," Dover Publications, New York, 1944.
- (22) Herzberg, G., "Spectra of Diatomic Molecules," 2nd ed., D. Van Nostrand, Princeton, 1950.
- (23) Honig, R. E., *Anal. Chem.* **25**, 1530 (1953).
- (24) Huffman, E. O., Tarbutton, G., Elmore, K., Cate, W., Walters, Jr., H., Elmore, G., *J. Am. Chem. Soc.* **76**, 6239 (1954).
- (25) Hugot, M. C., *Compt. Rend.* **139a**, 54 (1904).
- (26) Inghram, M., Drowart, J., "Proceedings of an International Symposium on High Temperature Technology," p. 226, McGraw-Hill, New York, 1960.
- (27) Janoff, W., *Z. Physik* **142**, 619 (1955).
- (28) Kane, J. S., Reynolds, J. H., *J. Chem. Phys.* **25**, 342 (1956).
- (29) Kerwin, L., *Can. J. Phys.* **32**, 757 (1954).
- (30) Klemm, W., Falkowski, I. V., *Z. Anorg. Chem.* **256**, 343 (1948).
- (31) Kohl, F. J., Uy, O. M., Carlson, K. D., Case Institute of Technology, unpublished research.
- (32) Krebs, H., Holz, W., Worms, K. H., *Ber.* **90**, 1031 (1957).
- (33) McCallum, K. J., Leiffer, E., *J. Chem. Phys.* **8**, 505 (1940).
- (34) Moldenhauer, W., Dorsam, H., *Ber.* **59B**, 926 (1926).
- (35) Moureu, H., Rocquet, P., *Compt. Rend.* **198**, 1691 (1934).
- (36) Moureu, H., Rocquet, P., *Compt. Rend.* **201**, 1381 (1935).
- (37) Moureu, H., Wetroff, G., *Bull. Soc. Chim.* **4**, 918 (1937).
- (38) Moureu, H., Wetroff, G., *Compt. Rend.* **204**, 51 (1937).
- (39) Moureu, H., Wetroff, G., *Compt. Rend.* **204**, 436 (1937).
- (40) Pauling, L., Simonetta, M., *J. Chem. Phys.* **20**, 29 (1952).
- (41) Reed, R. E., "Ion Production by Electron Impact," p. 49, Academic Press, New York, 1962.
- (42) Remy, H., Tiedeman, G., *Chem. Ber.* **94**, 472 (1961).
- (43) Renaud, R., *Ann. Chim.* **3**, 443 (1935).
- (44) Renaud, R., *Bull. Soc. Chim.* **53**, 692 (1933).
- (45) Samson, J. A. R., Cook, G. R., *Bull. Am. Phys. Soc. (II)* **4**, 454 (1959).
- (46) Saunders, G. A., Cooper, G., Miziumski, C., Lawson, A. W., *J. Phys. Chem. Solids* **26**, 533 (1965).
- (47) Schwartz, R., Jeanmaire, A., *Ber.* **65**, 1663 (1932).
- (48) Shih, C. H., Peretti, E. A., *Trans. Am. Soc. Metals* **48**, 709 (1956).
- (49) Siegel, B., *Quart. Rev.* **19**, 77 (1965).
- (50) Steger, E., *Chem. Ber.* **94**, 266 (1961).
- (51) Stevenson, D. P., Yost, D. M., *J. Chem. Phys.* **9**, 403 (1941).
- (52) Stock, A., Gomolka, E., *Ber.* **42**, 4519 (1909).
- (53) Stock, A., Hofmann, B., *Ber.* **36**, 314 (1903).
- (54) Trzebiatowski, W., Bryjak, E., *Z. Anorg. Chem.* **238**, 255 (1938).
- (55) Van Wazer, J. R., "Phosphorus and Its Compounds," p. 331, Interscience Publishers, New York, 1964.

- (56) Voronin, G. F., *Zh. Fiz. Khim* **40**, 1381 (1966).
- (57) Vought, R. H., *Phys. Rev.* **71**, 93 (1947).
- (58) Weessler, G. L., Samson, J. A. R., Ogawa, M., Cook, G. R., *J. Opt. Soc. Am.* **49**, 338 (1959).
- (59) Westmore, J. P., Mann, K. H., Tickner, A. W., *J. Phys. Chem.* **68**, 606 (1964).
- (60) Yosiyama, M., *J. Chem. Soc. Japan* **62**, 204 (1941).

RECEIVED November 2, 1966.

# Appearance Potentials, Ionization Potentials and Heats of Formation for Perfluorosilanes and Perfluoroborosilanes

J. D. McDONALD, C. H. WILLIAMS, J. C. THOMPSON,  
and J. L. MARGRAVE

Rice University, Houston, Texas

*A Bendix time-of-flight mass spectrometer has been used to measure appearance potentials and ionization potentials of species containing silicon, boron, and fluorine. From these data, a mutually consistent set of average bond energies and thermodynamic properties has been derived.*

In contrast to the large amount of data reported on the heats of formation and bond strengths of hydrocarbons and fluorocarbons, much less is known about the corresponding silicon and silicon-boron compounds. For the perfluorosilanes and boron compounds, heats of formation are reported for  $\text{SiF}_4$  (12),  $\text{SiF}_2$  and  $\text{SiF}$  (1, 13),  $\text{BF}_3$  (11),  $\text{BF}_2$  (5) and  $\text{BF}$  (3). The only value for the silicon-silicon bond strength is based on  $\text{Si}_2\text{H}_6$  data (7), and no measurements at all have been made on the silicon-boron bond. Average bond energies are used to derive the only published values of the heat of formation of  $\text{SiF}_3$  (8). In this paper, appearance potential studies, which lead to the ionization potentials and heats of formation of  $\text{Si}_2\text{F}_6$ ,  $\text{Si}_3\text{F}_6$ ,  $\text{Si}_2\text{BF}_7$ ,  $\text{BF}_2$ , and  $\text{SiF}_3$ , are reported. These are used to calculate bond dissociation energies which may be used to calculate thermodynamic properties of other fluorosilanes.

## *Experimental*

The appearance potentials given in this work were measured on a Bendix model 14-107 time-of-flight mass spectrometer. The ion source electronics were modified to provide operation according to the Retarding Potential Difference (RPD) method (2, 6). With the electron source filament at the electron energy potential below ground, the five electron grids of the standard model 14 ion source were connected as follows:

grid No. 1, biased at  $-5$  volts d.c., pulsed to  $+5$  volts with respect to the filament; grids No. 2 and 4,  $+1$  volt d.c. with respect to the filament; grid No. 3,  $-1.0$  or  $-1.1$  volt d.c. to the filament to provide a  $0.1$  volt RPD step; and grid No. 5, at ground potential.

This apparatus, when tested on  $O_2$ ,  $N_2$ , and the noble gases, gave results similar to those reported by Melton and Hamill (6), but when the silicon fluorides were introduced, some difficulty was encountered. The electron trap current, and hence the ion current, decreased with time, and the measured appearance potential of the standard ( $N_2$ ) dropped several tenths of an e.v. during the experiment. Both effects were probably caused by the thermal decomposition of the samples, depositing a silicon metal residue on the electron grids. The effect was minimized by operating at low sample pressures ( $1-2 \times 10^{-6}$  torr) and cleaning the ion source frequently. The lower signal-to-noise ratio caused by low sample pressure resulted in reducing the accuracy of measurement. The appearance potentials ( $AP$ ) were calibrated against  $N_2^+/N_2$ ,  $AP = 15.57$  volts and  $He^+/He$ ,  $AP = 24.58$  volts (4).

The  $SiF_4$  gas was purchased from Matheson and was freed of  $SO_2$  by passing it over iron at  $800^\circ C$ .  $SiF_2$  was produced by flowing the  $SO_2$ -free  $SiF_4$  over Si metal at  $1175^\circ C$ .; the gaseous products were leaked into the ion source of the mass spectrometer by a line-of-sight path. Attempts to detect  $SiF_3$  in the gaseous products were unsuccessful. The  $Si_2F_6$ ,  $Si_3F_8$ , and  $Si_2BF_7$  were fractionally distilled from the volatile products formed by heating a Si-F or Si-F-B polymer (9, 10); the sample fractions were about 97% pure.

### Calculations

The appearance potentials measured for the production of the various parent and fragment ions are listed in Table I; all have an experimental reproducibility of  $\pm 0.1$  volt. The process of formation of a given ion must be chosen to produce the most consistent set of results. In the calculations which follow the internal excitation energy and excess kinetic energy of the fragment ion are neglected. For this reason, only those fragmentation reactions likely to involve a minimum amount of internal excitation energy and excess kinetic energy were used in the calculations.

As an example of the method of computation, consider Process 6:



One has for the change in enthalpy,  $\Delta H$ , for this fragmentation reaction

$$\Delta H_r = \Delta H_f^\circ(SiF_2) + IP(SiF_2) + \Delta H_f^\circ(SiF_4) - \Delta H_f^\circ(Si_2F_6) = 13.02 \text{ e.v.}$$

Using the values for the heats of formation of  $SiF_2$  and  $SiF_4$  given in Table II and the appearance potential of  $SiF_2^+$  from  $SiF_2$  in Table I, this equation is solved for  $\Delta H_f^\circ(Si_2F_6) = -565$  kcal./mole. Subtracting

Process 6 from Process 10 gives



where

$$\Delta H_f^\circ = 2\Delta H_f^\circ(\text{Si}_2\text{F}_6) - \Delta H_f^\circ(\text{Si}_3\text{F}_8) - \Delta H_f^\circ(\text{SiF}_4) = 0.43 \text{ e.v.}$$

By inserting the value for  $\Delta H_f^\circ(\text{Si}_2\text{F}_6)$  calculated above and that for  $\Delta H_f^\circ(\text{SiF}_4)$  from Table II, the heat of formation of  $\text{Si}_3\text{F}_8$  is determined,  $\Delta H_f^\circ(\text{Si}_3\text{F}_8) = -754 \text{ kcal./mole}$ .

Table I. Appearance Potentials in Volts<sup>a</sup>

<i>Ion/Compound</i>	<i>SiF<sub>2</sub></i>	<i>SiF<sub>4</sub></i>	<i>Si<sub>2</sub>F<sub>6</sub></i>	<i>Si<sub>3</sub>F<sub>8</sub></i>	<i>Si<sub>2</sub>BF<sub>7</sub></i>
<i>Si<sub>3</sub>F<sub>8</sub><sup>+</sup></i>				10.84	
<i>Si<sub>3</sub>F<sub>7</sub><sup>+</sup></i>				15.62	
<i>Si<sub>2</sub>F<sub>6</sub><sup>+</sup></i>			12.89	11.77	12.97
<i>Si<sub>2</sub>F<sub>4</sub><sup>+</sup></i>				11.43	11.32
<i>SiF<sub>4</sub><sup>+</sup></i>		15.71			
<i>SiF<sub>3</sub><sup>+</sup></i>		16.20	14.30 (15.8)	15.51	15.42
<i>SiF<sub>2</sub><sup>+</sup></i>	11.29	27.35	13.02	13.45	13.21
<i>SiF<sup>+</sup></i>		28.75	14.16		11.56
<i>Si<sub>2</sub>BF<sub>6</sub><sup>+</sup></i>					15.36
<i>SiBF<sub>4</sub><sup>+</sup></i>					11.95
<i>BF<sub>2</sub><sup>+</sup></i>					14.67

<sup>a</sup> Experimental reproducibility =  $\pm 0.1 \text{ e.v.}$ ; Absolute accuracy =  $\pm 0.3 \text{ e.v.}$

It is now possible to set up two simultaneous equations involving  $D(\text{Si-F})_{\text{avg.}}$  and  $D(\text{Si-Si})_{\text{avg.}}$ :

$$\Delta H_f^\circ(\text{Si}_2\text{F}_6) = 6\Delta H_f^\circ(\text{F}) + 2\Delta H_f^\circ(\text{Si, gas}) - 6D(\text{SiF})_{\text{avg.}} - D(\text{Si-Si})_{\text{avg.}}$$

$$\Delta H_f^\circ(\text{Si}_3\text{F}_8) = 8\Delta H_f^\circ(\text{F}) + 3\Delta H_f^\circ(\text{Si, gas}) - 8D(\text{SiF})_{\text{avg.}} - 2D(\text{Si-Si})_{\text{avg.}}$$

By solving these, one finds  $D(\text{Si-F})_{\text{avg.}} = 138 \text{ kcal.}$  and  $D(\text{Si-Si})_{\text{avg.}} = 58 \text{ kcal.}$  From similar calculations on  $\text{SiF}_2$  and  $\text{SiF}_4$  one gets  $D(\text{SiF})_{\text{avg.}} = 141$  and  $142 \text{ kcal.}$  respectively. As a "best" value  $D(\text{Si-F})_{\text{avg.}} = 139 \pm 3$  is chosen. With this value in the above equations one obtains  $D(\text{Si-Si})_{\text{avg.}} = 55 \pm 10 \text{ kcal.}$

There is a break in the ionization efficiency curve for  $\text{SiF}_3^+$  from  $\text{Si}_2\text{F}_6$ . Below the break the ionization is attributed to ion pair production and above the break to more conventional dissociative ionization. With this latter interpretation, Process 5 combined with Process 1 gives  $\Delta H_f^\circ(\text{SiF}_3) = -253 \text{ kcal./mole}$  as compared with  $-254 \text{ kcal./mole}$  calculated on the basis of the average Si-F bond dissociation energy. By using  $\Delta H_f^\circ(\text{SiF}_3) = -253 \text{ kcal./mole}$  in Process 1, one calculates  $\text{IP}(\text{SiF}_3) = 13.3 \text{ volts}$ . Recent quantum mechanical calculations, however, strongly support  $\text{IP}(\text{SiF}_3) = 8.5 \pm 1 \text{ volts}$  [Hastie, J. W. Margrave,

J. L. (unpublished work, 1967-1968)] and yield through Process 1 the value  $\Delta H_f^\circ(\text{SiF}_3) = -235 \pm 20$  kcal./mole. Process 9 and this latter value for  $\text{SiF}_3$  give  $\Delta H_f^\circ(\text{Si}_2\text{F}_5) = -358 \pm 20$  kcal./mole and this heat in Process 4 yields  $\text{IP}(\text{Si}_2\text{F}_5) = 7.5 \pm 1$  volts. A combination of appearance potentials for Processes 8 and 12 yields  $\Delta H_f^\circ(\text{Si}_2\text{BF}_7) = -637 \pm 25$  kcal./mole. With this value and Process 14, one calculates  $\Delta H_f^\circ(\text{SiBF}_5) = -454 \pm 25$  kcal./mole and from Process 11 one derives  $\Delta H_f^\circ(\text{BF}_2) = -150 \pm 20$  kcal./mole. Process 15 yields  $\text{IP}(\text{BF}_2) = 9 \pm 1$  volts. By a process similar to that used for silicon, one computes  $D(\text{B-F})_{\text{avg.}} = 152 \pm 3$  kcal./mole and  $D(\text{B-Si})_{\text{avg.}} = 55 \pm 15$  kcal./mole.

The results of these calculations are summarized in Table III. The uncertainties listed are obtained by assigning an error of 0.1 volt or 2.3 kcal. to each appearance potential used in calculating a given quantity. The final data have been used to calculate an appearance potential for each of the reactions in Table III. Although in some processes the measured and calculated values agree to within 0.1 e.v., in others—*e.g.*, the production of  $\text{SiF}_2^+$  from  $\text{SiF}_4$ , internal excitation energy and excess kinetic energy considerations are important, and the difference between the measured appearance potential and that calculated for the "best fit" process is larger. Processes involving excited fragments were not used in the calculations of thermodynamic properties given in Table II.

**Table II. Heats of Formation and Ionization Potentials<sup>b</sup>**

Species	$\Delta H_f^\circ$ (kcal./mole <sup>-1</sup> )	IP (volts)
SiF	$-2 \pm 3$	$7.3 \pm 0.2^c$
SiF <sub>2</sub>	$-136 \pm 5$	$11.29 \pm 0.1$
SiF <sub>3</sub>	$-235 \pm 20$	$8.5 \pm 1^c$
SiF <sub>4</sub>	$-386.0 \pm 0.2$	$15.7 \pm 0.1$
Si <sub>2</sub> F <sub>5</sub>	$-358 \pm 25$	$7.5 \pm 1$
Si <sub>2</sub> F <sub>6</sub>	$-565 \pm 5$	$(10.6 \pm 1.0)^a$
Si <sub>3</sub> F <sub>8</sub>	$-754 \pm 10$	$10.84 \pm 0.1$
BF <sub>2</sub>	$-150 \pm 20$	$9 \pm 1^c$
SiBF <sub>5</sub>	$-454 \pm 20$	$(11 \pm 1.0)^a$
Si <sub>2</sub> BF <sub>7</sub>	$-637 \pm 25$	$(10.6 \pm 1)^a$

$D(\text{Si-F})_{\text{avg.}} = 139 \pm 3$  kcal./mole

$D(\text{Si-Si})_{\text{avg.}} = 55 \pm 10$  kcal./mole

$D(\text{B-F})_{\text{avg.}} = 152 \pm 3$  kcal./mole

$D(\text{B-Si})_{\text{avg.}} = 55 \pm 15$  kcal./mole

<sup>a</sup> Parent ion not observed.

<sup>b</sup> Other quantities used in calculations:

$$\Delta H_f^\circ(\text{F}) = 18.8 \pm 1 \text{ kcal./mole (4)}$$

$$\Delta H_f^\circ(\text{F}^-) = -64.8 \pm 1 \text{ (4)}$$

$$\Delta H_f^\circ[\text{Si(g)}] = 105 \pm \text{(4)}$$

$$\Delta H_f^\circ[\text{B(g)}] = 133 \pm 3 \text{ (4)}$$

$$\Delta H_f^\circ(\text{BF}_3) = -271 \pm 2 \text{ (11)}$$

<sup>c</sup> Hastie, J. W., Margrave, J. L. (unpublished work, 1967).

**Table III. Probable Fragmentation Reactions and Calculated Appearance Potentials**

<i>Process</i>	<i>Calc.<sup>a</sup> AP, volts</i>	<i>Meas. AP, volts</i>
1. $\text{SiF}_4 = \text{SiF}_3^+ + \text{F}$	$16.2 \pm 0.5$	16.20
2. $\text{SiF}_4 = \text{SiF}_2^+ + 2\text{F}$	$23.6 \pm 0.5$	27.35 <sup>b</sup>
3. $\text{SiF}_4 = \text{SiF}^+ + 3\text{F}$	$28.4 \pm 0.5$	28.75
4. $\text{Si}_2\text{F}_6 = \text{Si}_2\text{F}_5^+ + \text{F}^-$	$12.9 \pm 1.0$	12.89
5. $\text{Si}_2\text{F}_6 = \text{SiF}_3^+ + \text{SiF}_3$	$12 \pm 1$	15.8
6. $\text{Si}_2\text{F}_6 = \text{SiF}_2^+ + \text{SiF}_4$	$13.0 \pm 0.5$	13.02
7. $\text{Si}_3\text{F}_8 = \text{Si}_2\text{F}_5^+ + \text{SiF}_3$	$14 \pm 1$	11.77
8. $\text{Si}_3\text{F}_8 = \text{Si}_2\text{F}_4^+ + \text{SiF}_4$	—	11.43
9. $\text{Si}_3\text{F}_8 = \text{SiF}_3^+ + \text{Si}_2\text{F}_5$	$15.5 \pm 0.5$	15.51
10. $\text{Si}_3\text{F}_8 = \text{SiF}_2^+ + \text{Si}_2\text{F}_6$	$13.5 \pm 0.5$	13.45
11. $\text{Si}_2\text{BF}_7 = \text{Si}_2\text{F}_5^+ + \text{BF}_2$	$13 \pm 1$	12.97
12. $\text{Si}_2\text{BF}_7 = \text{Si}_2\text{F}_4^+ + \text{BF}_3$	—	11.32
13. $\text{Si}_2\text{BF}_7 = \text{SiF}_3^+ + \text{SiBF}_4$	$15.7 \pm 1.0$	15.42
14. $\text{Si}_2\text{BF}_7 = \text{SiF}_2^+ + \text{SiBF}_5$	$13 \pm 1$	13.21
15. $\text{Si}_2\text{BF}_7 = \text{BF}_2^+ + \text{Si}_2\text{F}_5$	$15 \pm 1$	14.67

<sup>a</sup> Based on Table II data.

<sup>b</sup> (Meas.-Calc. Values) > experimental error; fragment may possess kinetic energy, or may be in excited electronic or vibrational states, or the reaction products may be different than assumed.

### Conclusions

From these data, one can now predict the heats of formation of Si-B-F compounds based on the following average bond dissociation energies

$$D(\text{Si-F})_{\text{avg.}} = 139 \pm 3 \text{ kcal./mole}$$

$$D(\text{B-F})_{\text{avg.}} = 152 \pm 3 \text{ kcal./mole}$$

$$D(\text{Si-Si})_{\text{avg.}} = 55 \pm 10 \text{ kcal./mole}$$

$$D(\text{Si-B})_{\text{avg.}} = 55 \pm 15 \text{ kcal./mole}$$

For the monosilicon species one can calculate individual bond dissociation energies as follows:

$$D(\text{SiF}_3\text{-F}) = 170 \pm 10 \text{ kcal./mole}$$

$$D(\text{SiF}_2\text{-F}) = 118 \pm 10 \text{ kcal./mole}$$

$$D(\text{SiF-F}) = 153 \pm 5 \text{ kcal./mole}$$

$$D(\text{SiF}) = 130 \pm 3 \text{ kcal./mole}$$

### Acknowledgments

This work has been supported with funds from the Advanced Research Projects Agency, through the Army Research Office in Durham, and by the Robert A. Welch Foundation.

### Literature Cited

- (1) Ehlert, T. C., Margrave, J. L., *J. Chem. Phys.* **41**, 1066 (1966).
- (2) Fox, R. E., Hickam, W. M., Grove, D. J., Kjeldass, T., Jr., *Rev. Sci. Instr.* **26**, 1101 (1955).
- (3) Hildenbrand, D. L., Murad, E., *J. Chem. Phys.* **43**, 1400 (1965).
- (4) Kiser, R. W., "Tables of Ionization Potentials," *U. S. At. Energy Comm. TID-6142* (June, 1960).
- (5) Margrave, J. L., *J. Phys. Chem.* **66**, 1209 (1962).
- (6) Melton, C. E., Hamill, W. H., *J. Chem. Phys.* **41**, 546 (1964).
- (7) O'Neal, H. E., Ring, M. A., *Inorg. Chem.* **5**, 435 (1966).
- (8) Stull, D. R., editor, "JANAF Thermochemical Tables," No. PB-168-370, Clearinghouse for Federal Scientific and Technical Information, Springfield, Va., August, 1960.
- (9) Timms, P. L., Kent, R. A., Ehlert, T. C., Margrave, J. L., *J. Am. Chem. Soc.* **87**, 2824 (1965).
- (10) *Ibid.*, **87**, 3819 (1965).
- (11) Wise, S. S., Feder, H. M., Hubbard, W. N., Margrave, J. L., *J. Phys. Chem.* **67**, 2157 (1961).
- (12) *Ibid.*, **67**, 815 (1963).
- (13) Zmbov, K. F., Hastie, J. W., Uy, M., Margrave, J. L. (unpublished, 1967).

RECEIVED October 11, 1966.

# Mass Spectrometric Studies of Scandium, Yttrium, Lanthanum, and Rare-Earth Fluorides

K. F. ZMBOV and J. L. MARGRAVE

Rice University, Houston, Tex.

*A review is presented of recent mass spectrometric studies of the sublimation and vaporization processes for the rare-earth trifluorides. The rates of sublimation of the trifluorides have been measured, and the heats of sublimation have been determined. Mono- and difluorides of the rare-earths may be produced in the vapor phase either by vaporizing the trifluorides under reducing conditions, or by oxidizing the rare-earth metals with a fluorinating agent. Ionization potentials for rare-earth atoms, mono- and difluorides have been measured by the electron-impact method. Gaseous equilibria involving the atoms, subfluorides and trifluorides of the various metals have been studied and used to establish the bond strengths and other thermodynamic properties.*

Rare-earth trifluorides have been prepared in high purity for use in the production of pure rare-earth metals and for various optical applications, but until recently there have been no quantitative data on their sublimation and vaporization rates. The thermodynamic stabilities of these compounds have also been poorly known. There has been some spectroscopic evidence concerning the monofluorides of Sc, Y, and La, and attempts have been made to calculate dissociation energies by analyzing the spectral data. The uncertainties, however, were as high as 1.5 e.v. (2, 3, 7, 12, 14, 22, 30, 34).

Since the electronic configurations of the neutral rare-earth atoms differ only in the 4f-level, one might expect that vaporization properties, binding energies, etc. for the rare-earth metals and their compounds would be essentially identical, but this is far from the actual situation. Heats of vaporization of the rare-earth metals show a double periodicity

with increasing atomic number (13, 32, 35) and a similar behavior was found for the dissociation energies of rare-earth monoxides (36). It has been shown that there is appreciable variation in the heats of formation of the solid sesquioxides (15, 16). On the other hand, recent measurements of the heats of formation of some rare earth fluorides (28, 29) indicate only small differences.

This paper presents the results of an extensive mass spectrometric study of the sublimation rates for solid rare-earth trifluorides and of the stabilities of the various gaseous fluoride species which are present in equilibrium.

### *Experimental*

**Materials.** All of the chemicals used in this study were purchased from Semi-Elements, Inc., Saxonburg, Pa. and were used without further purification.

**Mass Spectrometer.** The mass spectrometer used for analysis of the vapors effusing from the Knudsen cell was a single-focusing, 12-inch radius of curvature, 60-degree instrument, equipped with a Knudsen cell assembly. The basic features and principles of operation of the apparatus have been described in several publications (17).

The high temperature assembly consisted of a cylindrical Knudsen cell, radiation shields, and a shutter plate. The Knudsen cell was made of tantalum and had a ratio of evaporation surface-to-orifice area of about 200. The cell was heated by electron bombardment, and the temperature was measured with a disappearing filament optical pyrometer sighted into a black-body hole through a calibrated flat quartz window. The optical pyrometer was calibrated by intercomparison with a similar pyrometer which had been calibrated by the U. S. National Bureau of Standards (25).

The molecules effusing from the Knudsen cell passed through the slit in the shutter plate and entered the ionization chamber of the ion source, where the neutral molecules were ionized by electrons. Ions formed were then accelerated and collimated by the ion lenses in the ion source, magnetically analyzed, and collected and amplified by a 16-stage Ag-Mg dynode electron multiplier whose output led to a Cary-vibrating-reed electrometer and a Leeds and Northrup pen-recorder. The instrument was also equipped with a movable plate in front of the first dynode of the electron multiplier, and this plate could be used for measurement of the multiplier gain.

### *Results*

**Sublimation Rates of Rare Earth Trifluorides.** The mass spectra of the vapors over solid rare-earth trifluorides were simple. The only peaks observed in the range of temperatures investigated were those corresponding to  $M^+$ ,  $MF^+$ , and  $MF_2^+$  ions. The intensity of  $MF_3^+$  ions was very small, and no polymeric species were detected. Ionization efficiency

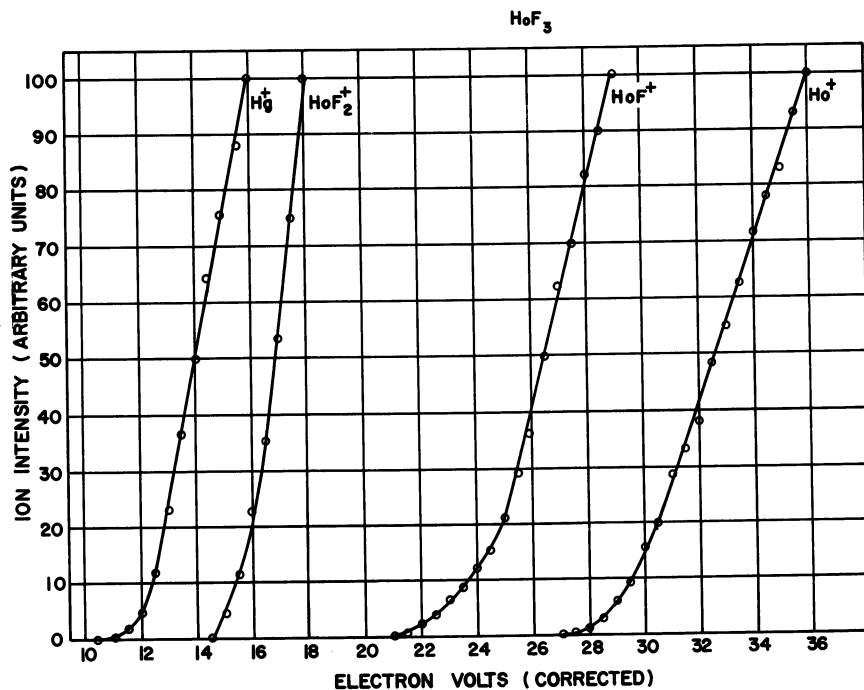


Figure 1. Ionization-efficiency curves for ions from  $\text{HoF}_3$ -vapors

curves for the various ions were measured. Figure 1 shows curves for the ions from  $\text{HoF}_3$ -vapor as a typical example of all the rare-earth fluorides.

The appearance potentials of the ions were measured by the vanishing current method, using the ionization potential of mercury, 10.43 e.v. (11) as a standard to calibrate the electron energy scale. The data are listed in Table I.

Both the shapes of the ionization-efficiency curves and the values of the appearance potentials served as a basis for concluding that the ions observed were formed by dissociative ionization of  $\text{MF}_3$  molecules. A very high probability of ion formation by dissociative ionization compared with simple ionization of the parent molecule is characteristic in this case as well as in many other metal halide systems (4, 10, 26).

After the identity of the vapor species was established, the sublimation rates of the trifluorides were determined by following the temperature dependence of the  $\text{MF}_2^+$ -ion intensity at a fixed energy of ionizing electrons. The data were plotted as  $\log(I^*T)$  vs.  $1/T$ , where  $I^*$  = ion intensity in arbitrary units,  $T$  = temperature in  $^\circ\text{K}$ . and the quantity  $(I^*T)$  is proportional to the absolute pressure,  $P$ , of the vapor (8). The

heats of sublimation were determined from the Clausius-Clapeyron relation:

$$\frac{d \ln(I^*T)}{d(1/T)} = -\frac{\Delta H^\circ_{s,T}}{R} \quad (1)$$

One can also, in principle, determine the heats of sublimation from the third-law since

$$\Delta F^\circ_{s,T} = -RT \ln P_T = \Delta H^\circ_{s,T} - T\Delta S^\circ_{s,T} \quad (2)$$

Where  $\Delta F^\circ_T$  and  $\Delta S^\circ_T$  are the changes in the free energy and the entropy for the sublimation process. This procedure requires that the absolute entropies of the solid and gaseous species be known. Neither low temperature nor high temperature heat capacity data are available for the solid trifluorides, and there are also no spectroscopic data or molecular structures known to provide the necessary information for calculation of the entropies; thus, third-law calculations were not made for these materials.

**Table I. Appearance Potentials of Ions from Rare-Earth Trifluoride Vapors**

Element	Appearance Potentials (e.v.) <sup>a</sup>		
	M <sup>+</sup>	MF <sup>+</sup>	MF <sub>2</sub> <sup>+</sup>
Sc	28.0	16.0	13.5
Y	28.0	21.5	13.5
La	26.5	18.5	12.0
Ce	28.0	20.5	13.0
Pr	27.5	19.0	12.5
Nd	25.5	19.8	12.9
Sm	26.0	19.0	13.0
Eu	27.0	19.5	13.5
Gd	26.5	20.0	14.5
Tb	27.0	19.5	13.0
Dy	27.4	20.0	13.5
Ho	28.0	21.0	14.5
Er	27.5	20.0	14.0
Tm	27.0	20.8	13.5
Yb	27.0	20.5	14.0
Lu	28.0	21.0	14.3

<sup>a</sup> Referred to the ionization potential of Hg,  $I.P. = 10.43$  e.v. (11), with an accuracy of  $\pm 0.7$  e.v.

Though second-law approaches, as used in this work for calculation of the heats of sublimation, require only a knowledge of the relative  $I^*T$ -values, the absolute pressures of several trifluorides have been measured by evaporating a weighed amount of a well outgassed sample at a constant temperature from the Knudsen cell and monitoring the MF<sub>2</sub><sup>+</sup>-ion

peak on the mass spectrometer. From the measured weight loss,  $\Delta m$ , in grams, the evaporation time,  $t$ , in seconds, the temperature  $T$  in  $^{\circ}\text{K}$ ., and the orifice area,  $s$ , in sq. cm., one may evaluate the absolute vapor pressure,  $P$ , in atm., from the Knudsen-Hertz equation (23).

$$P = \frac{\Delta m}{44.331} \left( \frac{1}{s \cdot t} \right) \left( \frac{T}{M} \right)^{\frac{1}{2}}$$

The absolute pressures thus obtained were used to calculate the machine-sensitivity constants relating the pressures and ion currents and thus, to yield absolute vapor pressure equations. The vapor pressure curves for  $\text{ScF}_3$ ,  $\text{YF}_3$ , and  $\text{LaF}_3$  (20) are shown in Figure 2.

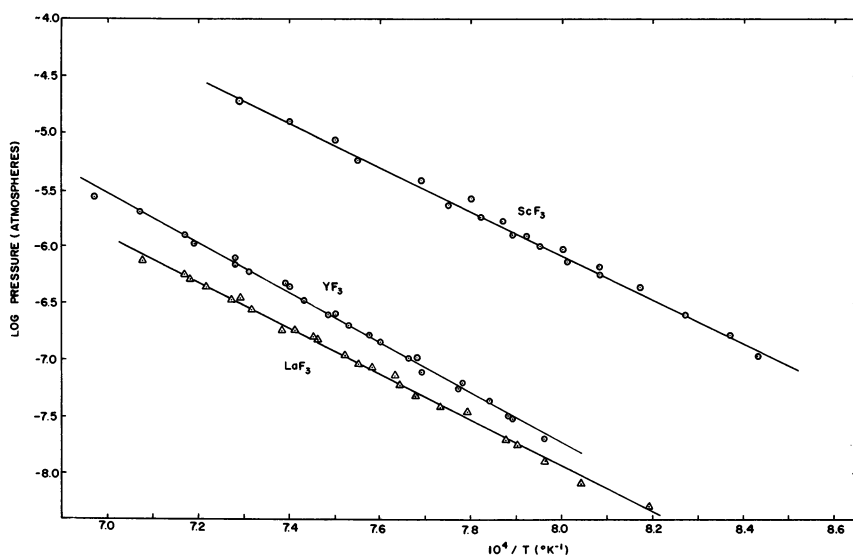


Figure 2. The Vapor Pressure Curves for  $\text{ScF}_3$ ,  $\text{YF}_3$ , and  $\text{LaF}_3$

Figure 3 shows the vapor pressure curve of  $\text{NdF}_3$ , and Figure 4 presents the curves for  $\text{YbF}_3$  and  $\text{LuF}_3$ . In Figure 5 second-law plots are presented for the sublimation of  $\text{SmF}_3$ ,  $\text{PrF}_3$ ,  $\text{GdF}_3$ ,  $\text{TbF}_3$ , and  $\text{TmF}_3$ .

From the slopes of these second-law plots one obtains the heats of sublimation at the average temperature of the measurements. The corrections to  $\Delta H^{\circ}_{298}$  were made by employing the estimated values,  $\Delta C_p = -7$  cal.  $\text{deg}^{-1}$   $\text{mole}^{-1}$ , for the sublimation process. The heats and entropies of sublimation for the rare-earth trifluorides are summarized in Table II.

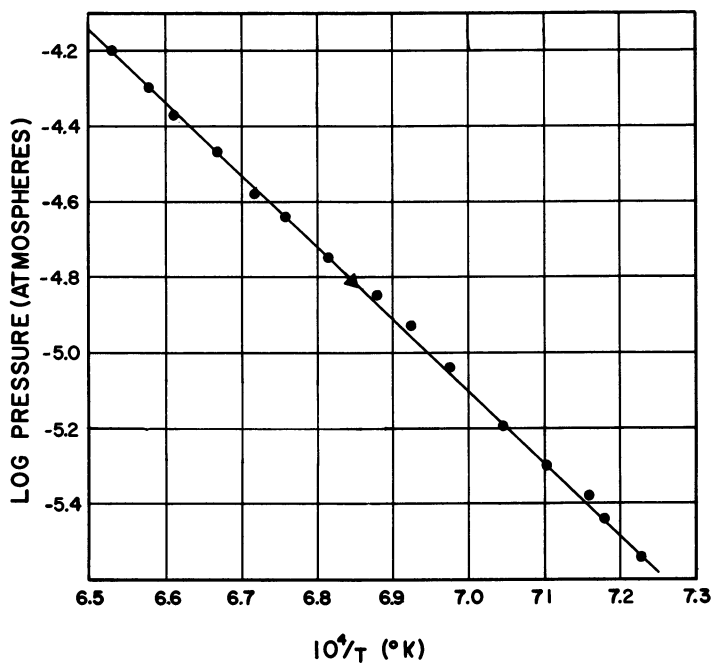
The usual uncertainties in the experimental determinations of the heats of sublimation, obtained as standard deviations from a least-squares treatment of the data were of the order of  $\pm 1$  kcal.  $\text{mole}^{-1}$ . The larger uncertainty  $\pm 5$  kcal.  $\text{mole}^{-1}$  at  $298^{\circ}\text{K}$ . in Table II reflects both possible

errors caused by temperature gradients in the crucible and errors in the estimation of the thermodynamic quantities.

**Stabilities of Rare-Earth Subfluorides.** Although the tripositive state is the most common valence state in the rare-earth series, the existence of difluorides of Sm, Eu, and Yb has long been recognized. There is also some spectroscopic evidence for the existence of the monofluorides of Sc, Y, and La (2, 3, 7, 12, 14, 22, 30, 34). It has been found that many subfluorides of the transition metals can be identified, in the vapor phase under reducing conditions by mass spectrometry.

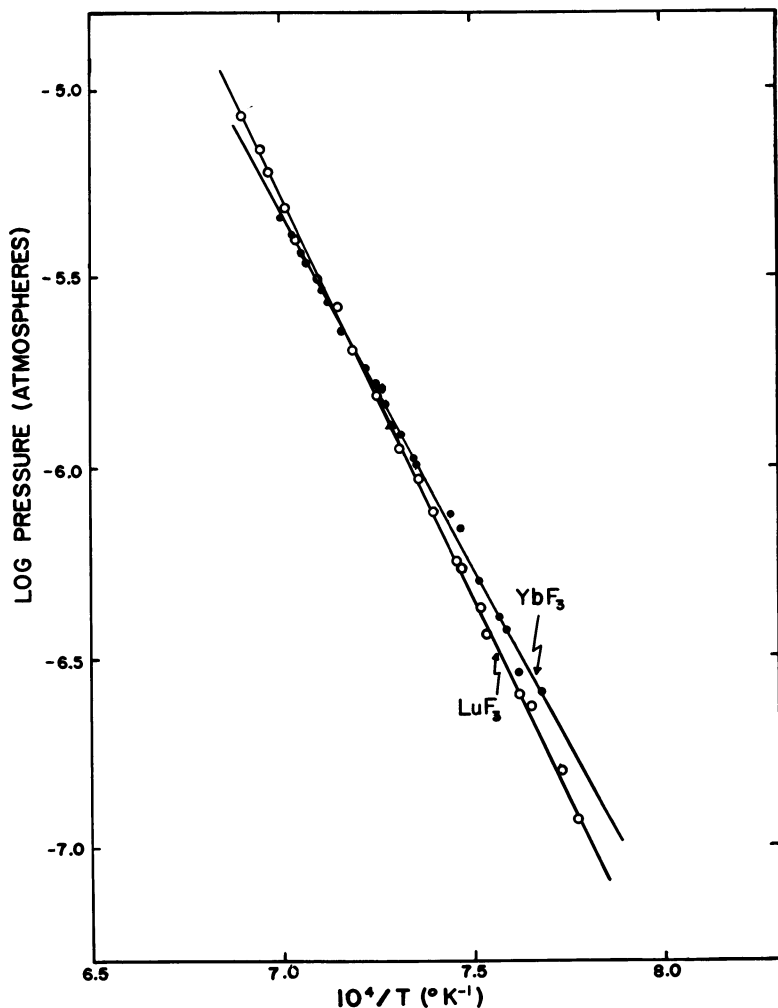
In this work an attempt was made to produce the various subfluorides of the rare-earths and to study fluorine-exchange reactions to determine the bond strengths. The rare-earth subfluorides were produced by heating appropriate mixtures of rare-earth trifluorides with a reducing metal, or rare-earth metals with a fluorinating agent in a tantalum Knudsen cell.

In the first experiment of this series, the system Nd + BaF<sub>2</sub> was studied (37). With the effusion cell at temperatures between 1330° and 1470°K., the ion species showing a clear shutter effect were Ba<sup>+</sup>, BaF<sup>+</sup>, Nd<sup>+</sup>, NdF<sup>+</sup>, and NdF<sub>2</sub><sup>+</sup>. The ionization efficiency curves for these ions are shown on Figure 6.



Journal of Chemical Physics

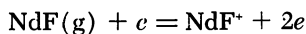
Figure 3. The Vapor Pressure Curve for NdF<sub>3</sub>



Journal of Less-Common Metals

Figure 4. The Vapor Pressure Curves for  $\text{YbF}_3$  and  $\text{LuF}_3$

The appearance potential of  $\text{Nd}^+$ -ion,  $5.6 \pm 0.3$  e.v., agrees well with the value obtained by the surface ionization method (18) and indicates the presence of Nd-atoms in the vapor. The  $\text{NdF}^+$  curve has a low energy tail, with the onset at  $5.0 \pm 0.5$  e.v. and a break at  $\sim 12.5 \pm 0.5$  e.v. This low-energy portion of the curve was attributed to a simple ionization process



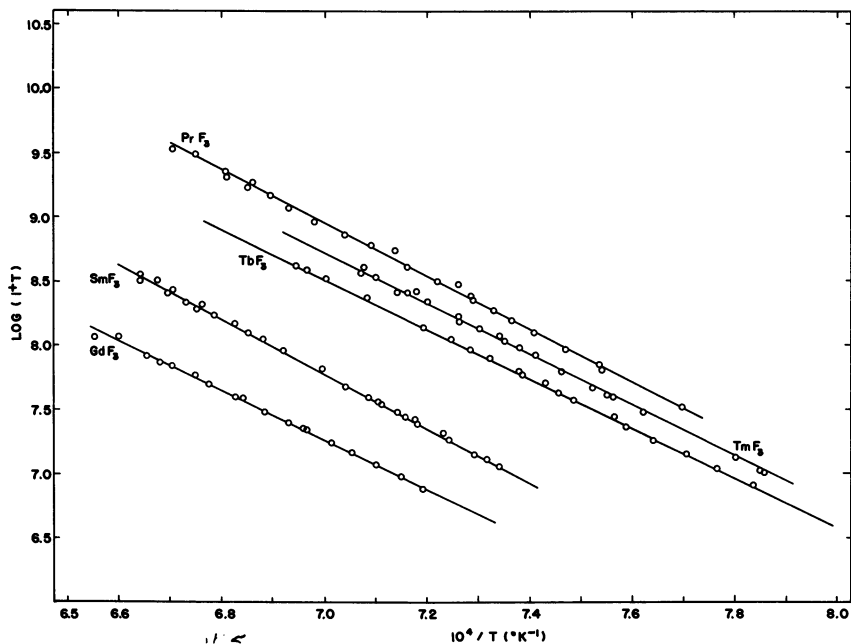


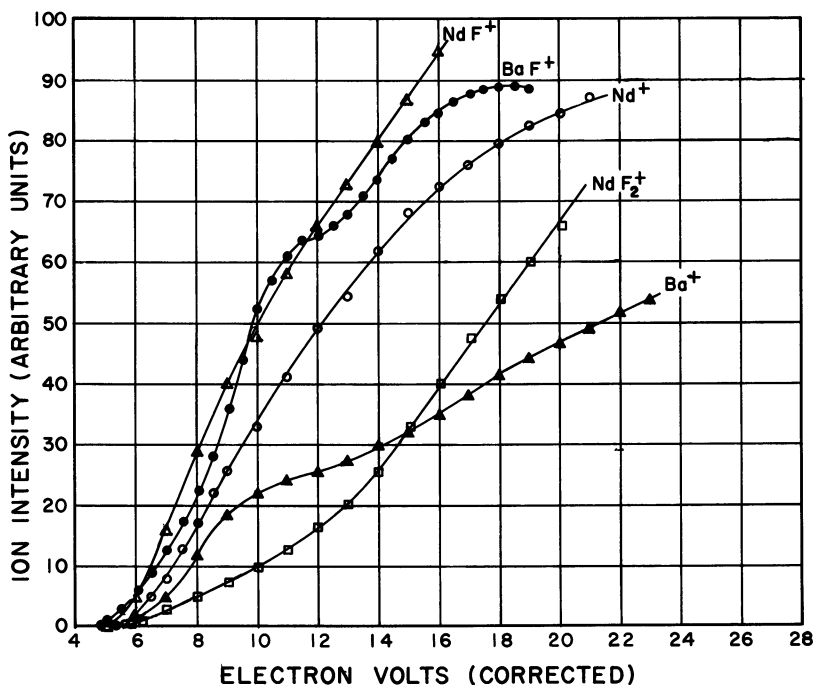
Figure 5. Clausius-Clapeyron Plots for the Variation of  $\text{SmF}_3^+$ ,  $\text{PrF}_3^+$ ,  $\text{GdF}_3^+$ ,  $\text{TbF}_3^+$  and  $\text{TmF}_3^+$  Ion Intensities with Temperature

Table II. Heats of Sublimation of Rare-Earth Trifluorides

Element	Temp. Range (°K.)	$\Delta H^\circ_{s,T}$	$\Delta H^\circ_{s,298}$	$\Delta S^\circ_{s,T}$
ScF <sub>3</sub>	1172-1323	88.7	101 ± 5	43.2 ± 1.5
YF <sub>3</sub>	1256-1434	100.0	115 ± 5	44.7 ± 1.0
LaF <sub>3</sub>	1303-1416	91.7	108 ± 5	37.5 ± 0.7
CeF <sub>3</sub>	1301-1485	91.2	99 ± 3	(38 ± 2)
PrF <sub>3</sub>	1327-1491	92.9	101 ± 5	(38 ± 2)
NdF <sub>3</sub>	1383-1520	85.7	95 ± 5	36.7 ± 0.8
SmF <sub>3</sub>	1362-1506	96.8	107 ± 5	(45 ± 2)
EuF <sub>3</sub>	1382-1522	92.0	100 ± 5	(43 ± 2)
GdF <sub>3</sub>	1391-1527	90.3	98 ± 5	(41 ± 2)
TbF <sub>3</sub>	992-1167	101.7	111 ± 5	(47 ± 2)
DyF <sub>3</sub>	1002-1170	107.5	115 ± 5	49.4 ± 1.1
HoF <sub>3</sub>	1023-1180	106.8	116 ± 5	49.8 ± 1.1
ErF <sub>3</sub>	1374-1521	111.5	120 ± 5	51.9 ± 1.5
TmF <sub>3</sub>	1273-1415	89.6	99 ± 5	37.7 ± 0.2
YbF <sub>3</sub>	1293-1428	85.5	95 ± 5	35.5 ± 1.0
LuF <sub>3</sub>	1287-1450	96.1	103 ± 5	43.1 ± 0.4

while the break at 12.5 e.v. corresponds to the formation of  $\text{NdF}^+$ -ions by dissociative ionization of  $\text{NdF}_2$ -molecules. The  $\text{NdF}_2^+$ -curve begins at  $5:6 \pm 0.5$  e.v., and has a break at  $13.5 \pm 0.6$  e.v. The latter value agrees with the appearance potential of  $\text{NdF}_2^+$  from  $\text{NdF}_3$  found in the sublimation studies, while it was assumed that  $\text{NdF}_2(\text{g})$  was the neutral precursor for  $\text{NdF}_2^+$ -ions at lower electron energies. The appearance potential curves for barium-containing ions were similar to those reported previously for the  $\text{BaF}_2\text{-Al}$  system (9).

The appearance potential and ionization efficiency measurements have established the presence of Ba, BaF, Nd, NdF,  $\text{NdF}_2$ , and  $\text{NdF}_3$  molecules in the gas phase over a  $\text{BaF}_2\text{-Nd}$  mixture. The relative intensities for Ba- and Nd-containing ions were measured at various temperatures, using low energy electrons, with voltages  $\sim 5$  e.v. above the thresholds. The portion of  $\text{NdF}_2^+$ -ion current corresponding to  $\text{NdF}_3$  molecules was obtained from measurements at 18 e.v. and by applying a correction for  $\text{NdF}_2^+$  from  $\text{NdF}_2(\text{g})$ , assuming a linear increase of the intensity with the electron energy.



Journal of Chemical Physics

Figure 6. Ionization efficiency curves in Nd-Ba-F System

The ion intensities were then used to calculate ion-current analogies of the equilibrium constants for various fluorine-exchange reactions. The equilibria studied are listed in Table III. Here again, the choice of a method for evaluating the reaction enthalpies from the experimental results was limited to the second-law procedure because of the lack of experimental data needed for calculating the thermal functions required in a third-law treatment.

Table III. Equilibrium Reactions in Ba-Nd-F System

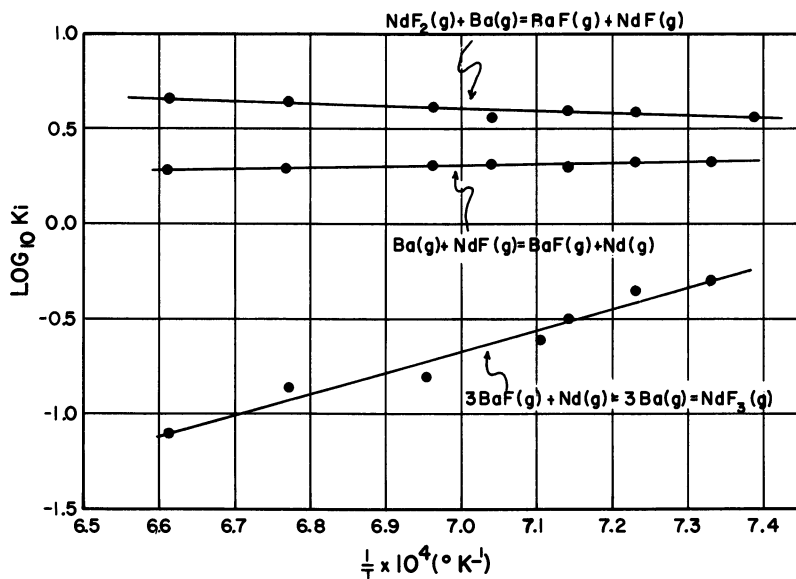
Reaction	T avg. (°K.)	$\Delta H^\circ_T$ kcal. mole <sup>-1</sup>	$\Delta H^\circ_{298}$ kcal. mole <sup>-1</sup>
(1) Ba(g) + NdF(g) = BaF(g) + Nd(g)	1428	-1.96 ± 0.85	-4.0 ± 1.0
(2) 2 BaF(g) + Nd(g) = 2 Ba(g) + NdF <sub>2</sub> (g)	1428	-3.0 ± 0.9	-4.5 ± 1.2
(3) 3 BaF(g) + Nd(g) = 3 Ba(g) + NdF <sub>3</sub> (g)	1428	-43.3 ± 5.0	-46.3 ± 5.0
(4) Ba(g) + NdF <sub>2</sub> (g) = BaF(g) + NdF(g)	1428	5.8 ± 1.7	8.2 ± 2.0
(5) 2 BaF(g) = Ba(g) + BaF <sub>2</sub> (s)	1428	-91.5 ± 3.6	-101.5 ± 3.6
(6) 3 NdF(g) = 2 Nd(g) + NdF <sub>3</sub> (s)	1455	-126.6 ± 5.1	-142.8 ± 5.1
(7) NdF <sub>3</sub> (g) + 2 Nd(g) = 3 NdF(g)	1455	34.0 ± 2.5	43.4 ± 3.0
(8) 2 NdF <sub>3</sub> (g) + Nd(g) = 3 NdF <sub>2</sub> (g)	1455	41.7 ± 2.8	45.2 ± 3.0

The plots of  $\log K_i$  vs.  $1/T$  for the reactions studied are presented in Figures 7, 8, and 9.

The heats of reaction obtained from the slopes of the curves are listed in Table III. Literature data for the heat capacities of Ba(g), BaF(g), BaF<sub>2</sub>(g), and Nd(g) (19), and estimated values for NdF(g), NdF<sub>2</sub>(g), and NdF<sub>3</sub>(g) were employed to calculate the enthalpy increments, ( $H_T - H_{298^\circ\text{K}}$ ). The results, corrected to 298°K., are shown in the last column of Table III.

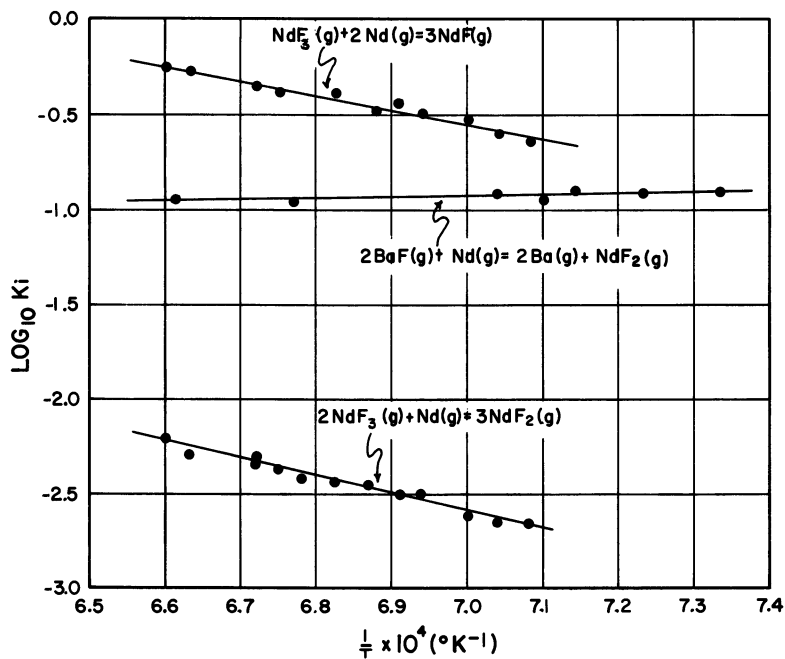
By combining the heat of Reaction 1, Table III, with the dissociation energy of BaF(g),  $D^\circ_{298}(\text{BaF}) = 134.3 \pm 2$  kcal. mole<sup>-1</sup> (10) one obtains  $D^\circ_{298}(\text{NdF}) = 130.3 \pm 3$  kcal. mole<sup>-1</sup> ( $5.65 \pm 0.13$  e.v.). Use of the same procedure with other data from Table III give  $\Delta H_{\text{atom}}[\text{NdF}_2(\text{g})] = 273.1 \pm 5$  kcal. mole<sup>-1</sup> and  $\Delta H_{\text{atom}}[\text{NdF}_3(\text{g})] = 437.4 \pm 10$  kcal. mole<sup>-1</sup>.

**Scandium and Yttrium Subfluorides.** In the experiments for determining the stabilities of Sc- and Y- subfluorides, these metals were heated with CaF<sub>2</sub> in the tantalum Knudsen cell. The appearance potential curves revealed the presence of Sc, ScF, ScF<sub>2</sub>, ScF<sub>3</sub>, and Ca and CaF



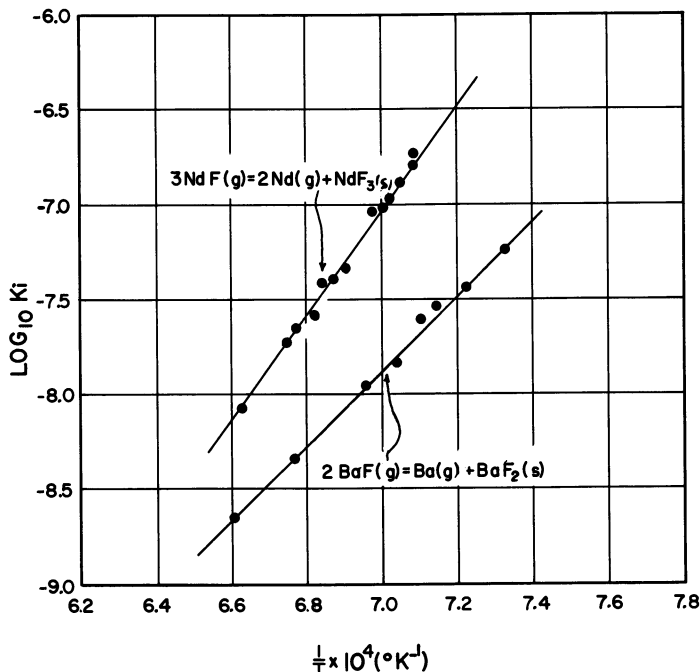
Journal of Chemical Physics

Figure 7. Second-law plots of data for Reactions 1, 3, and 4 (Table III)



Journal of Chemical Physics

Figure 8. Second-law plots of data for Reactions 2, 7, and 8 (Table III)

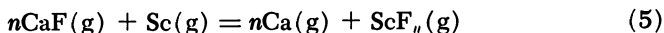


Journal of Chemical Physics

Figure 9. Second-law plots of data for Reactions 5 and 6 (Table III)

in the gas phase over the Sc-CaF<sub>2</sub> mixture, and of YF, YF<sub>2</sub>, YF<sub>3</sub>, and Ca and CaF over the Y-CaF<sub>2</sub> mixture (40).

In the Ca-Sc-F system, three simple fluorine-exchange reactions of the type



where ( $n = 1, 2, 3$ ) were considered. The heats of dissociation of scandium fluorides,  $\Delta H_{\text{atom}}[\text{ScF}_n(g)]$ , were derived from the reaction enthalpies,  $\Delta H^\circ_n$ , and the known dissociation energy of CaF,  $125.0 \pm 2$  kcal. mole<sup>-1</sup> (6):

$$\Delta H_{\text{atom}}(\text{ScF}_n) = -\Delta H^\circ_{n,298} + nD^\circ_{298}(\text{CaF}) \quad (6)$$

Second-law plots for various equilibria in the Ca-Sc-F system are presented in Figure 10, and reaction enthalpies are listed in Table IV.

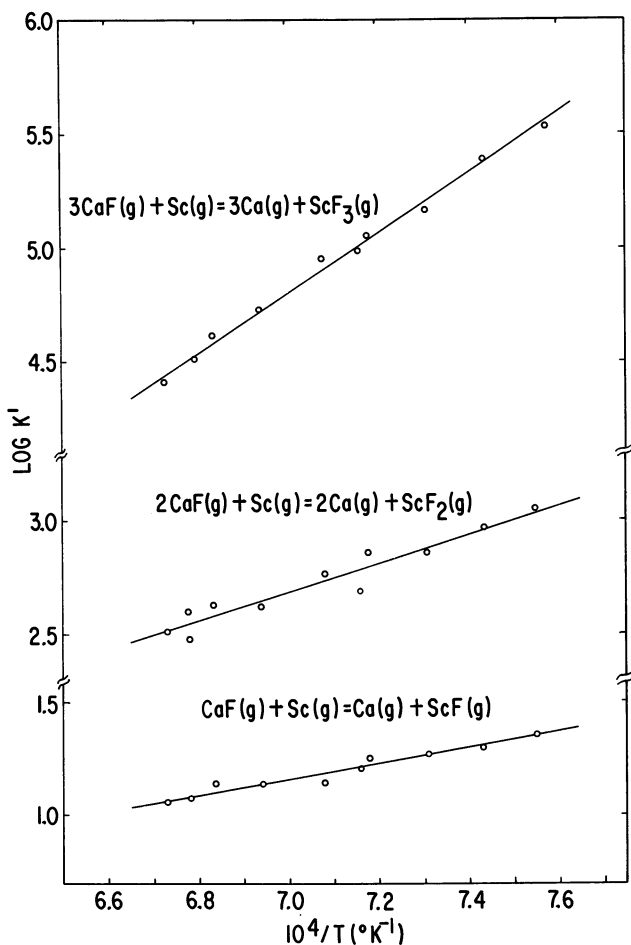
From the values of  $\Delta H_n$ ,  $D^\circ_{298}(\text{CaF})$  and by employing the Reaction 6, the atomization energies of the scandium fluorides are obtained:

$$D^\circ_{298}(\text{ScF}) = 140.8 \pm 3.2 \text{ kcal. mole}^{-1}$$

$$\Delta H_{\text{atom}}[\text{ScF}_2(g)] = 281.1 \pm 6 \text{ kcal. mole}^{-1}$$

$$\Delta H_{\text{atom}}[\text{ScF}_3(g)] = 438.1 \pm 6 \text{ kcal. mole}^{-1}$$

The lack of clear evidence for the existence of  $Y(g)$  species in the effusing vapors over  $Y-CaF_2$  mixtures made impossible a determination of the dissociation energies of yttrium fluorides from direct exchange reactions. As an alternative, use was made of data from fluorine bomb calorimetry which establish  $\Delta H^\circ_f[YF_3(s)] = -410.7 \pm 0.4 \text{ kcal. mole}^{-1}$  (28) and of equilibria which do not include yttrium atoms as reactants. The reactions studied and their enthalpies are given under numbers (d) and (e) in Table IV. The second-law plots of the equilibrium constants are shown in Figure 11.

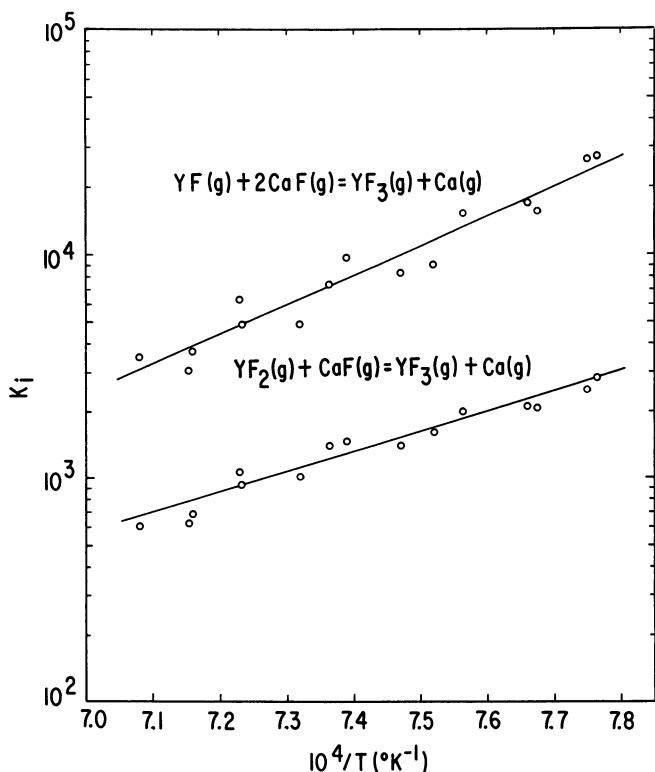


Journal of Chemical Physics

Figure 10. Second-law plots for data on the Sc-Ca-F System

Table IV. Heats of Reactions in Sc-Ca-F and Y-Ca-F Systems

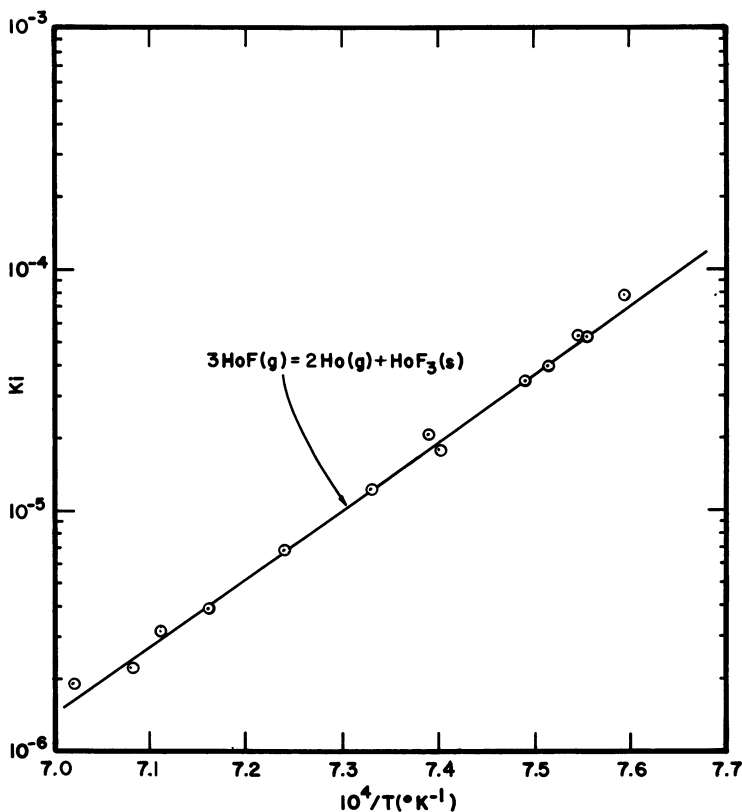
Number	Avg. Temp. (°C.)	Reaction	$\Delta H^\circ_T$ (kcal. mole <sup>-1</sup> )	$\Delta H^\circ_{298}$ (kcal. mole <sup>-1</sup> )
(a)	1410	$\text{CaF(g)} + \text{Sc(g)} = \text{Ca(g)} + \text{ScF(g)}$	$-15.8 \pm 1.2$	$-15.8 \pm 2$
(b)	1410	$2\text{CaF(g)} + \text{Sc(g)} = 2\text{Ca(g)} + \text{ScF}_2\text{(g)}$	$-28.9 \pm 2.6$	$-31.1 \pm 3$
(c)	1410	$3\text{CaF(g)} + \text{Sc(g)} = 3\text{Ca(g)} + \text{ScF}_3\text{(g)}$	$-60.3 \pm 1.7$	$-63.1 \pm 2$
(d)	1337	$\text{YF(g)} + 2\text{CaF(g)} = \text{YF}_3\text{(g)} + 2\text{Ca(g)}$	$-57.3 \pm 3.0$	$-59.7 \pm 5.0$
(e)	1337	$\text{YF}_2\text{(g)} + \text{CaF(g)} = \text{YF}_3\text{(g)} + \text{Ca(g)}$	$-38.5 \pm 3.0$	$-41.3 \pm 5.0$



Journal of Chemical Physics

Figure 11. Second-law plots of data for Y-Ca-F System

From the measured heat of Reaction d, Table IV, and available data for  $D^{\circ}_{298}(\text{CaF})$  (31),  $\Delta H^{\circ}_f(\text{YF}_3)$  (28),  $\Delta H^{\circ}_s(\text{YF}_3)$  (20),  $\Delta H^{\circ}_s(\text{Y})$  (13), and  $D^{\circ}_{298}(\text{F}_2)$  (31), one obtains  $D^{\circ}_{298}(\text{YF}) = 143.6 \pm 5 \text{ kcal. mole}^{-1}$  ( $6.2 \pm 0.2 \text{ e.v.}$ ). Similarly, one obtains from Reaction e the atomization energy of  $\text{YF}_2(\text{g})$ ,  $\Delta H_{\text{atom}}[\text{YF}_2(\text{g})] = 287.0 \pm 7.0 \text{ kcal. mole}^{-1}$ .



Journal of Physical Chemistry

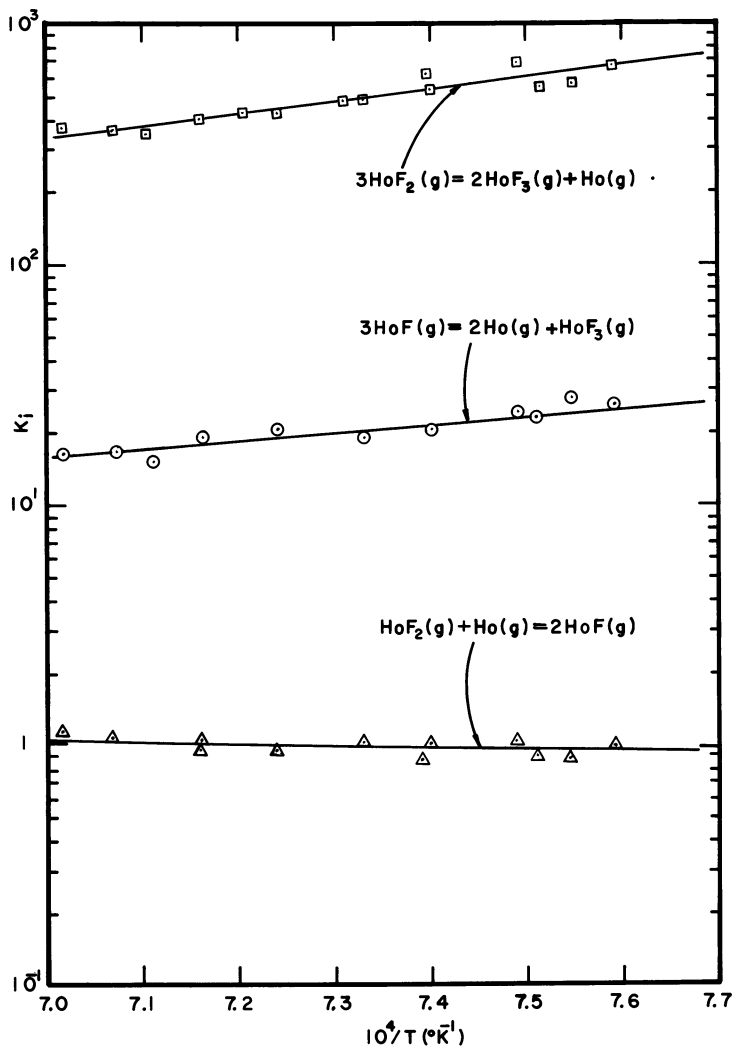
Figure 12. Second-Law Plot of the Mass Spectral Data for the Heterogeneous Reaction  $3\text{HoF}(\text{g}) = 2\text{Ho}(\text{g}) + \text{HoF}_3(\text{s})$

Table V. Equilibria in Ho–HoF<sub>3</sub> System

Avg. T No. (°K.)	Reaction	$\Delta H^{\circ}_T$ (kcal. mole <sup>-1</sup> )	$\Delta H^{\circ}_{298}$ (kcal. mole <sup>-1</sup> )
(1) 1369	$3 \text{ HoF}(\text{g}) = 2 \text{ Ho}(\text{g}) + \text{HoF}_3(\text{s})$	$-127.6 \pm 2.0$	$-141.8 \pm 5.0$
(2) 1369	$3 \text{ HoF}(\text{g}) = 2 \text{ Ho}(\text{g}) + \text{HoF}_3(\text{g})$	$-21.0 \pm 4.1$	$-31.2 \pm 6.0$
(3) 1369	$3 \text{ HoF}_2(\text{g}) = 2 \text{ HoF}_3(\text{g}) + \text{Ho}(\text{g})$	$17.0 \pm 2.3$	$22.0 \pm 5.9$

**Sm, Eu, Gd, Dy, Ho, and Er Subfluorides.** The known heat of formation of  $\text{HoF}_3$  (29) and the relatively high volatility of Ho-metal were crucial in designing experiments to determine the stabilities of Sm, Eu, Gd, Dy, Ho, and Er subfluorides (38, 39).

In the first experiment of this group,  $\text{HoF}_3$  was evaporated in the Knudsen cell in the presence of Ho-metal, and the Ho,  $\text{HoF}$ ,  $\text{HoF}_2$ , and



Journal of Physical Chemistry

Figure 13. Second-Law Plots of Data for Equilibria Involving the Subfluorides of Holmium

HoF<sub>3</sub> species were identified in the vapor through the appearance potential curves for the various ions. The equilibria among various gaseous species which were considered are listed in Table V. The second-law plots of the equilibrium constants are shown on Figures 12 and 13.

The heats of the various reactions and the available data for the  $\Delta H^\circ_f(\text{HoF}_3) = -405.8 \pm 4 \text{ kcal. mole}^{-1}$  (29),  $\Delta H_{\text{sub}}(\text{Ho}) = 70.6 \text{ kcal. mole}^{-1}$  (13),  $\Delta H_{\text{sub}}(\text{HoF}_3) = 116.2 \pm 3 \text{ kcal. mole}^{-1}$  (5), and  $D^\circ_{298}(\text{F}_2) = 37.7 \pm 0.3 \text{ kcal. mole}^{-1}$  (31), yielded  $D^\circ_{298}(\text{HoF}) = 129.6 \pm 3 \text{ kcal. mole}^{-1}$  (5.62  $\pm$  0.13 e.v.) and  $\Delta H_{\text{atom}}[\text{HoF}_2(\text{g})] = 265.4 \pm 8.0 \text{ kcal. mole}^{-1}$ .

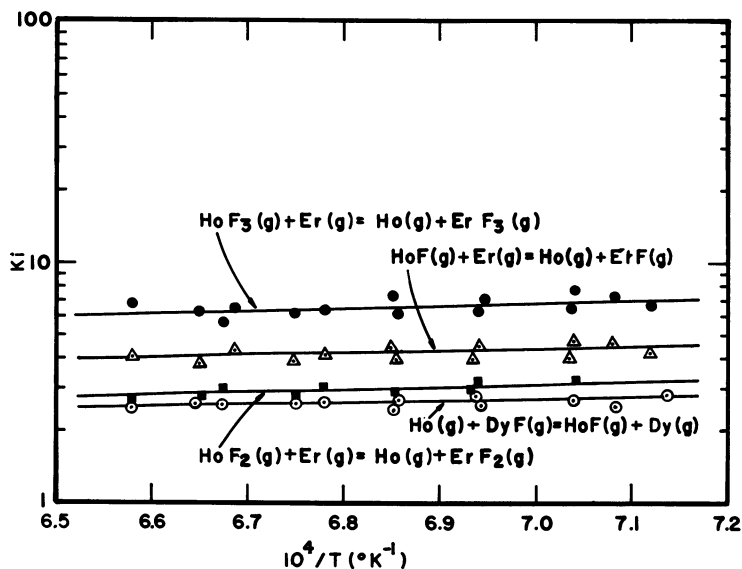
The dissociation energies of Sm, Eu, Gd, Dy, and Er subfluorides were determined from the study of fluorine-exchange reactions of these compounds with holmium:



The heats of these reactions actually represent the differences in the dissociation energies of the subfluorides of Ho and the corresponding element:

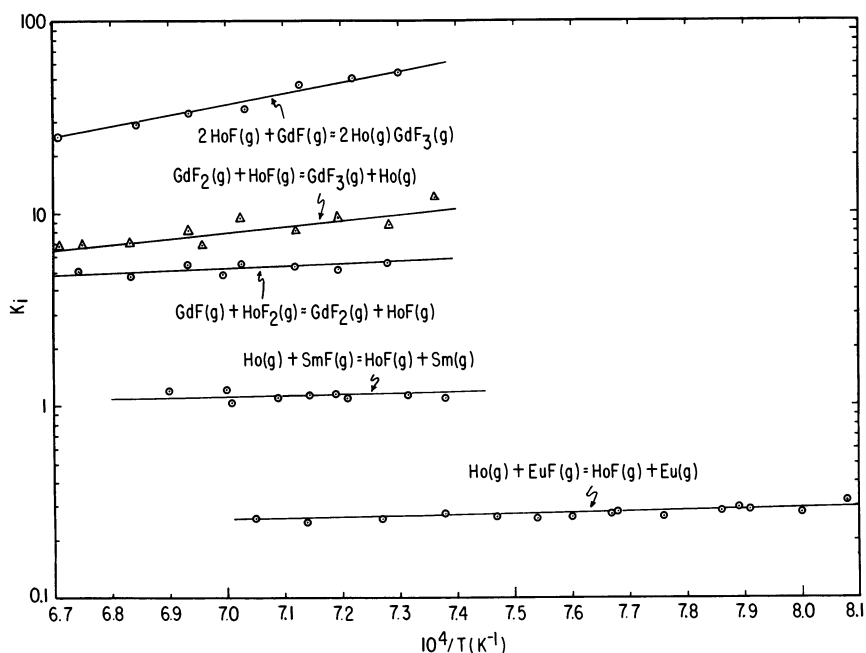
$$\Delta H_n = \Delta H_{\text{atom}}(\text{MF}_n) - \Delta H_{\text{atom}}(\text{HoF}_n) \quad (8)$$

Figures 14, 15, and 16 show the second-law plots of data for various equilibrium reactions, and Tables VI and VII give the heats of reactions.



Journal of Physical Chemistry

Figure 14. Second-law plots of data for exchange reactions between the subfluorides of Ho, Dy, and Er



Journal of Inorganic &amp; Nuclear Chemistry

Figure 15. Second-law plots of data for various equilibria involving subfluorides of Sm, Eu, and Gd

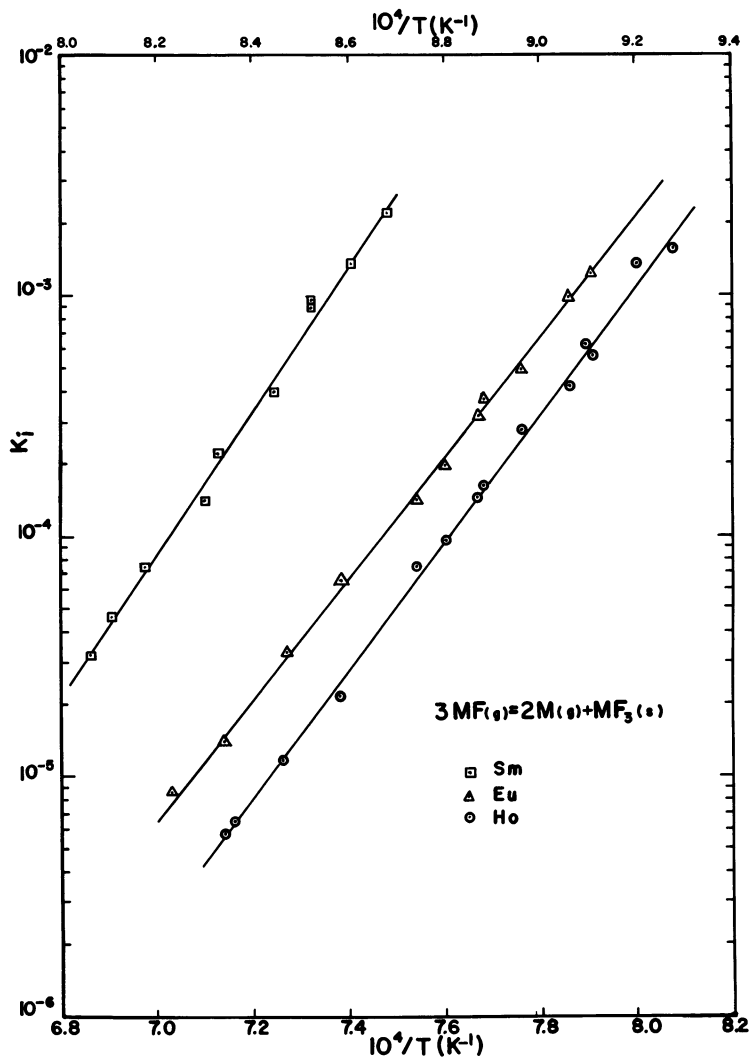
### Conclusions

This mass spectrometric study of the mono-, di-, and trifluorides of scandium, yttrium, lanthanum, and the rare-earth metals illustrates an experimental approach for providing an essentially complete energetic picture of several related systems. Ionization potentials, bond energies, atomization energies, heats of sublimation, and heats of formation are derived from the data and allow one to establish periodic effects across the rare-earth series as successive  $4f$ -electrons are added.

Table VIII lists the ionization potentials of the various atoms, mono- and difluorides. The values of the ionization potentials of the atoms (41) obtained in this work agree within the uncertainty of the experimental measurements with the surface-ionization data (1, 18) and with new spectroscopic data (27, 32).

There have not been any previous data on the ionization potentials of these mono- and difluorides, except for a qualitative indication of low values for the ionization potentials of  $\text{NdF}$  and  $\text{NdF}_2$  as revealed by the formation of  $\text{NdF}^+$  and  $\text{NdF}_2^+$  ions on heated tungsten surface (24).

Probably the most interesting observation about the data in Table VIII is that the ionization potentials of these monofluorides and difluorides are so low—comparable with the free metal atoms. Apparently, the bonding of either one or two fluorines to scandium, yttrium, lanthanum, or a rare-earth leaves outer electrons in orbitals similar to the outer orbitals of alkali or alkaline-earth atoms. A similar phenomenon was reported



Journal of Inorganic & Nuclear Chemistry

Figure 16. Second-law plots for heterogeneous equilibria between fluorides of Sm, Eu, and Ho (Upper scale for Sm-data; lower scale for Eu and Ho-data)

previously (6, 9) for the alkaline-earth monofluorides (MgF, CaF, SrF, and BaF) where only one of the easily ionized electrons is used for bonding and an ionic model, ( $M^+F^-$ ), yields calculated binding energies in excellent agreement with experimental data. One predicts that solid rare-earth subfluorides will be most active chemical reducing agents when they are isolated. Also, a high degree of ionic character is predicted for both the gaseous and condensed subfluorides.

Table IX summarizes the bond strengths for gaseous rare-earth fluorides as calculated from the equilibrium data. One can also calculate these bond energies, in principle, from the appearance potentials, but one must be cautious unless extreme care has been exerted to identify processes that use excess energy to produce excited products or species with kinetic energy. For ground-state species, for example,

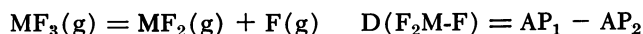
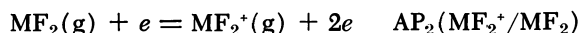
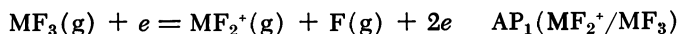


**Table VI. Heats of Reactions Involving Subfluorides of Ho, Dy, and Er**

No.	Avg. $T(^{\circ}K.)$	Reaction	$\Delta H^{\circ}_T$ <i>kcal. mole<sup>-1</sup></i>
(1)	1446	$Ho(g) + DyF(g) = HoF(g) + Dy(g)$	$-2.7 \pm 1.2$
(2)	1446	$Ho(g) + ErF(g) = HoF(g) + Er(g)$	$6.0 \pm 1.0$
(3)	1446	$Ho(g) + ErF_2(g) = HoF_2(g) + Er(g)$	$4.6 \pm 1.4$
(4)	1446	$Ho(g) + ErF_3(g) = HoF_3(g) + Er(g)$	$5.2 \pm 1.6$

**Table VII. Heats of Reactions Involving Subfluorides of Sm, Eu, Gd, and Ho**

No.	Avg. $T$ $(^{\circ}K.)$	Reaction	$\Delta H^{\circ}_T$ <i>kcal. mole<sup>-1</sup></i>	$\Delta H^{\circ}_{298}$ <i>kcal. mole<sup>-1</sup></i>
(1)	1401	$Ho(g) + SmF(g) =$ $HoF(g) + Sm(g)$	$-2.7 \pm 1.4$	$-2.7 \pm 1.4$
(2)	1321	$Ho(g) + EuF(g) =$ $HoF(g) + Eu(g)$	$-3.5 \pm 1.1$	$-3.5 \pm 1.1$
(3)	1401	$3HoF(g) =$ $2Ho(g) + HoF_3(s)$	$-126.2 \pm 2$	
(4)	1187	$3SmF(g) =$ $2Sm(g) + SmF_3(s)$	$-133.4 \pm 3$	
(5)	1321	$3EuF(g) =$ $Eu(g) + EuF_3(s)$	$-115.6 \pm 3$	
(6)	1428	$2HoF(g) + GdF =$ $2Ho(g) + GdF_3(g)$	$-32.6 \pm 2$	$-41.8 \pm 3.2$
(7)	1428	$GdF_2(g) + HoF(g) =$ $GdF_3(g) + Ho(g)$	$-22.1 \pm 4$	$-30.0 \pm 6$
(8)	1428	$GdF(g) + HoF_2(g) =$ $GdF_2(g) + HoF(g)$	$-6.1 \pm 1.1$	$-6.1 \pm 2$

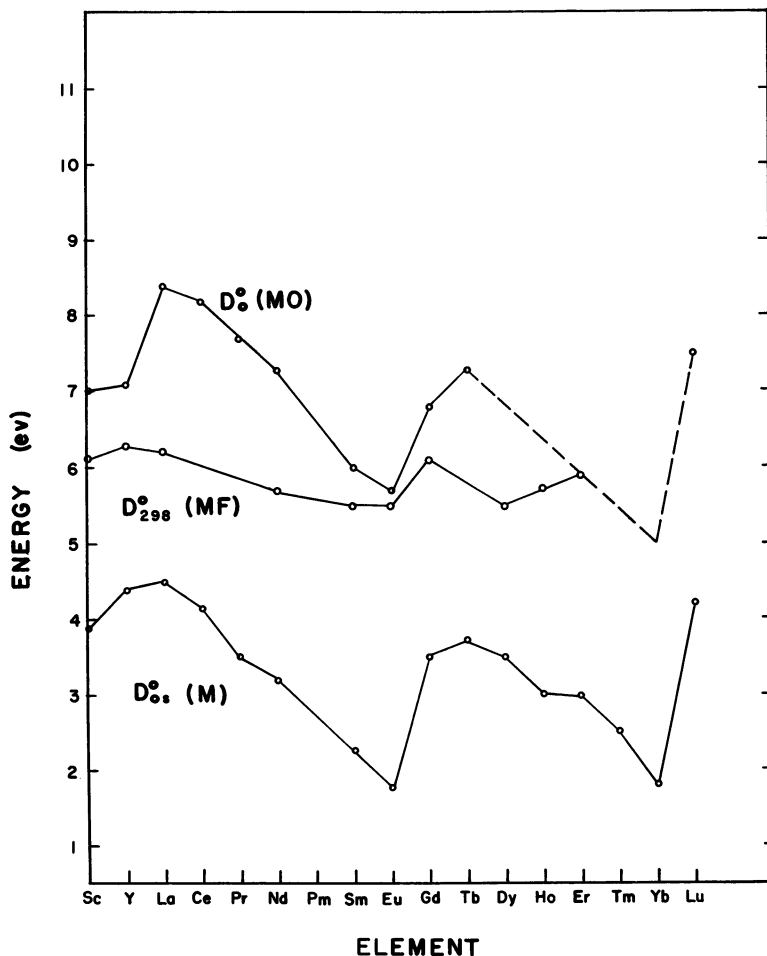


Figure 17. Variation of the dissociation energies of rare-earth monofluorides and monoxides and heats of sublimation of the metals with atomic number

From the available data in Tables I, VII, and IX, one finds several cases where the equilibrium heats and appearance potentials agree within experimental error. When there are discrepancies, one should regard the equilibrium studies as definitive and recognize the possibility of large errors ( $\geq 1$  e.v.) in reaction enthalpies calculated from appearance potential differences.

The variation of the dissociation energies of the rare-earth monofluorides (MF) as a function of atomic number is shown in Figure 17.  $D(\text{MF})$  values are contrasted with the dissociation energies of the rare-earth monoxides and the heats of sublimation of the rare-earth metals.

**Table VIII. Ionization Potentials of the Rare-Earth Metals, Monofluorides and Difluorides<sup>a</sup>**

<i>Element</i>	<i>Ionization Potentials (in electron volts), <math>\pm 0.3</math> e.v.</i>		
	<i>M</i>	<i>MF</i>	<i>MF<sub>2</sub></i>
Sc	6.7	6.5	7.0
Y	6.4	6.3	7.0
La	5.7	6.3	6.8
Ce	6.0	6.5	6.0
Pr	5.6	(6.0 $\pm$ 0.5)	(6.3 $\pm$ 0.5)
Nd	6.0	5.5	6.5
Pm	(5.8 $\pm$ 0.5)	(5.6 $\pm$ 0.5)	(6.5 $\pm$ 0.5)
Sm	5.6	5.7	(6.5 $\pm$ 0.5)
Eu	5.4	5.9	(6.5 $\pm$ 0.5)
Gd	6.0	6.2	6.5
Tb	6.0	(6.1 $\pm$ 0.5)	(6.6 $\pm$ 0.5)
Dy	5.8	6.0 $\pm$	6.7
Ho	5.9	6.1 $\pm$	6.9
Er	6.1	6.3 $\pm$	7.0
Tm	5.9	(6.5 $\pm$ 1.0)	(7 $\pm$ 1)
Yb	5.9	(6.5 $\pm$ 1.0)	(7 $\pm$ 1)
Lu	5.2	(6.5 $\pm$ 1.0)	(7 $\pm$ 1)

<sup>a</sup> The values in parentheses are estimated.**Table IX. Bond Dissociation Energies of Rare-Earth Fluorides<sup>a</sup>**

<i>Element</i>	<i>Bond Dissociation Energy (e.v.)</i>		
	<i>D<sup>o</sup><sub>298</sub>(M-F)</i>	<i>D(FM-F)</i>	<i>D(F<sub>2</sub>M-F)</i>
Sc	6.1	6.2	6.5
Y	6.3	6.5	7.2
La	(6.2 $\pm$ 0.5)	(6.3 $\pm$ 0.5)	(7.1 $\pm$ 0.5)
Ce	(6.0 $\pm$ 0.5)	(6.3 $\pm$ 0.5)	(7.1 $\pm$ 0.5)
Pr	(6.0 $\pm$ 0.5)	(6.2 $\pm$ 0.5)	(7.1 $\pm$ 0.5)
Nd	5.7	6.2	7.1
Pm	(5.6 $\pm$ 0.5)	(6.1 $\pm$ 0.5)	(7.0 $\pm$ 0.5)
Sm	5.5	(6.0 $\pm$ 0.5)	6.8
Eu	5.5	(6.0 $\pm$ 0.5)	6.4
Gd	6.1	6.2	6.9
Tb	(5.8 $\pm$ 0.5)	(6.0 $\pm$ 0.5)	(6.7 $\pm$ 0.5)
Dy	5.5	5.8	6.5
Ho	5.7	5.8	6.5
Er	5.9	5.8	6.5
Tm	(5.9 $\pm$ 0.5)	(5.9 $\pm$ 0.5)	(6.5 $\pm$ 0.5)
Yb	(5.9 $\pm$ 0.5)	(5.9 $\pm$ 0.5)	(6.5 $\pm$ 0.5)
Lu	(5.9 $\pm$ 0.5)	(5.9 $\pm$ 0.5)	(6.5 $\pm$ 0.5)

<sup>a</sup> The values in parentheses are estimated.

As one can see from the figure, there is a similar trend in all three quantities, but with much smaller differences among the extreme values of  $D(\text{MF})$ . Thus, while the differences between the maximum and minimum values in the cases of  $\Delta H^\circ_s(\text{M})$  and  $D^\circ_o(\text{MO})$  range up to 3 e.v., it is lower than 0.8 e.v. for  $D^\circ_{298}(\text{MF})$ .

### Acknowledgment

High temperature research at Rice University is sponsored by the U. S. Atomic Energy Commission, the U. S. Army Research Office, Durham, the National Aeronautics and Space Administration and by the Robert A. Welch Foundation.

### Literature Cited

- (1) Alekseev, N. I., Kaminskii, D. L., *Zh. Tekhn. Fiz.* **34**, 1521 (1964).
- (2) Barrow, R. F., Gissane, W. J. M., LeBargy, R. C., Rose, G. V. M., Ross, P. A., *Proc. Phys. Soc.* **83**, 889 (1964).
- (3) Barrow, R. F., Gissane, W. J. M., *Proc. Phys. Soc.* **84**, 615 (1964).
- (4) Berkowitz, J., Marquart, J. R., *J. Chem. Phys.* **37**, 1853 (1962).
- (5) Besenbruch, G., Charlu, T. V., Zmbov, K. F., Margrave, J. L., *J. Less-Common Metals* **12**, 375, 494 (1967).
- (6) Blue, G. D., Green, J. W., Bautista, R. G., Margrave, J. L., *J. Phys. Chem.* **67**, 877 (1963).
- (7) Carlson, K. D., Moser, K., *J. Chem. Phys.* **46**, 35 (1967).
- (8) Chupka, W. A., Inghram, M. G., *J. Phys. Chem.* **59**, 100 (1955).
- (9) Ehlert, T. C., Blue, G. D., Green, J. W., Margrave, J. L., *J. Chem. Phys.* **41**, 2250 (1964).
- (10) Ehlert, T. C., Blue, G. D., Green, J. W., Margrave, J. L., *J. Chem. Phys.* **41**, 2245 (1964).
- (11) Fox, R. E., *J. Chem. Phys.* **35**, 1379 (1961).
- (12) Gurvich, L. V., Shenyavskaya, E. A., *Opt. Spektroskopiya (USSR)* **14**, 307 (1963).
- (13) Habermann, C. E., Daane, A. H., *J. Chem. Phys.* **41**, 2818 (1964).
- (14) Hauge, R. A., Margrave, J. L., unpublished work (1965-66).
- (15) Huber, E. J. Jr., Head, E. L., Holley, C. E. Jr., *J. Phys. Chem.* **61**, 1021 (1957).
- (16) Huber, E. J. Jr., Matthews, C. O., Holley, C. E. Jr., *J. Am. Chem. Soc.* **77**, 6493 (1955).
- (17) Inghram, M. G., Drowart, J., "Proceedings of an International Symposium on High Temperature Technology," pp. 219-240. McGraw-Hill Book Co., Inc., New York, 1959.
- (18) Ionov, N. I., Mitsev, M. A., *Zhurn. Eksper. Teor. Fiz.* **38**, 1350 (1960).
- (19) Kelley, K. K., *U. S. Bur. of Mines, Bull.* **584** (1960).
- (20) Kent, R. A., Zmbov, K. F., Kana'an, A. S., McDonald, J. D., Margrave, J. L., *J. Inorg. Nucl. Chem.* **28**, 1419 (1966).
- (21) Kent, R. A., Margrave, J. L., *J. Chem. Engr. Data*, to be published (1968).
- (22) Mann, D. E., Ackquista, N., Linevsky, M. J., *Rare Earth Conf., 4th, Phoenix, Arizona*, 1964.
- (23) Margrave, J. L., "Physico-Chemical Measurements at High Temperatures," J. Bockris, J. White, and J. MacKenzie, eds., Butterworths, London, 1959.

- (24) Mitsev, M. A., *Zhurn. Tekhn. Fiz.* **10**, 1621 (1966).
- (25) *Natl. Bur. Stds. Test No. 184128*, July 13, 1965.
- (26) Porter, R. F., Schoonmaker, R. F., *J. Chem. Phys.* **29**, 1070 (1958).
- (27) Reader, J., private communication (1966).
- (28) Rudzitis, E., Feder, H. M., Hubbard, W. N., *J. Phys. Chem.* **63**, 2305 (1965).
- (29) Rudzitis, E., Van Deventer, E., private communication (1965).
- (30) Shenyavskaya, E. A., Gurvich, L. V., Mal'tsev, A. A., *Vestn. Mosk. Univ., Ser. II, Khim.* **4**, 10 (1965).
- (31) Stull, D. R., "JANAF Thermochemical Tables," Dow Chemical Co., Midland, Mich.
- (32) Sugar, J., Reader, J., *J. Opt. Soc. Amer.* **55**, 1286 (1965).
- (33) Trulson, O. C., Hudson, D. E., Spedding, F. H., *J. Chem. Phys.* **35**, 1081 (1961).
- (34) Weltner, W., private communication (1966).
- (35) White, D., Walsh, P. N., Goldstein, H. W., Dever, D. F., *J. Phys. Chem.* **65**, 1414 (1961).
- (36) White, D., Walsh, P. N., Ames, L. L., Goldstein, H. W., "Thermodynamics of Nuclear Materials," pp. 417-440, Intern. At. Energy Agency, Vienna, 1962.
- (37) Zmbov, K. F., Margrave, J. L., *J. Chem. Phys.* **45**, 3167 (1966).
- (38) Zmbov, K. F., Margrave, J. L., *J. Phys. Chem.* **70**, 3379 (1966).
- (39) Zmbov, K. F., Margrave, J. L., *J. Inorg. Nucl. Chem.* **29**, 59 (1967).
- (40) Zmbov, K. F., Margrave, J. L., *J. Chem. Phys.* **47**, 3122 (1967).
- (41) Zmbov, K. F., Margrave, J. L., *J. Phys. Chem.* **70**, 3014 (1966).

RECEIVED December 15, 1966.

# The "Mass" Effect of Electron Multipliers in High Temperature Mass Spectrometric Applications

KARL A. GINGERICH

Battelle Memorial Institute, Columbus Laboratories, Columbus, Ohio

*The electron multiplier gains of  $P^+$ ,  $As^+$ ,  $Sb^+$ ,  $Bi^+$ ,  $Co^+$ ,  $Pr^+$ , and  $U^+$  have been measured relative to that of  $Ag^+$  at constant ion energy under conditions commonly applied in high temperature mass spectrometry. With the exception of the results for  $P^+$ , the relative multiplier gains can be best described as being independent of mass. The deviations from the usually applied "inverse square root of mass" dependence of the multiplier gains are discussed using available literature data and the results of this investigation.*

The application of mass spectrometry to high temperature chemistry has developed during the past decade into one of the most important research techniques for studying the composition of vapors from condensed phases and the corresponding homogeneous and heterogeneous chemical reactions involving the vapor components (12).

For most of the thermochemical calculations, the ion intensities recorded by the mass spectrometer must be correlated with the respective absolute partial pressures. For this purpose it is necessary to calibrate the mass spectrometer to determine the proportionality constant that relates the measured ion current intensities to the corresponding partial pressures. A commonly used method for calibration is to vaporize a known amount of a standard material—*e.g.*, silver (6, 13) that is not reactive with the sample under investigation or with the container and effusion cell material. In such an experiment the calibration constant  $k_i = (IT)_i/P_i$ , which relates effective partial  $P_i$  pressure inside the Knudsen cell and the measured ion intensity  $I_i^+$  at the experimental temperature  $T_i$ , is determined by integrating the ion current with time in the usual way. This method requires knowledge of the relative ionization cross

sections and of the relative gain of the secondary electron multiplier that is commonly used as a detector for the resolved ion beam.

The relation between the known partial pressure  $P_i$  of the calibrating substance  $i$  and the partial pressure  $P_x$  of the vapor species  $x$  measured is given by (13)

$$\frac{P_i}{P_x} = \frac{(I^*T)_i (n\sigma\gamma)_x}{(I^*T)_x (n\sigma\gamma)_i} \quad (1)$$

where  $I^*$  is the measured ion current,  $T$  the absolute temperature,  $n$  the isotopic abundance correction factor,  $\sigma$  the relative ionization cross section, and  $\gamma$  the relative multiplier gain for the mass number of the ionic species measured. This relation shows that an uncertainty in the knowledge of the relative ionization cross section or multiplier efficiency results in a proportionate uncertainty of the corresponding partial pressure.

A set of calculated relative ionization cross sections at 75 e.v. has been given by Otvos and Stevenson (19) for most of the elements. In accounting for relative multiplier gains of monatomic ions, the variation with the mass of the primary ion at the experimental acceleration voltage is frequently estimated according to the suggestions given by Inghram and co-workers (14, 15), which were based on experimental data from alkali ions. The data suggests that at constant ion energy the multiplier gain is inversely proportional to the square root of mass of the isotope investigated. This relation appears to hold specifically for higher masses ( $> 100$  a.m.u.) and lower ion energies (2000-3000 e.v.), where the gain is a linear function of the ion energy. Higatsberger *et al.* (11) found that for the noble gas ions, except helium, the secondary electron emission by impact of ions, which is proportional to the electron multiplier gain, also varied approximately with the inverse square root of mass over the ion energy of 2000-6000 e.v. studied.

Ploch (20), as well as Ploch and Walcher (21) have shown experimentally that for the isotopic pairs  ${}^6\text{Li}$ - ${}^7\text{Li}$ ,  ${}^{20}\text{Ne}$ - ${}^{22}\text{Ne}$  and  ${}^{39}\text{K}$ - ${}^{41}\text{K}$  the secondary electron emission at ion energies between 600-6000 e.v. is within 1% proportional to the velocities of the isotopic ions—*i.e.*, inversely proportional to the square root of mass at constant ion energy. Higatsberger *et al.* (11) found an inverse square root of mass dependence at constant ion energy for the  ${}^{20}\text{Ne}$ - ${}^{22}\text{Ne}$  pair and the isotopic pair  ${}^{36}\text{Ar}$ - ${}^{40}\text{Ar}$ . The data for the krypton, xenon, and mercury isotopes by Higatsberger *et al.* also suggest the validity of the inverse square root of mass relation. In a study of the multiplier gains of the isotopic pairs  ${}^{107}\text{Ag}$ - ${}^{109}\text{Ag}$ ,  ${}^{185}\text{Re}$ - ${}^{187}\text{Re}$ , and  ${}^{203}\text{Tl}$ - ${}^{205}\text{Tl}$ , McKinney (18) also finds that at ion energies of 7000 e.v. the inverse square root of mass dependence applies within the experimental error.

In connection with high temperature mass spectrometric applications Ackerman *et al.* (1, 2) have measured the relative multiplier gains for  $\text{Ne}^+$ ,  $\text{Ar}^+$ ,  $\text{Kr}^+$ ,  $\text{Cu}^+$ ,  $\text{Ag}^+$ , and  $\text{Au}^+$  at ion energies of 4500 e.v. The results for these ions agree fairly well with the suggested inverse square root of mass dependence. From these results they constructed a calibration curve for the "mass dependence" of the multiplier gain. In subsequent publications, Drowart and co-workers have used this calibration curve extensively to estimate the multiplier gains of monatomic ions for which the gain was not measured. De Maria, Goldfinger, Malaspina, and Piacente (7) measured the relative multiplier gains for the ions  $\text{Zn}^+$ ,  $\text{Cd}^+$ ,  $\text{Ag}^+$ ,  $\text{Te}^+$ ,  $\text{Hg}^+$ , and  $\text{Pb}^+$  and found them to be nearly constant.

The present investigation is concerned with the combined mass effect and effect of electronic configuration (often simply referred to as "mass" effect) on the multiplier gain for several singly charged monatomic species. The measurements were made relative to  $^{107}\text{Ag}$  at constant ion energy. The experimental results are compared with measured and predicted literature data. The principal purpose of this contribution is to draw, by using the limited data available, attention to the fact that the "mass" effect in multiplier gain phenomena is not really understood and to stimulate further work on this matter.

### ***Experimental Method and Results***

The mass spectrometers used were  $60^\circ$  sector, 12-inch radius, directional focusing instruments built by Nuclide Analysis Associates that are similar to the one described by Inghram and co-workers (6, 22). The measurements correspond to conditions generally employed in high temperature mass spectrometric investigations in which Equation 1 is applied.

The grid collector and Faraday cup collector, respectively, in the two instruments used for the multiplier gain measurements, as well as the angle of incidence of the ion beam on the first dynode of the electron multiplier were used as supplied by the manufacturer. No attempt was made to study the many factors that enter the multiplier gain phenomena (14, 15). By keeping all experimental conditions constant and by relating the multiplier gain measured for a certain ion directly to that of the  $^{107}\text{Ag}^+$  ion measured in the same experiment, all these factors previously discussed (14, 15) except the contribution of the combined mass-effect and effect of electronic configuration are assumed to cancel out.

The multiplier gains were measured in connection with the study of the vaporization behavior of solids. The silver and the solid to be studied were contained in a Knudsen effusion cell. The silver was evaporated at the beginning of an experimental series, followed by the vaporization of the solid. Experimental details not pertinent to the measurement of the multiplier gain were similar to those previously described (10). Each series for which multiplier gains are presented was taken over a time period of no more than three days. Both instruments were equipped with a 16-stage pie-type electron multiplier that is magnetically shielded

(16, 17). It is similar to the one used by Inghram and co-workers (14, 15) but has Cu-Be dynodes with approximately 2% Be instead of Ag-Mg dynodes with 1.7% Mg. In one instrument used, the relative multiplier gain was measured with a grid-type dual collector similar to that described by Stevens and Inghram (23, 24). Advantages of this method are that grid and multiplier signals are recorded simultaneously, thus avoiding corrections for a drift in the ion intensity, and that a large number of measurements can be made conveniently. Multiplier gain measurements in Knudsen cell mass spectrometric applications, using a grid collector, have been described previously by Berkowitz and Chupka (3).

**Table I. Multiplier Gains at Ion Energies of 7.0 kv. for P<sup>+</sup>, As<sup>+</sup>, Sb<sup>+</sup>, Bi<sup>+</sup>, and U<sup>+</sup> Relative to Ag<sup>+</sup> Using a Grid Collector**

Substance Studied	Ion Measured	No. of Measurements	Average Gain $\gamma \times 10^{-5}$	S.D.	Deviation Factor	
					$\gamma_i / \gamma_{Ag^+}$	$\frac{\gamma_i \times M_i^{1/2}}{\gamma_{Ag^+} \times M_{Ag}^{1/2}}$
Ag + PrSB	Ag <sup>+</sup>	2	9.95	0.18	1.00	1.06
	Sb <sup>+</sup>	10	9.93	1.26		
Ag + TaP	Ag <sup>+</sup>	5	9.02	0.33	1.45	0.78
	P <sup>+</sup>	7	13.10	0.95		
Ag + UP + UO <sub>2</sub>	Ag <sup>+</sup>	7	9.11	0.48	1.39	0.75
	P <sup>+</sup>	22	12.70	0.62		
	U <sup>+</sup>	7	9.13	0.27		
Ag + PrAs	Ag <sup>+</sup>	6	9.06	0.46	1.14	0.95
	As <sup>+</sup>	17	10.35	0.88		
Ag + PrBi	Ag <sup>+</sup>	9	8.55	0.12	0.88	1.22
	Bi <sup>+</sup>	23	7.49	0.27		

In Table I the average values for the multiplier gains of Ag<sup>+</sup> and the monatomic ions investigated in the same experimental series are given together with the number of measurements taken, on which the weighed average was based, and the standard deviation for the average values. The kinetic energy of the ions impinging on the conversion dynode was 7000 e.v. The gains refer to the most abundant isotope of the element measured and have been corrected for the contribution of the other isotopes to the grid current. In the grid correction the mass effect on the multiplier gain for isotopes of the same element was neglected. For Ag<sup>+</sup> measured in connection with the study of PrSb, the error term represents the deviation of the two values from the mean value.

The multiplier gain was found to be constant within the standard deviation. For Ag<sup>+</sup> and P<sup>+</sup> in connection with the UP + UO<sub>2</sub> study, a decrease in multiplier gain with increasing multiplier output contributed significantly to the standard deviation. For Sb<sup>+</sup>, a decrease in gain that was a function of increase in ion current and of time contributed most to the standard deviation.

The accuracy of the measurement of the relative multiplier gains,  $\gamma_i/\gamma_{Ag^+}$  listed in Table I, is estimated to be within 10% for Bi<sup>+</sup> and U<sup>+</sup>, 15% for P<sup>+</sup> and As<sup>+</sup>, and 20% for Sb<sup>+</sup>. In this estimate a possible mass effect on the grid current, that may be caused by the constant setting for the suppressor potentials, was assumed to be small. The product of the multiplier gains with the square root of mass should be constant, if the inverse proportionality of gain with the square root of mass would be valid. These products  $\gamma_i M_i^{1/2}$  divided by  $\gamma_{Ag^+} M_{Ag}^{1/2}$  are listed in Table I as "deviation factors."

In another instrument the multiplier gains were measured similarly to the approach used by Ackerman *et al.* (1, 2) and De Maria *et al.* (7). Instead of measuring the ion current at the transmission grid, a Faraday cup collector was interposed between the final collimating slit and the electron multiplier. This way the current measured at the Faraday cup collector corresponds only to the isotope on which the multiplier is focused. There is, however, no direct record of the multiplier signal while the ion current is measured with the Faraday cup collector and the corresponding multiplier current must be obtained by interpolation, which may introduce an error in case of a drift in ion current during the measurement. In view of the high rate of evaporation at which multiplier gains must be measured, the time required for a single measurement also limits the number of measurements to a few determinations, and thus limits the accuracy obtained.

**Table II. Multiplier Gains at Ion Energies of 5.5 kv. for P<sup>+</sup> and Co<sup>+</sup> Relative to Ag<sup>+</sup> Using a Faraday Cup Collector**

Substance Studied	Ion Measured	No. of Measurements	Average Gain $\gamma \times 10^{-5}$	Deviation Factor	
				$\gamma_i/\gamma_{Ag^+}$	$\frac{\gamma_i \times M_i^{1/2}}{\gamma_{Ag^+} \times M_{Ag}^{1/2}}$
Ag + PrP	Ag <sup>+</sup>	4	3.74 ± 0.05	2.93	1.57
	P <sup>+</sup>	5	10.95 ± 0.75		
Ag + Mo-Co	Ag <sup>+</sup>	3	3.04 ± 0.06	0.98	0.72
	Co <sup>+</sup>	3	2.97 ± 0.07		

The results for Ag<sup>+</sup>, P<sup>+</sup>, and Co<sup>+</sup> are presented in Table II. The error term for the average values of the multiplier gains represents the maximum deviation from the mean value observed. For P<sup>+</sup> a decrease in multiplier gain similar to that for the data obtained for P<sup>+</sup> over UO<sub>2</sub> + UP by the grid method, was observed and accounted for approximately half of the uncertainty. The accuracy of the relative multiplier gain for Co<sup>+</sup> is estimated to be better than 10%, that of P<sup>+</sup> better than 20%. In this estimate the deviation of characteristics of the Faraday cup of the commercial instrument from those of an absolute collector was assumed to have a negligible effect on the relative multiplier gain measured.

For the type of multiplier used, the mass effect of stray magnetic fields on the multiplier gain has been found to be considerably less than

1% for the mass range 232–238 (5) and was in this investigation assumed to be negligible within the error indicated by the standard deviation. The angle of incidence and the position at which the ions impinge on the conversion dynode were kept constant for each instrument. Observations of declining gain with increasing ion current may have been in part caused by changes in surface conditions of the conversion dynode during the measurement. The observed time dependence of multiplier gain for  $Sb^+$  is most likely caused by such an effect.

The observed difference in the relative multiplier gains for  $P^+$  is possibly attributed to the difference in the conditions in the different instruments used, but no explanation can be given for its large size. It should be noted that a similar difference was observed for the  $P_2^+$  gains relative to  $Ag^+$  in measurements that were performed simultaneously with that for  $P^+$  reported in Tables I and II. The  $P_2^+$  values derived from Faraday cup measurements in connection with the study of  $AlP$  (8), which were obtained with the same instrument that was used by De Maria *et al.* (7) but with a reactivated multiplier, agreed with the values for  $P_2^+$  obtained with an instrument having the grid-collector. This agreement for the  $P_2^+$  gains would support the values for  $P^+$  obtained in this investigation with the grid-collector.

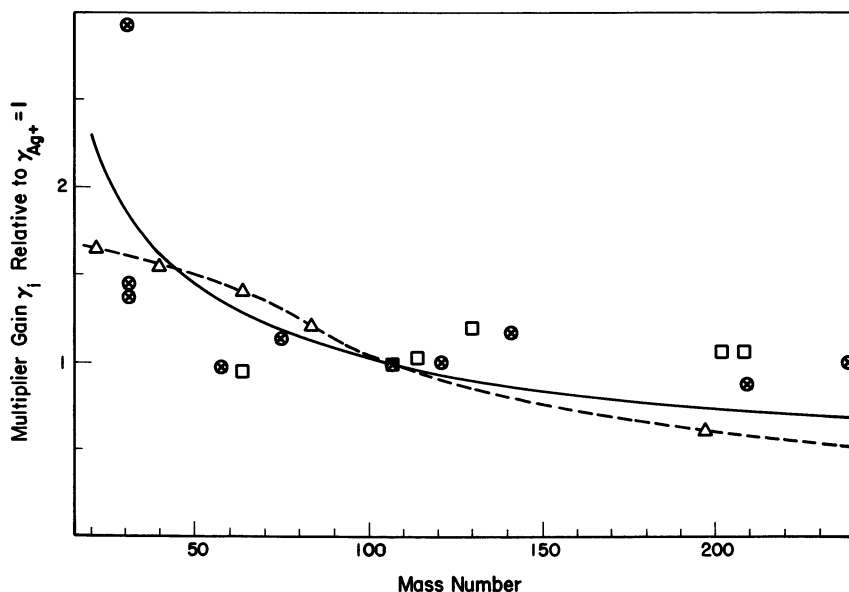


Figure 1. Multiplier gains  $\gamma_i$  relative to  $\gamma_{Ag^+}$  equal to unity, vs. mass number of various unipositive ions  $i$  of different elements

Inverse square root of mass relation —————

$\triangle$  - - - - Data by Ackerman *et al.* (1, 2)

$\square$  Data by De Maria *et al.* (7)

$\otimes$  Data from this investigation

In Figure 1 the relative multiplier gains measured in this investigation are compared with those obtained by Ackerman *et al.* (1, 2) and De Maria *et al.* (7). For comparison all values were normalized with respect to  $\gamma_{\text{Ag}^+}$ . In the normalization the effect of ion energy on the relative multiplier gains has been neglected. Assuming analogy with the results for alkali ions, this would introduce the larger errors for the lowest mass numbers because of their larger deviation from linearity of the multiplier gain with ion energy in the region investigated (14, 15).

The values by Ackerman *et al.* have been reproduced from a graph, which introduced additional uncertainties. It was also assumed that the gains measured by Ackerman *et al.* and by De Maria *et al.* correspond to the most abundant isotope of the respective element. The ion energy used by De Maria *et al.* (7) is assumed to be similar to that used for the AIP study (8)—*i.e.*, constant somewhere between 5000 and 6000 e.v. The solid curve of Figure 1 corresponds to the calculated  $M^{-1/2}$  values relative to the value for  $^{107}\text{Ag}$  equal to one; the dotted line represents the "calibration curve" by Ackerman *et al.*

The multiplier used by Ackerman *et al.* (1, 2) had Ag-Mg dynodes similar to the one used by Inghram and co-workers (14, 15). The multiplier used by De Maria *et al.* was of the same design, with Cu-Be dynodes, as the one used in the present investigation.

Also included in Figure 1 is a single value for  $\text{Pr}^+$  which was measured relative to  $\text{Ag}^+$  using a grid-collector in connection with the investigation of PrAs (*see* Table I). By analogy with the data for  $\text{As}^+$  its accuracy is estimated to be better than 30%.

### Discussion

The results of this investigation show that with the exception of  $\text{P}^+$  the relative multiplier gains at constant ion energy are constant within the accuracy of their determination. This is in agreement with the independent findings of De Maria *et al.* (7) and offers no support for the usually assumed inverse square root of mass dependence. The few values for ions with higher mass number by Ackerman *et al.* on the other hand indicate a somewhat stronger decrease in multiplier gain with increasing mass than is expected from the inverse square root of mass relationship. The deviation from the inverse square root of mass relationship is, however, smaller than 50% (with the exception of the high value for  $\text{P}^+$ ) for all data which are represented in Figure 1.

Since the inverse square root of mass dependence of the multiplier gain at constant ion energy or, more generally perhaps, the velocity dependence at constant electronic configuration has been documented for isotopic ions (11, 18, 20, 21), the effect of the difference in electronic configuration on the multiplier gain may be related to the observed deviation from the inverse square root of mass relation. Generally it may be observed that this deviation appears to be towards larger gain values

for larger masses and smaller values for smaller masses. While the available data are too limited for conclusive proof, this trend appears to be in the direction of a proportionality of the multiplier gain with the ionic volume as was first observed by Ploch for the alkali ions (20).

An influence of the material of the secondary emitting surface on the mass effect is considered unlikely on the basis of studies by Ploch (20). These studies have been performed with a variety of surfaces of different materials. Ploch found that the secondary electron yield varies significantly for different materials and for different states of activation of the same material. No influence of the target material or its state of activation could be detected on the mass effect for the yield of the secondary electron emission. Since the measurements by Ploch did not include exactly the same materials for which results are presented in this paper, the question of an influence of the dynode material on the mass effect of the multiplier gain in mass spectrometric investigations may warrant additional investigation. In this connection, it is interesting to note that in investigations where Ag-Mg dynodes were used as secondary emitting surfaces (1, 2, 14, 15) the inverse square root of mass relationship appears to be verified, whereas in the studies employing Cu-Be dynodes (Ref. 7, this investigation) an independence of the multiplier gain on the mass is indicated for higher mass numbers.

The trend toward lower multiplier gains than would be expected from the inverse square root of mass dependence for monatomic ions with low mass numbers is also apparent from other available data. De Maria *et al.* (8) found the multiplier gains of  $\text{Al}^+$  and  $\text{Hg}^+$  relative to that of  $\text{Ag}^+$  to be 1.12 and 0.58, for ion energies of 5300 e.v. Using a different multiplier at the same ion energy, a gain value of 1.02 for  $\text{Hg}^+$  relative to that of  $\text{Ag}^+$  was found in better agreement with that previously (7) obtained. The low value for  $\text{Al}^+$  is to be noted with respect to the deviation from the square root of mass relationship, while different values for  $\text{Hg}^+$  probably reflect the influence of different multipliers used.

Limited data obtained by Efimenko (9) for the multiplier gains of  $\text{O}^+$ , and  $\text{Be}^+$  relative to that for  $\text{Al}^+$  under the same conditions and with the same instrument as correspond to the data in Table I are 1.64 and 1.13, respectively. Multiplier gain values calculated from the data by Berkowitz and Chupka (4) for  $\text{Cl}^+$ ,  $\text{Br}^+$ , and  $\text{I}^+$  relative to that of  $\text{Mg}^+$  are 0.96, 1.23, and 0.80, respectively. Other relative multiplier gains involving singly charged monatomic ions have been measured by Trulson and Goldstein (25) who found 1.43 and 1.25 for  $\gamma_{\text{B}^+}/\gamma_{\text{Ag}^+}$  and  $\gamma_{\text{Zr}^+}/\gamma_{\text{Ag}^+}$ , respectively, and by Wiedemeier and Gilles (26) who give a value of 1.00 for  $\gamma_{\text{S}^+}/\gamma_{\text{Mn}^+}$ . Most of these values for the ions with masses smaller than 100 mass units tend to be lower than would be expected from the

inverse square root of mass dependence of the multiplier gain but higher than the gains for heavier ions of constant energy.

The information presently available indicates that there is little justification for assuming an inverse square root of mass dependence of the multiplier gain for the unipositive atoms of the various elements of constant energy or for using a calibration curve based on the measurements of a few elements. On the other hand, it appears that using either approach to estimate the relative multiplier gains for ions not measured will rarely lead to an error exceeding 100%.

It is expected that further information on relative electron multiplier gains will become available in the near future since many instruments are equipped for such measurements. If all investigators would give the conditions and the results under which they measure the multiplier gains in the course of their studies, a wealth of experimental material related to this property should become available soon for almost all elements, and this material could serve as a basis for better understanding and developing more accurate means of predicting the magnitude of secondary electron emission as a function of mass and electronic configuration.

### *Acknowledgments*

The experimental part of this work was in part supported under a subcontract of MIT Lincoln Laboratory, which is operated with support from the U.S. Army, Navy, and Air Force, and under AEC Contract No. At(30-1)-2541, both with the Pennsylvania State University. The author gratefully acknowledges the courtesy of the National Bureau of Standards for the use of the mass spectrometer with the grid-type collector in this investigation. The author also wishes to thank J. Efimenko for his help and interest in the mass spectrometric work, C. O. Shopay and H. G. Leonard for their help in the evaluation of the data, and R. J. Yinger and L. A. Cambey for valuable discussions.

### *Literature Cited*

- (1) Ackerman, M., Stafford, F. E., Drowart, J., "Vaporization of Compounds and Alloys at High Temperature," Part I WADD Tech. Rept. 60-782 (1960).
- (2) Ackerman, M., Stafford, F. E., Drowart, J., *J. Chem. Phys.* **33**, 1784 (1960).
- (3) Berkowitz, J., Chupka, W. A., *Ann. N. Y. Acad. of Sci.* **79**, 1073 (1960).
- (4) Berkowitz, J., Marquart, J. R., *J. Chem. Phys.* **37**, 1853 (1962).
- (5) Cambey, L. A., private communication (1966).
- (6) Chupka, W. A., Inghram, M. G., *J. Phys. Chem.* **59**, 100 (1955).
- (7) De Maria, G., Goldfinger, P., Malaspina, L., Piacente, V. (private communication, 1965).

- (8) De Maria, G., Gingerich, K. A., Malaspina, L., Piacente, V. (to be published).
- (9) Efimenko, J., private communication (August 1964).
- (10) Gingerich, K. A., Lee, P. K., *J. Chem. Phys.* **40**, 3520 (1964).
- (11) Higatsberger, M. J., Demorest, H. L., Nier, A. O., *J. Appl. Phys.* **25**, 883 (1954).
- (12) Inghram, M. G., Drowart, J., "High Temperature Technology," p. 219, McGraw-Hill, New York, 1960.
- (13) Inghram, M. G., Chupka, W. A., Porter, R. F., *J. Chem. Phys.* **23**, 2159 (1955).
- (14) Inghram, M. G., Hayden, R. J., Hess, D. C., *U. S. Natl. Bur. Std. Circ.* **522**, 257 (1953).
- (15) Inghram, M. G., Hayden, R. J., *Natl. Acad. Sci. Publ.* **311** (1954).
- (16) Marshall, D. J., Herzog, L. F., *Proc. Ann. Conf. Mass Spectrometry Allied Topics*, 8th, ASTM Committee E-14 (1960).
- (17) Marshall, D. J., Herzog, L. F., *Nuclide Analysis Assoc. Tech. Bull.* **EM-1** (1962).
- (18) McKinney, C. R., Maynes, D., *Proc. Ann. Conf. Mass Spectrometry Allied Topics*, 11th, ASTM Committee E-14, p. 403 (1963).
- (19) Otvos, J. W., Stevenson, D. P., *J. Am. Chem. Soc.* **78**, 546 (1956).
- (20) Ploch, W., *Z. Physik* **130**, 174 (1951).
- (21) Ploch, W., Walcher, W., *Rev. Sci. Instr.* **22**, 1028 (1951).
- (22) Porter, R. F., Schissel, P., Inghram, M. G., *J. Chem. Phys.* **23**, 339 (1955).
- (23) Stevens, C. M., Inghram, M. G., *Rev. Sci. Instr.* **24**, 987 (1953).
- (24) Stevens, C. M., Inghram, M. G., "Mass Spectrometer for Routine Solid Analysis," ANL-5251 (1954).
- (25) Trulson, O. C., Goldstein, H. W., *J. Phys. Chem.* **69**, 2531 (1965).
- (26) Wiedemeier, H., Gilles, P. W., *J. Chem. Phys.* **42**, 2765 (1965).

RECEIVED October 11, 1966.

# Application of Time Resolved Mass Spectrometry to Problems in High Temperature Chemistry

R. T. MEYER and L. L. AMES<sup>1</sup>

Sandia Laboratory, Albuquerque, N. M.

*Pulse heating and time resolved mass spectrometry were applied to the Langmuir vaporization of Ag, Zr, ZrO<sub>x</sub> and ZrO<sub>y</sub>N<sub>z</sub> at temperatures up to 2100°K. Numerical evaluation of "action" integrals permitted temperature-time measurements and identification of the  $\alpha$  to  $\beta$  transition for Zr. Vapor species identified were Ag, Zr, ZrO, ZrO<sub>2</sub>, N and N<sub>2</sub>. The relative ion intensities for ZrO<sub>2</sub><sup>+</sup> and ZrO<sup>+</sup> from air-oxidized Zr suggest that the Langmuir coefficient for ZrO is lower than for ZrO<sub>2</sub>. The mechanism of Zr combustion in N<sub>2</sub> + O<sub>2</sub> mixtures was explored by analysis of picomole quantities of gas contained in zirconia sacs, which are a product of the reaction. Nitrogen was the only gas detected. A nitrogen-release mechanism is suggested.*

**T**ime resolved mass spectrometry is becoming increasingly important as a research probe of chemical and physical phenomena. It has been widely applied to kinetic studies of shock wave initiated gaseous decompositions (6, 7, 9, 23, 33). Recently, it has been developed in our laboratory for the detection and analysis of fast gas phase reactions induced by flash photolysis (18, 19). Several investigators are also developing the technique for the study of flash and laser pyrolysis of elements (37, 39), plastics (8), and celluloses (15). We are now expanding the technique to studies of the high temperature chemistry of the refractory metals and their binary and ternary alloys and compounds with oxygen and nitrogen.

<sup>1</sup> Permanent Address: Department of Chemistry, New Mexico State University, Las Cruces, N. M.

The applications include: (1) thermodynamic measurements at temperatures greater than 2000°K., (2) vaporization kinetics, and (3) refractory metal combustion studies. In their present form, the first two involve vapor species identification and vapor pressure measurements in transient high temperature experiments, in which vapor density, temperature, and time are measured simultaneously. The third application involves the analysis of picomole quantities of gas contained in thin-walled oxide sacs, which are a product of flash heating metal droplets in oxidizing atmospheres (21).

The purpose of this paper is to describe the experimental techniques that are being developed and the preliminary results and implications. The latter are necessarily qualitative since only exploratory experiments have been performed. This is particularly true of the vaporization thermodynamics and kinetics research. The gas analyses for the refractory metal combustion studies are more advanced since the present mass spectrometry application has been preceded by several other directly related investigations.

The following discussion is divided into two principal sections. The first section (Vaporization Thermodynamics and Kinetics) combines the procedures and results for applications (1) and (2). The second section (Refractory Metal Combustion) describes application (3). The first two applications actually make use of the time resolving capability of the mass spectrometer during a transient high temperature experiment. The third application relies upon the fast response of the spectrometer for analyzing small but kinetically stable samples of gas at ambient temperature.

### *Vaporization Thermodynamics and Kinetics*

The principal advantages offered by time resolved mass spectrometry and pulse heating techniques are as follows: (1) both pulsed resistive and laser heating permit the attainment of temperatures greater than can be practically achieved by steady-state methods such as electron bombardment, direct current resistive, or radio-frequency induction; (2) reaction of the sample substance with supporting or containing materials is minimized or eliminated; (3) heat losses during heating are not appreciable; (4) vapor densities can be recorded as a function of temperature during a single transient experiment; and (5) the appearance of various vapor species, such as monomers, dimers, etc., can be observed as a function of time. Other special features of the pulse heating method have been cited by Baxter (1), Parker (32), and Cezairliyan (2).

It should be possible to obtain information on both nonequilibrium and equilibrium vaporization at temperatures appropriate to practical problems in ablation and reentry heating. The kinetic studies may provide

fundamental data pertinent to a surface-diffusion-controlled vaporization mechanism.

At present, our experimental efforts in high temperature chemistry are directed toward the thermodynamics and kinetics of the refractory metals, and their alloys with oxygen and nitrogen. The work to be described herein consists of preliminary studies on the vaporization of Zr,  $ZrO_x$ , and  $ZrO_yN_z$ . Some qualitative observations on Ag are also reported.

**Principles of Operation.** Langmuir vaporization conditions, pulsed resistive heating of wire samples, fast response temperature measurement, and time resolved mass spectrometry have been employed in the present investigation. The Langmuir vapor pressure  $P_L$  is given by

$$P_L = \frac{1}{S} \frac{dW}{dt} \left( \frac{2\pi RT}{M} \right)^{1/2} \quad (1)$$

where  $\frac{dW}{dt}$  is the steady-state rate of evaporation (weight loss) of a species of molecular weight  $M$  into a vacuum from a surface area  $S$  at temperature  $T$ . The Langmuir pressure is related to the equilibrium vapor pressure  $P_{eq}$  through the Langmuir sublimation coefficient  $\alpha_L$ :

$$P_L = \alpha_L P_{eq} \quad (2)$$

Chupka and Inghram (3) have shown that the mass spectrometer ion intensity  $I^+$  is related to the partial pressure of a vaporizing species by

$$I^+ = \frac{kP_L}{T} \quad (3)$$

where  $k$  is the calibration constant for the apparatus; further, a plot of  $\ln(I^+ \cdot T)$  vs.  $1/T$  yields  $-\Delta H_v/R$  from the slope where  $\Delta H_v$  is the heat of vaporization, if  $\alpha_L$  is independent of temperature. If  $\alpha_L$  is temperature dependent, the value of  $\Delta H_v$  obtained will be different from the true thermodynamic equilibrium value:

$$\Delta H_{v,L} = \Delta H_{v,eq} + \Delta H_v^* \quad (4)$$

where  $\Delta H_v^*$  is an activation enthalpy for vaporization. It can be shown that the Langmuir coefficient is a function of both an enthalpy and an entropy of activation:

$$\alpha_{L,T} = e^{-\frac{\Delta H^*}{RT}} \cdot e^{\frac{\Delta S^*}{R}} \quad (5)$$

Temperature dependent studies of  $\alpha_L$  will provide values of  $\Delta H^*$  and  $\Delta S^*$ , which should be useful in probing the mechanism of vaporization from a surface.

More direct information on vaporization kinetics may possibly be obtained from time resolved measurements of the growth of the vaporization rate to a steady state value. In principle this would be accomplished by subjecting the sample to a rectangular temperature pulse and observing the vapor density  $n$  as a function of time to give:

$$\frac{dn}{dt} = k(T, S, C), \quad (6)$$

where  $k$  may be a function of temperature  $T$ , surface structure  $S$ , and composition  $C$ .

Two methods of temperature measurement are being utilized: integration of the energy dissipated during the resistive heating pulse; and fast response optical pyrometry. The former method involves evaluation of experimental and theoretical "action" integrals, which are defined, respectively, as:

$$G_e = \int_0^t i^2 dt, \quad (7)$$

and

$$G_{th} = \frac{d_0 A_0^2}{M} \int_{T_0}^{T_1} \frac{\delta \cdot C_p}{\rho} dT + \left( \frac{d \cdot A^2 \cdot \Delta H_t}{M \rho_t} \right)_{T_1} + \frac{d_0 A_0^2}{M} \int_{T_1}^{T_2} \frac{\delta \cdot C_p}{\rho} dT \quad (8)$$

where  $i$  = current,  $C_p$  = heat capacity,  $\rho$  = resistivity,  $\Delta H_t$  = enthalpy of isothermal transition,  $\rho_t$  = averaged resistivity for transition state,  $d_0$  = density at initial temperature  $T_0$  (usually 300°K.),  $A_0$  = cross sectional area at  $T_0$ ,  $\delta$  = thermal expansion correction factor =  $l/l_0$  (ratio of linear dimension at  $T$  and  $T_0$ ), and  $M$  = molecular weight.

Tucker (36) and Cnare (5) have applied the action integrals successfully to the analysis of exploding metal wires. If the heat capacity, resistivity, and thermal expansion are known as a function of temperature, one needs only to integrate Equation 8 numerically to obtain  $G_{th}$  vs.  $T$ . Then an experimental measurement of filament current as a function of time provides  $G_e$  vs.  $t$ . Correlation of equivalent values of  $G_e$  and  $G_{th}$  gives the desired temperature vs. time dependence for the pulse heated filament. Radiative, conductive, and vaporization heat losses are negligible for energy pulses shorter than 1 msec. duration (1, 2, 32). The calculated action integral  $G_{th}$  is independent of the wire length but is dependent upon the cross-sectional area. Therefore, a measurement of the actual length of wire being heated is not required.

The fast response pyrometry is based on multicolor ratio methods reported by Mayfield (16) and Kottenstette (14). Planck's radiation law for monochromatic emissive power  $e_\lambda$  is

$$e_\lambda = \epsilon(\lambda) C_1 \lambda^{-5} [\exp(-C_2/\lambda T) - 1]^{-1} \quad (9)$$

where  $\epsilon(\lambda)$  is the spectral emissivity,  $C_1 = 4\pi c^2 h$  and  $C_2 = ch/k$ . For  $\lambda T$  products equal to or less than  $4 \times 10^3 \mu \cdot ^\circ\text{K}$ ., the above equation is well approximated by Wien's radiation formula:

$$e_\lambda = \epsilon(\lambda) C_1 \lambda^{-5} \exp(-C_2/\lambda T). \quad (10)$$

The ratio of power emitted at any two wavelengths is then given by

$$R = \frac{e_{\lambda_1}}{e_{\lambda_2}} = \frac{\epsilon(\lambda_1) \cdot \lambda_2^5}{\epsilon(\lambda_2) \cdot \lambda_1^5} \exp \left[ \frac{C_2}{T} \left( \frac{1}{\lambda_2} - \frac{1}{\lambda_1} \right) \right], \quad (11)$$

or

$$\ln R = \frac{A}{T} + B. \quad (12)$$

Calibration of the detectors against a blackbody source at known temperatures provides a determination of the constants A and B, which include correction factors for the finite bandwidth and spectral responsivity of the detectors. In the cases of a true blackbody or a greybody,  $\epsilon(\lambda_1) = \epsilon(\lambda_2)$  which simplifies the analysis. In a practical situation, however,  $\epsilon(\lambda)$  will not be constant with wavelength or temperature. Multicolor ratio pyrometry allows one to estimate this effect, since two or more ratio measurements will yield different temperatures if  $\epsilon(\lambda_1)$  and  $\epsilon(\lambda_2)$  are not approximately equal. The multicolor technique has the advantage that neither the absolute magnitude nor the temperature dependence of  $\epsilon(\lambda)$  is required to obtain an estimate of temperature.

A one-color ratio method is useful for experiments in which temperature varies rapidly with time,  $t$ . It is applicable if  $\epsilon(T)$  does not vary significantly for the temperature range being monitored ( $\epsilon(T_1) \simeq \epsilon(T_2)$ ) and if a temperature calibration point is available at some point in the heating pulse. The one-color ratio is defined from Equation 10 as

$$r(t_1, t_2) = \frac{e_{T_1(t_1)}}{e_{T_2(t_2)}} = \frac{\epsilon(T_1)}{\epsilon(T_2)} \exp \left[ \frac{C_2}{\lambda} \left( \frac{1}{T_2} - \frac{1}{T_1} \right) \right]. \quad (13)$$

The calibration point may be any identifiable phase transition, such as melting or a crystal structure change. In the event the emissive power does not change significantly or detectably at the transition, a correlation in time between the photodetector and action-detector records may provide the location of the transition.

**Experimental Techniques.** The time resolving mass spectrometer is basically the same apparatus which has been described for our gas phase flash photolysis experiments (18, 19). The operation will be briefly reviewed. The modifications required for the pulsed, resistive heating of samples are added.

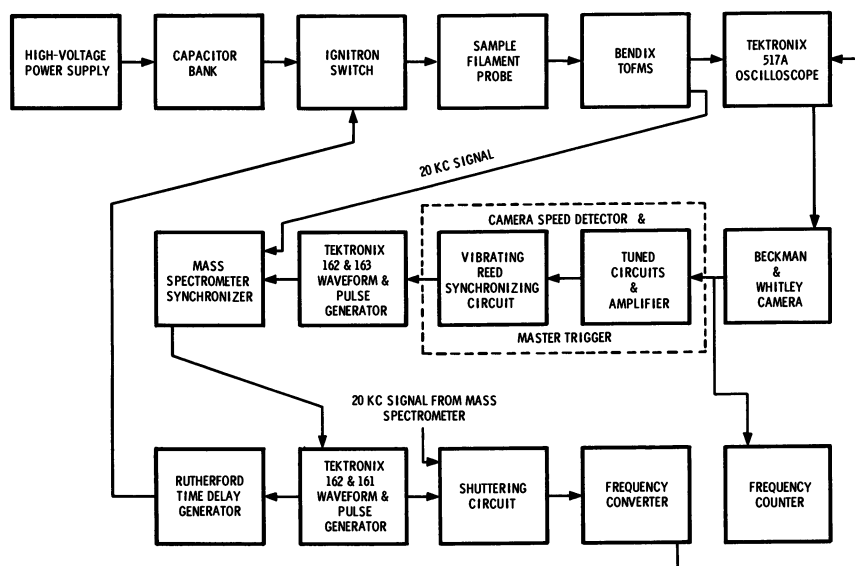


Figure 1. Block diagram of synchronized pulsed filament and mass spectrometer apparatus

A block diagram is presented in Figure 1. A capacitor-discharge energy source has been operated at 52.5  $\mu\text{f.}$ , 287  $\mu\text{h.}$ , and voltages up to 1.5 kv. This source provides a total discharge time of 385  $\mu\text{sec.}$  Current viewing resistors and voltage dividers provide an oscilloscope record of the time-dependent filament current and voltage pulses. A Bendix model 843A inlet probe provides the physical and electrical support for the filaments and the means of locating the sample within 6 mm. of the ion source electron beam (Figure 2). Pulsed heating of the filament generates a pulse of vapor which has a direct path to the ionization zone.

A Bendix model 14-101 time-of-flight mass spectrometer is utilized (38). The essential components of the spectrometer are an electron gun which ionizes the neutral molecules, an ion gun which focuses and accelerates the ions, a drift tube which mass resolves the ions by means of their time of flight, and an electron-multiplier detector which converts the ion bunches into electrical signals. It is the pulsed operation of the spectrometer at a 20-kHz frequency which provides the time resolving capability of the apparatus. The electron gun is operated with a pulse width of 1.4  $\mu\text{sec.}$  and produces a trap current in excess of 25  $\mu\text{A.}$  at 70 ev. The electron beam can be turned off to observe ions produced at the sample filament by surface ionization.

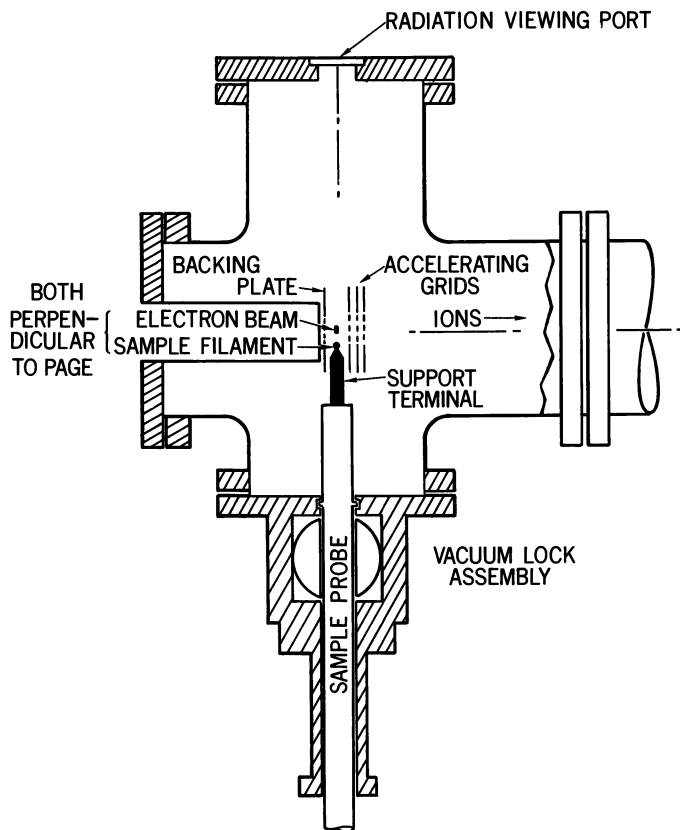


Figure 2. Geometry of sample probe and Bendix TOF mass spectrometer ion source

A Tektronix 517A oscilloscope displays the ion intensity *vs.* mass coordinates of the mass-spectral analysis. Complete mass-spectral patterns are displayed successively every 50  $\mu\text{sec.}$  before and after the single capacitor-discharge energy pulse. A Beckman and Whitley model 364-2 oscillographic drum camera time-resolves these scope traces and permanently records them on a strip of 35-mm. Agfa Isopan Record film (20). Total writing time can be varied from 6 msec. to 50 msec.

In addition to the drum camera, a more convenient data recording method involves Polaroid photographs of a number of superimposed mass spectra displayed on a Tektronix 545 oscilloscope. The number of traces displayed is controlled by the duration of the shuttering circuit gate pulse. The time delay between the start of the heating pulse and the first trace is varied by the time-delay generator. Normally, ten traces are recorded starting at 300  $\mu\text{sec.}$  and ending at 800  $\mu\text{sec.}$ , or starting at 1450  $\mu\text{sec.}$  and ending at 1950  $\mu\text{sec.}$

The partial vapor pressure sensitivity of the spectrometer for each cycle of operation has not been measured directly for the sample filament

and ion source geometry of Figure 2. It may be estimated, however, from the known spectrometer relative sensitivity and from an assumed molecular density distribution. From previous isotope abundance and ion intensity statistical fluctuation measurements (19), it had been determined that approximately 100,000 ions per cycle (every 50  $\mu$ sec.) could be produced, transmitted and detected. The relative sensitivity of 1 part per 100,000 was obtainable when an argon sample at 10.0 torr (300°K.) was expanded through a 0.051-mm. diameter gold orifice, located 3.3 mm. from the center of the ionizing electron beam. According to flow expansion analyses provided by Sherman (35) and by Diesen (6), the molecular density  $n_r$  along the centerline of an expanding jet of monatomic gas is given by the expression

$$n_r = 0.15 n_o (D/x)^2 \quad (14)$$

where  $x$  is the distance from the orifice to the ionization zone,  $D$  is the diameter of the orifice and  $n_o$  is the density on the high pressure side of the orifice. Thus, the limiting sensitivity at the ionization zone was  $1.1 \times 10^8$  atoms/cc. For the present situation of a vaporizing sample inside the spectrometer ion source, it is necessary to estimate the minimum vapor density required at the sample surface to produce a density of  $10^8$  molecules/cm.<sup>3</sup> at the ionization zone. Three possible geometrical distributions for the molecular density with distance  $d$  can be considered, depending upon the relative sizes of the sample surface and the effective area of the ionization zone. The density will be proportional to  $1/d^2$ ,  $1/d$  or  $1/1$ , according to whether the sample resembles a point source, an infinite wire, or an infinite plane, respectively. The size of the ionization zone is about 1.5 mm.  $\times$  10 mm. In the present operation, a wire with a typical radius of 0.125 mm. and a length of 10 mm. is located 6 mm. from the ionization zone. The longer dimensions of the wire and the zone are parallel. For this geometry, the density-distance dependence is probably intermediate between  $r^2/d^2$  and  $r/d$ , where  $r$  is the wire radius. Thus, the minimum vapor density required at the sample surface is between  $2.6 \times 10^{11}$  and  $5.5 \times 10^9$  molecules/cc. Since it is possible to utilize metal ribbons for samples, whose dimensions are equal to or greater than the ionization zone, we feel that the lower value is a valid representation of the spectrometer sensitivity. For a vapor at 2000°K., this density corresponds to a vapor pressure sensitivity of  $1 \times 10^{-6}$  torr. A demonstration of sensitivity is quoted later in this paper.

**Sample Preparation.** The samples consisted of 1-cm. lengths of wire ranging in diameter from 0.125 to 0.50 mm. The wire was strung over the sapphire insulators at the top of the stainless steel support terminals of the Bendix model 843A probe and fastened with screws for electrical contact. After mounting, the wire and support terminals were degreased in  $\text{CHCl}_3$  and  $\text{CH}_3\text{OH}$  baths and cleaned in an appropriate acid solution. The zirconium was ultra-high purity, triple zone refined (MRC Manufacturing Corp.). The silver wire was 99.9% pure (Handy and Harmon).

Oxygen and nitrogen alloys of the zirconium were crudely prepared by both d.c. and capacitor-discharge heating in an atmosphere of air. The degree of oxidation and nitridation was estimated by measuring the change in electrical resistance of the sample. Partial reaction corresponded to a change from 0.14 ohm (pure Zr) to 0.3 to 0.5 ohm. More

complete oxidation toward a  $ZrO_2$  stoichiometry was recognized by an actual burning of the sample and a resistance increase to 10 to 100 ohms. Techniques for preparation of controlled compositions are presently being developed.

Serious experimental complications have been encountered in the studies. These are mentioned here for two reasons. First, it is hoped that other individuals contemplating this line of research will benefit from our early experience. Second, it will provide an understanding of why the results reported herein are only qualitative.

Upon dissipating an energy pulse through a filament wire (Ag, Zr, or W), a large vapor pulse of hydrocarbon contamination was released from the filament surface and from surrounding surfaces. Time resolved mass spectra revealed that the hydrocarbon vapor generated rapidly as the filament was heated and decayed as the filament cooled radiatively. Neither organic solvent degreasing or acid cleaning of the wire substantially reduced the amount desorbed. Direct current heating of the filament at high temperatures under vacuum ( $5 \times 10^{-8}$  torr) prior to the capacitor-discharge showed some desorption but did not significantly help. Rapid, consecutive capacitor-discharges within 30 seconds of each other gave a substantial five-fold reduction in contamination between the first and second discharges. Most of the results presented in this paper were obtained in this way.

The high level of hydrocarbon contamination created two basic problems. The mass range below about 85 amu was completely masked, preventing identification of other vapor species. Second, the large impurity vapor pulse reduced the effective spectrometer sensitivity. In some cases, the vapor pulse was so large that arcing occurred between the ion accelerating grids, and the spectrum was lost for many milliseconds.

It appears that the source of wire contamination was hydrocarbon contamination (pump oil, etc.) in the spectrometer. The spectrometer pressure ( $5 \times 10^{-8}$ ) was sufficiently high to allow surface equilibration with the chemically cleaned or flash heated wire within a few seconds. Various techniques are being explored to reduce this contamination interference.

**Experimental Results and Discussion.** TEMPERATURE MEASUREMENT. The method of determining the temperature of a wire as a function of time by calculation of the action integrals has been discussed. Figure 3 shows the voltage and current waveforms of a capacitor-discharge heating pulse through a 0.25-mm. diameter Zr wire. It is noted that the current waveform exhibits a smooth shape while the voltage waveform shows a large step-like decrease in voltage at 175  $\mu$ sec. This abrupt decrease in voltage is believed to be caused by the  $\alpha$  to  $\beta$  transition of Zr metal, which is accompanied by a relatively large decrease in electrical resistivity. The ratio of resistance just before the transition to just after it, calculated from the current and voltage waveforms, is 1.15; this compares favorably with the value 1.17 obtained from the resistivities for the  $\alpha$  and  $\beta$  phase at the transition temperature tabulated by Goldsmith *et al.* (11). The reason the current waveform is unaffected by the transition is that the resistance of the wire is small compared with the total impedance of the discharge circuit.

Figure 4 shows the effect on the time position of the  $\alpha$  to  $\beta$  transition produced by a variation of the charging voltage while using a fixed

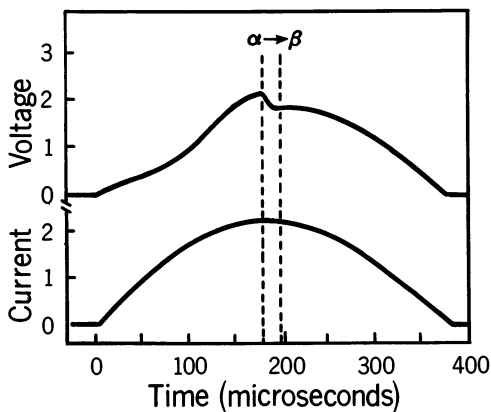


Figure 3. Voltage and current waveforms from a capacitor-discharge pulse through a 0.25-mm. diameter zirconium wire

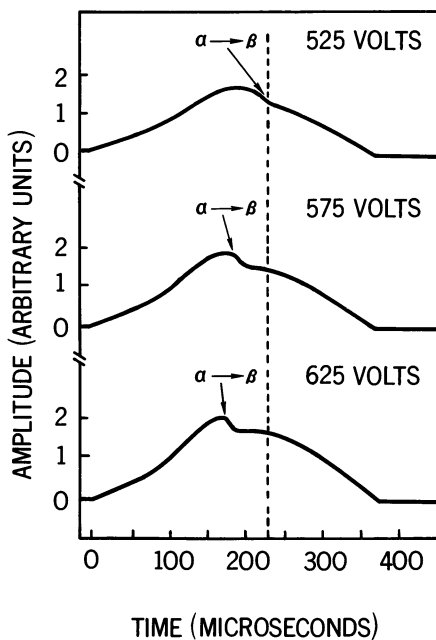


Figure 4. Voltage waveforms showing the change in the time position of the zirconium  $\alpha$  to  $\beta$  transition by a variation of the capacitor charging voltage

capacitance. The higher current caused by the larger voltage provided energy to the wire at a greater rate; thus, the transition occurred at an earlier point in time. By selecting the capacitance and charging voltage, the heating rate and peak temperature are reproducibly controlled. The amount of action  $G_0$ , measured at the observed time of transition for several 0.25-mm. Zr wires, including one that melted during the pulse, was constant within a few percent.

Table I. Theoretical Action for Zirconium Wire

$T$ °K.	$Cp^a$ Joule mole <sup>-1</sup> deg. <sup>-1</sup>	$\rho^b$ ohm cm. $\times 10^6$	$\delta^b$	$g_{th} = G_{th}/A_0^2$ Joule ohm <sup>-1</sup> cm. <sup>-4</sup> $\times 10^{-6}$
300	25.72	48	1.000	0.00
400	27.34	65	1.008	3.42
500	28.84	80	1.012	6.23
600	29.97	95	1.020	8.67
700	30.67	105	1.027	10.88
800	31.05	115	1.034	12.95
900	31.35	124	1.042	14.89
1000	31.80	131	1.050	16.73
1100	32.67	134	1.060	18.56
1143 ( $\alpha$ )	33.04	136	1.064	19.39
1143 ( $\beta$ )	32.09	112	1.036	21.82
1200	32.26	114	1.044	22.95
1300	32.56	116	1.054	25.03
1400	32.85	118	1.063	27.14
1500	33.14	121	1.073	29.24
1600	33.43	123	1.084	31.34
1700	33.73	125	1.093	33.44
1800	34.02	127	1.103	35.54
1900	34.31	129	1.113	37.65
2000	34.61	132	1.123	39.74
2100	34.91	134	1.133	41.86
2128 (m.p.)	34.99	135	1.136	42.45
2128 (melted)				53.25

<sup>a</sup> Ref. 12.

<sup>b</sup> Ref. 11.

The values of the action integral  $G_{th}$ , corrected for thermal expansion and the heat of the  $\alpha$  to  $\beta$  transition, for a Zr wire as a function of temperature are given in Table I. Given in Table II are the values of the action integral  $G_0$  as a function of time measured for a 0.25-mm. Zr wire from the current waveform shown in Figure 3. From a comparison of these two tables, a conversion of the data to a theoretical wire temperature as a function of time was made (Figure 5). The  $\alpha$  to  $\beta$  transition is observed to occur at a calculated temperature of about 1240°K., as compared with the known transition temperature of  $1143 \pm 5^\circ\text{K.}$  (12). Although part of this apparent error may be caused by radiation, conduction and vaporization heat losses, calculations have shown that these

losses are small ( $\ll 1\%$ ). The observed transition does not initiate until 11  $\mu\text{sec.}$  later than the predicted time. Utilizing the action supply rate near the  $\alpha$  to  $\beta$  transition (from Table II) and the amount of action required for the transition (from Table I), the time required for the transition to occur is calculated to be 10  $\mu\text{sec.}$  From the original data record corresponding to Figure 3, it is observed that the actual transition required about 13 to 14  $\mu\text{sec.}$  for the 1-cm. length. When these factors are considered in attempting to explain the high apparent transition temperature, two explanations can be presented.

Table II. Experimental Action for Zirconium Wire

Time $\mu\text{sec}$	$i$ amp	$g_e = G_e/A_0^2$ Joule $\text{ohm}^{-1} \text{cm.}^{-4} \times 10^{-6}$
0	0	—
16	30	0.04
36	73	0.32
56	110	1.14
76	143	2.66
96	171	5.02
116	193	8.24
136	211	12.17
156	221	16.64
166	223	19.00
176	225	21.40
186	224	23.80
196	223	26.19
216	217	30.84
236	203	35.08
256	186	38.74
276	163	41.67
296	137	43.84
316	107	45.29
336	75	46.09
356	45	46.44
383	0	46.53

First, the wire superheats and acquires all the energy of transition before the transformation starts; the transformation then propagates through the wire at a velocity of about  $7.4 \times 10^4$  cm./sec. Evidence for the occurrence of superheating does exist in the literature. Examples are the overheating of the solid to liquid phase transition of ice crystals by  $0.3^\circ\text{C.}$  (13), the superheating of the  $\alpha$  to  $\gamma$  transition for whiskers of iron (40) and the measurement of an activation energy (1.74 kcal./mole) for the  $\alpha$  to  $\beta$  transformation of a single crystal of *p*-dichlorobenzene (22).

Second, the temperature scale is high because of uncertainties in the values of the heat capacity, resistivity, etc.; the transition actually does initiate at  $1143^\circ\text{K.}$  and the degree of transformation is approximately proportional to the energy supplied. The JANAF (12) heat capacity data for Zr are quoted to be uncertain by 10% and 15% for the  $\alpha$  and  $\beta$

phases, respectively. Parker (32) and Cezairliyan (2) have both demonstrated that specific heat measurements from pulse heating experiments are in general agreement with the steady-state values. Furthermore, Parker has concluded, from studies on the  $\alpha$  to  $\beta$  transition of Ti, that the transition occurs in less than 200  $\mu\text{sec}$ . (5.5 cm. samples) and that the percentage transformation is a linear function of energy input. He also observed that the presence of small amounts of oxygen impurities required higher driving temperatures for phase change under rapid heating.

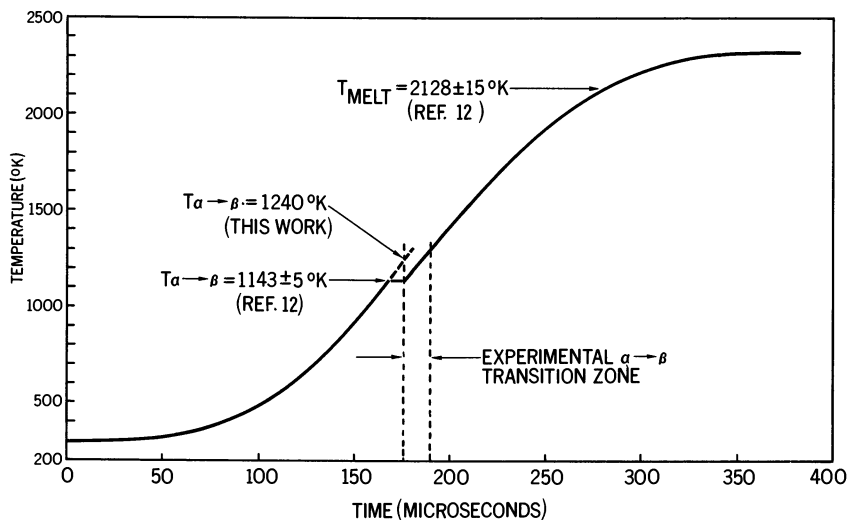


Figure 5. Theoretical temperature as a function of time for a pulse heated zirconium wire

The maximum calculated temperature is also seen in Figure 5 to exceed the melting point ( $2128^\circ\text{K}$ .) of Zr (12), although the wire did not melt. Whereas the heat of fusion has been neglected in the temperature calculation, the excess action available beyond that required to heat the wire to melting point is far short of that required for complete melting (Table I).

The light emitted from a pulse heated wire was monitored as a function of time with a 931 photomultiplier, which has a spectral response of 3000 to 6000  $\text{\AA}$ . and a maximum sensitivity near 4000  $\text{\AA}$ . Two things should be noted about the typical light vs. time curve for a Zr wire shown in Figure 6. The first is the relatively fast rise time and the comparatively long decay time. The long decay time verifies that the assumption of no heat loss in the action calculation is reasonable. Second, this type of heating cycle provides a relatively long time at high temperatures in which to record data by time resolved mass spectrometry. A large number of mass spectra at small temperature intervals could possibly be obtained from one heating pulse, giving the sublimation rate of a substance over a large temperature range from one experiment.

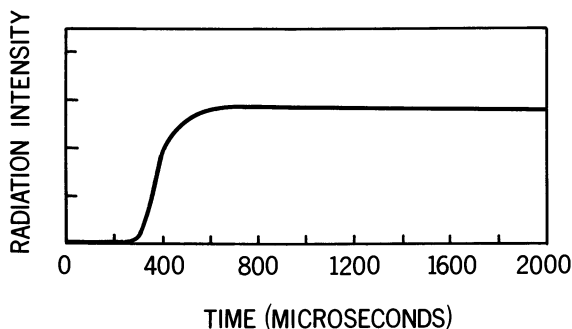


Figure 6. Emitted light response of 931 photomultiplier from pulse heated zirconium wire as a function of time

The adaptation of photodetectors to absolute temperature measurement is in the early stages of development. Therefore, there are no multi-color ratio results to report. Attempts are being made to establish correspondence between the response of a single detector and the action waveforms.

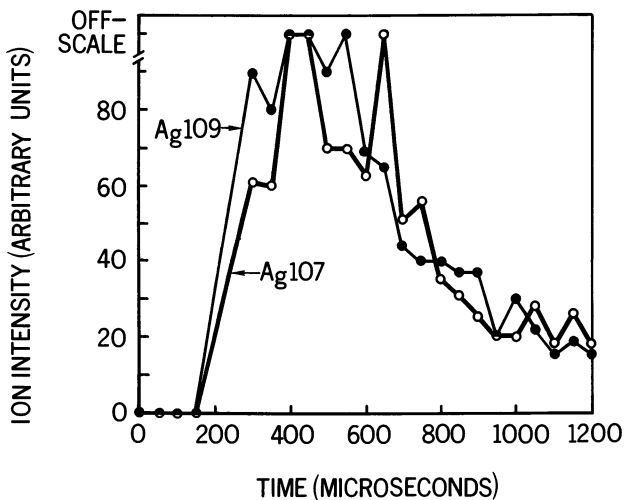


Figure 7. Time resolved ion intensities of silver isotopes from pulse heated silver wire; data obtained from drum camera record. Estimated maximum temperature is  $1150^{\circ}\text{K}$ .

**VAPORIZATION EXPERIMENTS.** Several 0.125-mm. silver wires were pulse heated to obtain a calibration for the mass spectrometer. During one such experiment, a time resolved mass spectrum of the vaporization

of silver was recorded on the drum camera. The variation of ion intensities with time for both isotopes 107 and 109 is shown in Figure 7. It is seen that the growth and decay for the two isotopes is similar and is in approximate agreement with the heating pulse. The two curves peak at about 400  $\mu\text{sec.}$ , while the energy input pulse terminated at 385  $\mu\text{sec.}$  It is estimated that the peak temperature achieved was about 1150°K.; this value is based upon the utilization of an input energy just below that required to melt (m.p. 1234°K.) the silver wire. It is observed from Figure 7 that the apparent vapor density of Ag falls off to about one-fifth of its peak value within 800  $\mu\text{sec.}$  Using the known heat of vaporization for Ag (68.1 kcal./mole (31)), the temperature decrease corresponding to the five-fold vapor density decrease is calculated to be about 60°K. However, calculations of heat losses caused by radiation, axial and radial conduction and vaporization show that the sum of these losses are much less than required for a 60°K. temperature decrease within 800  $\mu\text{sec.}$  It would appear, therefore, that the spectrometer sensitivity is varying rapidly with time. This is not unreasonable in view of the high and variable level of desorbed contaminates, which has been observed in almost every experiment. For the Ag vaporization experiments, the radiation intensity was too low to be monitored by the phototube employed (not the 931-photomultiplier).

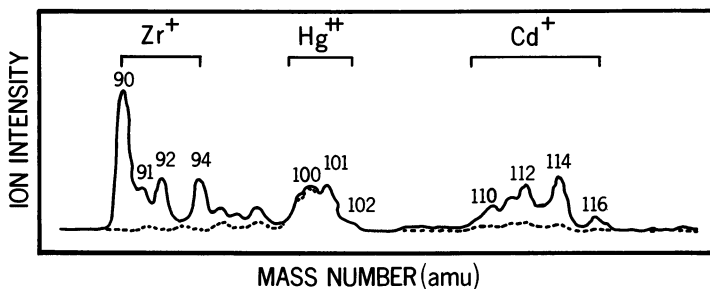


Figure 8. Mass spectral chart record of d.c. heated zirconium wire at about 2000°K. Solid line: heated wire; dashed line: background spectrum

To obtain the precise mass spectral position of Zr vapor by isotopic identification and to measure the sensitivity of the mass spectrometer for vapors from a hot wire, several Zr wires were heated continuously with a d.c. power supply. The solid line in Figure 8 shows an analog chart recorder trace of the mass spectral region of interest with a Zr wire heated to about 2000°K. ( $P_{\text{Zr}} \approx 10^{-5}$  torr), while the dashed line gives the background over the same region about a minute after power termination. The relative amplitudes of the 90, 91, 92, and 94 mass peaks are in good agreement with the accepted isotopic abundances. The Cd vapor seen in the mass spectrum came from a Cd-plated screw used to hold the Zr wire to the probe support terminal. Since this screw was heated only by the thermal conduction of heat from the hot Zr wire, it was found that the Cd grew in at a much slower rate than did the Zr. The  $\text{Hg}^{2+}$

spectrum is attributed to residual mercury in the ion source. Chemical cleanings of the ion source and the vacuum chamber completely eliminated it. Replacement of the Cd-plated screw with a stainless steel screw removed the Cd contamination.

Ion species detected by the superimposed oscilloscope-trace method consist of  $Zr^+$  from a pure Zr wire,  $Zr^+$  and  $ZrO^+$  from a slightly oxidized Zr wire, and  $ZrO^+$  and  $ZrO_2^+$  from a highly oxidized wire. The  $Zr^+$  peaks were observed when two strands of 0.25 mm. Zr wire were heated to about 2100°K. The time delay in this case was 300  $\mu$ sec. Because of the associated large hydrocarbon vapor pulse, the spectrometer sensitivity was limited to Zr vapor detection only near the melting point. The literature value for the equilibrium vapor pressure of Zr at 2100°K. is  $1.1 \times 10^{-5}$  torr (12). Thus, the spectrometer sensitivity must be at least  $5 \times 10^{10}$  molecules/cc.

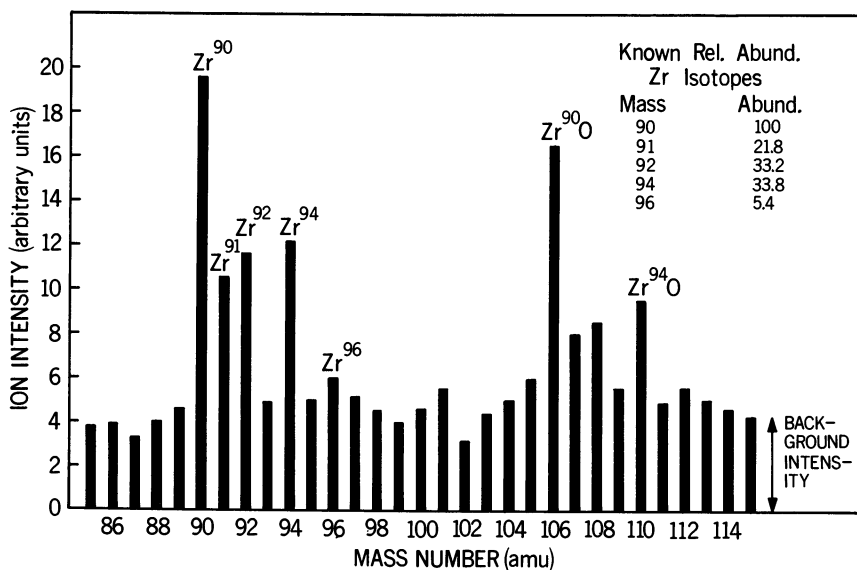


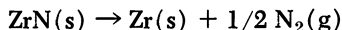
Figure 9.; Mass spectral bar graph obtained from pulse heating a slightly air-oxidized zirconium wire (0.3 to 0.5-ohm resistance)

The spectrum in which  $Zr^+$  and  $ZrO^+$  peaks were observed is reproduced in Figure 9 (time delay 1450  $\mu$ sec.). Since the  $Zr^+$  peaks are greater than the  $ZrO^+$  peaks, it can be assumed that both are parent ions. The relative abundance of these two species is reasonable, since the slightly oxidized wire from which these species were vaporized is a more oxygen deficient system than the  $Zr(s) + ZrO_2(s)$  mixture from which Chupka, Berkowitz, and Inghram (4) reported  $ZrO^+$  to be the major peak.

The intensity of  $ZrO_2^+$  observed from the pulse heating of a highly oxidized Zr wire was about twice that of  $ZrO^+$ . Since this mass spectrum was obtained using 70-volt ionizing electrons, it is possible that a sig-

nificant portion of the  $ZrO^+$  intensity is caused by fragmentation of  $ZrO_2(g)$ . The predominance of  $ZrO_2^+$  over  $ZrO^+$  is opposite to the results of Chupka, Berkowitz, and Inghram (4) and of Nakata, McKisson, and Pollock (24). Both groups reported  $ZrO^+$  to be about six times greater than  $ZrO_2^+$  when  $ZrO_2(s)$  was vaporized under equilibrium conditions. Because of the method used for the oxidation of the Zr wires, uniform oxidation to stoichiometric  $ZrO_2(s)$  could not be expected. In the highly oxidized wires, a center core of Zr, possibly alloyed with oxygen and nitrogen, must have provided the means for electrical conduction. In fact, some wires that were even more completely oxidized, as indicated by a high resistance, could not be heated effectively. Another possible explanation for the intensity difference is that the Langmuir vaporization coefficient for  $ZrO_2(g)$  may be considerably larger than that for  $ZrO(g)$  vaporized from  $ZrO_2(s)$ . Shchukarev and Semenov (34) observed the  $ZrO_2^+$  ion intensity to exceed the  $ZrO^+$  intensity for an interval of time prior to the establishment of equilibrium with  $ZrO_2(s)$  at  $2470^\circ C$ . The initial ratio ( $ZrO_2^+/ZrO^+$ ) was  $3/2$ , whereas the steady-state value was  $1/4$ .

A significant increase in masses 14 and 28 was observed in the case of a highly oxidized Zr wire. The signals appeared on a drum camera record at about  $300 \mu\text{sec.}$  after the initiation of the heating pulse and at an estimated temperature of  $1600$  to  $2000^\circ K$ . By approximately  $400 \mu\text{sec.}$ , the vapor pulse had become so great that complete mass spectrometer interference occurred. However, it is significant that no hydrocarbon contamination was observed in this experiment to mask the low mass range. Furthermore, since there was no corresponding increases at masses 16 and 32 as would be expected from an outgassing of air, it appears that both atomic and molecular nitrogen may have been released from the heated sample. Atomic nitrogen is considered because the 14:28 ratio was several times larger than that normally attributed to  $N_2$  fragmentation. Inasmuch as the Zr wire was oxidized by pulse heating above the ignition temperature in air, it is possible that a  $ZrO_xN_x$  type oxynitride compound was formed. Gilles (10) reported both the preparation of zirconium oxynitrides and their thermal decomposition by the elimination of nitrogen. The decomposition pressure of  $N_2$  over pure  $ZrN(s)$  at  $2000^\circ K$ . (12), calculated according to the reaction



is  $1 \times 10^{-5}$  torr, which is detectable in the present operation. Nelson (29) also reported that nitrogen is released during the latter stages of the combustion of freely falling zirconium droplets in mixtures of oxygen and nitrogen. This work will be referred to again later in this paper. The above evidence suggests that the observed nitrogen was released in the thermal decomposition of the sample.

**Summary of Vaporization Studies.** The implications of the semi-quantitative temperature measurement and qualitative vaporization results reported above are considered to be as follows. First, the good agreement (within 10%) between the temperature calculated from the action integral and the known temperatures of the  $\alpha$  to  $\beta$  transition in zirconium indicates it is possible to calculate reasonable temperature

values as a function of time for pulse heated wires. This is only true for samples for which the heat capacity, electrical resistivity, and linear expansion are known accurately as a function of temperature. However, by determining temperature independently, as by fast response optical pyrometry (2) and by controlling and measuring the energy discharged (32), it should be possible to measure heat capacities, resistivities, or  $C_p/\rho$  ratios by this method for nonstoichiometric conducting materials.

Second, the conclusion that superheating may have been observed for pulse heated Zr, both at the  $\alpha$  to  $\beta$  transition and at the melting point, suggests that it may be possible to measure vapor pressures for superheated states by time resolved mass spectrometry.

Third, the observed initial increase in vapor density for the two Ag isotopes confirms that the rate of vaporization can be followed for heating pulses of millisecond to microsecond duration.

Fourth, the preliminary results on pure Zr reflect both the ease of detecting vapor densities in the  $10^{10}$  molecules/cc. range and the ability to achieve temperatures of 2000°K. or greater by d.c. heating and by capacitor-discharge pulses.

Fifth, the detection of Zr, ZrO, and ZrO<sub>2</sub> vapors from air-oxidized Zr wires presents the motivation to explore the vapor species for both stoichiometric and nonstoichiometric substances.

Finally, it appears that the freedom from sample reactions with containers at high temperatures offered by the Langmuir geometry has been realized.

### ***Refractory Metal Combustion***

The high temperature research effort, described in the first section of this paper, was motivated by established studies on the combustion and explosion of refractory metal droplets in atmospheres of oxygen and nitrogen and by the absence of thermodynamic data on the metal-oxygen-nitrogen alloys at high temperatures. We now describe how mass spectrometry has been applied directly to the mechanism of the refractory metal combustion phenomenon.

Nelson (25, 28, 29) demonstrated that the burning of submillimeter droplets of zirconium in pure oxygen produces dense spheres of ZrO<sub>2</sub>. However, when small amounts of nitrogen are added to the oxygen atmosphere, the burning droplet explodes or forms a single thin-walled sac of ZrO<sub>2</sub>. He reasoned that the explosion and sac formation are gas driven and the gas is probably N<sub>2</sub> although no direct confirmation of gaseous N<sub>2</sub> formation within the liquid oxide droplet has been obtained.

If the explosions really are gas driven, the identification of the gas is essential to the interpretation of the reaction mechanism for Zr burning

at high temperature in a mixed  $N_2$  and  $O_2$  atmosphere. The gas analysis technique must be sensitive enough to detect the small quantities of gas ( $10^{15}$  molecules) expected to be encapsulated by the unexploded zirconia sacs. The fast response capability of the time-of-flight mass spectrometer offers the advantages of complete mass range coverage and many spectral analyses within one pass of the gas sample through the ionization zone. An analysis can be performed before the gas pulse expands into the spectrometer volume and is pumped away. This technique has been successfully adapted to the quantitative identification of gases contained in the zirconia sacs and in prepared capillaries, both containing  $10^{13}$  to  $10^{15}$  molecules. Nitrogen is the only gas observed in the sacs. The experimental technique and the implications of the nitrogen detection on the reaction mechanism are reviewed in the following paragraphs. A detailed report of this work is being published separately (21).

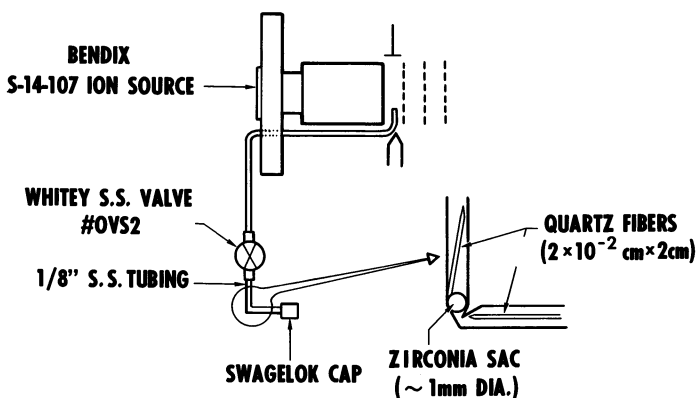


Figure 10. Sample holder and inlet system for zirconia sacs and gas calibration capillaries

**Sac Preparation and Analysis Procedures.** The apparatus used for observing the zirconium droplet explosions and for generating the unexploded zirconia sacs has been previously described (28, 30). A square of pure Zr foil is dropped through a flash lamp in a 625-torr atmosphere of  $N_2$  and  $O_2$ , for which the  $N_2/O_2$  ratio can be varied. When  $N_2/O_2$  equals or exceeds 0.04, the droplet explodes. Under a controlled threshold  $N_2/O_2$  ratio of 0.025, the metal becomes molten, burns, and inflates, but does not explode. The average sac diameter and volume are 1.0 mm. (range: 0.7 to 1.5 mm.) and  $0.5 \times 10^{-3}$  cc., respectively. The total time involved in the inflation and/or explosion is 150 milliseconds (25, 30). From separate experiments, it has been established that the explosions occur at temperatures around 3000°K. to 3500°K. (26, 27, 28).

Figure 10 shows the sample holder and inlet system. One or more sacs are loaded into the vertical arm of the thin wall stainless steel tubing, along with a quartz capillary which contains an inert gas such as

argon. The sacs and capillary are crushed simultaneously by hand to release the gases to the ion source. The sample holder volume is kept small, approximately 1 cc., to provide a short-duration, high-pressure pulse of gas. The inert gas generates a mass signal trigger pulse which synchronizes oscilloscope display circuitry. Capillaries containing known amounts of various gases are crushed in the horizontal arm of the holder to provide absolute calibrations.

Two methods of mass spectrum and ion intensity recording are used. One is to set the spectrometer analog circuits on two mass peaks and record the ion intensities as a function of time on a fast writing chart recorder. The other consists of displaying the complete mass spectrum on an oscilloscope for an interval of time at the peak intensity of the input pulse of gas. In the latter case, one mass selector analog is set on the inert gas and triggers a time delay generator upon the initial appearance of inert gas at the ion source. Thus, the 20-kHz trigger input to the oscilloscope is withheld and gated on for a typical duration of 25 msec. at the maximum of the gas pulse. The spectrum is photographed with a Polaroid camera.

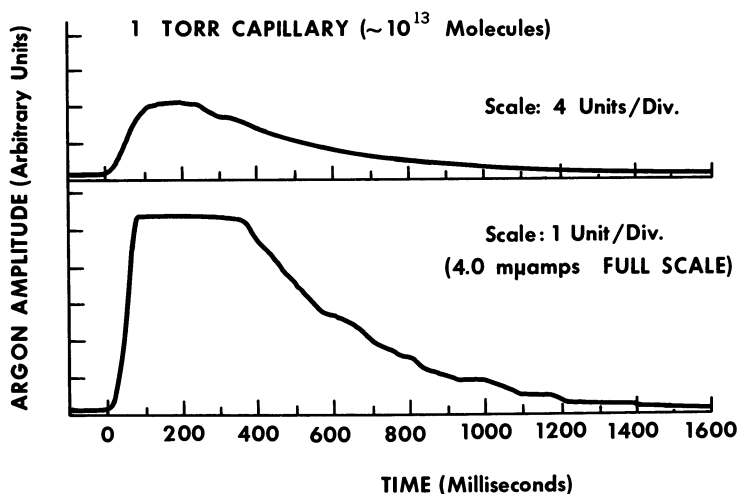


Figure 11. Analog chart recorder response of argon intensity vs. time for a 1-torr capillary

Figure 11 shows the recorder response of ion intensity versus time for a 1-torr capillary of argon which corresponds to approximately  $10^{13}$  atoms. The near peak of intensity is reached at 110 msec., and the signal persists beyond 1 sec. It is estimated that several orders of magnitude improvement in sensitivity could be achieved if the gas pulse were compressed in time from the 1.5-sec. duration of this analysis to a spike synchronized to one cycle of the spectrometer operation. The oscilloscope sensitivity presently is  $3 \times 10^{11}$  atoms; this value was ascertained from the oscilloscope detection of the  $^{36}\text{Ar}$  isotope in a 10-torr argon capillary.

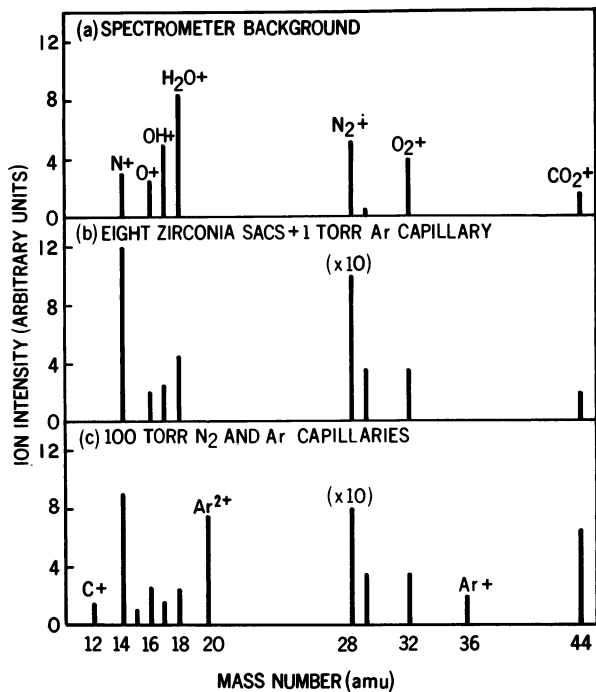


Figure 12. Bar graph reproduction of oscilloscope mass spectral display for zirconia sac gas content and for a  $N_2$  calibration capillary. In (b) and (c),  $N_2^+$  amplitudes must be multiplied by 10 to obtain 1:1 correspondence with the other ion intensities. Amplitudes of less than two units indicate presence of only trace quantities

**Quantitative Identification of Sac Gases.** The zirconia sacs have been analyzed both as single units and as several crushed simultaneously. Only one such analysis is presented here. Figure 12 shows bar graph reproductions of Polaroid film records of the mass spectra of eight zirconia sacs and of a 100-torr nitrogen calibration capillary. The top trace shows the spectrometer background gases, with masses 14, 16, 17, 18, 28, 32, and 44 readily recognizable. The argon trigger signal at mass 40 is absent from the oscilloscope record by virtue of its being gated out by the mass selector analog. The spectrum of the zirconia sacs, displayed in the middle trace, shows large increases in masses 14 and 28, but no other signal increases above background. The 100-torr  $N_2$  and Ar calibration capillaries (bottom trace) show ion intensities for masses 14 and 28 which are about 0.8 times those recorded for the zirconia sacs. Masses 20 and 44 are caused by Ar (doubly ionized) and  $CO_2$  (a capillary impurity). The maximum total volume of the eight zirconia sacs was 7.8

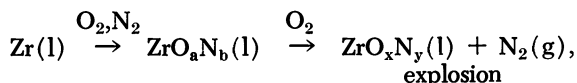
times the volume of the 100-torr N<sub>2</sub> capillary. Therefore, the average pressure per sac is equal to or greater than 16 torr. This value is a minimum because some of the sacs may have been prematurely broken during loading.

Altogether, 17 separate analyses have been performed on the zirconia sacs; four analyses utilized multiple numbers of sac, and the remainder utilized single sacs. Of this total, 11 analyses provided a positive detection of N<sub>2</sub> and a total absence of any other gases. One single sac analysis showed a N<sub>2</sub> pressure of approximately 100 torr, whereas most of the others were 10 torr or less. Although the sensitivity limit for O<sub>2</sub> was about 1 torr (N<sub>2</sub> was somewhat better than 1 torr), no O<sub>2</sub> was detected which could be attributed to the sac content. This distribution of values cannot be interpreted as a statistical distribution for several reasons, which are outlined in the detailed report (21). The principal factor is that very few of the individual sac preparations provide intact sacs; the majority of the preparations result in ruptured sacs or in dense spheres.

**Implications on Combustion Mechanism.** The positive identification of nitrogen and the absence of other gases support the hypothesis that the explosions are gas-driven and that the driving gas is nitrogen. Two facts suggest that the nitrogen is released at high temperature during the oxidation reaction. First, the absolute partial pressure measurements at 300°K. indicate that the sac pressure at 3000° to 3500°K. could be as high as 100 to 1000 torr; the higher values would approach the pressures required for an explosive rupture. Second, the detected N<sub>2</sub> to O<sub>2</sub> ratio within the sac was at least 100 to 1, whereas the N<sub>2</sub>/O<sub>2</sub> ratio for the reactant environment was 0.025. Thus, diffusion of gases from the atmosphere into a hollow sac cannot account for the presence or amount of nitrogen.

A nitrogen release mechanism was previously suggested by Nelson to describe sac formation and explosion. This model is based upon several independent observations: (1) the degree of explosion can be varied by changing the percentage of N<sub>2</sub> in O<sub>2</sub> (29); (2) no explosion occurs in pure O<sub>2</sub> or pure Ar (25, 29); and (3) there appears to be a high stability of ZrO<sub>2</sub> against a permanent reaction with N<sub>2</sub> (17). The present result, however, is the first direct evidence for the existence of N<sub>2</sub> as the driving gas.

The chemical processes that occur during the burning of the zirconium droplets are still obscure, but they may involve temperature and composition changes in the zirconium-oxygen-nitrogen system. At the present time, it is speculated that the reaction scheme might be represented as follows:



where  $0 < a < x < 2$  and  $b > y$  (both  $b$  and  $y$  being small). It is suggested that liquid zirconium reacts with oxygen and nitrogen to form intermediate oxygen-nitrogen alloys. As these alloys react further with oxygen, however, a critical set of temperature and composition conditions are attained, followed by the rapid release of nitrogen gas.

Other observations that seem to support this mechanism are as follows. It has been found that explosions occur if the zirconium metal is slightly nitrified first and then burned in a pure oxygen environment (29). The existence of intermediate oxynitride phases in quenched droplets was demonstrated by x-ray diffraction studies (25, 28). Further, the distinct possibility that a supersaturated phase is momentarily established is suggested by supercooling effects which have been identified in the reaction of zirconium droplets with pure oxygen (26).

The application of the techniques described here to the combustion of zirconium droplets suggests additional experiments for probing the reaction mechanism. For example, we plan to analyze sacs prepared from zirconium droplets of varied sizes and of controlled nitrogen alloying. In this way we hope to explore in detail the temperature and composition conditions for sac formation and explosion.

### *Acknowledgment*

The authors wish to express appreciation to J. M. Freese for assistance with the experiments, to H. S. Levine for many helpful discussions and to J. L. Margrave for encouragement in developing the techniques and for supplying valuable information and ideas.

The Associated Western Universities is acknowledged for granting an AWU-AEC Summer Fellowship, which permitted this cooperative research activity. The zirconia sacs were kindly provided by L. S. Nelson and N. L. Richardson.

### *Literature Cited*

- (1) Baxter, H. W., *Nature* **153**, 316 (1944).
- (2) Cezairliyan, A., "Advances in Thermophysical Properties At Extreme Temperatures and Pressures," pp. 253-263, The American Society of Engineers, New York, 1965.
- (3) Chupka, W. A., Inghram, M. G., *J. Phys. Chem.* **59**, 100 (1955).
- (4) Chupka, W. A., Berkowitz, J., Inghram, M. G., *J. Chem. Phys.* **26**, 1207 (1957).
- (5) Cnare, E. C., *Sandia Corporation Res. Rept. SC-4324 (TR)*, June 1959.
- (6) Diesen, R. W., *J. Chem. Phys.* **44**, 3662 (1966).
- (7) Dove, J. E., Moulton, D. McL., *Proc. Roy. Soc. (London)* **A283**, 216 (1965).
- (8) Friedman, H. L., Paper presented at *11th Ann. Conf. Mass Spectrometry Allied Topics*, San Francisco, Calif., May 1963.

- (9) Gay, I. D., Kern, R. D., Kistiakowsky, G. B., Niki, H., *J. Chem. Phys.* **45**, 2371 (1966).
- (10) Gilles, J. C., *Rev. Hautes Tempér. et Réfract.* **2**, 237 (1965).
- (11) Goldsmith, A., Waterman, T. E., Hirschhorn, H. J., "Handbook of Thermophysical Properties of Solid Materials," Vol. 1, The Macmillan Company, New York, 1961.
- (12) "JANAF Thermochemical Tables." The Dow Chemical Company, Midland, Michigan, December 31, 1961.
- (13) Kaesa, M., Magun, S., *Z. Krist.* **16**, 354 (1961).
- (14) Kottenstette, J. P., *ISA (Instr. Soc. Am.) Trans.* **4**, 270 (1965).
- (15) Lincoln, K. A., Werner, D. W., Paper presented at *15th Ann. Conf. Mass Spectrometry Allied Topics*, Denver, Colorado, May 1967.
- (16) Mayfield, E. B., "Exploding Wires," p. 147, Plenum Press, Inc., New York, 1959.
- (17) Meyer, H., *Ber. Deut. Keram. Ges.* **41**, 112 (1964).
- (18) Meyer, R. T., *J. Chem. Phys.* **46**, 967, 4146 (1967).
- (19) Meyer, R. T., *J. Sci. Instr.* **44**, 422 (1967).
- (20) Meyer, R. T., *Rev. Sci. Instr.* **35**, 1064 (1964).
- (21) Meyer, R. T., Nelson, L. S. (to be published).
- (22) Mnykh, Yu. V., Kitaigovskii, A. I., Asadov, Yu. G., *Zh. Eksperim. i Teor. Fiz.* **48**, 19 (1965).
- (23) Modica, A. P., La Graff, J. E., *J. Chem. Phys.* **44**, 3375 (1966).
- (24) Nakata, M. M., McKisson, R. L., Pollock, B. D., *Atomics Intern. Rept. NAA-SR-6095*, April 1961.
- (25) Nelson, L. S., "Eleventh Symposium (International) on Combustion," pp. 409-416, The Combustion Institute, Pittsburgh, 1967.
- (26) Nelson, L. S., *Nature* **210**, 410 (1966).
- (27) Nelson, L. S., Paper presented at *4th Interagency Chem. Rocket Propulsion Group Combust. Conf.*, Menlo Park, California, October 1967.
- (28) Nelson, L. S., *Pyrodynamics* **3**, 121 (1965).
- (29) Nelson, L. S., *Science* **148**, 1594 (1965).
- (30) Nelson, L. S., Richardson, N. L., *J. Phys. Chem.* **68**, 1268 (1964).
- (31) Panish, M. B., *J. Eng. Data* **6**, 592 (1961).
- (32) Parker, R., *Trans. Met. Soc. AIME* **233**, 1545 (1965).
- (33) Ryason, P. R., *Rev. Sci. Instr.* **38**, 607 (1967).
- (34) Shchukarev, S. A., Semenov, G. A., *Issled. v Obl. Khim. Silikatov I Okislov, Akad. Nauk SSSR, Sb. Statei*, 308 (1965).
- (35) Sherman, F. S., *Phys. Fluids* **8**, 773 (1965).
- (36) Tucker, T. J., *J. Appl. Phys.* **32**, 1894 (1961).
- (37) Vastola, F. J., Pirone, A. J., Knox, B. E., Paper presented at *14th Ann. Conf. Mass Spectrometry Allied Topics*, Dallas, Texas, May 1966.
- (38) Wiley, W. C., McLaren, I. H., *Rev. Sci. Instr.* **26**, 1150 (1955).
- (39) Zavitsanos, P. D., *Gen. Elec. Space Sci. Lab. Rept. R67SD11*, March 1967.
- (40) Zerwekh, P., Wayman, C. M., *Acta Met.* **13**, 99 (1965).

RECEIVED Sept. 5, 1967. This work was supported by the United States Atomic Energy Commission.

# INDEX

<b>A</b>	
Abnormal vibrational energy distributions .....	91
Absolute pressures, parent molecules and .....	252
Adiabatic hydrogen potential .....	85
Alkylboranes .....	201
Alkyl derivatives of carboranes ..	202
Alpha particle mass spectrometer ..	26
Amino borane, BH <sub>2</sub> NH <sub>2</sub> .....	150
Ammonia	
borane .....	144
competitive solvation of ammonium ion by water and ...	45
decomposition of .....	55
irradiation of .....	54, 56
Ammonium ion	
by water and ammonia, competitive solvation of .....	45
enthalpy of solvation of .....	29
entropy of solvation of .....	33
Analysis of boranes and carboranes	191
Antimony-arsenic systems .....	250-1
Appearance potentials ... 158, 162, 171, 183, 213, 252	
of the heteronuclear ions .....	3
for perfluorosilanes and perfluoroborosilanes .....	261
of rare-earth trifluorides .....	270
Arsenic .....	239
phosphorus system .....	247
vaporization of .....	231
AsN .....	247
As <sup>+</sup> , electron multiplier gain of ...	294
Atomic cross sections .....	122
Atomization energies of interpnictide molecules .....	257
Automated data acquisition in inorganic mass spectroscopy ...	127
<b>B</b>	
Barium system, ionization efficiency curves in .....	275
Beam intensity .....	70
B <sub>2</sub> H <sub>6</sub> .....	95
Bi <sup>+</sup> , electron multiplier gain of ...	294
BiN .....	247
B <sub>2</sub> O <sub>3</sub> .....	229
Bond dissociation energies .....	261
of rare-earth fluorides .....	288
Bond strengths .....	261
Borane carbonyls .....	141
Boranes .....	141
analysis of .....	191
and carboranes, comparison of ..	203
mass spectra of .....	199
Borane structures .....	194
Boron	
and carbon by <sup>13</sup> C-isotope analysis, determination of .....	204
chloride ions, solvation of .....	39
hydrides .....	15, 191
spectra, general characteristics of sulfide, conversion of metathio-boric acid to .....	211
sulfides .....	218, 228
high molecular weight .....	211
Boroxine .....	229
B <sub>8</sub> S <sub>16</sub> <sup>+</sup> .....	214, 220
B <sub>12</sub> S <sub>21</sub> <sup>+</sup> .....	228
<b>C</b>	
Cadmium .....	238
arsenide .....	241
vaporization of .....	231
selenide .....	242
vaporization of .....	231
vaporization of .....	231
Carbon by <sup>13</sup> C-isotope analysis, determination of boron and ...	204
Carbon-hydrogen system .....	150
Carboranes	
analysis of .....	191
comparison of boranes and ...	203
mass spectral profiles of .....	201
<i>closo</i> -Carborane .....	192, 201
structure .....	195
<i>nido</i> -Carborane .....	194, 203
structures .....	196
Catalytic laboratory, radiolytic and	48
Chemionization	
by reaction of electronically excited species .....	1
reactions of mercury .....	6
reactions, rates of .....	9
Chloride ion, solvation of .....	39
<sup>13</sup> C-isotope analysis, determination of boron and carbon by ...	204
Clastograms .....	157, 164, 170
logarithmic .....	157
Clausius-Clapeyron equation .....	159
C <sub>2</sub> O <sub>2</sub> <sup>+</sup> by chemionization .....	7
Co <sup>+</sup> , electron multiplier gain of ..	294
Collision-free sampling .....	181
Collision induced dissociation of D <sub>2</sub> <sup>+</sup> .....	92

Competitive solvation of ammonium ion by water and ammonia . . .	45	Entropy of solvation of ammonium ion . . . . .	33
Computer control, on-line . . . . .	134	Entropy of solvation of hydronium ion . . . . .	34
Consecutive unimolecular decompositions . . . . .	175	Erbium subfluorides . . . . .	282, 286
Cross sections		Europium subfluorides . . . . .	282, 286
atomic . . . . .	122	Excess energy of the ionizing electrons . . . . .	84
electron impact ionization . . . . .	115	Exploding metal wires . . . . .	304
ionization . . . . .	107, 112		
molecular ionization . . . . .	122		
		<b>F</b>	
<b>D</b>		Faraday cup collector . . . . .	295
Data acquisition in inorganic mass spectroscopy, automated . . . . .	127	Fast gas phase reactions . . . . .	301
$D_2^+$ , collision induced dissociation of . . . . .	92	Flames, direct sampling of . . . . .	76
$D^+/D_2^+$ ratio . . . . .	88	Flames, ions in . . . . .	12
Decomposition of ammonia . . . . .	55	Flash photolysis . . . . .	301
Deuterium ion reactions . . . . .	18	Fluorides, Sc, Yt, La, rare earth . . . . .	267
Deuterium-neon mixture, shock tube study of . . . . .	83	Fluorine-exchange reactions . . . . .	278
Diatomic ion formation . . . . .	10	Fluorosilanes . . . . .	261
Diatomic ions of the rare gases . . . . .	1	Formation, ionic heats of . . . . .	161
Diborane . . . . .	95	Formation of the gaseous noble metal oxides, heats of . . . . .	108
intermediates in the photochemical oxidation of . . . . .	94	Fragmentation	
Difluorides, ionization potentials of	288	mechanisms . . . . .	164, 175
Dimer species . . . . .	78	patterns . . . . .	73
$D_2^+$ ions with pentaborane, reaction of . . . . .	22	reactions . . . . .	265
$D^+$ ions with pentaborane, reactions of . . . . .	20	Fragmentive ionization . . . . .	115
Diphosphene-2 . . . . .	185	Franck-Condon principle . . . . .	84
Diphosphene-4 . . . . .	186	Free-jets . . . . .	69
Direct sampling of high pressure systems . . . . .	68	Free radicals . . . . .	64, 76
Direct sampling of flames . . . . .	76	Fluorine system, ionization efficiency curves in . . . . .	275
Dissociation energies of subfluorides of Dy, Er, Eu, Gd, Sm . . . . .	283		
rare-earth monofluorides . . . . .	287	<b>G</b>	
Dissociative charge transfer reaction . . . . .	92	Gadolinium subfluorides . . . . .	282, 286
Dissociative ionization . . . . .	167, 264	Gaseous noble metal oxide thermodynamics . . . . .	101
$D^+$ , pressure-dependent . . . . .	92	Gas flow into a mass spectrometer . . . . .	90
Dysprosium subfluorides . . . . .	282, 286	Gas phase, ion-solvent molecule interactions in the . . . . .	24
		Gas phase reactions, fast . . . . .	301
<b>E</b>		Glyoximates . . . . .	175
Effusion cell . . . . .	232	Grey selenium . . . . .	240
ion source . . . . .	235	Grid collector . . . . .	294
Effusion measurements, absolute . . . . .	256		
Electron beam mass spectrometer . . . . .	27	<b>H</b>	
Electronically excited species, chemionization by reaction of . . . . .	1	HBO <sub>2</sub> . . . . .	229
Electron impact ionization cross sections . . . . .	115	H <sub>2</sub> B <sub>2</sub> O <sub>3</sub> . . . . .	96
Electron multiplier gain of As <sup>+</sup> , Bi <sup>+</sup> , Co <sup>+</sup> , P <sup>+</sup> , Sb <sup>+</sup> , U <sup>+</sup> . . . . .	294	H <sub>3</sub> B <sub>3</sub> O <sub>3</sub> . . . . .	96
Electron multipliers, mass effect of	291	H <sub>3</sub> B <sub>3</sub> O <sub>3</sub> . . . . .	229
Enthalpy of solvation of ammonium ion . . . . .	29	HBS <sub>2</sub> . . . . .	218
Enthalpy of solvation of hydronium ion . . . . .	34	(HBS <sub>2</sub> ) <sub>2</sub> . . . . .	227
		(HBS <sub>2</sub> ) <sub>3</sub> . . . . .	226
		(HBS <sub>2</sub> ) <sub>3</sub> <sup>+</sup> . . . . .	217
		H <sub>2</sub> B <sub>2</sub> S <sub>5</sub> . . . . .	226
		H <sub>2</sub> B <sub>2</sub> S <sub>5</sub> <sup>+</sup> . . . . .	219
		H <sub>2</sub> B <sub>4</sub> S <sub>9</sub> <sup>+</sup> . . . . .	219
		H <sub>3</sub> BS <sub>3</sub> . . . . .	226
		Heats of formation . . . . .	264
		of the gaseous noble metal oxides for perfluorosilanes and perfluoroborosilanes . . . . .	108
		for positive ions . . . . .	162
		of rare earth fluorides . . . . .	268

- Heats of sublimation ..... 158  
 of rare-earth metals ..... 287  
 of rare-earth trifluorides ..... 274
- Heteronuclear ions, appearance potentials of the ..... 3
- High molecular weight boron sulfides ..... 211
- High pressure mass spectrometers ..... 27, 49
- High pressure systems, direct sampling of ..... 68
- High temperature  
 cell ..... 158  
 chemistry ..... 301  
 mass spectrometry ..... 137  
 vaporization ..... 231
- HoF<sub>3</sub>, ionization-efficiency curves for ..... 269
- Holmium subfluorides ..... 282, 286
- Homogeneous nucleation ..... 71
- H<sub>2</sub>S ..... 226
- H<sub>2</sub>S<sup>+</sup> ..... 219
- Hydrogen by water and methanol, solvation of ..... 39
- Hydronium ion, enthalpy of solvation of ..... 34
- Hydronium ion, entropy of solvation of ..... 34
- I**
- Inorganic halides ..... 153
- Inorganic mass spectroscopy, automated data acquisition in ... 127
- Interactions in the gas phase, ion-solvent molecule ..... 24
- Intermediates in the photochemical oxidation of diborane ..... 94
- Inter-pnictide molecules ..... 246  
 atomization energies of ..... 257
- Ionic decomposition ..... 218
- Ionic heats of formation ..... 161
- Ionic volume vs. multiplier gain .. 298
- Ionization  
 cross sections ..... 57, 107, 112  
 electron impact ..... 115  
 efficiency ..... 264  
 curve for diatomic ion of the rare gases ..... 2  
 curves ..... 129  
 curves for HoF<sub>3</sub> ..... 269  
 curves in Ba, F, and Nd systems ..... 275  
 curves, shape of ..... 118
- Otvos-Stevenson calculations .. 121
- potentials ..... 158, 264  
 for perfluorosilanes and perfluoroborosilanes ..... 261  
 of rare-earth metals ..... 288
- Ionizing electrons, excess energy of the ..... 84
- Ion fragmentation pattern ..... 83
- Ion-molecule reactions ..... 88  
 of pentaborane ..... 15
- Ion pair processes ..... 162
- Ion pair production ..... 264
- Ions in flames ..... 12
- Ion source gas density ..... 89
- Ion-solvent molecule interactions in the gas phase ..... 24
- Ion source pressure ..... 89
- Ion species, relative intensities .. 249
- Irradiation of ammonia ..... 54, 56
- Isothermal transpiration cells .... 77
- K**
- Knudsen cell ..... 101, 132, 232
- Knudsen number ..... 69
- Knudsen vaporization ..... 213
- L**
- Labile molecules ..... 137
- LaF<sub>3</sub>, vapor pressure curves for .. 271
- Langmuir vaporization ..... 303
- Lanthanum fluoride ..... 267
- Logarithmic clastogram ..... 172
- Logarithmic clastograms ..... 157
- LuF<sub>3</sub>, vapor pressure curves for .. 273
- M**
- Mach number ..... 70
- Mass effect ..... 293  
 of electron multipliers ..... 291
- Mass spectra of boranes ..... 199
- Mass spectral profiles of carboranes 201
- Mass spectrometry, time resolved . 301
- Mercuric halides ..... 168
- Mercury, chemionization reactions of ..... 6
- Metal  
 acetylacetonates ..... 175  
 alkyls ..... 175  
 carbonyl ..... 166, 175  
 wires, exploding ..... 304
- Metastable ion ..... 163
- Metastable ions ..... 214, 217
- Metastable transitions ..... 157, 170
- Metathiorboric acid to boron sulfide, conversion of ..... 211
- Methanol, solvation of hydrogen by water and ..... 39
- Modulated beams ..... 74
- Molecular beam formation ..... 69
- Molecular ionization cross sections 122
- Molecules of the nitrogen family .. 245
- Monofluorides, ionization potentials of ..... 288
- Monoisotopic mass spectrum ..... 169
- Multiplier gain, ionic volume vs. .. 298
- N**
- N<sub>4</sub><sup>+</sup> and C<sub>2</sub>O<sub>2</sub><sup>+</sup> by chemionization 7
- NdF<sub>3</sub>, vapor pressure curve for .. 272
- Neodymium system, ionization efficiency curves in ..... 275

Negative ion			
clastogram .....	173		
formation .....	169		
processes .....	163		
Negative ions .....	65, 163, 173		
solvation of .....	39		
Neon mixture, shock tube study of			
deuterium- .....	83		
Nickel carbonyl .....	143		
Niobium pentachloride .....	163		
Nitrogen family, molecules of the .	245		
Nitrogen with zirconium, reaction			
of .....	318		
$N^+/N_2^+$ vs. temperature .....	90		
Noble metal oxide			
thermodynamics, gaseous .....	101		
vaporization .....	107		
Noble metal oxides .....	101		
heats of formation of the gaseous	108		
Nuclear fusion .....	116		
Nucleation .....	78		
<b>O</b>			
On-line computer control .....	134		
Oscillator strength .....	121		
Otvos-Stevenson calculations .....	121		
Oxidation of diborane, intermedi-			
ates in the photochemical ....	94		
Oxygen system, ruthenium .....	101		
<b>P</b>			
Parent molecules and absolute pres-			
sures .....	252		
$P^+$ , electron multiplier gain of ...	294		
Pentaborane			
ion-molecule reactions of .....	15		
radiolysis of .....	15		
reaction of $D_2^+$ ions with .....	22		
reactions of $D^+$ ions with .....	20		
reactions of rare gas ions with ..	17		
Perfluoroborosilanes			
appearance potentials of .....	261		
heats of formation for .....	261		
ionization potentials for .....	261		
Perfluorosilanes			
appearance potentials for .....	261		
heats of formation for .....	261		
ionization potentials for .....	261		
Phase transition .....	309		
Phosphine .....	183		
Phosphorus			
hydrides .....	181		
tribromide .....	169		
trichloride .....	169		
Phosphoryl chloride .....	170		
Photochemical oxidation of dibor-			
ane, intermediates in the ....	94		
Plasmas .....	116		
PN .....	249		
$P_3N_5$ .....	246, 248, 252, 256		
Pnictide molecules, atomization en-			
ergies of inter- .....	257		
Pnictide molecules, inter- .....	246		
Pressure-dependent $D^+$ .....	92		
Proton beam mass spectrometer ..	27		
Pulse heating .....	302		
<b>Q</b>			
8-Quinolinolates .....	175		
<b>R</b>			
Radiation damage .....	116		
Radiolysis .....	49		
of pentaborane .....	15		
Radiolytic and catalytic laboratory	48		
Rare-earth			
fluorides .....	267		
bond dissociation energies of .	288		
heats of formation .....	268		
metals			
heats of sublimation of ....	287		
ionization potentials of .....	288		
monofluorides, dissociation ener-			
gies of .....	287		
subfluorides, stabilities of .....	272		
trifluorides .....	267		
appearance potentials of ....	270		
sublimation rates for solid ..	268		
Rare gases, diatomic ions of the ..	1		
Rare gas ions with pentaborane, re-			
actions of .....	17		
Rates of chemionization reactions .	9		
Reaction of $D_2^+$ ions with penta-			
borane .....	22		
Reaction of nitrogen with zirconium	318		
Reactions of $D^+$ ions with penta-			
borane .....	20		
Reactions of rare gas ions with			
pentaborane .....	17		
Reactive intermediates .....	137		
Refractory metal combustion ....	318		
Relative intensities of ion species ..	249		
Relative multiplier gain .....	292		
Resonance potentials .....	167		
Retarding potential difference ....	261		
Ruthenium-oxygen system .....	101		
<b>S</b>			
Samarium subfluorides .....	282, 286		
Sampling effects .....	73		
Sampling of high pressure systems,			
direct .....	68		
Sandwich compounds .....	175		
$Sb^+$ , electron multiplier gain of ...	294		
$SbN$ .....	247		
Scaling constant .....	256		
Scandium fluoride .....	267		
Scandium subfluorides .....	276		
$ScF_3$ , vapor pressure curves for ...	271		
Selenium .....	239		
vaporization of .....	231		
Shaft encoding .....	129		

Shape of ionization efficiency curves	118		
Shock tube study D <sub>2</sub> -Ne mixture	83		
Silicon-boron bond strengths	261		
Silicon-silicon bond strength	261		
Silver wire	314		
Sodium ion, solvation of	37		
Solar corona	116		
Solid phases	246		
Solvation of			
ammonium ion			
by water and ammonia, competitive	45		
enthalpy of	29		
entropy of	33		
chloride and boron chloride ions	39		
hydrogen by water and methanol	39		
hydronium ion	34		
enthalpy of	34		
entropy of	34		
negative ions	39		
sodium ion	37		
Stabilities of rare-earth subfluorides	272		
Stellar atmospheres	116		
Subfluorides of Dy, Er, Eu, Gd, Ho, Sm	286		
Sublimation rates of rare earth trifluorides	268		
Substituted acetylacetonates	175		
<b>T</b>			
Tantalum pentachloride	163		
Tetraborane carbonyl	141		
Temperature chemistry, high	301		
Temperature measurement	304		
Thermal ionization	63		
Thermodynamics, gaseous noble metal oxide	101		
Thiophosphoryl fluoride	170		
Time-of-flight mass spectrometer	83		
Time-of-flight measurements	75		
Time resolved mass spectrometry	301		
Titanium tetrachloride	161		
Transpiration cells, isothermal	77		
<b>U</b>			
U <sup>+</sup> , electron multiplier gain of	294		
Unstable species	137		
		<b>V</b>	
Vapor density	315		
Vapor pressure curves for NdF <sub>3</sub> , LaF <sub>3</sub> , LuF <sub>3</sub> , ScF <sub>3</sub> , YbF <sub>3</sub> , YF <sub>3</sub>	271-3		
Vapor species	248		
Vaporization			
of arsenic	231		
of cadmium	231		
arsenide	231		
arsenide, non-stoichiometric	241		
selenide	231		
effect	237		
of HBS <sub>2</sub>	217		
high temperature	231		
kinetics	304		
noble metal oxide	107		
of selenium	231		
of zinc	231		
Vibrational			
energy distributions, abnormal	91		
excitation	83		
relaxation	90		
		<b>W</b>	
Water and ammonia, competitive solvation of ammonium ion by	45		
Water and methanol, solvation of hydrogen by	39		
Weakly bound clusters	78		
Wide-range ion source	49		
		<b>Y</b>	
YbF <sub>3</sub> , vapor pressure curves for	273		
YF <sub>3</sub> , vapor pressure curves for	271		
Yttrium fluoride	267		
Yttrium subfluorides	276		
		<b>Z</b>	
Zinc	238		
bromide	166		
chloride	166		
vaporization of	231		
Zirconia sacs	319		
Zirconium	316		
oxide	316		
oxynitride	317		
reaction of nitrogen with	318		
wire	309		